Novel homoleptic and heteroleptic coordination polymers with flexible bis-pyridyl ligands

Hayder Dawood Jasim Arkawazi

Submitted in accordance with the requirements for the degree of
Doctor of Philosophy

The University of Leeds
School of Chemistry

March 2019

The candidate confirms that the work submitted is his own, except where work which has formed part of jointly-authored publication has been included. The contribution of the candidate and the other authors to this work has been explicitly indicated below. The candidate confirms that appropriate credit has been given within the thesis where reference has been made to the work of others. Further details of the jointly-authored publication and the contributions of the candidate and the other authors to the work should be included below this statement.

Reference for jointly authored publication

- H. D. J. Arkawazi, R. Clowes, A. I. Cooper, T. Konno, N. Kuwamura, C. M. Pask and M. J. Hardie, Complex Phase Behaviour and Structural Transformations of Metal-Organic Frameworks with Mixed Rigid and Flexible Bridging Ligands. *Chemistry A European Journal*. 2019, **25**(5), 1353-1362.

The work described within this publication is presented in Chapter 5 of this thesis. L3 ligand was designed, prepared and characterised by the candidate. The candidate also prepared the new MOFs, collected and solved seven crystal structures. Furthermore, the candidate scanned 107 crystals unit cells that requested for this publication. The weak diffracting crystals data were collected by Dr C. M. Pask and Mr. E. Britton using synchrotron radiation. Gas absorption/desorption properties were investigated at the University of Liverpool by Dr. R. Clowes and Prof. A. I. Copper. Ethanol sorption experiments were investigated at Osaka University by Dr. N. Kuwamura and Prof. T. Konno. Prof. M. J. Hardie directed the work and wrote the paper.

Acknowledgment

I would like to express my sincere gratitude to my supervisor Prof. Michaele J. Hardie for her time, patient, helping, encouragement, guiding and for her advice during my research time. I could not achieve this work without her unlimited support. I want to thank the Iraqi ministry of higher education and scientific research for funding. The Iraqi cultural attaché in London for their support during my research time. I would like to thank Prof. Malcolm Halcrow for his valuable advises, helping, support and efforts during my research time more especially when he spends long hours to correct my previous reports. I would like to thank my parents, my brother and my sister for their unconditional love, support, and encouragement. My dear parents, day after day, I realize how much you both sacrificed to give us a better life. I love you both from the bottom of my heart. I would like to thank my uncles Ali and Mohammed for their support and help during my studying time. Uncle Mohammed, you are always my best friend, and I wish that you were with us.

I would like to thank Prof. Patrick McGowan for his valuable corrections and feedback on my transfer report. I would like to thank Dr. C. Pask for his support and efforts for solving complicated crystal structures. I would like to thank Prof. Hardie research group past and present members for their help and support during my research time since day one, more especially, Dr. F. Thorp-Greenwood, Dr. J. Fowler, Dr. S. Oldknow, Dr. V. Pritchard and Mr. E. Britton. I am always grateful for all of you. I would like to thank Dr. C. Willans research group past and present members more especially, Dr. H. Abdulgawad, Dr. W. Rungtanapirom, Ms. F. Singer, Mr. H. Stephen and Ms. A. Frith for their support and kindness during my research time. I would like to thank Prof. M. Halcrow former and present research group members more especially, Dr. R. Kulmaczewski, Mr. I. Galadzhun, Mr. I. Capel, Ms. K. Burrows and Ms. N. Shahid. I would like to thank Prof. P. McGowan former and present research group members more especially, Dr. C. Madzivire and Mr. P. Caramés Méndez.

I would like to thank Mr. Abbas and Mr. Raheem Al-Saleem for their help with all my paperwork and financial transactions, I am grateful for both of you. I would like to thank Mr. A. Al-Fahdawai, Mr. H. Al-Khafaji and Mr. A. Akkady for their support and help during my studying time. I would like to thank Prof. J. Al-Zuhayri, Associated Prof. A. W. Salman, Associated Prof. S. Al-Bayati, Associated Prof. D. Al-Rekabi and Mrs. S. Hamed for guaranteeing me. I would like to thank my primary school teacher Mrs. Mayson who taught me my first Arabic letter. I still remember how she gently held my hand and help me to write my first ever letter. I would like to

thank Mr. Mohsen, my English language teacher. I wish that you were with us to show you my thesis. I would like to thank my master's degree supervisor Prof. S. Al-Kaylani I am always grateful for you. I would like to thank Mr. A. J. Noor and Mrs. S. B. Jassim for their support. I would like to thank my examiners Dr. T. Kee and Dr. S. Dalgarno for their long hours to read this thesis and for their valuable notes, corrections and feedback. I would like to thank all my friends that I missed to mention above. Finally, I would like to thank Dr. M. Howard, Mrs. A. Luty and all staff members at the University of Leeds.

Abstract

This thesis concerns the design, synthesis and characterisation of flexible and rigid bis-pyridyl ligands known as *N*,*N*′-bis-pyridin-3-ylmethylene-benzene-1,4-diamine ([a]L), *N*,*N*′-bis-pyridin-3-ylmethyl-benzene-1,4-diamine (L1), *N*,*N*′-bis-pyridin-4-ylmethylene-benzene-1,4-diamine ([b]L), *N*,*N*′-bis-pyridin-4-ylmethyl-benzene-1,4-diamine (L2), *N*,*N*′-bis(4-pyridinylmethylene)-2,5-dimethylbenzene-1,4-diamine ([c]L) and *N*,*N*′-bis(4-pyridinylmethyl)-2,5-dimethylbenzene-1,4-diamine (L3). Besides, the self-assembly process of new L1, L3 or the reported L2 with Mn(II), Fe(II), Fe(III), Co(II), Cu(II), Zn(II) or Cd(II) metal ions to produce a series of novel homoleptic coordination polymers and metal-organic frameworks. On the other hand, the self-assembly process of rigid dicarboxylic acid linkers such as, benzene-1,4-dicarboxylic acid, isophthalic acid or 4,4′-biphenyldicarboxylic acid with L1 or L3 and Co(II) or Cd(II) metal ions produced a series of new heteroleptic metal-organic frameworks. Furthermore, L3 ligand heteroleptic MOFs with Co(II) ion and benzene-1,4-dicarboxylic acid or 4,4′-biphenyldicarboxylic acid showed high thermal stability up to 450 °C, solvent exchange properties, high hydrogen gas uptake of 4.77 or 6.225 mmol/g and high ethanol uptakes of 97.16 or 91.36 cm^3/g respectively.

List of abbreviation

- *N*,*N*′-Bis-pyridin-3-ylmethylene-benzene-1,4-diamine (^{a}L)
- *N*,*N*′-Bis-pyridin-3-ylmethyl-benzene-1,4-diamine (L1)
- $([Mn_{0.5}(L1)Cl].MeOH)_n$ (**1**)
- $([Fe_{0.5}(L1)Cl].MeOH)_n$ (**2**)
- $([Co_{0.5}(L1)Cl].MeOH)_n$ (**3**)
- $([Cu(L1)Cl]\cdot CH_2Cl_2)_n$ (**4**)
- $([Zn(L1)(H_2O)_2].NO_3)_n$ (**5**)
- $([Cd(L1)_2(NO_3)_2])_n$ (**6**)
- $([Cd(L1)_{0.5}(isoph)(DMF)])_n$ (**7**)
- $([Cd_{1.5}(L1)_{0.5}(bdc)_{1.5}(DMF)])_n$ (**8**)
- *N*,*N*′-Bis-pyridin-4-ylmethylene-benzene-1,4-diamine (^{b}L)
- *N*,*N*′-Bis-pyridin-4-ylmethyl-benzene-1,4-diamine (L2)
- $([Mn_{0.5}(L2)_{0.5}Cl(DMSO)])_n$ (**9**)
- $([Co_{0.5}(L2)_{0.5}Cl(DMSO)])_n$ (**10**)
- $([Fe_{0.5}(L2)Cl])_n$ (**11**)
- $([Fe_{0.5}(L2)(SCN)].MeOH)_n$ (**12**)
- $([Co(L2)].NO_3.DMF)_n$ (**13**)
- *N*,*N*′-Bis(4-pyridinylmethylene)-2,5-dimethylbenzene-1,4-diamine (^{c}L)
- *N*,*N*′-Bis(4-pyridinylmethyl)-2,5-dimethylbenzene-1,4-diamine (L3)
- $([Fe_{0.5}(L3)Cl].MeOH)_n$ (**14**)
- $([Fe(L3)_{0.5}(SCN)])_n$ (**15**)
- $(Co(L3)(isoph)].DMF)_n$ (**16**)
- $(Cd(L3)(isoph)].DMF.H_2O)_n$ (**17**)
- $([Co(L3)(Meisoph)].DMF)_n$ (**18**)
- $([Cd(L3)(Meisoph)].DMF)_n$ (**19**)
- $(Co_2(L3)(bdc)_2.n(DMF))_n$ α-**20**(L)
- $(Co_2(L3)(bdc)_2.2DMF)_n$ β-**20**(S)
- $([Co_2(L3)(bdc)_2].(DMF).(H_2O))_n$ γ-**20**(L)
- $([Co(L3)_{0.5}(bdc)])_n$ δ-**20**(L)

- $([Co_2(L3)(bdc)_2].DMF.COMe_2)_n$ β-**20**(S)^{ace}
- $([Co(L3)_{0.5}(bdc)])_n$ ε-**20**(L)
- $([Co_2(L3)(bdc)_2].n(EtOH))_n$ γ-**20**(L)^{EtOH}
- $([Co_2(L3)(bdc)_2].2EtOH)_n$ ζ-**20**(S)^{EtOH}
- $([Co_2(L3)_2(bdc)_2].2H_2O)_n$ (**21**)
- $([Co_2(L3)(bpdc)_2])_n$ (**22**)
- $([Co_2(L3)(bpdc)_2])_n$ (**22**)^{a}
- $([Co_2(L3)(bpdc)_2].n(EtOH))_n$ (**22**)^{EtOH}
- $([Co_2(L3)(bpdc)_2].(H_2\text{-bpdc}).n(H_2O))_n$ (**22**)^{H_2O}
- $([Co(L3)_{0.5}(naph)].(H_2O).n(DMF))_n$ (**23**)
- $([Co(L3)_{0.5}(naph)].H_2O)_n$ MOF **23**^{H_2O}
- 1,3,5-Tris[((1,3-carboxylic acid-5-(4-(ethynyl)phenyl))ethynyl)phenyl]-benzene (H_6-LP)
- 1,3,5-Tris[(1,3-carboxylic acid-5-(4-(ethynyl)phenyl))butadiynyl]-benzene (H_6-LB)
- 1,4-Bis(4-pyridyl)-2,3-diaza-1,3-butadiene (4-bpdb)
- 2-Bromo-benzene-1,4-dicarboxylic acid (*o*-Br-H_2-bdc)
- 2-Hydroxypyrimidinolate (2-pymo)
- 2-Pyridinecarbaldehyde isonicotinoylhydrazone (HPCIH)
- 4,4′-Bipyridine (4,4′-bipy)
- 4,4′-Oxybis(benzoic acid) (H_2-oba)
- 4,4-Bipyneyldicarboxylic acid (H_2-bpdc)
- 4,4'-Sulfonyldibenzoate (sba)
- 5-(Isonicotinamido)isophthalic acid (H_2-ison)
- 5-(Nicotinamido)isophthalic acid (H_2-nica)
- 5-(Pyridin-3-ylamino)isophthalic acid (H_2-pyaiso)
- 5-(Pyridine-4-ylamino)isophthalic acid (H_2-pyiso)
- 5-(Pyrimidin-5-ylamino)isophthalic acid (H_2-pmiso)
- Benzene-1,3,5-tricarboxylic acid (H_3-btc)
- Benzene-1,3,5-tristetrazolate (btt^{3-})
- Benzene-1,4-dicarboxylic acid (H_2-bdc)
- Brunauer-Emmett-Teller (BET)

- Coordination polymers (CPs)
- Coupling constant (*J*)
- Dichloromethane (DCM)
- Dimethylsulfoxide (DMSO)
- Gram (g)
- Infrared radiation (IR)
- Isonicotinic acid (H-ina)
- Isophthalic acid (H_2-isoph)
- Kelvin (K)
- Lambda (λ)
- Ligand (L)
- Megahertz (MHz)
- Melting point (mp)
- Metal-organic frameworks (MOFs)
- Methyl (Me)
- *N,N'*-Bis(pyridin-4-yl)-2,2'-bipyridine-5,5'-dicarboxamide (2,2-bpbi)
- *N*,*N*-Diethylformamide (DEF)
- *N*,*N*-Dimethylformamide (DMF)
- Naphthalene-1,4-dicarboxylic acid (H_2-1,4-ndc)
- Naphthalene-1,6-dicarboxylic acid (H_2-naph)
- Nuclear magnetic resonance (NMR)
- Pyrazine (pyz)
- Pyridine (py)
- Scanning electron microscope (SEM)
- Solvent (solv)
- Thermal gravimetric analysis (TGA)
- Wave number ($\bar{\nu}$)

List of Contents

Chapter One

Coordination polymers and metal-organic frameworks; synthesis, properties and applications

1.1	Introduction	1
1.2	Overview	4
1.2.1	Prussian blue	4
1.2.2	The term metal-organic framework	5
1.2.3	HKUST-1 MOF	6
1.2.4	MIL-53 MOF	8
1.2.5	MOF-101	9
1.2.6	NU-109 and NU-110 MOFs	11
1.3	Coordination polymers and metal-organic frameworks synthesis methods	13
1.3.1	Solvothermal synthesis	13
1.3.2	Microwave synthesis	17
1.3.3	Mechanochemical synthesis	21
1.4	Coordination polymers and metal-organic frameworks applications	24
1.4.1	Chemical catalysts	24
1.4.2	Gas storage	28
1.5	Coordination polymers based on bis-pyridyl ligands	31
1.6	Conclusion	38
1.7	References	39

Chapter Two

***N,N'*-Bis-pyridin-3-ylmethyl-benzene-1,4-diamine (L1) coordination polymers and metal-organic frameworks**

2.1	Introduction	53
2.2	Experimental	54
2.2.1	Materials and instrumentation	54
2.2.2	Synthesis of *N,N'*-bis-pyridin-3-ylmethylene-benzene-1,4-diamine (^{a}L)	54
2.2.3	Synthesis of *N,N'*-bis-pyridin-3-ylmethyl-benzene-1,4-diamine (L1)	54

2.2.4 Synthesis of $([M_{0.5}(L1)Cl].MeOH)_n$ one-dimensional polymers (**1-3**) 55
2.2.5 Synthesis of $([Cu(L1)Cl].CH_2Cl_2)_n$ one-dimensional polymer (**4**) 55
2.2.6 Synthesis of $([Zn_{0.5}(L1)(H_2O)_2].NO_3)_n$ two-dimensional polymer (**5**) 56
2.2.7 Synthesis of $([Cd(L1)_2(NO_3)_2])_n$ two-dimensional polymer (**6**) 56
2.2.8 Synthesis of $([Cd(L1)_{0.5}(isoph)(DMF)])_n$ MOF (**7**) 56
2.2.9 Synthesis of $([Cd_{1.5}(L1)_{0.5}(bdc)_{1.5}(DMF)])_n$ MOF (**8**) 56
2.3 Crystallography experimental 57
2.4 Results and discussion 57
2.4.1 Synthesis of *N,N'*-bis-pyridin-3-ylmethylene-benzene-1,4-diamine (^{a}L) 57
2.4.2 Synthesis of *N,N'*-bis-pyridin-3-ylmethyl-benzene-1,4-diamine (L1) 59
2.4.3 Synthesis of new **1-8** CPs 61
2.5 Crystal structures 62
2.5.1 Crystal structure of *N,N'*-bis-pyridin-3-ylmethyl-benzene-1,4-diamine (L1) 62
2.5.2 Crystal structures of $([M_{0.5}(L1)Cl].MeOH)_n$ (**1-3**) CPs 64
2.5.3 Crystal structure of $([Cu(L1)Cl].DCM)_n$ coordination polymer (**4**) 70
2.5.4 Crystal structure of $([Zn(L1)(H_2O)_2].NO_3)_n$ coordination polymer (**5**) 74
2.5.5 Crystal structure of $([Cd(L1)_2(NO_3)_2])_n$ coordination polymer (**6**) 77
2.5.6 Crystal structure of $([Cd(L1)_{0.5}(isoph)(DMF)])_n$ MOF (**7**) 81
2.5.7 Crystal structure of $([Cd_{1.5}(L1)_{0.5}(bdc)_{1.5}(DMF)])_n$ MOF (**8**) 86
2.6 Conclusion 95
2.7 References 96

Chapter Three

***N,N'*-Bis-pyridin-4-ylmethyl-benzene-1,4-diamine (L2) complexes**

3.1 Introduction 104
3.2 Experimental 105
3.2.1 Synthesis of *N,N'*-bis-pyridin-4-ylmethylene-benzene-1,4-diamine (^{b}L) 105
3.2.2 Synthesis of *N,N'*-bis-pyridin-4-ylmethyl-benzene-1,4-diamine (L2) 105
3.2.3 Synthesis of $([Mn_{0.5}(L2)_{0.5}Cl(DMSO)])_n$ (**9**) and $([Co_{0.5}(L2)_{0.5}Cl(DMSO)])_n$ (**10**) 106
3.2.4 Synthesis of $([Fe_{0.5}(L2)Cl])_n$ coordination polymer (**11**) 106
3.2.5 Synthesis of $([Fe_{0.5}(L2)(SCN)].MeOH)_n$ coordination polymer (**12**) 106

3.2.6 Synthesis of $([Co(L2)].NO_3.DMF)_n$ complex (**13**) 106
3.3 Crystallography experimental 107
3.4 Results and discussion 107
3.4.1 Synthesis of *N,N'*-bis-pyridin-4-ylmethylene-benzene-1,4-diamine (^bL) 107
3.4.2 Synthesis of *N,N'*-bis-pyridin-4-ylmethyl-benzene-1,4-diamine (L2) 109
3.4.3 Synthesis of new complexes **9-13**. 111
3.5 Crystal structures 112
3.5.1 Crystal structure of *N,N'*-bis-pyridin-4-ylmethyl-benzene-1,4-diamine (L2) 112
3.5.2 Crystal structures of compounds (**9**) and (**10**) 114
3.5.3 Crystal structure of $([Fe_{0.5}(L2)Cl])_n$ coordination polymer (**11**) 118
3.5.4 Crystal structure of $([Fe_{0.5}(L2)(SCN)].MeOH)_n$ coordination polymer (**12**) 121
3.5.5 Crystal structure of $([Co(L2)].NO_3.DMF)_n$ complex (**13**) 127
3.6 Conclusion 132
3.7 References 133

Chapter Four

***N,N'*-Bis(4-pyridinylmethyl)-2,5-dimethylbenzene-1,4-diamine (L3) MOFs**

4.1 Introduction 137
4.2 Experimental 138
4.2.1 Synthesis of the new ligand (^cL) 138
4.2.2 Synthesis of the new ligand (L3) 138
4.2.3 Synthesis of $([Fe_{0.5}(L3)Cl].MeOH)_n$ MOF (**14**) 139
4.2.4 Synthesis of $([Fe(L3)_{0.5}(SCN)])_n$ MOF (**15**) 139
4.2.5 Synthesis of $(Co(L3)(isoph)].DMF)_n$ (**16**) and $(Cd(L3)(isoph)].DMF.H_2O)_n$ (**17**) 139
4.2.6 Synthesis of $([Co(L3)(Meisoph)].DMF)_n$ and $([Cd(L3)(Meisoph)].DMF)_n$ (**18-19**) 140
4.3 Crystallography experimental 140
4.4 Results and discussions 140
4.4.1 Synthesis of the new ligand (^cL) 140
4.4.2 Synthesis of the new ligand (L3) 142
4.4.3 Synthesis of new MOFs **14-19** 144
4.5 Crystal structures 145

4.5.1 Crystal structure of the new ligand (^{c}L) 145
4.5.2 Crystal structure of the new ligand (L3) 147
4.5.3 Crystal structure of $([Fe_{0.5}(L3)Cl].MeOH)_n$ MOF(**14**) 148
4.5.4 Crystal structure of $([Fe(L3)_{0.5}(SCN)])_n$ MOF (**15**) 153
4.5.5 Crystal structures of compounds (**16**) and (**17**) 158
4.5.6 Crystal structures of compounds (**18**) and (**19**) 165
4.6 Conclusion 175
4.7 References 177

Chapter Five

***N,N'*-Bis(4-pyridinylmethyl)-2,5-dimethylbenzene-1,4-diamine metal-organic frameworks**

5.1 Introduction 181
5.2 Experimental 182
5.2.1 Synthesis of $([Co_2(L3)(bdc)_2].n(DMF))_n$ (**20**) and $([Co_2(L3)_2(bdc)_2].2H_2O)_n$ (**21**) 182
5.2.2 Synthesis of $([Co_2(L3)(bpdc)_2])_n$ MOF (**22**) 182
5.2.3 Synthesis of $([Co(L3)_{0.5}(naph)].(H_2O).n(DMF))_n$ MOF (**23**) 182
5.3 Crystallography experimental 182
5.4 Results and discussions 183
5.5 Crystal structures 183
5.5.1 Crystal structures of (**20**) and (**21**) 183
5.5.1.1 Crystal structure of $(Co_2(L3)(bdc)_2.n(DMF))_n$ α-**20**(L) MOF 185
5.5.1.2 Crystal structure of $(Co_2(L3)(bdc)_2.2DMF)_n$ β-**20**(S) MOF 188
5.5.1.3 Crystal structure of $([Co_2(L3)(bdc)_2].(DMF).(H_2O))_n$ γ-**20**(L) MOF 193
5.5.1.4 Crystal structure of δ-**20**(L) MOF 197
5.5.1.5 Crystal structure of $([Co_2(L3)_2(bdc)_2].2H_2O)_n$ (**21**) MOF 201
5.5.1.6 Crystal structure of $([Co_2(L3)(bdc)_2].DMF.COMe_2)_n$ β-**20**$(S)^{ace}$ MOF 205
5.5.1.7 Crystal structure of $([Co(L3)_{0.5}(bdc)])_n$ ε-**20**(L) MOF 210
5.5.1.8 Crystal structure of $([Co_2(L3)(bdc)_2].n(EtOH))_n$ γ-**20**$(L)^{EtOH}$ MOF 214
5.5.1.9 Crystal structure of $([Co_2(L3)(bdc)_2].2EtOH)_n$ ζ-**20**$(S)^{EtOH}$ MOF 218
5.5.1.10 Crystal structure of compound **20** in water 222
5.5.2 Crystal structure of $([Co_2(L3)(bpdc)_2])_n$ MOF (**22**) 224

5.5.2.1 Crystal structure of $([Co_2(L3)(bpdc)_2])_n$ MOF (**22**) 225
5.5.2.2 Crystal structure of $([Co_2(L3)(bpdc)_2])_n$ MOF (**22**)[a] 229
5.5.2.3 Crystal structure of $([Co_2(L3)(bpdc)_2].n(EtOH))_n$ MOF (**22**)^{EtOH} 233
5.5.2.4 Crystal structure of $([Co_2(L3)(bpdc)_2].(H_2\text{-bpdc}).n(H_2O))_n$ MOF (**22**)^{H_2O} 236
5.5.3 Thermogravimetric analysis 239
5.5.3.1 Thermogravimetric analysis of compound **20** 239
5.5.3.2 Thermogravimetric analysis of compound **22** 240
5.5.4 Gas sorption studies 241
5.5.5 Crystal structure of $([Co(L3)_{0.5}(naph)])_n$ MOF 243
5.5.5.1 Crystal structure of $([Co(L3)_{0.5}(naph)].(H_2O).n(DMF))_n$ MOF (**23**) 243
5.5.5.2 Crystal structure of $([Co(L3)_{0.5}(naph)].H_2O)_n$ MOF **23**^{H_2O} 247
5.6 Conclusion 257
5.7 References 258

List of schemes

Scheme 1.1: Synthesis of 4-methoxy-biphenyl 25
Scheme 1.2: Cyanosilylation of aldehyde or ketone compounds 28
Scheme 2.1: Synthesis of *N,N′*-bis-pyridin-3-ylmethylene-benzene-1,4-diamine ([a]L) 58
Scheme 2.2: Synthesis of *N,N′*-bis-pyridin-3-ylmethyl-benzene-1,4-diamine ligand (L1) 60
Scheme 3.1: Synthesis of *N,N′*-bis-pyridin-4-ylmethylene-benzene-1,4-diamine ([b]L) 108
Scheme 3.2: Synthesis of *N,N′*-bis-pyridin-4-ylmethyl-benzene-1,4-diamine (L2) 110
Scheme 4.1: Synthesis of *N,N′*-bis(4-pyridinylmethylene)-2,5-dimethylbenzene-1,4-diamine ([c]L) 141
Scheme 4.2: Synthesis of *N,N′*-bis(4-pyridinylmethyl)-2,5-dimethylbenzene-1,4-diamine (L3) 143
Scheme 5.1: Phase behaviour of compound **20** as-synthesised, dried and in EtOH or H_2O 184
Scheme 5.2: Compound **22** as-synthesised, dried, in ethanol or water 224

List of Figures

Chapter One

Figure 1.1: One-dimensional coordination polymers common conformations 1

Figure 1.2: Two and three-dimensional coordination polymers common conformations 2

Figure 1.3: Coordination polymers and metal-organic frameworks publications 3

Figure 1.4: Rigid and flexible organic linkers examples 3

Figure 1.5: Dry solid, solid hydrated and soluble form of Prussian blue 5

Figure 1.6: Crystal structure of $[Co(btc)_3(py)_2].2/3(py)$ MOF 6

Figure 1.7: HKUST-1 MOF building block and four-fold symmetry 7

Figure 1.8: HKUST-1 MOF Kagome structure 8

Figure 1.9: MIL-53ht MOF crystal structure 9

Figure 1.10: MOF-101 square secondary building unit 10

Figure 1.11: NU-109 and NU-110 MOFs organic linkers 12

Figure 1.12: NU-109 and NU-110 three-dimensional open networks 12

Figure 1.13: NU-109 and NU-110 MOFs nitrogen gas sorption data 13

Figure 1.14: SEM images of HCC-1 resultant crystals 14

Figure 1.15: [Zn(bdc)(DMF)], ($[Zn(bdc)(H_2O)](DMF)$) and ($[Zn(HCO_2)_3](C_2H_8N)$) MOFs crystal structures 15

Figure 1.16: ($[In(OH)(1,4\text{-}ndc)].2H_2O$) MOF 17

Figure 1.17: ($H[In(1,4\text{-}ndc)_2].2(H_2O).1.5(DMF)$) MOF 17

Figure 1.18: SEM image of MOF-199 18

Figure 1.19: CYCU-1 and CYCU-2 MOFs coordination environments 19

Figure 1.20: CYCU-1 MOF cross-section and diagonal distances 20

Figure 1.21: $[Cu_2(pyz)_2SO_4(H_2O)_2]$ MOF coordination sphere 21

Figure 1.22: Resulted and calculated powder XRD patterns of $[Cu(ina)_2]$ MOF 22

Figure 1.23: HKUST-1 MOF mechanochemical reaction 23

Figure 1.24: XRD patterns for TMU-8 and TMU-9 MOFs 24

Figure 1.25: $[Pd(2\text{-}pymo)_2]_n$ MOF crystal structure 25

Figure 1.26: $[(Cu_4O_{0.27}Cl_{0.73})_3(H_{0.5}btt)_8]$ MOF crystal structure 27

Figure 1.27: $Cu(ison).(solv)_n$ and $Cu(nica).(solv)_n$ MOFs Kagome structure 29

Figure 1.28: Cu(pyiso).(solv)$_n$, Cu(pyaiso).(solv)$_n$ and Cu(pmiso).(solv)$_n$ MOFs 30
Figure 1.29: [($Cu_4O_{0.27}Cl_{0.73}$)$_3$($H_{0.5}$btt)$_8$] (Cu-MOF1') 31
Figure 1.30: Crystal structure of 2,2-bpbi 32
Figure 1.31: Crystal structure of {[Cu_5(2,2-bpbi)$_6$]}$_\infty$ MOF 32
Figure 1.32: {[Cu_5(2,2-bpbi)$_6$]$_\infty$.(NO_3)$_{10}$.(H_2O)$_{18}$}$_\infty$ MOF crystal structure 33
Figure 1.33: {[Fe_xCu_y(2,2-bpbi)$_6$]$_\infty$.(NO_3)$_{10}$.(H_2O)$_{18}$}$_\infty$ MOF crystal structure 34
Figure 1.34: {[Co(2,2-bpbi)Cl_2].DMF}$_\infty$ MOF coordination environment 34
Figure 1.35: Interpenetrating of {[Co(2,2-bpbi)Cl_2].DMF}$_\infty$ MOF 2D networks 35
Figure 1.36: {Cd(2,2-bpbi)(NO_3)$_2$}$_\infty$ MOF crystal structure 35
Figure 1.37: {Cd(2,2-bpbi)(NO3)$_2$}$_\infty$ MOF two-dimensional networks 36
Figure 1.38: [Zn(iso)(2,2-bpbi)].2(DMF) MOF spiral chains 37
Figure 1.39: [Zn(iso)(2,2-bpbi)].2(DMF) MOF crystal structures 37

Chapter Two

Figure 2.1: ^{1}H NMR (400 MHz, DMSO-d_6) spectrum of ^{a}L ligand 58
Figure 2.2: ^{13}C{^{1}H} NMR (101 MHz, DMSO-d_6) spectrum of ^{a}L ligand 59
Figure 2.3: ^{1}H NMR (300 MHz, DMSO-d_6) spectrum of L1 ligand 60
Figure 2.4: ^{13}C{^{1}H} NMR (75 MHz, DMSO-d_6) spectrum of L1 ligand 61
Figure 2.5: L1 ligand asymmetric unit of the crystal structure 62
Figure 2.6: Crystal structure of L1 ligand 63
Figure 2.7: ([($Mn_{0.5}$(L1)Cl].MeOH)$_n$ CP asymmetric unit of the crystal structure 65
Figure 2.8: ([$Mn_{0.5}$(L1)Cl].MeOH)$_n$ CP rectangle cavities 66
Figure 2.9: ([$Mn_{0.5}$(L1)Cl].MeOH)$_n$ CP hydrogen bond interactions 66
Figure 2.10: Packing diagram of ([$Mn_{0.5}$(L1)Cl].MeOH)$_n$ CP 67
Figure 2.11: Calculated and powder XRD patterns of compound **1** 69
Figure 2.12: Calculated and powder XRD patterns of compound **2** 69
Figure 2.13: Calculated and powder XRD patterns of compound **3** 69
Figure 2.14: ([Cu(L1)Cl].DCM)$_n$ asymmetric unit of the crystal structure 71
Figure 2.15: [Cu_2(μ-L1)$_2$] Coordination chains 71
Figure 2.16: ([Cu(L1)Cl]·CH_2Cl_2)$_n$ CP 2D layers 72
Figure 2.17: Packing diagram of ([Cu(L1)Cl]·CH_2Cl_2)$_n$ CP 72

Figure 2.18: Calculated and powder XRD patterns of compound **4** 73
Figure 2.19: $([Zn_{0.5}(L1)(H_2O)_2].NO_3)_n$ CP asymmetric unit of the crystal structure 75
Figure 2.20: $([Zn_{0.5}(L1)(H_2O)_2].NO_3)_n$ two-dimensional polymer network 75
Figure 2.21: $([Zn_{0.5}(L1)(H_2O)_2].NO_3)_n$ CP topology 76
Figure 2.22: Calculated and powder X-ray pattern of compound **5** 77
Figure 2.23: $([Cd(L1)_2(NO_3)_2])_n$ CP asymmetric unit of the crystal structure 78
Figure 2.24: $([Cd(L1)_2(NO_3)_2])_n$ two-dimensional network 79
Figure 2.25: Packing diagram of $([Cd(L1)_2(NO_3)_2])_n$ CP 79
Figure 2.26: Calculated and powder XRD patterns of compound **6** 80
Figure 2.27: $([Cd(L1)_{0.5}(isoph)(DMF)])_n$ MOF asymmetric unit of the crystal structure 82
Figure 2.28: Cd(II) and isophthalate two-dimensional network top view 82
Figure 2.29: Cd(II) and isophthalate two-dimensional network topology 83
Figure 2.30: $([Cd(L1)_{0.5}(isoph)(DMF)])_n$ MOF coordination environment 83
Figure 2.31: $([Cd(L1)_{0.5}(isoph)(DMF)])_n$ MOF after symmetrical expanding 84
Figure 2.32: Calculated and powder XRD patterns of compound **7** 85
Figure 2.33: $([Cd_{1.5}(L1)_{0.5}(bdc)_{1.5}(DMF)])_n$ MOF asymmetric unit of the crystal structure 87
Figure 2.34: Cd(II)-bdc^{2-} linear trimeric coordination centres 87
Figure 2.35: Cd(II)-bdc^{2-} two-dimensional network 88
Figure 2.36: $([Cd_{1.5}(L1)_{0.5}(bdc)_{1.5}(DMF)])_n$ MOF coordination environment 88
Figure 2.37: Chemdraw of $([Cd_{1.5}(L1)_{0.5}(bdc)_{1.5}(DMF)])_n$ MOF 89
Figure 2.38: $([Cd_{1.5}(L1)_{0.5}(bdc)_{1.5}(DMF)])_n$ MOF after symmetrical expanding 89
Figure 2.39: Calculated and powder XRD patterns of compound **8** 91

Chapter Three

Figure 3.1: ^1H NMR (300 MHz, DMSO-d_6) spectrum of ^bL ligand 108
Figure 3.2: $^{13}C\{^1H\}$ NMR (75 MHz, DMSO-d_6) spectrum of ^bL ligand 109
Figure 3.3: ^1H NMR (300 MHz, DMSO-d_6) spectrum of L2 ligand 110
Figure 3.4: $^{13}C\{^1H\}$ NMR (75 MHz, DMSO-d_6) spectrum of L2 ligand 111
Figure 3.5: L2 ligand asymmetric unit of the crystal structure 112
Figure 3.6: Crystal structure of L2 ligand 113
Figure 3.7: $([Mn_{0.5}(L2)_{0.5}Cl(DMSO)])_n$ CP asymmetric unit of the crystal structure 115

Figure 3.8: Packing diagram of ($[Mn_{0.5}(L2)_{0.5}Cl(DMSO)]$)$_n$ CP 115
Figure 3.9: Calculated and powder XRD patterns of compound **9** 117
Figure 3.10: Calculated and powder XRD patterns of compound **10** 117
Figure 3.11: ($[Fe_{0.5}(L2)Cl]$)$_n$ CP asymmetric unit of the crystal structure 119
Figure 3.12: ($[Fe_{0.5}(L2)Cl]$)$_n$ CP two-dimensional network structure 119
Figure 3.13: Packing diagram of ($[Fe_{0.5}(L2)Cl]$)$_n$ CP 120
Figure 3.14: Calculated and powder XRD patterns of compound **11** 121
Figure 3.15: ($[Fe_{0.5}(L2)(SCN)].MeOH$)$_n$ CP asymmetric unit of the crystal structure 123
Figure 3.16: ($[Fe_{0.5}(L2)(SCN)].MeOH$)$_n$ CP 4^4 network topology 124
Figure 3.17: Two-fold interpenetrating of ($[Fe_{0.5}(L2)(SCN)].MeOH$)$_n$ 2D networks 124
Figure 3.18: Packing diagram of ($[Fe_{0.5}(L2)(SCN)].MeOH$)$_n$ 2D networks 125
Figure 3.19: Magnetic susceptibility measurement of ($[Fe_{0.5}(L2)(SCN)].MeOH$)$_n$ CP 125
Figure 3.20: Calculated and powder XRD patterns of compound **12** 127
Figure 3.21: ($[Co(L2)].NO_3.DMF$)$_n$ complex asymmetric unit of the crystal structure 128
Figure 3.22: ($[Co(L2)].NO_3.DMF$)$_n$ complex after symmetrical expanding 128
Figure 3.23: Calculated and powder XRD pattern of ($[Co(L2)].NO_3.DMF$)$_n$ complex 129

Chapter Four

Figure 4.1: ^{1}H NMR (300 MHz, $CDCl_3$) spectrum of ^{c}L ligand 141
Figure 4.2: $^{13}C\{^1H\}$ NMR (75 MHz, $CDCl_3$) spectrum of ^{c}L ligand 142
Figure 4.3: ^{1}H NMR (300 MHz, DMSO-d_6) spectrum of L3 ligand 143
Figure 4.4: $^{13}C\{^1H\}$ NMR (75 MHz, DMSO-d_6) spectrum of L3 ligand 144
Figure 4.5: ^{c}L ligand asymmetric unit of the crystal structure 145
Figure 4.6: Crystal structure of ^{c}L ligand 146
Figure 4.7: L3 ligand asymmetric unit of the crystal structure 147
Figure 4.8: Packing diagram of L3 ligand 147
Figure 4.9: ($[Fe_{0.5}(L3)Cl].MeOH$)$_n$ CP asymmetric unit of the crystal structure 150
Figure 4.10: ($[Fe_{0.5}(L3)Cl].MeOH$)$_n$ CP network 150
Figure 4.11: Packing diagram of ($[Fe_{0.5}(L3)Cl].MeOH$)$_n$ CP 151
Figure 4.12: Hydrogen bond interactions in compound **14** 151
Figure 4.13: Calculated and powder XRD patterns of compound **14** 153

Figure 4.14: $([Fe(L3)_{0.5}(SCN)])_n$ MOF asymmetric unit of the crystal structure 154
Figure 4.15: Compound **15** distorted octahedral coordination centre 154
Figure 4.16: $([Fe(L3)_{0.5}(SCN)])_n$ MOF hexagonal channels 155
Figure 4.17: Cross and H-shape channels of compound **15** 155
Figure 4.18: $([Fe(L3)_{0.5}(SCN)])_n$ crystal structure after symmetrical expanding 156
Figure 4.19: Calculated and powder XRD patterns of $([Fe(L3)_{0.5}(SCN)])_n$ MOF 156
Figure 4.20: Compounds **16** and **17** asymmetric units of crystal structures 160
Figure 4.21: Compounds **16** and **17** M(II)-isophthalate coordination chains 160
Figure 4.22: $(Co)_8(L3)_4(isoph)_4$ and $(Cd)_8(L3)_4(isoph)_4$ tetragonal structures 161
Figure 4.23: Packing diagram of compounds **16** and **17** 161
Figure 4.24: Compound **16** calculated and powder XRD patterns 164
Figure 4.25: Compound **17** calculated and powder XRD patterns 164
Figure 4.26: Compounds **18** and **19** asymmetric unit of crystal structures 166
Figure 4.27: Co(II) or Cd(II) and 5-methylisophthalate coordination chains 167
Figure 4.28: Compounds **18** and **19** tetragonal structures 167
Figure 4.29: Compounds **18** and **19** 2D networks 168
Figure 4.30: Compound **18** calculated and powder XRD patterns 169
Figure 4.31: Compound **19** calculated and powder XRD patterns 169

Chapter Five

Figure 5.1: Compounds **20** and **21** crystals as-synthesised in DMF and after separation 184
Figure 5.2: Compound α-**20**(L) asymmetric unit of the crystal structure 186
Figure 5.3: Compound α-**20**(L) $(Co_2)_8(L3)_4(bdc)_8$ tetragonal structure 187
Figure 5.4: Compound β-**20**(S) asymmetric unit of the crystal structure 189
Figure 5.5: β-**20**(S) MOF coordination environment 190
Figure 5.6: β-**20**(S) MOF open network structure 191
Figure 5.7: β-**20**(S) MOF crystal structure with solvent guest molecules 192
Figure 5.8: Compound γ-**20**(L) asymmetric unit of the crystal structure 194
Figure 5.9: Compound γ-**20**(L) tetragonal structure 195
Figure 5.10: Compound γ-**20**(L) interpenetrating three-dimensional networks 196
Figure 5.11: Compound δ-**20**(L) asymmetric unit of the crystal structure 198

Figure 5.12: Compound δ-**20**(L) coordination environment 198
Figure 5.13: Compound δ-**20**(L) three-dimensional open network 199
Figure 5.14: Compounds **20** calculated and powder XRD patterns 200
Figure 5.15: Compound **21** asymmetric unit of the crystal structure 202
Figure 5.16: Co(II)-bdc^{2-} two-dimensional network 202
Figure 5.17: Compound **21** three-dimensional open network 203
Figure 5.18: Compound **21** calculated and powder XRD patterns 203
Figure 5.19: Compound β-**20**$(S)^{ace}$ asymmetric unit of the crystal structure 206
Figure 5.20: Co(II) ion coordination environment in compound β-**20**$(S)^{ace}$ 207
Figure 5.21: β-**20**$(S)^{ace}$ MOF three-dimensional open network 208
Figure 5.22: β-**20**$(S)^{ace}$ MOF two-fold interpenetrating networks 209
Figure 5.23: ε-**20**(L) MOF asymmetric unit of the crystal structure 211
Figure 5.24: ε-**20**(L) MOF paddlewheel structure, square unit and tetragonal structures 211
Figure 5.25: ε-**20**(L) MOF three-dimensional open network 212
Figure 5.26: β-**20**$(S)^{ace}$ MOF calculated powder XRD pattern 213
Figure 5.27: γ-**20**$(L)^{EtOH}$ MOF asymmetric unit of the crystal structure 215
Figure 5.28: Co(II) ion coordination environment in γ-**20**$(L)^{EtOH}$ MOF 216
Figure 5.29: γ-**20**$(L)^{EtOH}$ MOF three-dimensional open network structure 217
Figure 5.30: ζ-**20**$(S)^{EtOH}$ MOF asymmetric unit of crystal structure 219
Figure 5.31: ζ-**20**$(S)^{EtOH}$ MOF paddlewheel structure 219
Figure 5.32: ζ-**20**$(S)^{EtOH}$ MOF three-dimensional open network 220
Figure 5.33: Ethanol molecules in ζ-**20**$(S)^{EtOH}$ MOF 221
Figure 5.34: ζ-**20**$(L)^{EtOH}$ and γ-**20**$(L)^{EtOH}$ MOFs calculated and powder XRD patterns 221
Figure 5.35: Compound $(L3.2H_2O)_n$ asymmetric unit of the crystal structure 223
Figure 5.36: Compound **22** asymmetric unit of the crystal structure 226
Figure 5.37: Compound **22** paddlewheel structure 226
Figure 5.38: Compound **22** Co(II)-$bpdc^{2-}$ two and three-dimensional networks 227
Figure 5.39: Compound **22** three-dimensional open network 228
Figure 5.40: Compound $\mathbf{22}^{a}$ asymmetric unit of the crystal structure 230
Figure 5.41: Compound $\mathbf{22}^{a}$ paddlewheel structure 230

Figure 5.42: Compound **22**[a] two and three-dimensional networks 231
Figure 5.43: **22**[a] Co(II)-bpdc^{2-} 3D open network rectangle, square and rhombic channels 232
Figure 5.44: Compound **22**^{EtOH} asymmetric unit of the crystal structure 234
Figure 5.45: Compound **22**^{EtOH} paddlewheel structure 234
Figure 5.46: Compound **22**^{EtOH} 3D network structure 235
Figure 5.47: Compound **22**^{H_2O} asymmetric unit of the crystal structure 237
Figure 5.48: Compound **22**^{H_2O} paddlewheel structure 237
Figure 5.49: Compound **22**^{H_2O} one-dimensional open network 238
Figure 5.50: Calculated and powder XRD pattern for compounds **22** 238
Figure 5.51: Thermal gravimetric analysis trace of compound **20** 240
Figure 5.52: Thermal gravimetric analysis trace of compound **22** 241
Figure 5.53: Gas sorption properties of activated compound **20** 242
Figure 5.54: Gas sorption properties of activated compound **22** 242
Figure 5.55: Ethanol isotherms of Compounds **20** and **22** at 298 K 243
Figure 5.56: Compound **23** asymmetric unit of the crystal structure 244
Figure 5.57: Compound **23** paddlewheel structure 245
Figure 5.58: Compound **23** three-fold interpenetrating network 246
Figure 5.59: Compound **23**^{H_2O} asymmetric unit of the crystal structure 248
Figure 5.60: Compounds **23** calculated and powder XRD patterns 249
Figure 5.61: Compound **23** thermal gravimetric analysis trace 250
Figure 5.62: Activated compound **23** nitrogen and hydrogen gases isotherms 250

List of Tables

Chapter Two

Table 2.1: Selected bond lengths (Å) and angles (°) for L1 ligand 63

Table 2.2: Selected torsion angles (°) for L1 ligand 63

Table 2.3: Selected bond lengths (Å) and angles (°) for compounds (**1-3**) 67

Table 2.4: Selected torsion angles (°) for compounds (**1-3**) 68

Table 2.5: Selected torsion angles (°) for compound **4** 71

Table 2.6: Selected bond lengths (Å) and angles (°) for compound **4** 73

Table 2.7: Selected bond lengths (Å) and angles (°) for compound **5** 76

Table 2.8: Selected torsion angles (°) for compound **5** 77

Table 2.9: Selected bond lengths (Å) and angles (°) for compound **6** 79

Table 2.10: Selected torsion angles (°) for compound **6** 80

Table 2.11: Selected bond lengths (Å) and angles (°) for compound **7** 84

Table 2.12: Selected torsion angles (°) for compound **7** 85

Table 2.13: Selected bond lengths (Å) and angles (°) for compound **8** 90

Table 2.14: Selected torsion angles (°) for compound **8** 90

Table 2.15: Crystallographic data of compounds L1, **1** and **2** 92

Table 2.16: Crystallographic data of compounds **3**, **4** and **5** 93

Table 2.17: Crystallographic data of compounds **6**, **7** and **8** 94

Chapter Three

Table 3.1: Selected bond lengths (Å) and angles (°) for L2 ligand 113

Table 3.2: Selected torsion (°) angles for L2 ligand 113

Table 3.3: Selected bond lengths (Å) and angles (°) for compounds **9** and **10** 116

Table 3.4: Selected torsion angles (°) for compounds **9** and **10** 116

Table 3.5: Selected bond lengths (Å) and angles (°) for compound **11** 120

Table 3.6: Selected torsion angles (°) for compound **11** 121

Table 3.7: Selected bond lengths (Å) and angles (°) for compound **12** 126

Table 3.8: Selected torsion angles (°) for compound **12** 126

Table 3.9: Selected bond lengths (Å) and angles (°) for compound **13** 129

Table 3.10: Selected torsion angles (°) for compound **13** 129

Table 3.11: The crystallographic data of compounds L2, **9** and **10** 130

Table 3.12: The crystallographic data of compounds **11**, **12** and **13** 131

Chapter Four

Table 4.1: Selected bond lengths (Å) and angles (°) for ^{c}L ligand 146

Table 4.2: Selected torsion angles (°) for ^{c}L ligand 146

Table 4.3: Selected bond lengths (Å) and angles (°) for L3 ligand 148

Table 4.4: Selected torsion angles (°) for L3 ligand 148

Table 4.5: Selected bond lengths (Å) and angles (°) for compound **14** 152

Table 4.6: Selected torsion angles (°) for compound **14** 152

Table 4.7: Selected bond lengths (Å) and angles (°) for compound **15** 157

Table 4.8: Selected torsion angles (°) for compound **15** 158

Table 4.9: Selected bond lengths (Å) and angles (°) for compounds **16** and **17** 162

Table 4.10: Selected torsion angles (°) for compounds **16** and **17** 163

Table 4.11: Selected bond lengths (Å) and angles of compounds **18** and **19** 170

Table 4.12: Selected torsion angles (°) for compounds **18** and **19** 171

Table 4.13: The crystallographic data of compounds ^{c}L, L3 and **14** 172

Table 4.14: The crystallographic data of compounds **15**, **16** and **17** 173

Table 4.15: The crystallographic data of compounds **18** and **19** 174

Chapter Five

Table 5.1: Selected bond lengths (Å) and angles (°) for α-**20**(L) MOF 186

Table 5.2: Selected torsion angles (°) for α-**20**(L) MOF 187

Table 5.3: Selected bond lengths (Å) and angles (°) for β-**20**(S) MOF 189

Table 5.4: Selected torsion angles for β-**20**(S) MOF 192

Table 5.5: Selected torsion angles (°) for γ-**20**(L) MOF 194

Table 5.6: Selected bond lengths (Å) and angles (°) for γ-**20**(L) MOF 195

Table 5.7: Selected bond lengths (Å) and angles (°) for δ-**20**(L) MOF 199

Table 5.8: Selected torsion angles (°) for δ-**20**(L) MOF 200

Table 5.9: Selected bond lengths (Å) and angles (°) for compound **21** 204

Table 5.10: Selected torsion angles (°) for compound **21** 204

Table 5.11: Selected bond lengths (Å) and angles (°) for β-**20**(S)^{ace} MOF 206

Table 5.12: Selected torsion angles (°) for β-**20**(S)^{ace} MOF 209
Table 5.13: Selected bond lengths (Å) and angles (°) for ε-**20**(L) MOF 213
Table 5.14: Selected torsion angles (°) for ε-**20**(L) MOF 213
Table 5.15: Selected bond lengths (Å) and angles (°) for γ-**20**(L)^{EtOH} MOF 215
Table 5.16: Selected torsion angles (°) for γ-**20**(L)^{EtOH} MOF 218
Table 5.17: Selected bond lengths (Å) and angles (°) for ζ-**20**(S)^{EtOH} MOF 222
Table 5.18: Selected torsion angle (°) for ζ-**20**(S)^{EtOH} MOF 222
Table 5.19: Selected bond lengths (Å), angles and torsion angles (°) of (L3.2H_2O)$_n$ 223
Table 5.20: Selected bond lengths (Å) and angles (°) for compound **22** 226
Table 5.21: Selected torsion angles (°) for compound **22** 227
Table 5.22: Selected torsion angles (°) for compound **22**^{a} 230
Table 5.23: Selected bond lengths (Å) and angles (°) for compound **22**^{a} 233
Table 5.24: Selected bond lengths (Å) and angles (°) for compound **22**^{EtOH} 235
Table 5.25: Selected torsion angles (°) for compound **22**^{EtOH} 235
Table 5.26: Selected bond lengths (Å) and angles (°) for compound **22**^{H_2O} 239
Table 5.27: Selected torsion angles (°) for compound **22**^{H_2O} 239
Table 5.28: Selected bond lengths (Å) and angles (°) for compound **23** 245
Table 5.29: Selected torsion angles (°) for compound **23** 246
Table 5.30: Selected torsion angles (°) for compound **23**^{H_2O} 248
Table 5.31: Selected bond lengths (Å) and angles (°) for compound **23**^{H_2O} 249
Table 5.32: Crystallographic data of compounds α-**20**(L), β-**20**(S) and γ-**20**(L) 251
Table 5.33: Crystallographic data of compounds δ-**20**(L), **21** and β-**20**(S)^{ace} 252
Table 5.34: Crystallographic data of compounds ε-**20**(L), γ-**20**(L)^{EtOH} and ζ-**20**(S)^{EtOH} 253
Table 5.35: Crystallographic data of compounds L3.2H_2O, **22** and **22**^{a} 254
Table 5.36: Crystallographic data of compounds **22**^{EtOH} and **22**^{H_2O} 255
Table 5.37: Crystallographic data of compounds **23** and **23**^{H_2O} 256

Coordination polymers and metal-organic frameworks; synthesis, properties and applications

1.1 Introduction

Coordination polymers (CPs) are inorganic-organic compounds with infinite repeated structures constructed from metal nodes or clusters and multidentate organic ligands [1-15]. The organic ligand in coordination polymers may extend in one, two or three dimensions to produce one-dimensional coordination polymer (figure 1.1), two-dimensional coordination polymer or three-dimensional coordination polymer where 2D and 3D materials are also known as metal-organic frameworks (MOFs) (figure 1.2) [2-9, 14-19]. CPs and MOFs have received a considerable attention in recent years, as indicated by the high number of publications (figure 1.3) [17]. CPs and MOFs high number of publications could due to their high thermal stability [20-29], bonding properties [30-39] and architecture systems [40-49]. CPs form from coordination bonding [50-59] and may also form other chemical interaction such as hydrogen bonding [60-66], π-π interactions [67-76], ionic interactions [77-86] and Van Der Waals forces [87-93]. The variety of chemical bonding, physical forces/interactions, and structures can lead to a wide range of possible applications in chemical catalysis [94-101], gas or liquid storage and separation [102-114], spin crossover [115-123], luminescence [124-133], nanochemistry [134-143] and drug delivery [144-153]. Other unique properties of MOFs are due to the pore sizes and significant surface area that MOFs can provide for guest molecules [11-13, 84, 108, 111, 154]. Some of the most common rigid and flexible organic linkers that utilise in coordination polymers and metal-organic frameworks synthesis are included in figure 1.4 [19, 114, 155, 156].

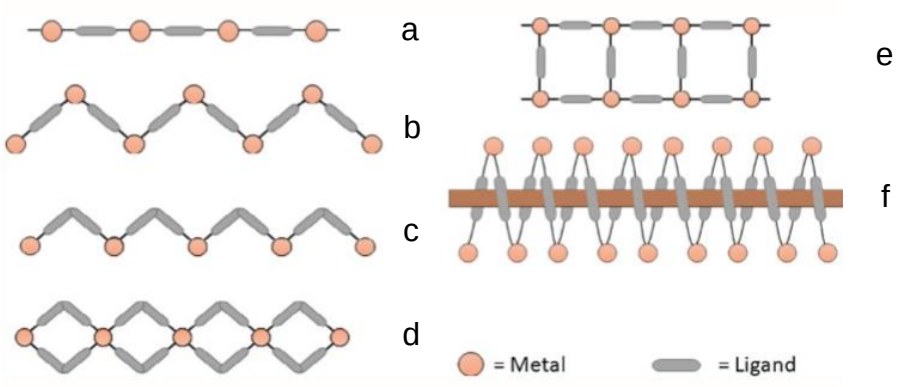

Figure 1.1: One-dimensional coordination polymers common conformations. (a) Linear chain, (b-c) zigzag chain, (d) ribbon, (e) ladder and (f) helical [17]. Reproduced by permission of Taylor and Francis.

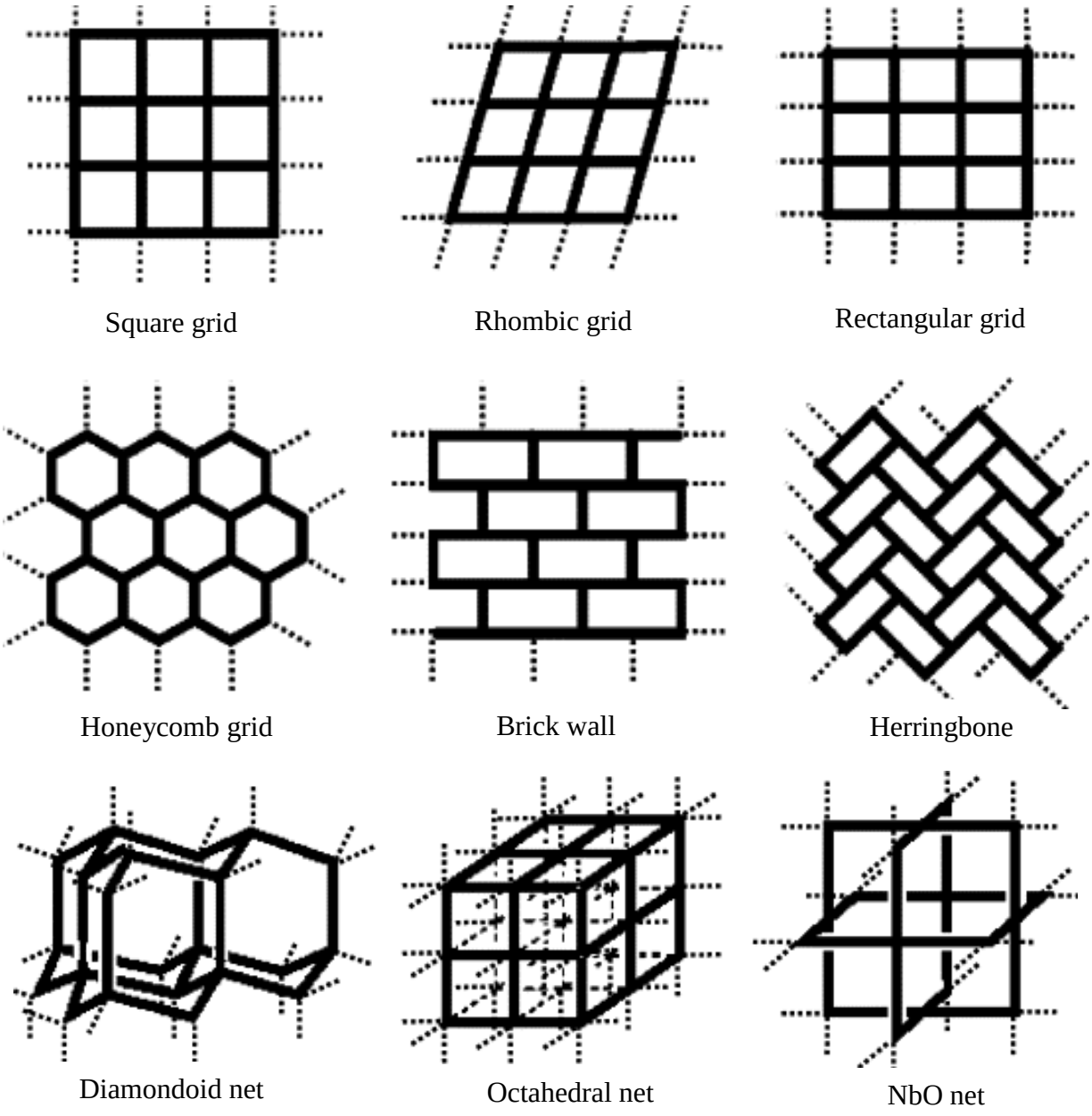

Figure 1.2: Two and three-dimensional coordination polymers common conformations [18]. Reproduced by permission of Science Direct.

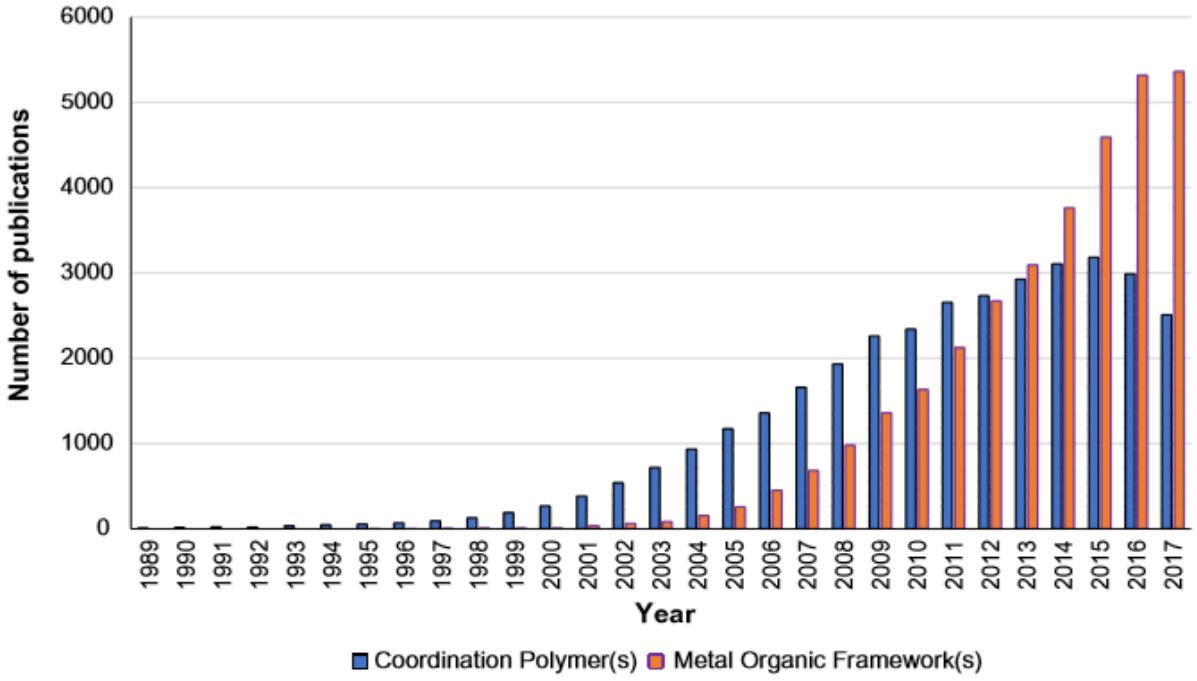

Figure 1.3: Coordination polymers and metal-organic frameworks publications per year until November 2017 [17]. Reproduced by permission of Taylor and Francis.

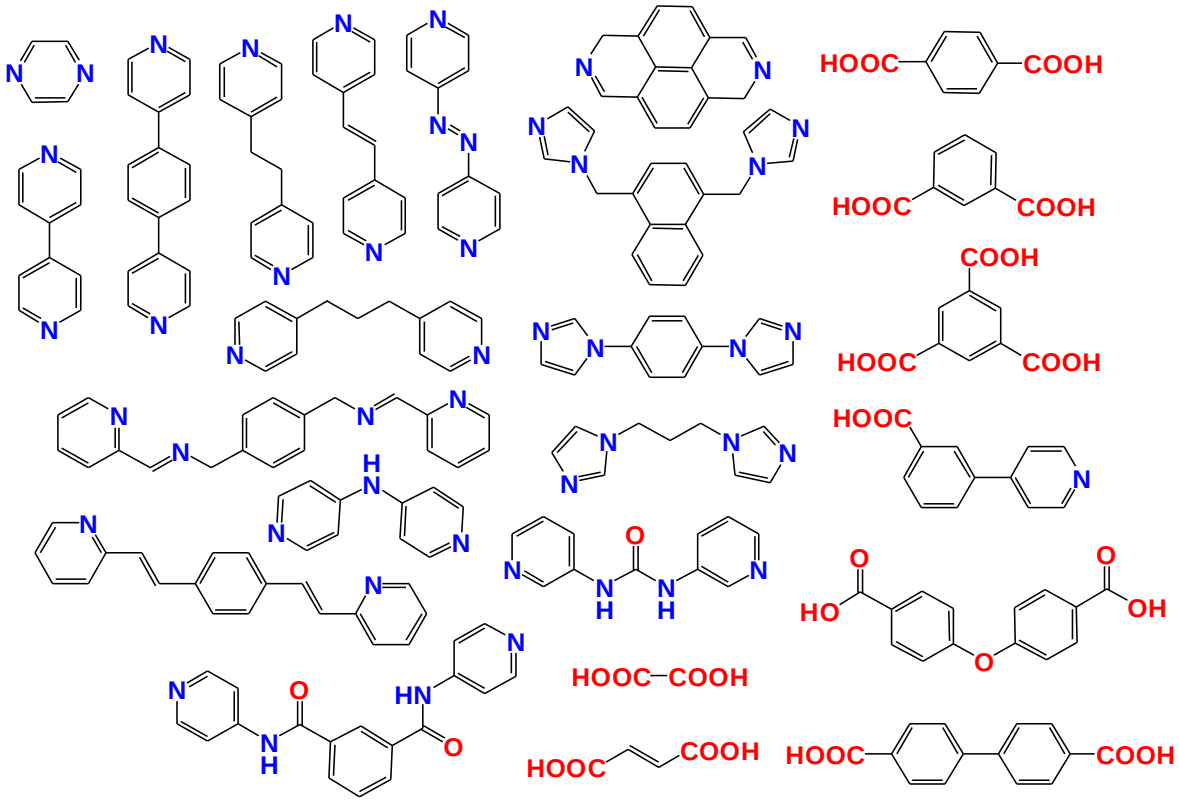

Figure 1.4: Rigid and flexible organic linkers examples that utilised in coordination polymers and MOFs synthesis [114, 155, 156].

1.2 Overview of some important MOF materials

1.2.1 Prussian blue

In 1706 a colour maker named Johann Jacob Von Diesbach was trying to make a red pigment called Florentine lake [157]. The original recipe was simple, potash and carminic acid [157]. Diesbach added iron(II) sulphate to the original recipe to produce a red pigment with more violet shade [157]. The potash pot was mislabelled from the supplier Johann Conrad Dippel by his young assistant Rösser and contaminated with ox blood [157]. The resulted pigment was pale and turned to a deep blue colour with higher concentration [158]. According to Buser et al. and Batten et al. Prussian blue is the first ever synthetic coordination polymer or coordination compound [158-159]. After 271 years, Prussian blue modified crystal structure model was reported by Buser and co-workers [159]. The modified version was solved in cubic face-centred unit cell O_h^1-*Pm*3*m* and shows corresponding average distances of 1.92, 1.13 or 2.03 Å for Fe(II)-C, C≡N and Fe(III)-N [159]. Fe(II) ion shows low spin state and is coordinated by carbon atoms of cyanide molecules. On the other hand, Fe(III) ion shows high spin state and coordinated by nitrogen atoms of cyanide molecules (–N≡C–Fe(II)–C≡N–Fe(III)–N≡C–) [157]. Prussian blue can display more than one crystal lattice structure with different chemical compositions. The first crystal lattice structure is ($Fe_4[Fe(CN)_6]_3$) the typical solid dry structure, where $[Fe(CN)_6]_3^{12-}$ negative coordination sphere is neutralised by four Fe(III) ions (Fe(II)-C= 1.92 Å) and (Fe(III)-N= 2.03 Å) [157]. The second coordination lattice structure is ($Fe_4[Fe(CN)_6]_3.nH_2O$) the solid hydrated lattice that contains between 14-15 water molecules (Fe(III)-O= 2.138 Å) [157, 159]. The third coordination lattice is ($KFe[Fe(CN)_6]$) the soluble form (colloid solution) where potassium cations occupy the resulted lattice channels. Prussian blue dry, hydrated and soluble structures are demonstrated in (figure 1.5) [157, 160].

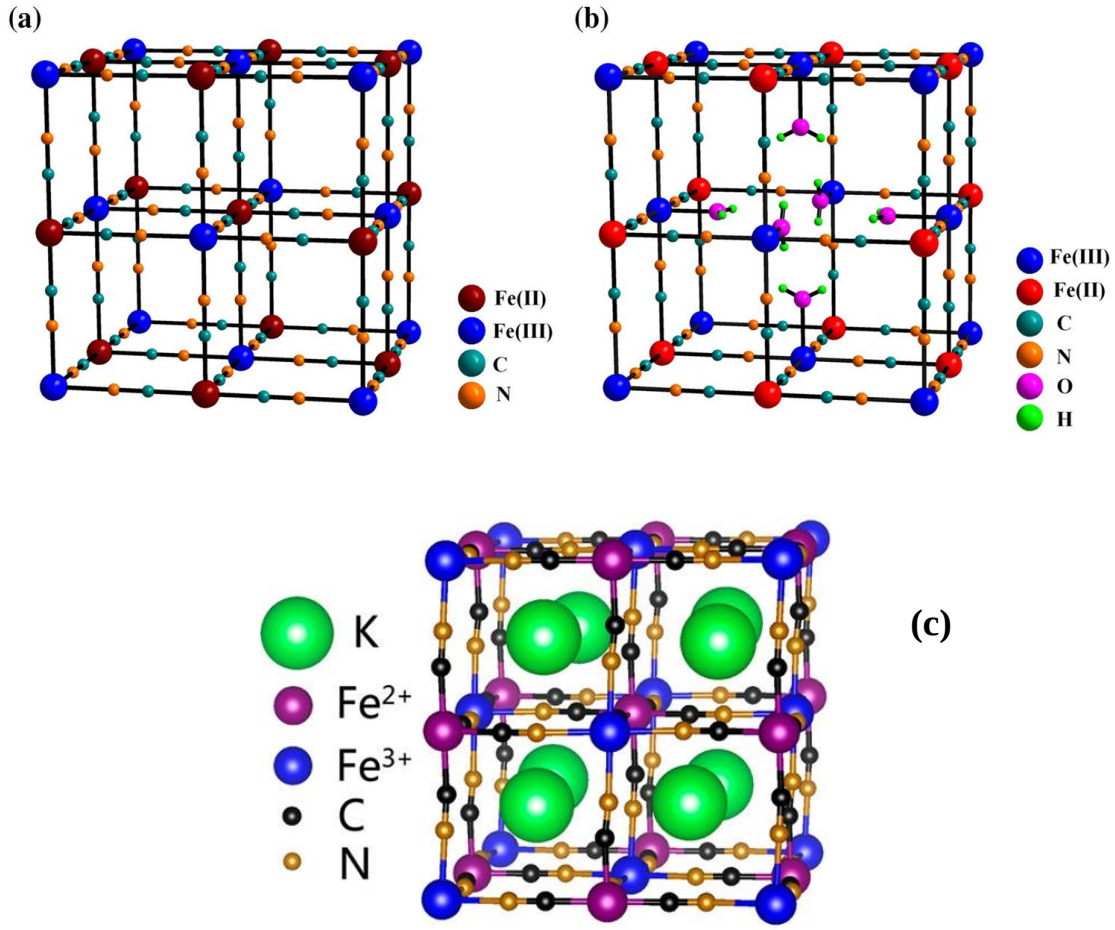

Figure 1.5: (a) The dry solid crystal lattice of Prussian blue, (b) solid hydrated crystal lattice of Prussian blue. (c) The soluble form of Prussian blue crystal lattice [157, 160]. Reproduced by permission from Springer and the American Chemical Society.

1.2.2 The term metal-organic framework

In December 1995, the term Metal-Organic Framework was first reported by Yaghi and co-workers [14]. The reported MOF was based on pyridine, cobalt(II) nitrate and benzene-1,3,5-tricarboxylic acid (H_3-btc). Yaghi used the rigid organic linker because it has three carboxylic acid groups oriented symmetrically around the aromatic ring and behave either as monodentate or bidentate ligands towards metal ions (figure 1.6). Yaghi diffused pyridine (py) into a mixture of benzene-1,3,5-tricarboxylic acid and cobalt(II) nitrate in alcohol for 72 hours to produce pink cubic crystals. The resultant crystals were thermally stable up to 350 °C even after removing guest molecules and insoluble in water or other organic solvents. Single crystal X-ray analysis confirmed the complex formula $[Co(btc)_3(py)_2].2/3(py)$ which shows distortion octahedral geometry around

Co(II) ions. Cobalt(II) cations and btc^{3-} anions form a planar layer where each btc^{3-} bridges between three Co(II) cations and each Co(II) ion is coordinated by three btc^{3-} ligands. There are *trans* coordinated pyridine ligands on the Co(II) ions. The resulting layers stack to form 7 × 10 Å rectangle channels structure with additional uncoordinated pyridine guest molecules in the channels. The resulting MOF structure shows 3.5 Å between uncoordinated pyridine guest molecules and phenyl rings of deprotonated btc^{3-} molecules that due to π-π stacking interaction. Moreover, Co(II) MOF shows absorb selectivity to aromatic guest molecules, for example, benzene, nitrobenzene, cyanobenzene and chlorobenzene, but not chloroform, acetonitrile or nitromethane.

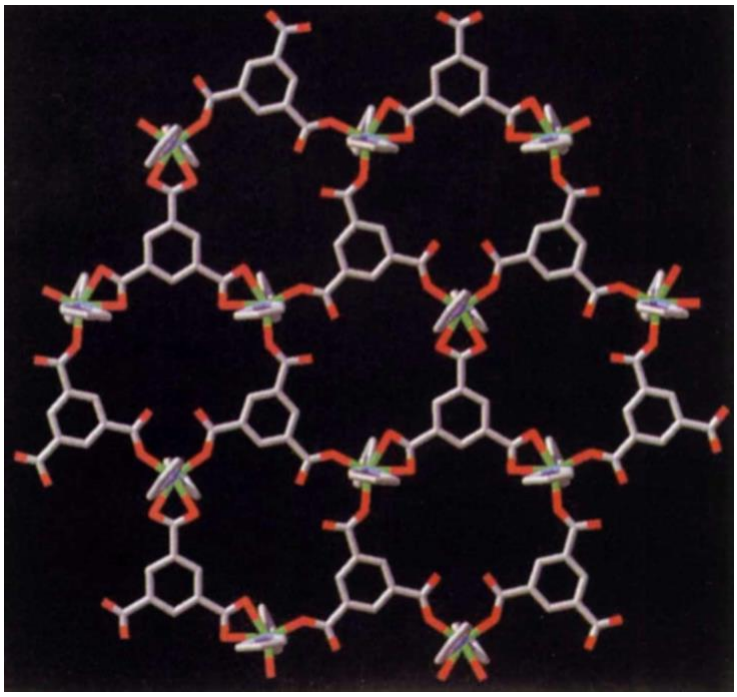

Figure 1.6: Crystal structure of $[Co(btc)_3(py)_2].2/3(py)$ MOF along the *x-y* plane. Each Co(II) ion is coordinated to three different btc^{3-} molecules on the equatorial axes and two pyridine molecules on the axial axes. btc^{3-} molecules are fully deprotonated and behave either as tridentate ligands or as hexadentate ligands to three different Co(II) ions [14]. Reprodued by permission from Springer Nature.

1.2.3 HKUST-1 MOF

In 1999 Chui and co-workers [161] reported a three-dimensional metal-organic framework ($[Cu_3(btc)_2(H_2O)_3]_n$) known as HKUST-1. HKUST-1 MOF was formed in a high yield of 80 % and thermally stable up to 240 °C. The structure has a three-dimensional open network with

channels of one nanometre in size giving about 40 % accessible space in the solid state. Furthermore, water guest molecules in these channels can be replaced by other solvent such as pyridine without the network collapsing. The neutral $[Cu_3(btc)_2(H_2O)_3]_n$ building unit was formed by four carboxylate groups from four different btc^{3-} molecules behave as bidentate bridging ligands for two copper (II) ions in a dimer style (Cu-O= 1.952(3) Å) (Cu(II) to Cu(II)= 2.628(2) Å). Moreover, each Cu(II) ion has a coordinated water molecule on the axial axes (Cu-OH_2= 2.165(8) Å) to produce the pseudoctahedral geometry (figure 1.7).

HKUST-1 MOF has a face-centred cubic structure with large square pores of volume 9 × 9 Å containing up to ten water molecules per formula unit and displays one nanometer-sized channel for the four-fold symmetry (figure 1.7). The four-fold symmetry results from oxygen atoms of carboxylate groups that producing a square structure with measurements of 9.5 Å for edge and 13.3 Å across its diagonal. The nanochannels are overlapping to produce a three-dimensional network with open connected pores. The three-dimensional network shows a Kagome structure containing 18 Å hexagonal windows formed by six copper(II) dimers and six btc^{3-} ions intersections (figure 1.8). Nitrogen gas adsorption/desorption experiments of HKUST-1 MOF shows 692.2 m^2/g for Brunauer-Emmett-Teller (BET) surface area and 917.6 m^2/g for Langmuir surface area.

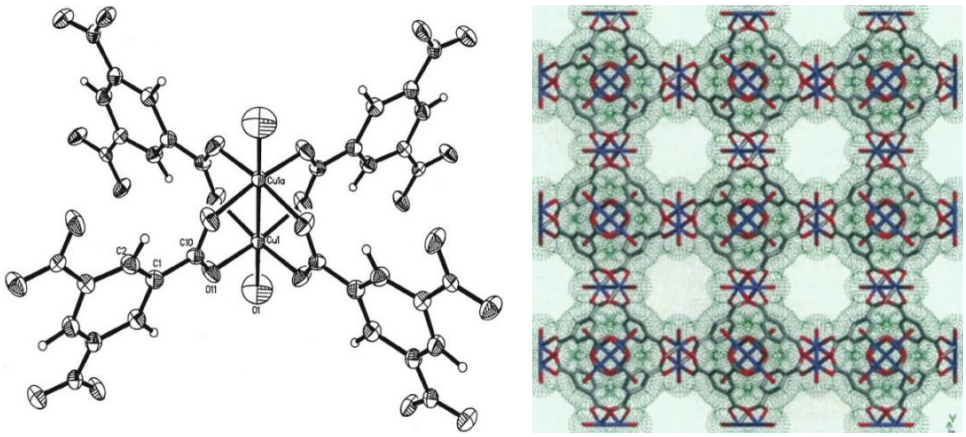

Figure 1.7: (left) HKUST-1 building block, (right) four-fold symmetry of HKUST-1 MOF [161]. Reproduced by permission from the American Association for the Advancement of Science.

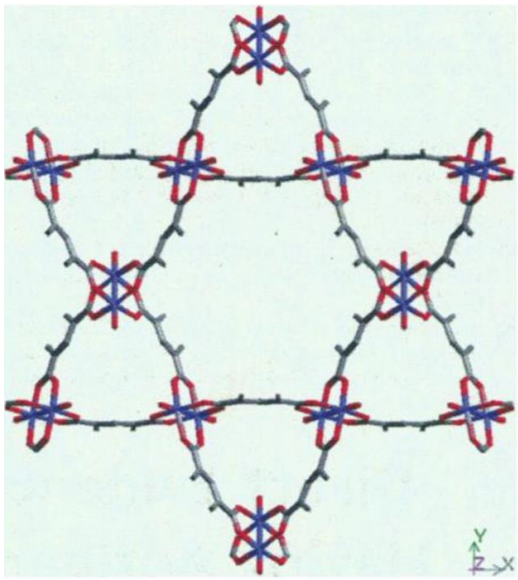

Figure 1.8: HKUST-1 Kagome structure that has 18 Å hexagonal windows [161]. Reproduced by permission from the American Association for the Advancement of Science.

1.2.4 MIL-53 MOF

In 2002 Millange and co-workers [162] reported a new MOF based on chromium(III) nitrate hydrate and benzene-1,4-dicarboxylic acid (H_2-bdc) known as (MIL-53as). MIL-53as MOF is the first MOF example of chromium(III) ion and dicarboxylate organic ligand. MIL-53as MOF was synthesised by the hydrothermal reaction of $Cr(NO_3)_3.nH_2O$, H_2-bdc, HF and water in molar ratios of 1:1:1:280 at 220 °C for 72 hours. The reaction mixture was kept in a very high acidic medium (pH was less than one) through the synthesis process as the pH level has a significant effect on single crystals growth. The resultant solid purple crystals were recovered by filtration, washed with deionized water and dried at ambient temperature to produce $[Cr^{III}(OH).(bdc)].(H_2\text{-}bdc)_{0.75}$ MOF (MIL-53as). The crystal structure of MIL-53as MOF was confirmed by single crystal X-ray analysis and shows one-dimensional open channels that represent a good example of non-interpenetrated porous MOF. On the other hand, powder X-ray analysis of MIL-53as MOF showed that the resulted bulk sample is contaminated with H_2-bdc starting material traces, the contamination was also confirmed by elemental microanalysis.

Thermal gravimetric analysis (TGA) of MIL-53as MOF displayed two weight losses; the first weight loss was equal to 28 % of the sample weight and happened at 249.58 °C due to the removal of uncoordinated H_2-bdc molecules to produce $[Cr^{III}(OH).(bdc)]$ MOF (MIL-53ht). The second weight loss was equal to 50 % of the sample weight and occurred at 449.85 °C due to MOF

decomposition. MIL-53ht MOF rapidly absorbs atmospheric water to produce ($[Cr^{III}(OH)\cdot(bdc)]\cdot H_2O$) MOF (MIL-53lt). TGA of MIL-53ht MOF showed two weight losses. The first weight loss was equal to 7 % of the sample weight and occurred at 79.85 °C due to the release of water guest molecules. The second weight loss was equal to 58 % of the sample weight and occurred at 449.85 °C due to MIL-53lt MOF decomposition. MIL-53as and MIL-53ht MOFs have identical topology of three-dimensional network accumulated from Cr(III) and bdc^{2-} molecules. Cr(III) coordination centres share the axial bridging hydroxyl groups to produce Cr(III)-OH linear chains. The resulted chains are further linked by bdc^{2-} molecules along the equatorial axes to create the one-dimensional open network structure. Furthermore, MIL-53as and MIL-53ht crystal structures show 8.3 × 12 or 9.4 × 11.4 Å rhombic channels (figure 1.9). Nitrogen absorption/desorption experiments showed Langmuir surface area over 1500 m^2/g for MIL-53as MOF and 1150 m^2/g for MIL-53ht MOF.

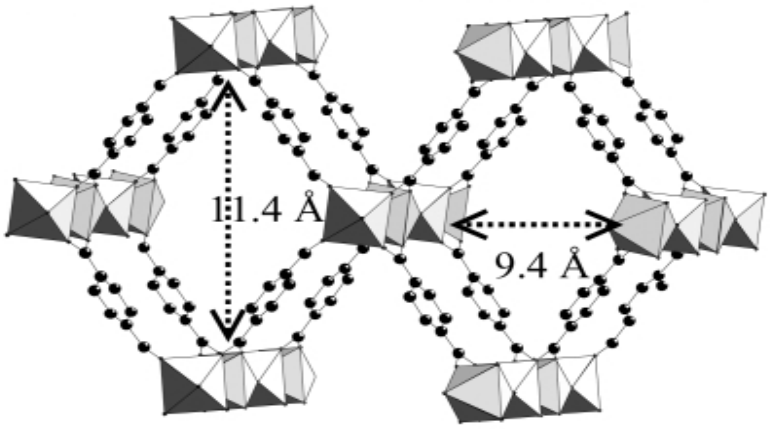

Figure 1.9: MIL-53ht crystal structure that shows 11.4 × 9.4 Å rhombic channels and Cr(III) distortion octahedral coordination centres [162]. Reproduced by permission from the Royal Society of Chemistry.

1.2.5 MOF-101

In 2002 Eddaoudi and co-workers [163] reported a new metal-organic framework that has NbO-type structure based on 2-bromo-benzene-1,4-dicarboxylic acid (*o*-Br-H_2-bdc) and copper(II) nitrate hydrate ($[Cu_2(o\text{-Br-bdc})_2(H_2O)_2].(DMF)_8(H_2O)_2$) known as (MOF-101). MOF-101 was synthesised by a self-assembly process of the metal salt precursor and the organic linker in *N*,*N*-dimethylformamide (DMF) at ambient temperature to produce MOF-101 as blue cubic

crystals. MOF-101 resultant crystals are insoluble in the common organic solvents for example, MeOH, EtOH, THF, MeCN and DCM but sensitive to H_2O.

Single crystal X-ray analysis shows that MOF-101 features as paddlewheel structure with two Cu(II) ions surrounding by four coordinated carboxylate groups behaving as bidentate ligands (Cu-O= 1.954(8) Å). In addition, there are two coordinated axial water molecules (Cu-OH_2= 2.135(18) Å) to produce Cu(II) square pyramid coordination centres (figure 1.10). The organic linker in MOF-101 shows right angle links between (Cu-O-C) bonds to produce the square building units that extend the NbO like network. Moreover, the square planar node in NbO is replaced by a square secondary building unit and spaced away from another node by the organic linker to form the three-dimensional open network structure. MOF-101 has 12-14 Å diameter cross-section, and 19-21 Å diameters of spherical internal voids contain at least eight DMF and one water guest molecules per formula unit (figure 1.10).

Thermal gravimetric analysis for MOF-101 at a fixed average of heating 5 °C per minute shows three weight losses. The first weight loss was below 100 °C and due to a release of all guest molecules. The second weight loss was between 100-300 °C and due to release of coordinated water molecules. The third weight loss was between 300-400 °C and due to MOF-101 decomposition. Moreover, MOF-101 guest molecules could be replaced by other organic solvents molecules, for example, CH_3OH, $CHCl_3$, DMSO, MeCN and THF without destruction of the MOF structure.

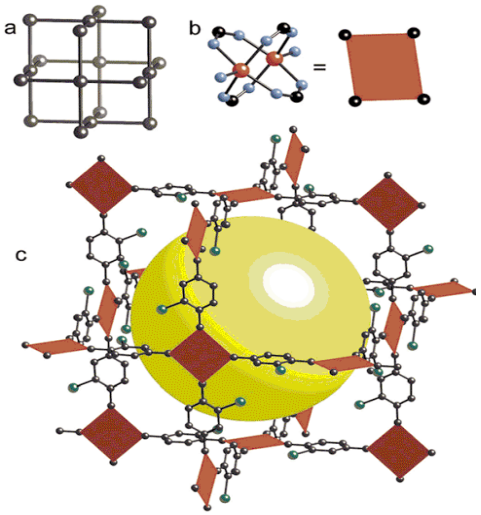

Figure 1.10: (a) MOF-101 square secondary building unit, (b) the right angle between carboxylate groups in *o*-Br-bdc^{2-} molecules. (c) The NbO-type structure is noninterpenetrating [163]. Reproduced by permission of the American Chemical Society.

1.2.6 NU-109 and NU-110 MOFs

In 2012 Farha and co-workers [164] reported two new MOFs based on 1,3,5-tris[(1,3-carboxylic acid-5-(4-(ethynyl)phenyl))butadiynyl]-benzene (H_6-LB) or 1,3,5-tris[((1,3-carboxylic acid-5-(4-(ethynyl)phenyl))ethynyl)phenyl]-benzene (H_6-LP) (figure 1.11) and copper(II) nitrate hydrate known as NU-109 and NU-110. These new MOFs were obtained by solvothermal reaction of (H_6-LB) or (H_6-LP) and copper(II) nitrate hydrate in a mixture of DMF, EtOH and a few drops of HCl at 75 °C for two days to produce $[Cu_3(LB)(H_2O)_3]_n$ (NU-109) or $[Cu_3(LP)(H_2O)_3]_n$ (NU-110) MOFs teal color crystals. NU-109 MOF crystal structure was solved in cubic space group $Fm\bar{3}m$ and shows two copper(II) ions in a dimer style (Cu to Cu= 3.194 Å) coordinated to four carboxylate groups from four different organic ligands along the equatorial axes (Cu-O= 1.98(4) Å) to produce $Cu_2(COO)_4$ paddlewheel structure. Cu(II) ions are also coordinated to two water molecules along the axial axes which were not well resolved in the single crystal X-ray analysis. Each (LB^{6-}) ligand behaves as a dodeca dentate ligand to six Cu(II) dimers by three fully deprotonated isophthalate molecules. However, 24 isophthalate groups and 12 Cu(II) dimers are connected to produce the cuboctahedral building cage that extends to produce a three-dimensional open network (figure 1.12). On the other hand, NU-110 MOF has similar Cu(II) and (LP^{6-}) coordination environments in comparison with NU-109 MOF and shows 1.720(9) Å for Cu-O coordination bond lengths and 2.067(8) Å between Cu(II) ions in the paddlewheel structure.

Thermal gravimetric analysis traces for NU-109 and NU-110 MOFs are similar with two main weight losses. The first mass loss at 100 °C is due to the release of guest molecules. Then, the resultant crystals were thermally stable up to 325 °C and showed the second weight loss after 325 °C that due to NU-109 or NU-110 MOFs decomposition. NU-109 and NU-110 MOFs as-synthesised crystals were soaked in 100 % EtOH for 24 hours. Then, soaking solutions were replaced every 24 hours for 72 hours to produce ethanol containing samples. Ethanol containing samples were placed inside the dryer where ethanol was replaced with liquid carbon dioxide after 10 hours. Then, the temperature was raised, and carbon dioxide was evaporated under supercritical conditions to produce the activated dried MOFs. Nitrogen adsorption/desorption isotherms experiments at 77 K showed phenomenal uptakes of 2480 and 2845 cm^3/g for NU-109 and NU-110 activated MOFs (figure 1.13). Moreover, activated NU-109 and NU-110 MOFs have the highest recorded BET surface areas of 7010 and 7104 m^2/g and total pore volumes of 3.75 and 4.40 cm^3/g [164].

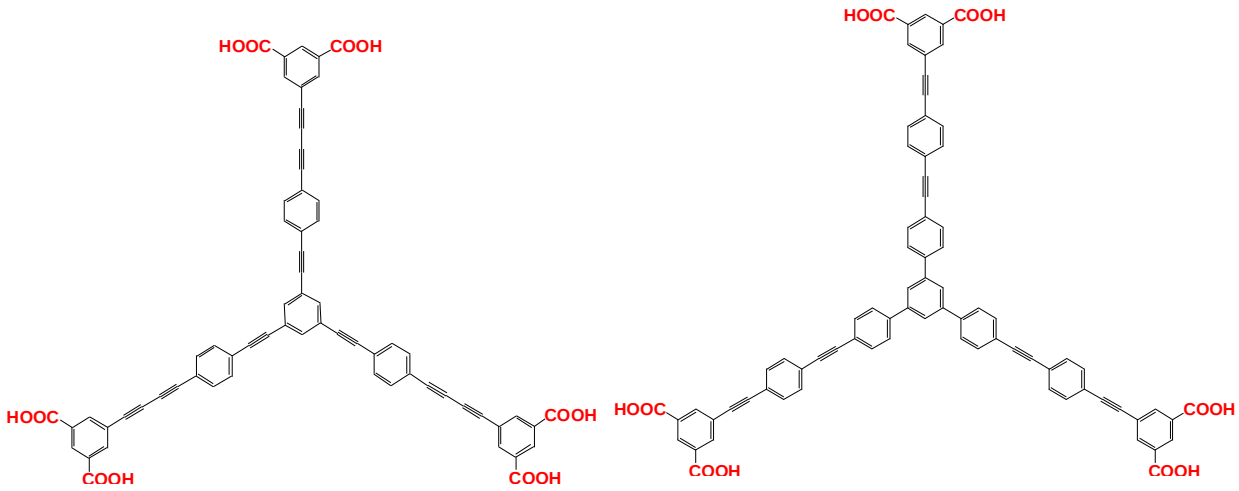

Figure 1.11: (left) 1,3,5-Tris[(1,3-carboxylic acid-5-(4-(ethynyl)phenyl))butadiynyl]-benzene ligand (H_6-LB), (right) 1,3,5-tris[((1,3-carboxylic acid-5-(4-(ethynyl)phenyl))ethynyl)phenyl]-benzene ligand (H_6-LP) [164].

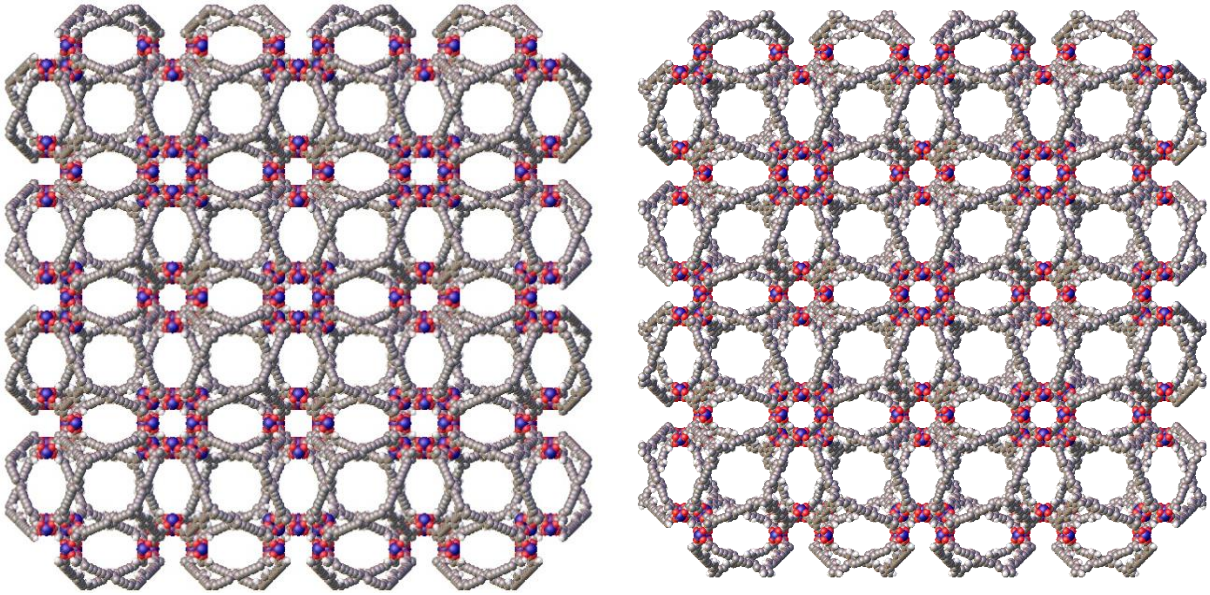

Figure 1.12: (left) NU-109 three-dimensional open network. (right) NU-110 3D open network [164].

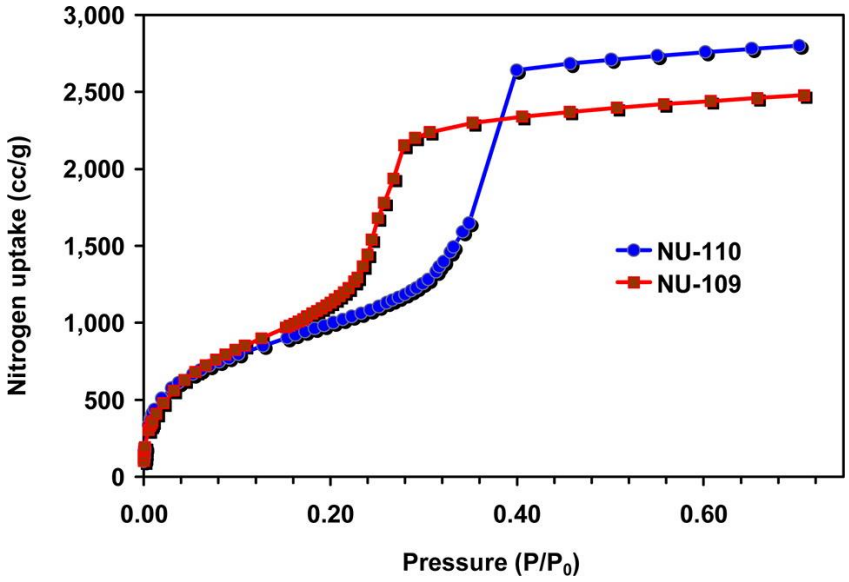

Figure 1.13: NU-109 and NU-110 MOFs nitrogen gas sorption data [164]. Reproduced by the permission from the American Chemical Society.

1.3 Coordination polymers and metal-organic frameworks synthesis methods

Solvent and solvent-free synthesis are the two main methods to produce coordination polymers and MOFs [14, 163, 165-172]. The main aims of these different types of synthesis methods are to produce pure compounds in large quantities, reduce the reaction time and obtain thermally stable products. Classical synthesis procedures can produce CPs or MOFs below 100 °C for example, the solvent slow evaporation method, self-assembly process at ambient temperature and solvothermal synthesis for some reported CPs or MOFs [14, 163, 170, 173, 174]. However, CPs and MOFs can be synthesised by solvothermal methods if the reaction temperature is above 100 °C for example, hydrothermal synthesis or microwave synthesis method [162, 173].

1.3.1 Solvothermal synthesis

Solvothermal synthesis of CPs or MOFs involves dissolving of the organic ligand/ligands and the metal salt precursor in an appropriate solvent or in a mixture of solvents and heating the reaction mixture in a sealed container from one to seven days. Although this procedure can produce high quality crystals suitable for single X-ray analysis in a good yield, it has cost limitation for some solvents such as *N*,*N*-diethylformamide (DEF) and scale limitation above one gram [175]. In 2011 Kim and co-workers [174] reported IRMOF-16 modified version based on 1,4-di(4-carboxy-2-hydroxyphenyl)benzene and $Zn(NO_3)_2.6H_2O$ known as HCC-1 MOF. HCC-1 MOF was synthesised by the reaction of 1,4-di(4-carboxy-2-hydroxyphenyl)benzene and

$Zn(NO_3)_2.6H_2O$ in *N*,*N*-dimethylformamide (DMF) at 85 °C for 86 hours. Then, HCC-1 MOF resultant block crystals were washed with fresh DMF to remove any possible unreacted starting materials. Kim prepared the same MOF by using DEF solvent with fixed conditions. The synthesis process was less effective in comparison with DMF process, and the resultant crystals were smaller and don't have DMF solvent crystals of regular shape and size. HCC-1 resultant crystals from the solvothermal synthesis in DMF are thermally stabile up to 250 °C and show an average size of 500 µm. Furthermore, HCC-1 MOF has 4724 m^2/g for BET surface area (figure 1.14).

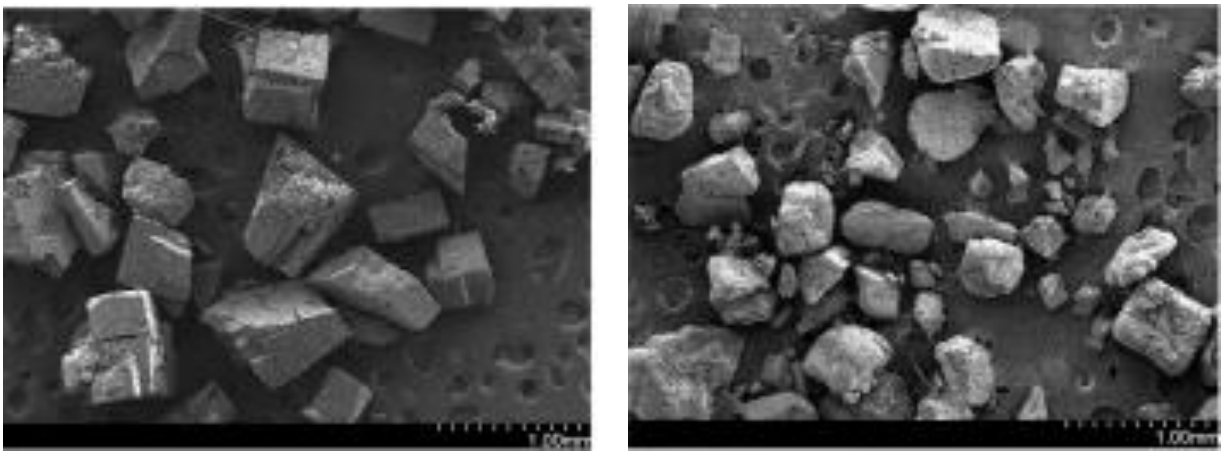

Figure 1.14: (left) SEM images of HCC-1 resultant crystals in DMF, (right) in DEF [174]. Reproduced by permission from Science Direct.

In 2005 Clausen and co-workers [176] reported two new MOF structures based on $Zn(NO_3)_2.6H_2O$, benzene-1,4-dicarboxylic acid and DMF. Clausen used the solvothermal synthesis method to produce various final products from the same starting materials by changing the reaction conditions, for example, reaction temperature or reaction time. The main product is [Zn(bdc)(DMF)] MOF (figure 1.15), that converts to ($[Zn(bdc)(H_2O)](DMF)$) MOF after one year (figure 1.15). In addition to the secondary product, the new 3D metal-organic framework ($[Zn(HCO_2)_3](C_2H_8N)$) (figure 1.15). Moreover, HCO_2^- and $C_2H_8N^+$ ions were resulted from the solvent decomposition at high temperature. The solvothermal synthesis process involved dissolving of the starting materials in DMF and raising the temperature to 107 °C for 96 hours. The resultant colourless crystals of [Zn(bdc)(DMF)] and ($[Zn(HCO_2)_3](C_2H_8N)$) MOFs were kept in the solution and re-examined after one year. Then, a single crystal of ($[Zn(bdc)(H_2O)](DMF)$) MOF was picked from the sample solution.

Single crystal analysis of [Zn(bdc)(DMF)] MOF shows a pair of Zn(II) ions coordinated to four fully deprotonated carboxylate groups from four different bdc^{2-} ligands (Zn-O1= 2.042(5) Å) and (Zn-O2= 2.014(4) Å). Zn(II) ion is also coordinated to one DMF solvent molecule (Zn-O10= 2.000(7) Å) to produce a distorted Zn(II) square pyramid structure. The ($[Zn(HCO_2)_3](C_2H_8N)$) MOF single crystal structure shows an octahedral structure around Zn(II) ions, that consist of six coordination oxygen atoms from six different formate ions (Zn-O1= 2.1072(7) Å). Moreover, ($[Zn(HCO_2)_3](C_2H_8N)$) MOF crystal structure shows dimethylammonium molecules located in the voids of the three-dimensional frameworks and forms hydrogen bonding interaction with the anionic framework (O1-N1= 2.886 Å).

The ($[Zn(bdc)(H_2O)](DMF)$) MOF structure is similar to the [Zn(bdc)(DMF)] MOF structure but it has axial coordinated water molecules to Zn(II) instead of the coordinated DMF molecules (Zn(II)-bdc^{2-} = 2.009(19) Å) and (Zn(II)-OH_2= 1.960(15) Å). Moreover, coordinated water molecules form new hydrogen bonding interactions with DMF solvent molecules (O5-O6= 2.886 Å) (figure 1.15).

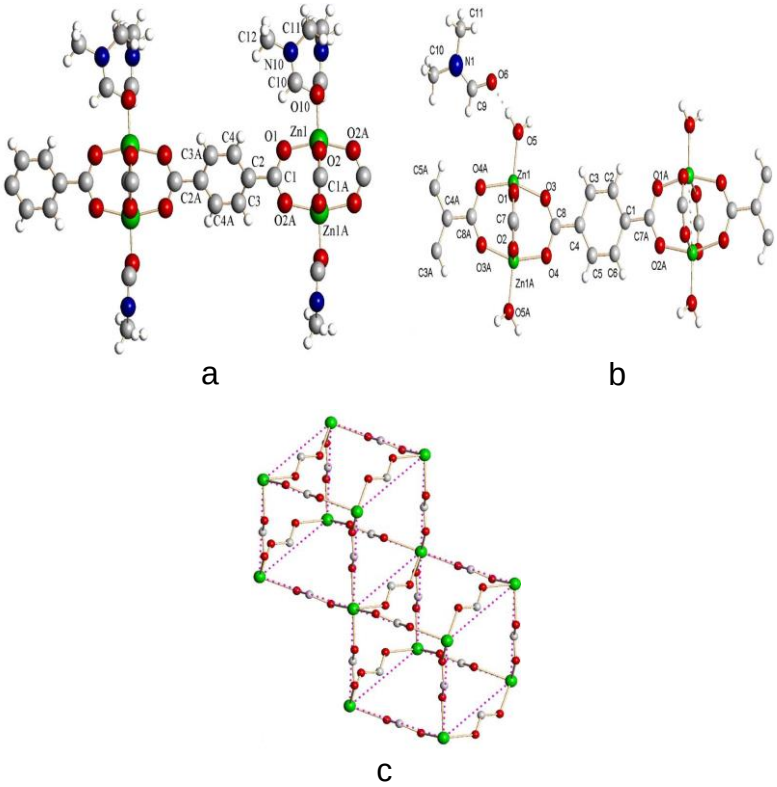

Figure 1.15: (a) 2D layer structure of [Zn(bdc)(DMF)] MOF. (b) 2D layer structure of ($[Zn(bdc)(H_2O)](DMF)$) MOF. (c) ($[Zn(HCO_2)_3](C_2H_8N)$) MOF 3D network [176]. Reproduced by permission of Science Direct.

In 2012, Wang and co-workers [177] reported two new metal-organic frameworks based on $InCl_3.4H_2O$ and naphthalene-1,4-dicarboxylic acid (H_2-1,4-ndc) referred as ([In(OH)(1,4-ndc)].$2H_2O$) and (H[In(1,4-ndc)$_2$].2(H_2O).1.5(DMF)) MOFs. [In(OH)(1,4-ndc).$2H_2O$] MOF was synthesised by the reaction of naphthalene-1,4-dicarboxylic acid, sodium hydroxide aqueous solution and indium(III) chloride in acetonitrile for 72 hours at 100 °C to result in the colourless needle shape crystals. Whereas (H[In(1,4-ndc)$_2$].2(H_2O).1.5(DMF)) MOF was synthesised by the reaction of naphthalene-1,4-dicarboxylic acid, Et_4NBr and $InCl_3.4H_2O$ in DMF for 72 hours at 100 °C to produce (H[In(1,4-ndc)$_2$].2(H_2O).1.5(DMF)) MOF colourless block crystals.

([In(OH)(1,4-ndc)].$2H_2O$) MOF has a three-dimensional network structure consisting from two kinds of square shape channels with 10.89 × 10.89 Å or 6.46 × 6.46 Å diameter resulting from In(III)-OH coordination chains and 1,4-ndc^{2-} molecules (figure 1.16). On the other hand, (H[In(1,4-ndc)$_2$].2(H_2O).1.5(DMF)) MOF has a 3D anion framework structure with two-fold interpenetrating diamond topology completed by connection of four organic linker molecules to indium(III) nodes (figure 1.17). ([In(OH)(1,4-ndc)].$2H_2O$) MOF shows distorted octahedral coordination centres, where each carboxylate group of 1,4-ndc^{2-} molecule is coordinated to two indium(III) centres and each indium (III) is coordinated by four oxygen atoms from four carboxylate groups, in addition of two bridging hydroxyl groups (figure 1.16).

(H[In(1,4-ndc)$_2$].2(H_2O).1.5(DMF)) MOF shows a dodecahedral structure, where each indium (III) cation is coordinated by eight oxygen atoms from four different deprotonated bidentate carboxylate groups. This coordination style represents a good example of a high steric number for the main group elements (figure 1.17). The 3D network is completed by linking of four linear 1,4-ndc^{2-} ligands and four Indium(III) nodes, in addition to the free water and solvent molecules. The free voids in the resulting MOF are filled by another separate framework to generate a two-fold interpenetrating three-dimensional anionic network that is balanced by a proton (figure 1.17). These explain all illustrate that the exact conditions of a solvothermal synthesis are critical in determining the nature of the MOF produced.

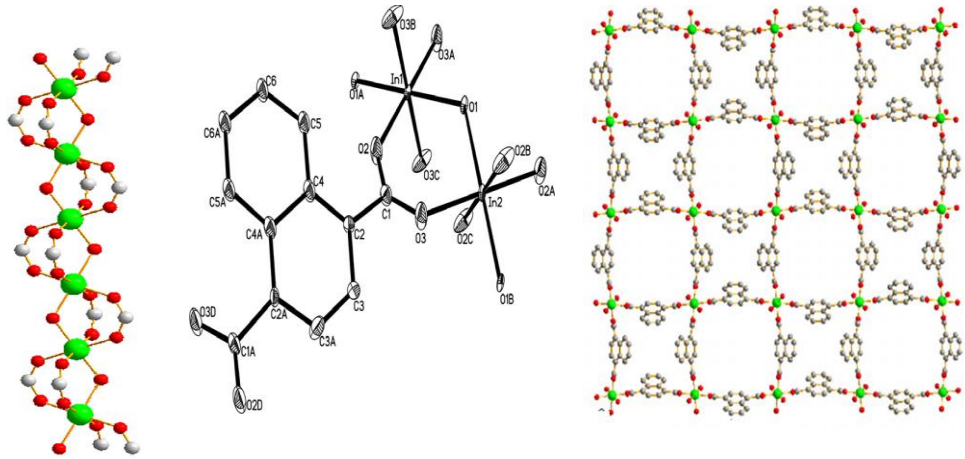

Figure 1.16: (left) In(III) chain. (centre) ([In(OH)(1,4-ndc)].2H_2O) MOF SBU. (right) Two types of ([In(OH)(1,4-ndc)].2H_2O) MOF square-shaped channels [177]. Reproduced by permission from Science Direct.

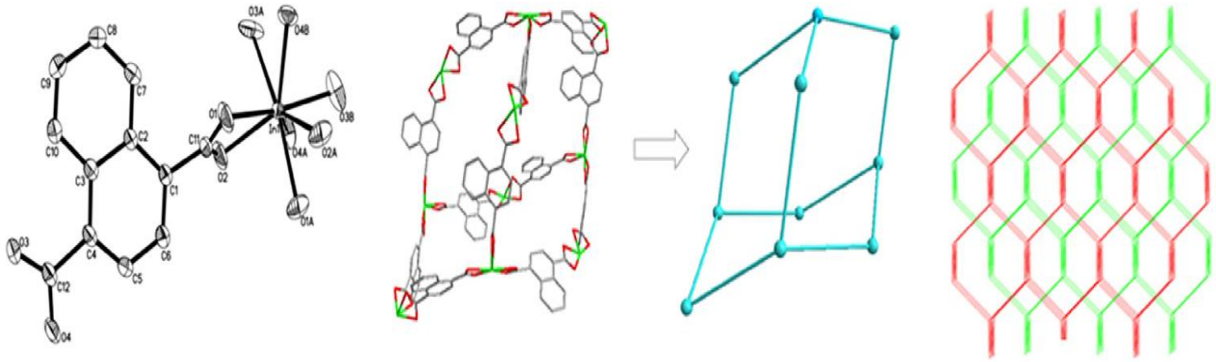

Figure 1.17: (left) In(III) dodecahedral coordination environment. (centre) Diamond structure of In(III)-1,4-ndc network. (right) Two two-fold interpenetrating 3D diamond net [177]. Reproduced by permission from Science Direct.

1.3.2 Microwave synthesis

Microwave synthesis and microwave-assisted processes can form high yields of CPs and porous MOF materials in short times in comparison with other synthesis methods [178-181]. Microwave synthesis can employ both solvent-based and solvent-free synthesis methods to synthesise CPs or MOFs in periods from a few seconds to minutes [177-183]. Microwave-assisted processes may involve dissolving the mixture of the metal salt precursor and the organic bridging linker/linkers in an appropriate solvent or a mixture of solvents followed by a heating process. Solvent-free microwave synthesis involves grinding a mixture of the metal salt with the bridging

ligand together to guarantee homogeneity of the mixture, followed by a microwave heating process [177-183]. Although these methods allow a high yield production of CPs or MOFs in a short time, the resultant crystal size is usually from 5 to 20 nm because of rapid synthesis, and not suitable for single crystal X-ray analysis studies [177-183].

In 2014 Lanchas and co-workers [178] reported the microwave synthesis of four previously reported MOFs known as ZIF-67, MOF-199, MIL-100(Fe/Cl) and MIL-100(Fe/NO_3) based on 2-methylimidazole, benzene-1,3,5-tricarboxylic acid, cobalt(II) hydroxide, copper(II) acetate hydrate, iron(III) chloride hydrate and iron(III) nitrate hydrate. The first step was grinding the organic ligand with the metal salt to ensure homogeneity of the mixture, then heating the reaction mixture between 120-170 °C from 1 to 20 minutes and finally wash the resulted MOFs with ethanol to remove any unreacted starting materials. ZIF-67 and MOF-199 yields were between 90-97 % after six minutes, while the same MOFs from solvothermal synthesis in DMF yield only 78 %. On the other hand, MIL-100(Fe/Cl) and MIL-100(Fe/NO_3) yields were between 80-83 % after three to four minutes. However, microwave synthesis method produced MOFs with low surface areas and small crystals not large enough for single X-ray analysis (figure 1.18).

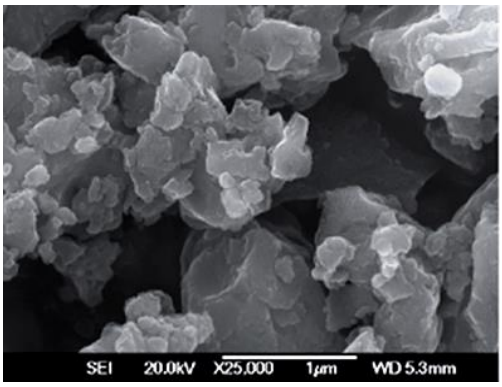

Figure 1.18: SEM image of MOF-199 prepared by microwave heating for 7.5 minutes [178]. Reproduced by permission from the Royal Society of Chemistry.

In 2012, Yeh and co-workers [184] reported two new MOFs based on 4,4'-sulfonyldibenzoate (sba) and $Ca(NO_3)_2.4H_2O$ or $Sr(NO_3)_2$ known as $[Ca(sba)].0.45H_2O$ (CYCU-1) and $[Sr(sba)].0.2H_2O$ (CYCU-2). CYCU-1 MOF was synthesised by dissolving of 1:2 molar ratios from the organic linker and calcium nitrate in the solution of ethanol and water. Then, heating the reaction mixture in an autoclave at 150 °C for 20 minutes to produce a 74 % yield of $[Ca(sba)].0.45H_2O$ MOF. CYCU-2 synthesis process was similar to CYCU-1 MOF but used a 1:4

molar ratio from the organic linker and strontium nitrate in the solution of ethanol and water, under hydrothermal conditions.

Single crystal X-ray analysis confirmed that CYCU-1 and CYCU-2 MOFs have a similar 3D network structure, where each metal centre has seven coordination bonds with six different ligands. The metal centre is coordinated by four oxygen atoms from four different carboxylate groups, two oxygen atoms from one carboxylate group and another coordinated oxygen atom from the sulfonyl groups (figure 1.19). The organic linker behaves as a hexadentate ligand to six metal ions through five oxygen donor atoms. A carboxylate group behaves as a bidentate ligand for two metal centres. Another carboxylate group behaves as a tetradentate ligand for three metal centres, in addition to one coordinated oxygen atom from the SO_2 group (figure 1.19).

The prepared MOFs have 1D zigzag chains structure resulted from the triangular edge-sharing of MO_7 monocapped trigonal prisms. The 1D chains are coordinated by the S-O-M bonds in two directions to create 3D MOFs having the guest molecules in the rhomboidal and zigzag channels. CYCU-1 MOF has 8.5 × 8.4 Å distances between the aromatic rings in the rhomboidal channels and approximately 12 Å diagonal distances inside the porous zigzag chains. The channels are located along the *b*-axis and can provide approximately 17.6 % free space from the unit cell (figure 1.20). CYCU-2 MOF has 8.8 × 8.8 Å distance between the aromatic rings in the rhomboidal channels along the *b*-axis and provide approximately 19.3 % free space from the unit cell. Thermal gravimetric analysis for CYCU-1 and CYCU-2 displayed two weight losses. The first weight loss was between 50-240 °C and due to release of guest molecules, while the second weight loss was at 450 °C and due to decomposition.

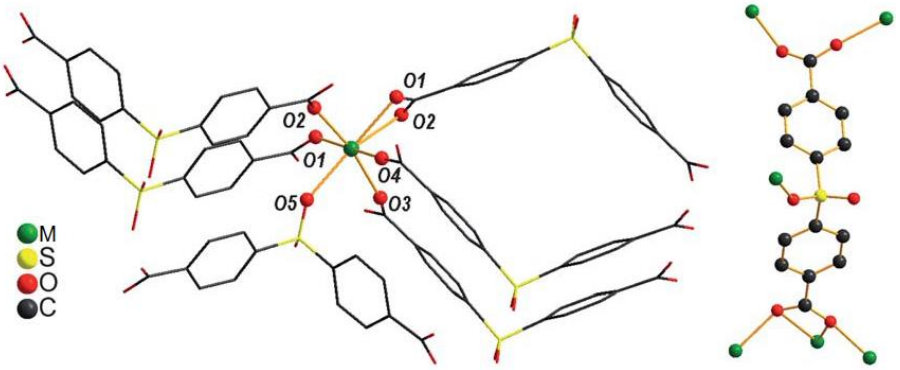

Figure 1.19: (left) Ca(II) and Sr(II) coordination environment, (right) the organic ligand coordination environment [184]. Reproduced by permission from the Royal Society of Chemistry.

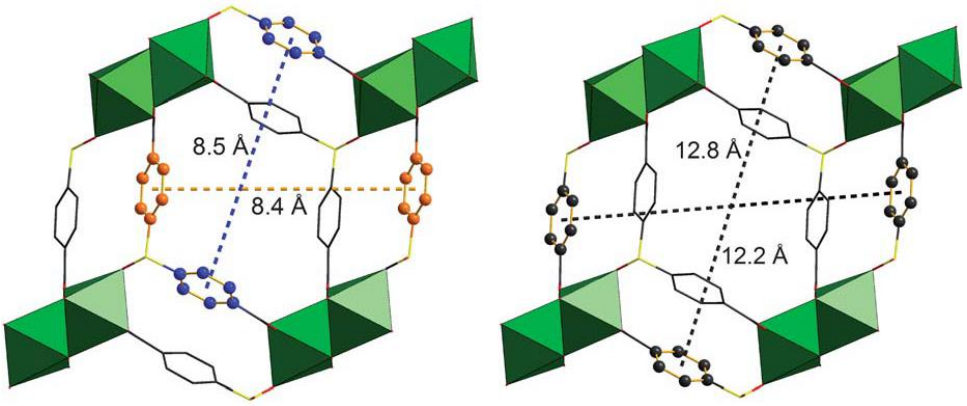

Figure 1.20: (left) CYCU-1 MOF cross-section. (right) CYCU-1 MOF diagonal distances [184]. Reproduced by permission from the Royal Society of Chemistry.

In 2007, Ochoa and co-workers [185] reported a novel copper(I) MOF based on copper(II) sulphate and pyrazine (pyz) of general formula $[Cu_2(pyz)_2SO_4(H_2O)_2]_n$. Ochoa successfully synthesised the novel MOF by the conventional hydrothermal method and the microwave irradiation method. The hydrothermal synthesis process uses equivalent amounts of copper(II) sulphate, pyrazine and benzoic acid, heated at 180 °C for 24 hours to produce a 46 % yield of Cu(I) MOF red crystals. Alternatively, the $[Cu_2(pyz)_2SO_4(H_2O)_2]$ microwave synthesis process uses the same amount of the reagents in a microwave-specified TFM autoclave, sealed and placed in a microwave reactor. The reaction mixture was heated at 180 °C for six hours and cool down to room temperature to produce Cu(I) MOF red crystals. Then the resultant red crystals were washed by warm water and dried under vacuum to produce a 37.6 % yield of Cu(I) MOF pure red crystals based on copper(II) sulphate starting material.

The resultant compounds from the microwave synthesis processes are dependent on the reaction time. For example, the 60 minutes reaction time produced only the blue crystals of $[Cu(pyz)SO_4(H_2O)]_n$ one-dimensional polymer, whereas the three hours reaction time produce the one-dimensional polymer in addition to 8.7 % from $[Cu_2(pyz)_2SO_4(H_2O)_2]$ MOF. Single crystal X-ray analysis of $[Cu_2(pyz)_2SO_4(H_2O)_2]$ MOF shows that the Cu(I) ion is coordinated to one bridging sulphate ion, two bridging pyrazine molecules and one water molecule to form Cu(I) distorted tetrahedral structure (figure 1.21). The resultant MOF has a complex construction based on three independent three-dimensional networks, where the resulted voids from one network are filled by the other two networks that form a three-fold interpenetrated net. Moreover, Cu(I) MOF shows four different bond distances between sulphate, pyrazine and water coordinated molecules

(Cu-N1= 1.984(17) Å), (Cu-N11= 1.955(16) Å), (Cu-O1= 2.109(14) Å) and (Cu-Ow= 2.1762(15) Å) (figure 1.21).

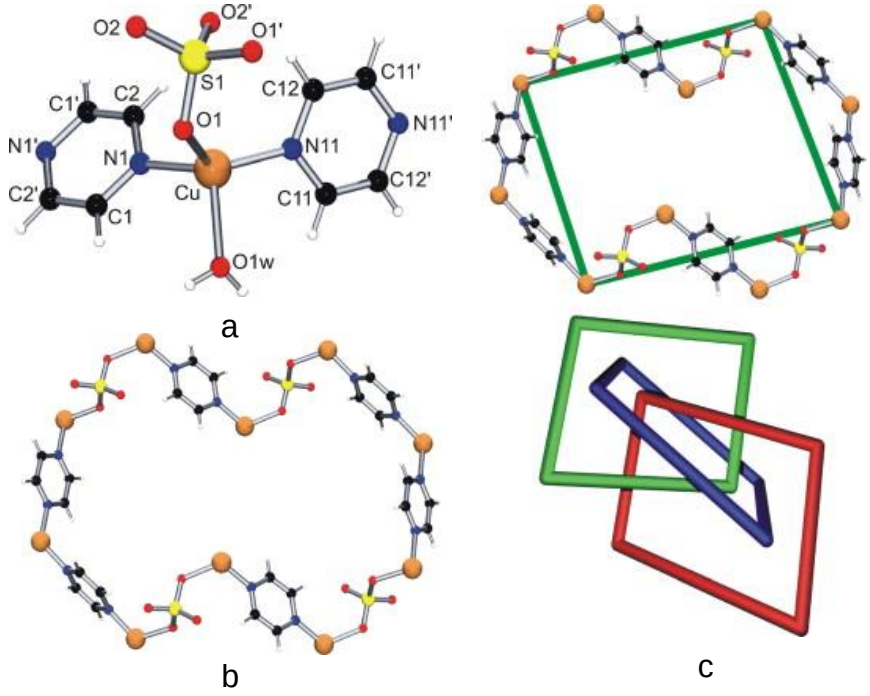

Figure 1.21: (a) $[Cu_2(pyz)_2SO_4(H_2O)_2]$ MOF coordination sphere, (b) $Cu_{10}(pyz)_6(SO_4)_4$ coordination ring, H_2O and shared pyrazine molecules were removed for clarity. (c) Interpenetrating of three independent 3D networks [185]. Reproduced by permission of Science Direct.

1.3.3 Mechanochemical synthesis

Mechanochemical synthesis or mechanosynthesis refers to the grinding reaction between the solid organic bridging ligand/ligands and the metal salt in a ball mill to produce coordination polymers or porous MOFs [186-188]. Mechanochemical synthesis can produce quantitative amounts of CPs or MOFs in a short time under ambient temperature either in solvent-free synthesis or with the addition of low amounts of the solvent in specific steps [186-188].

Solvent-free synthesis of microporous $[Cu(ina)_2]$ MOF (H-ina= isonicotinic acid) was reported in 2006 by Pichon and co-workers [189]. $[Cu(ina)_2]$ MOF was prepared by grinding of copper (II) acetate and isonicotinic acid for 10 minutes in a ball mill. The synthesis procedure was solvent-free and performed without any heating to produce the 3D crystalline MOF $[Cu(ina)_2]H_2O.2(CH_3COOH)$ (material one). This material was subsequently heated to 200 °C for three hours to give a quantitative yield of the empty crystalline microporous MOF $[Cu(ina)_2]$

(material two). During the 10 minutes of the grinding, material one reaction was indicated by the colour changing from green to blue and no liquid phase was observed when the grinding was stopped or when transferring material one to the reaction vessel [189]. Moreover, powder X-ray analysis indicated phase purity, and there are no traces for the unreacted starting materials (figure 1.22).

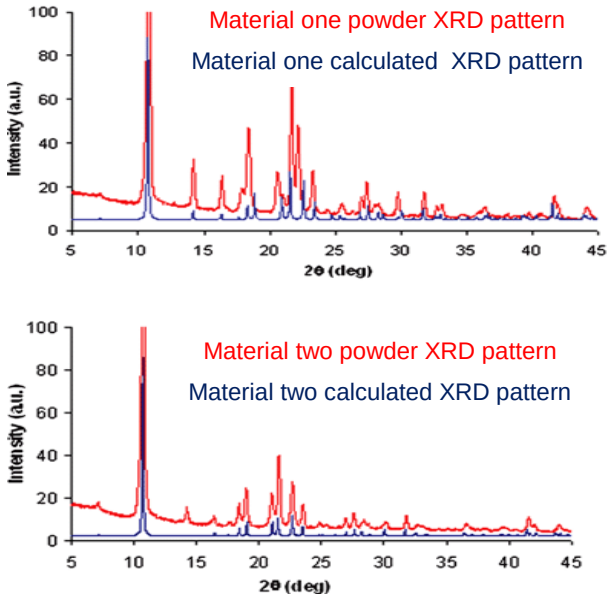

Figure 1.22: Comparison between resulted and calculated powder XRD patterns of material one and material two [189]. Reproduced by permission from the Royal Society of Chemistry.

In 2010, Yuan et al. [190] reported the mechanochemical synthesis and properties of HKUST-1 MOF prepared by the grinding reaction of copper(II) acetate hydrate and benzene-1,3,5-tricarboxylic acid. HKUST-1 MOF synthesis process involved grinding of 1.5 mmol from the metal salt precursor and one mmol from the organic linker for 15 minutes in a ball mill without solvent addition and washing the resulting product with fresh ethanol (figure 1.23). The washing process involved a total immersion for 20 minutes in ethanol on a Buchner funnel to remove the unreacted starting materials that blocked the 3D open network.

Nitrogen gas absorption/desorption experiments indicated that the resultant HKUST-1 MOF from the mechanochemical reaction before washing has a very low BET surface area of approximately 278 m^2/g in comparison with 900-2200 m^2/g BET surface area for HKUST-1 MOF from the conventional synthesis method. However, HKUST-1 from the mechanochemical method has a 1364 m^2/g BET surface area after washing with ethanol. A thermogravimetric analysis for

HKUST-1 from the mechanochemical synthesis method shows a similar result to HKUST-1 synthesised by conventional methods. The TGA showed two mass losses, the first mass loss at 270 °C due to loss of acetic acid and water guest molecules, while the second mass loss at 300 °C is due to MOF decomposition.

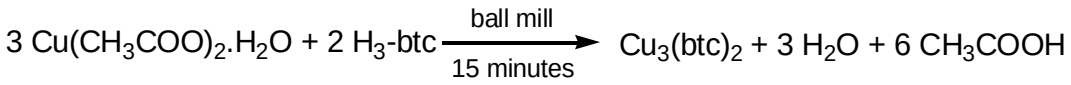

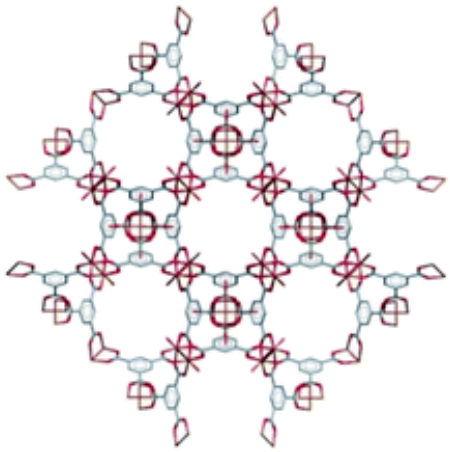

Figure 1.23: HKUST-1 MOF mechanochemical reaction, HKUST-1 MOF structure as reported by Chui [190]. Reproduced by permission from the Royal Society of Chemistry.

In 2015 Masoomi and co-worker [191] reported the synthesis of $[Cd_2(oba)_2(4\text{-}bpdb)_2]_n.(DMF)_x$ (TMU-8) and $[Cd(oba)(4,4'\text{-}bipy)]_n.(DMF)_y$ (TMU-9) heteroleptic MOFs by the conventional and the mechanochemical methods, where (H_2-oba)= 4,4′-oxybis(benzoic acid), (4-bpdb)= 1,4-bis(4-pyridyl)-2,3-diaza-1,3-butadiene and (4,4′-bipy)= 4,4′-bipyridine. The TMU-8 and TMU-9 conventional synthesis procedure involved dissolving of cadmium nitrate hydrate and the organic linkers in DMF and heating the mixture for 72 hours at 80 °C to result in 65 % yield of TMU-8 MOF yellow crystals and 63 % yield of TMU-9 MOF colourless crystals. On the other hand, the $[Cd_2(oba)_2(4\text{-}bpdb)_2]_n$ MOF mechanochemical synthesis procedure involved hand grinding of cadmium(II) acetate and the organic linkers for 25 minutes and washing the resulted powder with small amounts of DMF to remove any possible unreacted starting materials. Then, TMU-8 MOF powder was dried for 24 hours at 80 °C. $[Cd(oba)(4,4'\text{-}bipy)]_n$ MOF synthesis process involved hand grinding of the metal salt and the organic linkers for 20 minutes, and washing the resulted powder with DMF, then drying the MOF powder for 24 hours at 100 °C.

The thermogravimetric analysis for the resulting TMU-8 and TMU-9 MOFs from the conventional method displayed two main weight losses. The first weight loss was between 50-260 or 50-290 °C due to the release of guest molecules, while the second weight loss was above 260 or 290 °C due to ligand decomposition. However, TMU-8 and TMU-9 MOFs from the mechanochemical methods showed only the MOF decomposition at 260 or 290 °C. Furthermore, TMU-8 and TMU-9 MOFs from the conventional method and the mechanochemical method have similar powder X-ray patterns (figure 1.24).

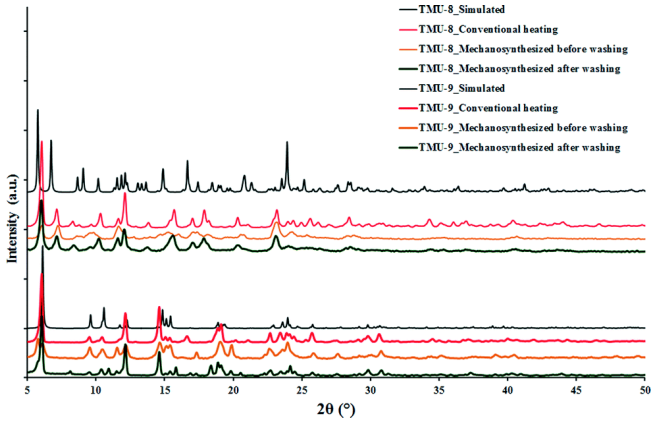

Figure 1.24: Comparison of XRD patterns for TMU-8 and TMU-9: simulated, conventional heating and mechanosynthesised MOFs before and after washing with DMF [191]. Reproduced by permission from the Royal Society of Chemistry.

1.4 Applications of coordination polymers and metal-organic frameworks

CP and MOF applications are diverse, numerous and extending in a high number of fields, for example, industrial [192-195], biological [142, 196-198] and medicinal applications [199-201]. The diversity of CP and MOF applications are due to the unique properties that each CP or MOF can supply. These properties depend on the repeated organic linkers, metal ions, synthesis method and resulting structures. MOFs can provide solutions for scientific and industrial problems [173]. Problems can be solved by MOF application directly or indirectly [173], for examples gas storage and separation [11, 12, 61, 102-114], synthesis of new catalyst [6, 16, 94-101] and synthesis of thermally stable microporous compounds [20-29].

1.4.1 Chemical catalysts

MOFs are highly active catalysts for different types of chemical reactions such as Suzuki coupling, alkenes hydrogenation, and alcohol oxidation because of their thermal stability, nanochannel and nanocavity systems [202]. In 2007, Xamena and co-workers [202] reported an

active, reusable and shape-selective 3D MOF based on Pd(II) ions and 2-hydroxypyrimidinolate (2-pymo) of general formula $[Pd(2\text{-pymo})_2]_n$. The prepared MOF has 600 m^2/g BET surface area and is insensitive to moisture because it was originally synthesised in an aqueous medium. Moreover, the synthesised MOF could supply 42 % of its 3D overall structure to guest molecules because of the four-membered and six-membered ring window arrangements (figure 1.25).

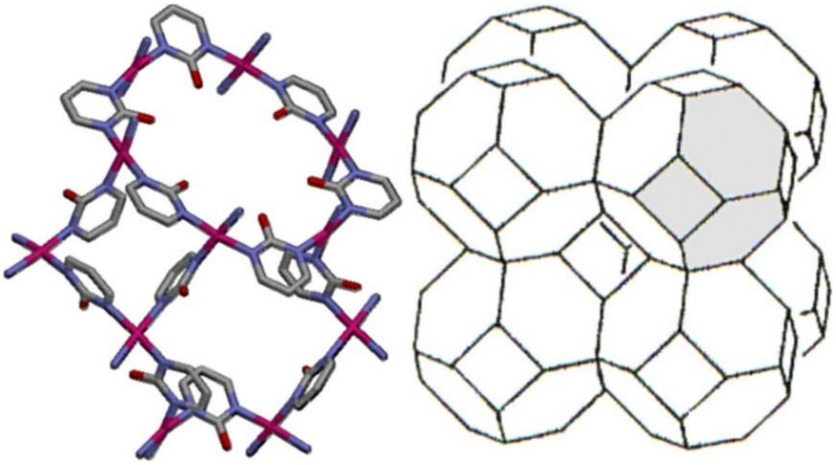

Figure 1.25: (left) Detail of Pd-MOF, showing the 4-membered and the two 6-membered rings. (right) The 3D arrangement of the sodalite cages in sodalite-type frameworks [202]. Reproduced by permission from Science Direct.

The catalytic activity of the synthesised Pd-MOF was tested in a Suzuki-Miyaura reaction between phenylboronic acid and 4-bromoanisole (scheme 1.1). These compounds represent a good example for carbon-carbon coupling reactions between boron aromatic organic compounds and organic aromatic halides compounds, which it has been suggested as a reference reaction for highly active Pd catalysts. The 4-methoxy-biphenyl product was obtained in a 99 % yield after five hours of using Pd-MOF in DMF at 150 °C. The X-ray analysis for the used Pd-MOF was almost identical to the fresh sample after recovery showing the MOF was very stable.

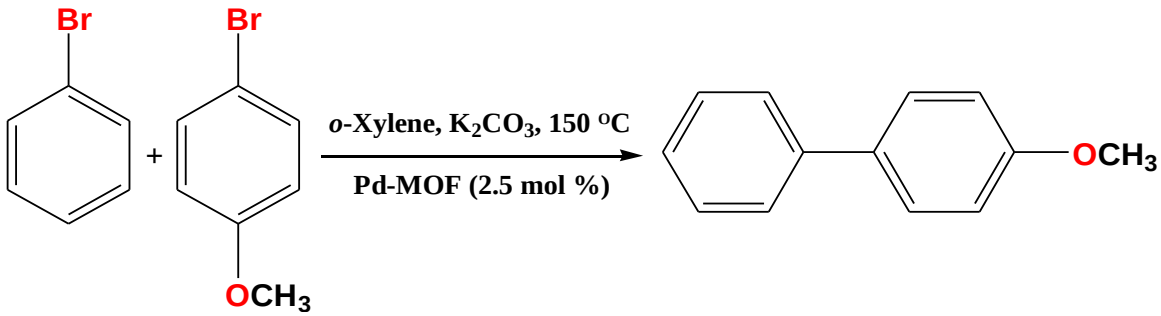

Scheme 1.1: Synthesis of 4-methoxy-biphenyl [202].

1-Octene and cyclododecene were used to test the structure selectivity and the hydrogenation activity of the synthesised Pd-MOF in comparison with a classical palladium catalyst which has no structure selectivity. The Pd-MOF converts 59 % of 1-octene to octane after 40 minutes, and after 120 minutes the secondary alkene 2-octene was completely converted to octane, whereas cyclododecene was not converted to cyclododecane even after five hours. The results indicate that the active centres are in the internal surface area of the prepared MOF and accessible only for the linear octene molecules through the pores.

Hydrogenation of 2-furfuraldehyde to 2-furfuryl alcohol has been reported as a challenge for selective hydrogenation catalysis for two reasons [203]. The first reason is that 2-furfuryl alcohol can be polymerised by its methylene group. The second is that 2-furfuryl alcohol also can be hydrogenated to tetrahydrofurfuryl alcohol. In 2015 Yang and co-workers [203] reported the hydrogenation of 2-furfuraldehyde to 2-furfuryl alcohol using Zr(IV) MOFs known as UiO-66, MIL-140A, MIL-140B, UiO-67 and MIL-140C used benzene-1,4-dicarboxylic acid, 4,4'-biphenyldicarboxylic acid and naphthalene-2,6-dicarboxylic acid as organic linkers that loaded with ruthenium(III) nanoparticles. Catalysis with the Ru(III) loaded MOF gave only 2-furfuryl alcohol as the final product and was thermally stable up to 450 °C because of the strong bonding between the zirconium(IV) metal ions and carboxylate groups. Moreover, Ru/Zr (UiO-66) MOF selectivity was nearly 94.9 % and reusable five times without significant loss in performance [203].

In 2015 Zhang and co-workers [204] reported a new solvent-free heterogeneous catalyst for carbon-carbon formation reactions by cyanosilylation of aldehyde or ketone compounds. Zhang used the modified $[(Cu_4O_{0.27}Cl_{0.73})_3(H_{0.5}btt)_8]$ MOF (Cu-MOF1′) as a heterogeneous catalyst which resulted from the dehydration of $[(Cu_4O_{0.27}Cl_{0.73})_3(H_{0.5}btt)_8(H_2O)_{12}]$.3(MeOH).9(DMF) MOF ($btt^{3-}$ = benzene-1,3,5-tristetrazolate). The MOF synthesis process involved a solvothermal reaction between a methanolic solution of copper(II) acetate hydrate contains nitric acid and a DMF solution of H_3btt.2HCl at 85 °C for 48 hours to produce 80 % yield of Cu-MOF1 green crystals. Cu-MOF1' synthesis process involved washing of Cu-MOF1 green crystals by fresh methanol several times to remove the guest molecules and drying the green crystals under vacuum for 12 hours.

Single crystal X-ray analysis of Cu-MOF1 shows that the Cu(II) ion is coordinated by four equatorial nitrogen atoms from four different btt^{3-} ligands and an axial oxygen atom from the coordinated water molecules. Cu-O1 and Cu-Cl1 coordinated atoms occupy the same axial

position to produce the distorted octahedral coordination centre. Cu(II) metal ions and O1, Cl1 atoms are coordinated to form a planar structure that has the axial coordination water molecules to generate the tetracopper cluster based secondary building unit (figure 1.26). The btt^{3-} organic linker is connected to six Cu(II) ions by two nitrogen atoms from the tertazyl groups, and each tetracopper cluster planar structure is coordinated to eight btt^{3-} organic linkers. Moreover, each ligand is coordinated to three copper cluster to generate the 3D connected net (figure 1.26).

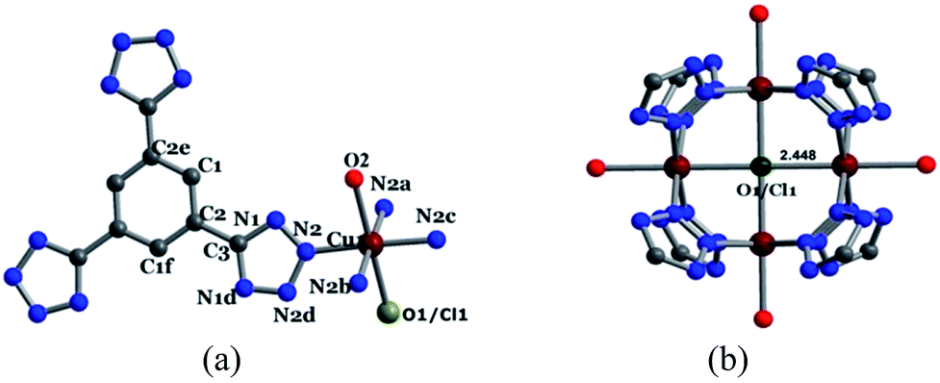

Figure 1.26: (a) Cu-MOF1 distortion octahedral structure Cu-N= 2.018(3) Å, Cu-O2= 2.396(9) Å and Cu-O1/Cl1= 2.448 Å. (b) Tetracopper cluster based secondary building unit [204]. Reproduced by permission from the Royal Society of Chemistry Publishing.

The cyanosilylation catalyst reaction test involved the addition of 0.005 mmol of Cu-MOF1' to a mixture of 0.5 mmol of benzaldehyde and one mmol of Me_3SiCN and heating the mixture at 40 °C for 19 hours under nitrogen (scheme 1.2). This cyanosilylation catalyst reaction leads to a 96 % conversion of benzaldehyde after the 19 hours. However, another catalyst test involved removing the Cu-MOF1′ by filtration after two hours, and the reaction mixture could continue heating for another 17 hours. Zhang determined the conversion process of the aldehyde or the ketone compounds during the reaction time by gas chromatography analysis. The GC analysis results showed that, when the catalyst is present the conversion of the aldehyde or ketone compounds was 50 %, and no more conversion was occurred after removing the catalyst even after 17 hours. Cu-MOF1' shows high catalytic activity to convert benzaldehyde, 2-furfural, pentanal and cyclohexanone to cyanosilylated compounds with 96 % conversion for benzaldehyde and 99 % for the other compounds. The catalyst can be used five times without an obvious decrease in activity. Moreover, the catalysts recycling process involves filtration from the mixture solution, washing by fresh MeOH and drying for 12 hours under vacuum.

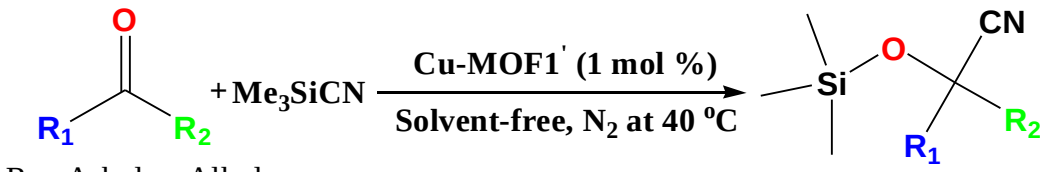

R_1= Arkyl or Alkyl
R_2= H or Alkyl

Scheme 1.2: Cyanosilylation of aldehyde or ketone compounds [204].

1.4.2 Gas storage

Gas storage and separation by high surface area materials such as metal-organic frameworks are promising research fields and have had great attention in recent years [205, 206]. This attention is due to MOFs high storage capacities for different gases, MOFs high thermal stability, and MOFs potential behaviour as fully reversible microporous materials for gas adsorption and desorption [205-207]. Moreover, MOFs have been reported as carbon dioxide storage and hydrocarbon gas separation materials [205].

In 2015 Chen and co-workers reported carbon dioxide gas storage materials. Besides, separation materials for hydrocarbon gases such as methane, ethane and propane [205]. Chen prepared five novel MOFs materials based on copper nitrate with 5-(isonicotinamido)isophthalic acid (H_2-ison), 5-(nicotinamido)isophthalic acid (H_2-nica), 5-(pyridine-4-ylamino)isophthalic acid (H_2-pyiso), 5-(pyridin-3-ylamino)isophthalic acid (H_2-pyaiso) and 5-(pyrimidin-5-ylamino)isophthalic acid (H_2-pmiso) as bridging ligands.

Copper nitrate and (H_2-ison) ligand were used to synthesise the Cu(ison).$(solv)_n$ MOF (n= 0-∞) by the solvothermal reaction method. The MOF synthesis method involved dissolving the metal salt and the organic linker in *N*,*N*-dimethylacetamide and acetic acid then heating the mixture up to 115 °C for 24 hours. The resulted green block crystals were investigated by single crystal X-ray analysis and showed the hourglass structure for the prepared MOF. The organic linker in the synthesised MOF behaves as a three connected node and the paddlewheel molecular building blocks as six connected octahedral building units. In addition, the synthesised MOF has three-membered ring windows with 7.8 Å diameter linked to six-member ring windows with 10.5 Å diameter to produce hourglass-shaped channels that can provide 59.6 % free space from the overall calculated volume after removing the solvent guest molecules (figure 1.27).

Copper nitrate was reacted with (H_2-nica) under fixed conditions to produce Cu(nica).$(solv)_n$ MOF. The prepared MOF Kagome structure was confirmed by single crystal X-

ray analysis results, which has three-member rings and six-member rings cavities, smaller by 0.2 and 0.7 Å diameters compared to the first prepared Cu(ison).$(solv)_n$ MOF. Moreover, the thermogravimetric analyses for the two prepared MOFs to have similar thermal stability below 249.8 °C.

Chen synthesised three additional metal-organic frameworks based on (H_2-pyiso), (H_2-pyaiso) or (H_2-pmiso) and copper(II) nitrate in general formulas Cu(pyiso).$(solv)_n$, Cu(pyaiso).$(solv)_n$ and Cu(pmiso).$(solv)_n$. The organic linkers in the synthesised MOFs behave as three connected nodes and the paddlewheel molecular building blocks as six connected octahedral building units. The resulting square lattice metal-organic frameworks layers include four-member ring windows arranged in a 1,2-alternate fashion and correlating with neighbouring two dimensional square lattice MOF layers to generate 2.9 × 7.1 Å channels for Cu(pyiso).$(solv)_n$ and 3.55 × 5.6 Å channels for Cu(pyaiso).$(solv)_n$ and Cu(pmiso).$(solv)_n$ MOFs. However, Cu(pyiso).$(solv)_n$ MOF can provide 51.9 % free space from the overall calculated volume after removing the solvent guest molecules (figure 1.28).

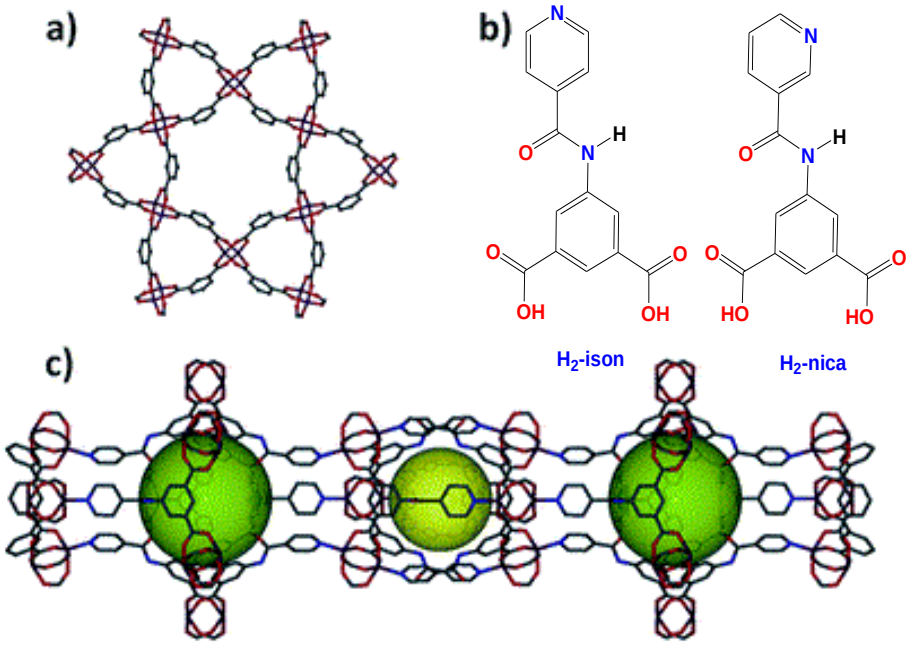

Figure 1.27: (a) Cu(ison).$(solv)_n$ and Cu(nica).$(solv)_n$ MOFs Kagome structure, (b) 5-(isonicotinamido)isophthalic acid (H_2-ison), 5-(nicotinamido)isophthalic acid (H_2-nica) organic linkers. (c) Hourglass shape structure channels [205]. Reproduced by permission from the Royal Society of Chemistry.

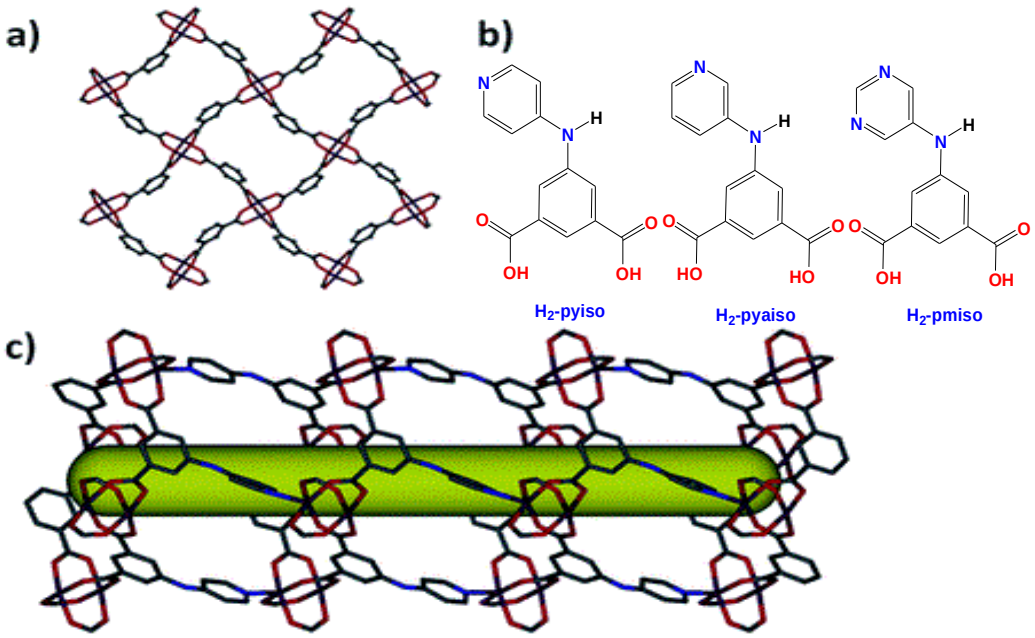

Figure 1.28: (a) Square lattice metal-organic frameworks layers. (b) 5-(Pyridine-4-ylamino)-isophthalic acid (H_2-pyiso), 5-(pyridin-3-ylamino)isophthalic acid (H_2-pyaiso) and 5-(pyrimidin-5-ylamino)isophthalic acid (H_2-pmiso) organic linkers. (c) Square shape channels [205]. Reproduced by permission from the Royal Society of Chemistry.

Cu(ison).(solv)$_n$ and Cu(nica).(solv)$_n$ MOFs permanent porosity properties were confirmed by Argon gas adsorption and desorption experiments at 87 K and from 0 to 800 Torr pressure. Cu(ison).(solv)$_n$ MOF is a fully reversible microporous material with 1860 m^2/g Langmuir surface area and has a 0.65 cm^3/g pore volume which agrees 98.48 % with the calculated crystal structure pore volume. Cu(nica).(solv)$_n$ showed 1200 m^2/g Langmuir surface area and had 96.29 % pore volume in agreement with the calculated crystal structure. On the other hand, the CO_2 adsorption for Cu(ison).(solv)$_n$ MOF is 0.56 or 3 mmol/g in 298 K at 0.15 or 1 bar pressure, while CO_2 adsorption for Cu(nica).(solv)$_n$ MOF is 0.94 or 4.5 mmol/g under the same conditions. However, the two prepared MOFs showed similar nitrogen and methane gas adsorption of 0.18 and 0.9 mmol/g at 298 K and 1 bar pressure, while ethane and propane gas uptake for Cu(ison).(solv)$_n$ MOF is 5.21 and 5.99 mmol/g are higher than 4.31 and 4.77 mmol/g for Cu(nica).(solv)$_n$ MOF at 1 bar pressure and 298 K [205].

In 2015 Zhang and co-workers [204] reported porosity and gas sorption experiments on $[(Cu_4O_{0.27}Cl_{0.73})_3(H_{0.5}btt)_8]$ (Cu-MOF1'). Gas sorption experiments were performed at 77 K for hydrogen, nitrogen, and oxygen gases. The synthesised Cu-MOF1 was immersed in CH_3OH for 24 hours to remove any guest molecules and washed by fresh methanol five times, then heated

under vacuum at 393 K overnight to produce the de-solvated Cu-MOF1'. Hydrogen gas adsorption experiment results indicated that the Cu-MOF1' shows fully reversible gas uptake of 1.44 weight at 1.05 bar and has 226.58 m^2/g Langmuir surface area. Oxygen and nitrogen absorption measurements of Cu-MOF1' displayed micro-mesoporous material properties with 736 m^2/g and 1223.04 cm^2/g for BET and Langmuir surface areas (figure 1.29).

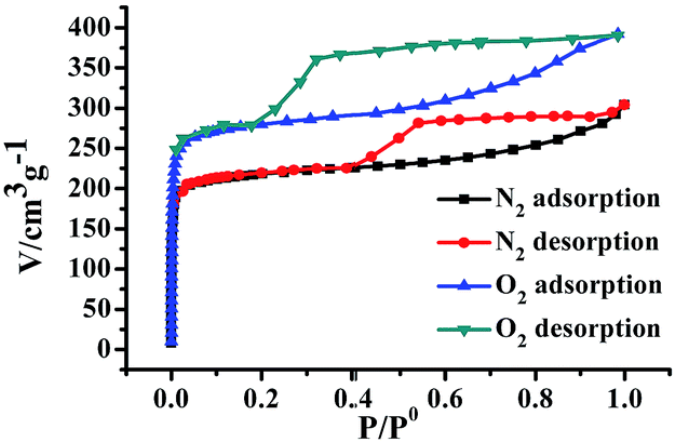

Figure 1.29: Cu-MOF1' adsorption/desorption experiments uptake for oxygen and nitrogen gases at 77 K [204]. Reproduced by permission from the Royal Society of Chemistry Publishing.

1.5 Coordination polymers based on bis-pyridyl ligands.

In 2012, T. Jacobs and M. J. Hardie [208] reported five new homoleptic metal-organic frameworks based on $Fe(BF_4)_2.6H_2O$, $CoCl_2.6H_2O$, $Cu(NO_3)_2.2.5H_2O$, $Zn(NO_3)_2.6H_2O$ or $Cd(NO_3)_2.4H_2O$ and the new ligand *N,N'*-bis(pyridin-4-yl)-2,2'-bipyridine-5,5'-dicarboxamide (2,2-bpbi). The new organic ligand synthesis process involved two steps. The first step was oxidation of 5,5'-dimethyl-2,2'-bipyridine to 5,5'-dicarboxylic acid-2,2'-bipyridine by potassium dichromate in sulfuric acid. The second synthesis step involved the addition of thionyl chloride to convert the prepared 2,2'-bipyridine-5,5'-dicarboxylic acid to acid chloride form. Then, treatment with 4-aminopyridine to produce the new organic linker (figure 1.30). Jacobs synthesised three-dimensional metal-organic frameworks in general formula $\{[M_5(2,2\text{-bpbi})_6]\}_\infty$ where M= Cu(II), Zn(II) or a mixture of Fe(II) and Cu(II) ions, in addition to $\{[Co(2,2\text{-bpbi})Cl_2].DMF\}_\infty$ and $\{Cd(2,2\text{-bpbi})(NO_3)_2\}_\infty$ two-dimensional sheets.

$\{[Cu_5(2,2\text{-bpbi})_6]_\infty.(NO_3)_{10}.(H_2O)_{18}\}_\infty$ MOF was obtained by solvent diffusion process of the metal salt precursor and the organic ligand in DMF with diethyl ether as an antisolvent at ambient temperature to produce the new MOF blue-purple crystals after one week. Furthermore,

the same procedure was followed to produce $\{[Zn_5(2,2\text{-bpbi})_6]_\infty.(NO_3)_{10}.(H_2O)_{18}\}_\infty$ and $\{[Fe_xCu_y(2,2\text{-bpbi})_6]_\infty.(NO_3)_{10}.(H_2O)_{18}\}_\infty$ MOFs ($x+y= 5$). $\{[Cu_5(2,2\text{-bpbi})_6]_\infty.(NO_3)_{10}.(H_2O)_{18}\}_\infty$ MOF crystal structure was solved in body centred space group *I*432 and shows two separate copper(II) octahedral coordination centres. Cu(1) coordination centre is coordinated to three different ligands by nitrogen atoms of 2,2-bipyridine rings (Cu1-N= 2.117(2) Å). Whereas Cu(2) coordination centre is coordinated to four equatorial 4-pyridyl rings from four different ligand molecules (Cu-N= 2.011(2) Å) and two axial water molecules (Cu-O= 2.309(4) or 2.760(5) Å) to produce Cu(2) distorted octahedral coordination centre (figure 1.31). After symmetrical expansion $\{[Cu_5(2,2\text{-bpbi})_6]_\infty.(NO_3)_{10}.(H_2O)_{18}\}_\infty$ MOF shows a three-dimensional open network structure (figure 1.32).

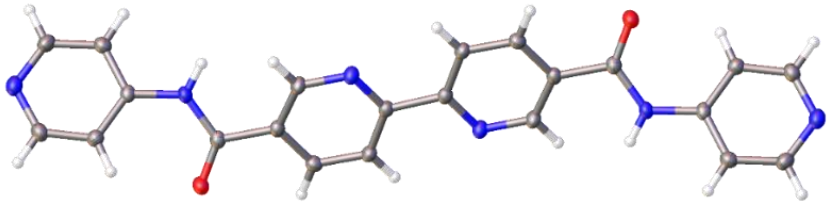

Figure 1.30: Crystal structure of *N,N'*-bis(pyridin-4-yl)-2,2'-bipyridine-5,5'-dicarboxamide ligand [208].

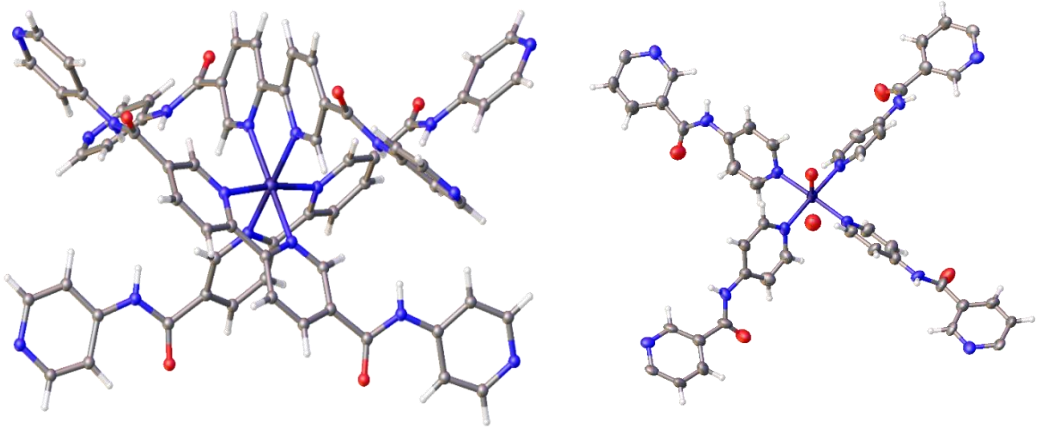

Figure 1.31: (left) Cu1 octahedral coordination environment. (right) Cu2 octahedral coordination environment [208].

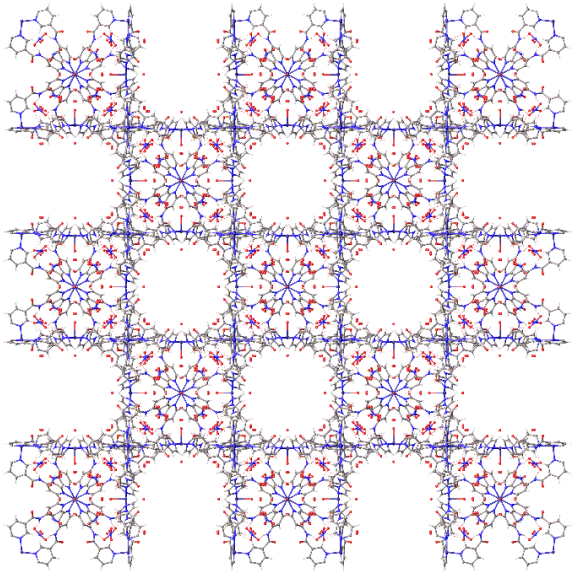

Figure 1.32: $\{[Cu_5(2,2\text{-bpbi})_6]_\infty.(NO_3)_{10}.(H_2O)_{18}\}_\infty$ MOF three-dimensional open network structure [208].

$\{[Zn_5(2,2\text{-bpbi})_6]_\infty.(NO_3)_{10}.(H_2O)_{18}\}_\infty$ and $\{[Fe_xCu_y(2,2\text{-bpbi})_6]_\infty.(NO_3)_{10}.(H_2O)_{18}\}_\infty$ MOFs are isostructural with $\{[Cu_5(2,2\text{-bpbi})_6]_\infty.(NO_3)_{10}.(H_2O)_{18}\}_\infty$ MOF. Zn(II)-MOF also shows two Zn(II) coordination centres. Zn(1) ion is coordinated to three different (2,2-bpbi) ligand molecules by nitrogen atoms of 2,2-bipyridine rings (Zn1-N1= 2.157(3) Å) to produce Zn(II) octahedral coordination centre. Whereas Zn(2) is coordinated to four equatorial 4-pyridyl rings from four different (2,2-bpbi) ligands (Zn2-N13= 2.182(3) Å) and two axial water molecules (Zn2-O3= 2.209(7) Å) or (Zn2-O4= 2.231(16) Å) to produce Zn(II) distorted octahedral coordination centre.

Fe(II) ions in $\{[Fe_xCu_y(2,2\text{-bpbi})_6]_\infty.(NO_3)_{10}.(H_2O)_{18}\}_\infty$ MOF are coordinated to three (2,2-bpbi) ligand molecules by nitrogen atoms of 2,2′-bipyridine rings to produce Fe(II) octahedral coordination centre (Fe-N1= 2.114(2) Å) (figure 1.33). On the other hand, Cu(II) ion is coordinated to four 4-pyridyl rings from four different (2,2-bpbi) molecules and two axial water molecules Cu2-N1= 2.040(2), Cu2-O3= 2.724(5) and Cu2-O4= 2.465(4) Å to produce Cu(II) distorted octahedral coordination centre (figure 1.33).

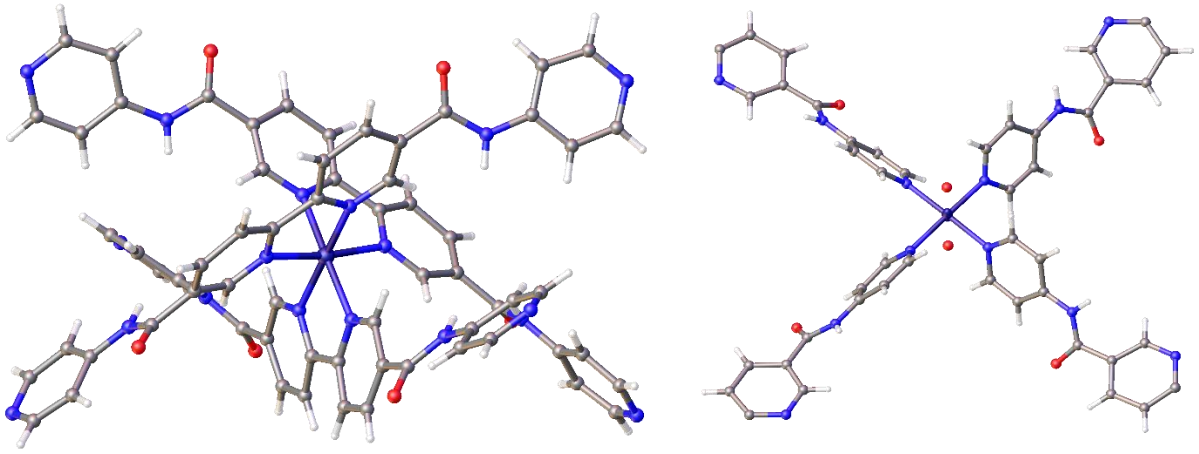

Figure 1.33: (left) Fe(II) octahedral coordination centre in{[Fe_xCu_y(2,2-bpbi)$_6$]$_\infty$.(NO_3)$_{10}$.(H_2O)$_{18}$}$_\infty$ MOF, (right) Cu(II) octahedral coordination centre in {[Fe_xCu_y(2,2-bpbi)$_6$]$_\infty$.(NO_3)$_{10}$.(H_2O)$_{18}$}$_\infty$ MOF [208].

Co(II) ions in {[Co(2,2-bpbi)Cl_2].DMF}$_\infty$ MOF are coordinated to three different (2,2-bpbi) ligand molecules by nitrogen atoms of pyridyl rings and two chloride ions in *cis* arrangement to produce Co(II) distorted octahedral coordination centre (figure 1.34). The resultant crystal structure shows coordination bond lengths of 2.217(2) and 2.188(2) Å between Co(II) and 2-pyridyl rings. In addition to 2.441(7) and 2.445(7) Å between Co(II) and Cl^- ions and 2.238(19) or 2.216(2) Å between Co(II) and 4-pyridyl rings. After symmetry expansion {[Co(2,2-bpbi)Cl_2].DMF}$_\infty$ MOF shows two-dimensional square lattice structure that has 13.099 × 11.925 Å sides and 18.239 × 16.306 Å diagonals between Co(II) coordination centres (figure 1.35). Moreover, the resulted two-dimensional square lattice is packing with other 2D networks to produce a two-fold interpenetrating structure (figure 1.35).

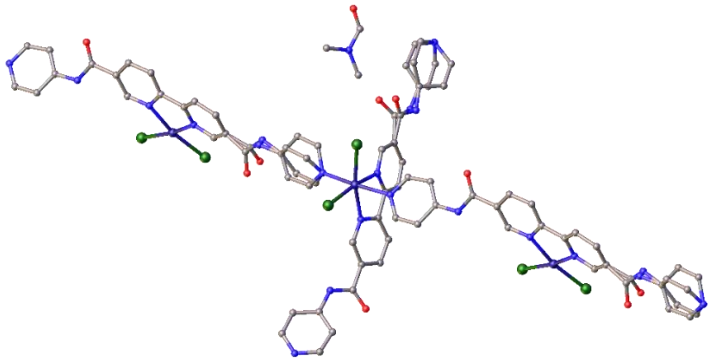

Figure 1.34: Co(II) ion in {[Co(2,2-bpbi)Cl_2].DMF}$_\infty$ MOF coordination environment [208].

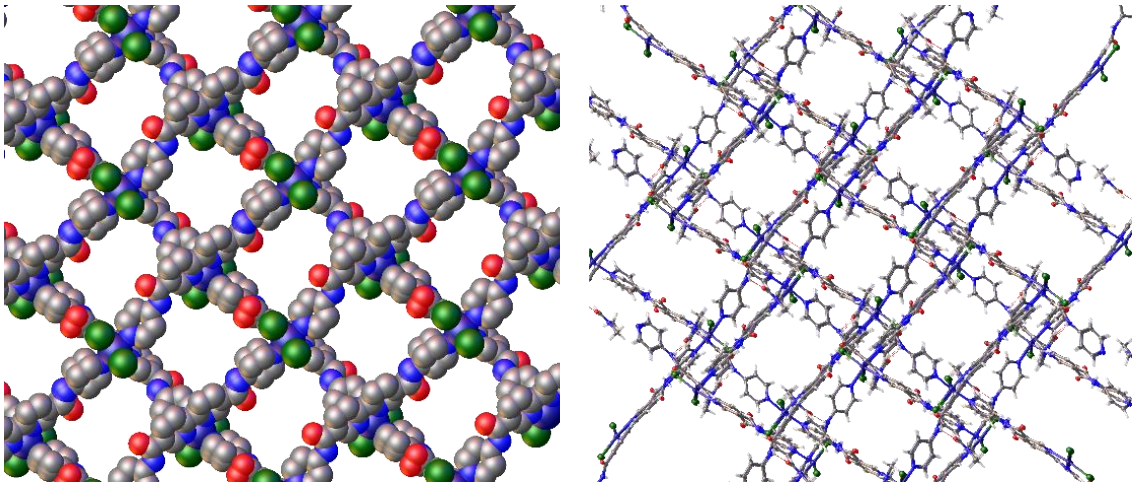

Figure 1.35: (left) $\{[Co(2,2\text{-bpbi})Cl_2].DMF\}_\infty$ MOF 2D network. (right) Interpenetrating of $\{[Co(2,2\text{-bpbi})Cl_2].DMF\}_\infty$ MOF 2D networks [208].

$\{Cd(2,2\text{-bpbi})(NO_3)_2\}_\infty$ two-dimensional coordination polymer crystal structure was solved in monoclinic space group $P2_1$ and shows one Cd(II) ion on a general position, two coordinated nitrate ions and one (2,2-bpbi) ligand molecule per asymmetric unit (figure 1.36). Cd(II) ion is coordinated to one (2,2-bpbi) ligand molecule by its 2,2-bipyridyl rings (Cd-N= 2.340(2)-2.467(4) Å), two other (2,2-bpbi) molecules by 4-pyridyl rings (Cd-N= 2.234(4) or 2.306(4) Å) and two nitrate molecules (Cd-O= 2.412(3)-2.455(3) Å) to produce Cd(II) distorted pentagonal bipyramid coordination centre (figure 1.36). Moreover, the resulted two-dimensional coordination network shows 12.784 Å sides and 19.029 × 14.922 Å diagonals between Cd(II) centres (figure 1.37).

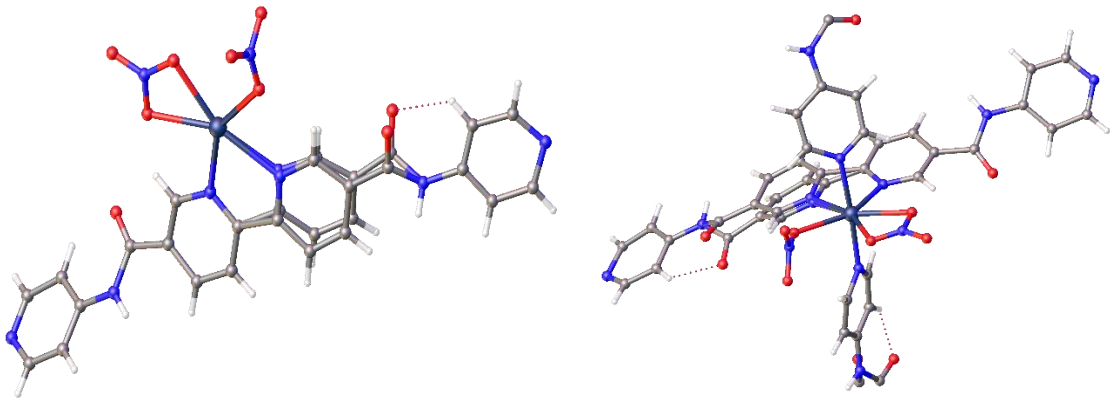

Figure 1.36: (left) $\{Cd(2,2\text{-bpbi})(NO_3)_2\}_\infty$ MOF asymmetric unit of the crystal structure, (right) Cd(II) pentagonal bipyramid coordination centre [208].

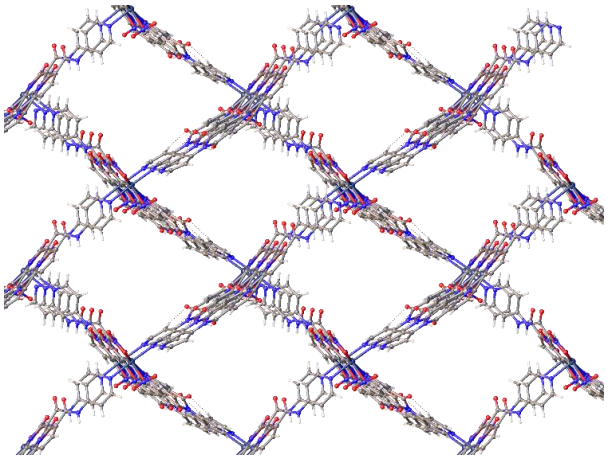

Figure 1.37: $\{Cd(2,2\text{-bpbi})(NO_3)_2\}_\infty$ MOF two-dimensional networks [208].

A three-dimensional metal-organic framework based on zinc(II) nitrate hexahydrate, isophthalate (iso) and *N,N'*-bis(pyridin-4-yl)-2,2'-bipyridine-5,5'-dicarboxamide (2,2-bpbi) was reported in 2012 by Jacobs and co-workers [209]. The [Zn(iso)(2,2-bpbi)].2(DMF) MOF synthesis process involved dissolving equivalent molar ratio of the starting materials in DMF and elevating the temperature to produce crystals large enough and suitable for single crystal X-ay analysis. The resulted MOF yellow crystals have a novel network topology and uncoordinated 2,2-bipyridine groups that can use as post-synthetic modification material. The divalent zinc cation is coordinated to two bridging isophthalate molecules behave as monodentate ligands (Zn-O= 1.987(7) Å). In addition to two coordinated *N,N'*-bis(pyridin-4-yl)-2,2'-bipyridine-5,5'-dicarbox-amide ligands through the nitrogen atoms of 4-pyridyl rings (Zn-N= 2.062(7) Å) to produce Zn(II) tetrahedral coordination centres (figure 1.38).

The bridging isophthalate anions and the divalent zinc cation centres generate a spiral chain on the three-fold screw axis, where the monodentate ligands are creating a planar structure with their aromatic rings all perpendicular, and each resulting chain is surrounded by three other spiral chains (figure 1.38). The 2,2,-bipyridine of (2,2-bpbi) ligand did not coordinate to the Zn(II) ion and this site can be metallated a post-synthesis modification process. [Zn(iso)(2,2-bpbi)].2(DMF) MOF the post-modification process involved soaking the MOF resultant crystals into copper(II) chloride or copper(II) tetrafluoroborate DMF solutions for 21 days to obtain $[ZnCu_{1/3}(iso)(2,2\text{-bpbi})]\cdot_{1/3}Cl\cdot[CuCl_2]_{0.3}.n(DMF)$ MOF as yellow crystals (figure 1.39). Moreover, the single crystal analysis result shows a distorted tetrahedral structure for copper(I) and (II) coordination centres (Cu-N= 2.066 Å) (figure 1.39).

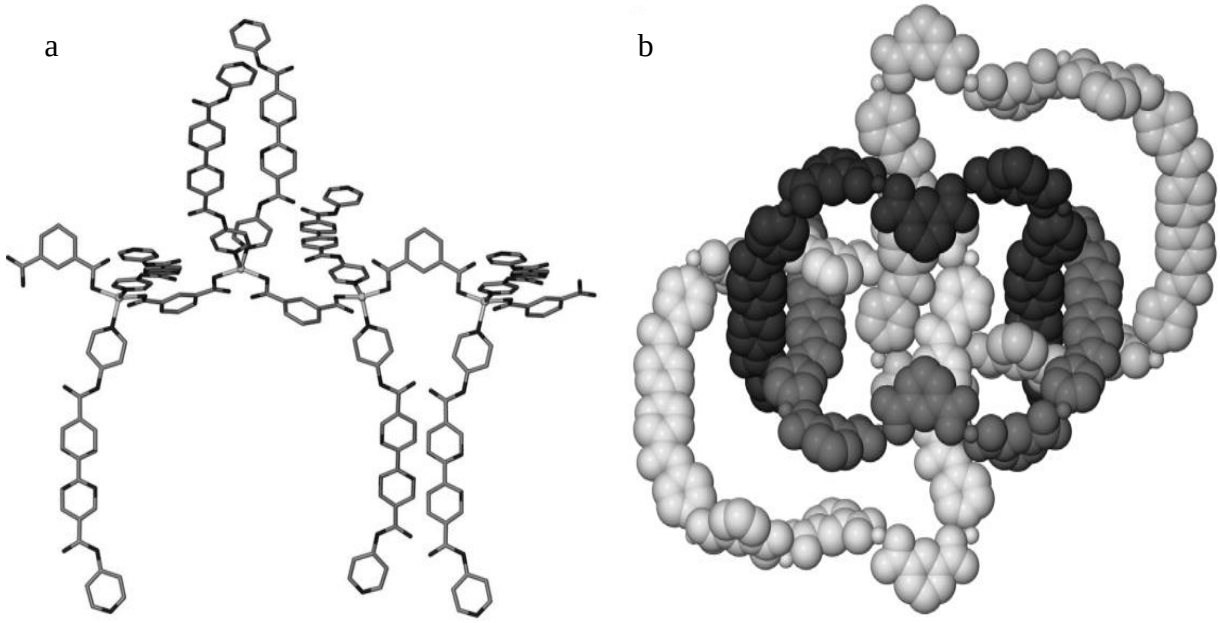

Figure 1.38: (a) Zn(II) tetrahedral coordination centres. (b) [Zn(iso)(2,2-bpbi)].2(DMF) MOF spiral chain surrounded by three other spiral chains [209]. Reproduced by permission of John Wiley and Sons.

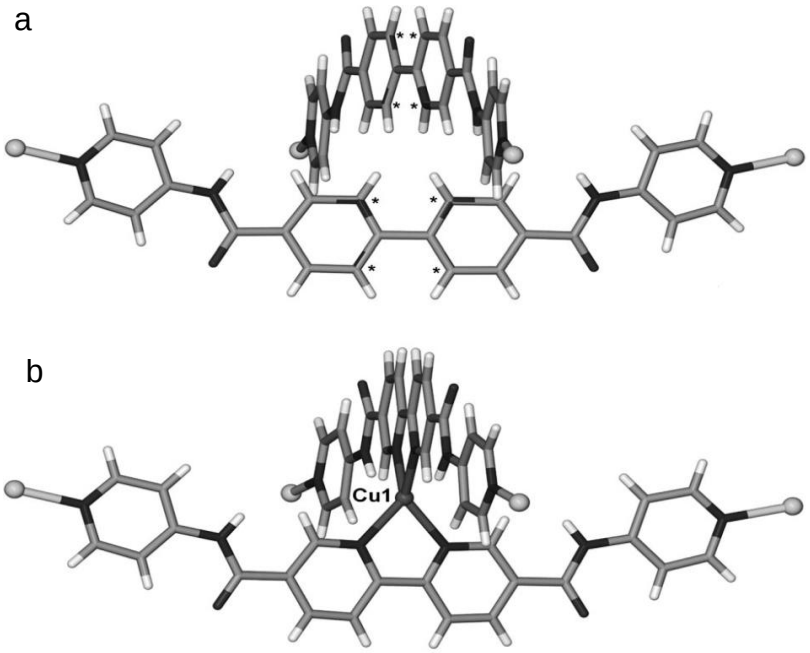

Figure 1.39: (a) [Zn(iso)(2,2-bpbi)].2(DMF) MOF crystal structures showing non-coordinating 2,2-bipy sites. (b) $[ZnCu_{1/3}(iso)(2,2\text{-}bpbi)]\cdot_{1/3}Cl\cdot[CuCl_2]_{0.3}.n(DMF)$ MOF coordination environment [209]. Reproduced by permission of John Wiley and Sons.

1.6 Conclusion

In conclusion coordination polymers and metal-organic frameworks are hybrid inorganic-organic compounds resulted from the self-assembly process of organic ligand/ligands with the metal ion or metal ion clusters by solvent or solvent-free synthesis [1-15]. CPs can be classified according to their organic linker/linkers and metal ions extending to 1D, 2D or 3D. Multi-pyridyl, carboxylate or pyridyl and carboxylate organic ligands are promising ligand systems in coordination polymers synthesis and that may due to their stability, synthesis methods and cost efficiency [114, 155, 156]. Coordination polymers have a great attention because of their high thermal stability [20-29], chemical bonding and physical interactions [50-59] and architecture systems [40-49]. These unique properties lead to a wide range of possible application in chemical catalysis [6, 16, 94-101], gas or liquid storage and separation [102-114], luminacins [124-133], spin crossover [115-123] and drug delivery [144-153]. Three-dimensional coordination polymers (MOFs) are the most interesting class of coordination polymers and that could be indicated by increasing publications number per year [17]. MOFs are interesting materials because of their synthesis methods, stability, resulted in structures, porosity and the high surface areas that they can provide for guest molecules [164].

1.7 Project aims

The project main aim is the design, synthesis, and characterisation of new flexible ligand systems based on primary amine and pyridyl compounds, for example, *p*-phenylenediamine, 2,5-dimethyl-benzene-1,4-diamine, 3-pyridinecarboxaldehyde or 4-pyridinecarboxaldehyde and their self-assembly with metal cations to produce novel homoleptic coordination polymers, metal-organic frameworks or cage systems. Furthermore, the self-assembly process of the novel bis-pyridyl ligands with rigid dicarboxylic acids, and metal ions to obtain novel heteroleptic coordination polymers and metal-organic frameworks. The new CPs or MOFs will be characterised by standard and suitable methods such as single X-ray analysis, powder X-ray analysis diffraction, IR analysis, and micro elemental-analysis. Then, utilised in gas adsorption/desorption, liquids storage or separation; spin crossover, chemical catalysis, and host chemistry.

1.8 References

1. H. D. J. Arkawazi, R. Clowes, A. I. Cooper, T. Konno, N. Kuwamura, C. M. Pask and M. J. Hardie, Complex Phase Behaviour and Structural Transformations of Metal-Organic Frameworks with Mixed Rigid and Flexible Bridging Ligands. *Chemistry A European Journal*. 2019, **25**(5), 1353-1362.
2. A. Lázaro and R. S. Forgan, Application of zirconium MOFs in drug delivery and biomedicine. *Coordination Chemistry Reviews*. 2019, **380**, 230-259.
3. M. Pander, A. Zelichowska and W. Bury, Probing mesoporous Zr-MOF as drug delivery system for carboxylate functionalized molecules. *Polyhedron*. 2018, **156**, 131-137.
4. X. Yang and Q. Xu, Bimetallic Metal-Organic Frameworks for Gas Storage and Separation. *Crystal Growth and Design*. 2017, **17**(4), 1450-1455.
5. R. E. Morris and L. Brammer, Coordination change, lability and hemilability in metal-organic frameworks. *Chemical Society Reviews*. 2017, **46**(17), 5444-5462.
6. Y. B. Huang, J. Liang, X. S. Wanga and R. Cao, Multifunctional metal-organic framework catalysts: synergistic catalysis and tandem reactions. *Chemical Society Reviews*. 2017, **46**(1), 126-157.
7. M. I. Nandasiri, S. R. Jambovanea, B. P. Mc Grail, H. T. Schaef and S. K. Nuneb, Adsorption, separation, and catalytic properties of densified metal-organic frameworks. *Coordination Chemistry Reviews*. 2016, **311**, 38-52.
8. Q. L. Zhu and Q. Xu, Metal-organic framework composites. *Chemical Society Reviews*. 2014, **43**(16), 5468-5512.
9. C. R. Murdock, B. C. Hughes, Z. Lu and D. M. Jenkins, Approaches for synthesizing breathing MOFs by exploiting dimensional rigidity. *Coordination Chemistry Reviews*. 2014, **258-259**, 119-136.
10. J. D. Rocca, D. Liu and W. Lin, Nanoscale Metal-Organic Frameworks for Biomedical Imaging and Drug Delivery. *Accounts of Chemical Research*. 2011, **44**(10), 957-968.
11. H. Furukawa, N. Ko, Y. B. Go, N. Aratani, S. B. Choi, E. Choi, A. O Yazaydin, R. Q. Snurr, M. O'Keeffe, J. Kim and O. M. Yaghi, Ultrahigh Porosity in Metal-Organic Frameworks. *Science*. 2010, **329**(5990), 424-428.
12. O. K. Farha, A. O. Yazaydın, I. Eryazici, C. D. Malliakas, B. G. Hauser, M. G. Kanatzidis, S. B. T. Nguyen, R. Q. Snurr and J. T. Hupp, De novo synthesis of a metal-organic framework material featuring ultrahigh surface area and gas storage capacities. *Nature Chemistry*. 2010, **2**, 944-948.
13. S. L. James, Metal-organic frameworks. *Chemical Society Reviews*. 2003, **32**(5), 276-288.
14. O. M. Yaghi, G. Li and H. Li, Selective binding and removal of guests in a microporous metal-organic framework. *Nature*. 1995, **378**(6558), 703-706.
15. W. L. Leong and J. J. Vittal, One-Dimensional Coordination Polymers: Complexity and Diversity in Structures, Properties, and Applications. *Chemical Reviews*. 2011, **111**(2), 688-764.
16. L. Ma, C. Abney and W. Lin, Enantioselective catalysis with homochiral metal-organic frameworks. *Chemical Society Reviews*. 2009, **38**(5), 1248-1256.
17. E. Loukopoulos and G. E. Kostakis, Review: Recent advances of one-dimensional coordination polymers as catalysts. *Journal of Coordination Chemistry*. 2018, **71**(3), 371-410.
18. A. Y. Robin and K. M. Fromm, Coordination polymer networks with O- and N-donors: What they are, why and how they are made. *Coordination Chemistry Reviews*. 2006, **250**(15), 2127-2157.

19. S. Kitagawa, R. Kitaura and S. Noro, Functional porous coordination polymers. *Angewandte Chemie International Edition*. 2004, **43**(18), 2334-2375.
20. P. Yang, L. Yang, J. Yang, X. Luo and G. Chang, Synthesis of a metal-coordinated N-substituted polybenzimidazole pyridine sulfone and method for the nondestructive analysis of thermal stability. *High Performance Polymers*. 2019, **31**(2), 238-246.
21. H. L. Wang, H. Yeh, Y. C. Chen, Y. C. Lai, C. Y. Lin, K. Y. Lu, R. M. Ho, B. H. Li, C. H. Lin and D. H. Tsai, Thermal Stability of Metal-Organic Frameworks and Encapsulation of CuO Nanocrystals for Highly Active Catalysis. *ACS Applied Materials and Interfaces*. 2018, **10**(11), 9332-9341.
22. T. A. Makal, X. Wang and H. C. Zhou, Tuning the Moisture and Thermal Stability of Metal-Organic Frameworks through Incorporation of Pendant Hydrophobic Groups. *Crystal Growth and Design*. 2013, **13**(11), 4760-4768.
23. I. J. Kang, N. A. Khan, E. Haque and S. H. Jhung, Chemical and thermal stability of isotypic metal-organic frameworks: effect of metal ions. *Chemistry A European Journal*. 2011, **17**(23), 6437-6442.
24. W. Kleist, M. Maciejewski and A. Baiker, MOF-5 based mixed-linker metal-organic frameworks: Synthesis, thermal stability and catalytic application. *Thermochimica Acta*. 2010, **499**(1), 71-78.
25. Y. Wei, Y. Yu, R. Sa, Q. Lia and K. Wu, Two cobalt(II) coordination polymers $[Co_2(H_2O)_4(Hbidc)_2]_n$ and $[Co(Hbidc)]_n$ (Hbidc= 1H-benzimidazole-5,6-dicarboxylate): syntheses, crystal structures, and magnetic properties. *Crystal Engineering Communications*. 2009, **11**(6), 1054-1060.
26. X. J. Zhang, Y. H. Xing, J. Han, X. Q. Zeng, M. F. Ge and S. Y. Niu, A Series of Novel Ln-Succinate-Oxalate Coordination Polymers: Synthesis, Structure, Thermal Stability, and Fluorescent Properties. *Crystal Growth and Design*. 2008, **8**(10), 3680-3688.
27. P. Ren, W. Shi and P. Cheng, Synthesis and Characterization of Three-Dimensional 3d−3d and 3d−4f Heterometallic Coordination Polymers with High Thermal Stability. *Crystal Growth and Design*. 2008, **8**(4), 1097-1099.
28. S. Ma, X. S. Wang, D. Yuan and H. C. Zhou, A coordinatively linked Yb metal-organic framework demonstrates high thermal stability and uncommon gas-adsorption selectivity. *Angewandte Chemie International Edition*. 2008, **47**(22), 4130-4133.
29. J. H. Cavka, S. Jakobsen, U. Olsbye, N. Guillou, C. Lamberti, S. Bordiga and K. P. Lillerud, A New Zirconium Inorganic Building Brick Forming Metal Organic Frameworks with Exceptional Stability. *Journal of the American Chemical Society*. 2008, **130**(42), 13850-13851.
30. I. Ahmed and S. H. Jhung, Applications of metal-organic frameworks in adsorption/separation processes via hydrogen bonding interactions. *Chemical Engineering Journal*. 2017, **310**, 197-215.
31. Z. J. Wang, L. Qin, J. X. Chen and H. G. Zheng, H-Bonding Interactions Induced Two Isostructural Cd(II) Metal-Organic Frameworks Showing Different Selective Detection of Nitroaromatic Explosives. *Inorganic Chemistry*. 2016, **55**(21), 10999-11005.
32. J. V. A. Requena, E. M. López, R. P. Herrera and D. D. Díaz, Metal-organic frameworks (MOFs) bring new life to hydrogen-bonding organocatalysts in confined spaces. *Crystal Engineering Communications*. 2016, **18**(22), 3985-3995.
33. S. Saha and U. Becker, The effect of the aliphatic carboxylate linkers on the electronic structures, chemical bonding and optical properties of the uranium-based metal-organic frameworks. *RSC Advances*. 2015, **5**(34), 26735-26748.

34. J. Wang, X. Jing, Y. Cao, G. Li, Q. Huoa and Y. Liu, Structural diversity and magnetic properties of three metal-organic frameworks assembled from a T-shaped linker. *Crystal Engineering Communications*. 2014, **17**(3), 604-611.
35. B. Liu, F. Yang, Y. Zou and Y. Peng, Adsorption of Phenol and *p*-Nitrophenol from Aqueous Solutions on Metal-Organic Frameworks: Effect of Hydrogen Bonding. *Journal of Chemical and Engineering Data*. 2014, **59**(5), 1476-1482.
36. W. Li, S. Henke and A. K. Cheetham, Research Update: Mechanical properties of metal-organic frameworks-Influence of structure and chemical bonding. *APL Materials*. 2014, **2**(12), 123902-123902-9.
37. P. P. Cui, Y. Zhao, G. C. Lv, Q. Liu, X. L. Zhao, Y. Lu and W. Y. Sun, Synthesis, characterization and selective hysteretic sorption property of metal-organic frameworks with 3,5-di(pyridine-4-yl)benzoate. *Crystal Engineering Communications.* 2014, **16**(28), 6300-6308.
38. Y. Hu, Z. Huang, J. Liao and G. Li, Chemical Bonding Approach for Fabrication of Hybrid Magnetic Metal-Organic Framework-5: High Efficient Adsorbents for Magnetic Enrichment of Trace Analytes. *Analytical Chemistry*. 2013, **85**(14), 6885-6893.
39. X. M. Ouyang, Z. W. Li, T. Okamura, Y. Z. Li, W. Y. Sun. W. X. Tang and N. Ueyama, Construction of metal-organic frameworks through coordination and hydrogen bonding interactions: Syntheses, structures and photoluminescent properties of metal complexes with macrocyclic ligand. *Journal of Solid State Chemistry*. 2004, **177**(1), 350-360.
40. T. Yang, L. Feng, B. Chen, L. Tang, J. Wang, Z. Ning, J. Bi, D. Gao, X. Lai and W. Li, Magnolia-like terbium-based metal-organic frameworks hierarchical architectures: Solvent-induced synthesis, microstructure and enhanced luminescent properties. *Optical Materials*. 2018, **81**, 64-70.
41. M. Wen, K. Mori, Y. Kuwahara, T. An and H. Yamashita, Design and architecture of metal organic frameworks for visible light enhanced hydrogen production. *Applied Catalysis B: Environmental*. 2017, **218**, 555-569.
42. M. Lammert, M. T. Wharmby, S. Smolders, B. Bueken, A. Lieb, K. A. Lomachenko, D. D. Vosc and N. Stock, Cerium-based metal organic frameworks with UiO-66 architecture: synthesis, properties and redox catalytic activity. *Chemical Communications*. 2015, **51**(63), 12578-12581.
43. H. Guo, T. Li, W. Chen, L. Liu, J. Qiao and J. Zhang, Self-assembly formation of hollow Ni-Fe-O nanocage architectures by metal-organic frameworks with high-performance lithium storage. *Scientific Reports*. 2015, **5**(1), 13310.
44. T. Yamada, K. Otsubo, R. Makiurac and H. Kitagawa, Designer coordination polymers: dimensional crossover architectures and proton conduction. *Chemical Society Reviews*. 2013, **42**(16), 6655-6669.
45. J. Reboul, S. Furukawa, N. Horike, M. Tsotsalas, K. Hirai, H. Uehara, M. Kondo, N. Louvain, O. Sakata and S. Kitagawa, Mesoscopic architectures of porous coordination polymers fabricated by pseudomorphic replication. *Nature Materials*. 2012, **11**(8), 717-723.
46. S. Chen, F. Wang and J. Zhang, Metal-Organic Framework Architecture with Polyhedron-in-Polyhedron and Further Polyhedral Assembly. *Crystal Engineering Communications*. 2013, **15**, 1036-1038.
47. R. Makiura, S. Motoyama, Y. Umemura, H. Yamanaka, O. Sakata and H. Kitagawa, Surface nano-architecture of a metal-organic framework. *Nature Materials*. 2010, **9**(7), 565-571.

48. J. C. Dai, X. T. Wu, Z. Y. Fu, C. P. Cui, S. M. Hu, W. X. Du, L. M. Wu, H. H. Zhang and R. Q. Sun, Synthesis, Structure, and Fluorescence of the Novel Cadmium(II)-Trimesate Coordination Polymers with Different Coordination Architectures. *Inorganic Chemistry*. 2002, **41**(6), 1391-1396.
49. R. K. Kumar, S. Balasubramanian and I. Goldberg, Supramolecular Multiporphyrin Architecture. Coordination Polymers and Open Networks in Crystals of Tetrakis(4-cyanophenyl)- and Tetrakis(4-nitrophenyl)metalloporphyrin. *Inorganic Chemistry*. 1998, **37**(3), 541-552.
50. V. A. Kawade, S. S. Bhat, S. B. Tayade and A. S. Kumbhar, A one-dimensional self-assembled porous coordination polymer poly[bis(picolinato-N,O)(*μ*-1,2-bis(4-pyridyl)ethane-*N,N'*)cobalt(II)] dimethanol. *Inorganica Chimica Acta*. 2018, **483**, 539-543.
51. C. M. Wang, M. F. Pan, Y. C. Chen, H. M. Lin, M. Y. Chung, Y. S. Wen and K. H. Lii. Two Polymorphs of an Organic-Zincophosphate Incorporating a Terephthalate Bridging Ligand in an Unusual Bonding Mode. *Inorganic Chemistry*. 2017, **56**(14), 7602-7605.
52. C. Hopa and I. Cokay, Synthesis, structural characterization and thermal properties of a new copper(II) one-dimensional coordination polymer based on bridging *N,N*'-bis(2-hydroxybenzylidene)-2,2-dimethylpropane-1,3-diamine and dicyanamide ligands. *Acta Crystallographica Section C*. 2016, **72**(2), 149-154.
53. M. S. Gargari, G. Mahmoudi, S. R. Batten, V. Stilinović, D. Butler, L. Beauvais, W. S. Kassel, W. G. Dougherty and D. V. Derveer, Control of Interpenetration in Two-Dimensional Metal-Organic Frameworks by Modification of Hydrogen Bonding Capability of the Organic Bridging Subunits. *Crystal Growth and Design*. 2015, **15**(3), 1336-1343.
54. M. S. Gargari, V. Stilinović, A. Bauzá, A. Frontera, P. M. Ardle, D. V. Derveer, S. W. Ng and G. Mahmoudi, Design of Lead(II) Metal-Organic Frameworks Based on Covalent and Tetrel Bonding. *Chemistry A European Journal*. 2015, **21**(49), 17951-17958.
55. Y. Hanifehpour, B. Mirtamizdoust, B. Khomami and S. W. Joo, Effects of Halogen Bonding in Chemical Activity of Lead(II) Electron Pair: Sonochemical Synthesis, Structural Studies, and Thermal Analysis of Novel Lead(II) Nano Coordination Polymer. *Journal of Inorganic and General Chemistry*. 2015, **641**(14), 2466-2472.
56. Y. Yang, J. Yang, P. Du, Y. Y. Liu and J. F. Ma, A series of metal-organic frameworks based on a semi-rigid bifunctional ligand 5-[(1H-1,2,4-triazol-1-yl)methoxy] isophthalic acid and flexible N-donor bridging ligands. *Crystal Engineering Communications*. 2014, **16**(28), 6380-6390.
57. G. Nandi and I. Goldberg, The effects of halogen bonding and molecular design on the self-assembly of coordination polymers of Mn(III)-tetraarylporphyrin with axial bridging ligands. *Crystal Engineering Communications*. 2014, **16**(36), 8327-8333.
58. J. Li and H. Zhou, Bridging-ligand-substitution strategy for the preparation of metal-organic polyhedra. *Nature Chemistry*. 2010, **2**(10), 893-898.
59. X. Xue, X. S. Wang, L. Z. Wang, R. G. Xiong, B. F. Abrahams, X. Z. You, Z. L. Xue and C. M. Che, Hydrothermal preparation of novel Cd(II) coordination polymers employing 5-(4-pyridyl)tetrazolate as a bridging ligand. *Inorganic Chemistry*. 2002, **41**(25), 6544-6546.
60. G. Smith and U. D. Wermuth, The coordination complex structures and hydrogen bonding in the three-dimensional alkaline earth metal salts (Mg, Ca, Sr and Ba) of (4-aminophenyl)arsonic acid. *Acta Crystallographica Section C*. 2017, **73**(1), 61-67.

61. I. Ahmed, M. Tong, J. W. Jun, C. Zhong and S. H. Jhung, Adsorption of Nitrogen-Containing Compounds from Model Fuel over Sulfonated Metal-Organic Framework: Contribution of Hydrogen-Bonding and Acid-Base Interactions in Adsorption. *The Journal of Physical Chemistry C*. 2016, **120**(1), 407-415.
62. S. S. Yu, G. J. Yuan and H. B. Duan, The low dielectric constant and relaxation dielectric behavior in hydrogen-bonding metal-organic frameworks. *RSC Advances*. 2015, **5**(56), 45213-45216.
63. M. Sadakiyo, T. Yamada, K. Honda, H. Matsui and H. Kitagawa, Control of crystalline proton-conducting pathways by water-induced transformations of hydrogen-bonding networks in a metal-organic framework. *Journal of the American Chemical Society*. 2014, **136**(21), 7701-7707.
64. Z. Hasan, M. Tong, B. K. Jung, I. Ahmed, C. Zhong and S. H. Jhung, Adsorption of Pyridine over Amino-Functionalized Metal-Organic Frameworks: Attraction via Hydrogen Bonding versus Base-Base Repulsion. *The Journal of Physical Chemistry C*. 2014, **118**(36), 21049-21056.
65. R. Custelcean, B. A. Moyer, V. S. Bryantsev and B. P. Hay, Anion Coordination in Metal-Organic Frameworks Functionalized with Urea Hydrogen-Bonding Groups. *Crystal Growth and Design*. 2006, **6**(2), 555-563.
66. S. K. Ghosh, J. Ribas and P. K. Bharadwaj, Characterization of 3-D Metal-Organic Frameworks Formed through Hydrogen Bonding Interactions of 2-D Networks with Rectangular Voids by Co^{II}- and Ni^{II}-Pyridine-2,6-dicarboxylate and 4,4‘-Bipyridine or 1,2-Di(pyridyl)ethylene. *Crystal Growth and Design*. 2005, **5**(2), 623-629.
67. Q. Huang, T. Wei, M. Zhang, L. Z. Dong, A. M. Zhang, S. L. Li, W. J. Liu, J. Liua and Y. Q. Lan, A highly stable polyoxometalate-based metal-organic framework with π-π stacking for enhancing lithium ion battery performance. *Journal of Materials Chemistry*. 2017, **5**(18), 8477-8483.
68. Y. W. Dong, R. Q. Fan, X. M. Wang, P. Wang, H. J. Zhang, L. G. Wei, Y. Song, X. Du, W. Chen and Y. L. Yang, Topological Evolution in Mercury(II) Schiff Base Complexes Tuned through Alkyl Substitution-Synthesis, Solid-State Structures, and Aggregation-Induced Emission Properties. *European Journal of Inorganic Chemistry*. 2016, **2016**(22), 3598-3610.
69. A. J. Calahorro, E. S. Sebastián, A. S. Castillo, J. M. Seco, C. M. Fierro, B. Fernándeza and A. R. Diéguez, Effect of π-π stacking interactions on the emission properties of cadmium metal-organic frameworks based on 1,4-bis(4-pyridyl)-2,3-diaza-1,3-butadiene. *Crystal Engineering Communications*. 2015, **17**(19), 3659-3666.
70. W. Wu, A. Kirillov, X. Yan, P. Zhou, W. Liu and Y. Tang, Enhanced Separation of Potassium Ions by Spontaneous K+-Induced Self-Assembly of a Novel Metal-Organic Framework and Excess Specific Cation-π Interactions. *Angewandte Chemie International Edition*. 2014, **53**(40), 10649-10653.
71. R. Saha, S. Goswami, S. Biswas, I. M. Steele, K. Dey, A. D. Jana and S. Kumara, A dynamic metal-organic supramolecular host based on weak π-stacking interactions incorporating 2D water-chloride-methanolic supramolecular sheet. *Inorganica Chimica Acta*. 2014, **423**, 123-132.
72. L. Liu, J. Hao, Y. Shi, J. Qiua and C. Hao, Roles of hydrogen bonds and π-π stacking in the optical detection of nitro-explosives with a luminescent metal-organic framework as the sensor. *RSC Advances*. 2014, **5**(4), 3045-3053.
73. X. L. Wu, X. M. Zhang, S. Y. Huang, W. N. Zhou and Z. C. Wang, A novel two-dimensional metal-organic supramolecular framework including π-π stacking and hydrogen-bond interactions. *Acta Crystallographica Section C*. 2013, **69**(7), 730-733.

74. H. Cai, Y. Guo and J. G. Li, Controllable assembly of a three-dimensional metal-organic supramolecular framework including π-π stacking interactions. *Acta Crystallographica, Section C*. 2013, **69**(1), 8-10.
75. K. H. Wang, M. C. Zhu, L. Liu, E. J. Gao, D. Y. Hou, G. Xin and T. C. Li, A novel 3D water network containing adamantane-type $(H_2O)_{24}$ water cluster trapped in metal-organic framework constructed via π…π and CH…π Interactions. *Russian Journal of Coordination Chemistry*. 2012, **38**(1), 29-35.
76. D. L. Reger, J. Horger, M. D. Smitha and Gary J. Long, Homochiral, helical metal-organic framework structures organized by strong, non-covalent π-π stacking interactions. *Chemical Communications*. 2009, **41**, 6219-6221.
77. R. Dutta and A. Kumar, Ion transport dynamics in ionic liquid incorporated CuBTC-metal-organic framework based composite polymer electrolyte. *Journal of Materials Science: Materials in Electronics*. 2019, **30**(2), 1117-1132.
78. V. Nozari, M. Zeeshan, S. Keskin and A. Uzun, Effect of methylation of ionic liquids on the gas separation performance of ionic liquid/metal-organic framework composites. *Crystal Engineering Communications*. 2018, **20**(44), 7137-7143.
79. X. L. Sun, W. H. Deng, H. Chen, H. L. Han, J. M. Taylor, C. Q. Wan and G. Xu, A Metal-Organic Framework Impregnated with a Binary Ionic Liquid for Safe Proton Conduction above 100 °C. *Chemistry A European Journal*. 2017, **23**(6), 1248-1252.
80. A. Karmakar, A. V. Desai and S. K. Ghosh, Ionic metal-organic frameworks (iMOFs): Design principles and applications. *Coordination Chemistry Reviews*. 2016, **307**, 313-341.
81. K. Fujie and H. Kitagawa, Ionic liquid transported into metal-organic frameworks. *Coordination Chemistry Reviews*. 2016, **307**, 382-390.
82. N. R. Dhumal, M. P. Singh, J. A. Anderson, J. Kiefer and H. J. Kim, Molecular Interactions of a Cu-Based Metal-Organic Framework with a Confined Imidazolium-Based Ionic Liquid: A Combined Density Functional Theory and Experimental Vibrational Spectroscopy Study. *The Journal of Physical Chemistry C*. 2016, **120**(6), 3295-3304.
83. Q. Dai, J. Ma, S. Ma, S. Wang, L. Li, X. Zhu and X. Qiao, Cationic Ionic Liquids Organic Ligands Based Metal-Organic Frameworks for Fabrication of Core-Shell Microspheres for Hydrophilic Interaction Liquid Chromatography. *ACS Applied Materials and Interfaces*. 2016, **8**(33), 21632-21639.
84. K. Fujie, K. Otsubo, R. Ikeda, T. Yamadab and H. Kitagawa, Low temperature ionic conductor: ionic liquid incorporated within a metal-organic framework. *Chemical Science*. 2015, **6**(7), 4306-3410.
85. J. S. Qin, S. R. Zhang, D. Y. Du, P. Shen, S. J. Bao, Y. Q. Lan and Z. M. Su, A Microporous Anionic Metal-Organic Framework for Sensing Luminescence of Lanthanide(III) Ions and Selective Absorption of Dyes by Ionic Exchange. *Chemistry A European Journal*. 2014, **20**(19), 5625-5630.
86. N. A. Khan, Z. Hasan and S. H. Jhung, Ionic Liquids Supported on Metal-Organic Frameworks: Remarkable Adsorbents for Adsorptive Desulfurization. *Chemistry A European Journal*. 2014, **20**(2), 376-380.
87. T. M. Tovar, I. Iordanov, D. F. S. Gallis and J. B. D. Coste, Enhancing Van der Waals Interactions of Functionalized UiO-66 with Non-polar Adsorbates: The Unique Effect of para Hydroxyl Groups. *Chemistry A European Journal*. 2018, **24**(8), 1931-1937.
88. B. Vlaisavljevich, J. Huck, Z. Hulvey, K. Lee, J. A. Mason, J. B. Neaton, J. R. Long, C. M. Brown, D. Alfèo, A. Michaelides and B. Smit, Performance of van der Waals Corrected Functionals for Guest

Adsorption in the M_2(dobdc) Metal-Organic Frameworks. *The Journal of Physical Chemistry A*. 2017, **121**(21), 4139-4151.

89. A. Varadwaj, P. R. Varadwaj and K. Yamashita, Hybrid organic-inorganic $CH_3NH_3PbI_3$ perovskite building blocks: Revealing ultra-strong hydrogen bonding and mulliken inner complexes and their implications in materials design. *Journal of Computational Chemistry*. 2017, **38**(32), 2802-2818.
90. D. Schwarz, Y. Noda, J. Klouda, K. S. Pecková, J. Tarábek, J. Rybáček, J. Janoušek, F. Simon, M. V. Opanasenko, J. Čejka, A. Acharjya, J. Schmidt, S. Selve, V. R. Scherer, N. Severin, J. P. Rabe, P. Ecorchard, J. He, M. Polozij, P. Nachtigall and M. J. Bojdys, Twinned Growth of Metal-Free, Triazine-Based Photocatalyst Films as Mixed-Dimensional (2D/3D) van der Waals Heterostructures. *Advanced Materials*. 2017, **29**(40), 1703399 (1-9).
91. S. Zuluaga, P. Canepa, K. Tan, Y. J. Chabal and T. Thonhauser, Study of van der Waals bonding and interactions in metal organic framework materials. *Journal of physics: Condensed Matter*. 2014, **26**(13), 133002.
92. S. V. Aradhya, M. Frei, M. S. Hybertsen and L. Venkataraman, Van der Waals interactions at metal/organic interfaces at the single-molecule level. *Nature Materials*. 2012, **11**(10), 872-876.
93. A. Tkatchenko, L. Romaner, O. T. Hofmann, E. Zojer, C. A. Draxl and M. Scheffler, Van der Waals Interactions Between Organic Adsorbates and at Organic/Inorganic Interfaces. *MRS Bulletin*. 2010, **35**(6), 435-442.
94. L. Zhu, X. Q. Liu, H. L. Jiang and L. B. Sun, Metal-Organic Frameworks for Heterogeneous Basic Catalysis. *Chemical Reviews*. 2017, **117**(12), 8129-8176.
95. Q. Yang, Q. Xu and H. L. Jiang, Metal-organic frameworks meet metal nanoparticles: synergistic effect for enhanced catalysis. *Chemical Society Reviews*. 2017, **46**(15), 4774-488.
96. X. Chen, Y. Peng, X. Han, Y. Liu, X. Lin and Y. Cui, Sixteen isostructural phosphonate metal-organic frameworks with controlled Lewis acidity and chemical stability for asymmetric catalysis. *Nature Communications*. 2017, **8**(1), 1-9.
97. S. Wang, J. Lin and X. Wang, Semiconductor-redox catalysis promoted by metal-organic frameworks for CO_2 reduction. *Physical Chemistry Chemical Physics*. 2014, **16**(28), 14656-14660.
98. F. Song, C. Wang and W. Lin, A chiral metal-organic framework for sequential asymmetric catalysis. *Chemical Communications*. 2011, **47**(29), 8256-8258.
99. M. Ranocchiari and J. A. V. Bokhoven, Catalysis by metal-organic frameworks: fundamentals and opportunities. *Physical Chemistry Chemical Physics*. 2011, **13**(14), 6388-6396.
100. X. Gu, Z. H. Lu, H. L. Jiang, T. Akita and Q. Xu, Synergistic catalysis of metal-organic framework-immobilized Au-Pd nanoparticles in dehydrogenation of formic acid for chemical hydrogen storage. *Journal of the American Chemical Society*. 2011, **133**(31), 11822-11825.
101. D. Dang, P. Wu, C. He, Z. Xie and C. Duan, Homochiral metal-organic frameworks for heterogeneous asymmetric catalysis. *Journal of the American Chemical Society*. 2010, **132**(41), 14321-14323.
102. H. Li, K. Wang, Y. Sun, C. T. Lollar, J. Li and H. C. Zhou, Recent advances in gas storage and separation using metal-organic frameworks. *Materials Today*. 2018, **21**(2), 108-121.
103. K. Chen, L. Zhang and W. Zhang, Preparation and evaluation of open-tubular capillary column combining a metal-organic framework and a brush-shaped polymer for liquid chromatography. *Journal of Separation Science*. 2018, **41**(11), 2347-2353.

104. M. P. Singh, N. R. Dhumal, H. J. Kim, J. Kiefer and J. A. Anderson, Removal of Confined Ionic Liquid from a Metal Organic Framework by Extraction with Molecular Solvents. *The Journal of Physical Chemistry C*. 2017, **121**(19), 10577-10586.
105. A. Singh, R. Vedarajan and N. Matsumi, Modified Metal Organic Frameworks (MOFs)/Ionic Liquid Matrices for Efficient Charge Storage. *Journal of The Electrochemical Society*. 2017, **164**(8), H5169-H5174.
106. M. S. Shah, M. Tsapatsis and J. I. Siepmann, Hydrogen Sulfide Capture: From Absorption in Polar Liquids to Oxide, Zeolite, and Metal-Organic Framework Adsorbents and Membranes. *Chemical Reviews*. 2017, **117**(14), 9755-9803.
107. J. Cho and Y. Ishida, Macroscopically Oriented Porous Materials with Periodic Ordered Structures: From Zeolites and Metal-Organic Frameworks to Liquid-Crystal-Templated Mesoporous Materials. *Advanced Materials*. 2017, **29**(25), 1605974.
108. H. Furukawa, U. Müller and O. M. Yaghi, "Heterogeneity within order" in metal-organic frameworks. *Angewandte Chemie International Edition*. 2015, **54**(11), 3417-3430.
109. H. C. J. Zhou and S. Kitagawa, Metal-Organic Frameworks (MOFs). *Chemical Society Reviews*. 2014, **43**(16), 5415-5418.
110. L. Li, S. Tang, C. Wang, X. Lv, M. Jiang, H. Wua and X. Zhao, High gas storage capacities and stepwise adsorption in a UiO type metal-organic framework incorporating Lewis basic bipyridyl sites. *Chemical Communications*. 2014, **50**(18), 2304-2307.
111. H. Furukawa, K. E. Cordova, M. O. Keeffe and O. M. Yaghi, The Chemistry and Applications of Metal-Organic Frameworks. *Science*. 2013, **341**(6149), 974-974.
112. M. Yadav and Q. Xu, Liquid-phase chemical hydrogen storage materials. *Energy and Environmental Science*. 2012, **5**(12), 9698-9725.
113. G. Férey and C. Serre, Large breathing effects in three-dimensional porous hybrid matter: facts, analyses, rules and consequences. *Chemical Society Reviews*. 2009, **38**(5), 1380-1899.
114. S. Kitagawa and R. Matsuda, Chemistry of coordination space of porous coordination polymers. *Coordination Chemistry Reviews*. 2007, **251**(21), 2490-2509.
115. X. L. Lia, G. Z. Liu, L. Y. Xin and L. Y. Wang, Binuclear and tetranuclear Mn(II) clusters in coordination polymers derived from semirigid tetracarboxylate and N-donor ligands: syntheses, new topology structures and magnetism. *Journal of Solid State Chemistry*. 2017, **246**, 252-257.
116. Y. Garcia, N. N. Adarsh and A. D. Naik, Crystal Engineering of Fe^{II} Spin Crossover Coordination Polymers Derived from Triazole or Tetrazole Ligands. *CHIMIA International Journal for Chemistry*. 2013, **67**(6), 411-418.
117. X. Zhu, X. Y. Wang, B. L. Li, J. Wang and S. Gao, Syntheses, structures and magnetic properties of five iron(II) coordination polymers with flexible bis(imidazole) and bis(triazole) ligands. *Polyhedron*. 2012, **31**(1), 77-81.
118. X. Yin, T. T. Xiao, J. Fan, S. R. Zheng, N. Wang, S. L. Cai, J. B. Tana and W. G. Zhang, Assembly of two new Mn(II) coordination polymers based on 5-aminoisophthalate: Structural diversity and properties. *Inorganic Chemistry Communications*. 2012, **22**, 93-97.
119. P. Grondin, D. Siretanu, O. Roubeau, M. F. Achard and R. Clérac, Liquid-Crystalline Zinc(II) and Iron(II) Alkyltriazoles One-Dimensional Coordination Polymers. *Inorganic Chemistry*. 2012, **51**(9), 5417-5426.

120. A. Białońska and R. Bronisz, High Spin and Spin-Crossover Two-Dimensional Coordination Polymers Containing $Fe^{II}(tetrazol\text{-}2\text{-}yl)_4(solv)_2$(solv= Ethanol, Acetonitrile) Cores Linked by Flexible/Elastic Spacers. *Inorganic Chemistry*. 2010, **49**(10), 4534-4542.
121. A. Bialoriska, R. Bronisz and M. Weselski, A New Family of Spin-Crossover Complexes Based on a $Fe^{II}(Tetrazolyl)_4(MeCN)_2$-Type Core. *Inorganic Chemistry*. 2008, **47**(11), 4436-4438.
122. G. J. Halder, C. J. Kepert, B. Moubaraki, K. S. Murray and J. D. Cashion, Guest-dependent spin crossover in a nanoporous molecular framework material. *Science*. 2002, **298**(5599), 1762-1765.
123. S. Noro, M. Kondo, T. Ishii, S. Kitagawa and H. Matsuzaka, Syntheses and crystal structures of iron coordination polymers with 4,4′-bipyridine (4,4′-bpy) and 4,4′-azopyridine (azpy). Two-dimensional networks supported by hydrogen bonding, $\{[Fe(azpy)(NCS)_2(MeOH)_2]\cdot azpy\}_n$ and $\{[Fe(4,4'\text{-}bpy)(NCS)_2(H_2O)_2]\cdot 4,4'\text{-}bpy\}_n$. *Dalton Transactions*. 1999, (**10**), 1569-1574.
124. Y. Wang, R. Huang, J. Zhang, G. Cheng and H. Yang, Lanthanide(Tb^{3+}, Eu^{3+})-functionalized a new one dimensional Zn-MOF composite as luminescent probe for highly selectively sensing Fe^{3+}. *Polyhedron*. 2018, **148**, 178-183.
125. Q. Liu and W. Liu, A new luminescent Pb(II) coordination polymer based on designed pyridinecarboxylate ligand. *Inorganic and Nano-Metal Chemistry*. 2017, **47**(5), 768-771.
126. S. S. Jin, X. Han, J. Yang, H. M. Zhang, X. L. Liu and J. F. Ma, Luminescent coordination polymers based on a new resorcin[4]arene-functionalized tetracarboxylate: Highly selective luminescent detection of metal cations, anions and small organic molecules. *Journal of Luminescence*. 2017, **188**, 346-355.
127. L. Croitor, E. B. Coropceanu, G. Duca, A. V. Siminel and M. S. Fonari, Nine Mn(II), Zn(II) and Cd(II) mixed-ligand coordination networks with rigid dicarboxylate and pyridine-n-aldoxime ligands: Impact of the second ligand in the structures' dimensionality and solvent capacity. *Polyhedron*. 2017, **129**, 9-21.
128. L. Zhu and Z. An, A New Luminescent Cd(II) Coordination Polymer Based on Mixed Ligands. *Synthesis and Reactivity in Inorganic, Metal-Organic, and Nano-Metal Chemistry*. 2016, **46**(7), 1065-1068.
129. B. Song, Q. Liu, W. Liu, Z. Cao, Y. Ren, Q. Zhou and L. Zhang, Two new luminescent Zn(II) coordination polymers with different interpenetrated motifs. *Journal of Molecular Structure*. 2015, **1099**, 49-53.
130. J. Duan, C. Zou, Q. Lia and W. Jin, New luminescent porous coordination polymers with an acylamide-decorated linker for anion recognition and reversible I_2 accommodation. *Crystal Engineering Communications*. 2015, **17**(43), 8226-8230.
131. Y. Cheng and J. Gao, Employing Trinuclear $[Zn_3(COO)_4]$ Cluster as Building Subunits to Construct a New Luminescent Coordination Polymer. *Synthesis and Reactivity in Inorganic, Metal-Organic, and Nano-Metal Chemistry*. 2015, **45**(3), 333-336.
132. Y. R. Liu, X. Zhang and G. R. Liang, Hydrogen-bond directed 2D→3D polythreading of a new luminescent Cd(II) coordination polymer. *Inorganic Chemistry Communications*. 2013, **37**, 1-3.
133. H. Y. Wang, J. Y. Cheng, J. P. Ma, Y. B. Dong and R. Q. Huang, Synthesis and characterization of new coordination polymers with tunable luminescent properties generated from bent 1,2,4-triazole-bridged *N,N'*-dioxides and Ln(III) salts. *Inorganic Chemistry*. 2010, **49**(5), 2416-2426.
134. K. Lu, T. Aung, N. Guo, R. Weichselbaum and W. Lin, Nanoscale Metal-Organic Frameworks for Therapeutic, Imaging, and Sensing Applications. *Advanced Materials*. 2018, **30**(37), 1707634.
135. H. Yoo, A. Welle, W. Guo, J. Choi and E. Redel, Electrodeposition of WO_3 nanoparticles into surface mounted metal-organic framework HKUST-1 thin films. *Nanotechnology*. 2017, **28**(11), 115605.

136. C. Prochowicz, A. Kornowicz and J. Lewiński, Interactions of Native Cyclodextrins with Metal Ions and Inorganic Nanoparticles: Fertile Landscape for Chemistry and Materials Science. *Chemical Reviews*. 2017, **117**(22), 13461-13501.
137. J. Liu and C. Wöll, Surface-supported metal-organic framework thin films: fabrication methods, applications, and challenges. *Chemical Society Reviews*. 2017, **46**(19), 5730-5770.
138. M. Zhao, Y. Wang, Q. Ma, Y. Huang, X. Zhang, J. Ping, Z. Z. Q. Lu, Y. Yu, H. Xu, Y. Zhao and H. Zhang, Ultrathin 2D Metal-Organic Framework Nanosheets. *Advanced Materials*. 2015, **27**(45), 7372-7378.
139. K. Liu, Z. R. Shen, Y. Li, S. D. Han, T. L. Hu, D. S. Zhang, X. H. Bu and W. J. Ruan, Solvent induced rapid modulation of micro/nano structures of metal carboxylates coordination polymers: mechanism and morphology dependent magnetism. *Scientific Reports*. 2014, **4**(1), 6023.
140. K. M. Choi, H. M. Jeong, J. H. Park, Y. B. Zhang, J. K. Kang and O. M. Yaghi, Supercapacitors of nanocrystalline metal-organic frameworks. *ACS Nano*. 2014, **8**(7), 7451-7457.
141. B. Yilmaz, N. Trukhan and U. Muller, Industrial Outlook on Zeolites and Metal Organic Frameworks. *Chinese Journal of Catalysis*. 2012, **33**(1), 3-10.
142. N. J. Hinks, A. C. McKinlay, B. Xiao, P. S. Wheatley and R. E. Morris, Metal organic frameworks as NO delivery materials for biological applications. *Microporous and Mesoporous Materials*. 2010, **129**(3), 330-334.
143. M. Oh and C. A. Mirkin, Ion exchange as a way of controlling the chemical compositions of nano- and microparticles made from infinite coordination polymers. *Angewandte Chemie International Edition*. 2006, **45**(33), 5492-5494.
144. Z. He, P. Zhang, Y. Xiao, J. Li, F. Yang, Y. Liu, J. R. Zhang and J. J. Zhu, Acid-degradable gadolinium-based nanoscale coordination polymer: A potential platform for targeted drug delivery and potential magnetic resonance imaging. *Nano Research*. 2018, **11**(2), 929-939.
145. J. Zhao, Y. Yang, X. Han, C. Liang, J. Liu, X. Song, Z. Ge and Z. Liu, Redox-Sensitive Nanoscale Coordination Polymers for Drug Delivery and Cancer Theranostics. *ACS Applied Materials and Interfaces*. 2017, **9**(28), 23555-23563.
146. M. X. Wu and Y. W. Yang, Metal-Organic Framework (MOF)-Based Drug/Cargo Delivery and Cancer Therapy. *Advanced Materials*. 2017, **29**(23), 1606134.
147. L. Tang, J. Shi, X. Wang, S. Zhang, H. Wu, H. Sun and Z. Jiang, Coordination polymer nanocapsules prepared using metal-organic framework templates for pH-responsive drug delivery. *Nanotechnology*. 2017, **28**(27), 275601.
148. L. Wang, W. Wang and Z. Xie, Tetraphenylethylene-based fluorescent coordination polymers for drug delivery. *Journal of Materials Chemistry B*. 2016, **4**(24), 4263-4266.
149. F. Novio, J. Lorenzo, F. Nador, K. Wnuk and D. R. Molina, Carboxyl Group (-CO_2H) Functionalized Coordination Polymer Nanoparticles as Efficient Platforms for Drug Delivery. *Chemistry A European Journal*. 2014, **20**(47), 15443-15450.
150. H. Y. Lian, M. Hu, C. H. Liu, Y. Yamauchi and K. C. W. Wu, Highly biocompatible, hollow coordination polymer nanoparticles as cisplatin carriers for efficient intracellular drug delivery. *Chemical Communications*. 2012, **48**(42), 5151-5553.
151. Z. Ma and B. Moulton, Recent advances of discrete coordination complexes and coordination polymers in drug delivery. *Coordination Chemistry Reviews*. 2011, **255**(15), 1623-1641.

152. I. Imaz, M. R. Martínez, L. G. Fernández, F. García, D. R. Molina, J. Hernando, V. Puntesa and D. Maspoch, Coordination polymer particles as potential drug delivery systems. *Chemical Communications*. 2010, **46**(26), 4737-4739.
153. W. J. Rieter, K. M. Pott, K. M. L. Taylor and W. Lin, Nanoscale Coordination Polymers for Platinum-Based Anticancer Drug Delivery. *Journal of the American Chemical Society*. 2008, **130**(35), 11584-11585.
154. H. C. Zhou, J. R. Long and O. M. Yaghi, Introduction to Metal-Organic Frameworks. *Chemical Reviews*. 2012, **112**(2), 673-674.
155. N. Li, R. Feng, J. Zhu, Z. Chang and X. H. Bu, Conformation versatility of ligands in coordination polymers: From structural diversity to properties and applications. *Coordination Chemistry Reviews*. 2018, **375**, 558-586.
156. O. Drath, R. W. Gable, B. Moubaraki, K. S. Murray, G. Poneti, L. Sorace and C. Boskovic, Valence Tautomerism in One-Dimensional Coordination Polymers. *Inorganic Chemistry*. 2016, **55**(9), 4141-4151.
157. A. J. C. Kraft, What a chemistry student should know about the history of Prussian blue. *ChemTexts*. 2018, **4**(4), 16.
158. Stuart R. Batten, Suzanne M. Neville and David R. Turner, Coordination polymers: design, analysis and application. 2009. Royal Society of Chemistry.
159. H. J. Buser, D. Schwarzenbach, W. Petter and A. Ludi, The crystal structure of Prussian Blue: $Fe_4[Fe(CN)_6]_3.xH_2O$. *Inorganic Chemistry*. 1977, **16**(11), 2704-2710.
160. A. Eftekhari, Z. Jian and X. Ji, Potassium Secondary Batteries. *ACS Applied Materials and Interfaces*. 2017, **9**(5), 4404-4419.
161. S. S. Y. Chui, S. M.F. Lo, J. P. H. Charmant, A. G. Orpen and I. D. Williams, A Chemically Functionalizable Nanoporous Material $[Cu_3(TMA)_2(H_2O)_3]_n$. *Science*. 1999, **283**(5405), 1148-1150.
162. F. Millange, C. Serre and G. Férey, Synthesis, structure determination and properties of MIL-53as and MIL-53ht: the first Cr^{III} hybrid inorganic-organic microporous solids: $Cr^{III}(OH)\cdot\{O_2C\text{-}C_6H_4\text{-}CO_2\}\cdot\{HO_2C\text{-}C_6H_4\text{-}CO_2H\}_x$. *Chemical Communications*. 2002, (**8**), 822-823.
163. M. Eddaoudi, J. Kim, M. O'Keeffe and O. M. Yaghi, $Cu_2[o\text{-}Br\text{-}C_6H_3(CO_2)_2]_2(H_2O)_2\cdot(DMF)_8(H_2O)_2$: A Framework Deliberately Designed To Have the NbO Structure Type. *Journal of the American Chemical Society*. 2002, **124**(3), 376-377.
164. O. K. Farha, I. Eryazici, N. C. Jeong, B. G. Hauser, C. E. Wilmer, A. A. Sarjeant, R. Q. Snurr, S. B. T. Nguyen, A. O. Yazaydin and J. T. Hupp, Metal-organic framework materials with ultrahigh surface areas: is the sky the limit?. *Journal of the American Chemical Society*. 2012, **134**(36), 15016-15021.
165. S. Singha, A. Saha, S. Goswami, S. K. Dey, S. Payra, S. Banerjee, S. Kumar and R. Saha, A Metal-Organic Framework to CuO Nanospheres of Uniform Morphology for the Synthesis of α-Aminonitriles under Solvent-Free Condition along with Crystal Structure of the Framework. *Crystal Growth and Design*. 2018, **18**(1), 189-199.
166. B. Notash and B. R. Kheirkhah, The effect of solvent on one-dimensional cadmium coordination polymers. *New Journal of Chemistry*. 2018, **42**(18), 15014-15021.
167. Z. H. Li, L. P. Xue, S. B. Miao and B. T. Zhao, Assembly of 4-, 6- and 8-connected Cd(II) pseudo-polymorphic coordination polymers: Synthesis, solvent-dependent structural variation and properties. *Journal of Solid State Chemistry*. 2016, **240**, 9-15.

168. X. M. Wang, R. Q. Fan, P. Wang, L. S. Qiang, Y. L. Yang and Y. L. Wang, Auxiliary ligand-assisted two novel one-dimensional indium coordination polymers: Synthesis, crystal structures and photoluminescence characterization effected by solvent and temperature. *Inorganic Chemistry Communications*. 2015, **51**, 29-35.
169. A. Zurawski, J. C. Rybak, L. V. Meyer, P. R. Matthes, V. Stepanenko, N. Dannenbauer, F. Würthnerb and K. M. Buschbaum, Alkaline earth imidazolate coordination polymers by solvent free melt synthesis as potential host lattices for rare earth photoluminescence: $^{x}_{\infty}[AE(Im)_2(ImH)_{2\text{-}3}]$, Mg, Ca, Sr, Ba, *x* = 1-2. *Dalton Transactions*. 2012, **41**(14), 4067-4078.
170. A. L. Garay, A. Pichon and S. L. James, Solvent-free synthesis of metal complexes. *Chemical Society Reviews*. 2007, **36**(6), 846-855.
171. I. S. Lee, D. M. Shin and Y. K. Chung, Novel supramolecular isomerism in coordination polymer synthesis from unsymmetrical bridging ligands: solvent influence on the ligand placement orientation and final network structure. *Chemistry A European Journal*. 2004, **10**(13), 3158-3165.
172. M. A. Withersby, A. J. Blake, N. R. Champness, P. A. Cooke, P. Hubberstey, W. S. Li and M. Schroder, Solvent Control in the Synthesis of 3,6-Bis(pyridin-3-yl)-1,2,4,5-tetrazine-Bridged Cadmium(II) and Zinc(II) Coordination Polymers. *Inorganic Chemistry*. 1999, **38**(10), 2259-2266.
173. G. Férey, Hybrid porous solids: past, present, future. *Chemical Society Reviews*. 2008, **37**(1), 191-214.
174. J. Kim, D. O. Kim, D. W. Kim and K. Sagong, Synthesis of MOF having functional side group. *Inorganica Chimica Acta*. 2011, **370**(1), 76-81.
175. S. T. Meek, J. A. Greathouse and M. D. Allendorf, Metal-organic frameworks: a rapidly growing class of versatile nanoporous materials. *Advanced Materials*. 2011, **23**(2), 249-267.
176. H. F. Clausen, R. D. Poulsen, A. D. Bond, M. A. S. Chevallier and B. B. Iversen, Solvothermal synthesis of new metal organic framework structures in the zinc-terephthalic acid-dimethyl formamide system. *Journal of Solid State Chemistry*. 2005, **178**(11), 3342-3351.
177. L. Wang, L. Zhang, T. Song, C. Li, J. Xu and Li Wang, Solvothermal syntheses, structures and properties of two new In-MOFs based on rigid 1,4-naphthalenedicarboxylate ligand. *Microporous and Mesoporous Materials*. 2012, **155**, 281-286.
178. M. Lanchas, S. Arcediano, A. T. Aguayo, G. Beobide, O. Castillo, J. Cepeda, D. V. Sánchez and A. Luque, Two appealing alternatives for MOFs synthesis: solvent-free oven heating vs. microwave heating. *RSC Advances*. 2014, **4**(104), 60409-60412.
179. H. K. Liu, T. H. Tsao, Y. T. Zhang and C. H. Lin, Microwave synthesis and single-crystal-to-single-crystal transformation of magnesium coordination polymers exhibiting selective gas adsorption and luminescence properties. *Crystal Engineering Communications*. 2009, **11**(7), 1462-1468.
180. S. Diring, S. Furukawa, Y. Takashima, T. Tsuruoka and S. Kitagawa, Controlled Multiscale Synthesis of Porous Coordination Polymer in Nano/Micro Regimes. *Chemistry of Materials*. 2010, **22**(16), 4531-4538.
181. A. C. Kathalikkattil, D. W. Kim, J. Tharun, H. G. Soek, R. Roshana and D. W. Park, Aqueous-microwave synthesized carboxyl functional molecular ribbon coordination framework catalyst for the synthesis of cyclic carbonates from epoxides and CO_2. *Green Chemistry*. 2014, **16**(3), 1607-1616.
182. Z. Ni and R. I. Masel, Rapid production of metal-organic frameworks via microwave-assisted solvothermal synthesis. *Journal of the American Chemical Society*. 2006, **128**(38), 12394-12395.

183. Y. Yoo and H. K. Jeong, Rapid fabrication of metal organic framework thin films using microwave-induced thermal deposition. *Chemical Communications*. 2008, (**21**), 2441-2443.
184. A. T. Yeh, W. C. Lin, S. H. Lo, C. C. Kao, C. H. Lin and C. C. Yang, Microwave synthesis and gas sorption of calcium and strontium metal-organic frameworks with high thermal stability. *Crystal Engineering Communications*. 2012, **14**(4), 1219-1222.
185. P. A. Ochoa, G. Givaja, P. J. S. Miguel, O. Castillo and F. Zamora, Microwave assisted hydrothermal synthesis of a novel Cu^{I}-sulfate-pyrazine MOF. *Inorganic Chemistry Communications*. 2007, **10**(8), 921-924.
186. S. L. James, C. J. Adams, C. Bolm, D. Braga, P. Collier, T. Friščić, F. Grepioni, K. D. M. Harris, G. Hyett, W. Jones, A. Krebs, J. Mack, L. Maini, A. G. Orpen, I. P. Parkin, W. C. Shearouse, J. W. Steed and D. C. Waddell, Mechanochemistry: opportunities for new and cleaner synthesis. *Chemical Society Reviews*. 2011, **41**(1), 413-447.
187. V. Cabras, M. Pilloni, A. Scano, R. Lai, M. C. Aragoni, S. J. Coles and G. Ennas, Mechanochemical Reactivity of Square-Planar Nickel Complexes and Pyridyl-Based Spacers for the Solid-State Preparation of Coordination Polymers: The Case of Nickel Diethyldithiophosphate and 4,4'-Bipyridine. *European Journal of Inorganic Chemistry*. 2017, **2017**(13), 1908-1914.
188. M. Y. Masoomi, S. Beheshti and A. Morsali, Mechanosynthesis of new azine-functionalized Zn(II) metal-organic frameworks for improved catalytic performance. *Journal of Materials Chemistry A*. 2014, **2**(40), 16863-16866.
189. A. Pichon, A. L. Garay and S. L. James, Solvent-free synthesis of a microporous metal-organic framework. *Crystal Engineering Communications*. 2006, **8**(3), 211-214.
190. W. Yuan, A. L. Garay, A. Pichon, R. Clowes, C. D. Wood, A. I. Cooper and S. L. James, Study of the mechanochemical formation and resulting properties of an archetypal MOF: $Cu_3(BTC)_2$ (BTC= 1,3,5-benzenetricarboxylate). *Crystal Engineering Communications*. 2010, **12**(12), 4063-4065.
191. M. Y. Masoomi, A. Morsali and P. C. Junk, Rapid mechanochemical synthesis of two new Cd(II)-based metal-organic frameworks with high removal efficiency of Congo red. *Crystal Engineering Communications*. 2015, **17**(3), 686-692.
192. A. Wang, L. H. Xie, X. Wang, X. M. Liu, J. Li and J. R. Li, Applications of metal-organic frameworks for green energy and environment: New advances in adsorptive gas separation, storage and removal. *Green Energy and Environment*. 2018, **3**(3), 191-228.
193. A. A. U. Czaja, N. Trukhan and U. Muller, Industrial applications of metal-organic frameworks. *Chemical Society Reviews*. 2009, **38**(5), 1284-1293.
194. U. Mueller, M. Schubert, F. Teich, H. Puetter, K. S. Arndta and J. Pastréa, Metal-organic frameworks-prospective industrial applications. *Journal of Materials Chemistry*. 2006, **16**(7), 626-636.
195. D. B. Leznoff and J. Lefebvre, Coordination polymers with cyanoaurate building blocks: Potential new industrial applications for gold. *Gold Bulletin*. 2005, **38**(2), 47-54.
196. S. M. Sheta, S. M. El-Sheikh and M. M. Abd-Elzaher, Simple synthesis of novel copper metal-organic framework nanoparticles: biosensing and biological applications. *Dalton Transactions*. 2018, **47**(14), 4847-4855.
197. H. Tan, L. Zhang, C. Ma, Y. Song, F. Xu, S. Chen and L. Wang, Terbium-based coordination polymer nanoparticles for detection of ciprofloxacin in tablets and biological fluids. *ACS Applied Materials and Interfaces*. 2013, **5**(22), 11791-11796.

198. J. H. Jung, J. H. Lee, J. R. Silverman and G. John, Coordination polymer gels with important environmental and biological applications. *Chemical Society Reviews*. 2013, **42**(3), 924-936.
199. R. K. Ameta, R. R. Koshti, A. Vyas, C. Rane, N. K. Sharma and M. Singh, $[Fe(CN)_6]^{4-}$/$[Fe(CN)_6]^{3-}$ based metal organic ionic frameworks and impact of Fe^{2+}/Fe^{3+} on material-medicinal-properties. *Journal of Molecular Liquids.* 2018, **268**, 677-684.
200. H. Oh, T. Li and J. An, Drug Release Properties of a Series of Adenine-Based Metal-Organic Frameworks. *Chemistry A European Journal*. 2015, **21**(47), 17010-17015.
201. S. M. Cohen, New approaches for medicinal applications of bioinorganic chemistry. *Current Opinion in Chemical Biology*. 2007, **11**(2), 115-120.
202. X. Françesc, L. Xamena, A. Abad, A. Corma and H. Garcia, MOFs as catalysts: Activity, reusability and shape-selectivity of a Pd-containing MOF. *Journal of Catalysis*. 2007, **250**(2), 294-298.
203. Q. Yuan, D. Zhang, L. V. Haandel, F. Ye, T. Xue, E. J. M. Hensen and Y. Guan, Selective liquid phase hydrogenation of furfural to furfuryl alcohol by Ru/Zr-MOFs. *Journal of Molecular Catalysis A: Chemical*. 2015, **406**, 58-64.
204. L. J. Zhang, C. Y. Han, Q. Q. Dang, Y. H. Wang and X. M. Zhang, Solvent-free heterogeneous catalysis for cyanosilylation in a modified sodalite-type Cu(II)-MOF. *RSC Advances*. 2015, **5**(31), 24293-24298.
205. Z. Chen, K. Adil, L. J. Weseliński, Y. Belmabkhout and M. Eddaoudi, A supermolecular building layer approach for gas separation and storage applications: the eea and rtl MOF platforms for CO_2 capture and hydrocarbon separation. *Journal of Materials Chemistry A*. 2015, **3**(12), 6276-6281.
206. A. R. Millward and O. M. Yaghi, Metal-organic frameworks with exceptionally high capacity for storage of carbon dioxide at room temperature. *Journal of the American Chemical Society*. 2005, **127**(51), 17998-17999.
207. Y. Ren, G. H. Chia and Z. Gao, Metal-organic frameworks in fuel cell technologies. *Nano Today*. 2013, **8**(6), 577-597.
208. T. Jacobs and M. J. Hardie, Construction of metal-organic frameworks: versatile behaviour of a ligand containing mono and bidentate coordination sites. *Chemistry A European Journal*. 2012, **18**(1), 267-276.
209. T. Jacobs, R. Clowes, A. I. Cooper and M. J. Hardie, A Chiral, Self-Catenating and Porous Metal-Organic Framework and its Post-Synthetic Metal Uptake. *Angewandte Chemie International Edition*. 2012, **51**(21), 5192-5195.

N,N′-Bis-pyridin-3-ylmethyl-benzene-1,4-diamine (L1) coordination polymers and metal-organic frameworks

2.1 Introduction

Coordination polymers (CPs) have a great attention and play an important role in the development of coordination chemistry applications fields, for example, chemical catalysis [1-8], host chemistry [9-14] and gas absorption-desorption materials [15-22]. CPs important role might due to the high stability [23-29], synthesis methods [30-35] or resulted in architectures [30, 36-40]. Ligands based on 3-pyridyl, homocyclic or heterocyclic substituted compounds are common in coordination polymers and widely investigated over the past years [41-50]. 3-Pyridyl organic ligands are common because of the strong chelating properties, cost-efficiency, resulted in structures and possible applications [41-50]. 3-Pyridyl organic ligands may be utilised in different CPs applications fields, such as nanochemistry [35, 51-54], photoluminescence [55-57], computational chemistry and electrochemical studies [55-61].

The present chapter reports the synthesis and characterisation of the new ligand *N,N′*-bis-pyridin-3-ylmethyl-benzene-1,4-diamine (L1) and its reaction with $MnCl_2.4H_2O$, $FeCl_3.6H_2O$, $CoCl_2.6H_2O$, $CuCl_2.2H_2O$, $Zn(NO_3)_2.6H_2O$, $Cd(NO_3)_2.4H_2O$, isophthalic acid (H_2-isoph) or benzene-1,4-dicarboxylic acid (H_2-bdc) to produce a series of new coordination polymers and metal-organic frameworks. Self-assembly of L1 with Mn(II), Fe(III), Co(II), Cu(II), Zn(II) or Cd(II) metal salts in methanol or in a mixture of methanol and dichloromethane at room temperature produced $([Mn_{0.5}(L1)Cl].MeOH)_n$ (**1**), $([Fe_{0.5}(L1)Cl].MeOH)_n$ (**2**), $([Co_{0.5}(L1)Cl].MeOH)_n$ (**3**) and $([Cu(L1)Cl]\cdot CH_2Cl_2)_n$ (**4**) one-dimensional polymers; $([Zn(L1)(H_2O)_2].NO_3)_n$ (**5**) and $([Cd(L1)_2(NO_3)_2])_n$ (**6**) two-dimensional polymers. On the other hand, solvothermal reaction of L1 ligand, Cd(II) nitrate, isophthalic acid or benzene-1,4-dicarboxylic acid in *N,N*-dimethylformamide (DMF) at 115 °C produced $([Cd(L1)_{0.5}(isoph)(DMF)])_n$ (**7**) or $([Cd_{1.5}(L1)_{0.5}(bdc)_{1.5}(DMF)])_n$ (**8**) MOFs.

L1 shows bent L-shape for compounds **1-4**, bent U-shape for compound **5** and bent S-shape for compounds **6-8**. Compounds **1-4** are homoleptic CPs with one-dimensional open channels occupied by methanol guest molecules (compounds **1-3)** or dichloromethane (compound **4**). Compounds **5** and **6** are homoleptic two-dimensional CPs and display M-shape or rhombic cavities that occupied by nitrate molecules for compound **5** and Cd(II) coordination centres for compound **6**. Compounds **7** and **8** are heteroleptic three-dimensional coordination polymers with no open channels along the three axes because of L1 ligand bent S-shape and $isoph^{2-}$ or bdc^{2-} coordination angles.

2.2 Experimental

2.2.1 Materials and instrumentation

All chemicals were supplied by Sigma-Aldrich, Aldrich, VWR Chemicals, Acros Organics, Euriso-Top, Fisher Scientific and Thomas Baker companies and used without further purification. Elemental microanalyses were performed at the micro-analysis laboratory at the University of Leeds or at London Metropolitan University. FTIR spectra were recorded as solid-state samples on Perkin-Elmer FTIR spectrometer. Mass spectra were recorded by using UltiMate 3000 spectrometer. ^{1}H NMR and ^{13}C{^{1}H} NMR spectra were acquired in DMSO-d_6 solution using a Bruker DPX 300 MHz spectrometer or a Bruker Ascend^{TM} 400 MHz spectrometer. Single crystal X-ray structures were obtained from an Agilent SuperNova single crystal X-ray diffractometer at 120 K. Powder X-ray patterns were obtained from a D2-Phaser Burker powder X-ray diffractometer.

2.2.2 Synthesis of *N,N′*-bis-pyridin-3-ylmethylene-benzene-1,4-diamine (^{a}L)

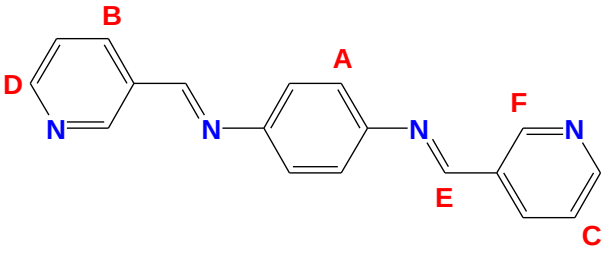

3-Pyridinecarboxaldehyde (1.96 g, 18.4 mmol) was dissolved in ethanol (50 ml) and added dropwise to *p*-phenylenediamine (1 g, 9.2 mmol) in ethanol (50 ml) and heated at reflux for 5 hours at 70 °C. The solvent was evaporated under vacuum to result in a yellow solid product. The product was washed with acetone and dried under vacuum to form 2.4 g, 91 % yield of the prepared ligand ^{a}L, mp= 172 °C. ^{1}H NMR (400 MHz, DMSO-d_6) δ(ppm): 9.09 (dd, 2H, F, *J*= 2.2, 0.9 Hz); 8.80 (s, 2H, E); 8.72 (dd, 2H, D, *J*= 4.8, 1.7 Hz); 8.34 (dt, 2H, C, *J*= 7.9, 2.0 Hz); 7.57 (dd, 2H, B, *J*= 7.9, 4.8 Hz) and 7.43 (s, 4H, A); ^{13}C{^{1}H} NMR (101 MHz, DMSO-d_6) δ(ppm): 158.59, 152.41, 150.91, 149.74, 135.43, 132.07, 124.55 and 122.67; ESI-MS: *m/z* 287 {M+H}$^{+}$. IR (solid state): $\bar{\nu}$ (cm^{-1}) 3023, 2884, 1617 and 1567. Microanalysis found: C, 74.90; H, 5.10; N, 19.60 %, calculated for $C_{18}H_{14}N_4$: C, 75.50; H, 4.93; N, 19.57 %.

2.2.3 Synthesis of *N,N′*-bis-pyridin-3-ylmethyl-benzene-1,4-diamine (L1)

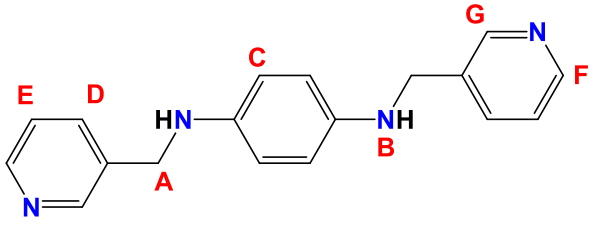

Sodium borohydride (2 g, 54 mmol) was added gradually to a pale yellow methanolic solution (250 ml) containing ^{a}L ligand (2.5 g, 8.7 mmol) at room temperature and left stirring overnight. The solvent was evaporated under vacuum, and the resulted powder was dissolved in deionized water (300 ml)

with the addition of aqueous 1M HCl solution. Then, the reaction pH was increased to pH 12 by aqueous 2M sodium hydroxide solution. Subsequently, the ligand was precipitated from the basic solution, filtered, washed by water 4×100 ml, and dried under vacuum to result in 2.2 g, 87 % yield of L1, mp= 183 ºC. ^{1}H NMR (300 MHz, DMSO-d_6) δ(ppm): 8.55 (dd, 2H, G, *J*= 2.2, 0.9 Hz); 8.41 (dd, 2H, F, *J*= 4.8, 1.7 Hz); 7.71 (dt, 2H, E, *J*= 7.8, 2.0 Hz); 7.31 (ddd, 2H, D, *J*= 7.8, 4.8, 0.8 Hz); 6.43 (s, 4H, C); 5.46 (t, 2H, B, *J*= 6.2 Hz) and 4.16 (d, 4H, A, *J*= 5.9 Hz); ^{13}C{^{1}H} NMR (75 MHz, DMSO-d_6) δ(ppm): 148.90, 147.73, 139.84, 136.12, 135.01, 123.28, 113.94 and 45.15 ; ESI-MS: *m/z* 291 {M+H}$^{+}$. IR (solid state): $\bar{\nu}$ (cm^{-1}) 3235, 3022, 2883, 1633 and 1510. Microanalysis found: C, 69.30; H, 6.40; N, 18.30 %, calculated for $C_{18}H_{18}N_4.H_2O$: C, 70.11; H, 6.54; N, 18.17 %.

2.2.4 Synthesis of $([M_{0.5}(L1)Cl].MeOH)_n$ one-dimensional polymers (1-3)

A solution of L1 (30 mg, 0.1 mmol) in methanol (4 ml) was added dropwise to $MnCl_2.4H_2O$, $FeCl_3.6H_2O$ or $CoCl_2.6H_2O$ (19 mg, 27 mg or 23 mg, 0.1 mmol) solutions in methanol (3 ml). The reaction vials were heated for a few seconds, sealed and left standing to give 41, 38 or 34 mg of $([Mn_{0.5}(L1)Cl].MeOH)_n$ (**1**), $([Fe_{0.5}(L1)Cl].MeOH)_n$ (**2**) or $([Co_{0.5}(L1)Cl].MeOH)_n$ (**3**) yellow or yellow reddish crystals after a few days. IR (solid state) for compound **1**: $\bar{\nu}$ (cm^{-1}) 3322, 3050, 2820, 1599, 1517 and 519. IR (solid state) for compound **2**: $\bar{\nu}$ (cm^{-1}) 3330, 3017, 2820, 1598, 1516 and 511. IR (solid state) for compound **3**: $\bar{\nu}$ (cm^{-1}) 3347, 3025, 2814, 1600, 1514 and 510. Microanalysis found: C, 60.32; H, 4.87; N, 15.68 %, calculated for $([Mn(L1)_2Cl_2].MeOH)_n$: C, 60.17; H, 5.46; N, 15.17 %. Found: C, 58.51; H, 5.40; N, 15.37 %, calculated for $([Fe(L1)_2Cl_2].2H_2O)_n$: C, 58.16; H, 5.42; N, 15.07 %. Found: C, 59.98; H, 5.31; N, 15.55 %, calculated for $([Co(L1)_2Cl_2].MeOH)_n$: C, 59.84; H, 5.43; N, 15.09 %.

2.2.5 Synthesis of $([Cu(L1)Cl].CH_2Cl_2)_n$ one-dimensional polymer (4)

A pale yellow solution of the ligand (L1) (30 mg, 0.1 mmol) in dichloromethane (DCM) (5 ml) was added dropwise to a vial containing $CuCl_2.2H_2O$ (17 mg, 0.1 mmol) solution in methanol (4 ml). The reaction vial was heated for a few seconds, sealed and left to stand at room temperature to result in $([Cu(L1)Cl].CH_2Cl_2)_n$ yellow reddish crystals (32 mg) after five weeks. IR (solid state): $\bar{\nu}$ (cm^{-1}) 3322, 3052, 1602, 1515 and 511. Microanalysis found: C, 44.26; H, 3.21; N, 11.13 %, calculated for $([Cu(L1)Cl_2].CH_2Cl_2)_n$: C, 44.77; H, 3.95; N, 10.99 %.

2.2.6 Synthesis of $([Zn(L1)(H_2O)_2].NO_3)_n$ two-dimensional polymer (5)

A solution of the ligand (L1) (30 mg, 0.1 mmol) in methanol (4 ml) was added dropwise to a vial containing $Zn(NO_3)_2.6H_2O$ (29 mg, 0.1 mmol) in methanol (3 ml). Then, the reaction vial was heated for a few seconds, sealed and left to stand at room temperature to result in $([Zn(L1)(H_2O)_2].NO_3)_n$ pale yellow crystals (33 mg) after six weeks. IR (solid state): $\bar{\nu}$ (cm^{-1}) 3400-3000, 3397, 3354, 3050, 1604, 1515, 645 and 521. Microanalysis found: C, 53.61; H, 5.22; N, 17.25 %, calculated for $([Zn(L1)_2(H_2O)_2].2NO_3)_n$: C, 53.64; H, 5.00; N, 17.38 %.

2.2.7 Synthesis of $([Cd(L1)_2(NO_3)_2])_n$ two-dimensional polymer (6)

A solution of the ligand (L1) (30 mg, 0.1 mmol) in methanol (4 ml) was added dropwise to a vial containing $Cd(NO_3)_2.4H_2O$ (30 mg, 0.1 mmol) in methanol (3 ml). Then, the reaction vial was heated for a few seconds, sealed and left stand at room temperature to result in $([Cd(L1)_2(NO_3)_2])_n$ pale yellow crystals (35 mg) after one week. IR (solid state): $\bar{\nu}$ (cm^{-1}) 3295, 3009, 2915, 1602, 1584, 527 and 420. Microanalysis found: C, 51.69; H, 4.63; N, 16.50 %, calculated for $([Cd(L1)_2(NO_3)_2].H_2O)_n$: C, 51.77; H, 4.59; N, 16.77 %.

2.2.8 Synthesis of $([Cd(L1)_{0.5}(isoph)(DMF)])_n$ MOF (7)

A pale yellow solution of the ligand (L1) (29 mg, 0.1 mmol) and isophthalic acid (H_2-isoph) (16 mg, 0.1 mmol) in *N*,*N*-dimethylformamide (DMF) (4 ml) was added dropwise to a vial containing $Cd(NO_3)_2.4H_2O$ (30 mg, 0.1 mmol) colourless solution in DMF (3 ml). Then, the reaction vial was sealed and placed in a thermal block and left for solvothermal reaction at 115 °C to result in $([Cd(L1)_{0.5}(isoph)(DMF)])_n$ (45 mg) pale yellow crystals after 24 hours. IR (solid state): $\bar{\nu}$ (cm^{-1}) 3365, 3068, 2932, 1643, 1598, 1556, 1368, 518 and 437. Microanalysis found: C, 48.02; H, 4.19; N, 8.98 %, calculated for $([Cd_2(L1)(isoph)_2(DMF)_2])_n$: C, 48.55; H, 4.07; N, 8.49 %.

2.2.9 Synthesis of $([Cd_{1.5}(L1)_{0.5}(bdc)_{1.5}(DMF)])_n$ MOF (8)

A solution of the ligand (L1) (29 mg, 0.1 mmol) and benzene-1,4-dicarboxylic acid (H_2-bdc) (16 mg, 0.1 mmol) in DMF (4 ml) was added dropwise to a vial containing a colorless solution of $Cd(NO_3)_2.4H_2O$ (30 mg, 0.1 mmol) in DMF (3 ml). Then, the reaction vial was sealed and placed in the thermal block and left for solvothermal reaction at 115 °C to result in $([Cd_{1.5}(L1)_{0.5}(bdc)_{1.5}(DMF)])_n$ (48 mg) pale yellow crystals after 24 hours. IR (solid state): $\bar{\nu}$ (cm^{-1}) 3401, 3048, 2927, 1648, 1551, 1510, 1366, 522 and 413. Microanalysis found: C, 43.82; H, 3.97; N, 6.50 %, calculated for $([Cd_{1.5}(L1)_{0.5}(bdc)_{1.5}(DMF)].H_2O)_n$: C, 44.23; H, 3.68; N, 6.45 %.

2.3 Crystallography experimental

Crystals were mounted under inert oil on a MiTeGen tip and flash frozen to 120(1) K using an OxfordCryosystems low temperature device. X-ray diffraction data were collected using Cu-*Ka* (λ= 1.54184 Å) radiation using an Agilent Supernova dual-source diffractometer with Atlas S2 CCD detector and fine-focus sealed tube generator. Structures were solved by charge flipping methods using SUPERFLIP or by direct methods using SHELXS, and refined by olex2.refine, ShelXL or by full-matrix least-squares on F^2 using SHELXL. All non-hydrogen atoms were refined as anisotropic, and hydrogen positions were included at geometrically estimated positions. Summary of data collections and refinements are given in tables 2.15, 2.16 and 2.17. Further details of refinements are given below [62-66].

2.4 Results and discussion

2.4.1 Synthesis of *N,N'*-bis-pyridin-3-ylmethylene-benzene-1,4-diamine (^{a}L)

^{a}L ligand was reported for the first time in 1981 by Grasso and co-workers [61] and then by Aragoni et al. [67-71]. The ligand was synthesised *via* its imine according to scheme 2.1. The FTIR spectrum of the free ligand displayed differences in comparison with starting materials spectrums. The most important to note is bands disappearing at 1720 cm^{-1}, 3409 cm^{-1} and 3371 cm^{-1} that are due to aldehyde or amine groups of 3-pyridinecarboxaldehyde and *p*-phenylenediamine starting materials respectively [72-73]. Furthermore, appearance of new band at 1567 cm^{-1} [72-74], which is due to the imine group formation in comparison with starting materials spectra. These changes provide strong evidence of Schiff base formation [75-77]. The ^{1}H NMR spectrum of the prepared ligand shows disappearance of the aldehyde peak at δ 10.11 ppm and the amine peak at δ 4.18 ppm for 3-pyridinecarboxaldehyde and *p*-phenylenediamine starting materials. Moreover, the free ligand ^{1}H NMR spectrum shows a new singlet peak at δ 8.80 ppm at typical chemical shift for azomethine group (figure 2.1) [74, 78-80]. ^{13}C{^{1}H} NMR spectrum for ^{a}L ligand shows disappearance of the aldehyde group peak at δ 192 ppm and appearance of the imine peak at δ 158.59 ppm (figure 2.2) [72-74, 81].

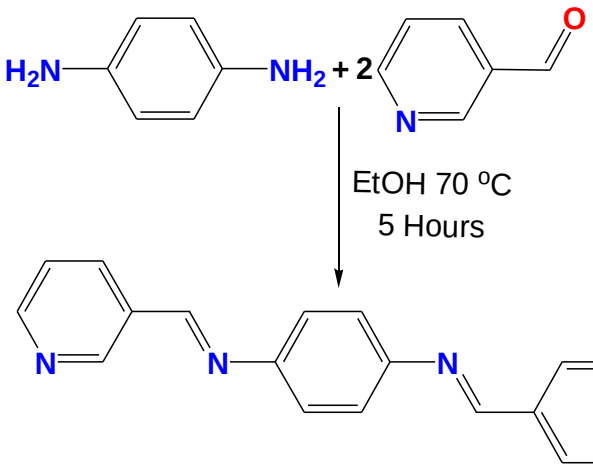

Scheme 2.1: Synthesis of *N*,*N'*-bis-pyridin-3-ylmethylene-benzene-1,4-diamine ([a]L).

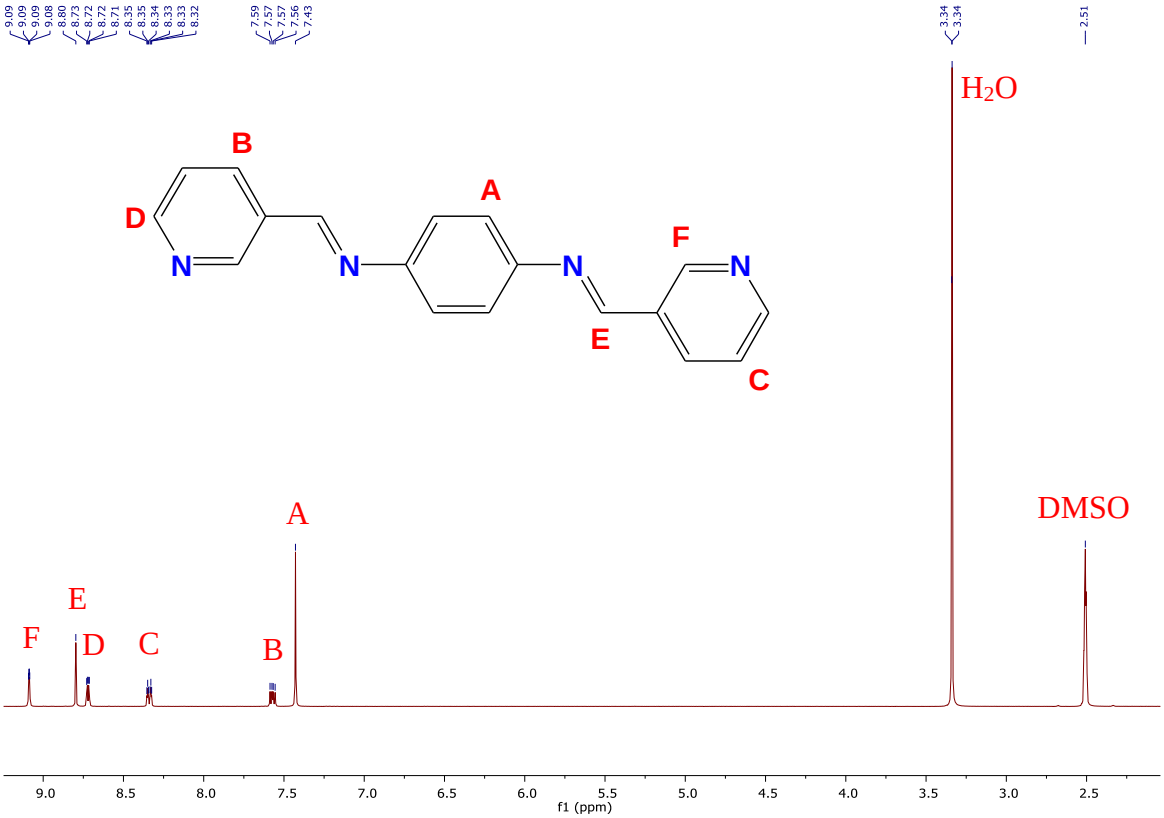

Figure 2.1: ^{1}H NMR (400 MHz, DMSO-d_6) spectrum of *N*,*N'*-bis-pyridin-3-ylmethylene-benzene-1,4-diamine ([a]L).

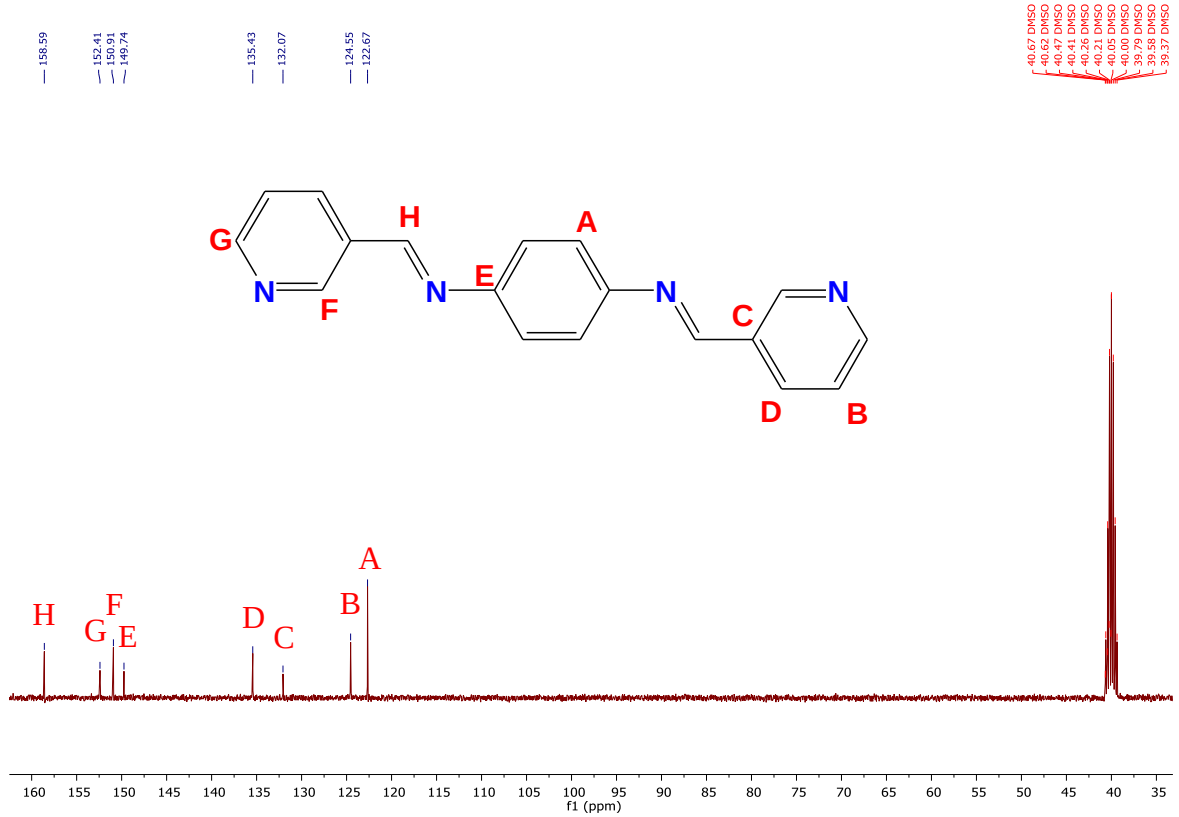

Figure 2.2: $^{13}C\{^{1}H\}$ NMR (101 MHz, DMSO-d_6) spectrum of *N,N'*-bis-pyridin-3-ylmethylene-benzene-1,4-diamine (^{a}L).

2.4.2 Synthesis of *N,N'*-bis-pyridin-3-ylmethyl-benzene-1,4-diamine (L1)

The new ligand L1 was prepared by reduction of *N,N'*-bis-pyridin-3-ylmethylene-benzene-1,4-diamine in methanol solution by $NaBH_4$ for 12 hours according to scheme 2.2 [82, 83]. The FTIR spectrum of the free ligand shows bands changing in comparison with ^{a}L ligand spectrum. The most important to note is the band disappearing at 1567 cm^{-1} which is due to the imine group and appearance of the new band at 3235 cm^{-1} which is due to the secondary amine group formation [73, 74]. These changes provide strong evidence of Schiff base reduction and formation of the secondary amine compound. ^{1}H NMR spectrum of the prepared ligand shows disappearance of the imine peak at δ 8.80 ppm and appearance of methylene and secondary amine functional group peaks at δ 4.16 ppm and at δ 5.46 ppm (figure 2.3) [73, 74, 80]. $^{13}C\{^{1}H\}$ NMR spectrum shows a new peak at δ 45.15 ppm which is due to methylene functional group formation and disappearing of the imine group at δ 158.59 ppm (figure 2.4) [74].

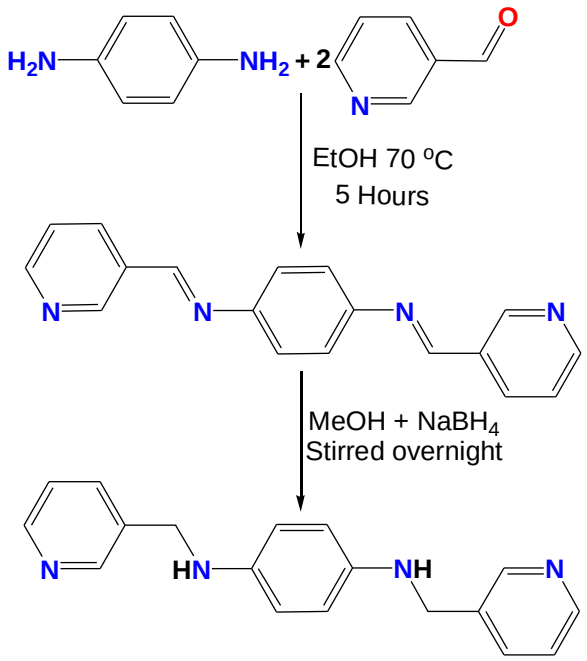

Scheme 2.2: Synthesis of *N*,*N*′-bis-pyridin-3-ylmethyl-benzene-1,4-diamine ligand (L1).

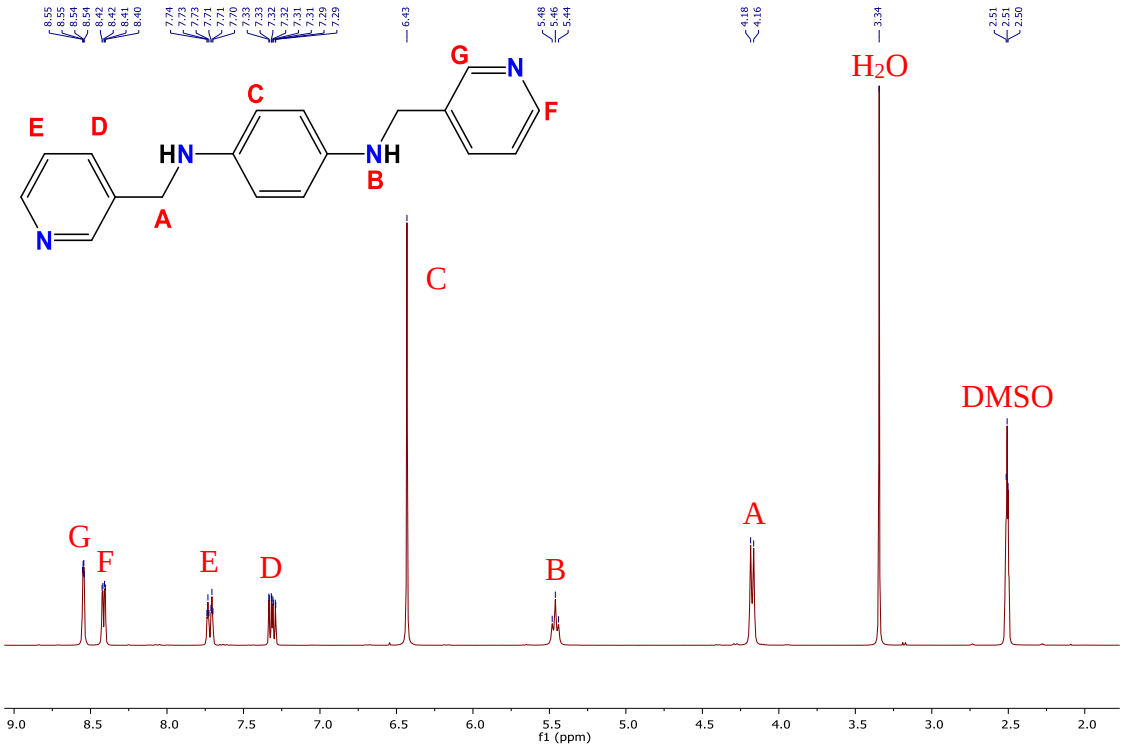

Figure 2.3: ^{1}H NMR (300 MHz, DMSO-d_6) spectrum of *N*,*N*′-bis-pyridin-3-ylmethyl-benzene-1,4-diamine (L1).

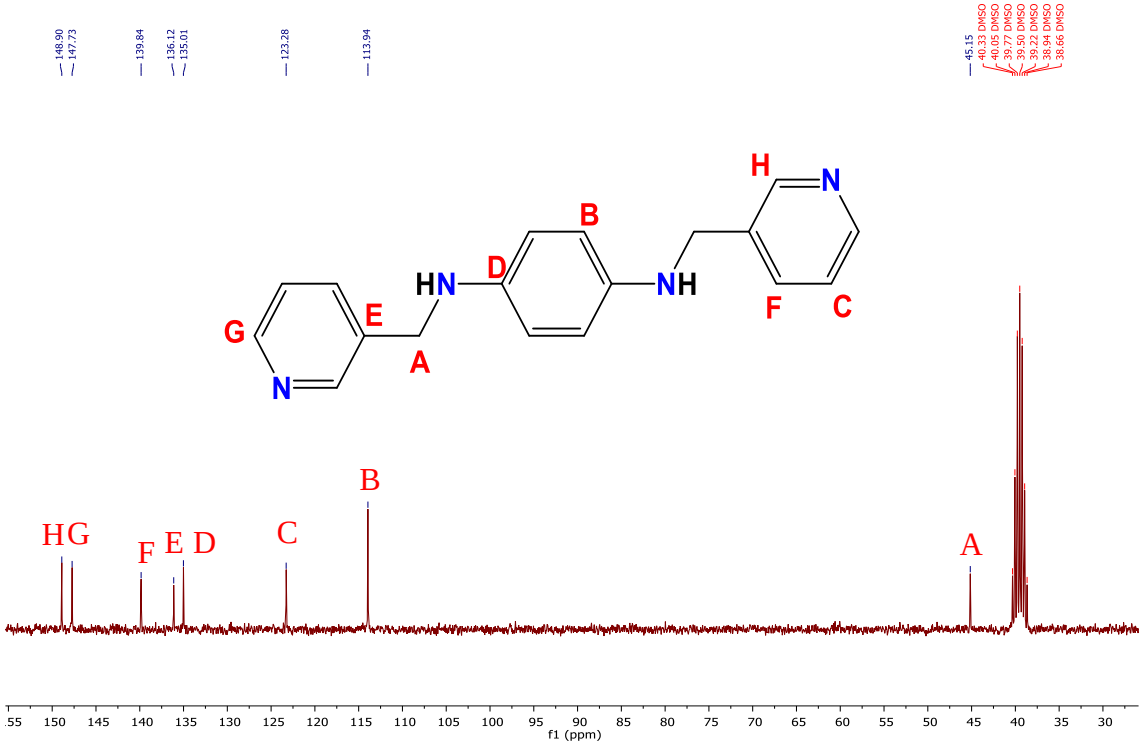

Figure 2.4: $^{13}C\{^{1}H\}$ NMR (75 MHz, DMSO-d_6) spectrum of *N*,*N'*-bis-pyridin-3-ylmethyl-benzene-1,4-diamine (L1).

2.4.3 Synthesis of new 1-8 CPs

The reaction of L1 ligand with $MnCl_2.4H_2O$, $FeCl_3.6H_2O$, $CoCl_2.6H_2O$, $CuCl_2.2H_2O$, $Zn(NO_3)_2.6H_2O$, $Cd(NO_3)_2.4H_2O$, isophthalic acid or benzene-1,4-dicarboxylic acid produced a series of new coordination polymers $([Mn_{0.5}(L1)Cl].MeOH)_n$ (**1**), $([Fe_{0.5}(L1)Cl].MeOH)_n$ (**2**), $([Co_{0.5}(L1)Cl].MeOH)_n$ (**3**) and $([Cu(L1)Cl]\cdot CH_2Cl_2)_n$ (**4**) one-dimensional polymers. $([Zn(L1)(H_2O)_2].NO_3)_n$ (**5**) and $([Cd(L1)_2(NO_3)_2])_n$ (**6**) two-dimensional polymers; $([Cd(L1)_{0.5}(isoph)(DMF)])_n$ (**7**) and $([Cd_{1.5}(L1)_{0.5}(bdc)_{1.5}(DMF)])_n$ (**8**) three-dimensional polymers. Compounds **1-6** were obtained from self-assembly process in methanol or in a mixture of methanol and dichloromethane at room temperature. Whereas compounds **7** and **8** were synthesised by solvothermal reaction in DMF at 115 °C. The resultant crystals of **1-6** are soluble and decomposed to starting materials in hot MeOH, EtOH, MeCN and DCM, or in DMSO, DMF and $CHCl_3$ at room temperature. On the other hand, compounds **7** and **8** crystals are insoluble in common organic and inorganic solvents. Therefore, compounds **1-8** were characterised as solid materials by single crystal X-ray analysis, powder X-ray analysis, microanalysis of the elements and FTIR analysis.

IR spectra for complexes **1-3** shows main peaks between 3347-3322, 3050-3017, 2820-2814, 1600-1598 and 1517-1514 cm^{-1} due to νN-H, νC-$H_{Ar,}$ νC-H_{Al}, νC=C and νC-N functional

groups [72-74, 84]. Complexes spectra also showed new bands between 519-510 cm^{-1} due to νM-N coordination bond [84, 85]. FTIR spectrum for complex **4** shows main bands at 3322, 3052, 1602, 1515 and 511 cm^{-1} due to νN-H, νC-$H_{Ar,}$ νC=C, νC-N and νM-N functional groups and coordination bond [72-74, 79, 86]. The IR spectrum of complex **5** display main peaks at 3400-3000, 3397, 3354, 3050, 1604, 1515, 645 and 521cm^{-1} due to νO-H, νN-H, νC-H_{Ar}, νC=C, νC-N, νM-N and νM-O functional groups and coordination bonds [74, 84]. Compound **6** IR spectrum display main bands at 3295, 3009, 2915, 1602, 1584, 527 and 420 cm^{-1} due to νN-H, νC-$H_{Ar,}$ νC-H_{Al}, νC=C, νC-N, νM-N and νM-O functional groups and coordination bonds [72-74, 79, 87]. Complexes **7** and **8** IR spectra show main bands between 3401-3365, 3068-3048, 2932-2927, 1648-1643, 1598-1551, 1556-1510, 1368-1366, 522-518 and 437-413 cm^{-1} due to νN-H, νC-$H_{Ar,}$ νC-H_{Al}, νC=O, νC=C, νC-N, νCH_3, νM-N and νM-O functional groups and coordination bonds [73, 74, 84, 85].

2.5 Crystal structures

2.5.1 Crystal structure of the new ligand *N,N'*-bis-pyridin-3-ylmethyl-benzene-1,4-diamine (L1)

N,N'-Bis-pyridin-4-ylmethyl-benzene-1,4-diamine was synthesised and characterised as discussed in sections 2.2.3 and 2.4.2. The ligand was dissolved in dichloromethane and left to evaporate slowly to afford yellow single crystals after 24 hours. A suitable crystal was selected for structure determination by X-ray diffraction. The structure was solved in the monoclinic space group $P2_1/c$ [62-66]. The asymmetric unit shows half of L1 ligand molecule (figure 2.5), and after symmetry expansion, the ligand shows torsion angle of -178.20(16) ° between the phenyl and 3-pyridyl rings. The ligand crystal structure also shows 3.819 Å distance between 3-pyridyl rings in the crystal lattice that due to π-π stacking interaction (figure 2.6). Selected bond lengths, angles and torsion angles for L1 ligand are listed in tables 2.1 and 2.2.

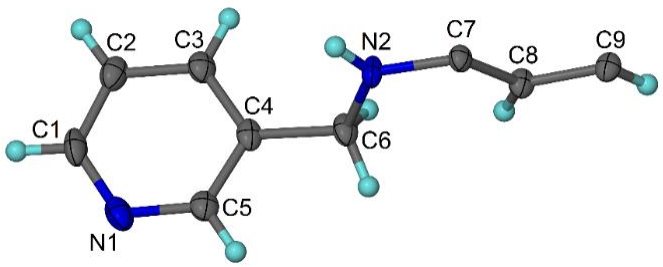

Figure 2.5: *N,N'*-Bis-pyridin-3-ylmethyl-benzene-1,4-diamine asymmetric unit of the crystal structure. Ellipsoids shown at 50 % probability levels.

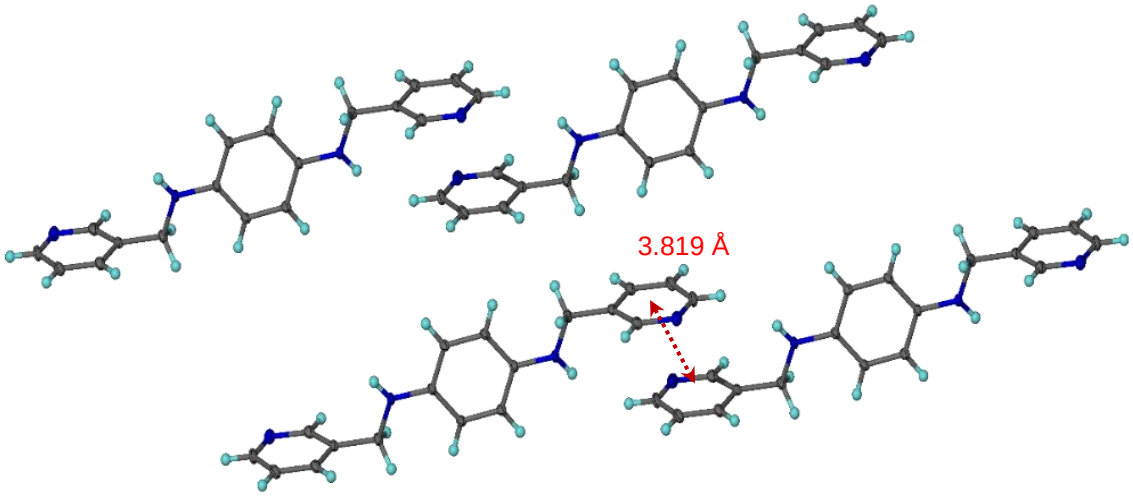

Figure 2.6: Crystal structure of L1 shows torsion angle of -178.20(16) ° between the phenyl and 3-pyridyl rings, 3.819 Å distance between L1 ligand molecules that due to π-π stacking interaction.

Table 2.1: Selected bond lengths (Å) and angles (°) for L1 ligand.

N1-C1	1.344(3)	C1-C2-C3	118.76(17)
C1-C2	1.381(3)	C2-C3-C4	119.34(17)
C2-C3	1.381(2)	C3-C4-C5	117.10(17)
C3-C4	1.395(3)	C4-C5-N1	124.68(17)
C4-C5	1.390(2)	C5-N1-C1	116.54(15)
C5-N1	1.347(2)	C4-C6-N2	110.61(14)
C4-C6	1.507(2)	C6-N2-C7	117.37(14)
N2-C6	1.458(2)	N2-C7-C8	123.39(14)
N2-C7	1.407(9)	C7-C8-C9	120.70(16)
C7-C8	1.396(3)	C3-C4-C6	120.90(16)
C8-C9	1.392(2)	C5-C4-C6	121.99(16)
N1-C1-C2	123.53(16)		

Table 2.2: Selected torsion angles (°) for L1 ligand.

N2-C7-C8-C9	178.88(18)
C2-C3-C4-C6	-179.73(17)
C3-C4-C6-N2	74.2(2)
C5-C4-C6-N2	-106.4(2)
C6-N2-C7-C8	13.2(3)
C6-N2-C7-C9[1]	-168.11(18)
C7-N2-C6-C4	-178.20(16)

2.5.2 Crystal structures of ($[M_{0.5}(L1)Cl].MeOH)_n$ (1-3) CPs

Complexes **1-3** are isostructural with coordination polymer structures. Their structures were solved in the triclinic space group $P\bar{1}$ [62-66] and display half of Mn(II), Fe(II) or Co(II) ion on an inversion centre. There is one L1 ligand molecule, one coordinated chloride ion and one MeOH molecule per asymmetric unit which is shown for complex **1** in figure 2.7. M^{2+} ions are coordinated to four L1 ligand molecules and show two coordination distances between nitrogen atoms of 3-pyridyl rings and M^{2+} cations (Mn-N1= 2.338(2) Å), (Mn-N4= 2.314(2) Å), (Fe-N1= 2.273(18) Å), (Fe-N4= 2.254(19) Å) or (Co-N1= 2.202(19) Å) and (Co-N4= 2.222(2) Å). The divalent metals are also coordinated to two chloride ions in a *trans* arrangement to produce distorted octahedral coordination centres (Mn-Cl1= 2.515(6) Å), (Fe-Cl1= 2.443(5) Å) or (Co-Cl1= 2.453(6) Å).

In 1995 Araya and co-workers [88] reported the crystal structure of $MnCl_2(py)_4$ complex that shows coordination bond lengths of 2.342(6), 2.341(6) and 2.514(2) Å for Mn-N1, Mn2-N3 and Mn-Cl1 [88]. Another example based on Mn(II) chloride and pyridine-2,6-diylbis((pyridin-3-yl)methanone was reported in 2013 by Liu [89]. Liu's reported complex shows coordination bond lengths of 2.330(18), 2.320(18) and 2.472(6) Å for Mn1-N1, Mn1-N3 and Mn1-Cl1 [89]. $([Fe_{0.5}(L1)Cl].MeOH)_n$ complex was synthesised from Iron(III) but reduced to Fe(II) by methanol and water [90]. Complex **2** coordination bond lengths are similar to Karsten's reported crystal structure of [(bis(1,8-diazabicyclo[5.4.0]undec-7-en-8-ium)trans-dichlorotetra(pyridine-N)iron(II)dichloride)] that shows M-N or M-Cl coordination bond lengths of 2.279(3), 2.273(3) and 2.406(8) Å for Fe1-N1, Fe1-N2 and Fe1-Cl1 [91]. Compound **2** also has a good agreement with Ton's Fe(II) chloride and pyridine reported complex that shows coordination bond lengths of 2.218(7) Å for Fe1-N1 and 2.424(4) Å for Fe1-Cl1 [92]. The $([Co_{0.5}(L1)Cl].MeOH)_n$ CP shows similar coordination bond lengths in comparison with Kansikas's Co(II) chloride and 3,5-dimehtyl-pyridine reported structure that has coordination bond lengths of 2.455(2) Å for Co-Cl and 2.186(4) Å for Co-N [93]. In 2015 Tradin and co-workers reported a crystal structure based on Co(II) chloride and 3-pyridinemethanol that shows coordination bond lengths between 2.188(13)-2.234(13) Å for Co-N, and 2.487(4) Å for Co-Cl [94].

The ligand L1 is coordinated *via* nitrogen atoms of 3-pyridyl rings to two different M^{2+} ions and shows torsion angles of -174.4(2) and -92.2(3) ° for compound **1**, 175.0(19) and 92.2(3) ° for compound **2** or -93.7(3) and -175.0(2) ° for compounds **3** between the phenyl and 3-pyridyl rings to produce L1 bent-L shape between M(II) coordination centres figure 2.7 and

table 2.4. Each L1 ligand bridges between two Mn(II) centres to form a double bridged coordination chain structure (Mn-L1-Mn= 15.478 Å), (Fe-L1-Fe= 15.414 Å) and (Co-L1-Co= 15.410 Å). L1 also shows M_2L_2 metallacycle motif with distances of 12.372, 12.278 or 12.306 Å between 3-pyridyl rings and 9.123, 9.028 or 8.908 Å between phenyl rings for complexes **1-3** figures 2.8 and 2.9. The resulted one-dimensional chains are packing in the crystal lattice to form one-dimensional channels occupied by methanol guest molecules (figure 2.10). The resulted crystal structure shows hydrogen bond interaction between methanol guest molecules and L1 secondary amines HN···O= 2.944, 2.940 or 2.933 Å for compound **1-3**. The crystal structure shows another hydrogen bond interaction between the secondary amines and the coordinated chloride ions from different coordination chains -HN···Cl= 3.244, 3.238 or 3.234 Å. In addition to π-π stacking interaction between 3-pyridyl rings from different coordination chains 3-py to 3-py= 3.961, 4.004 or 3.979 Å (figure 2.9). Powder XRD of dried samples are consistent with each other but do not match the calculated diffraction patterns from the single crystal structures. This indicates that there is a change of structure on the loss of methanol from these compounds. This new phase is crystalline, but the structure could not be determined as the materials did not stay as a single crystal on drying out. Moreover, the experimental pattern of complex **3** shows some amorphous materials in present (figure 2.13).

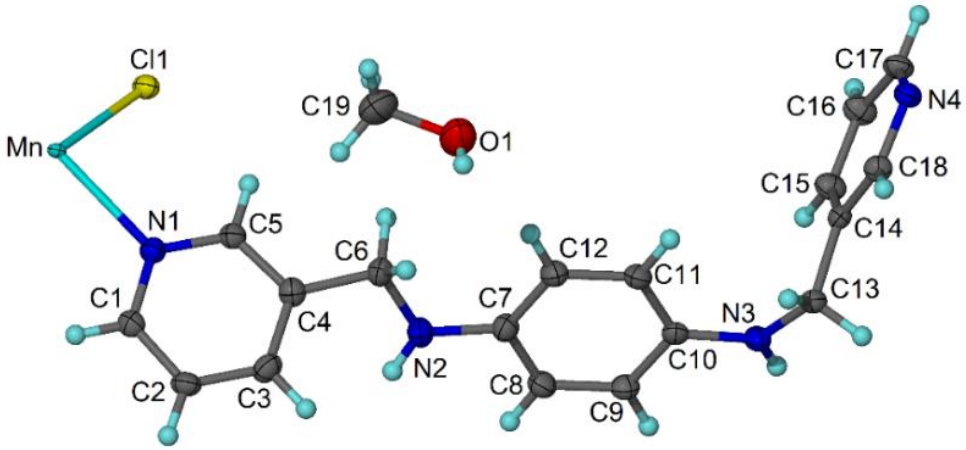

Figure 2.7: $([(Mn_{0.5}(L1)Cl].MeOH)_n$ CP asymmetric unit of the crystal structure. Ellipsoids shown at 50 % probability levels.

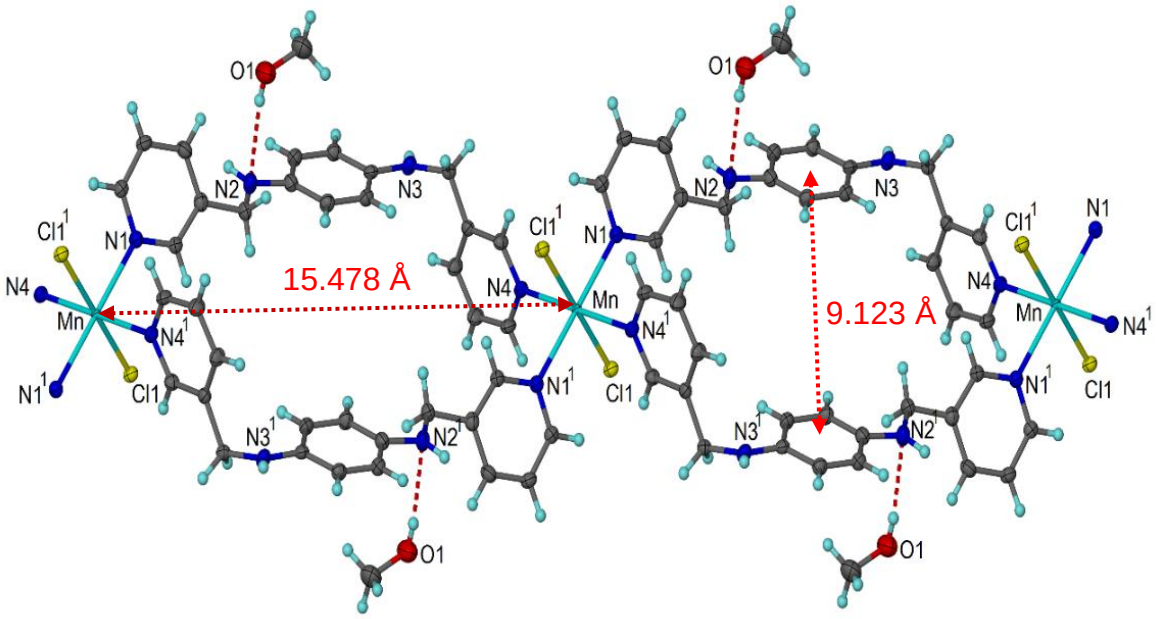

Figure 2.8: $([Mn_{0.5}(L1)Cl].MeOH)_n$ CP rectangle cavities (Mn-L1-Mn= 15.478 Å), (Fe-L1-Fe= 15.414 Å) or (Co-L1-Co= 15.410 Å), 9.123, 9.028 or 8.908 Å between phenyl rings. Hydrogen bond interaction between the secondary amines and methanol guest molecules.

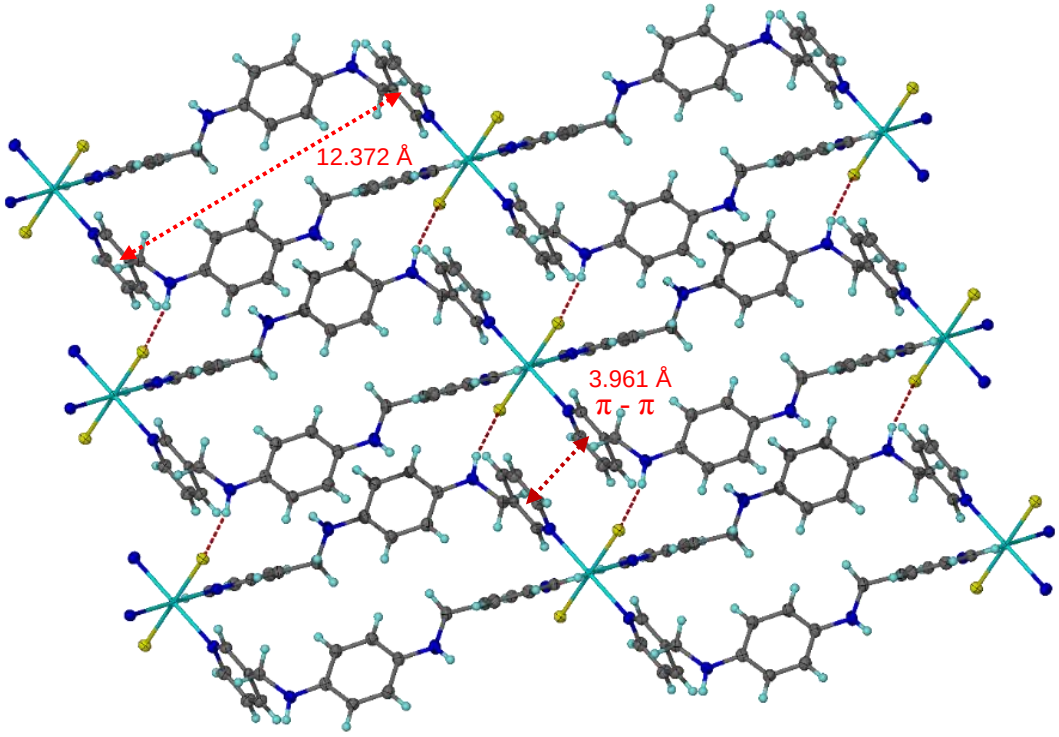

Figure 2.9: $([Mn_{0.5}(L1)Cl].MeOH)_n$ CP hydrogen bond interactions between the secondary amines and the coordinated chloride ions from different coordination chains, 12.372, 12.278 or 12.306 Å between 3-pyridyl rings. π-π Stacking interaction between 3-pyridyl rings.

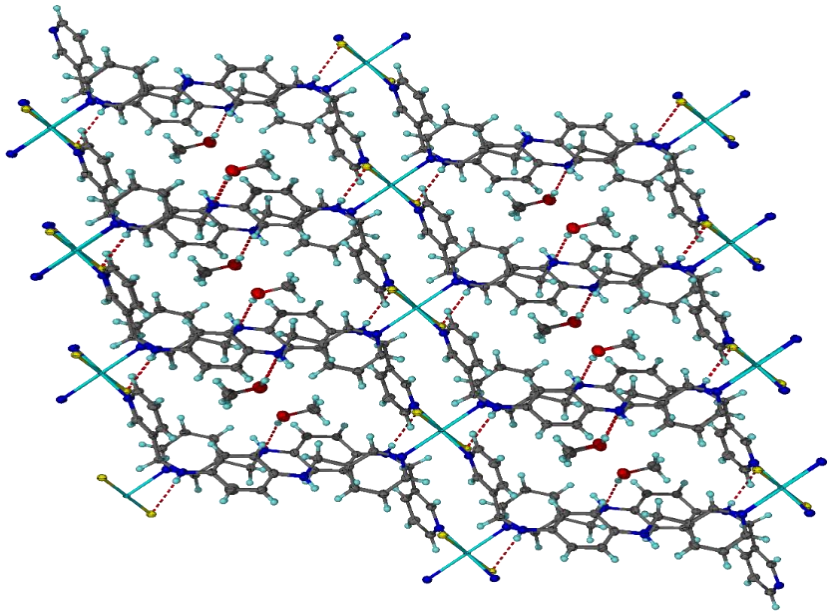

Figure 2.10: Packing diagram of $([Mn_{0.5}(L1)Cl].MeOH)_n$ CP.

Table 2.3: Selected bond lengths (Å) and angles (°) for compounds (**1-3**).

(1)		**(2)**		**(3)**	
Mn-Cl1	2.515(6)	Fe-Cl1	2.443(5)	Co-Cl1	2.453(6)
Mn-N1	2.338(2)	Fe-N1	2.273(18)	Co-N1	2.202(19)
Mn-N4	2.314(2)	Fe-N4	2.254(19)	Co-N4	2.222(2)
N2-C6	1.460(3)	N2-C6	1.457(3)	N2-C6	1.445(3)
N3-C13	1.440(3)	N3-C13	1.443(3)	N3-C13	1.457(3)
$Cl1^1$-Mn-Cl1	180.00(3)	$Cl1^1$-Fe-Cl1	180.0	Cl1-Co-$Cl1^1$	180.0
N1-Mn-$Cl1^1$	88.29(5)	N4-Fe-$Cl1^1$	88.74(5)	$N1^1$-Co-Cl1	88.83(5)
N1-Mn-Cl1	91.71(5)	N4-Fe-Cl1	91.26(5)	N1-Co-Cl1	91.17(5)
$N1^1$-Mn-Cl1	88.29(5)	$N4^1$-Fe-$Cl1^1$	91.26(5)	N1-Co-$Cl1^1$	88.83(5)
$N1^1$-Mn-$Cl1^1$	91.71(5)	$N4^1$-Fe-Cl1	88.74(5)	$N1^1$-Co-$Cl1^1$	91.17(5)
N1-Mn-$N1^1$	180.0	$N4^1$-Fe-N4	180.0	$N1^1$-Co-N1	180.00(11)
N4-Mn-$Cl1^1$	88.29(6)	N4-Fe-N1	93.91(7)	$N1^1$-Co-N4	93.83(7)
$N4^1$-Mn-Cl1	88.29(6)	N4-Fe-$N1^1$	86.09(7)	$N1^1$-Co-$N4^1$	86.17(7)
$N4^1$-Mn-$Cl1^1$	91.71(6)	$N4^1$-Fe-$N1^1$	93.91(7)	N1-Co-$N4^1$	93.83(7)
N4-Mn-Cl1	91.71(6)	$N4^1$-Fe-N1	86.09(7)	N1-Co-N4	86.17(7)
N4-Mn-$N1^1$	86.56(7)	$N1^1$-Fe-Cl1	88.64(5)	N4-Co-Cl1	88.83(5)
N4-Mn-N1	93.44(7)	N1-Fe-Cl1	91.35(5)	N4-Co-$Cl1^1$	91.17(5)
$N4^1$-Mn-$N1^1$	93.44(7)	$N1^1$-Fe-$Cl1^1$	91.36(5)	$N4^1$-Co-Cl1	91.17(5)
$N4^1$-Mn-N1	86.56(7)	N1-Fe-$Cl1^1$	88.65(5)	$N4^1$-Co-$Cl1^1$	88.83(5)
$N4^1$-Mn-N4	180.0	N1-Fe-$N1^1$	180.0	N4-Co-$N4^1$	180.00(4)
C4-C6-N2	110.03(2)	C4-C6-N2	109.98(2)	C4-C6-N2	115.01(2)
C6-N2-C7	118.47(2)	C6-N2-C7	118.73(2)	C6-N2-C7	123.00(16)
C10-N3-C13	122.64(2)	C10-N3-C13	122.66(2)	C10-N3-C13	118.80(2)
N3-C13-C14	114.76(2)	N3-C13-C14	114.94(18)	N3-C13-C14	110.35(2)

Table 2.4: Selected torsion angles (°) for compounds (**1-3**).

(1)		**(2)**		**(3)**	
Mn-N1-C1-C2	-179.1(2)	Fe-N1-C1-C2	-178.69(18)	Co-N1-C1-C2	178.8(2)
Mn-N1-C5-C4	178.4(2)	Fe-N1-C5-C4	178.96(18)	Co-N1-C5-C4	-178.00(18)
Mn^{1}-N4-C17-C16	179.7(2)	Fe^{1}-N4-C18-C14	178.18(17)	Co^{1}-N4-C17-C16	-179.05(18)
Mn^{1}-N4-C18-C14	-178.78(19)	Fe^{1}-N4-C17-C16	-178.99(19)	Co^{1}-N4-C18-C14	178.56(18)
C7-N2-C6-C4	-174.4(2)	C7-N2-C6-C4	175.02(19)	C7-N2-C6-C4	-93.7(3)
C10-N3-C13-C14	-92.2(3)	C10-N3-C13-C14	92.2(3)	C10-N3-C13-C14	-175.0(2)
N3-C13-C14-C15	-17.5(4)	N3-C10-C9-C8	180.0(2)	N2-C7-C8-C9	179.8(2)
N3-C13-C14-C18	165.3(2)	C18-C14-C13-N3	-165.5(2)	N2-C7-C12-C11	179.9(2)
C3-C4-C6-N2	52.6(3)	N2-C7-C8-C9	-175.2(2)	N3-C10-C11-C12	175.4(2)
C5-C4-C6-N2	-128.1(3)	C11-C12-C7-N2	175.7(2)	N3-C13-C14-C15	52.2(3)
C6-N2-C7-C8	-177.5(2)	C12-C11-C10-N3	-179.7(2)	N3-C13-C14-C18	-128.9(2)
C6-N2-C7-C12	6.2(4)	C5-C4-C6-N2	128.5(2)	C3-C4-C6-N2	-18.3(3)
C13-N3-C10-C9	-163.8(2)	C3-C4-C6-N2	-52.7(3)	C5-C4-C6-N2	165.2(2)
C13-N3-C10-C11	16.5(4)	C13-N3-C10-C11	164.7(2)	C6-N2-C7-C8	-163.9(2)
C13-C14-C18-N4	176.1(2)	C13-N3-C10-C9	-16.4(3)	C6-N2-C7-C12	16.2(4)
C13-C14-C15-C16	-176.6(2)	C15-C14-C13-N3	17.9(3)	C8-C9-C10-N3	-175.9(2)
N3-C10-C9-C8	-179.8(2)	C6-N2-C7-C12	176.9(2)	C13-N3-C10-C9	-176.2(2)
N3-C10-C11-C12	179.5(2)	C6-N2-C7-C8	-6.8(3)	C13-N3-C10-C11	7.0(4)

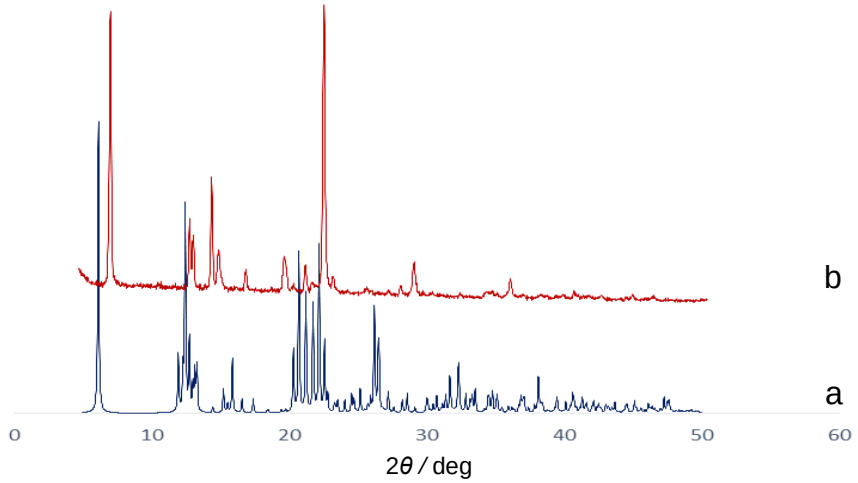

Figure 2.11: (a) Calculated powder XRD pattern of compound **1**. (b) Powder XRD pattern of compound **1**.

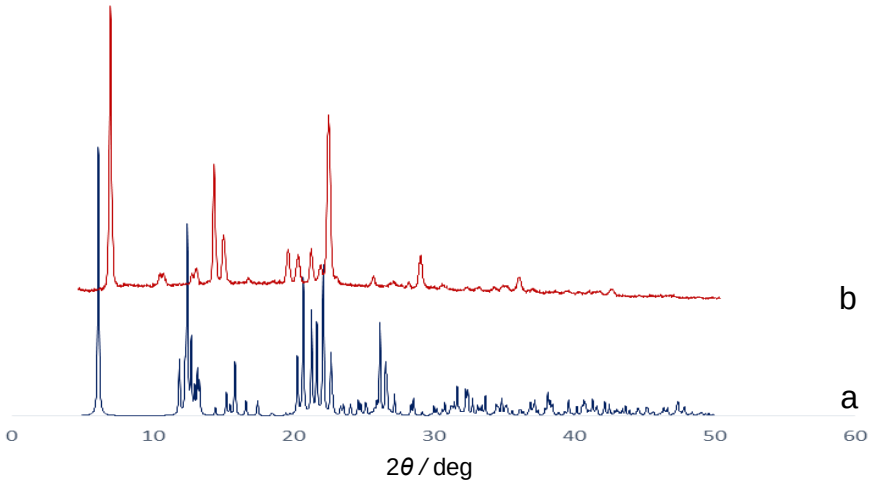

Figure 2.12: (a) Calculated powder XRD pattern of compound **2**. (b) Powder XRD pattern of compound **2**.

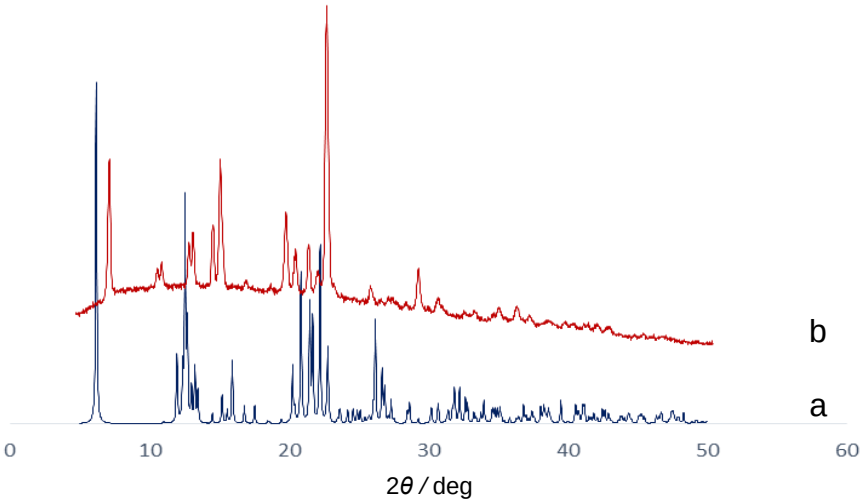

Figure 2.13: (a) Calculated powder XRD pattern of compound **3**. (b) Powder XRD pattern of compound **3**.

2.5.3 Crystal structure of $([Cu(L1)Cl].DCM)_n$ coordination polymer (4)

The complex $([Cu(L1)Cl]\cdot CH_2Cl_2)_n$ crystallises with a triclinic unit cell and the structure was solved in space group $P\bar{1}$ [62-66]. The asymmetric unit of the structure has one L1 ligand, one Cu(I) centre on a general position, one Cl^- ligand and a molecule of CH_2Cl_2 (figure 2.14). The complex is a coordination chain with a $[Cu_2(\mu\text{-}Cl)_2]$ dimer. The Cu(I) centre is approximately tetrahedral in geometry and is coordinated by two symmetry-equivalent bridging Cl ions at Cu-Cl distances of 2.455(17) and 2.346(17) Å, and pyridyl groups of two L1 ligands related by an inversion centre at Cu-N distances of 2.036(5) and 2.026(5) Å. A bond valence sum calculation is consistent with the Cu(I) oxidation state [90, 95-97]. The Cu···Cu distance across the $[Cu_2(\mu\text{-}Cl)_2]$ dimer is 2.769(2) Å, and the dimer features a particularly acute Cu-Cl-Cu angle of 70.38(5) °. The Cu…Cu separation in $[Cu(L1)Cl]\cdot CH_2Cl_2$ is shorter than for most other examples of $[Cu^I_2(\mu\text{-}Cl)_2(py)_4]$ complexes where py is a monodentate pyridyl-type ligand and Cu..Cu distances are typically 3 Å or more [97-99], however is consistent with the short Cu…Cu and Cu-Cl-Cu angle reported by Yang and Houser for complex $[Cu^I_2(\mu\text{-}Cl)_2(N\text{-}(2\text{-pyridylmethyl})acetamide)_4]$ [86].

The ligand is asymmetric showing two distinct torsion angles of 69.5(7) and 176.2(6) ° to produce the L1 ligand an overall bent L-shape. Each L-ligand bridge between two Cu(I) centres such that $[Cu_2(\mu\text{-}L1)_2]$ metallacycles are formed and these are linked into a coordination chain through the $[Cu_2(\mu\text{-}Cl)_2]$ dimers (figure 2.15). The metallacycles show significant internal space approximately 13 Å across and two molecules of CH_2Cl_2 solvent occupy these spaces. The motif of $Cu_2(L1)_2$ metallacycles linked by further μ-Cl bridges is unusual and there are no examples in the Cambridge crystallographic data centre (CCDC) of such structures with Cu(I) and N-donor ligands. Closest contacts between coordination chains occur with pair-wise N-H…Cl interactions at N…Cl separation 3.307 Å. These result in formation of a 2D layer (figure 2.16). The closest coplanar arene…arene separation is 4.623 Å between centroids which is too far to indicate π-π stacking. The layers stack along the *y* axis such that channels are evident when the structure is viewed down the *b* crystallographic cell length which are filled with CH_2Cl_2 (figure 2.17). Powder X-ray analysis for compound **4** doesn't match the calculated pattern, during the data collection of compound **4** the dried powder sample was observed to degrade under X-ray exposure and crystals color changed from yellow reddish to black (figure 2.18). Selected bond lengths, angles and torsion angles for compound **4** are listed in tables 1.5 and 1.6.

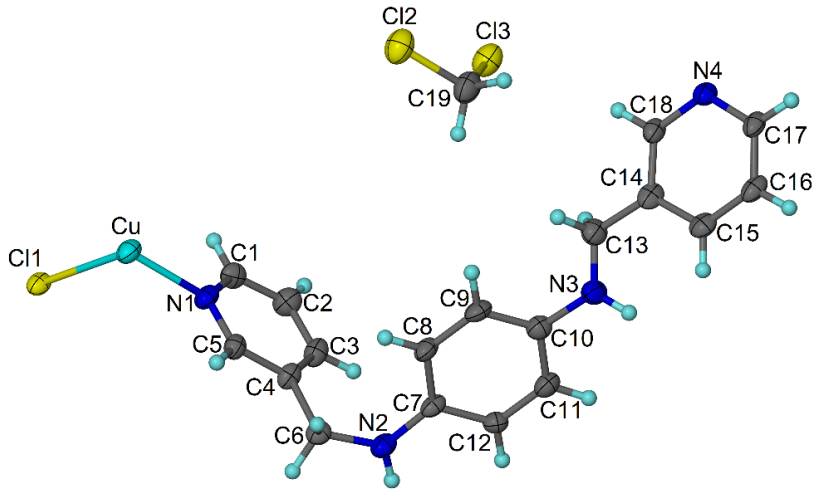

Figure 2.14: $([Cu(L1)Cl].DCM)_n$ CP asymmetric unit of the crystal structure. Ellipsoids shown at 50 % probability levels.

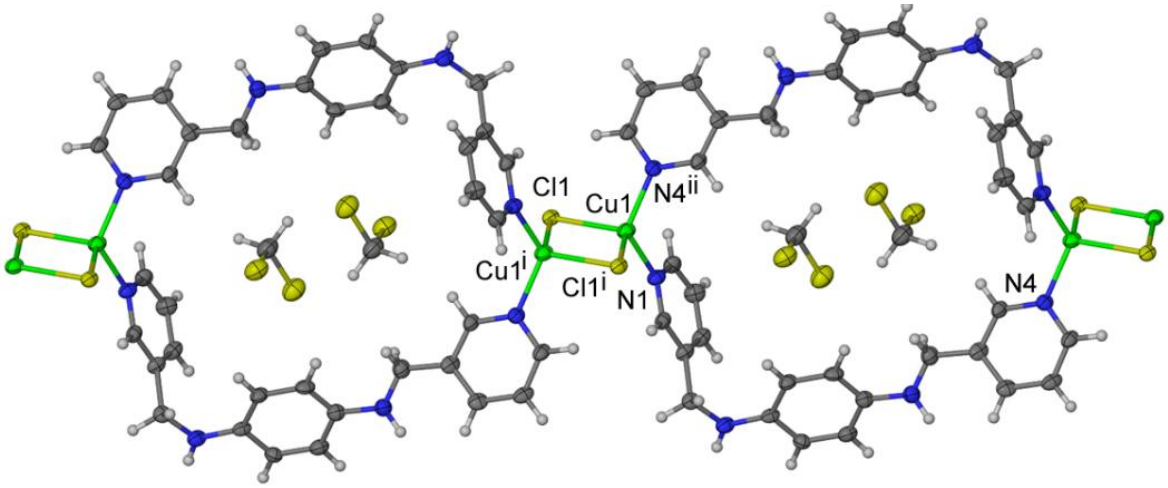

Figure 2.15: From the crystal structure of complex **4** showing $[Cu_2(\mu\text{-}L1)_2]$ metallacycle motifs linked into a coordination chain by $[Cu_2(\mu\text{-}Cl)_2]$ dimers. Solvent CH_2Cl_2 occupy the interior of the metallacycles. Ellipsoids are shown at 50 % probability level.

Table 2.5: Selected torsion angles (°) for compound **4**.

Cu-N1-C1-C2	177.9(5)	C5-C4-C6-N2	-162.3(5)
Cu-N1-C5-C4	-177.7(4)	C6-N2-C7-C8	1.1(9)
Cu^1-N4-C17-C16	178.2(5)	C6-N2-C7-C12	179.4(6)
Cu^1-N4-C18-C14	179.2(5)	C7-N2-C6-C4	69.5(7)
N2-C7-C8-C9	-179.8(6)	C8-C9-C10-N3	-175.5(6)
N2-C7-C12-C11	-177.8(6)	C13-N3-C10-C9	-42.3(10)
N3-C10-C11-C12	178.2(6)	C13-N3-C10-C11	142.1(7)
N3-C13-C14-C15	-7.4(10)	C10-N3-C13-C14	176.2(6)
N3-C13-C14-C18	171.8(6)		

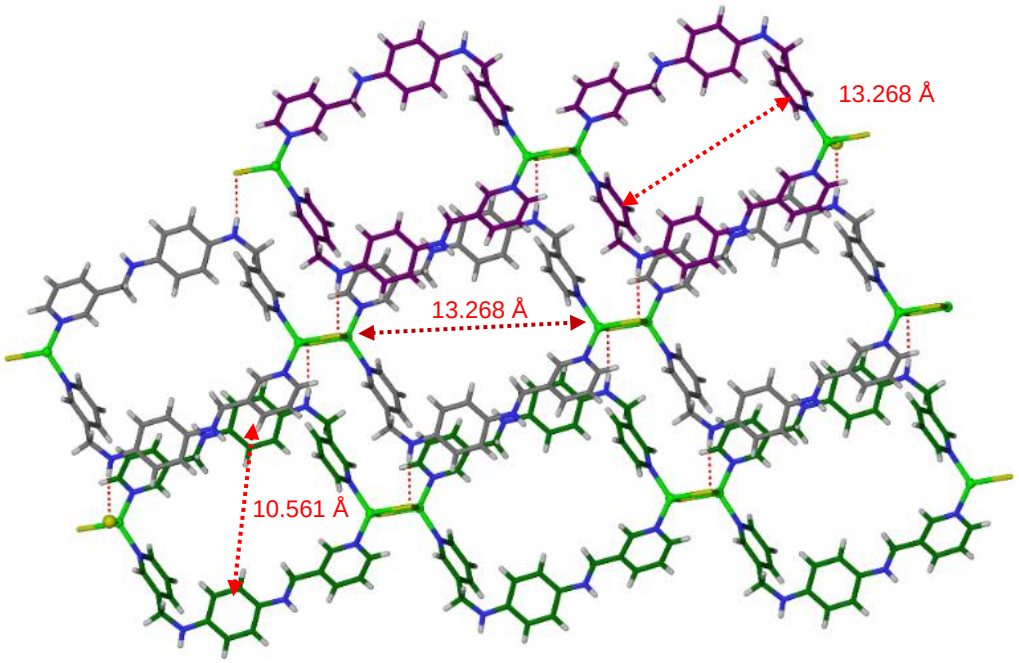

Figure 2.16: From the crystal structure of complex [Cu(L1)Cl]·CH_2Cl_2 showing formation of 2D layers with N-H…Cl interactions (dotted lines) between [Cu(L1)Cl] chains, (3-py to 3-py= 13.268 Å) and (phenyl to phenyl= 10.561 Å).

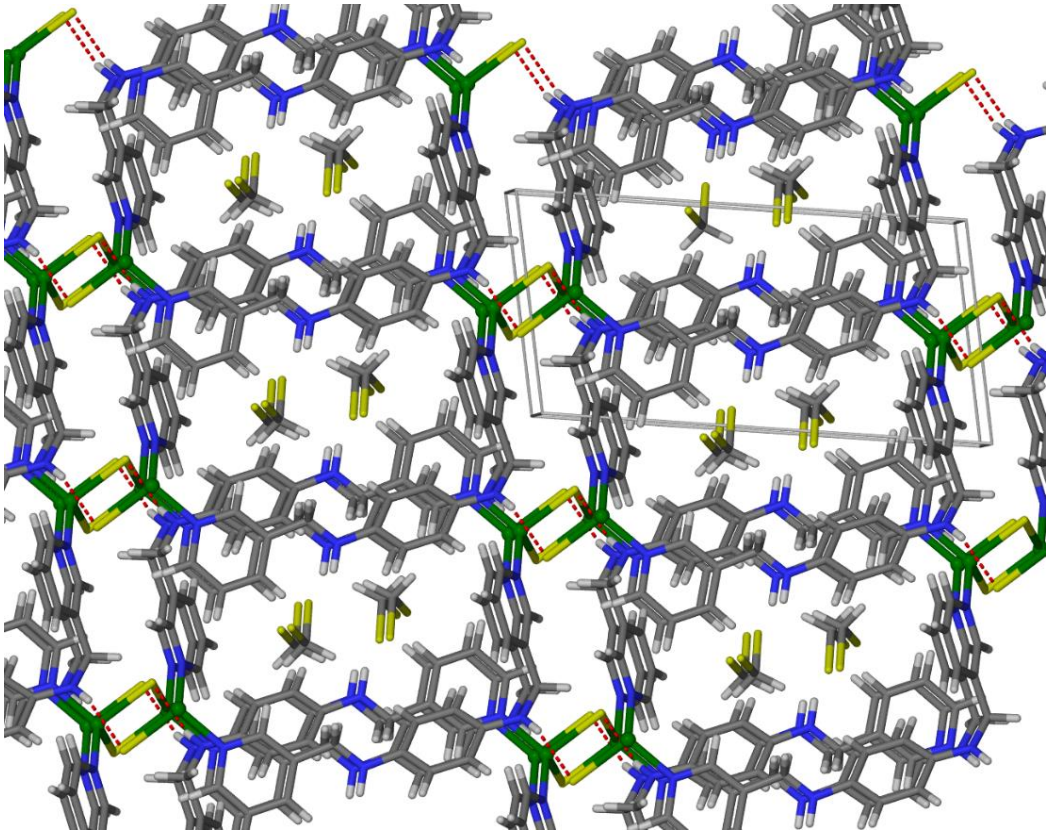

Figure 2.17: Packing diagram of [Cu(L1)Cl]·CH_2Cl_2 CP viewed down *b* unit cell axis.

Table 2.6: Selected bond lengths (Å) and angles (°) for compound **4**.

Cu-Cu^1	2.769(2)	N4^1-Cu-Cu^1	127.25(15)
Cu-Cl1	2.455(17)	N4^1-Cu-Cl1	100.51(15)
Cu-Cl1^1	2.346(17)	N4^1-Cu-Cl1^1	121.55(15)
Cu-N1	2.036(5)	N4^1-Cu-N1	113.1(2)
Cu-N4	2.026(5)	Cu^1-Cl1-Cu	70.38(5)
Cl1-Cu^1	2.3470(17)	C1-N1-Cu	118.9(4)
N2-C6	1.441(8)	C5-N1-Cu	123.7(4)
N2-C7	1.371(8)	C5-N1-C1	117.4(5)
N3-C10	1.410(8)	C7-N2-C6	122.9(5)
N3-C13	1.267(9)	C13-N3-C10	121.3(6)
N4-Cu^1	2.026(5)	C17-N4-Cu^1	122.4(4)
N4-C17	1.347(8)	C17-N4-C18	115.8(5)
N4-C18	1.356(8)	C18-N4-Cu^1	121.8(4)
Cl1^1-Cu-Cu^1	56.65(5)	N2-C6-C4	113.2(5)
Cl1-Cu-Cu^1	52.98(5)	N2-C7-C8	123.6(5)
Cl1^1-Cu-Cl1	109.62(5)	N2-C7-C12	119.0(5)
N1-Cu-Cu^1	117.77(16)	N3-C10-C11	118.4(5)
N1-Cu-Cl1^1	104.95(16)	C9-C10-N3	123.6(6)
N1-Cu-Cl1	106.19(15)	N3-C13-C14	120.4(6)

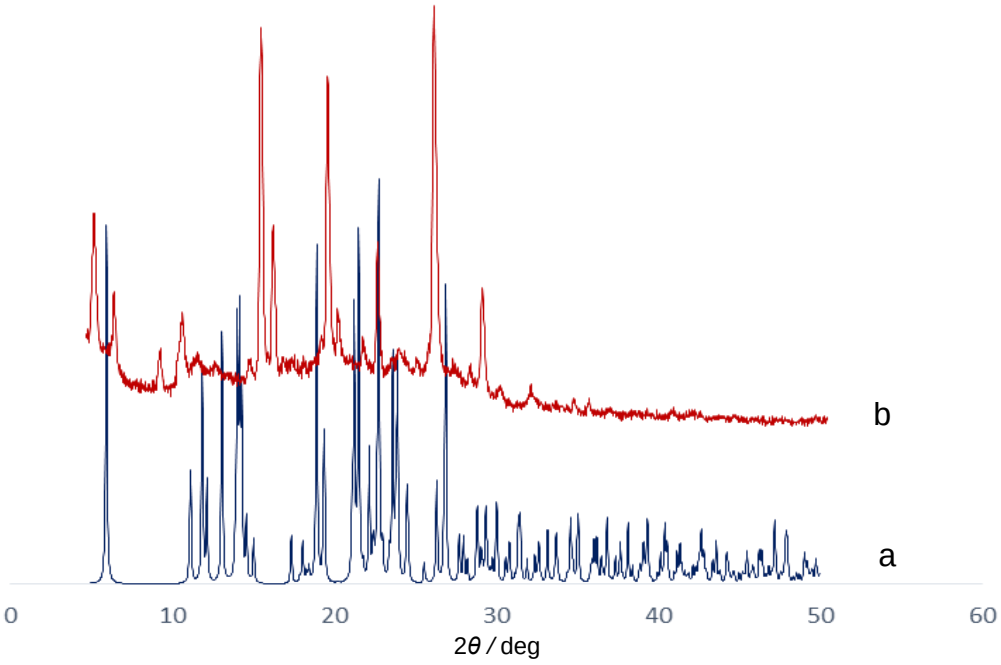

Figure 2.18: (a) Calculated powder XRD pattern of compound **4**. (b) Powder XRD pattern of compound **4**.

2.5.4 Crystal structure of $([Zn(L1)(H_2O)_2].NO_3)_n$ coordination polymer (5)

$([Zn(L1)(H_2O)_2].NO_3)_n$ crystal structure was solved in orthorhombic space group *Pbcn* [62-66] and shows one zinc(II) ion on two-fold position, one coordinated L1 ligand molecule, two coordinated water molecules and one nitrate anion per asymmetric unit (figure 2.19). Zn(II) is coordinated to four L1 ligand molecules along the equatorial axes and shows two M-N coordination distances (Zn-N1= 2.189(19) Å) and (Zn-N4= 2.170(2) Å). The metal cation is also coordinated to two water molecules in a *trans* arrangement and shows two M-O coordination distances (Zn-O1= 2.080(2) Å) and (Zn-O2= 2.174(2) Å) to produce Zn(II) distorted octahedral coordination centres. Moreover, coordinated water molecules show hydrogen bond interaction with nitrate anions and display two hydrogen bond interaction distances (O1···O3= 2.774 and O2···O5= 2.732 Å) figure 2.19.

In 2004 Turner et. al [100] reported a crystal structure based on Zn(II) sulphate and 1-(3-Pyridinyl)-3-(4-methylphenyl)urea. Turner's Zn(II) complex shows similar octahedral coordination environment to compound **5** with M-O and M-N coordination distances of 2.120(6), 2.186(7) or 2.170(17) Å for Zn1-O1, Zn1-O2 and Zn1-N1 [100]. Another example based on Zn(II) perchlorate and 25,26,27,28-tetrakis((pyridin-3-yl)methoxy)calix[4]arene was reported in 2016 by Brancatelli [101]. Brancatelli's structure shows M-N and M-O coordination bond lengths of 2.133(11), 2.179(5) and 2.121(8) Å for Zn1-N10, Zn1-O40 and Zn1-O1.

Each L1 ligand is coordinated to two Zn(II) ions by nitrogen atoms of the 3-pyridyl rings and shows two torsion angles of -88.2(3) and -85.0(3) ° between the phenyl and 3-pyridyl rings to produce L1 bent U-shape between Zn(II) coordination centres figure 2.19 and table 2.8. Four L1 ligand molecules are coordinated to four Zn(II) coordination centres to produce the M-shape cavity that expand to produce the two-dimensional network (figure 2.20). The resulted network shows 10.436 Å sides and 9.267 × 18.703 Å diagonals between Zn(II) coordination centres. Furthermore, the two-dimensional network shows 5.014 × 9.881 Å M-shape cavities occupied by nitrate ions (figure 2.20). Powder X-ray analysis for compound **5** shows a good match with the calculated pattern which indicates phase purity and compound stability (figure 2.22). Selected bond lengths, angles and torsion angles for compound **5** are listed in tables 2.7 and 2.8.

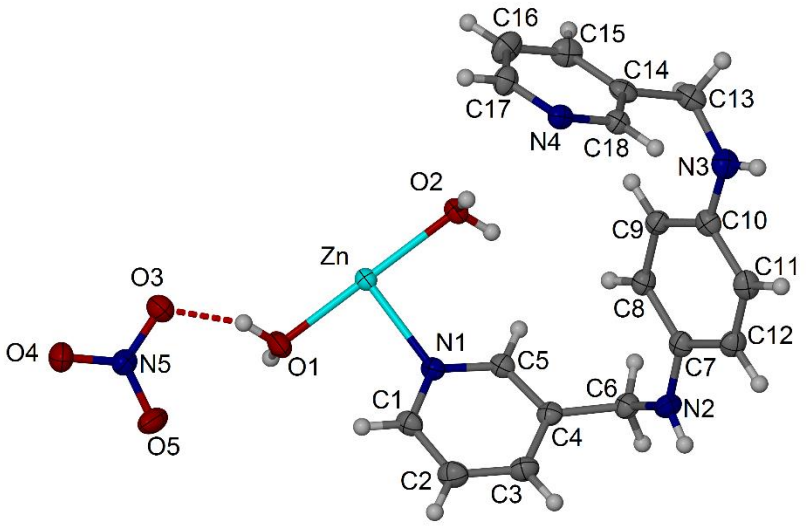

Figure 2.19: $([Zn(L1)(H_2O)_2].NO_3)_n$ CP asymmetric unit of the crystal structure. Ellipsoids shown at 50 % probability levels.

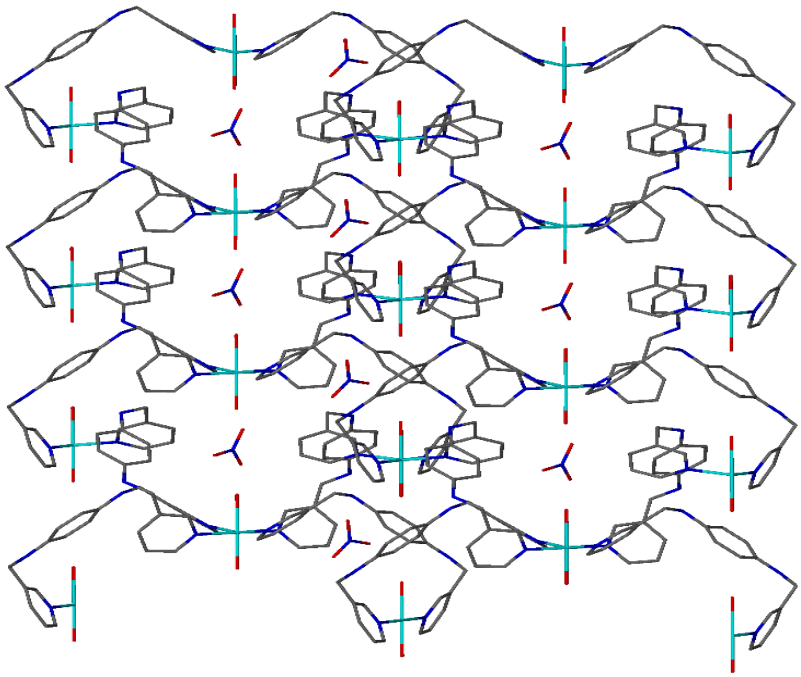

Figure 2.20: $([Zn(L1)(H_2O)_2].NO_3)_n$ two-dimensional polymer network that has (5.014 × 9.881 Å) M-shape cavities and occupied by nitrate ions.

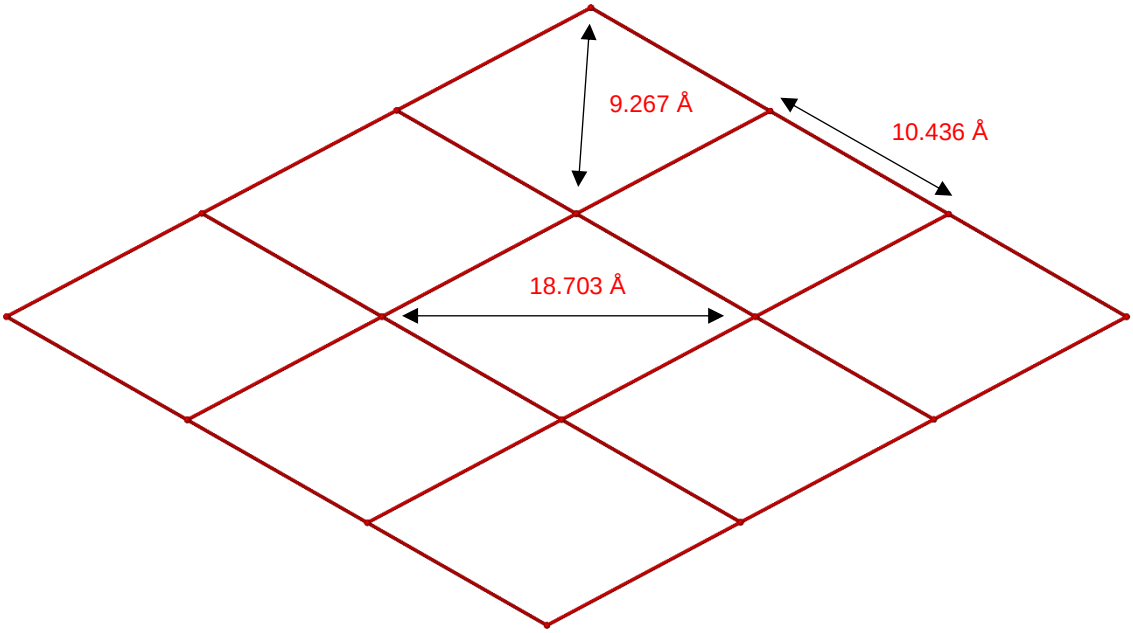

Figure 2.21: $([Zn(L1)(H_2O)_2].NO_3)_n$ CP network that has 10.436 Å sides and 9.267 × 18.703 Å diagonals between Zn(II) coordination centres.

Table 2.7: Selected bond lengths (Å) and angles (°) for compound **5**.

Zn-O1	2.080(2)	C9-C10	1.383(3)	$N4^1$-Zn-N1	89.93(7)
Zn-O2	2.174(2)	C10-C11	1.409(3)	$N4^1$-Zn-N4	166.71(10)
$Zn-N1^1$	2.189(19)	C11-C12	1.377(4)	C1-N1-Zn	121.19(15)
Zn-N1	2.189(19)	C13-C14	1.515(3)	C1-N1-C5	117.3(2)
Zn-N4	2.170(2)	C14-C15	1.382(4)	C5-N1-Zn	120.57(15)
$Zn-N4^1$	2.170(2)	C14-C18	1.390(3)	C7-N2-C6	121.01(19)
N1-C1	1.342(3)	C15-C16	1.391(4)	C10-N3-C13	123.0(2)
N1-C5	1.352(3)	C16-C17	1.381(4)	C17-N4-Zn	122.33(16)
N2-C6	1.457(3)	O3-N5	1.255(3)	C17-N4- C18	117.4(2)
N2-C7	1.397(3)	O4-N5	1.247(3)	C18-N4-Zn	119.17(16)
N3-C10	1.399(3)	O5-N5	1.249(3)	N1-C1- C2	122.9(2)
N3-C13	1.440(3)	O1-Zn-O2	180.0	N1-C5-C4	123.7(2)
N4-Zn	2.169(19)	$O1-Zn-N1^1$	89.89(5)	N2-C6-C4	112.58(19)
N4-C17	1.341(3)	O1-Zn-N1	89.89(5)	N2-C7-C8	123.7(2)
N4-C18	1.347(3)	$O1-Zn-N4^1$	96.65(5)	N2-C7-C12	118.9(2)
C1-C2	1.381(4)	$O1-Zn-N4^1$	96.65(5)	N3-C10-C11	118.8(2)
C2-C3	1.386(4)	$O2-Zn-N1^1$	90.11(5)	C9-C10-N3	123.0(2)
C3-C4	1.384(3)	O2-Zn-N1	90.11(5)	N3-C13-C14	113.7(2)
C4-C5	1.386(3)	$N1-Zn-N1^1$	179.77(9)	N4-C17-C16	122.7(2)
C4-C6	1.511(3)	$N4^1$-Zn-O2	83.35(5)	N4-C18-C14	124.1(2)
C7-C8	1.400(3)	$N4^1$-Zn-O2	83.35(5)	O4-N5-O3	120.3(2)
C7-C12	1.407(3)	$N4^1-Zn-N1^1$	89.93(7)	O4-N5-O5	120.2(2)
C8-C9	1.400(3)	$N4^1$-Zn-N1	90.10(7)	O5-N5-O3	119.5(2)

Table 2.8: Selected torsion angles (°) for compound **5**.

Zn1-N1-C1-C2	-167.76(19)	C5-C4-C6-N2	125.1(2)
Zn1-N1-C5-C4	166.28(17)	C6-N2-C7-C8	15.6(3)
Zn1[1]-N4-C17-C16	166.2(2)	C6-N2-C7-C12	-165.9(2)
Zn1[1]-N4-C18-C14	-166.84(17)	C6-C4-C5-N1	-177.5(2)
N1-C1-C2-C3	1.1(4)	C7-N2-C6-C4	-88.2(3)
N2-C7-C8-C9	177.3(2)	C8-C9-C10-N3	177.9(2)
N2-C7-C12-C11	-177.4(2)	C10-N3-C13-C14	85.0(3)
N3-C10-C11-C12	-177.9(2)	C13-N3-C10-C9	0.0(4)
N3-C13-C14-C15	-147.0(2)	C13-N3-C10-C11	177.8(2)
N3-C13-C14-C18	35.6(3)	C13-C14-C18-N4	177.5(2)
C1-N1-C5-C4	-2.6(3)	C15-C14-C18-N4	-0.1(3)
C3-C4-C5-N1	2.0(3)	C15-C16-C17-N4	0.5(4)
C3-C4-C6-N2	-54.3(3)	C17-N4-C18-C14	1.5(3)
C5-N1-C1-C2	1.1(3)	C18-N4-C17-C16	-1.7(4)

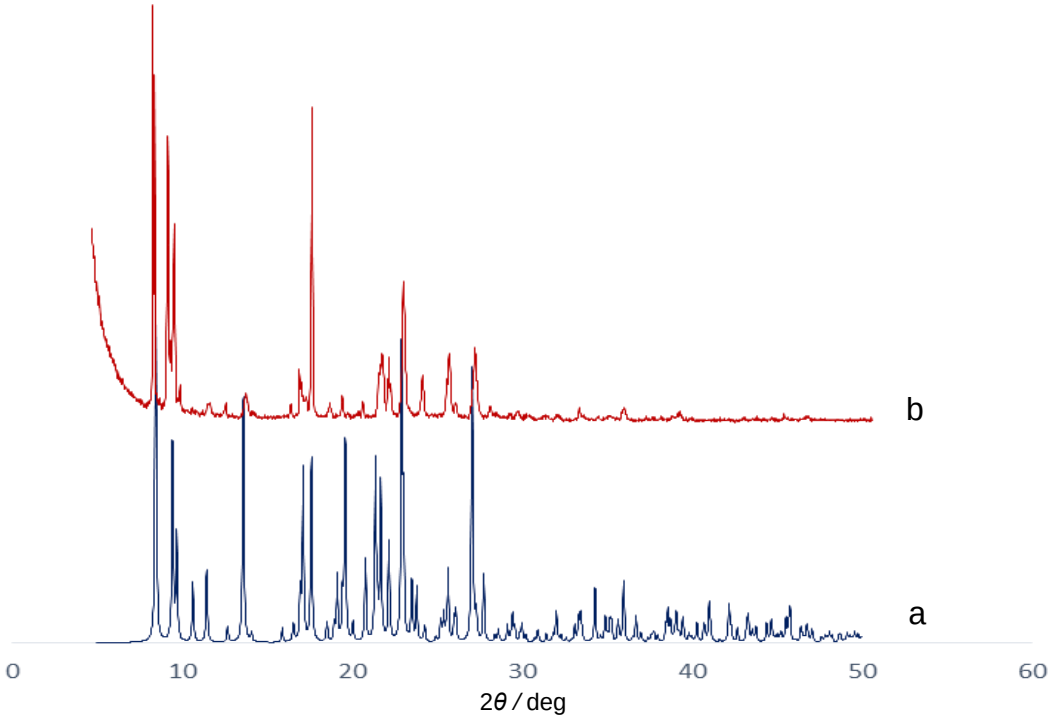

Figure 2.22: (a) Calculated powder X-ray pattern of compound **5**. (b) Powder XRD pattern of compound **5**.

2.5.5 Crystal structure of $([Cd(L1)_2(NO_3)_2])_n$ coordination polymer (6)

$([Cd(L1)_2(NO_3)_2])_n$ crystal structure was solved in triclinic space group $P\bar{1}$ [62-66] and shows two L1 ligand molecules, one cadmium(II) ion on a general position and two coordinated nitrate ions per asymmetric unit (figure 2.23). Cd(II) is coordinated to four L1 ligand molecules and shows four coordination distances (Cd-N1= 2.399(2) Å), (Cd-N4= 2.313(2) Å), (Cd-N5= 2.418(2) Å) and (Cd-N8= 2.308(2) Å). Cd(II) is also coordinated to two nitrate ions in a *trans*

arrangement with two different coordination styles. In the first coordinated style, the nitrate anion behaves as a bidentate ligand and shows two M-O coordination distances (Cd-O1= 2.644(2) Å) and (Cd-O2= 2.572(2) Å). Whereas in the second coordinated style, the nitrate anion behaves as a monodentate ligand and shows one coordination distance of 2.527(2) Å for Cd-O4 to produce Cd(II) distorted pentagonal bipyramidal coordination centres (figure 2.24). In 2013 Wan and co-workers [102] reported a crystal structure based on Cd(II) nitrate and 2,6-pyridinediylbis(3-pyridinyl)-methanone that shows coordination bond lengths between 2.359(2)-2.383(2) Å for Cd-N and 2.403(2) or 2.431(2) Å for Cd-O. Shanmugaraju et al. [103] reported a crystal structure based on Cd(II) nitrate and (bis-[*N*-(3-pyridyl)methyl)]-9,18-methano-1,8-naphthalimide-[b,f][1,5]diazocine that shows coordination bond lengths from 2.398(5) to 2.327(5) Å for Cd-N and 2.305(6) Å for Cd-O.

The ligand L1 is coordinated to two different Cd(II) coordination centres by nitrogen atoms of 3-pyridyl rings and shows four torsion angles of -150.0(2), 82.6(3), -174.0(2) and -64.2(3) ° between the phenyl and 3-pyridyl substituted rings to produce L1 bent S-shape figure 2.23 and table 2.10. Four L1 ligand molecules are coordinated to four Cd(II) coordination centres to produce M_4-$(L1)_4$ rhombic structure that expand to produce the two-dimensional network. The resulted two-dimensional network shows 15.925 × 13.744 Å sides and 13.066 × 26.726 Å diagonals between Cd(II) coordination centres. Furthermore, the resulted 2D network has 4^4 topology and 5.844 × 13.744 Å rhombic cavities that occupied by Cd(II) coordination centre from another two-dimensional network figures 2.24 and 2.25. Powder X-ray analysis for compound **6** showed a good match between calculated and experimental patterns which indicates phase purity and material stability (figure 2.26). Selected bond lengths, angles and torsion angles for compound **6** are listed in tables 1.9 and 1.10.

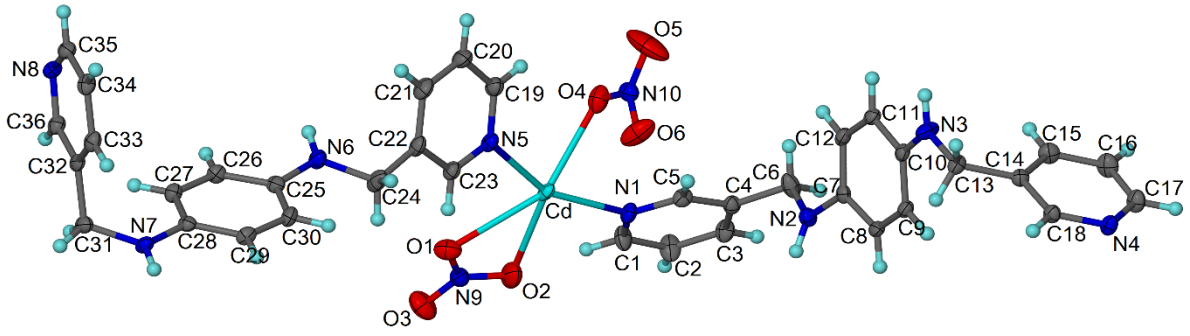

Figure 2.23: $([Cd(L1)_2(NO_3)_2])_n$ CP asymmetric unit of the crystal structure. Ellipsoids shown at 50 % probability levels.

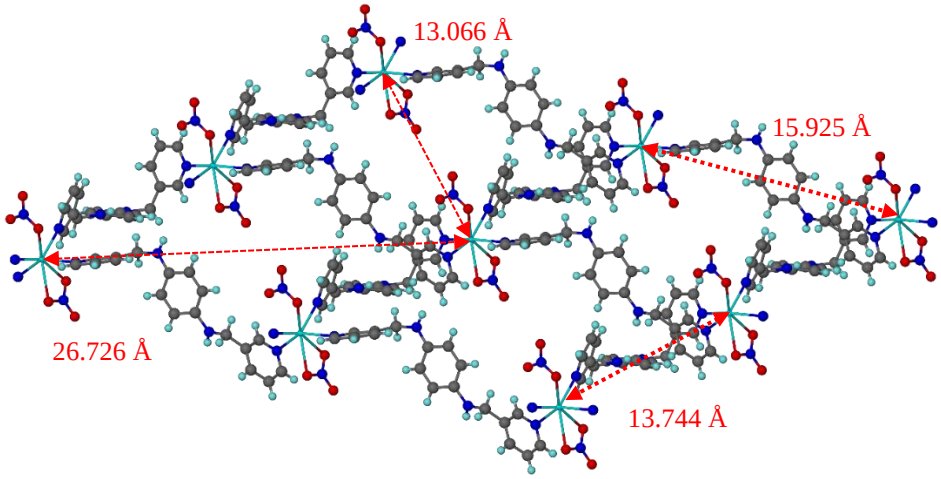

Figure 2.24: $([Cd(L1)_2(NO_3)_2])_n$ two-dimensional network which has 15.925 × 13.744 Å sides and 13.066 × 26.726 Å diagonals between Cd(II) coordination centres.

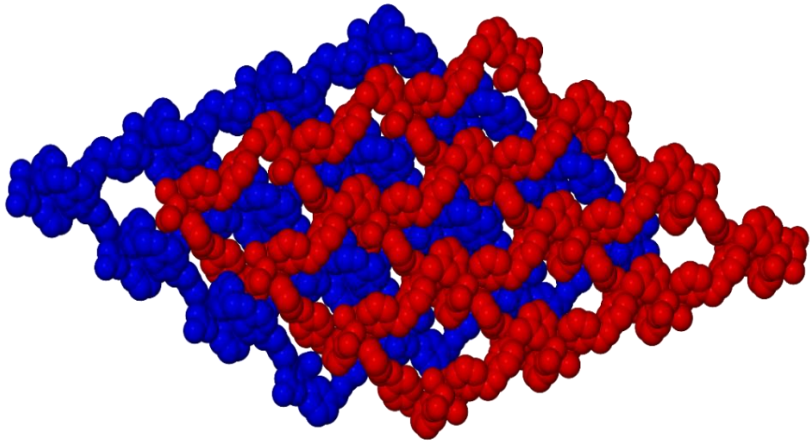

Figure 2.25: Packing diagram of $([Cd(L1)_2(NO_3)_2])_n$ CP.

Table 2.9: Selected bond lengths (Å) and angles (°) for compound **6**.

Cd-O1	2.644(2)	O2-Cd-O1	48.44(6)	N8-Cd-O1	82.42(7)
Cd-O2	2.572(2)	O4-Cd-O1	149.90(6)	N8-Cd-O2	89.53(8)
Cd-O4	2.527(2)	O4-Cd-O2	143.81(7)	N8-Cd-O4	117.94(7)
Cd-N1	2.399(2)	N1-Cd-O1	124.71(7)	N8-Cd-N1	95.76(7)
Cd-N4	2.313(2)	N1-Cd-O2	76.37(7)	N8-Cd-N4	162.02(8)
Cd-N5	2.418(2)	N1-Cd-O4	77.73(7)	N8-Cd-N5	85.97(7)
Cd-N8	2.308(2)	N1-Cd-N5	157.06(8)	C7-N2-C6	121.6(2)
N2-C6	1.451(3)	N4-Cd-O1	80.03(7)	N2-C6-C4	110.3(2)
N2-C7	1.402(3)	N4-Cd-O2	81.74(8)	N3-C13-C14	114.1(2)
N3-C10	1.383(3)	N4-Cd-O4	77.00(7)	C10-N3-C13	123.2(2)
N3-C13	1.436(3)	N4-Cd-N1	97.39(7)	N6-C24-C22	111.1(2)
N6-C24	1.457(3)	N4-Cd-N5	86.68(7)	C25-N6-C24	117.9(2)
N6-C25	1.409(3)	N5-Cd-O1	78.23(7)	C28-N7-C31	119.4(2)
N7-C28	1.412(3)	N5-Cd-O2	126.57(7)	N7-C31-C32	113.9(2)
N7-C31	1.463(3)	N5-Cd-O4	81.26(7)		

Table 2.10: Selected torsion angles (°) for compound **6**.

Cd-O1-N9-O2	13.0(2)	N7-C28-C29-C30	179.0(2)
Cd-O1-N9-O3	-168.0(2)	N7-C31-C32-C33	-61.0(3)
Cd-O2-N9-O1	-13.4(2)	N7-C31-C32-C36	118.0(3)
Cd-O2-N9-O3	167.5(2)	C3-C4-C6-N2	-114.3(3)
Cd-O4-N10-O5	-164.6(2)	C6-N2-C7-C8	-155.6(2)
Cd-O4-N10-O6	13.6(3)	C6-N2-C7-C12	30.6(3)
Cd-N1-C1-C2	176.4(2)	C7-N2-C6-C4	-150.0(2)
Cd-N1-C5-C4	-174.91(19)	C8-C9-C10-N3	176.1(2)
Cd-N4-C17-C16	-171.6(2)	C10-N3-C13-C14	82.6(3)
Cd-N4-C18-C14	170.60(18)	C13-N3-C10-C9	-2.5(4)
Cd-N5-C19-C20	-179.5(2)	C13-N3-C10-C11	177.3(2)
Cd-N5-C23-C22	179.56(19)	C21-C22-C24-N6	56.1(4)
Cd-N8-C35-C34	-173.94(18)	C23-C22-C24-N6	-125.7(3)
Cd-N8-C36-C32	172.24(18)	C24-N6-C25-C26	-165.1(2)
N2-C7-C8-C9	-169.9(2)	C24-N6-C25-C30	18.9(4)
N2-C7-C12-C11	170.7(2)	C25-N6-C24-C22	-174.0(2)
N3-C10-C11-C12	-175.0(2)	C26-C27-C28-N7	-178.9(2)
N3-C13-C14-C15	7.8(3)	C28-N7-C31-C32	-64.2(3)
N3-C13-C14-C18	-175.0(2)	C31-N7-C28-C27	-13.2(3)
N6-C25-C26-C27	-173.8(2)	C31-N7-C28-C29	169.6(2)
N6-C25-C30-C29	173.6(2)		

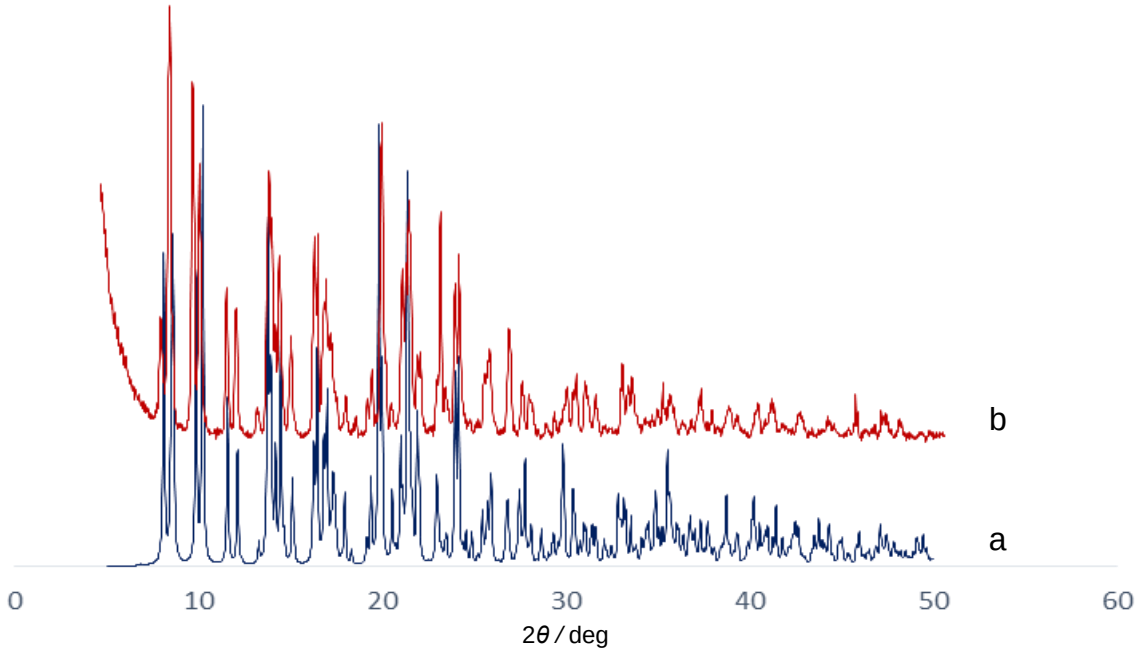

Figure 2.26: (a) Calculated powder XRD pattern of compound **6**. (b) Powder XRD pattern of compound **6**.

2.5.6 Crystal structure of $([Cd(L1)_{0.5}(isoph)(DMF)])_n$ compound (7)

Crystal structure of $([Cd(L1)_{0.5}(isoph)(DMF)])_n$ MOF was solved in monoclinic space group $P2_1/n$ [62-66] and shows one cadmium(II) ion on a general position, one isophthalate anion, half L1 ligand molecule and one coordinated DMF molecule per asymmetric unit (figure 2.27). Cd(II) ion is coordinated to four oxygen atoms from three different isophthalate molecules and shows four M-O coordination distances (Cd-O1= 2.324(2) Å), (Cd-O2= 2.480(2) Å), (Cd-$O2^1$= 2.356(2) Å) and (Cd1-O3= 2.220(2) Å). Cd(II) ion is also coordinated to one DMF molecule (Cd-O5= 2.293(3) Å), and one L1 ligand molecule (Cd-N1= 2.323(3) Å) on axial positions to produce Cd(II) distorted octahedral coordination centres. Each isophthalate anion behaves as a tetra-dentate ligand by the deprotonated carboxylate groups to three Cd(II) coordination centres. One of the carboxylate groups behaves as a tridentate ligand to two Cd(II) metal centres and shows three M-O bond length (Cd-O1= 2.324(2) Å), (Cd-O2= 2.480(2) Å) and (Cd-$O2^1$= 2.356(2) Å). The other carboxylate group behaves as a monodentate ligand and shows one M-O bond length (Cd-O3= 2.220(2) Å). The resulted Cd(II) and isophthalate two-dimensional network shows 3^6 topology and approximately 10.997 × 13.031 Å sides between Cd(II) coordination centres (figure 2.28). To the best of our knowledge and according to CCDC the coordination style between isophthalate molecules and Cd(II) ions in compound **7** was not reported before although a high number of examples based on Cd(II) and isophthalate were reported before [104-113]. Other common coordination styles between Cd(II) and isophthalate ion shows that the first carboxylate group behaves as a bidentate ligand to one Cd(II) ion and the second carboxylate group behaves either as a mono-dentate ligand to one Cd(II) or as a bidentate ligand to two Cd(II) coordination centres [104-115].

The ligand L1 behaves as bidentate ligand by nitrogen atoms of the 3-pyridyl rings and linking between two different Cd(II)-$isoph^{2-}$ two-dimensional networks (Cd-L1-Cd= 13.404 Å). L1 ligand shows torsion angle of -56.4 ° between the phenyl and 3-pyridyl rings to produce L1 bent S-shape (figure 2.30) and (table 2.12). Moreover, the crystal structure shows 8.017 Å as the closest distance between two different Cd(II)-isophthalate 2D coordination networks (figure 2.31). The resulted MOF structure is not porous along the three axes because of $isoph^{2-}$ coordination angles and the L1 ligand bent S-shape between Cd(II) coordination centres. Powder X-ray analysis of compound **7** shows a good match between calculated and experimental patterns which indicates phase purity and the new MOF stability (figure 2.32). Selected bond lengths, angles and torsion angles for compound **7** are listed in tables 2.11 and 2.12.

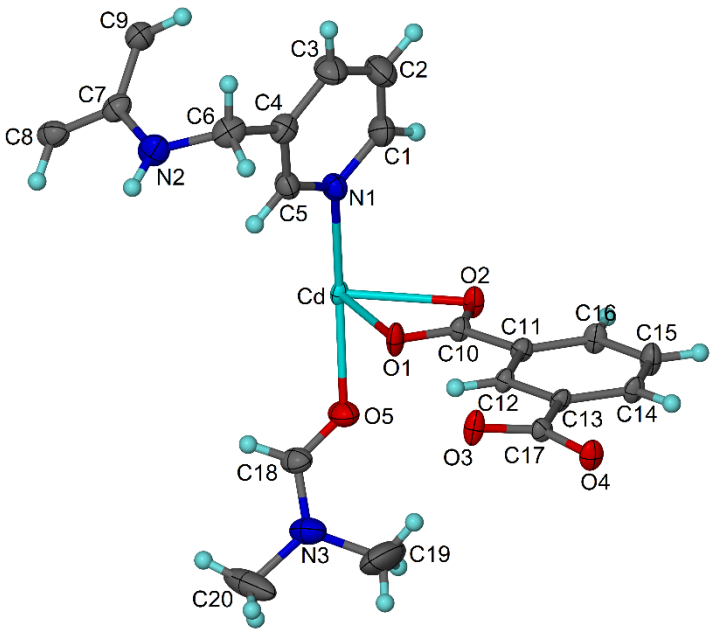

Figure 2.27: $([Cd(L1)_{0.5}(isoph)(DMF)])_n$ MOF asymmetric unit of the crystal structure. Ellipsoids shown at 50 % probability levels.

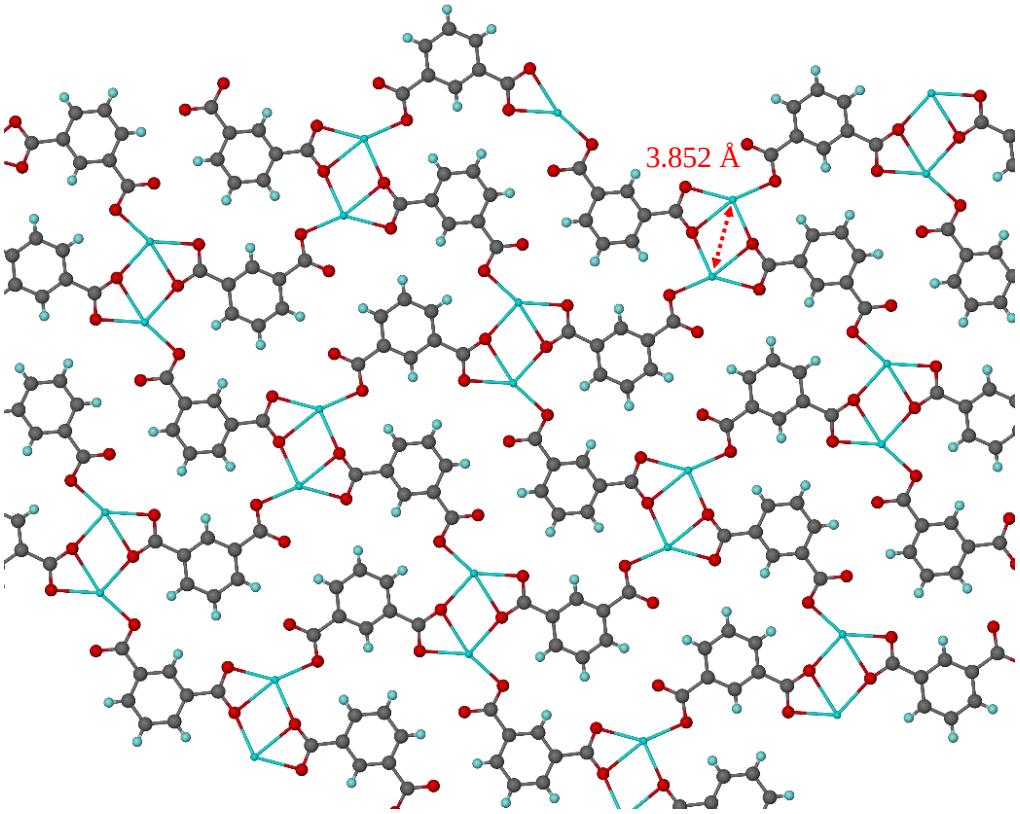

Figure 2.28: Cd(II) and isophthalate 2D network top view (Cd to Cd= 3.852 Å).

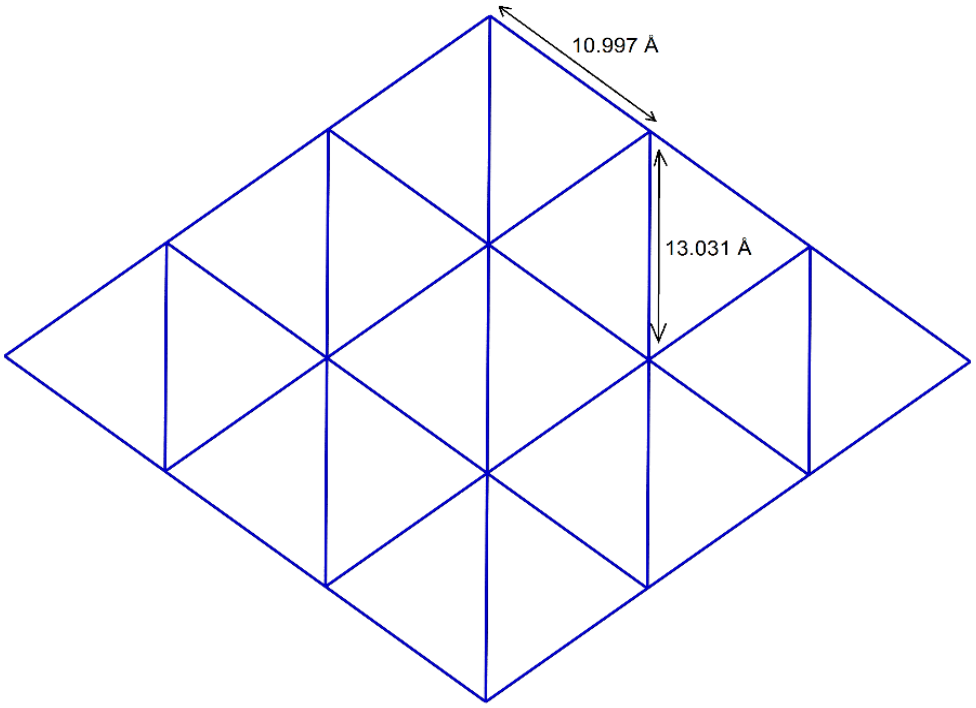

Figure 2.29: Cd(II) and isophthalate two-dimensional network which has approximately 10.997 × 13.031 Å sides between Cd(II) dimeric coordination centres and shows 3^6 network topology.

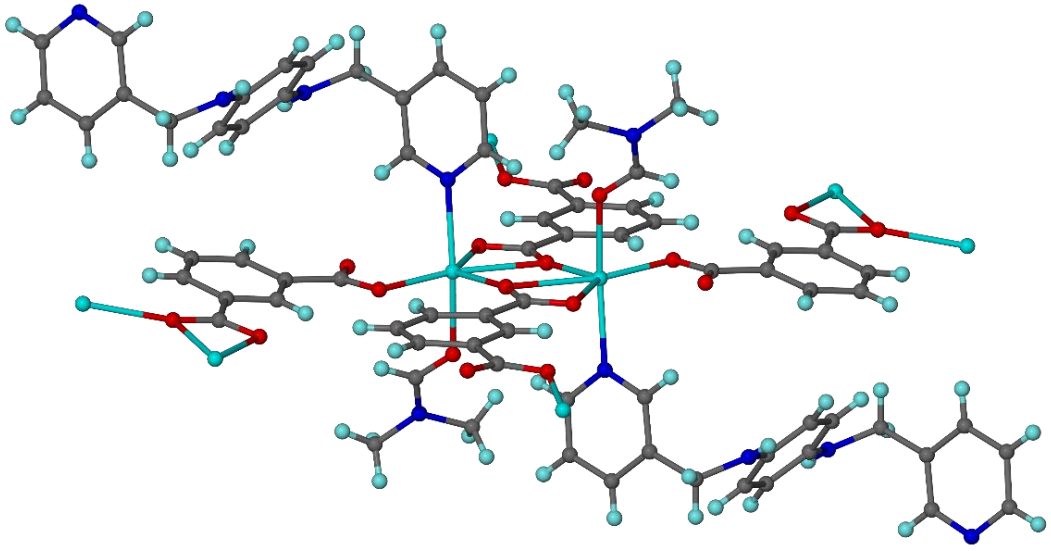

Figure 2.30: $([Cd(L1)_{0.5}(isoph)(DMF)])_n$ MOF after highlighting coordination environment of Cd(II).

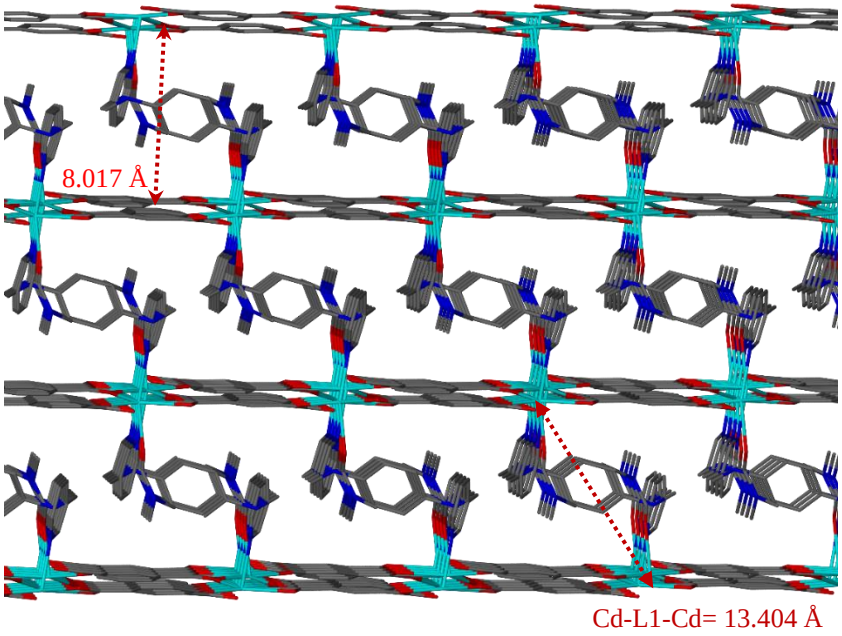

Figure 2.31: $([Cd(L1)_{0.5}(isoph)(DMF)])_n$ MOF after symmetrical expanding, L1 ligand is connecting between two different Cd(II)-$isoph^{2-}$ networks.

Table 2.11: Selected bond lengths (Å) and angles (°) for compound **7**.

Cd-O1	2.324(2)	O5-Cd-O2	86.78(10)
Cd-$O2^1$	2.356(2)	O5-Cd-$O2^1$	101.29(10)
Cd-O2	2.480(2)	O5-Cd-N1	162.14(11)
Cd-$O3^1$	2.220(2)	N1-Cd-O1	82.02(11)
Cd-O5	2.293(3)	N1-Cd-$O2^1$	94.92(11)
Cd-N1	2.323(3)	N1-Cd-O2	90.43(10)
O1-C10	1.251(4)	C10-O1-Cd	95.8(2)
O2-Cd^1	2.356(2)	Cd^1-O2-Cd	105.59(9)
O2-C10	1.275(4)	C10-O2-Cd	87.9(2)
O3-Cd^1	2.220(2)	C10-O2-Cd^1	165.4(2)
O3-C17	1.273(4)	C17-O3-Cd^1	105.3(2)
O4-C17	1.249(4)	C18-O5-Cd	127.3(3)
O5-C18	1.222(5)	C1-N1-Cd	124.6(3)
N1-C1	1.337(5)	C1-N1-C5	117.0(4)
N1-C5	1.339(5)	C5-N1-Cd	118.0(3)
N2-C6	1.455(6)	C7-N2-C6	120.3(4)
N2-C7	1.397(5)	N2-C6-C4	114.9(3)
O1-Cd-O2	54.56(8)	N2-C7-C9	122.0(4)
O1-Cd-$O2^1$	128.74(9)	C8-C7-N2	120.0(4)
$O2^1$-Cd-O2	74.41(9)	O1-C10-O2	121.7(3)
$O3^1$-Cd-O1	140.48(9)	O1-C10-C11	118.1(3)
$O3^1$-Cd-O2	164.56(9)	O2-C10-C11	120.2(3)
$O3^1$-Cd-$O2^1$	90.77(9)	O3-C17-C13	117.0(3)
$O3^1$-Cd-O5	92.03(11)	O4-C17-O3	122.9(3)
$O3^1$-Cd-N1	95.23(11)	O4-C17-C13	120.2(3)
O5-Cd-O1	82.00(11)	O5-C18-N3	125.3(4)

Table 2.12: Selected torsion angles (°) for compound **7**.

Cd-O1-C10-O2	-0.8(4)	N1-C1-C2-C3	1.4(7)
Cd-O1-C10-C11	178.9(3)	N2-C7-C8-C9[1]	176.9(4)
Cd-O2-C10-O1	0.8(4)	N2-C7-C9-C8[1]	-176.8(4)
Cd[1]-O2-C10-O1	159.0(8)	C3-C4-C6-N2	130.9(4)
Cd[1]-O2-C10-C11	-20.7(12)	C5-N1-C1-C2	-2.5(6)
Cd-O2-C10-C11	-178.9(3)	C5-C4-C6-N2	-48.4(6)
Cd[2]-O3-C17-O4	8.2(4)	C6-N2-C7-C8	165.2(4)
Cd[2]-O3-C17-C13	-171.9(2)	C6-N2-C7-C9	-18.4(6)
Cd-O5-C18-N3	-155.2(3)	C7-N2-C6-C4	-56.4(5)
Cd-N1-C1-C2	-174.3(4)	C12-C13-C17-O3	-7.7(5)
Cd-N1-C5-C4	173.1(3)	C12-C13-C17-O4	172.1(3)
O1-C10-C11-C12	1.0(5)	C14-C13-C17-O3	169.7(3)
O1-C10-C11-C16	-178.0(4)	C14-C13-C17-O4	-10.5(5)
O2-C10-C11-C12	-179.3(3)	C19-N3-C18-O5	6.0(8)
O2-C10-C11-C16	1.7(5)	C20-N3-C18-O5	-173.4(5)

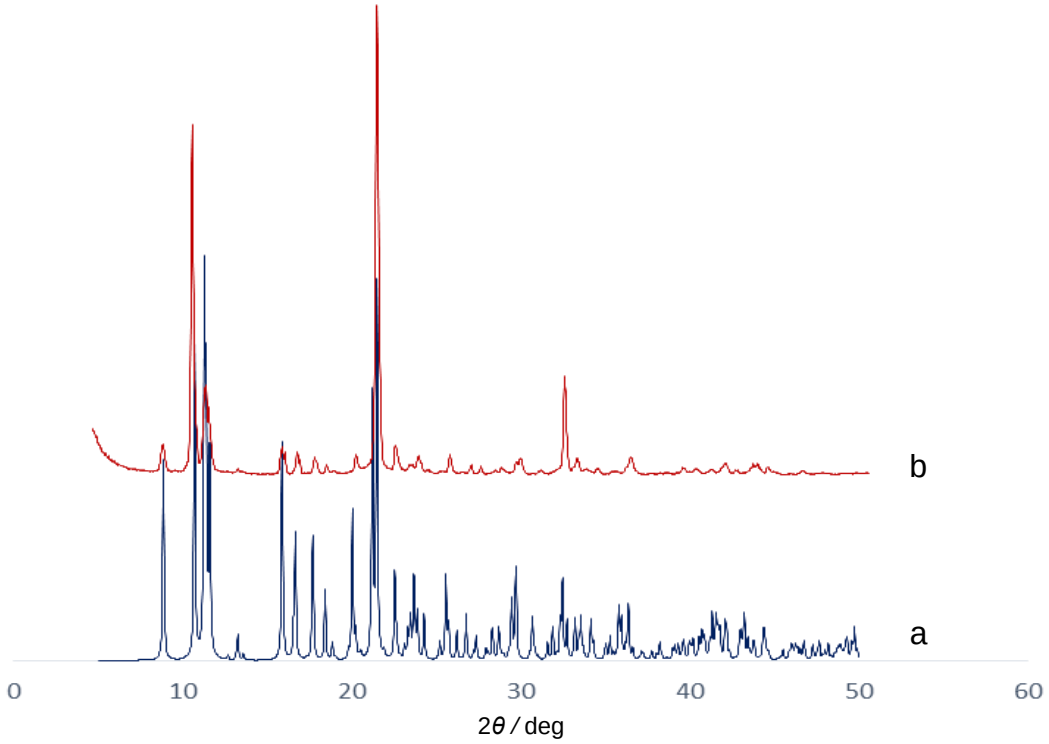

Figure 2.32: (a) Calculated powder XRD pattern of compound **7**. (b) Powder XRD pattern of compound **7**.

2.5.7 Crystal structure of $([Cd_{1.5}(L1)_{0.5}(bdc)_{1.5}(DMF)])_n$ MOF (8)

$([Cd_{1.5}(L1)_{0.5}(bdc)_{1.5}(DMF)])_n$ MOF crystal structure was solved in monoclinic space group $P2_1/n$ [62-66] and display one and a half of bdc^{2-} molecules, half of L1 ligand molecule, one cadmium(II) ion on a general position, half of Cd(II) ion on an inversion centre and one coordinated DMF molecule per asymmetric unit (figure 2.33). Cd1 is coordinated to four oxygen atoms from three different bdc^{2-} molecules and shows four M-O coordination bond lengths (Cd1-O2= 2.230(2) Å), (Cd1-O3= 2.253(2) Å), (Cd1-O6= 2.385(2) Å) and (Cd1-O7= 2.351(2) Å). Cd1 is also coordinated to an oxygen atom from a DMF solvent molecule (Cd1-O5= 2.399(2) Å), in addition to one nitrogen atom from L1 ligand molecule (Cd1-N1= 2.301(3) Å) to produce Cd1 distorted octahedral coordination centres. Cd2 is coordinated to six oxygen atoms from six different bdc^{2-} molecules and shows three M-O bond lengths (Cd2-O1= 2.198(2) Å), (Cd2-O4= 2.291(2) Å) and (Cd2-O6= 2.292(2) Å) to produce Cd2 distorted octahedral coordination centres.

Each bdc^{2-} molecule behaves as a penta-dentate ligand and coordinated to four Cd(II) coordination centres by the deprotonated carboxylate groups. One of the carboxylate groups behaves as a bidentate ligand to two Cd(II) metal centres and shows four M-O bond lengths (Cd1-O2= 2.230(2) Å), (Cd1-O3= 2.253(2) Å), (Cd2-O1= 2.198(2) Å) and (Cd2-O4= 2.291(2) Å). The other carboxylate group behaves as a tridentate ligand to two Cd(II) metal centres and shows three M-O bond lengths (Cd1-O6= 2.385(2) Å), (Cd1-O7= 2.351(2) Å) and (Cd2-O6= 2.292(2) Å). The resulted Cd(II) and bdc^{2-} two-dimensional network has 3^6 topology and shows approximately 6.6 × 10.4 Å distances between Cd(II) linear trimeric coordination centres (figure 2.35).

A similar MOF based on Cd(II), bdc^{2-} and *N*,*N*-(oxybis(4,1-phenylene))bis(1-(pyridin-4-yl)-methanimine) was reported in 2017 by Rouhani et. al [114]. Each bdc^{2-} is coordinated to four Cd(II) coordination centres by the deprotonated carboxylate groups and shows two different coordination styles. In the first coordination style the deprotonated carboxylate groups behaves as a tridentate ligand to two Cd(II) coordination centres and show three M-O bond lengths of 2.389(8), 2.479(8) and 2.292(8) Å. In the second coordination style the first carboxylate group behaves as a bidentate ligand to two Cd(II) ions Cd-O= 2.282(8)-2.209(8) Å. Whereas the second carboxylate group behaves as a tridentate ligand to two Cd(II) coordination centres and shows three M-O coordination bond lengths of 2.342(7), 2.475(8) and 2.405(7) [114]. Another Cd(II) and bdc^{2-} linear trimeric MOF was reported in 2015 by Wang et. al [115]. The bdc^{2-} is coordinated to four Cd(II) coordination centres by the deprotonated carboxylate groups. The first carboxylate group behaves as a bidentate ligand to two Cd(II)

centres and the second carboxylate group behaves as a tridentate ligand to two Cd(II) coordination centres (M-O= 2.184(3)-2.515(3) Å) [115].

The ligand L1 behaves as a bidentate ligand by nitrogen atoms of 3-pyridyl rings and coordinated to two linear trimeric Cd(II) coordination centres from two different Cd(II)-bdc^{2-} 2D networks (Cd1-L1-Cd1= 12.393 Å) (figure 2.38). The ligand L1 shows torsion angle of 84.0(4) ° between the phenyl and 3-pyridyl rings to produce L1 bent S-shape between Cd(II) coordination centres (table 2.14). $([Cd_{1.5}(L1)_{0.5}(bdc)_{1.5}(DMF)])_n$ MOF is not porous along *a*, *b* or *c* axes, because of bdc^{2-} coordination angles and L1 bent S-shape between coordination centres. Furthermore, powder X-ray analysis for compound **8** shows a good match between calculated and experimental patterns which indicate phase purity and the new MOF stability (figure 2.39). Selected bond lengths, angles and torsion angles for compound **8** are listed in tables 2.13 and 2.14.

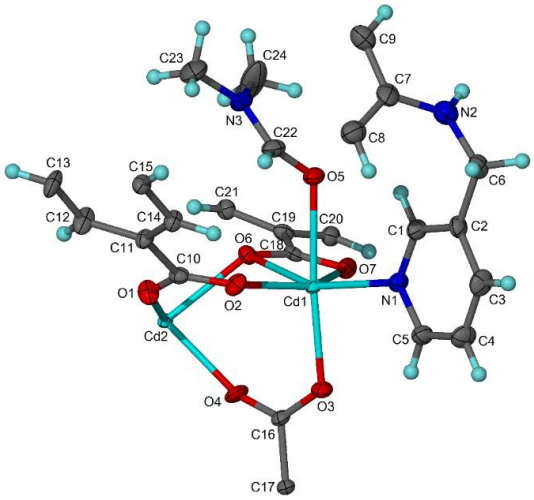

Figure 2.33: $([Cd_{1.5}(L1)_{0.5}(bdc)_{1.5}(DMF)])_n$ MOF asymmetric unit of the crystal structure. Ellipsoids shown at 50 % probability levels (Cd1 to Cd2= 3.763 Å).

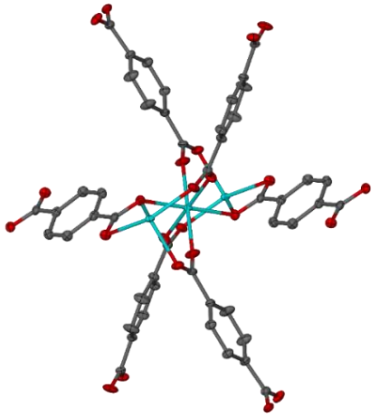

Figure 2.34: Cd(II)-bdc^{2-} linear trimeric coordination centres.

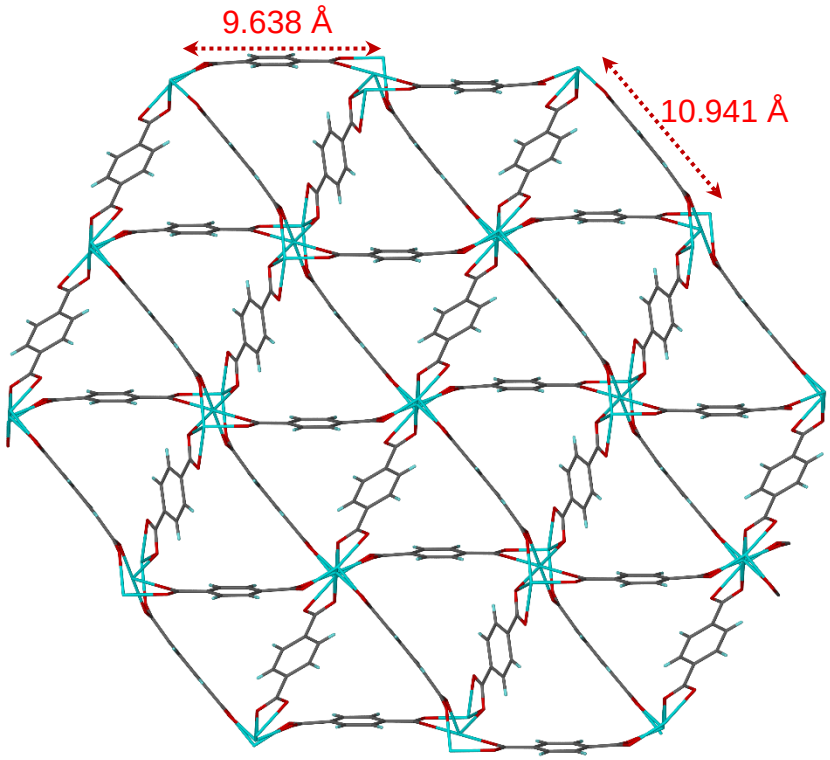

Figure 2.35: Cd(II)-bdc^{2-} two-dimensional network which has approximately 6.638 × 10.491 Å sides between Cd(II) trimeric coordination centres.

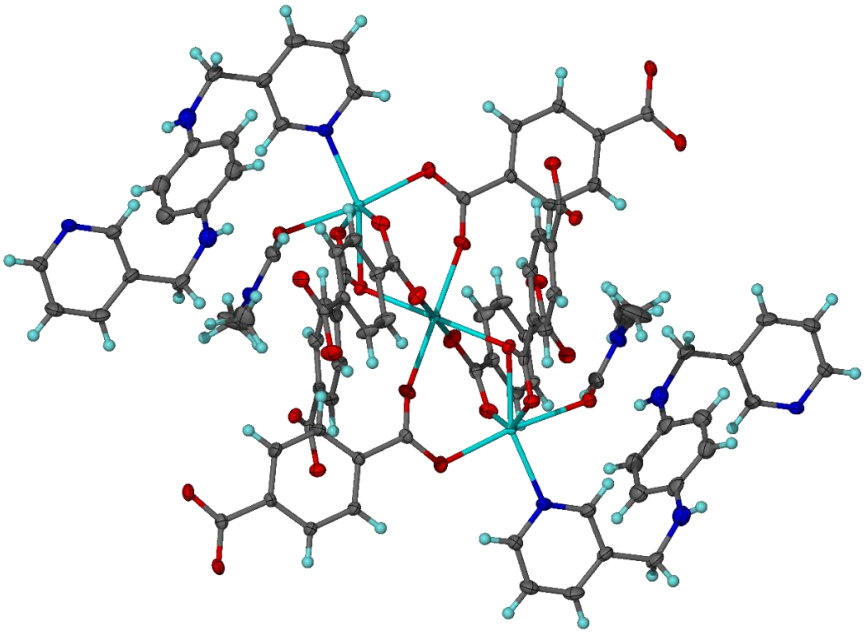

Figure 2.36: $([Cd_{1.5}(L1)_{0.5}(bdc)_{1.5}(DMF)])_n$ MOF coordination environment.

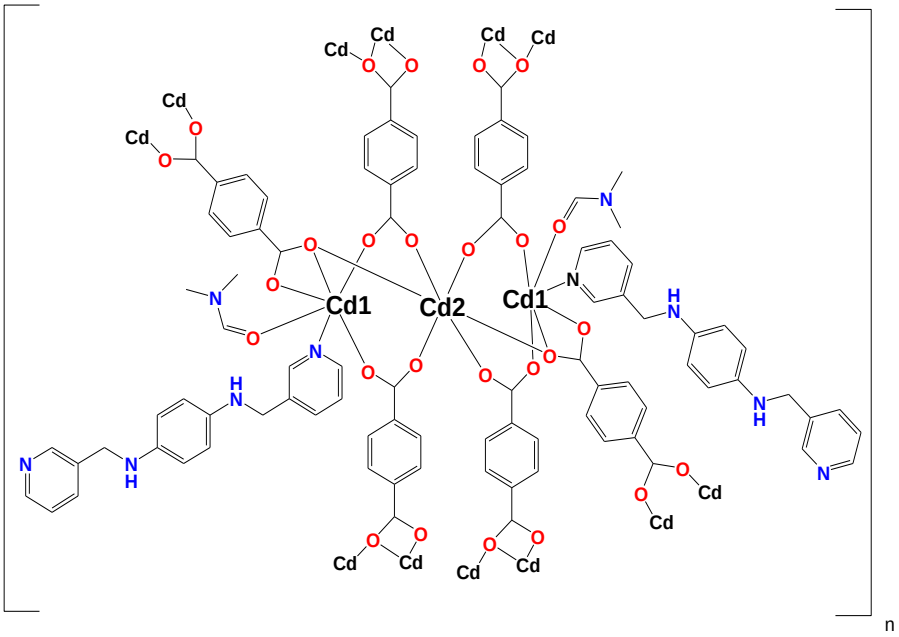

Figure 2.37: Chemdraw of $([Cd_{1.5}(L1)_{0.5}(bdc)_{1.5}(DMF)])_n$ MOF showing the ligands bridging mode.

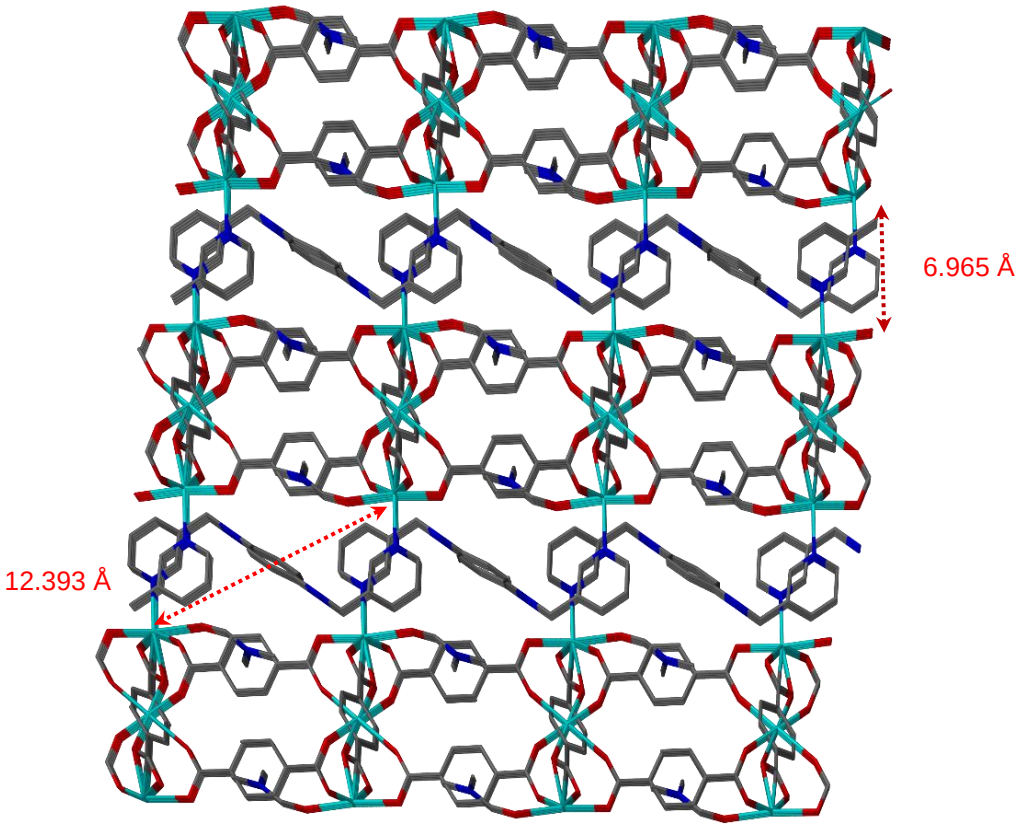

Figure 2.38: $([Cd_{1.5}(L1)_{0.5}(bdc)_{1.5}(DMF)])_n$ MOF after symmetrical expanding, L1 ligand is connecting between two trimeric Cd(II) coordination centres (Cd1-L1-Cd1= 12.393 Å). The closest distance between two Cd(II)-bdc^{2-} networks is 6.965 Å.

Table 2.13: Selected bond lengths (Å) and angles (°) for compound **8**.

Cd1-O2	2.230(2)	O7- Cd1-O6	55.70(7)
Cd1-O3	2.253(2)	N1- Cd1-O5	84.91(8)
Cd1-O5	2.399(2)	N1- Cd1-O6	156.27(8)
Cd1-O6	2.385(2)	N1- Cd1-O7	107.82(8)
Cd1-O7	2.351(2)	O1- Cd2-O1^{1}	180.0
Cd1-N1	2.301(3)	O1- Cd2-O4^{1}	85.83(9)
Cd2-O1	2.198(2)	O1^{1}- Cd2-O4^{1}	94.16(9)
Cd2-O4	2.291(2)	O1- Cd2-O4	94.17(9)
Cd2-O6	2.292(2)	O1^{1}- Cd2-O4	85.83(9)
C6-N2	1.445(5)	O1^{1}- Cd2-O6	93.23(8)
O2- Cd1-O3	94.60(8)	O1- Cd2-O6^{1}	93.23(8)
O2- Cd1-O5	86.34(8)	O1^{1}- Cd2-O6^{1}	86.76(7)
O2- Cd1-O6	92.17(7)	O1- Cd2-O6	86.77(7)
O2- Cd1-O7	147.82(7)	O4^{1}- Cd2-O4	180.0
O2- Cd1-N1	102.03(9)	O4- Cd2-O6^{1}	95.39(8)
O3- Cd1-O5	173.42(8)	O4^{1}- Cd2-O6	95.39(8)
O3- Cd1-O6	109.39(7)	O4- Cd2-O6	84.61(8)
O3- Cd1-O7	97.87(8)	O4^{1}- Cd2-O6^{1}	84.61(8)
O3- Cd1-N1	88.53(9)	O6- Cd2-O6^{1}	180.0(10)
O6- Cd1-O5	77.05(7)	C2-C6-N2	114.7(3)
O7- Cd1-O5	84.61(7)	C6-N2-C7	122.0(3)

Table 2.14: Selected torsion angles (°) for compound **8**.

Cd1-O2-C10-O1	35.9(4)	Cd2-O1-C10-C11	158.2(2)
Cd1-O2-C10-C11	-142.7(2)	Cd2-O4-C16-O3	-18.5(9)
Cd1-O3-C16-O4	-1.4(4)	Cd2-O4-C16-C17	161.5(5)
Cd1-O3-C16-C17	178.56(19)	Cd2-O6-C18-O7	-110.9(3)
Cd1-O5-C22-N3	-129.1(3)	Cd2-O6-C18-C19	71.3(3)
Cd1-O6-C18-O7	1.3(3)	N2-C7-C8-C9^{1}	-179.2(3)
Cd1-O6-C18-C19	-176.6(2)	N2-C7-C9-C8^{1}	179.2(3)
Cd1-O7-C18-O6	-1.3(3)	C1-C2-C6-N2	6.6(5)
Cd1-O7-C18-C19	176.6(2)	C3-C2-C6-N2	-172.5(3)
Cd1-N1-C1-C2	164.7(3)	C6-N2-C7-C8	-11.5(5)
Cd1-N1-C5-C4	-164.3(3)	C6-N2-C7-C9	170.0(3)
Cd2-O1-C10-O2	-20.5(5)	C7-N2-C6-C2	84.0(4)

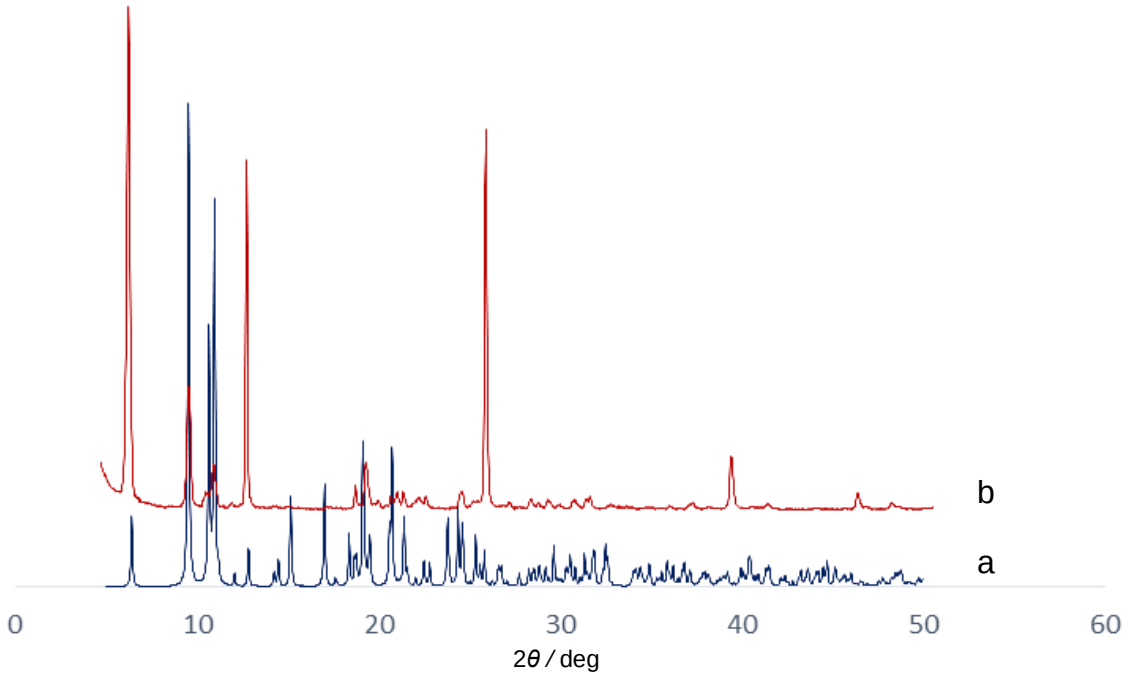

Figure 2.39: (a) Calculated powder XRD pattern of compound **8**. (b) Powder XRD pattern of compound **8**.

Table 2.15: Crystallographic data of compounds L1, **1** and **2**.

Identification code	L1	**1**	**2**
Empirical Formula	$C_{18}H_{18}N_4$	$C_{19}H_{22}ClMn_{0.5}N_4O$	$C_{19}H_{22}ClFe_{0.5}N_4O$
Formula weight	290	385.32	385.78
Temperature/*K*	120(2)	119.94(10)	120.00(10)
Crystal system	Monoclinic	Triclinic	Triclinic
Space group	$P2_1/c$	$P\bar{1}$	$P\bar{1}$
a/Å	9.5469(5)	7.9017(5)	7.8834(5)
b/Å	9.7629(3)	8.9877(5)	8.9901(6)
c/Å	8.8790(5)	14.6874(9)	14.6236(10)
α/°	90	80.117(5)	79.792(6)
β/°	116.961(6)	80.433(5)	80.415(6)
γ/°	90	64.594(6)	64.473(7)
Volume/Å^3	737.63(7)	923.19(11)	915.68(12)
Z	2	2	2
ρ_{calc}g/cm^3	1.307	1.386	1.333
μ/mm^{-1}	0.630	4.605	4.998
F(000)	308.0	403.0	364.0
Crystal size/mm^3	0.081 × 0.172 × 0.250	0.157 × 0.271 × 0.376	0.130 × 0.250 × 0.532
Radiation	Cu*Kα* (λ = 1.54184)	Cu*Kα* (λ = 1.54184)	Cu*Kα* (λ = 1.54184)
2*Θ* range for data collection/°	10.396 to 147.17	6.142 to 147.422	6.172 to 147.404
Index ranges	-7 ≤ h ≤ 10, -11 ≤ k ≤ 11, -10 ≤ l ≤ 8	-9 ≤ h ≤ 9, -10 ≤ k ≤ 8, -18 ≤ l ≤ 18	-8 ≤ h ≤ 9, -10 ≤ k ≤ 11, -16 ≤ l ≤ 18
Reflections collected	2164	6643	6677
Independent reflections	1231 [R_{int} = 0.0272, R_{sigma} = 0.0365]	3471 [R_{int} = 0.0279, R_{sigma} = 0.0342]	3443 [R_{int} = 0.0306, R_{sigma} = 0.0378]
Data/restraints/parameters	1231/0/100	3471/0/234	3443/0/234
Goodness-of-fit on F^2	1.299	1.034	1.044
Final *R* indexes [*I*>=2*σ* (*I*)]	R_1 = 0.0580, wR_2 = 0.1737	R_1 = 0.0440, wR_2 = 0.1164	R_1 = 0.0409, wR_2 = 0.1092
Final *R* indexes [all data]	R_1 = 0.0655, wR_2 = 0.1847	R_1 = 0.0460, wR_2 = 0.1190	R_1 = 0.0441, wR_2 = 0.1125
Largest diff. peak/hole / e Å^{-3}	0.64/-0.48	0.73/-0.53	0.57/-0.55

Table 2.16: Crystallographic data of compounds **3**, **4** and **5**.

Identification code	**3**	**4**	**5**
Empirical Formula	$C_{19}H_{22}ClCo_{0.5}N_4O$	$C_{19}H_{20}Cl_3CuN_4$	$C_{36}H_{40}N_{10}O_8Zn$
Formula weight	387.32	474	806.18
Temperature/*K*	119.94(10)	120.15	120(2)
Crystal system	Triclinic	Triclinic	Orthorhombic
Space group	$P\bar{1}$	$P\bar{1}$	*Pbcn*
a/Å	7.8730(5)	8.0301(14)	18.7029(5)
b/Å	8.9875(6)	8.7023(16)	9.2673(2)
c/Å	14.5708(10)	15.507(3)	20.8929(6)
α/°	92.034(6)	101.930(15)	90
β/°	99.236(6)	96.873(15)	90
γ/°	115.831(7)	108.503(16)	90
Volume/Å^3	909.49(12)	985.2(3)	3621.26(16)
Z	2	2	7
ρ_{calc}g/cm^3	1.414	1.599	1.479
μ/mm^{-1}	5.422	5.401	1.515
F(000)	405.0	484.0	1680.0
Crystal size/mm^3	0.093 × 0.153 × 0.175	0.059 × 0.125 × 0.143	0.101 × 0.131 × 0.456
Radiation	Cu*Kα* (λ = 1.54184)	Cu*Kα* (λ = 1.54184)	Cu*K*α (λ = 1.54184)
2*Θ* range for data collection/°	6.19 to 147.206	11.104 to 148.55	9.458 to 147.554
Index ranges	-9 ≤ h ≤ 8, -10 ≤ k ≤ 11, -15 ≤ l ≤ 18	-9 ≤ h ≤ 6, -8 ≤ k ≤ 10, -19 ≤ l ≤ 18	-15 ≤ h ≤ 22, -11 ≤ k ≤ 9, -21 ≤ l ≤ 25
Reflections collected	6414	7008	9323
Independent reflections	3410 [R_{int} = 0.0372, R_{sigma} = 0.0464]	3687 [R_{int} = 0.0768, R_{sigma} = 0.0943]	3571 [R_{int} = 0.0407, R_{sigma} = 0.0368]
Data/restraints/parameters	3410/0/234	3687/0/244	3571/0/252
Goodness-of-fit on F^2	1.052	1.041	1.037
Final *R* indexes [*I*>=2*σ* (*I*)]	R_1 = 0.0409, wR_2 = 0.0984	R_1 = 0.0806, wR_2 = 0.2017	R_1 = 0.0494, wR_2 = 0.1342
Final *R* indexes [all data]	R_1 = 0.0465, wR_2 = 0.1028	R_1 = 0.1060, wR_2 = 0.2292	R_1 = 0.0573, wR_2 = 0.1459
Largest diff. peak/hole / e Å^{-3}	0.55/-0.48	1.13/-0.77	0.66/-0.70

Table 2.17: Crystallographic data of compounds **6**, **7** and **8**.

Identification code	**6**	**7**	**8**
Empirical Formula	$C_{36}H_{36}CdN_{10}O_6$	$C_{20}H_{20}CdN_3O_5$	$C_{24}H_{22}Cd_{1.5}N_3O_7$
Formula weight	817	494.40	633.07
Temperature/*K*	120.00	120.03(16)	120.01(10)
Crystal system	Triclinic	Monoclinic	Monoclinic
Space group	$P\bar{1}$	$P2_1/n$	$P2_1/n$
a/Å	11.7212(5)	9.4255(2)	15.8305(5)
b/Å	13.0058(4)	13.0307(3)	9.6381(2)
c/Å	13.7443(5)	15.5713(3)	17.5237(5)
α/°	70.374(3)	90	90
β/°	87.500(3)	93.3942(19)	112.274(3)
γ/°	63.550(4)	90	90
Volume/Å^3	1752.90(13)	1909.13(7)	2474.18(13)
Z	3	4	4
ρ_{calc}g/cm^3	1.548	1.721	1.699
μ/mm^{-1}	5.512	9.502	10.843
F(000)	836.0	996.0	1260.0
Crystal size/mm^3	0.184 × 0.345 × 0.473	0.085 × 0.110 × 0.118	0.092 × 0.169 × 0.363
Radiation	Cu*Kα* (λ = 1.54184)	Cu*Kα* (λ = 1.54184)	Cu*Kα* (λ = 1.54184)
2*Θ* range for data collection/°	6.882 to 147.914	8.856 to 147.802	6.418 to 147.806
Index ranges	-14 ≤ h ≤ 13, -15 ≤ k ≤ 16, -14 ≤ l ≤ 16	-11 ≤ h ≤ 11, -14 ≤ k ≤ 16, -15 ≤ l ≤ 19	-16 ≤ h ≤ 19, -11 ≤ k ≤ 8, -21 ≤ l ≤ 20
Reflections collected	14298	7605	9674
Independent reflections	6615 [R_{int} = 0.0417, R_{sigma} = 0.0364]	3715 [R_{int} = 0.0315, R_{sigma} = 0.0431]	4833 [R_{int} = 0.0226, R_{sigma} = 0.0266]
Data/restraints/parameters	6615/0/478	3715/0/264	4833/0/324
Goodness-of-fit on F^2	1.031	1.044	1.032
Final *R* indexes [I>=2σ (I)]	R_1 = 0.0341, wR_2 = 0.0879	R_1 = 0.0311, wR_2 = 0.0699	R_1 = 0.0278, wR_2 = 0.0732
Final *R* indexes [all data]	R_1 = 0.0346, wR_2 = 0.0884	R_1 = 0.0448, wR_2 = 0.0757	R_1 = 0.0313, wR_2 = 0.0757
Largest diff. peak/hole / e Å^{-3}	0.99/-1.39	0.77/-0.72	1.37/-0.82

2.6 Conclusion

In conclusion, this chapter includes synthesis and characterisation of the new flexible ligand *N,N'*-bis-pyridin-3-ylmethyl-benzene-1,4-diamine (L1) as an organic linker with $MnCl_2.4H_2O$, $FeCl_3.6H_2O$, $CoCl_2.6H_2O$, $CuCl_2.2H_2O$, $Zn(NO_3)_2.6H_2O$, $Cd(NO_3)_2.4H_2O$, isophthalic acid (H_2-isoph) or benzene-1,4-dicarboxylic acid (H_2-bdc) to produce a series of new coordination polymers and metal-organic frameworks. $([Mn_{0.5}(L1)Cl].MeOH)_n$ (**1**), $([Fe_{0.5}(L1)Cl].MeOH)_n$ (**2**), $([Co_{0.5}(L1)Cl].MeOH)_n$ (**3**) and $([Cu(L1)Cl]\cdot CH_2Cl_2)_n$ (**4**) one-dimensional polymers; $([Zn(L1)(H_2O)_2].NO_3)_n$ (**5**) and $([Cd(L1)_2(NO_3)_2])_n$ (**6**) two-dimensional polymers; $([Cd(L1)_{0.5}(isoph)(DMF)])_n$ (**7**) and $([Cd_{1.5}(L1)_{0.5}(bdc)_{1.5}(DMF)])_n$ (**8**) three-dimensional polymers. Compounds **1-4** are homoleptic one-dimensional coordination polymers contains rectangle cavities of $M_2(L1)_2$ that occupied by solvents guest molecules. Compounds **5** and **6** are homoleptic MOFs containing M-shape or rhombic cavity consisting of four L1 ligand molecules and four Zn(II) or Cd(II) ions that extend to produce the two-dimensional network structures. Compound **5** resulted M-shape cavities occupied by nitrate anions, whereas compound **6** resulted rhombic cavities occupied by Cd(II) coordination centre from another two-dimensional network. On the other hand, compounds **7** and **8** are heteroleptic MOFs synthesised by solvothermal method in DMF with repeated structure of Cd(II)-isoph^{2-} or Cd(II)-bdc^{2-} networks that linked by L1 ligand molecules. Compounds **7** and **8** are not porous along *a*, *b* or *c* axes because of L1 ligand bent S-shape and Cd(II)-isoph^{2-} or Cd(II)-bdc^{2-} coordination angles. According to CCDC Cd(II)-isoph^{2-} coordination style in compound **7** was not reported before and compound **8** represent another rare example of Cd(II) linear trimeric heteroleptic MOF.

2.7 References

1. L. Wang, D. C. Tranca, J. Zhang, Y. Qi, S. Sfaelou, T. Zhang, R. Dong, X. Zhuang, Z. Zheng and G. Seifert, Toward Activity Origin of Electrocatalytic Hydrogen Evolution Reaction on Carbon-Rich Crystalline Coordination Polymers. *Small*. 2017, **13**(37), 1700783.
2. K. Vellingiria, L. Philipa and K. Kim, Metal-organic frameworks as media for the catalytic degradation of chemical warfare agents. *Coordination Chemistry Reviews*. 2017, **353**, 159-179.
3. S. E. H. Etaiw, A. S. Badr El-din and S. N. Abdou, Structure and catalytic activity of host-guest coordination polymers constructed from copper(I) cyanide nets and 1,4-diaminobutane or 1,5-diaminopentane in the presence of water. *Transition Metal Chemistry*. 2016, **41**(4), 413-425.
4. Q. Sun, Z. Dai, X. Menga and F. Xiao, Porous polymer catalysts with hierarchical structures. *Chemical Society Reviews*. 2015, **44**(17), 6018-6034.
5. D. X. Li, Z. G. Ren, D. J. Young and J. P. Lang, Synthesis of Two Coordination Polymer Photocatalysts and Significant Enhancement of Their Catalytic Photodegradation Activity by Doping with Co^{2+} Ions. *European Journal of Inorganic Chemistry*. 2015, **2015** (11), 1981-1988.
6. F. X. Bu, M. Hu, L. Xu, Q. Meng, G. Y. Mao, D. M. Jianga and J. S. Jiang, Coordination polymers for catalysis: enhancement of catalytic activity through hierarchical structuring. *Chemical Communications*. 2014, **50**(62), 8543-8546.
7. H. Kim, M. C. Cha, H. W. Park and J. Y. Chang, Preparation of a Yb(III)-Incorporated porous polymer by post-Coordination: Enhancement of gas adsorption and catalytic activity. *Polymer Chemistry*. 2013, **51**(24), 5291-5297.
8. M. K. Sharma, P. P. Singh and P. K. Bharadwaj, Two-dimensional rhombus grid coordination polymer showing heterogeneous catalytic activities. *Journal of Molecular Catalysis A: Chemical*. 2011, **342-343**, 6-10.
9. R. Ohtani and S. Hayami, Guest-Dependent Spin-Transition Behavior of Porous Coordination Polymers. *Chemistry A European Journal*. 2017, **23**(10), 2236-2248.
10. Z. Chen, J. Lv, K. Yu, H. Zhang, C. Wang, C. Wang and B. Zhou, Self-assembly, bifunctional electrocatalytic behavior, and photocatalytic property of host–guest metal-oxide-based coordination polymers. *Journal of Coordination Chemistry*. 2016, **69**(1), 39-47.
11. S. Jana, K. Harms and S. Chattopadhyay, In situ assembly of a host-guest linked, mixed valence copper(II)-copper(I) coordination polymer $[Cu(1,2\text{-en})_2(\mu_3\text{-I})_2Cu_2(\mu_2\text{-I})_2]_n$ *via* partial reduction of copper(II) under ambient conditions. *Journal of Coordination Chemistry*. 2014, **67**(17), 2954-2966.
12. J. J. Henkelis, S. A. Barnett, L. P. Harding and M. J. Hardie, Coordination Polymers Utilizing N-Oxide Functionalized Host Ligands. *Inorganic Chemistry*. 2012, **51**(20), 10657-10674.
13. R. Yu, X. F. Kuang, X. Y. Wu, C. Z. Lu and J. P. Donahue, Stabilization and immobilization of polyoxometalates in porous coordination polymers through host-guest interactions. *Coordination Chemistry Reviews*. 2009, **253**(23), 2872-2890.
14. R. Ahmad and M. J. Hardie, Propeller-shaped chain and 2D grid coordination polymers with the host molecule cyclotriveratrylene and $(CB_9H_5Br_5)^-$. *New Journal of Chemistry*. 2004, **28**(11), 1315-1319.
15. P. Mani, K. M. Ranjith, S. Mandal and A. K. Paul, Comparative Studies on Optical and Electronic Behavior of Lanthanide-based Coordination Polymers: Synthesis, Structure, Absorption-Emission and Magnetic Properties. *Journal of Chemical Sciences*. 2018, **130**(6), 60.

16. D. Geng, M. Zhang, X. Hang, W. Xie, Y. Qin, Q. Li, Y. Bi and Z. Zheng, A 2D metal-thiacalix[4]arene porous coordination polymer with 1D channels: gas absorption/separation and frequency response. *Dalton Transactions*. 2018, **47**(27), 9008-9013.
17. Y. Y. Xu, X. X. Wu, Y. Y. Wang, X. M. Su, S. X. Liu, Z. Z. Zhu, B. Ding, Y. Wang, J. Z. Huo and G. X. Du, Hydrothermal syntheses of a series of cluster-based micro-porous luminescent cadmium(II) metal-organic frameworks with 4-amino-benzene-1,2,4-triazole: topological diversity, gas absorption and photo-luminescent characterization. *Royal Society of Chemistry Advances*. 2014, **4**(48), 25172-25182.
18. L. Lu, X. R. Wu, J. Q. Liu, J. M. Wu, Q. L. Li, J. H. Man, Y. Hu, M. S. Li, J. Wang, M. Lin, O. Guillou and N. S. Weng, Synthesis, luminescence and gas absorption of a new polythreading coordination polymer. *Inorganic Chemistry Communications*. 2014, **46**, 268-272.
19. J. T. Culp, L. Sui, A. Goodman and D. Luebke, Carbon dioxide (CO_2) absorption behavior of mixed matrix polymer composites containing a flexible coordination polymer. *Journal of Colloid and Interface Science*. 2013, **393**, 278-285.
20. N. Yanai, K. Kitayama, Y. Hijikata, H. Sato, R. Matsuda, Y. Kubota, M. Takata, M. Mizuno, T. Uemura and S. Kitagawa, Gas detection by structural variations of fluorescent guest molecules in a flexible porous coordination polymer. *Nature Materials*. 2011, **10**, 787-793.
21. J. L. C. Rowsell, E. C. Spencer, J. Eckert, J. A. K. Howard and O. M. Yaghi, Gas Adsorption Sites in a Large-Pore Metal-Organic Framework. *Science*. 2005, **309**(5739), 1350-1354.
22. J. Y. Lee, J. Li and J. Jagiello, Gas sorption properties of microporous metal organic frameworks. *Journal of Solid State Chemistry*. 2005, **178**(8), 2527-2532.
23. W. Liu, X. Bao, J. Y. Li, Y. L. Qin, Y. C. Chen, Z. P. Ni and M. L. Tong, High-Temperature Spin Crossover in Two Solvent-Free Coordination Polymers with Unusual High Thermal Stability. *Inorganic Chemistry*. 2015, **54**(6), 3006-3011.
24. Y. Liu and H. X. He, Structural and thermal stability of mesoporous alumina synthesized by Al-based coordination polymer. *Microporous and Mesoporous Materials*. 2013, **165**, 27-31.
25. Y. L. Hou, G. Xiong, P. F. Shi, R. R. Cheng, J. Z. Cui and B. Zhao, Unique (3,12)-connected coordination polymers displaying high stability, large magnetocaloric effect and slow magnetic relaxation. *Chemical Communications*. 2013, **49**(54), 6066-6068.
26. P. Ren, W. Shi and P. Cheng, Synthesis and Characterization of Three-Dimensional 3d-3d and 3d-4f Heterometallic Coordination Polymers with High Thermal Stability. *Crystal Growth and Design*. 2008, **8**(4), 1097-1099.
27. Y. Li, G. Xu, W. Q. Zou, M. S. Wang, F. K. Zheng, M. F. Wu, H. Y. Zeng, G. C. Guo and J. S. Huang, A Novel Metal-Organic Network with High Thermal Stability: Nonlinear Optical and Photoluminescent Properties. *Inorganic Chemistry*. 2008, **47**(18), 7945-7947.
28. J. Zhang, R. G. Xiong, X. T. Chen, C. M. Che, Z. Xue and X. Z. You, Two Luminescent 2D Layered Copper(I)−Olefin Coordination Polymers with High Thermal Stability. *Organometallics*. 2001, **20**(19), 4118-4121.
29. R. G. Xiong, J. L. Zuo, X. Z. You, B. F. Abrahams, Z. P. Bai, C. M. Che and H. K. Fun, Opto-electronic multifunctional chiral diamondoid-network coordination polymer: bis{4-[2-(4-pyridyl)ethenyl]benzoato}zinc with high thermal stability. *Chemical Communications*. 2000, **20**, 2061-2062.
30. Q. M. Qiu, L. Gu, H. Ma, L. Yan, M. Liu and H. Li, Double layer zinc–UDP coordination polymers: structure and properties. *Dalton Transactions*. 2018, **47**(40), 14174-14178.

31. S. Q. Bai, I. H. K. Wong, N. Zhang, K. L. Ke, M. Lin, D. J. Young and T. S. A. Hor, A new 3-D coordination polymer as a precursor for CuI-based thermoelectric composites. *Dalton Transactions*. 2018, **47**(45), 16292-16298.
32. C. X. Bezuidenhout, C. Esterhuysen and L. J. Barbour, Solvatochromism as a probe to observe the solvent exchange process in a 1-D porous coordination polymer with 1-D solvent accessible channels. *Chemical Communications*. 2017, **53**(41), 5618-5621.
33. H. J. Jeon, R. Matsuda, P. Kanoo, H. Kajiro, L. Li, H. Sato, Y. Zheng and S. Kitagawa, The densely fluorinated nanospace of a porous coordination polymer composed of perfluorobutyl-functionalized ligands. *Chemical Communications*. 2014, **50**(74), 10861-10863.
34. C. Tamain, B. A. Chapelet, M. Rivenet, F. Abraham and S. Grandjean, Single Crystal Synthesis Methods Dedicated to Structural Investigations of Very Low Solubility Mixed-Actinide Oxalate Coordination Polymers. *Crystal Growth and Design*. 2012, **12**(11), 5447-5455.
35. L. Hashemi and A. Morsali, Synthesis and Characterization of a New Nano Lead(II) Two-dimensional Coordination Polymer by Sonochemical Method: A Precursor to Produce Pure Phase Nano-sized Lead(II) Oxide. *Journal of Inorganic Organometallic Polymers and Materials*. 2010, **20**(4), 856-861.
36. I. Bassanetti, C. Atzeri, D. A. Tinonin and L. Marchiò, Silver(I) and Thioether-bis(pyrazolyl)methane Ligands: The Correlation between Ligand Functionalization and Coordination Polymer Architecture. *Crystal Growth and Design.* 2016, **16**(6), 3543-3552.
37. T. Yamada, K. Otsubo, R. Makiura and H. Kitagawa, Designer coordination polymers: dimensional crossover architectures and proton conduction. *Chemical Society Reviews*. 2013, **42**(16), 6655-6669.
38. J. Reboul, S. Furukawa, N. Horike, M. Tsotsalas, K. Hirai, H. Uehara, M. Kondo, N. Louvain, O. Sakata and S. Kitagawa, Mesoscopic architectures of porous coordination polymers fabricated by pseudomorphic replication. *Nature Materials*. 2012, **11**, 717-723.
39. A. Zharkouskaya, A. Buchholz and W. Plass, A New Coordination Polymer Architecture with (10,3)-a Network Containing Chiral Hydrophilic 3-D Channels. *European Journal of Inorganic Chemistry.* 2005, **2005** (24), 4875-4879.
40. J. C. Dai, X. T. Wu, Z. Y. Fu, C. P. Cui, S. M. Hu, W. X. Du, L. M. Wu, H. H. Zhang and R. Q. Sun, Synthesis, Structure, and Fluorescence of the Novel Cadmium(II)-Trimesate Coordination Polymers with Different Coordination Architectures. *Inorganic Chemistry*. 2002, **41**(6), 1391-1396.
41. M. Garai and K. Biradha, One-Dimensional Coordination Polymers of Bis(3-pyridyl-acrylamido)ethane: Influence of Anions and Metal Ions on Their Solid State [2 + 2] Photochemical Polymerization and Dimerization Reactions. *Crystal Growth and Design*. 2017, **17**(2), 925-932.
42. M. C. Aragoni, M. Arca, V. Cabras, S. J. Coles, G. Ennas, F. Isaia, R. Lai, V. Lippolis and E. Podda, Coordination polymers based on dithiophosphato/dithiophosphonato nickel complexes and linear 1,4-di(3-pyridyl)buta-1,3-diyne ligand. *Supramolecular Chemistry*. 2017, **29**(11), 853-864.
43. H. Lin, M. Le, D. Liu, G. Liu, X. Wang and S. Duan, Four Cu(II)/Co(II) coordination polymers based on *N,N*′-di(3-pyridyl)sebacicdiamide: influence of different carboxylate ancillary ligands on structures and properties. *Journal of Coordination Chemistry*. 2016, **69**(6), 934-946.
44. X. D. Hu and Y. M. Guo, Synthesis, Structures, and Properties of Ni^{II}, Co^{II}, Cu^{II}, Mn^{II}, and Zn^{II} Coordination Polymers Based on 5-Aminoisophthalate and 4-Amino-3,5-bis(3-pyridyl)-1,2,4-

triazole. *Synthesis and Reactivity in Inorganic, Metal-Organic, and Nano-Metal Chemistry*. 2016, **46**(4), 522-528.

45. Q. Chen, Y. Bi and J. Chen, Pseudohalide-directed Assembly of Two Zinc(II) Coordination Polymers with a 3,4-Bis(3-pyridyl)-5-(4-pyridyl)-1,2,4-triazole Tecton. *Journal of Inorganic and General Chemistry*. 2016, **642**(24), 1445-1449.
46. J. Chen, M. Z. Li, N. Sun and J. H. Guo, Influence of pseudohalide anions on the structural assembly of Cd(II) coordination polymers with 3,4-bis(3-pyridyl)-5-(4-pyridyl)-1,2,4-triazole. *Journal of Molecular Structure*. 2016, **1105**, 273-278.
47. S. R. Zheng, Z. Z. Wen, Y. Y. Chen, S. L. Cai, J. Fan and W. G. Zhang, Two new three-dimensional (3,4)-connected lanthanide (III) coordination polymers based on 2-(3-Pyridyl)-1H-imidazole-4, 5-dicarboxylate: Structures and luminescent properties. *Inorganic Chemistry Communications*. 2015, **55**, 165-168.
48. H. Kim, M. Park, H. Lee and O. S. Jung, Construction of helical coordination polymers *via* flexible conformers of bis(3-pyridyl)cyclotetramethylenesilane: metal(II) and halogen effects on luminescence, thermolysis and catalysis. *Dalton Transactions*. 2015, **44**(17), 8198-8204.
49. K. Liu, X. Zhu, J. Wang, B. Li and Y. Zhang, Four coordination polymers derived from 4-amino-3,5-bis(3-pyridyl)-1,2,4-triazole and copper sulfate. *Inorganic Chemistry Communications*. 2010, **13**(8), 976-980.
50. M. B. Zaman, M. D. Smith, D. M. Ciurtin and H. C. Loye, New Cd(II)-, Co(II)- and Cu(II)-Containing Coordination Polymers Synthesized by Using the Rigid Ligand 1,2-Bis(3-pyridyl)ethyne(3,3‘-DPA). *Inorganic Chemistry*. 2002, **41**(19), 4895-4903.
51. X. K. Yang, M. N. Chang, J. F. Hsing, M. L. Wu, C. T. Yang, C. H. Hsu and J. D. Chen, Synthesis, crystal structures and thermal properties of six Co(II) and Ni(II) coordination polymers with mixed ligands: Formation of a quadruple-strained helical nanotube. *Journal of Molecular Structure*. 2018, **1171**, 340-348.
52. M. Khanpour and A. Morsali, Synthesis and Characterization of ZnS and ZnO Nanoparticles *via* Thermal Decomposition of Two New Synthesized One-Dimensional Coordination Polymers at Two Different Temperatures. *Journal of Inorganic, Organometallic Polymers, and Materials.* 2010, **20**(4), 692-697.
53. F. Bigdeli, A. Morsali and P. Retailleau, Syntheses and characterization of different zinc(II) oxide nano-structures from direct thermal decomposition of 1D coordination polymers. *Polyhedron*. 2010, **29**(2), 801-806.
54. Y. Zhang, K. Zhang and H. Ma, Electrochemical DNA biosensor based on silver nanoparticles/poly(3-(3-pyridyl) acrylic acid)/carbon nanotubes modified electrode. *Analytical Biochemistry*. 2009, **387**(1), 13-19.
55. S. A. Tovstun, E. G. Martyanova, S. B. Brichkin, M. G. Spirin, V. Yu Gak, A. V. Kozlov and V. F. Razumov, Förster electronic excitation energy transfer upon adsorption of meso-tetra(3-pyridyl)porphyrin on InP@ZnS colloidal quantum dots. *Journal of Luminescence*. 2018, **200**, 151-157.
56. A. M. Al-Soliemy, O. I. Osman, M. A. Hussein, A. M. Asiri and S. A. El-Daly, Fluorescence, Photophysical Behaviour and DFT Investigation of E,E-2,5-bis[2-(3-pyridyl)ethenyl]pyrazine (BPEP). *Journal of Fluorescence*. 2016, **26**(4), 1199-1209.
57. A. Bharti, M. K. Bharty, S. Kashyap, U. P. Singh, R. J. Butcher and N. K. Singh, Hg(II) complexes of 4-phenyl-5-(3-pyridyl)-1,2,4-triazole-3-thione and 5-(4-pyridyl)-1,3,4-oxadiazole-2-thione

and a Ni(II) complex of 5-(thiophen-2-yl)-1,3,4-oxadiazole-2-thione: Synthesis and X-ray structural studies. *Polyhedron*. 2013, **50**(1), 582-591.

58. M. Al-Anber, S. Vatsadze, R. Holze, H. Lang and W. R. Thiel, π-Conjugated N-heterocyclic compounds: correlation of computational and electrochemical data. *Dalton Transactions*. 2005, **22**, 3632-3637.
59. M. Al-Anber, T. Stein, S. Vatsadze and H. Lang, Organometallic π-tweezers incorporating pyrazine-and pyridine-based bridging units*. Inorganica Chimica Acta*. 2005, **358**(1), 50-56.
60. S. Z. Vatsadze, V. N. Nuriev, A. V. Chernikov and N. V. Zyk, Synthesis of novel linear exo-bidentate bispyridine ligands and their complexes with silver(I) tetrafluoroborate. *Russian Chemical Bulletin*. 2002, **51**(10), 1957-1958.
61. D. Grasso, G. Buemi, S. Fasone and C. Gandolfo, Electronic Spectra and Dipole Moments of *p*-phenylendiamine-*N*-*N*′-dibenzylidene and Its Aza-derivatives. *Croatica Chemica Acta*. 1981, **54**(1), 85-90.
62. L. J. Bourhis, O. V. Dolomanov, R. J. Gildea, J. A. K. Howardd and H. Puschmannb, The anatomy of a comprehensive constrained, restrained refinement program for the modern computing environment-Olex2 dissected. *Acta Crystallographica Section A*. 2015, **71**(1), 59-75.
63. L. Palatinus, S. J. Prathapab and S. V. Smaalen, EDMA: a computer program for topological analysis of discrete electron densities. *Journal of Applied Crystallography*. 2012, **45**(3), 575-580.
64. O. V. Dolomanov, L. J. Bourhis, R. J. Gildea, J. A. K. Howarda and H. Puschmann, OLEX2: a complete structure solution, refinement and analysis program. *Journal of Applied Crystallography*. 2009, **42**(2), 339-341.
65. L. Palatinus and A. V. D. Lee, Symmetry determination following structure solution in P1. *Journal of Applied Crystallography*. 2008, **41**(6), 975-984.
66. L. Palatinus and G. Chapuis, SUPERFLIP- a computer program for the solution of crystal structures by charge flipping in arbitrary dimensions. *Journal of Applied Crystallography*. 2007, **40**(4), 786-790.
67. S. J. Musevi, E. Şahin and A. Aslani, Synthesis of PbO and $PbBr_2$ nanopowders from nano-sized 2D lead(II) coordination polymers. *Powder Technology*. 2012, **229**, 30-36.
68. K. Ha, A centrosymmetric monoclinic polymorph of N^1,N^4-bis(pyridin-3-ylmethylidene)benzene-1,4-diamine. *Acta Crystallographica Section E Structure Reports Online*. 2011, **67**(9), o2250-o2250.
69. Y. H. Liu, Q. A. Xu and Z. Y. Han, Catena-Poly[[(nitrato-κ^2O,O')silver(I)]-μ-*N,N*′-bis(3-pyridylmethylidene)benzene-1,4-diamine]. *Acta Crystallographica Section E Structure Reports Online*. 2010, **66**, M903-U423.
70. S. Vatsadze, M. Al-Anber, W. R. Thiel, H. Lang and R. Holze, Electrochemical studies and semiempirical calculations on π-conjugated dienones and heterocyclic nitrogen containing donor ligand molecules. *Journal of Solid State Electrochemistry*. 2005, **9**(11), 764-777.
71. M. C. Aragoni, M. Arca, N. R. Champness, A. V. Chernikov, F. A. Devillanova, F. Isaia, V. Lippolis, N. S. Oxtoby, G. Verani, S. Z. Vatsadze and C. Wilson, Designed Assembly of Low-dimensional Molecular Units: Novel Neutral Coordination Polymers Based on (Phosphonodithioato)Ni^{II} Complexes. *European Journal of Inorganic Chemistry*. 2004, **2004**(10), 2008-2012.
72. Robert M. Silverstein, Francis X. Webster and David J. Kiemle, Spectrometric identification of organic compounds: 7th Edition. 2005. John Wiley and Sons, Inc.

73. Dudley H. Williams and Ian Fleming, Spectroscopic methods in organic chemistry: 6th Edition. 2008. McGraw-Hill Education. McGraw-Hill Education.
74. Donald L. Pavia, Gary M. Lampman and George S. Kriz, Introduction to spectroscopy: a guide for students of organic chemistry. 2nd Edition. 1996. Harcourt Brace College Publishers.
75. I. Kaya and E. Kilavuz, Novel Multicolor Schiff Base Polymers Prepared *via* Oxidative Polycondensation. *Journal of Fluorescence*. 2015, **25**(3), 663-673.
76. A. Atahan and S. Durmus, 1-Amino-2-hydroxy-4-naphthalenesulfonic acid based Schiff bases or naphtho[1,2-d]oxazoles: Selective synthesis and photophysical properties. *Spectrochimica Acta Part A: Molecular and Biomolecular Spectroscopy*. 2015, **144**, 61-67.
77. A. Barth, Infrared spectroscopy of proteins. *Biochimica et Biophysica Acta (BBA)-Bioenergetics*. 2007, **1767**(9), 1073-1101.
78. Y. M. Issa, H. B. Hassib and H. E. Abdelaal, ^{1}H NMR, ^{13}C NMR and mass spectral studies of some Schiff bases derived from 3-amino-1,2,4-triazole. *Spectrochimica Acta Part A: Molecular and Biomolecular Spectroscopy*. 2009, **74**(4), 902-910.
79. R. M. Issa, A. M. Khedr and H. F. Rizk, UV-vis, IR and ^{1}H NMR spectroscopic studies of some Schiff bases derivatives of 4-aminoantipyrine. *Spectrochimica Acta Part A: Molecular and Biomolecular Spectroscopy*. 2005, **62**(1-3), 621-629.
80. R. J. Abraham, J. Fisher and P. Loftus, Introduction to NMR spectroscopy. 1988. John Wiley and Sons, Inc.
81. M. Zahedi, B. Shaabani, M. Aygün and C. Kazak, Construction of one dimensional Co(II) and Zn(II) coordination polymers based on expanded *N,N'*-donor ligands*. Inorganica Chimica Acta*. 2018, **469**, 461-468.
82. Y. Yang, S. Liu, J. Li, X. Tian, X. Zhen and J. Han, Convenient Method for Reduction of C-N Double Bonds in Oximes, Imines, and Hydrazones Using Sodium Borohydride-Raney Ni System. *Synthetic Communications*. 2012, **42**(17), 2540-2554.
83. G. W. Gribble, Sodium borohydride in carboxylic acid media: a phenomenal reduction system. *Chemical Society Reviews*. 1998, **27**(6), 395-404.
84. X. Yin, T. T. Xiao, J. Fan, S. R. Zheng, N. Wang, S. L. Cai, J. B. Tan and W. G. Zhang, Assembly of two new Mn(II) coordination polymers based on 5-aminoisophthalate: Structural diversity and properties. *Inorganic Chemistry Communications*. 2012, **22**, 93-97.
85. J. R. Ferraro, L. J. Basile and D. L. Kovacic, The Infrared Spectra of Rare Earth Metal Chloride Complexes of 2,2'-Bipyridyl and 1,10-Phenanthroline from 650 to 70 cm^{-1}. *Inorganic Chemistry*. 1966, **5**(3), 391-395.
86. L. Yang and R. P. Houser, Copper(I) coordination chemistry of (pyridylmethyl)amide ligands. *Inorganic Chemistry*. 2006, **45**(23), 9416-9422.
87. A. K. Brisdon, Inorganic Spectroscopic Methods. 1998. Oxford University Press.
88. M. A. Araya, F. A. Cotton, J. H. Matonic and C. A. Murillo, An Efficient Reduction Process Leading to Titanium(II) and Niobium(II): Preparation and Structural Characterization of *trans*-$MCl_2(py)_4$ Compounds, M = Ti, Nb, and Mn. *Inorganic Chemistry*. 1995, **34**(22), 5424-5428.
89. B. Liu, dichloro-bis(pyridine-2,6-diylbis((pyridin-3-yl)methanone))-manganese(II). *New Crystal Structures*. 2013, **228**, 385-386.
90. T. Iwasita, Electrocatalysis of methanol oxidation. *Electrochimica Acta*. 2002, **47**(22-23), 3663-3674.

91. P. Karsten and J. Strahle, Bis(1,8-diazabicyclo[5.4.0]undec-7-en-8-ium)*trans*-Dichlorotetra(pyridine-N)iron(II) Dichloride. *Acta Crystallographica Section C*. 1998, **54**(10), 1406-1408.
92. T. M. U. Ton, C. Tejo, S. Tania, J. W. W. Chang and P. W. H. Chan, Iron(II)-Catalyzed Amidation of Aldehydes with Iminoiodinanes at Room Temperature and under Microwave-Assisted Conditions. *The Journal of Organic Chemistry*. 2011, **76**, 4894-4904.
93. J. Kansikas, M. Leskela, G. Kenessey, P. E. Werner and G. Liptay, Pyridine-Type Complexes of Transition-Metal Halides. VI. Preparation and Characterization of 2,6- and 3,5-Dimethylpyridine Complexes of Cobalt(II) Halides; the Crystal Structure of Di(2,6-dimethylpyridinium) Tetrachlorocobaltate(II) and Dichlorotetrakis(3,5-dimethylpyridine)cobalt(II). *Acta Chemica Scandinavica*. 1994, **48**, 951-959.
94. M. Trdin, I. Leban and N. Lah, Three Concomitant Crystal Forms of Monomeric Cobalt Chloride with 3-Pyridinemethanol. *Acta Chimica Slovenica*. 2015, **62**(2), 249-254.
95. N. E. Brese and M. Okeeffe, Bond-Valance Parameters for Solids. *Acta Crsyallographica Section B-Structural Science*. 1991, **47**(2), 192-197.
96. J. C. Dyason, L. M. Engelhardt, P. C. Healy, C. Pakawatchai and A. H. White, Lewis base adducts of group 11 metal compounds. 14. Crystal structures of the 1:2 binuclear adducts of copper(I) halides with some 2(4)-mono- and dimethyl-substituted pyridine bases and quinoline. *Inorganic Chemistry*. 1985, **24**(12), 1950-1957.
97. W. T. Liu and H. H. Thorp, Bond Valance Sum Analysis of Metal-Ligand Bond Lengths in Metalloenzymes and Model Complexes .2. Refind Distances and Other Enzymes. *Inorganic Chemistry*. 1993, **32**(19), 4102-4105.
98. T. J. Boyle, l. M. Ottley and R. Raymond, Unusual structurally characterized pyridine carbinoxide copper(II) coordination compounds, isolated from organic solvents. *Journal of Coordination Chemistry*. 2010, **63**(4), 545-557.
99. P. C. Healy, J. D. Kildea, B. W. Skelton, A. F. Waters and A. H. White, Lewis-Base Adducts of Group 11 Metal(I) Compounds .60. Binuclear Adducts of Copper(I) Halides With 2-Hindered Pyridine Bases. *Acta Crystallographica Section C-Crystal Structre Communications*. 1991, **47**(8), 1721-1723.
100. D. R. Turner, M. B. Hursthouse, M. E. Light and J. W. Steed, Linear distortion of octahedral metal centres by multiple hydrogen bonds in modular ML_4 systems. *Chemical Communications*. 2004, **12**, 1354-1355.
101. G. Brancatelli, C. Bonaccorso and S. Geremia, bis(25,26,27,28-tetrakis((pyridin-3-yl)methoxy)calix[4]arene)-diaqua-zinc(II) diperchlorate methanol unknown solvate. *Experimental Crystal Structure Determination*. 2016.
102. C. Q. Wan, A. M. Li, S. A. Al-Thabaiti and T. C. W. Mak, Group 12 Metal Complexes of Semirigid 2,6-Pyridinediylbis(3-pyridinyl)methanone: Role of Counteranions and Solvent in Product Formation. *Crystal Growth and Design*. 2013, **13**, 1926−1936.
103. S. Shanmugaraju, C. S. Hawes, A. J. Savyasachi, S. Blasco, J. A. Kitchen and T. Gunnlaugsson, Supramolecular coordination polymers using a close to 'V-shaped' fluorescent 4-amino-1,8-naphthalimide Tröger's base scaffold. *Chemical Communications*. 2017, **53**(93), 12512-12515.
104. J. Pan, D. Zhang, Z. Z. Xue, L. Wei, S. D. Han and G. M. Wang, Three d10 coordination polymers assembled from 3,5-bis(imidazole-1-yl)pyridine and different polycarboxylates: Syntheses, structures and luminescence properties. *Solid State Sciences*. 2017, **73**, 13-18.

105. A. E. Meyers, R. K. Randolph and R. L. L. Duca, Divergent topologies in luminescent zinc and cadmium substituted isophthalate coordination polymers constructed from long-spanning dipyridylamide ligand precursors. *Inorganica Chimica Acta*. 2017, **467**, 330-342.

106. K. Li, V. A. Blatov, T. Fan, T. R. Zheng, Y. Q. Zhang, B. L. Li and B. Wu, A series of Cd(II) coordination polymers based on flexible bis(triazole) and multicarboxylate ligands: topological diversity, entanglement and properties. *Crystal Engineering Communications*. 2017, **19**(38), 5797-5808.

107. X. L. Wang, X. T. Sha, G. C. Liu, N. L. Chen, C. H. Gong and Y. Qu, Assembly, Structures, and Properties of a Series of Metal-Organic Coordination Polymers Derived from a Semi-rigid Bis-pyridyl-bis-amideLigand. *Journal of Inorganic and General Chemistry*. 2015, **641**(7), 1274-1281.

108. Q. Huang, W. Tang, C. Liu, X. Su and X. Meng, Syntheses, structures, and properties of two 2-D Cd(II) complexes based on 2-(1H-imidazol-1-methyl)-1H-benzimidazole and polycarboxylate ligands. *Journal of Coordination Chemistry*. 2014, **67**(1), 149-161.

109. D. Zhao, Y. Xiu, X. L. Zhou and X. R. Meng, Syntheses, structures, and fluorescent properties of two new d10-metal coordination polymers containing 1-((benzotriazol-1-yl)methyl)-1-H-1,2,4-triazole ligand. *Journal of Coordination Chemistry*. 2012, **65**(1), 112-121.

110. X. Wang, X. H. Qiao, G. Jin and X. Meng, Syntheses, Structures and Luminescence Properties of Two Cd(II) Complexes Based on 2-((1H-1,2,4-Triazol-1-yl)methyl)-1H-benzimidazole and Aromatic Polycarboxylate Ligands*. Journal of Natural Sciences B*. 2012, **67b**, 783-790.

111. J. Chen, C. P. Li and M. Du, Substituent effect of R-isophthalates (R = –H, –CH3, –OCH3, –tBu, –OH, and $–NO_2$) on the construction of Cd^{II} coordination polymers incorporating a dipyridyl tecton 2,5-bis(3-pyridyl)-1,3,4-oxadiazole. *Crystal Engineering Communications*. 2011, **13**(6), 1885-1893.

112. Y. Y. Liu, J. F. Ma, J. Yang and Z. M. Su, Syntheses and Characterization of Six Coordination Polymers of Zinc(II) and Cobalt(II) with 1,3,5-Benzenetricarboxylate Anion and Bis(imidazole) Ligands. *Inorganic Chemistry*. 2007, **46**(8), 3027-3037.

113. J. Tao, X. M. Chen, R. B. Huang and L. S. Zheng, Hydrothermal syntheses and crystal structures of two rectangular grid coordination polymers based on unique prismatic $[M_8(ip)_8(4,4'\text{-bipy})_8]$ building blocks [M=Ni(II) or Cd(II), ip=isophthalate, bipy=bipyridine]. *Journal of Solid State Chemistry*. 2003, **170**(1), 130-134.

114. F. Rouhani and A. Morsali, Highly effective Brønsted base/lewis acid cooperative catalysis: a new Cd metal-organic framework for the synthesis of Hantzsch 1,4-DHPs at ambient temperature. *New Journal of Chemistry*. 2017, **41**(24), 15475-15484.

115. Z. J. Wang, L. Qin, X. Zhang, J. X Chen and H. G. Zheng, Syntheses, Characterizations, Luminescent Properties, and Controlling Interpenetration of Five Metal–Organic Frameworks Based on Bis(4-(pyridine-4-yl)phenyl)amine. *Crystal Growth and Design*. 2015, **15**(3), 1303-1310.

N,N′-Bis-pyridin-4-ylmethyl-benzene-1,4-diamine (L2) complexes

3.1 Introduction

N,N′-Bis-pyridin-4-ylmethylene-benzene-1,4-diamine (^{b}L) was reported for the first time in 1981 by Grasso et. al and utilised for electronic and dipole moment studies [1]. Then, the ligand was reported for mechanochemical synthesis, heteroleptic MOF synthesis, organic catalysis, heterogeneous catalysis, nanostructure MOF synthesis, high adsorption MOF materials, electrochemical studies, novel crystal structures synthesis, and gas adsorption-desorption materials [2-29]. On the other hand, *N,N′*-bis-pyridin-4-ylmethyl-benzene-1,4-diamine (L2) was reported for the first time in 2011 by Zhou and co-workers [30]. Then, the ligand was reported by Abedi et. al [10] and Bigdeli et. al [12] for mechanochemical synthesis, heteroleptic MOFs synthesis, basic catalysis and heterogeneous catalysts synthesis [10, 12].

The current chapter reports the crystal structure of L2 ligand for the first time. In addition to, L2 self-assembly with $MnCl_2.4H_2O$, $FeCl_3.6H_2O$, $Fe(SCN)_3$, $CoCl_2.6H_2O$ or $Co(NO_3)_2.6H_2O$ to produce $([Mn_{0.5}(L2)_{0.5}Cl(DMSO)])_n$ (**9**) and $([Co_{0.5}(L2)_{0.5}Cl(DMSO)])_n$ (**10**) one-dimensional polymers; $([Fe_{0.5}(L2)Cl])_n$ (**11**) and $([Fe_{0.5}(L2)(SCN)].MeOH)_n$ (**12**) two-dimensional polymers and $([Co(L2)].NO_3.DMF)_n$ complex (**13**). Compounds **9** and **10** are isostructural CPs, obtained from solvent diffusion process of $MnCl_2.4H_2O$ or $CoCl_2.6H_2O$ and L2 ligand in DMSO with acetone as antisolvent. Moreover, compounds **9** and **10** crystal structures show zig-zag shape for L2 ligand molecules between M^{2+} coordination centres. Compound **11** represent the first example of iron(II) chloride and 4-pyridyl substituted ligands two-dimensional coordination polymer. Furthermore, the resulted two-dimensional network has 4^4 topology and packing in an inter-digitated style with other networks left no significant free space. Compound **12** has a two-dimensional network structure and represent another example of iron(II) thiocyanate and 4-pyridyl ligands two-dimensional network. The resulted two-dimensional network is interpenetrating with another two-dimensional network in two-fold 2D-2D fashion and shows free spaces occupied by MeOH solvent molecules. Magnetic susceptibility measurements for compound **12** indicated Fe(II) high spin state from 300 to 5 K and zero field splitting below 5 K. Compound **13** crystal structure represents another rare example of Co(I) and 4-pyridyl substituted ligands and shows unexpected rectangle structure consisting of two Co(I) cations and two L2 ligand molecules that perhaps due to the synthesis method or L2 ligand flexibility.

3.2 Experimental

3.2.1 Synthesis of *N,N'*-bis-pyridin-4-ylmethylene-benzene-1,4-diamine (^{b}L)

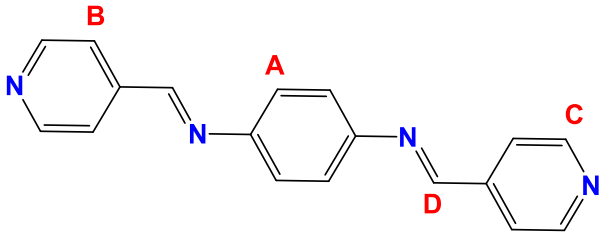

4-Pyridinecarboxaldehyde (1.96 g, 18.4 mmol) was dissolved in ethanol (30 ml) and added dropwise with stirring to *p*-phenylenediamine (1 g, 9.2 mmol) in ethanol (40 ml) and heated under reflux for 5 hours at 70 °C. The solvent was evaporated under vacuum to result in a yellow solid product. The product was washed with acetone and dried under vacuum to form 2.40 g, 90.90 % yield of the prepared ligand ^{b}L, mp= 184-186 ºC. ^{1}H NMR (300 MHz, DMSO-d_6) δ(ppm): 8.78 (s, 2H, D); 8.76 (d, 4H, C, *J*= 3 Hz); 7.87 (m, 4H, B) and 7.47 (s, 4H, A) [10, 25, 26]; ^{13}C{^{1}H} NMR (75 MHz, DMSO-d_6) δ(ppm): 158.97, 150.46, 149.12, 142.45, 122.39 and 122.16; ESI-MS: *m/z* 287{M+H}$^{+}$ [10, 12, 25, 26, 29]. IR (solid state): $\bar{\nu}$ (cm^{-1}) 3029, 2888, 1630 and 1619. Microanalysis found: C, 75.00; H, 5.00; N, 19.60 %, calculated for $C_{18}H_{14}N_4$: C, 75.50; H, 4.93; N, 19.57 %. The resulted ^{1}H NMR, IR and mass data are consisted with reported literatures by Al-Anber and Abedi [10, 25, 26].

3.2.2 Synthesis of *N,N'*-bis-pyridin-4-ylmethyl-benzene-1,4-diamine (L2)

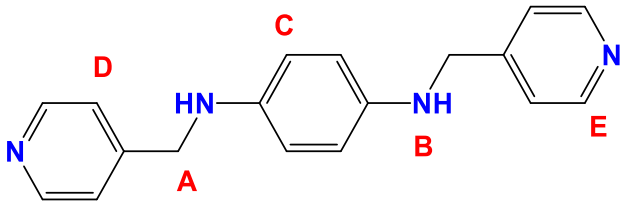

Sodium borohydride (2 g, 54 mmol) was added gradually to a pale yellow methanolic solution (250 ml) containing ^{b}L (2.5 g, 8.7 mmol) at room temperature and left stirring overnight. The solvent was evaporated under vacuum, and the resulted powder was dissolved in deionized water (250 ml) by the addition of aqueous 1M HCl solution. Then, the reaction pH was increased to pH 12 by aqueous 2M sodium hydroxide solution. The ligand was precipitated from the basic solution, filtered, washed by water 4×100 ml and dried under vacuum to result in 2.0 g, 79.05 % yield of L2, mp= 170-171 ºC. ^{1}H NMR (300 MHz, DMSO-d_6) δ(ppm): 8.46 (d, 4H, E, *J*= 5.0 Hz); 7.32 (d, 4H, D, *J*= 5.0 Hz); 6.39 (s, 4H, C); 5.57 (t, 2H, B, *J*= 6.3 Hz); and 4.18 (d, 4H, A, *J*= 6.2 Hz) [10, 12]; ^{13}C{^{1}H} NMR (75 MHz, DMSO-d_6) δ(ppm): 150.31, 149.32, 139.75, 122.33, 113.81 and 46.52; ESI-MS: *m/z* 291 {M+H}$^{+}$. IR (solid state): $\bar{\nu}$ (cm^{-1}) 3265, 3029, 2817, 1604, 1510 and 1417. Microanalysis found: C, 73.70; H, 6.30; N, 19.60 %, calculated for $C_{18}H_{18}N_4$: C, 74.46; H, 6.25; N, 19.30 %.

3.2.3 Synthesis of ($[Mn_{0.5}(L2)_{0.5}Cl(DMSO)])_n$ (9) and ($[Co_{0.5}(L2)_{0.5}Cl(DMSO)])_n$ (10) one-dimensional polymers

A solution of the ligand (L2) (29 mg, 0.1 mmol) in DMSO (1 ml) was added dropwise to $MnCl_2.4H_2O$ or $CoCl_2.6H_2O$ (19 mg or 23 mg, 0.1 mmol) solutions in DMSO (1 ml) and heated for a few seconds. Then, the reaction vials were placed in larger vials containing acetone as antisolvent and left for solvent diffusion process to give $([Mn_{0.5}(L2)_{0.5}Cl(DMSO)])_n$ (28 mg) or $([Co_{0.5}(L2)_{0.5}Cl(DMSO)])_n$ (35 mg) yellow and yellow reddish crystals after a few days. IR (solid state) for compound **9**: $\bar{\nu}$ (cm^{-1}) 3305, 2999, 2827, 1608, 1512, 498 and 430. IR (solid state) for compound **10**: $\bar{\nu}$ (cm^{-1}) 3296, 3001, 2802, 1611, 1513, 500 and 440. Microanalysis found: C, 46.17; H, 5.47; N, 9.61 %, calculated for $([Mn(L2)Cl_2(DMSO)_2])_n$: C, 46.16; H, 5.28; N, 9.79 %. Found: C, 45.82; H, 5.47; N, 9.55 %, calculated for: $([Co(L2)Cl_2(DMSO)_2])_n$: C, 45.84; H, 5.25; N, 9.72 %.

3.2.4 Synthesis of $([Fe_{0.5}(L2)Cl])_n$ coordination polymer (11)

A solution of the ligand (L2) (29 mg, 0.1 mmol) in MeOH (3 ml) was added dropwise to a vial containing $FeCl_3.6H_2O$ (27 mg, 0.1 mmol) in MeOH (2 ml). The reaction vial was heated for a few seconds, sealed and left to stand at room temperature to result in $([Fe_{0.5}(L2)Cl])_n$ (42 mg) red crystals after 24 hours. IR (solid state): $\bar{\nu}$ (cm^{-1}) 3301, 3058, 2852, 1608, 1509 and 489. Microanalysis found: C, 60.14; H, 5.49; N, 15.01 %, calculated for $([Fe(L2)_2Cl_2].H_2O)_n$: C, 59.60; H, 5.28; N, 15.45 %.

3.2.5 Synthesis of $([Fe_{0.5}(L2)(SCN)].MeOH)_n$ coordination polymer (12)

A solution of the ligand (L2) (29 mg, 0.1 mmol) in MeOH (2 ml) was added dropwise to a vial containing $Fe(SCN)_3$ (23 mg, 0.1 mmol) in MeOH (4 ml). Then, the reaction vial was heated for a few seconds, sealed and left to stand at room temperature to result in $([Fe_{0.5}(L2)(SCN)].MeOH)_n$ (29 mg) yellow reddish crystals after three days. IR (solid state): $\bar{\nu}$ (cm^{-1}) 3317, 3052, 2862, 2048, 1664, 1513 and 500. Microanalysis found: C, 58.86; H, 4.43; N, 17.74 %, calculated for $([Fe(L2)_2(SCN)_2].2MeOH)_n$: C, 58.82; H, 5.43; N, 17.15 %.

3.2.6 Synthesis of $([Co(L2)].NO_3.DMF)_n$ complex (13)

A solution of the ligand (L2) (29 mg, 0.1 mmol) in DMF (2 ml) was added dropwise to a vial containing $Co(NO_3)_2.6H_2O$ (29 mg, 0.1 mmol) in DMF (2 ml). The reaction vial was sealed and placed in a thermal block and left for the solvothermal reaction at 115 °C to give a brownish red solution after three days. The solution was left at ambient temperature to result in $([Co(L2)].NO_3.DMF)_n$ (38 mg) red crystals after a few days. IR (solid state): $\bar{\nu}$ (cm^{-1}) 3400-

3050, 3344, 3100, 2880, 1597, 1352 and 476. Microanalysis found: C, 50.10; H, 4.90; N, 16.60 %, calculated for $([Co(L2)].NO_3.DMF.H_2O)_n$: C, 50.20; H, 5.42; N, 16.73 %.

3.3 Crystallography experimental

For the prepared compounds a suitable crystal was selected and mounted under inert oil on a MiTeGen tip and flash frozen to 120(1) K using an OxfordCryosystems low temperature device. X-ray diffraction data were collected using Cu-*Ka* (λ= 1.54184 Å) or Mo-*Ka* (λ= 0.71073 Å) radiation using an Agilent Supernova dual-source diffractometer with Atlas S2 CCD detector and fine-focus sealed tube generator. Data were corrected for Lorenztian and polarization effects, and absorption corrections were applied. The structures were solved by charge flipping methods using SUPERFLIP or by direct methods using SHELXS, and refined by olex2.refine, ShelXL or by full-matrix least-squares on F^2 using SHELXL. All non-hydrogen atoms were refined as anisotropic, and hydrogen positions were included at geometrically estimated positions [31-35]. Summary of data collections and refinements are given in tables 3.11 and 3.12.

3.4 Results and discussion

3.4.1 Synthesis of *N,N′*-bis-pyridin-4-ylmethylene-benzene-1,4-diamine (^{b}L)

The Ligand (^{b}L) was reported for the first time in 1981 by Grasso and co-workers [1]. Then in 1990 by Kunitake et. al [29], other authors [3-16, 17-28] and finally in 2018 by Zahedi et. al [2]. The ligand ^{b}L was prepared by the condensation reaction of *p*-phenylenediamine and 4-pyridinecarboxaldehyde in ethanol (scheme 3.1). The FTIR spectrum of ^{b}L ligand shows bands disappearance at 3409, 3371 and 1720 cm^{-1} that are due to primary amine and aldehyde group of the starting materials [36-38]. Moreover, the FTIR spectrum shows a new band at 1619 cm^{-1} which is due to azomethine group formation [36-38]. The ^{1}H NMR spectrum shows peaks disappearance at δ 10.14 ppm and at δ 4.18 ppm that due to aldehyde or amine groups of 4-pyridinecarboxaldehyde and *p*-phenylenediamine starting materials [36-39]. Furthermore, the ^{1}H NMR spectrum (figure 3.1) shows a new singlet peak at δ 8.78 ppm which is due to azomethine group formation [37, 38, 40]. The $^{13}C\{^1H\}$ NMR spectrum shows peak disappearance at δ 193.08 ppm which is due to the aldehyde group of 4-pyridinecarboxaldehyde. The spectrum also shows a new peak appearance at δ 158.97 ppm that due to the imine group formation (figure 3.2) [30, 36-39]. The resulted ^{1}H NMR, IR and mass data are consistent with reported literatures by Al-Anber and Abedi [10, 25, 26].

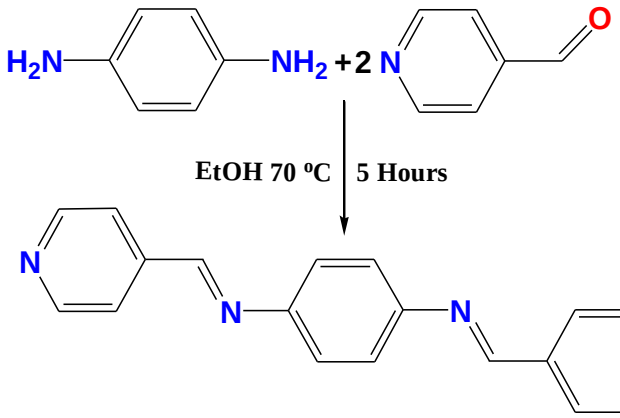

Scheme 3.1: Synthesis of *N,N'*-bis-pyridin-4-ylmethylene-benzene-1,4-diamine (^{b}L).

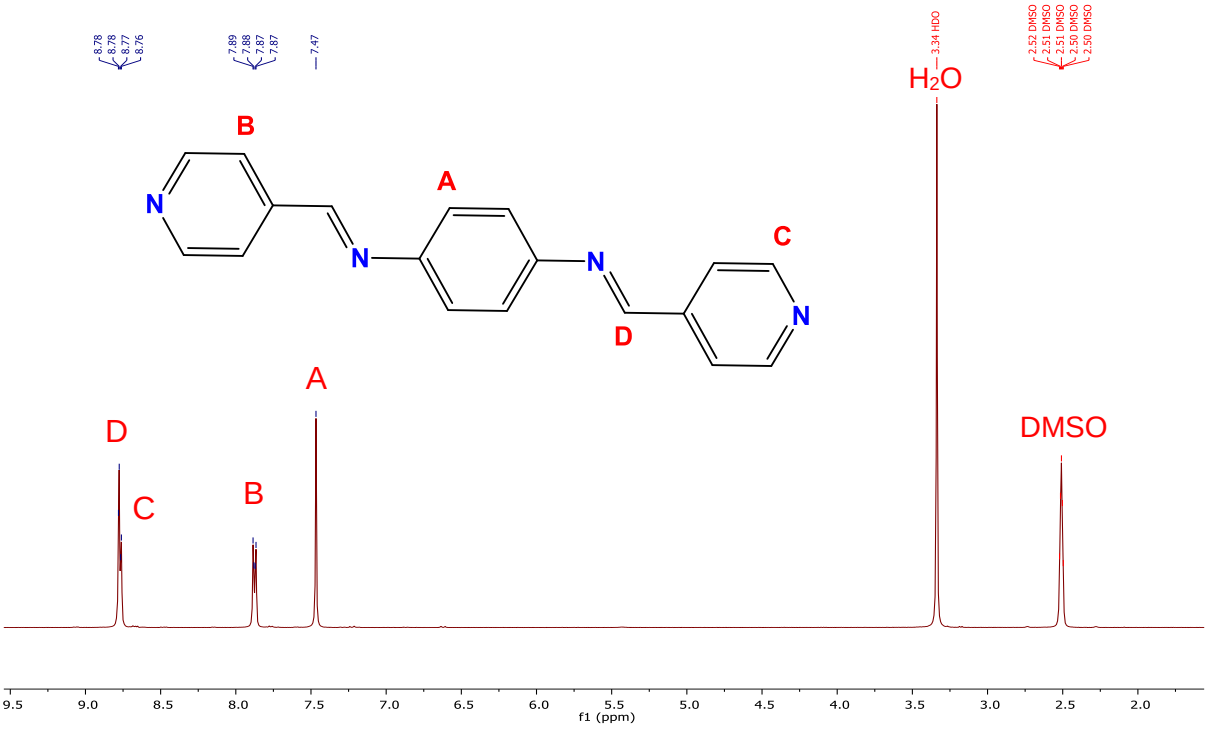

Figure 3.1: ^{1}H NMR (300 MHz, DMSO-d_6) spectrum of *N,N'*-bis-pyridin-4-ylmethylene-benzene-1,4-diamine (^{b}L).

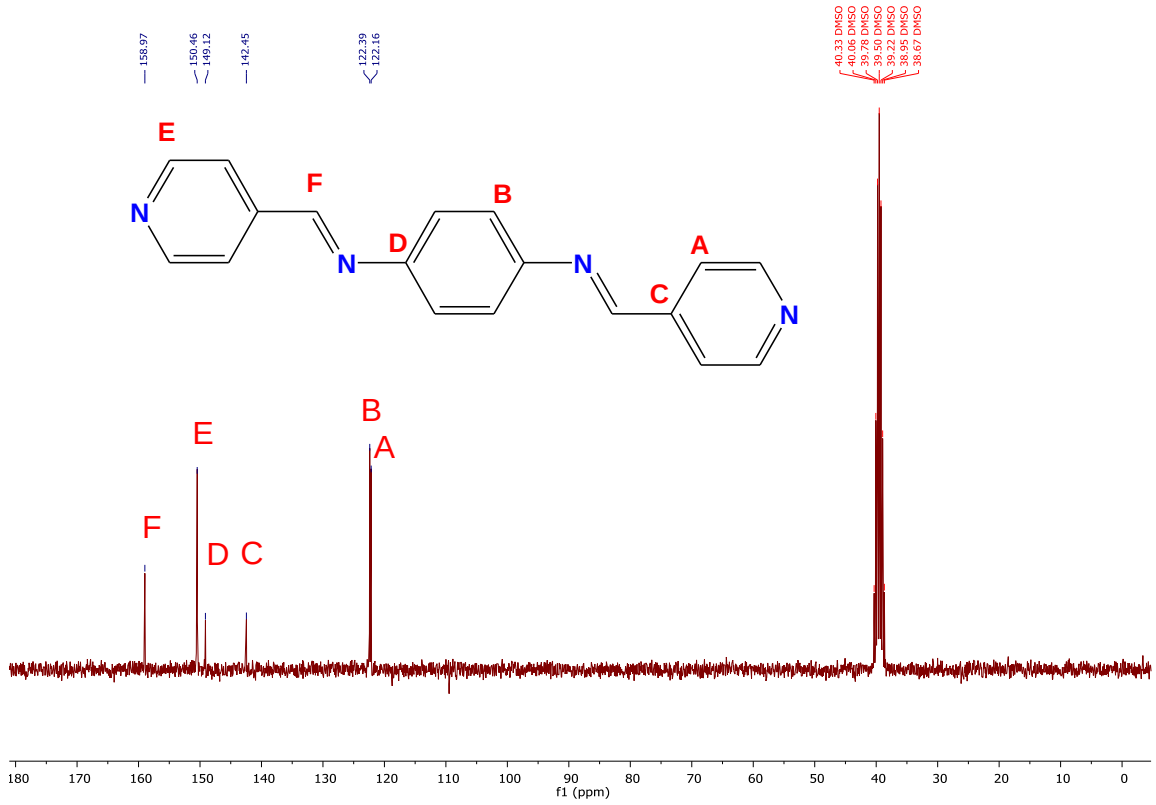

Figure 3.2: $^{13}C\{^{1}H\}$ NMR (75 MHz, DMSO-d_6) spectrum of *N,N'*-bis-pyridin-4-ylmethylene-benzene-1,4-diamine (^{b}L).

3.4.2 Synthesis of *N,N'*-bis-pyridin-4-ylmethyl-benzene-1,4-diamine (L2)

N,N'-Bis-pyridin-4-ylmethyl-benzene-1,4-diamine was reported for the first time in 2011 by Zhou and co-workers [30], then by Abedi et. al [10] and Bigdeli et. al [12]. The ligand was prepared by reduction of *N,N'*-bis-pyridin-4-ylmethylene-benzene-1,4-diamine in methanol solution by $NaBH_4$ for 12 hours (scheme 3.2). The FTIR spectrum of the prepared ligand shows band disappearance at 1619 cm^{-1} which is due to azomethine group [25, 26] and appearance of new bands at 3256 and 1417 cm^{-1} that due to the secondary amine and the methylene groups formation [37, 38]. The ^{1}H NMR spectrum shows disappearance of the azomethine singlet peak at δ 8.78 ppm [10] and appearance of methylene and secondary amine peaks at δ 4.18 ppm and δ 5.57 ppm (figure 3.3) [36-39]. $^{13}C\{^{1}H\}$ NMR spectrum shows appearance of a new peak at δ 46.52 ppm which is due to the methylene group formation and disappearing of the imine group peak at δ 158.97 ppm (figure 3.4) [36-39].

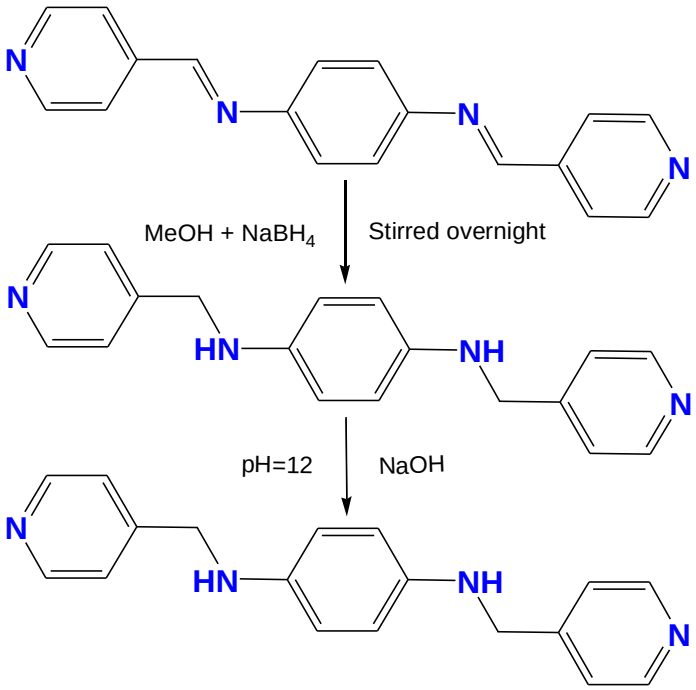

Scheme 3.2: Synthesis of *N*,*N*′-bis-pyridin-4-ylmethyl-benzene-1,4-diamine (L2).

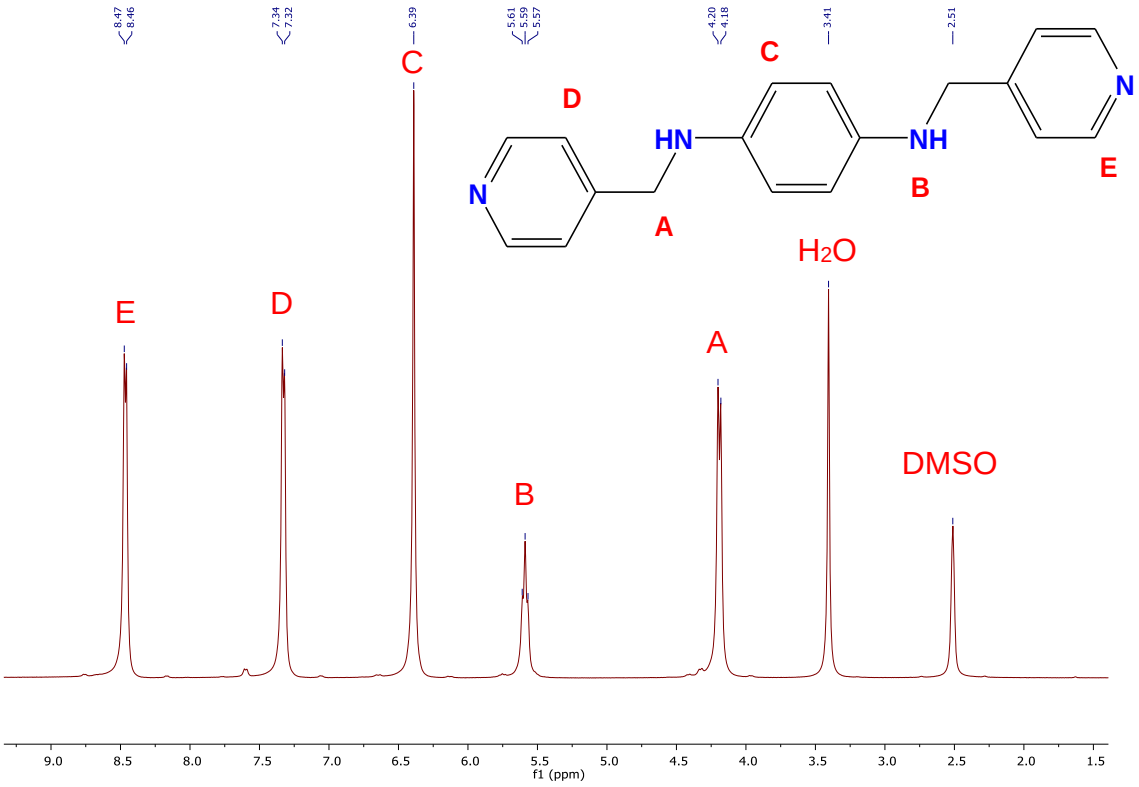

Figure 3.3: ^{1}H NMR (300 MHz, DMSO-d$_6$) spectrum of *N*,*N*′-bis-pyridin-4-ylmethyl-benzene-1,4-diamine (L2).

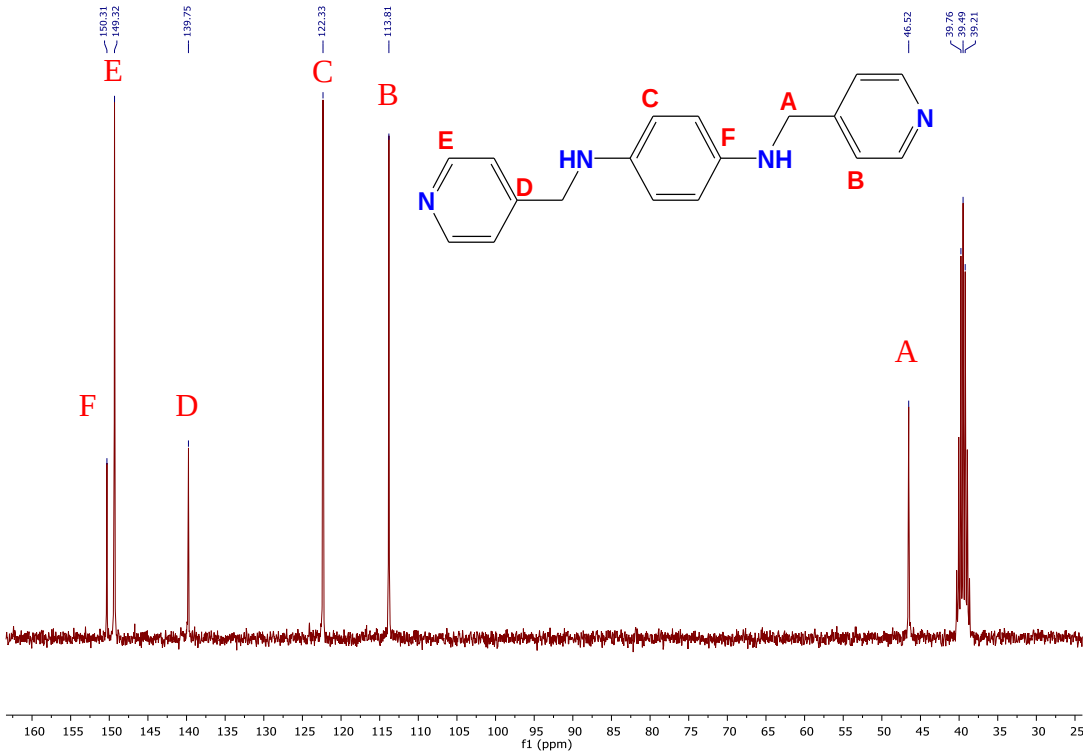

Figure 3.4: $^{13}C\{^{1}H\}$ NMR (75 MHz, DMSO-d_6) spectrum of *N*,*N'*-bis-pyridin-4-ylmethyl-benzene-1,4-diamine (L2).

3.4.3 Synthesis of new complexes 9-13.

A series of novel complexes were synthesised from reaction of L2 with $MnCl_2.4H_2O$, $FeCl_3.6H_2O$, $Fe(SCN)_3$, $CoCl_2.6H_2O$ or $Co(NO_3)_2.6H_2O$ to produce, $([Mn_{0.5}(L2)_{0.5}Cl(DMSO)])_n$ (**9**) and $([Co_{0.5}(L2)_{0.5}Cl(DMSO)])_n$ (**10**) one-dimensional polymers; $([Fe_{0.5}(L2)Cl])_n$ (**11**) and $([Fe_{0.5}(L2)(SCN)].MeOH)_n$ (**12**) MOFs and $([Co(L2)].NO_3.DMF)_n$ complex (**13**). Compounds **9** and **10** were obtained from solvent diffusion process in DMSO with acetone as antisolvent. Compounds **11** and **12** were obtained from self-assembly process in methanol at room temperature. Compound **13** was synthesised by solvothermal reaction in DMF at 115 °C. The resultant crystals of **9-12** are soluble and decomposed to starting materials in hot MeOH, EtOH, MeCN, DCM, DMSO, DMF or $CHCl_3$ solvents. On the other hand, compound **13** crystals are insoluble in common organic and inorganic solvents. Therefore, compounds **9-13** were characterised as solid materials by single crystal X-ray analysis, powder X-ray analysis, microanalysis of the elements and FTIR analysis.

IR spectra for compounds **9** and **10** shows main peaks between 3305-3296, 3001-2999, 2827-2802, 1611-1608 and 1513-1512 cm^{-1} due to νN-H, νC-$H_{Ar,}$ νC-H_{Al}, νC=C and νC-N functional groups [36-38]. The resulted spectra also show new bands between 500-498 cm^{-1}

and 440-430 cm^{-1} that due to νM-N or νM-O coordination bonds [2, 40]. IR spectrum for compound **11** shows main bands at 3301, 3058, 2852, 1608, 1509 and 489 cm^{-1} due to νN-H, $\nu C\text{-}H_{Ar,}$ $\nu C\text{-}H_{Al}$, νC=C, νC-N and νM-N functional groups and coordination bond [28, 36-38, 40]. IR spectrum of complex **12** display main peaks at 3317, 3052, 2862, 2048, 1664, 1513 and 500 cm^{-1} due to νN-H, $\nu C\text{-}H_{Ar}$, $\nu C\text{-}H_{Al}$, νS-C≡N, νC=C, νC-N and νM-N functional groups and coordination bond [36-38, 41-43]. Complex **13** IR spectrum display main bands at 3400-3050, 3344, 3100, 2880, 1597, 1352 and 476 cm^{-1} due to νO-H, νN-H, $\nu C\text{-}H_{Ar,}$ $\nu C\text{-}H_{Al}$, νNO_3^-, νCH_2 and νM-N functional groups and coordination bond [36-38, 40, 43].

3.5 Crystal structures

3.5.1 Crystal structure of *N,N′*-bis-pyridin-4-ylmethyl-benzene-1,4-diamine (L2)

N,N′-Bis-pyridin-4-ylmethyl-benzene-1,4-diamine was reported for the first time in 2011 by Zhou et. al [30], then by Abedi et. al, and finally by Bigdeli et. al [2, 12]. Herein, we report the crystal structure of L2 ligand for the first time, in addition to the standard characterisation techniques that were discussed before in sections 3.2.2 and 3.4.2. The ligand L2 was dissolved in dichloromethane and left to slowly evaporate to afford yellow single crystals after a few days. A suitable crystal was selected for structure determination by single X-ray diffraction. The crystal structure was solved in triclinic space group $P\bar{1}$ [31-35] with an asymmetric unit of half of the L2 molecule (figure 3.5). On symmetry expansion the ligand shows a torsion angle of 179.73(18) ° between the phenyl and 4-pyridyl rings. Furthermore, in the crystal lattice the ligand molecules show 3.607 Å distance between 4-pyridyl rings centres that due to π-π stacking interaction (figure 3.6). Selected bond lengths, angles and torsion angles for L2 ligand are listed in tables 3.1 and 3.2.

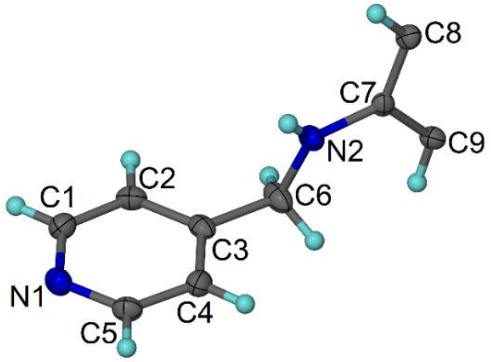

Figure 3.5: *N,N′*-Bis-pyridin-4-ylmethyl-benzene-1,4-diamine asymmetric unit of the crystal structure. Ellipsoids shown at 50 % probability levels.

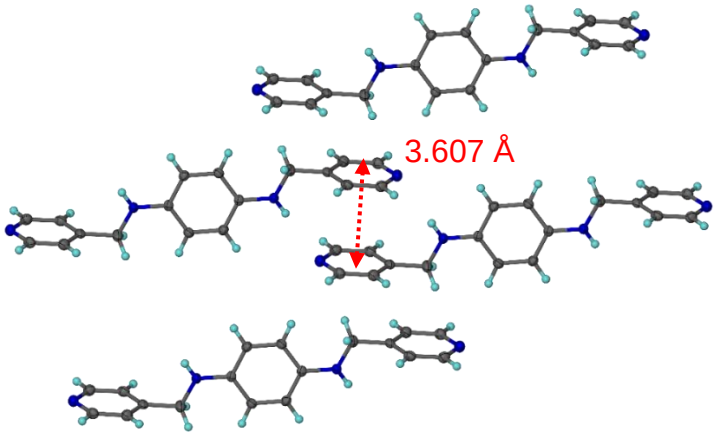

Figure 3.6: Crystal structure of L2 ligand shows torsion angle of 179.73(18) ° between the phenyl and 4-pyridyl rings, 3.607 Å distance between 4-pyridyl rings centres that due to π-π interaction.

Table 3.1: Selected bond lengths (Å) and angles (°) for L2 ligand.

N1-C1	1.337(3)	C7-N2-C6	118.56(17)
N1-C5	1.343(3)	N1-C1-C2	124.0(2)
N2-C6	1.447(3)	C1-C2-C3	119.4(2)
N2-C7	1.403(3)	C2-C3-C6	120.6(2)
C1-C2	1.382(3)	C4-C3-C2	117.25(19)
C2-C3	1.385(3)	C4-C3-C6	122.1(2)
C3-C4	1.384(3)	C5-C4-C3	119.7(2)
C3-C6	1.506(3)	N1-C5-C4	123.4(2)
C4-C5	1.384(3)	N2-C6-C3	110.77(17)
C7-C8	1.398(3)	C8-C7-N2	119.24(18)
C7-C9	1.395(3)	C9-C7-N2	122.89(18)
C8-C91	1.392(3)	C9-C7-C8	117.72(19)
C9-C81	1.392(3)	C91-C8-C7	121.53(19)
C1-N1-C5	116.24(18)	C81-C9-C7	120.75(19)

Table 3.2: Selected torsion (°) angles for L2 ligand.

N1-C1-C2-C3	-0.7(3)	C4-C3-C6-N2	-82.5(3)
N2-C7-C8-C91	175.74(18)	C5-N1-C1-C2	0.7(3)
N2-C7-C9-C81	-175.58(18)	C6-N2-C7-C8	167.7(2)
C1-N1-C5-C4	0.0(3)	C6-N2-C7-C9	-16.7(3)
C1-C2-C3-C4	0.0(3)	C6-C3-C4-C5	-178.89(18)
C1-C2-C3-C6	179.53(18)	C7-N2-C6-C3	179.73(18)
C2-C3-C4-C5	0.6(3)	C8-C7-C9-C81	0.1(3)
C2-C3-C6-N2	98.0(2)	C9-C7-C8-C91	-0.1(3)
C3-C4-C5-N1	-0.7(3)		

3.5.2 Crystal structures of $([Mn_{0.5}(L2)_{0.5}Cl(DMSO)])_n$ (9) and $([Co_{0.5}(L2)_{0.5}Cl(DMSO)])_n$ (10) coordination polymers

$([Mn_{0.5}(L2)_{0.5}Cl(DMSO)])_n$ (**9**) and $([Co_{0.5}(L2)_{0.5}Cl(DMSO)])_n$ (**10**) are isostructural coordination polymer structures. Compounds **9** and **10** were synthesised by a solvent diffusion process of $MnCl_2.4H_2O$ or $CoCl_2.6H_2O$ and L2 in DMSO with acetone as the antisolvent. The resulting CPs crystal structures were solved in triclinic space group $P\bar{1}$ [31-35] and display half of M^{2+} ion on an inversion centre, half L2 ligand molecule, one coordinated chloride anion and one coordinated DMSO molecule per asymmetric unit as shown in figure 3.7 for compound **9**. The metal is coordinated to two L2 molecules by nitrogen atoms of 4-pyridyl rings (Mn-N1= 2.555(3) Å) or (Co-N1= 2.137(2) Å), two DMSO molecules (Mn-O= 2.200(3) Å) or (Co-O= 2.133(2) Å) and two coordinated chloride anions (Mn-Cl= 2.549(9) Å) or (Co-Cl= 2.496(4) Å) in a *trans* arrangement to produce the distorted octahedral coordination centres figure 3.8 for compound **9**.

In 2003 Armstrong and co-workers [44] reported Mn(II) trimeric complex crystal structure based on Mn(II) chloride, DMSO and 2-pyridinecarbaldehyde isonicotinoylhydrazone (HPCIH) $[\{MnCl_2(DMSO)(HPCIH)\}_2Mn(DMSO)_2Cl_2]$. The resulted crystal structure has one similar Mn(II) coordination environment in comparison with complex **9** and shows coordination bond lengths of 2.292(5), 2.499(2) and 2.311(4) Å for Mn1-N4, Mn1-Cl1 and Mn1-O2 [44]. In 1998 Lu and co-workers reported a one-dimensional coordination polymer based on Co(II) chloride, DMSO and 4,4-bipyridine $[CoCl_2(DMSO)_2(4,4'\text{-bipy})]$ that shows coordination bond lengths of 2.152(2), 2.470(5) and 2.129(2) Å for Co-N, Co-Cl and Co-O [45].

Each L2 ligand molecule behaves as a bidentate ligand and bridges between two M^{2+} coordination centres to produce a one-dimensional coordination chain that shows 16.573 or 16.537 Å distance between Mn(II) or Co(II) coordination centres (figure 3.8). Moreover. The ligand L2 shows torsion angle of -83.3(4) or 83.6(3) ° between the phenyl and 4-pyridyl rings to produce L2 zigzag shape between M^{2+} coordination centres (figure 3.8) and (table 3.3). L2 ligand molecules show weak electrostatic bonding interaction between the secondary amines and the coordinated chloride ions from two different coordination chains (-NH···Cl= 3.397 Å) for compound **9** and (-NH···Cl= 3.390 Å) for compound **10** [46]. Powder X-ray analysis of dried compounds **9** and **10** shows a good agreement between calculated and experimental patterns figures 3.9 and 3.10 which indicate new materials stability and phase purity. Moreover,

compound **10** experimental pattern shows some amorphous materials is present. Selected bond lengths, angles and torsion angles for compounds **9** and **10** are listed in tables 3.3 and 3.4.

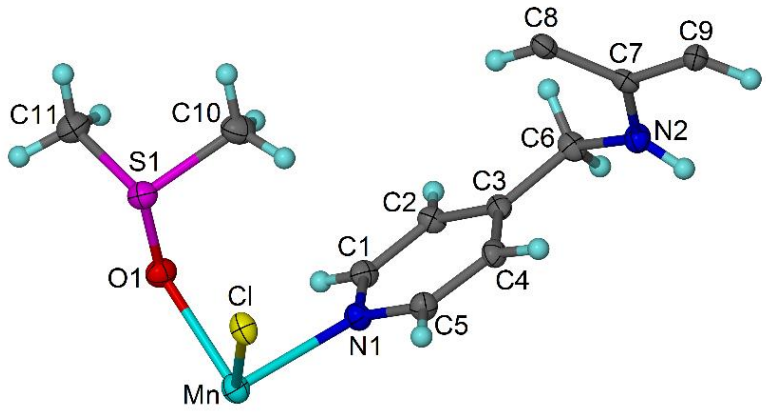

Figure 3.7: $([Mn_{0.5}(L2)_{0.5}Cl(DMSO)])_n$ CP asymmetric unit of the crystal structure. Ellipsoids shown at 50 % probability levels.

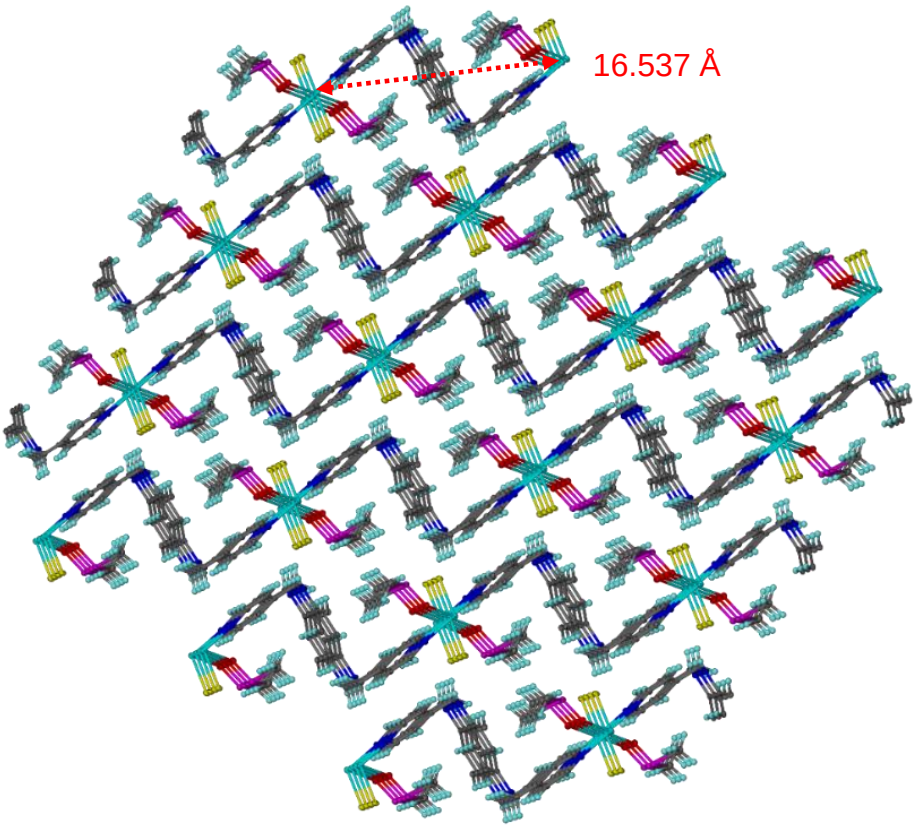

Figure 3.8: Packing diagram of $([Mn_{0.5}(L2)_{0.5}Cl(DMSO)])_n$ CP that shows 16.537 Å between Mn(II) coordination centres in 1D coordination chain.

Table 3.3: Selected bond lengths (Å) and angles (°) for compounds **9** and **10**.

(**9**)		(**10**)	
Mn-Cl	2.549(9)	Co-Cl	2.496(7)
Mn-O	2.200(3)	Co-O	2.133(2)
Mn-N1	2.255(3)	Co-N1	2.137(2)
N2-C6	1.451(5)	N2-C6	1.452(4)
N2-C7	1.398(5)	N2-C7	1.401(4)
Cl^1-Mn-Cl	180.0	Cl-Co-Cl^1	180.0
O^1-Mn-Cl	91.09(7)	O^1-Co-Cl	90.33(6)
O-Mn-Cl	88.91(7)	O-Co-Cl	89.67(6)
O^1-Mn-O1	180.00(8)	O^1-Co-O	180.0
O^1-Mn-N1	91.28(10)	O-Co-$N1^1$	89.41(9)
O-Mn-N1	88.72(10)	O-Co-N1	90.59(9)
$N1^1$-Mn-Cl^1	90.57(8)	N1-Co-Cl^1	89.51(7)
N1-Mn-Cl	90.58(8)	N1-Co-Cl	90.49(7)
N1-Mn-Cl^1	89.43(8)	$N1^1$-Co-N1	180.0
N1-Mn-$N1^1$	180.00(14)	S-O-Co	123.23(12)
S-O-Mn	125.24(15)	C1-N1-Co	121.52(19)
C1-N1-Mn	120.9(2)	C5-N1-Co	120.38(19)
C5-N1-Mn	121.9(2)	C7-N2-C6	120.0(2)
C7-N2-C6	120.7(3)	N2-C6-C3	114.9(2)
N2-C6-C3	114.6(3)	N2-C7-C9	123.2(3)
N2-C7-C8	123.1(3)	C8-C7-N2	119.6(3)

Table 3.4: Selected torsion angles (°) for compounds **9** and **10**.

(**9**)		(**10**)	
Mn-N1-C1-C2	170.9(3)	Co-N1-C1-C2	173.1(2)
Mn-N1-C5-C4	-171.3(3)	Co-N1-C5-C4	-173.1(2)
N2-C7-C8-$C9^1$	177.9(3)	C10-S-O-Co	81.81(17)
N2-C7-C9-$C8^1$	-178.0(3)	C11-S-O-Co	-175.12(15)
C2-C3-C6-N2	179.3(3)	C3-C6-N2-C7	83.6(3)
C4-C3-C6-N2	-1.0(5)	C9-C7-N2-C6	-18.6(4)
C6-N2-C7-C8	17.2(5)	C8-C7-N2-C6	163.7(3)
C6-N2-C7-C9	-164.5(3)	C4-C3-C6-N2	-178.8(3)
C7-N2-C6-C3	-83.3(4)	C2-C3-C6-N2	1.6(4)
C10-S-O-Mn	81.4(2)	N2-C7-C8-$C9^1$	178.1(3)
C11-S-O-Mn	-175.43(19)	N2-C7-C9-$C8^1$	-178.0(3)

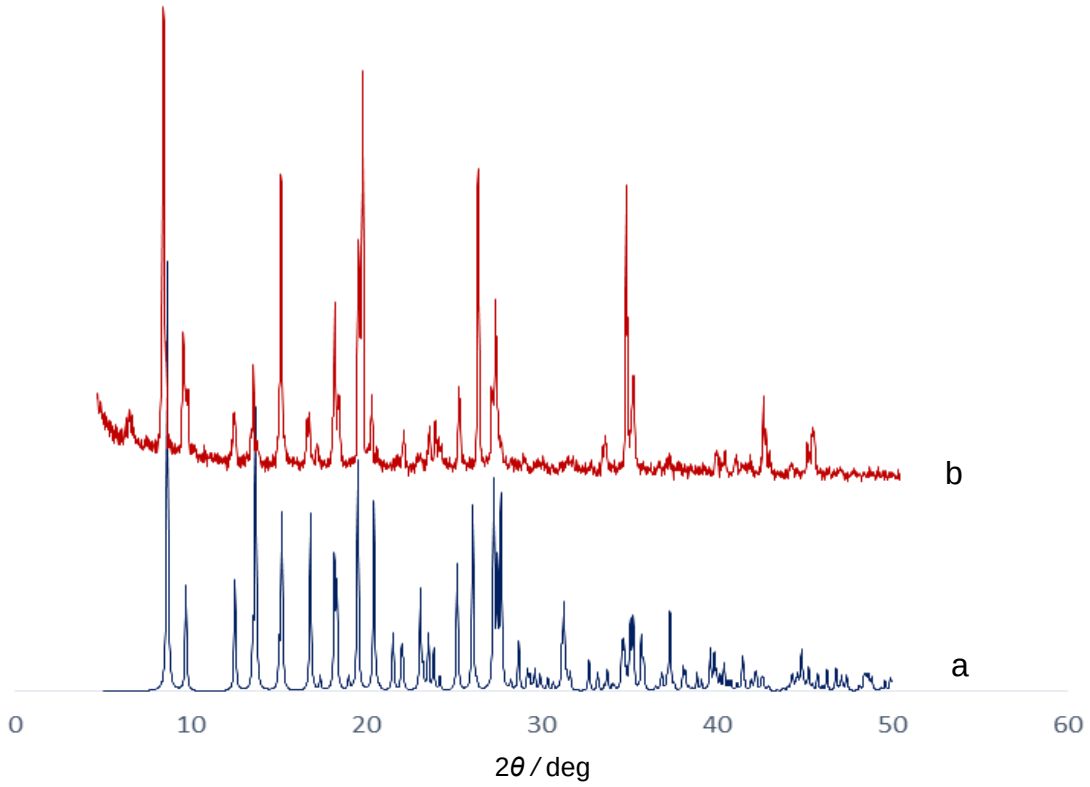

Figure 3.9: (a) Calculated powder XRD pattern of compound **9**. (b) Powder XRD pattern for compound **9**.

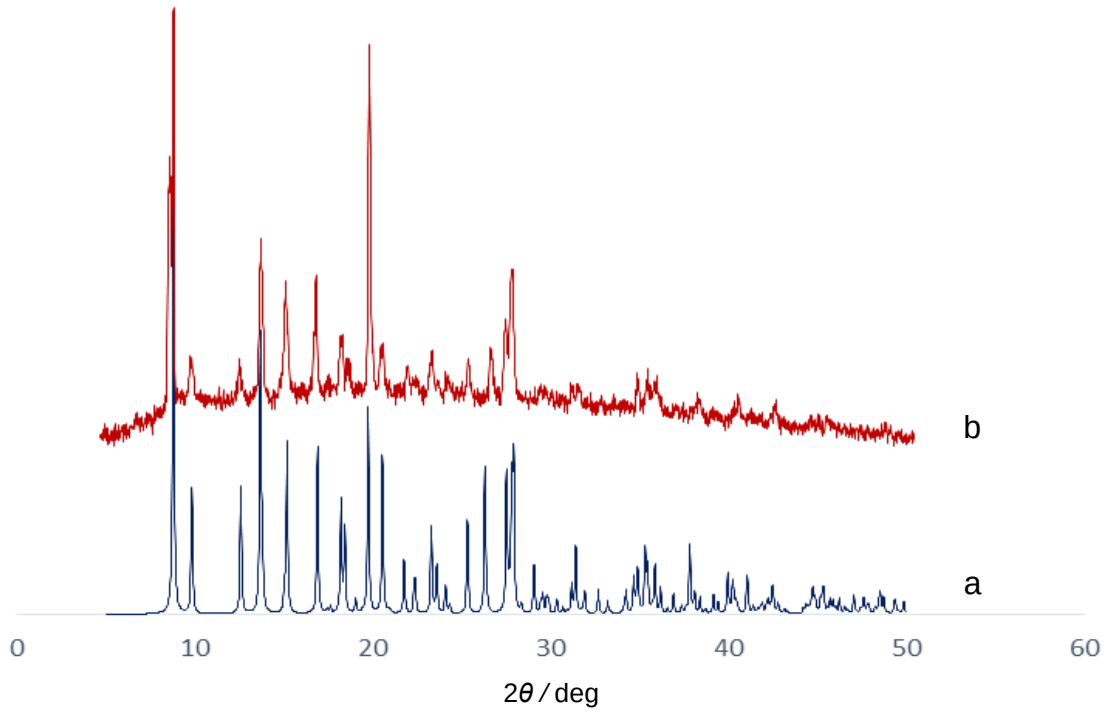

Figure 3.10: (a) Calculated powder XRD pattern of compound **10**. (b) Powder XRD pattern of compound **10**.

3.5.3 Crystal structure of $([Fe_{0.5}(L2)Cl])_n$ coordination polymer (11)

$([Fe_{0.5}(L2)Cl])_n$ crystal structure was solved in monoclinic space group $P2_1/n$ [31-35] and shows half of Fe(II) ion on an inversion centre, one L2 ligand molecule and one coordinated chloride anion per asymmetric unit (figure 3.11). Fe(II) ion is coordinated to four L2 ligand molecules by nitrogen atoms of 4-pyridyl rings and shows two M-N coordination bond lengths (Fe-N1= 2.327(3) Å) and (Fe-N4= 2.211(3) Å). Fe(II) ion is also coordinated to two chloride anions (Fe-Cl= 2.421(8) Å) in a *trans* arrangement to produce Fe(II) distorted octahedral coordination centres.

$([Fe_{0.5}(L2)Cl])_n$ coordination polymer was synthesised from Iron(III) but reduced to Fe(II) by methanol and water [47]. $([Fe_{0.5}(L2)Cl])_n$ complex shows longer M-N and M-Cl coordination bond lengths in comparison with Hosterˈs $Fe(py)_3Cl_3$ reported complex that shows coordination bond lengths of 2.168(5) or 2.274(5) Å for Fe-N and 2.306(2) or 2.326(1) Å for Fe-Cl [48]. Compound **11** shows similar Fe-N and Fe-Cl coordination bond lengths in comparison with Longˈs $Fe(py)_4Cl_2$ and $Fe(py)_4Cl_2.H_2O$ reported structures (Fe-N= 2.229(6) or 2.257(4) Å) and (Fe-Cl= 2.430(3) or 2.417(2) Å) [49]. $([Fe_{0.5}(L2)Cl])_n$ coordination bond lengths are similar to Karstenˈs reported crystal structure of (bis(1,8-diazabicyclo[5.4.0]undec-7-en-8-ium)trans-dichlorotetra(pyridine-N)iron(II)dichloride) complex that shows 2.279(3) or 2.273(3) Å for Fe-N and 2.406(8) Å for Fe-Cl coordination bonds [50].

L2 ligand behaves as a bidentate ligand and coordinates to two Fe(II) coordination centres *via* nitrogen atoms of 4-pyridyl rings. L2 ligand shows two torsion angles of -168.9(3) and -93.6(3) ° between the phenyl and 4-pyridyl rings to produce L2 ligand bent L-shape between iron(II) coordination centres (Fe-L2-Fe= 16.976 Å) (figure 3.11). The ligand L2 also shows hydrogen bond interactions between the secondary amine groups and the coordinated chloride anions from different interpenetrating 2D networks (-HN⋯Cl= 3.293 Å). Four L2 ligand molecules are coordinate to four Fe(II) ions to produce 18.188 × 28.188 Å rhombic cavity that extending to produce the 4^4 network topology (figure 3.12). The resulted networks are packing in an inter-digitated fashion, and there are no significant channels in the lattice (figure 3.13). To the best of our knowledge and according to CCDC compound **11** represent the first example of Fe(II) chloride two-dimensional coordination polymer with 4-pyridyl substituted organic ligands. Powder X-ray analysis for compound **11** shows a good agreement between calculated and experimental patterns which indicates material stability and phase purity (figure 3.15). Selected bond lengths, angles and torsion angles for compound **11** are listed in tables 3.5 and 3.6.

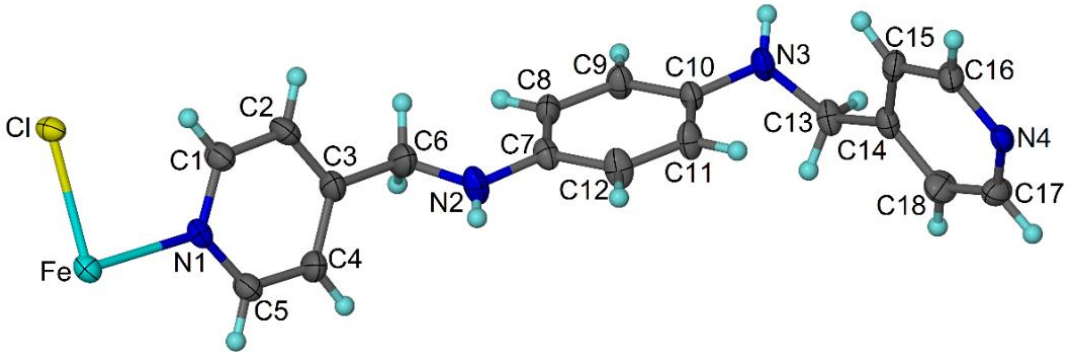

Figure 3.11: $([Fe_{0.5}(L2)Cl])_n$ asymmetric unit of the crystal structure. Ellipsoids shown at 50 % probability levels.

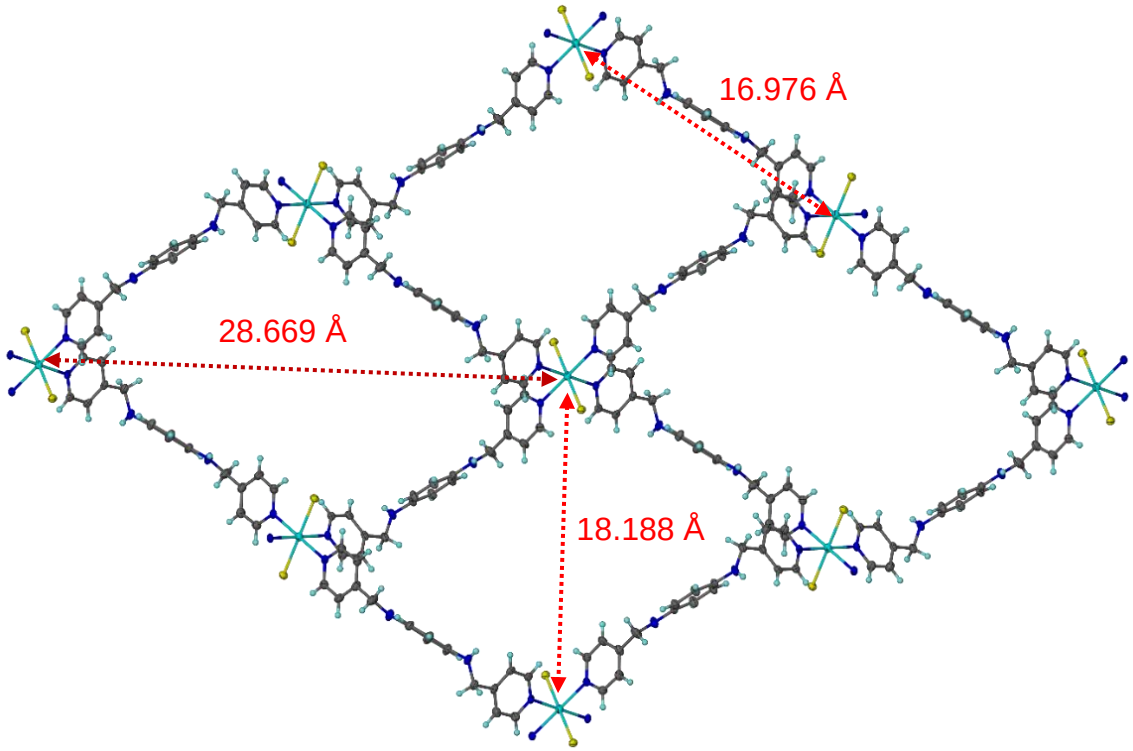

Figure 3.12: Two-dimensional network of $([Fe_{0.5}(L2)Cl])_n$ CP which has 16.976 Å sides and 18.188 × 28.669 Å diagonals between Fe(II) coordination centres.

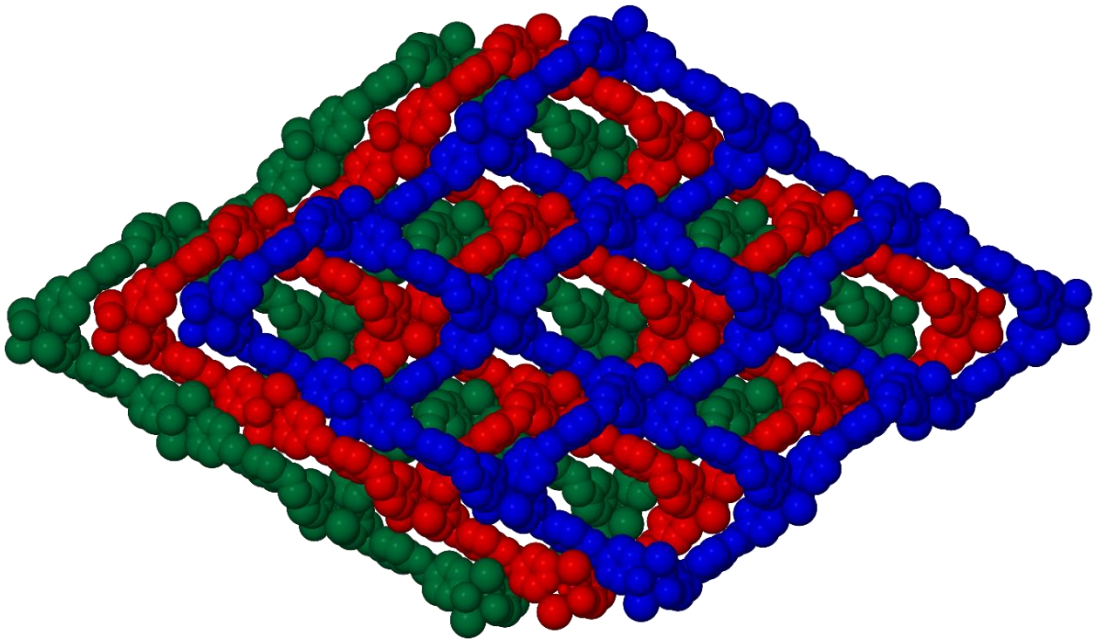

Figure 3.13*:* Packing diagram of $([Fe_{0.5}(L2)Cl])_n$ CP, each rhombic cavity is occupied by two Fe(II) coordination centres from two different 2D networks.

Table 3.5: Selected bond lengths (Å) and angles (°) of compound **11**.

Fe-Cl	2.421(8)	$N1^1$-Fe-N1	180.0
Fe-N1	2.327(3)	$N4^1$-Fe-Cl^1	90.51(8)
Fe-N4	2.211(3)	$N4^1$-Fe-Cl	89.49(8)
N2-C6	1.426(5)	$N4^1$-Fe-N1	90.85(10)
N2-C7	1.404(4)	$N4^1$-Fe-N1	89.15(10)
N3-C10	1.411(4)	$N4^1$-Fe-$N1^1$	90.85(10)
N3-C13	1.445(5)	N4-Fe-$N4^1$	180.0
C3-C6	1.517(5)	C7-N2-C6	117.3(3)
C13-C14	1.517(5)	C10-N3-C13	118.1(3)
Cl^1-Fe-Cl	180.0	N2-C6-C3	110.6(4)
$N1^1$-Fe-Cl	88.62(7)	C8-C7-N2	123.3(3)
N1-Fe-Cl	91.38(7)	N3-C13-C14	115.6(3)

Table 3.6: Selected torsion angles (°) for compound **11**.

Fe-N1-C1-C2	-179.0(3)	C2-C3-C6-N2	113.7(4)
Fe-N1-C5-C4	178.6(3)	C4-C3-C6-N2	-67.4(5)
Fe-N4-C16-C15	178.8(3)	C6-N2-C7-C8	-9.1(5)
Fe-N4-C17-C18	178.6(3)	C6-N2-C7-C12	172.0(4)
N2-C7-C8-C9	-178.5(4)	C7-N2-C6-C3	-168.9(3)
N2-C7-C12-C11	178.9(4)	C8-C9-C10-N3	-177.1(3)
N3-C10-C11-C12	177.4(4)	C10-N3-C13-C14	-93.6(4)
N3-C13-C14-C15	-18.9(5)	C13-N3-C10-C9	-128.7(4)
N3-C13-C14-C18	163.4(3)	C13-N3-C10-C11	53.6(5)

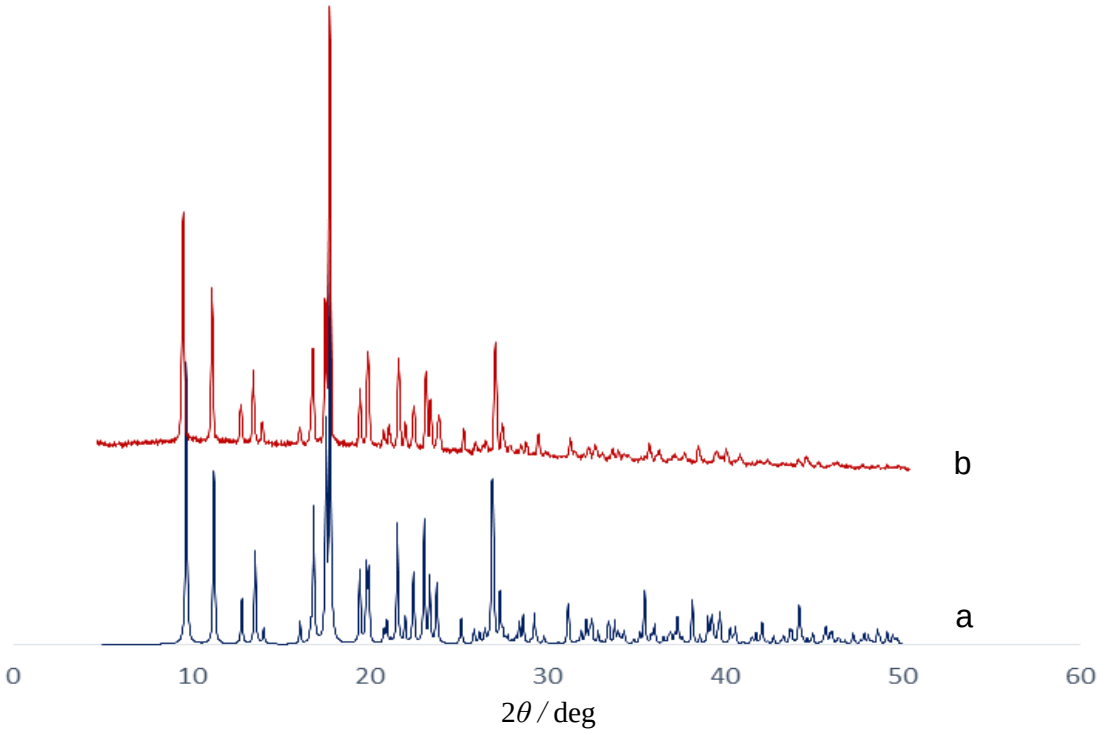

Figure 3.14: (a) Calculated powder XRD pattern of compound **11**. (b) Powder XRD pattern of compound **11**.

3.5.4 Crystal structure of $([Fe_{0.5}(L2)(SCN)].MeOH)_n$ coordination polymer (12)

$([Fe_{0.5}(L2)(SCN)].MeOH)_n$ crystal structure was solved in monoclinic space group *C2/c* [31-35] and shows half of Fe(II) ion on an inversion centre, two halves of L2 ligand molecules, one coordinated thiocyanate anion and one methanol solvent molecule per asymmetric unit (figure 3.15). Fe(II) ion is coordinated to four L2 ligand molecules by nitrogen atoms of 4-pyridyl rings and shows two M-N coordination bond lengths of 2.210(2) Å and 2.268(2) Å for Fe-N1 and Fe-N3. Fe(II) ion is also coordinated to two thiocyanate anions in a *trans* arrangement (Fe-N5= 2.122(2) Å) to produce the distorted Fe(II) octahedral coordination centres (figure 3.16).

A similar two-dimensional coordination polymer based on iron(II) thiocyanate and 1,3-di(4-pyridyl)propane [Fe(1,3-di(4-pyridyl)propane)$_2$(NCS)$_2$]$_2$ was reported in 2016 by Luo and co-workers [51]. The reported crystal structure shows coordination bond lengths from 2.189(12) to 2.267(15) Å for Fe-(4-py), and between 2.084(15)-2.139(16) Å for Fe-NCS [51]. ([Fe$_{0.5}$(L2)(SCN)].MeOH)$_n$ complex shows similar coordination bond lengths in comparison with Halder reported complex of [Fe$_2$(azpy)$_4$(NCS)$_4$].(EtOH) (azpy= *trans*-4,4-azopyridin). Halder's complex shows coordination bond lengths between 2.199(5)-2.221(5) Å for Fe-azpy, and from 2.080(5) to 2.086(5) Å for Fe-NCS at 150 K [52].

The ligand L2 is coordinated to two Fe(II) coordination centres by nitrogen atoms of 4-pyridyl rings. One of the coordinated L2 molecules shows torsion angle of -74.8(5) ° between the phenyl and 4-pyridyl rings to produce L2 bent U-shape between iron(II) coordination centres (Fe-L2-Fe= 12.657 Å). The second coordinated L2 molecule is approximately linear and shows torsion angle of 172.8(2) ° between the phenyl and 4-pyridyl rings (Fe-L2-Fe= 19.868 Å) tables 3.7 and 3.8. Four L2 ligand molecules are coordinated to four Fe(II) coordination centres to produce M$_4$-(L2)$_4$ rectangle cavity. The structure is extending to form a two-dimensional network that has 12.657 or 19.868 Å sides, and 17.376 × 28.424 Å diagonals between Fe(II) coordination centres (figure 3.16). Furthermore, the cyclic unit of four Fe(II) ions and four L2 ligand molecules is interpenetrating with another two-dimensional network in two-fold 2D-2D fashion (figure 3.17).

Magnetic susceptibility measurements for a two-dimensional coordination polymer based on Fe(II) thiocyanate and *trans*-4,4`-azopyridine (azpy) was investigated in 2002 by Halder and co-workers [52]. Fe$_2$(azpy)$_2$(NCS)$_4$.(EtOH) CP has two-dimensional network structure that interpenetrated with another 2D network perpendicularly. The resulted CP showed effective magnetic moment value equal to 5.3 μ_B from 300 to 150 K and 3.65 μ_B at 50 K. The dried Fe$_2$(azpy)$_2$(NCS)$_4$ material shows effective magnetic moment value equal to 5.2 μ_B at 300 K, 5.1 μ_B at 50 K, 4.0 μ_B at 4 K and zero-field splitting at lower temperature. After immersion Fe$_2$(azpy)$_2$(NCS)$_4$ in dry MeOH the material showed effective magnetic moment value equal to 5.2 μ_B from 300 to 150 K and 3.5 μ_B at 50 K. Immersion of Fe$_2$(azpy)$_2$(NCS)$_4$ in anhydrous propanol resulted Fe$_2$(azpy)$_2$(NCS)$_4$.(PrOH) material that shows Fe(II) high spin state with effective magnetic moment value equal to 5.0 μ_B from 300 to 140 K, 4.65 μ_B from 130 to 110 K and 3.8 μ_B at 70 K. Another example of Fe(II) two-dimensional coordination polymer was reported in 2016 by Yang and co-workers [51]. [(Fe(1,3-di(4-pyridyl)propane)$_2$(SCN)$_2$]$_2$ coordination polymer has 4^4 grid structure and shows effective

magnetic moment value equal to 3.0 μ_B at 200 K, 2.8 μ_B at 50 K, 2.0 μ_B at 5 K and finally zero-field splitting at a lower temperature.

Solid state magnetic susceptibility measurements for compound **12** was investigated using a Quantum Design SQUID/VSM magnetometer in an applied field of 5000 G and a temperature ramp of 5 K per minute [53, 54]. $([Fe_{0.5}(L2)(SCN)].MeOH)_n$ coordination polymer showed Fe(II) high spin state and effective magnetic moment value equal to 3.5 μ_{BM} at 300 K or 3.25 μ_{BM} at 98 K [51]. Then, the μ_{eff} value was decreased gradually to 2.0 μ_{BM} at 5 K, and finally to zero field splitting below 5 K (figure 3.19). The experimental powder X-ray analysis for compound **12** do not match the calculated pattern from the single crystal. The new phase is crystalline, but the structure could not be determined as the materials did not stay as a single crystal on drying out (figure 3.20). Selected bond lengths, angles and torsion angles for compound **12** are listed in tables 3.7 and 3.8.

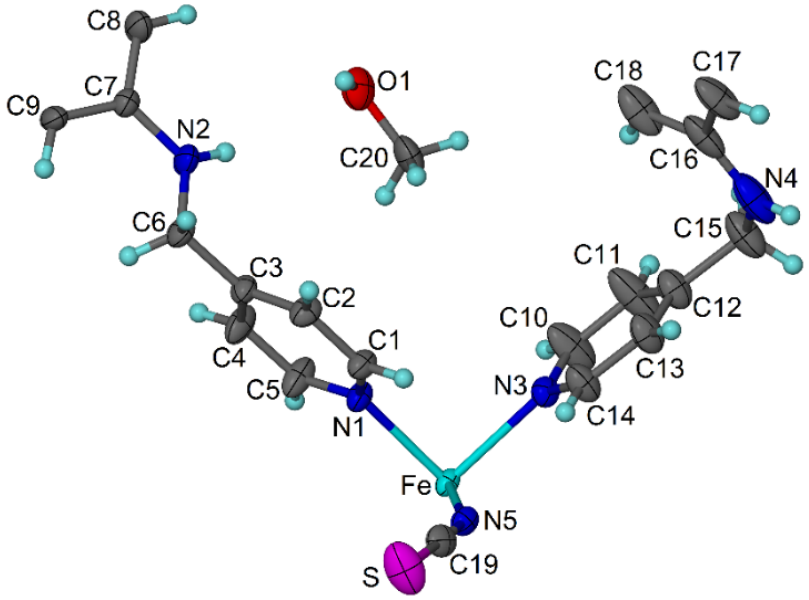

Figure 3.15: $([Fe_{0.5}(L2)(SCN)].MeOH)_n$ two-dimensional coordination polymer asymmetric unit of the crystal structure. Ellipsoids shown at 50 % probability levels.

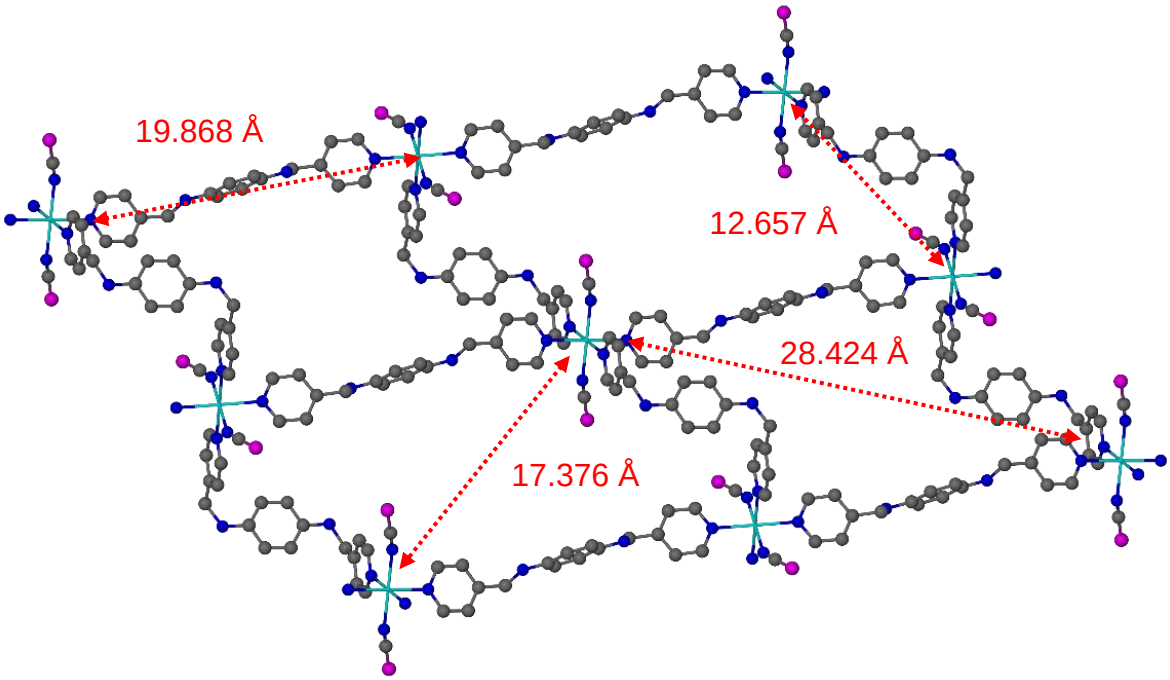

Figure 3.16: $([Fe_{0.5}(L2)(SCN)].MeOH)_n$ CP 4^4 network topology that has 12.657 or 19.868 Å sides and 17.376 × 28.424 Å diagonals between Fe(II) coordination centres.

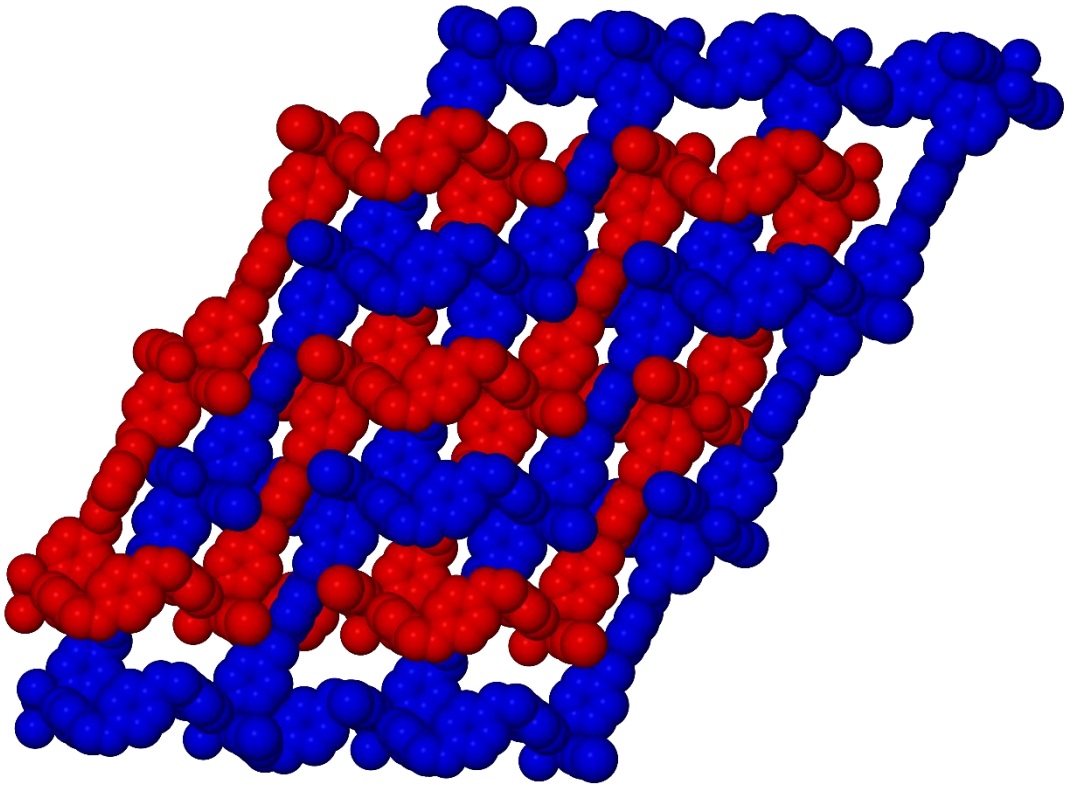

Figure 3.17: Two-fold interpenetrating of $([Fe_{0.5}(L2)(SCN)].MeOH)_n$ 2D networks.

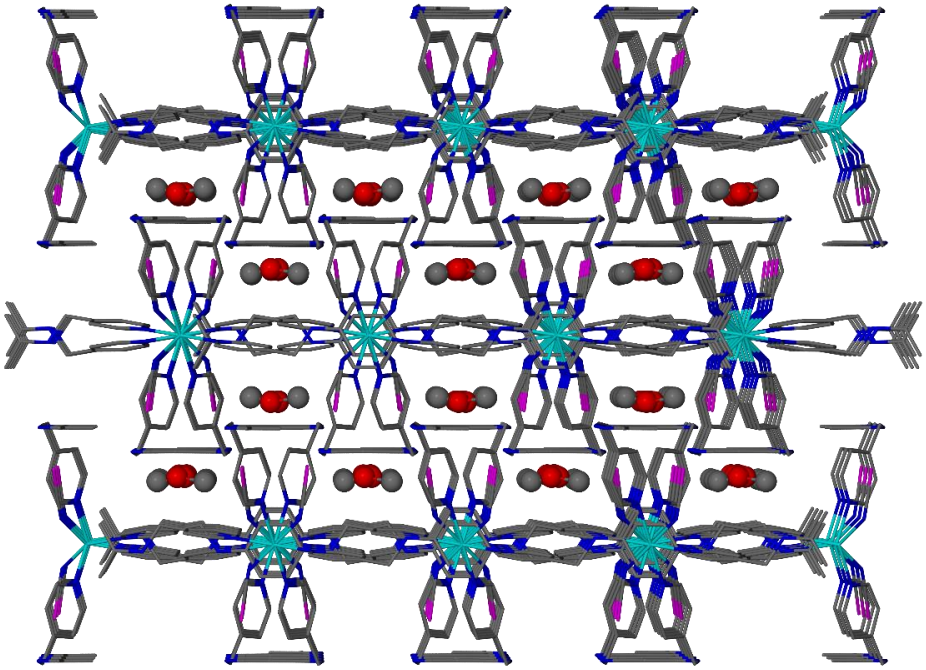

Figure 3.18: Packing diagram of $([Fe_{0.5}(L2)(SCN)].MeOH)_n$ 2D networks, hydrogen atoms were removed for clarity.

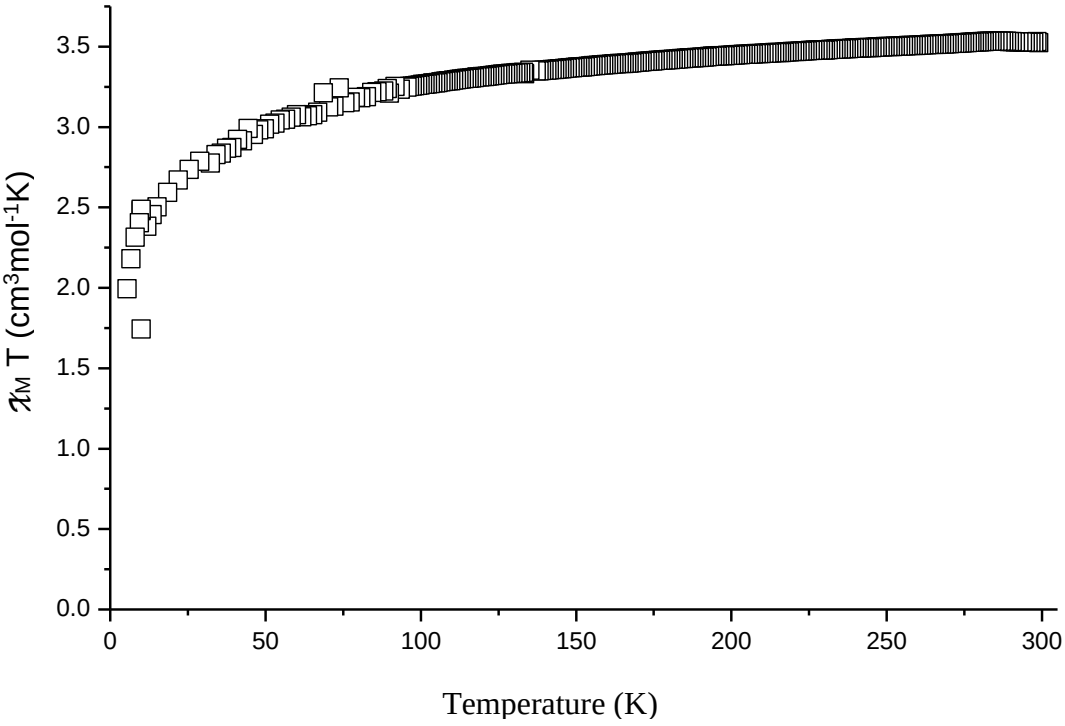

Figure 3.19: Magnetic susceptibility measurement of $([Fe_{0.5}(L2)(SCN)].MeOH)_n$ coordination polymer.

Table 3.7: Selected bond lengths (Å) and angles (°) for $([Fe_{0.5}(L2)(SCN)].MeOH)_n$ CP.

Fe-N1	2.210(2)	N1-Fe-N3	90.43(8)
Fe-N3	2.268(2)	N3-Fe-N3^1	180.0
Fe-N5	2.122(2)	N5^1-Fe-N1	91.36(9)
S-C19	1.637(3)	N5-Fe-N1	88.64(9)
N5-C19	1.153(4)	N5-Fe-N3	89.87(8)
N2-C6	1.449(4)	N5-Fe-N3^1	90.13(8)
N2-C7	1.407(4)	N5-Fe-N5^1	180.0
N4-C15	1.465(4)	C7-N2-C6	118.7(2)
N4-C16	1.398(6)	C16-N4-C15	120.1(4)
N1-Fe-N1^1	180.0	N2-C6-C3	110.4(2)
N1-Fe-N3^1	89.58(8)	N4-C15-C12	113.9(3)
N1^1-Fe-N3^1	90.42(8)	N5-C19-S	177.9(3)
N1^1-Fe-N3	89.57(8)	Fe-N5-C19	152.1(2)

Table 3.8: Selected torsion angles (°) for $([Fe_{0.5}(L2)(SCN)].MeOH)_n$ CP.

Fe-N1-C1-C2	-179.0(2)	C6-N2-C7-C9	-15.4(4)
Fe-N1-C5-C4	179.6(3)	C7-N2-C6-C3	172.8(2)
Fe-N3-C10-C11	-175.2(4)	N4-C16-C17-C18^1	179.7(3)
Fe-N3-C14-C13	174.7(3)	N4-C16-C18-C17^1	-179.6(3)
N2-C7-C8-C8^1	178.1(4)	C11-C12-C15-N4	146.5(5)
N2-C7-C9-C9^1	-177.9(3)	C13-C12-C15-N4	-33.0(6)
C2-C3-C6-N2	112.9(3)	C15-N4-C16-C17	-174.8(3)
C4-C3-C6-N2	-69.3(4)	C15-N4-C16-C18	5.6(5)
C6-N2-C7-C8	166.3(3)	C16-N4-C15-C12	-74.8(5)

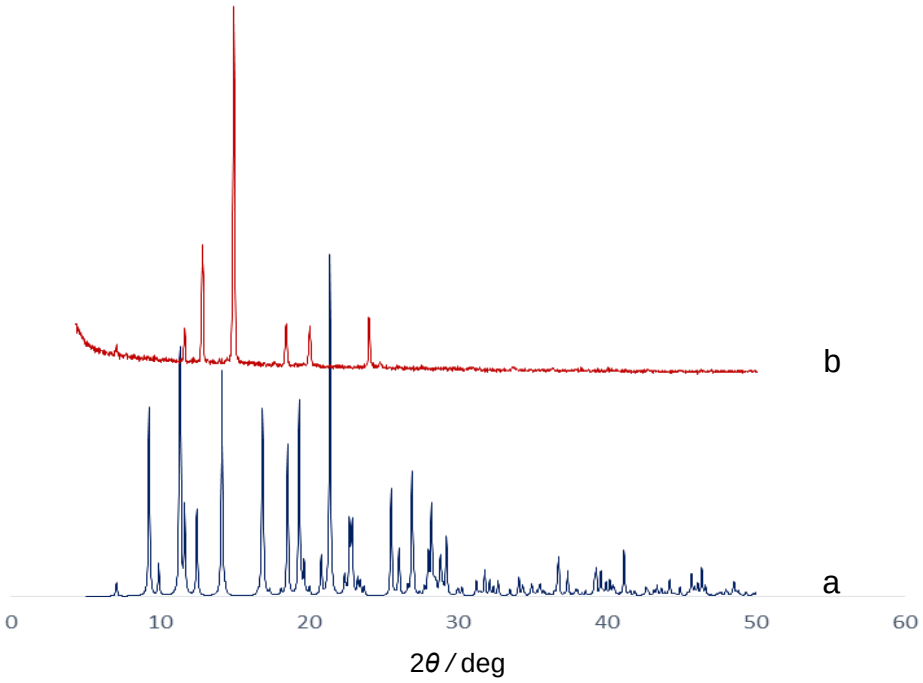

Figure 3.20: (a) Calculated powder XRD pattern of compound **12**. (b) Powder XRD pattern of compound **12**.

3.5.5 Crystal structure of $([Co(L2)].NO_3.DMF)_n$ complex (13)

$([Co(L2)].(NO_3).DMF)_n$ complex was synthesised by solvothermal reaction of L2 ligand and $Co(NO_3)_2.6H_2O$ in DMF as described before in section 3.2.6. The crystal structure was solved in monoclinic space group $P2_1/n$ [31-35] and shows one L2 ligand molecule, one cobalt(I) ion on a general position, one nitrate anion and one distorted DMF solvent molecule per asymmetric unit (figure 3.21). Co(I) is coordinated to two L2 ligand molecules by nitrogen atoms of 4-pyridyl rings and shows two different coordination distances (Co-N1= 1.888(9) Å) and (Co-N4= 1.900(9) Å) to produce Co(I) linear coordination centre (figure 3.22). This coordination model is very rare to the best of our knowledge and occurred only with bulk ligand systems [55]. Moreover, Co(I) also has ionic interactions with the nitrate anions and shows two ionic distances (Co-O2= 2.655 Å) and (Co-O3= 2.800 Å).

The ligand L2 behaves as a bidentate ligand and coordinated to two Co(I) coordination centres *via* nitrogen atoms of 4-pyridyl rings. L2 ligand molecule shows two torsion angles of 85.70(13) and -81.0(13) ° between the phenyl and 4-pyridyl rings to produce L2 ligand bent U-shape between Co(I) coordination centres (figure 3.20) and (table 3.9). After growing the structure, a rectangular complex structure of $[Co_2L_2]$ metallacycle was obtained. The new structure has 7.844 × 13.478 Å cavity that occupied by two DMF guest molecules (figure 3.22). The experimental powder X-ray analysis for complex **13** do not match with the calculated powder XRD pattern of the single crystal structure. The resulted phase is solid, but the structure

could not be determined as the complex did not stay as a single crystal on drying out (figure 3.23). Selected bond lengths, angles and torsion angles for complex 13 are listed in tables 3.9 and 3.10.

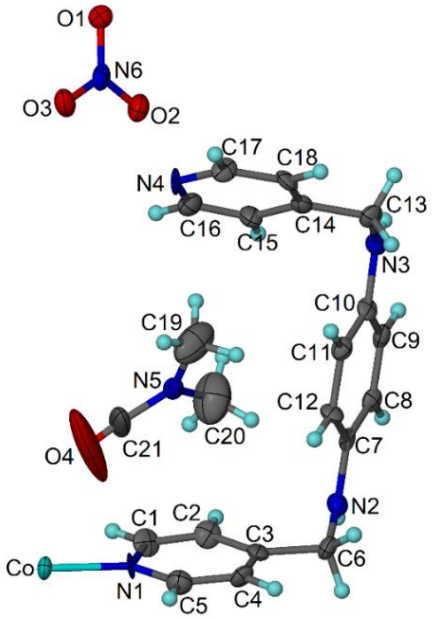

Figure 3.21: $([Co(L2)].NO_3.DMF)_n$ complex asymmetric unit of the crystal structure. Ellipsoids shown at 50 % probability levels.

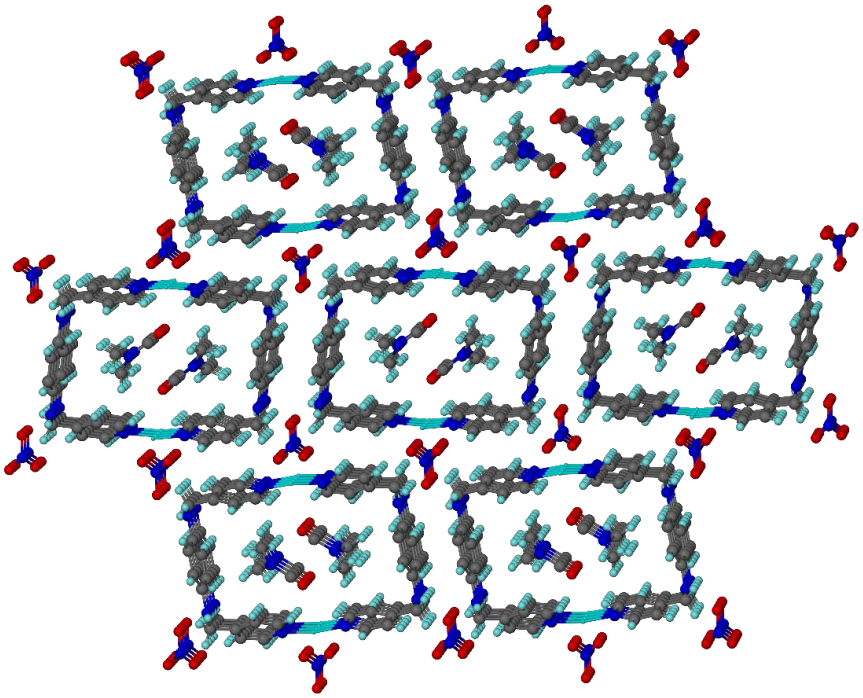

Figure 3.22: $([Co(L2)].NO_3.DMF)_n$ complex after symmetrical expanding, the resulted rectangular cavities are occupied by two DMF molecules.

Table 3.9: Selected bond lengths (Å) and angles (°) for compound **13**.

Co-N1	1.888(9)	C16-N4-Co	119.2(9)
Co-N4	1.900(9)	C17-N4-Co	122.8(9)
N2-C6	1.434(16)	C7-N2-C6	119.0(10)
N2-C7	1.415(15)	N2-C6-C3	114.0(10)
N3-C13	1.434(15)	N4-C16-C15	124.4(12)
N3-C10	1.392(15)	N3-C13-C14	113.2(10)
N1-Co-N4^{1}	170.70(10)	C8-C7-N2	122.4(11)
C5-N1-Co	1.22.20(9)	C12-C7-N2	118.7(10)
C1-N1-Co	119.8(9)	N3-C10-C11	118.7(11)
C10-N3-C13	120.40(10)	C9-C10-N3	124.3(10)

Table 3.10: Selected torsion angles (°) for $([Co(L2)].NO_3.DMF)_n$ complex.

Co-N1-C1-C2	174.5(11)	C2-C3-C6-N2	21.8(17)
Co-N1-C5-C4	-175.4(10)	C4-C3-C6-N2	-160.2(11)
Co^{1}-N4-C16-C15	-178.5(10)	C6-N2-C7-C8	-16.6(16)
Co^{1}-N4-C17-C18	178.6(9)	C6-N2-C7-C12	164.5(10)
N2-C7-C8-C9	-179.2(10)	C7-N2-C6-C3	85.7(13)
N2-C7-C12-C11	179.1(10)	C8-C9-C10-N3	177.6(11)
N3-C10-C11-C12	-177.9(11)	C10-N3-C13-C14	-81.7(13)
N3-C13-C14-C15	-3.4(16)	C13-N3-C10-C9	12.9(17)
N3-C13-C14-C18	176.0(11)	C13-N3-C10-C11	-171.5(10)

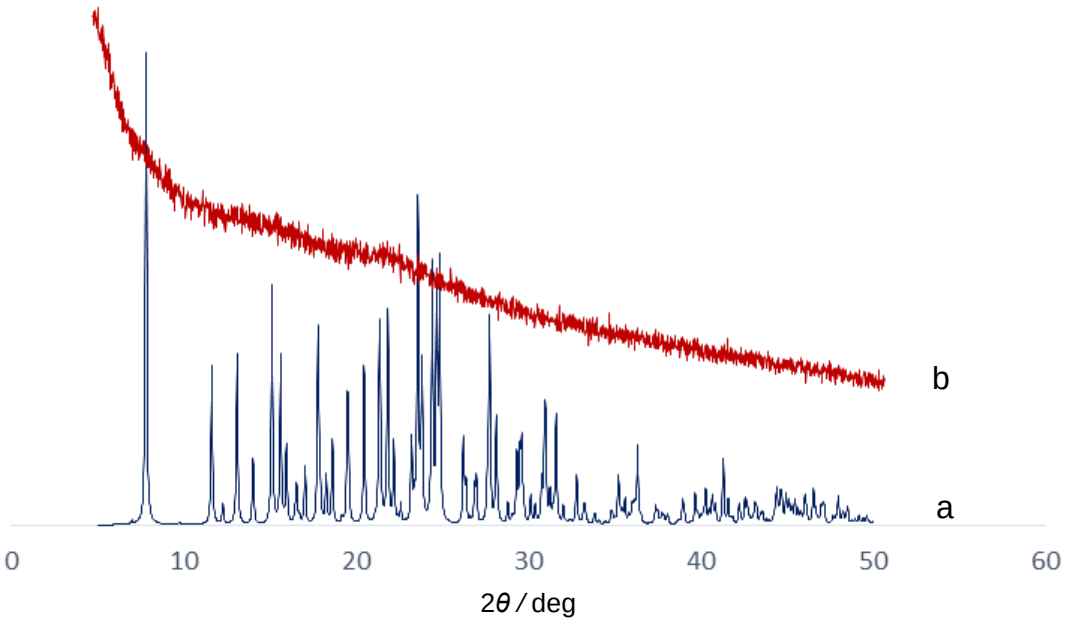

Figure 3.23: (a) Calculated powder XRD pattern of $([Co(L2)].NO_3.DMF)_n$ complex. (b) Powder XRD pattern of complex **13**.

Table 3.11: The crystallographic data of compounds L2, **9** and **10**.

Identification code	L2	**9**	**10**
Empirical Formula	$C_{18}H_{18}N_4$	$C_{10}H_{15}ClMn_{0.5}N_2OS$	$C_{10}H_{15}ClCo_{0.5}N_2OS$
Formula weight	290.36	273.70	275.96
Temperature/K	119.99(13)	119.99(10)	119.99(11)
Crystal system	Triclinic	Triclinic	Triclinic
Space group	$P\bar{1}$	$P\bar{1}$	$P\bar{1}$
a/Å	6.9995(10)	6.6463(7)	6.6700(5)
b/Å	7.5918(11)	9.2681(11)	9.1886(5)
c/Å	7.9588(11)	10.3253(12)	10.2064(5)
α/°	112.230(13)	92.885(9)	93.525(4)
β/°	101.539(12)	98.238(9)	98.399(5)
γ/°	94.915(12)	100.660(9)	100.880(5)
Volume/Å^3	377.46(10)	616.67(12)	605.13(6)
Z	1	3	2
ρ_{calc}g/cm^3	1.277	1.541	1.582
μ/mm^{-1}	0.615	0.949	9.439
F(000)	154.0	297.0	299.0
Crystal size/mm^3	0.073 × 0.125 × 0.310	0.076 × 0.111 × 0.190	0.066 × 0.071 × 0.087
Radiation	*CuKα* (*λ* = 1.54184)	*MoKα* (*λ* = 0.71073)	*CuKα* (*λ* = 1.54184)
2*Θ* range for data collection/°	12.416 to 146.986	3.998 to 52.536	8.794 to 147.902
Index ranges	-7 ≤ h ≤ 8, -9 ≤ k ≤ 9, -8 ≤ l ≤ 9	-8 ≤ h ≤ 6, -11 ≤ k ≤ 11, -8 ≤ l ≤ 12	-8 ≤ h ≤ 8, -11 ≤ k ≤ 9, -8 ≤ l ≤ 12
Reflections collected	2375	4058	4768
Independent reflections	1418 [R_{int} = 0.0364, R_{sigma} = 0.0490]	2319 [R_{int} = 0.0473, R_{sigma} = 0.0559]	2292 [R_{int} = 0.0368, R_{sigma} = 0.0458]
Data/restraints/parameters	1418/0/100	2319/0/153	2292/0/153
Goodness-of-fit on F^2	1.046	1.064	1.052
Final *R* indexes [*I*>=2*σ* (*I*)]	R_1 = 0.0669, wR_2 = 0.1756	R_1 = 0.0590, wR_2 = 0.1582	R_1 = 0.0467, wR_2 = 0.1224
Final *R* indexes [all data]	R_1 = 0.0775, wR_2 = 0.1926	R_1 = 0.0656, wR_2 = 0.1664	R_1 = 0.0486, wR_2 = 0.1245
Largest diff. peak/hole / e Å^{-3}	0.63/-0.63	0.88/-1.03	0.55/-0.47

Table 3.12: The crystallographic data of compounds **11**, **12** and **13**.

Identification code	**11**	**12**	**13**
Empirical Formula	$C_{18}H_{18}ClFe_{0.5}N_4$	$C_{20}H_{22}Fe_{0.5}N_5OS$	$C_{21}H_{25}CoN_6O$
Formula weight	353.42	408.41	484.40
Temperature/K	120.00(10)	120.01(17)	119.97(14)
Crystal system	Monoclinic	Monoclinic	Monoclinic
Space group	$P2_1/n$	$C2/c$	$P2_1/n$
a/Å	8.6951(2)	8.68801(18)	6.1606(5)
b/Å	18.1883(5)	19.1203(4)	22.6195(15)
c/Å	10.4986(3)	25.3135(5)	15.2559(11)
α/°	90	90	90
β/°	93.267(3)	98.8117(19)	94.439(7)
γ/°	90	90	90
Volume/Å^3	1657.65(8)	4155.37(15)	2119.5(3)
Z	1	8	4
ρ_{calc}g/cm^3	1.417	1.280	1.495
μ/mm^{-1}	0.656	4.207	6.692
F(000)	736.0	1676.0	993.0
Crystal size/mm^3	0.126 × 0.178 × 0.246	0.063 × 0.070 × 0.160	0.077 × 0.114 × 0.286
Radiation	*MoKα* (λ = 0.71073)	*CuKα* (λ = 1.54184)	*CuKα* (λ = 1.54184)
2Θ range for data collection/°	4.478 to 52.532	7.068 to 147.656	7.004 to 148.172
Index ranges	-10 ≤ h ≤ 8, -22 ≤ k ≤ 15, -12 ≤ l ≤ 12	-7 ≤ h ≤ 10, -23 ≤ k ≤ 19, -31 ≤ l ≤ 28	-6 ≤ h ≤ 7, -24 ≤ k ≤ 27, -17 ≤ l ≤ 18
Reflections collected	6299	9048	8703
Independent reflections	3267 [R_{int} = 0.0391, R_{sigma} = 0.0493]	3939 [R_{int} = 0.0243, R_{sigma} = 0.0287]	4146 [R_{int} = 0.1020, R_{sigma} = 0.1229]
Data/restraints/parameters	3267/0/214	3939/0/252	4146/0/291
Goodness-of-fit on F^2	1.119	1.049	1.134
Final R indexes [I>=2σ (I)]	R_1 = 0.0620, wR_2 = 0.1616	R_1 = 0.0535, wR_2 = 0.1534	R_1 = 0.1301, wR_2 = 0.3240
Final R indexes [all data]	R_1 = 0.0698, wR_2 = 0.1683	R_1 = 0.0603, wR_2 = 0.1597	R_1 = 0.1998, wR_2 = 0.3596
Largest diff. peak/hole / e Å^{-3}	0.O82/-0.62	0.81/-0.56	1.08/-1.04

3.6 Conclusion

This chapter reports the synthesis and characterisation of the ligand *N*,*N'*-bis-pyridin-4-ylmethyl-benzene-1,4-diamine (L2) as an organic linker with Mn(II), Fe(III) and Co(II) metal salts to produce $([Mn_{0.5}(L2)_{0.5}Cl(DMSO)])_n$ and $([Co_{0.5}(L2)_{0.5}Cl(DMSO)])_n$ one-dimensional polymers. $([Fe_{0.5}(L2)Cl])_n$ and $([Fe_{0.5}(L2)(SCN)].MeOH)_n$ two-dimensional polymers, and $([Co(L2)].NO_3.DMF)_n$ complex. Compounds **9** and **10** are isostructural one-dimensional coordination polymers with a zig-zag structure for L2 molecules between M^{2+} coordination centres. Compound **11** is a two-dimensional coordination polymer that has 4^4 network topology. The resulted 2D network is packed with two other networks in an inter-digitated fashion and there are no significant channels in the lattice. According to CCDC compound **11** represent the first example of iron(II) chloride and 4-pyridyl ligands two-dimensional coordination polymer. Compound **12** has a two-dimensional 4^4 network topology and the cyclic unit of four Fe(II) ions and four ligand molecules is interpenetrating with another two-dimensional network in two-fold 2D-2D fashion. Magnetic susceptibility measurements for compound **12** shows iron(II) high spin state properties from 300 to 5 K and zero field splitting below 5 K. Complex **13** forms unexpected Co(I) M_2L_2 metallacycle that could due to the synthesis process or L2 ligand flexibility.

3.7 References

1. D. Grasso, G. Buemi, S. Fasone and C. Gandolfo, Electronic Spectra and Dipole Moments of *p*-Phenylendiamine-*N*-*N*'-dibenzylidene and Its Aza-derivatives. *Croatica Chemica Acta*. 1981, **45**(1), 85-90.
2. M. Zahedi, B. Shaabani, M. Aygün and C. Kazak, Construction of one dimensional Co(II) and Zn(II) coordination polymers based on expanded *N,N'*-donor ligands. *Inorganica Chimica Acta*. 2018, **469**, 461-468.
3. R. Sanii, A. Bajpai, E. P. Kaźmierczak and M. J. Zaworotko, High Yield, Low-Waste Synthesis of a Family of Pyridyl and Imidazolyl-Substituted Schiff Base Linker Ligands. *ACS Sustainable Chemistry and Engineering*. 2018, **6**(11), 14589-14598.
4. R. Jangir, A. C. Kalita, D. Kaleeswaran, S. K. Gupta and R. Murugavel, A [4+2] Condensation Strategy to Imine-Linked Single-Crystalline Zeolite-Like Zinc Phosphate Frameworks. *Chemistry A European Journal.* 2018, **24**(23), 6178-6190.
5. L. Esrafili, V. Safarifard, E. Tahmasebi, M. D. Esrafili and A. Morsali, Functional group effect of isoreticular metal-organic frameworks on heavy metal ion adsorption. *New Journal of Chemistry*. 2018, **42**(11), 8864-8873.
6. N. R. Yousefnia, B. Shaabani, M. Kubicki, M. S. Zakerhamidi and A. M. Grzeskiewicz, 2D holodirected lead(II) halide coordination polymers based on rigid *N,N'*-bis(4-pyridylmethylidyne) phenylene-1,4-diamine ligand: Syntheses, crystal structures, NBO studies and luminescence properties. *Polyhedron*. 2017, **129**, 38-45.
7. H. Amanzadeh, Y. Yamini, M. Y. Masoomi and A. Morsali, Nanostructured metal-organic frameworks, TMU-4, TMU-5, and TMU-6, as novel adsorbents for solid phase microextraction of polycyclic aromatic hydrocarbons. *New Journal of Chemistry*. 2017, **41**(20), 12035-12043.
8. V. Safarifard, S. R. Hermida, V. Guillerm, I. Imaz, M. Bigdeli, A. A. Tehrani, J. Juanhuix, A. Morsali, M. E. Casco, J. S. Albero, E. V. R. Fernandez and D. Maspoch, Influence of the Amide Groups in the CO_2/N_2 Selectivity of a Series of Isoreticular, Interpenetrated Metal-Organic Frameworks. *Crystal Growth and Design*. 2016, **16**(10), 6016-6023.
9. E. Tahmasebi, M. Y. Masoomi, Y. Yamini and A. Morsali, Application of a Zn(II) based metal-organic framework as an efficient solid-phase extraction sorbent for preconcentration of plasticizer compounds. *RSC Advances*. 2016, **6**(46), 40211-40218.
10. S. Abedi, A. A. Tehrani, H. Ghasempoura and A. Morsali, Interplay between hydrophobicity and basicity toward the catalytic activity of isoreticular MOF organocatalysts. *New Journal of Chemistry*. 2016, **40**(8), 6970-6976.
11. M. Y. Masoomi, M. Bagheri and A. Morsali, High adsorption capacity of two Zn-based metal-organic frameworks by ultrasound assisted synthesis. *Ultrasonics Sonochemistry*. 2016, **33**, 54-60.
12. F. Bigdeli, S. Abedi, H. H. Monfared and A. Morsali, An investigation of the catalytic activity in a series of isoreticular Zn(II)-based metal-organic frameworks. *Inorganic Chemistry Communications*. 2016, **72**, 122-127.
13. Tehrani, H. Ghasempour, A. Morsali, G. Makhloufi and C. Janiak, Effects of Extending the pi-Electron System of Pillaring Linkers on Fluorescence Sensing of Aromatic Compounds in Two Isoreticular Metal-Organic Frameworks. *Crystal Growth and Design*. 2015, **15**(11), 5543-5547.

14. M. Y. Masoomi, S. Beheshti and A. Morsali, Shape Control of Zn(II) Metal-Organic Frameworks by Modulation Synthesis and Their Morphology-Dependent Catalytic Performance. *Crystal Growth and Design*. 2015, **15**(5), 2533-2538.
15. E. Tahmasebi, M. Y. Masoomi, Y. Yamini and A. Morsali, Application of Mechanosynthesized Azine-Decorated Zinc(II) Metal-Organic Frameworks for Highly Efficient Removal and Extraction of Some Heavy-Metal Ions from Aqueous Samples: A Comparative Study. *Inorganic Chemistry*. 2015, **54**(2), 425-433.
16. A. Ghorai, J. Mondal, R. Chandra and G. K. Patra, A reversible fluorescent-colorimetric imino-pyridyl bis-Schiff base sensor for expeditious detection of Al^{3+} and HSO_3^- in aqueous media. *Dalton Transactions*. 2015, **44**(29), 13261-13271.
17. M. Y. Masoomi, S. Beheshti and A. Morsali, Mechanosynthesis of new azine-functionalized Zn(II) metal-organic frameworks for improved catalytic performance. *Journal of Materials Chemistry A*. 2014, **2**(40), 16863-16866.
18. D. Sek, M. Siwy, K. Bijak, M. G. Zajac, G. Malecki, K. Smolarek, L. Bujak, S. Mackowski and E. S. Balcerzak, Comparative Studies of Structural, Thermal, Optical, and Electrochemical Properties of Azines with Different End Groups with Their Azomethine Analogues toward Application in (Opto)Electronics. *The Journal of Physical Chemistry A*. 2013, **117**(40), 10320-10332.
19. H. Lang, K. Döring, D. Taher, U. Siegert, B. Walfort, T. Rüffer and R. Holze, Linear homobimetallic palladium complexes with end-capped SC(O)Me units. *Journal of Organometallic Chemistry*. 2009, **694**(1), 27-35.
20. J. J. Jang, L. Li, T. Yang, D. B. Kuang, W. Wang and C. Y. Su, Self-assembly of 2D Borromean networks through hydrogen-bonding recognition. *Chemical Communications*. 2009, (**17**), 2387-2389.
21. J. J. Jiang, S. R. Zheng, Y. Liu, M. Pan, W. Wang and C. Y. Su, Self-Assembly of Triple Helical and meso-Helical Cylindrical Arrays Tunable by Bis-Tripodal Coordination Converters. *Inorganic Chemistry*. 2008, **47**(22), 10692-10699.
22. Q. Wang, D. Q. Wang and Y. Y. Sun, *N,N′*-Bis(4-pyridylmethylene)benzene-1,4-diamine monohydrate. *Acta Crystallographica Section E*. 2007, **63**(12), o4665-o4665.
23. Q. F. Hou, L. Ye and S. M. Jiang, *N,N′*-Bis(4-pyridylmethyl-ene)benzene-1,4-diamine. *Acta Crystallographica Section E*. 2007, **63**(2), o939-o940.
24. S. Vatsadze, M. Al-Anber, W. R. Thiel, H. Lang and R. Holze, Electrochemical studies and semiempirical calculations on π-conjugated dienones and heterocyclic nitrogen containing donor ligand molecules. *Journal of Solid State Electrochemistry*. 2005, **9**(11), 764-777.
25. M. Al-Anber, S. Vatsadze, R. Holze, H. Lang and W. R. Thiel, π-Conjugated N-heterocyclic compounds: correlation of computational and electrochemical data. *Dalton Transactions*. 2005, (**22**), 3632-3737.
26. M. Al-Anber, T. Stein, S. Vatsadze and H. Lang, Organometallic π-tweezers incorporating pyrazine- and pyridine-based bridging units. *Inorganica Chimica Acta*. 2005, **358**(1), 50-56.
27. S. Z. Vatsadze, V. N. Nuriev, A. V. Chernikov and N. V. Zyk, Synthesis of novel linear exo-bidentate bispyridine ligands and their complexes with silver(I) tetrafluoroborate. *Russian Chemical Bulletin*. 2002, **51**(10), 1957-1958.
28. T. Moriuchi, S. Bandoh, M. Kamikawa and T. Hirao, Palladium Homobimetallic Complexes with Bridging π-Conjugated Ligands. *Chemistry Letters*. 2000, **29**(2), 148-149.

29. M. Kunitake, K. Akiyoshi, K. Kawatana, N. Nakashima and O. Manabe, Transmembrane electron transfer through a new hydrophobic mediator incorporated in monolayer assemblies on metal electrodes. *Journal of Electroanalytical Chemistry*. 1990, **292**(1), 277-280.
30. H. Zhou, C. X. Chua and Y. Z. Li, Poly[[aquatris(*μ*-benzene-1,4-dicarboxylato)tricobalt(II)] methanol monosolvate monohydrate]. *Acta Crystallographica Section E: Structure Reports Online*. 2011, **67**(7), m841-m842.
31. L. J. Bourhis, O. V. Dolomanov, R. J. Gildea, J. A. K. Howardd and H. Puschmannb, The anatomy of a comprehensive constrained, restrained refinement program for the modern computing environment-Olex2 dissected. *Acta Crystallographica Section A.* 2015, **71**(1), 59-75.
32. L. Palatinus, S. J. Prathapab and S. V. Smaalen, EDMA: a computer program for topological analysis of discrete electron densities. *Journal of Applied Crystallography*. 2012, **45**(3), 575-580.
33. O. V. Dolomanov, L. J. Bourhis, R. J. Gildea, J. A. K. Howarda and H. Puschmann, OLEX2: a complete structure solution, refinement and analysis program. *Journal of Applied Crystallography*. 2009, **42**(2), 339-341.
34. L. Palatinus and A. V. D. Lee, Symmetry determination following structure solution in *P*1. *Journal of Applied Crystallography*. 2008, **41**(6), 975-984.
35. L. Palatinus and G. Chapuis, SUPERFLIP-a computer program for the solution of crystal structures by charge flipping in arbitrary dimensions. *Journal of Applied Crystallography*. 2007, **40**(4), 786-790.
36. Robert M. Silverstein, Francis X. Webster and David J. Kiemle, Spectrometric identification of organic compounds: 7th Edition. 2005. John Wiley and Sons, Inc.
37. Donald L. Pavia, Gary M. Lampman and George S. Kriz, Introduction to spectroscopy: a guide for students of organic chemistry: 3rd Edition. 2001. Harcourt College Publishers.
38. Dudley H. Williams and Ian Fleming, Spectroscopic methods in organic chemistry: 6th Edition. 1995. McGraw-Hill Companies, Inc.
39. R. J. Abraham, J. Fisher and P. Loftus, Introduction to NMR spectroscopy: 1988. John Wiley and Sons, Inc.
40. J. R. Ferraro, L. J. Basile and D. L. Kovacic, The Infrared Spectra of Rare Earth Metal Chloride Complexes of 2,2'-Bipyridyl and 1,10-Phenanthroline from 650 to 70 cm^{-1}. *Inorganic Chemistry*. 1966, **5**(3), 391-395.
41. C. Baer and J. Pike, Infrared Spectroscopic Analysis of Linkage Isomerism in Metal-Thiocyanate Complexes. *Journal of Chemical Education*. 2010, **87**(7), 724-726.
42. M. Kabesova and J. Gazo, Structure and classification of thiocyanates and the mutual influence of their ligands. *Chemické Zvesti*. 1980, **34**(6), 800-841.
43. L. H. Jones, Infrared Spectrum and Structure of the Thiocyanate Ion. *The Journal of Chemical Physics*. 1956, **25**(5), 1069-1072.
44. C. M. Armstrong, P. V. Bernhardt, P. Chin and D. R. Richardson, Structural Variations and Formation Constants of First-Row Transition Metal Complexes of Biologically Active Aroylhydrazones. *European Journal of Inorganic Chemistry*. 2003, **2003**(6), 1145-1156.
45. J. Lu, C. Yu, T. Niu, T. Paliwala, G. Crisci, F. Somosa and A. J. Jacobson, One-Dimensional Coordination Polymers of Cobalt with 4,4‘-Bipyridine: Syntheses and Structures. *Inorganic Chemistry*. 1998, **37**(18), 4637-4640.
46. Gautam. R. Desiraju and Thomas Steiner, The weak hydrogen bond in structural chemistry and biology: 2001. Oxford University Press.

47. T. Iwasita, Electrocatalysis of methanol oxidation. *Electrochimica Acta*. 2002, **47**(22-23), 3663-3674.
48. A. Hoser and Z. Kaluski, Structure of the Pyridine-Ferric Chloride (4:1) Complex, $Fe(C_5H_5N)_3Cl_3.C_5H_5N$, at 190 K. *Acta Crystallographica Section C: Structural Chemistry*. 1983, C**39**, 1039-1041.
49. G. J. Long and P. J. Clarke, Crystal and Molecular Structures of *trans*-Tetrakis(pyridine)dichloroiron(II), -nickel(II), and -cobalt(II) and *trans*-Tetrakis(pyridine)dichloroiron(II) Monohydrate. *Inorganic Chemistry*. 1978, **17**(6), 1394-1401.
50. P. Karsten and J. Strahle, Bis(1,8-diazabicyclo[5.4.0]undec-7-en-8-ium) *trans*-Dichlorotetra(pyridine-N)iron(II) Dichloride. *Acta Crystallographica Section C*. 1998, **54**(10), 1406-1408.
51. Y. H. Luo, D. E. Qian, Y. W. Zhang, Y. H. Jiang, H. S. Wu and B. W. Sun, Investigation of two 2D interpenetration iron(II) coordination polymers. *Polyhedron*. 2016, **110**, 241-246.
52. G. J. Halder, C. J. Kepert, B. Moubaraki, K. S. Murray and J. D. Cashion, Guest-dependent spin crossover in a nanoporous molecular framework material. *Science*. 2002, **298**(5599), 1762-1765.
53. K. E. Burrows, S. E. M. Grath, R. Kulmaczewski, O. Cespedes, S. A. Barrett and M. A. Halcrow, Spin States of Homochiral and Heterochiral Isomers of $[Fe(PyBox)_2]^{2+}$ Derivatives. *Chemistry A European Journal*. 2017, **23**(38), 9067-9075.
54. K. E. Burrows, R. Kulmaczewski, O. Cespedes, S. A. Barrett and M. A. Halcrow, The speciation of homochiral and heterochiral diastereomers of homoleptic cobalt(II) and zinc(II) PyBox complexes. *Polyhedron*. 2018, **149**, 134-141.
55. C. B. Ni, T. A. Stich, G. J. Long and P. P. Power, Unusual magnetic properties of a two-coordinate heteroleptic linear cobalt(II) complex. *Chemical Communications*. 2010, **46**(25), 4466-4468.

N,N′-Bis(4-pyridinylmethyl)-2,5-dimethylbenzene-1,4-diamine (L3) MOFs

4.1 Introduction

Synthesis of new ligands plays an important role in the development of coordination chemistry that could be indicated by the high publication's number in recent years. New ligand systems based on pyridyl substituted compounds are well known in coordination polymers chemistry [1-8], that might due to the simple synthesis methods [2,9-11], stability [12-14] or resulted architecture [15-17]. Imine, amide, azo or amine ligands contains 4-pyridyl rings have a considerable attention in coordination polymers chemistry and utilised in different fields such as chemical catalysis [2, 3, 18], gas storage and separation [19-22], luminescence [15, 23, 24], spin crossover [8, 25] and biological activities [26-28].

This chapter reports designing, synthesis and characterisation of new ligand based on 4-pyridinecarboxaldehyde and 2,5-dimethyl-benzene-1,4-diamine and the new ligand reaction with iron(II) thiocyanate, iron(III) chloride, cobalt(II) nitrate, cadmium(II) nitrate, isophthalic acid (H_2-isoph) or 5-methylisophthalic acid (H_2-Meisoph) to produce a series of new coordination polymers. We selected 2,5-dimethyl-benzene-1,4-diamine to control the resulted ligand structure and torsion angles as the substituted aromatic amine may result in a linear linker ligand. To the best of our knowledge, only one similar ligand based on isonicotinoyl chloride hydrochloride and 2,5-dimethyl-benzene-1,4-diamine was reported in 2016 by Vardhan and co-workers [29].

Self-assembly process of L3 ligand with $FeCl_3.6H_2O$ or $Fe(SCN)_2$ produced $([Fe_{0.5}(L3)Cl].MeOH)_n$ (**14**) or $([Fe(L3)_{0.5}(SCN)])_n$ (**15**) coordination polymers, where L3 is approximately linear in compound **14** and shows bent S-shape in compound **15**. On the other hand, reaction of L3, isophthalic acid, 5-methylisophthalic acid, $Co(NO_3)_2.6H_2O$ or $Cd(NO_3)_2.4H_2O$ in DMF at 115 °C for 24 hours produced $([Co(L3)(isoph)].DMF)_n$ (**16**), $(Cd(L3)(isoph)].DMF.H_2O)_n$ (**17**), $([Co(L3)(Meisoph)].DMF)_n$ (**18**) or $([Cd(L3)(Meisoph)].DMF)_n$ (**19**) two-dimensional coordination polymers where L3 is approximately linear and connecting between two different M(II)-isoph or M(II)-Meisoph 2D networks. The resulted compounds **16-19** are structurally stable and showed one-dimensional open network channels that occupied by solvent molecules for compounds **16**, **18** and **19** or water and solvent molecules for compound **17**.

4.2 Experimental

4.2.1 Synthesis of the new ligand *N,N'*-bis(4-pyridinylmethylene)-2,5-dimethylbenzene-1,4-diamine (^{c}L)

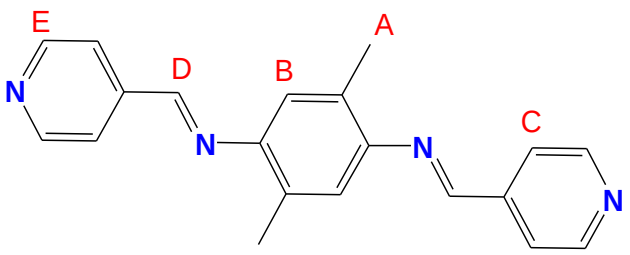

4-Pyridinecarboxaldehyde (1.57 g, 14.67 mmol) was dissolved in methanol (40 ml) and added dropwise with stirring to 2,5-dimethyl-benzene-1,4-diamine (1 g, 7.3 mmol) in methanol (40 ml) and heated under reflux for 5 hours at 70 °C. The solvent was evaporated under vacuum to result in a yellow solid product. The product was washed with acetone two times and dried under vacuum to form 1.90 g, 82.42 % yield of the new ligand ^{c}L, mp= 227.5-229 °C. ^{1}H NMR (300 MHz, $CDCl_3$) δ (ppm): δ 8.78 (m, 4H, E); 8.43 (s, 2H, D); 7.79 (m, 4H, C); 6.92 (s, 2H, B) and 2.41 (s, 6H, A); $^{13}C\{^{1}H\}$ NMR (75 MHz, $CDCl_3$) δ (ppm): 156.29, 150.57, 148.35, 143.03, 131.41, 122.19, 119.31 and 17.48; ESI-MS: *m/z* 315 $\{M+H\}^{+}$. IR (solid state): $\bar{\nu}$ (cm^{-1}) 3056, 2878, 1624, 1594 and 1410. Microanalysis found: C, 75.90; H, 5.80; N, 17.90 %, calculated for $C_{20}H_{18}N_4$: C, 76.41; H, 5.77; N, 17.82 %.

4.2.2 Synthesis of the new ligand *N,N'*-bis(4-pyridinylmethyl)-2,5-dimethylbenzene-1,4-diamine (L3)

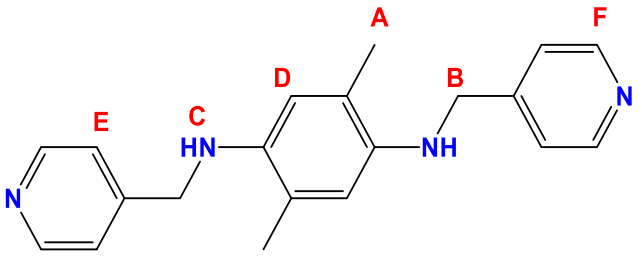

Sodium borohydride (2.5 g, 67 mmol) was added gradually to a pale yellow methanolic solution (250 ml) containing ^{c}L ligand (1.8 g, 5.7 mmol) at room temperature and left stirring overnight. The solvent was evaporated under vacuum, and the resulted powder was dissolved in deionized water (300 ml) by the addition of aqueous 1M HCl solution. Then, the reaction pH was increased to pH 13 by aqueous 2M sodium hydroxide solution. The ligand was precipitated from the basic solution, filtered, washed by water 4×100 ml and dried under vacuum to result in 1.56 g, 85.57 % yield of L3 ligand, mp= 186-187 °C. ^{1}H NMR (300 MHz, DMSO-d_6) δ(ppm): 8.46 (m, 4H, F); 7.33 (m, 4H, E); 6.12 (s, 2H, D); 4.91 (t, 2H, C, *J*= 6.2 Hz); 4.25 (d, 4H, B, *J*=5.9 Hz) and 2.00 (s, 3H, A); $^{13}C\{^{1}H\}$ NMR (75 MHz, DMSO-d_6) δ(ppm): 150.59, 149.31, 136.95, 122.22, 120.32, 113.40, 46.32 and 17.73; ESI-MS: *m/z* 319 $\{M+H\}^{+}$. IR (solid state): $\bar{\nu}$ (cm^{-1}) 3411, 3071, 2871, 1598, 1524, 1414 and 1361.

Microanalysis Found: C, 74.50; H, 6.70; N, 17.20 %, calculated for $C_{20}H_{22}N_4$: C, 75.44; H, 6.96; N, 17.60 %.

4.2.3 Synthesis of $([Fe_{0.5}(L3)Cl].MeOH)_n$ MOF (14)

A solution of the ligand (L3) (31 mg, 0.1 mmol) in MeOH (2 ml) was added dropwise to a vial containing $FeCl_3.6H_2O$ (27 mg, 0.1 mmol) in MeOH (2 ml). The reaction vial was heated for a few seconds, sealed and left to stand at room temperature to result in $([Fe_{0.5}(L3)Cl].MeOH)_n$ (28 mg) red crystals after a few days. IR (solid state): $\bar{\nu}$ (cm^{-1}) 3451, 3311, 3253, 3057, 2839, 1613, 1491, 1418, 1356 and 478. Microanalysis found: C, 61.76; H, 5.91; N, 13.95 %, calculated for $([Fe(L3)_2Cl_2].MeOH)_n$: C, 61.89; H, 6.08; N, 14.08 %.

4.2.4 Synthesis of $([Fe(L3)_{0.5}(SCN)])_n$ MOF (15)

A solution of the ligand (L3) (31 mg, 0.1 mmol) in MeOH (2 ml) was added dropwise to a vial containing $Fe(SCN)_2$ (17 mg, 0.1 mmol) in MeOH (2 ml). Then, the reaction vial was heated for a few seconds, sealed and left to stand at room temperature to result in $([Fe(L3)_{0.5}(SCN)])_n$ (23 mg) red crystals after a few weeks. IR (solid state): $\bar{\nu}$ (cm^{-1}) 3348, 3025, 2867, 2064, 1615, 1563, 1440, 1340 and 482. Microanalysis found: C, 58.62; H, 5.31; N, 15.71 %, calculated for $([Fe(L3)_2(SCN)_2].3H_2O)_n$: C, 58.46; H, 5.84; N, 16.23 %.

4.2.5 Synthesis of $(Co(L3)(isoph)].DMF)_n$ (16) and $(Cd(L3)(isoph)].DMF.H_2O)_n$ (17) MOFs

A pale yellow solution of the ligand (L3) (31 mg, 0.1 mmol) and isophthalic acid (H_2-isoph) (17 mg, 0.1 mmol) in DMF (3.5 ml) was added dropwise to $Co(NO_3)_2.6H_2O$ or $Cd(NO_3)_2.4H_2O$ (29 mg or 30 mg, 0.01 mmol) solution in *N*,*N*-dimethylformamide (DMF) (2 ml). Then, the reaction vials were sealed and placed in a thermal block and left for solvothermal reaction at 115 °C to result in $([Co(L3)(isoph)].DMF)_n$ (45 mg) or $(Cd(L3)(isoph)].DMF.H_2O)_n$ (38 mg) crystals after 24 hours. IR (solid state) for compound **16**: $\bar{\nu}$ (cm^{-1}) 3406, 3066, 2929, 1713, 1600, 1547, 1441, 1372, 526 and 420. IR (solid state) for compound **17**: $\bar{\nu}$ (cm^{-1}) 3300, 3050, 2918, 2854, 1671, 1609, 1571, 1444, 1393, 524 and 412. Microanalysis found: C, 60.37; H, 5.83; N, 11.18 %, calculated for $([Co(L3)(isoph)].DMF])_n$: C, 60.59; H, 5.41; N, 11.40 %. Found: C, 54.95; H, 5.80; N, 11.11 %, calculated for $([Cd(L3)(isoph)].2DMF])_n$: C, 55.10; H, 5.44; N, 11.34 %.

4.2.6 Synthesis of ([Co(L3)(Meisoph)].DMF)$_n$ (18) and ([Cd(L3)(Meisoph)].DMF)$_n$ (19) coordination polymers

A pale yellow solution of the ligand (L3) (31 mg, 0.1 mmol) and 5-methylisophthalic acid (H_2-Meisoph) (18 mg, 0.1 mmol) in DMF (4 ml) was added dropwise to $Co(NO_3)_2.6H_2O$ or $Cd(NO_3)_2.4H_2O$ (29 mg or 30 mg, 0.1 mmol) in DMF (3 ml). Then, the reaction vials were sealed and placed in the thermal block and left for solvothermal reaction at 115 °C to result in ([Co(L3)(Meisoph)].DMF)$_n$ (42 mg) or ([Cd(L3)(Meisoph)].DMF)$_n$ (32 mg) crystals after 24 hours. IR (solid state) for compound **18**: $\bar{\nu}$ (cm^{-1}) 3325, 3054, 2917, 2848, 1670, 1613, 1578, 1419, 1381, 525 and 450. IR (solid state) for compound **19**: $\bar{\nu}$ (cm^{-1}) 3324, 3040, 2918, 2851, 1671, 1610, 1542, 1416, 1372, 522 and 429. Microanalysis found: C, 60.97; H, 5.72; N, 11.06 %, calculated for ([Co(L3)(Meisoph)].DMF)$_n$: C, 61.14; H, 5.61; N, 11.14 %. Found: C, 55.97; H, 5.59; N, 10.06 %, calculated for ([Cd(L3)(Meisoph)].DMF)$_n$: C, 56.35; H, 5.17; N, 10.27 %.

4.3 Crystallography experimental

Crystals were mounted under inert oil on a MiTeGen tip and flash frozen to 120(1) using an OxfordCryosystems low temperature device. X-ray diffraction data were collected using Cu-*Ka* (λ= 1.54184 Å) radiation using an Agilent Supernova dual-source diffractometer with Atlas S2 CCD detector and fine-focus sealed tube generator. Data were corrected for Lorenztian and polarization effects, and absorption corrections were applied. The structures were solved by charge flipping methods using SUPERFLIP or by direct methods using SHELXS and refined by olex2.refine or by full-matrix least-squares on F^2 using SHELXL. All non-hydrogen atoms were refined as anisotropic, and hydrogen positions were included at geometrically estimated positions [30-34]. Summary of data collections and refinements are given in tables 4.13, 4.14 and 4.15. Further details of refinements are given below.

4.4 Results and discussions

4.4.1 Synthesis of the new ligand *N,N'*-bis(4-pyridinylmethylene)-2,5-dimethylbenzene-1,4-diamine (^{c}L)

The new ligand was synthesised by the reaction of 4-pyridinecarboxaldehyde and 2,5-dimethyl-benzene-1,4-diamine in MeOH according to scheme 4.1. The FTIR spectrum of the new ligand shows bands disappearance at 3396, 3306, 3219 and 1720 cm^{-1} that are due to amine or carbonyl group of 2,5-dimethyl-benzene-1,4-diamine or 4-pyridinecarboxaldehyde starting materials respectively [35-38]. Furthermore, the FTIR spectrum shows a new band at 1594 cm^{-1} that is due to imine group formation [35-38]. The ^{1}H NMR spectrum of the prepared ligand

shows disappearance of the aldehyde peak at δ 10.08 ppm and the amine peak at δ 3.91 ppm. Moreover, the ligand ^{1}H NMR spectrum shows a new singlet peak at δ 8.43 ppm which is due to the imine functional group formation (figure 4.1) [35-40]. The ^{13}C{^{1}H} NMR spectrum shows disappearance of the aldehyde peak at δ 193.11 ppm and appearance of the imine peak at δ 156.29 ppm (figure 4.2) [35-40].

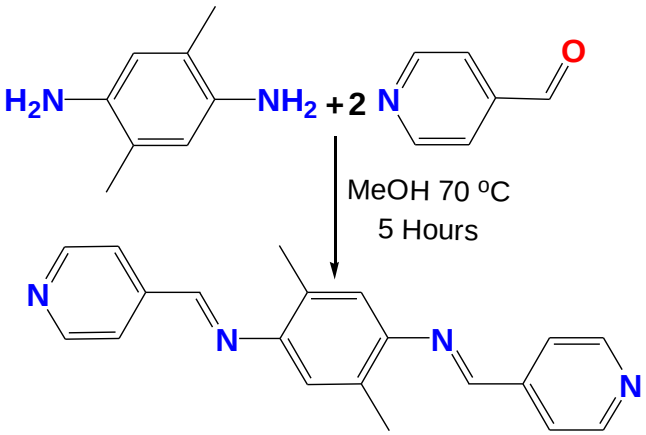

Scheme 4.1: Synthesis of the new ligand *N*,*N'*-bis(4-pyridinylmethylene)-2,5-dimethylbenzene-1,4-diamine (^{c}L).

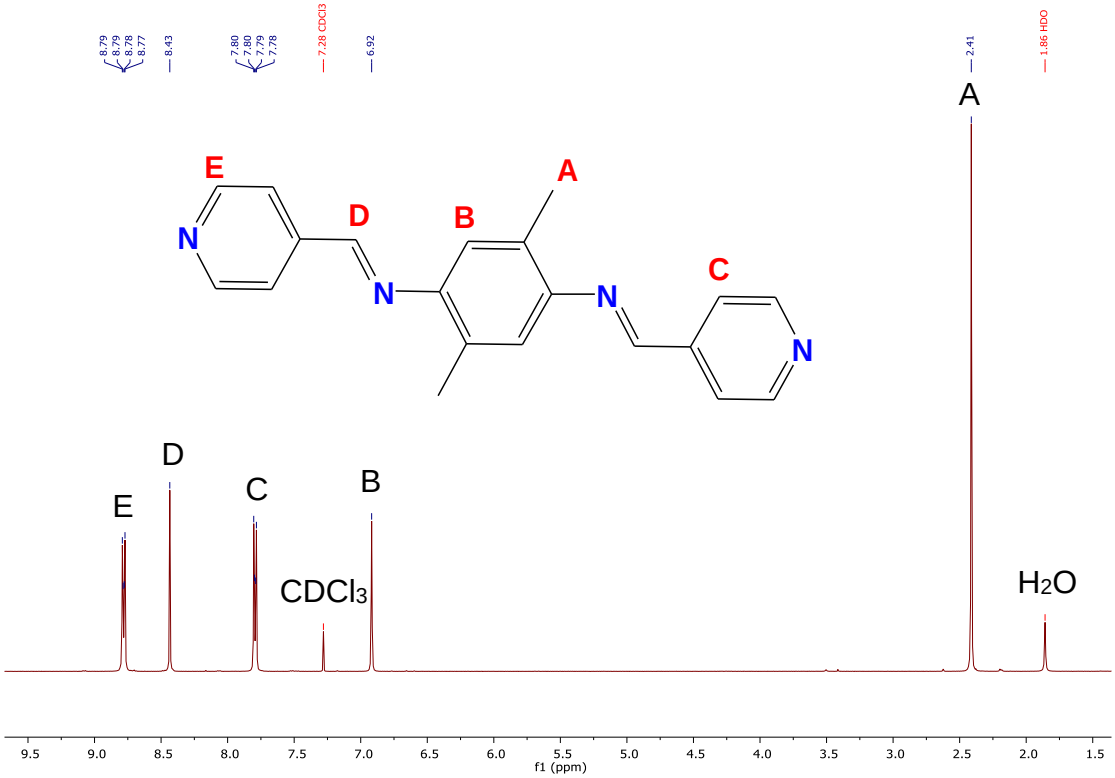

Figure 4.1: ^{1}H NMR (300 MHz, $CDCl_3$) spectrum of *N*,*N'*-bis(4-pyridinylmethylene)-2,5-dimethylbenzene-1,4-diamine (^{c}L).

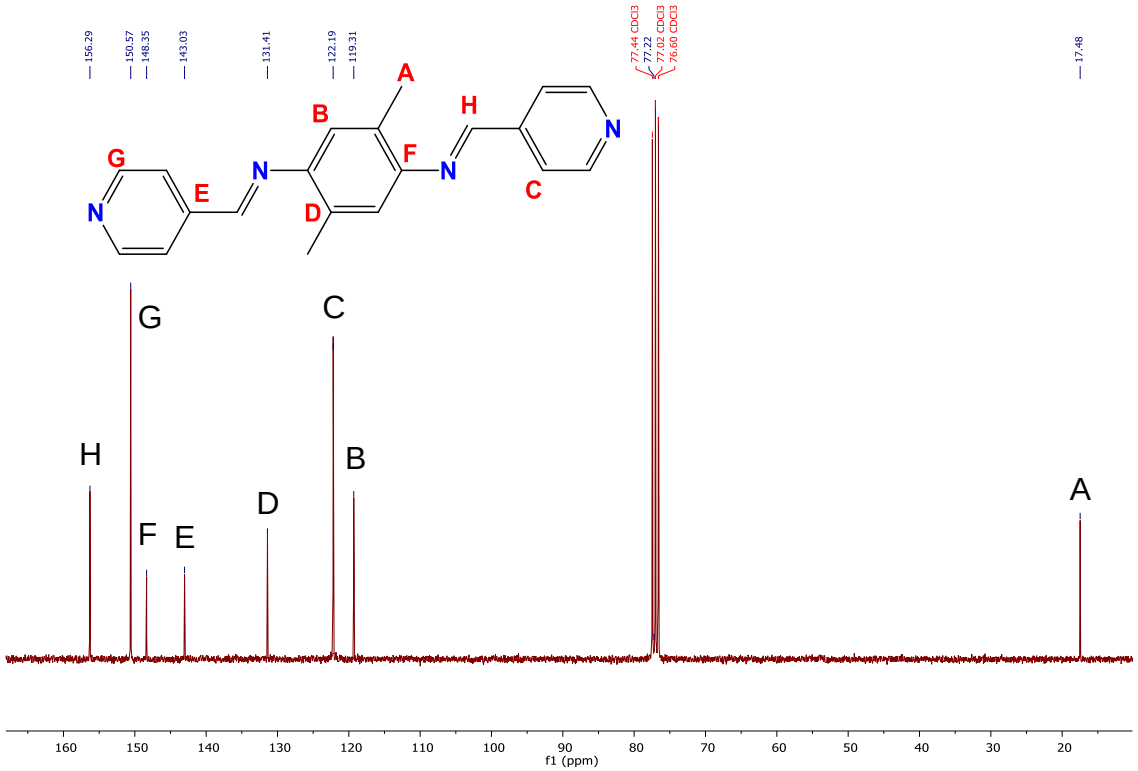

Figure 4.2: $^{13}C\{^{1}H\}$ NMR (75 MHz, $CDCl_3$) spectrum of *N*,*N*′-bis(4-pyridinylmethylene)-2,5-dimethylbenzene-1,4-diamine (^{c}L).

4.4.2 Synthesis of the new ligand *N*,*N*′-bis(4-pyridinylmethyl)-2,5-dimethylbenzene-1,4-diamine (L3)

The new ligand was prepared by reduction of *N*,*N*′-bis(4-pyridinylmethylene)-2,5-dimethylbenzene-1,4-diamine in methanol by sodium borohydride according to scheme 4.2 [41, 42]. The FTIR spectrum of the new ligand shows bands changing in comparison with ^{c}L ligand spectrum. The most important to note is the imine group band disappearing at 1594 cm^{-1} and appearance of a new band at 3411 cm^{-1} which is due to the secondary amine group formation [35, 37, 38]. The ^{1}H NMR spectrum of the prepared ligand shows disappearance of the imine peak at δ 8.43 ppm and appearance of the methylene and the secondary amine peaks at δ 4.25 ppm and at δ 4.91 ppm (figure 4.3) [35, 37, 38, 40]. The $^{13}C\{^{1}H\}$ NMR spectrum shows a new peak at δ 46.32 ppm which is due to the methylene group formation and disappearing of the imine group peak at δ 156.29 ppm (figure 4.4) [35, 37, 38, 40].

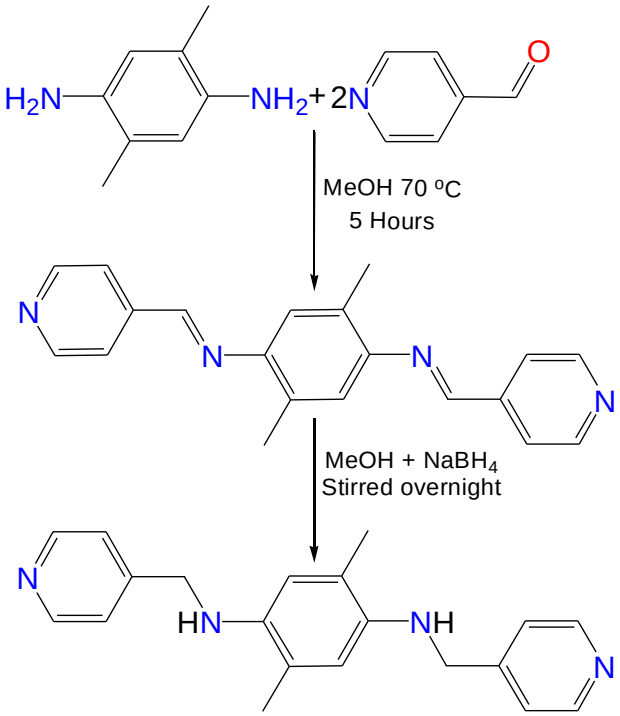

Scheme 4.2: Synthesis of new ligand *N*,*N*′-bis(4-pyridinylmethyl)-2,5-dimethylbenzene-1,4-diamine (L3).

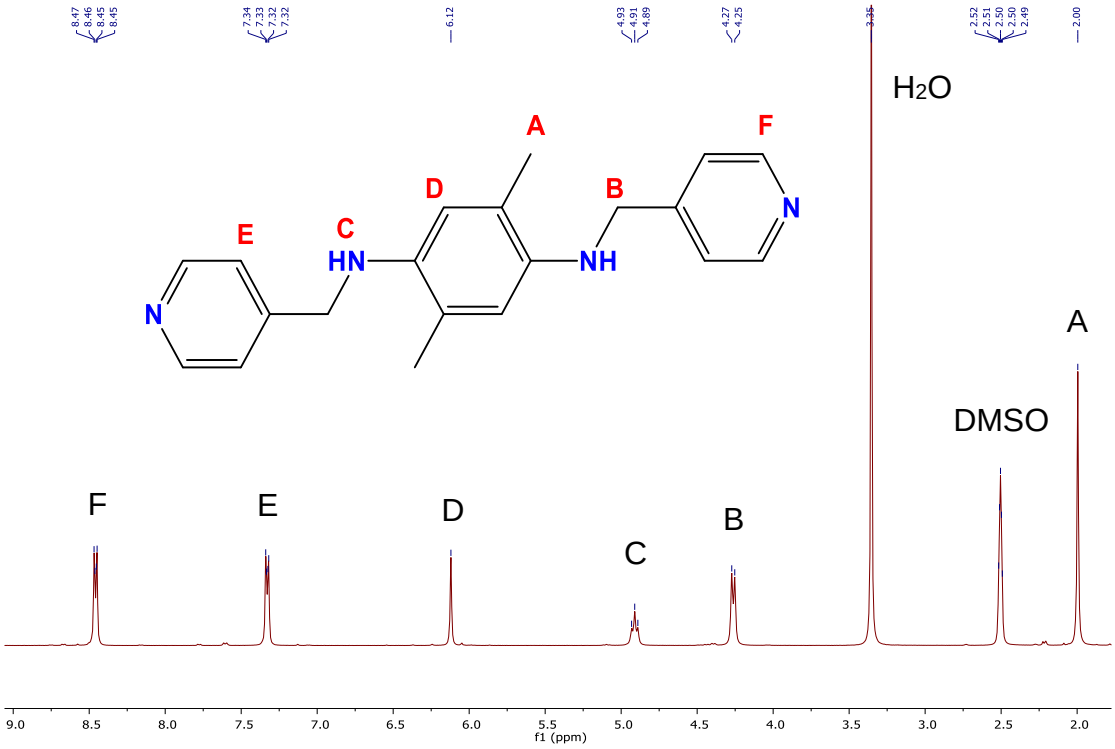

Figure 4.3: ^{1}H NMR (300 MHz, DMSO-d_6) spectrum of *N*,*N*′-bis(4-pyridinylmethyl)-2,5-dimethylbenzene-1,4-diamine (L3).

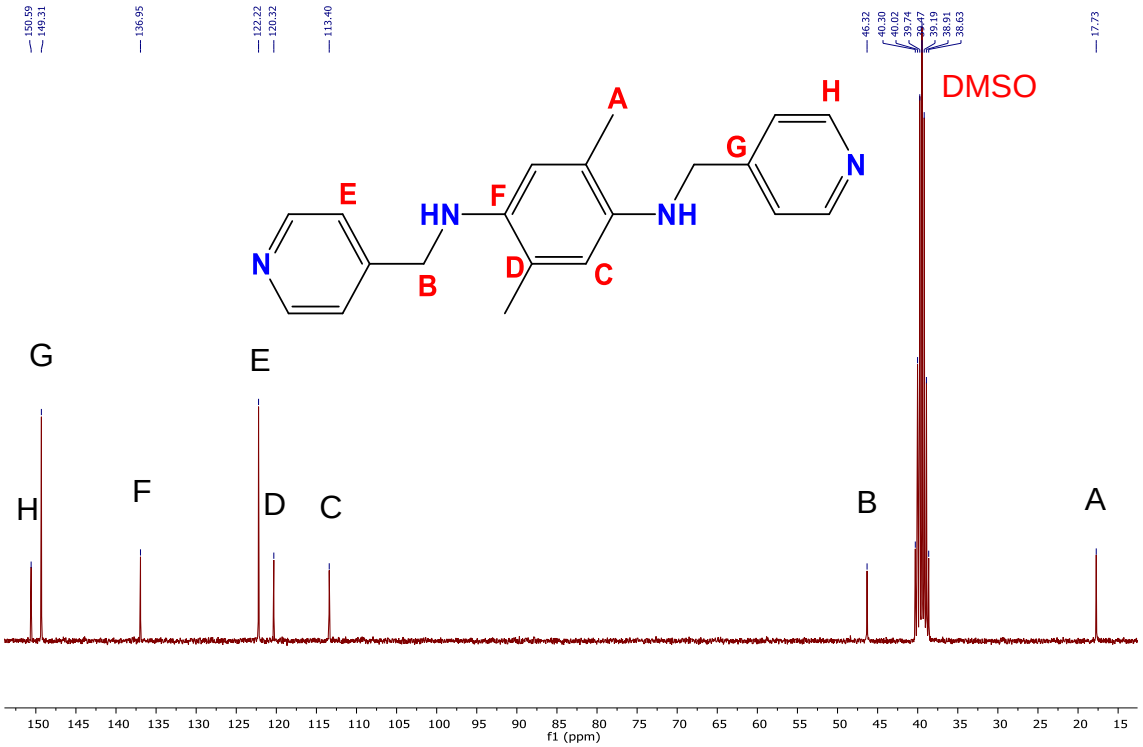

Figure 4.4: $^{13}C\{^{1}H\}$ NMR (75 MHz, DMSO-d_6) spectrum of *N*,*N*′-bis(4-pyridinylmethyl)-2,5-dimethylbenzene-1,4-diamine (L3).

4.4.3 Synthesis of new MOFs 14-19

A series of novel coordination polymers were synthesised from the reaction of L3, $FeCl_3.6H_2O$, $Fe(SCN)_2$, $Co(NO_3)_2.6H_2O$, $Cd(NO_3)_2.4H_2O$, isophthalic acid or 5-methylsophthalic acid to produce $([Fe_{0.5}(L3)Cl].MeOH)_n$ (**14**) and $([Fe(L3)_{0.5}(SCN)])_n$ (**15**) MOFs; $(Co(L3)(isoph)].DMF)_n$ (**16**), $(Cd(L3)(isoph)].DMF.H_2O)_n$ (**17**), $([Co(L3)(Meisoph)].DMF)_n$ (**18**) or $([Cd(L3)(Meisoph)].DMF)_n$ (**19**) MOF. Compounds **14** and **15** were obtained from self-assembly process in methanol at room temperature. Whereas compounds **16-19** were synthesised by solvothermal reaction in DMF at 115 °C for 24 hours. The resultant crystals of **14** and **15** are soluble and decomposed to starting materials in hot MeOH, EtOH, MeCN, DCM, DMSO, DMF or $CHCl_3$ solvents. On the other hand, compounds **16-19** crystals are insoluble in common organic and inorganic solvents. Therefore, compounds **14-19** were characterised as solid materials by single crystal X-ray diffraction, powder X-ray diffraction, microanalysis of the elements and FTIR.

IR spectrum of compound **14** shows main peaks at 3451, 3311, 3253, 3057, 2839, 1613, 1491, 1418 and 1356 cm^{-1} due to νN-H, νC-$H_{Ar,}$ νC-H_{Al}, νC=C, νC-N, νCH_2 and νCH_3 functional groups [35, 37, 38, 43]. The spectrum also shows a new band at 478 cm^{-1} which due to νM-N coordination bond [43-45]. The IR spectrum of compound **15** shows main bands at 3348, 3025, 2867, 2064, 1615, 1563, 1440, 1340 and 482 cm^{-1} which due to νN-H, νC-$H_{Ar,}$ νC-

H_{Al}, νS-C≡N, νC=C, νC-N, νCH_2, νCH_3 and νM-N functional groups and coordination bond [35, 37, 38, 43-46]. Complexes **16** and **17** IR spectra display main peaks at 3406-3300, 3066-3050, 2929-2918, 2854, 1713-1671, 1609-1600, 1571-1547, 1444-1441, 1393-1372, 526-524 and 420-412 cm^{-1} due to νN-H, $\nu C\text{-}H_{Ar}$, $\nu C\text{-}H_{Al}$, νC=O, νC=C, νC-N, νCH_2, νCH_3, νM-N and νM-O functional groups and coordination bonds [35, 37, 38, 43, 47-49]. Compounds **18** and **19** IR spectra display main bands at 3325-3324, 3054-3040, 2918-2917, 2851-2848, 1671-1670, 1613-1610, 1578-1542, 1419-1416, 1381-1372, 525-522 and 450-429 cm^{-1} due to νN-H, $\nu C\text{-}H_{Ar,}$ $\nu C\text{-}H_{Al}$, νC=O, νC=C, νC-N, νCH_2, νCH_3, νM-N and νM-O functional groups and coordination bonds [37, 38, 43, 50-53].

4.5 Crystal structures

4.5.1 Crystal structure of the new ligand *N,N'*-bis(4-pyridinylmethylene)-2,5-dimethylbenzene-1,4-diamine (^{c}L)

The new ligand was dissolved in dichloromethane and left to evaporate slowly to afford yellow single crystals after a few days. A suitable crystal was selected for structure determination by X-ray diffraction. The crystal structure was solved in monoclinic space group $P2_1/c$ [30-34] and shows half of ^{c}L ligand molecule per asymmetric unit (figure 4.5). After symmetry expansion the ligand molecule is approximately linear and shows torsion angle of 178.78(11) ° between the phenyl and 4-pyridyl rings (figure 4.6). The resulted crystal structure also shows 4.003 or 4.021 Å distance between the phenyl and the 4-pyridyl ring from different ligand molecules which is too far for π-π stacking interaction (figure 4.6). Selected bond lengths, angles and torsion angles for ^{c}L ligand crystal structure are given in tables 4.1 and 4.2.

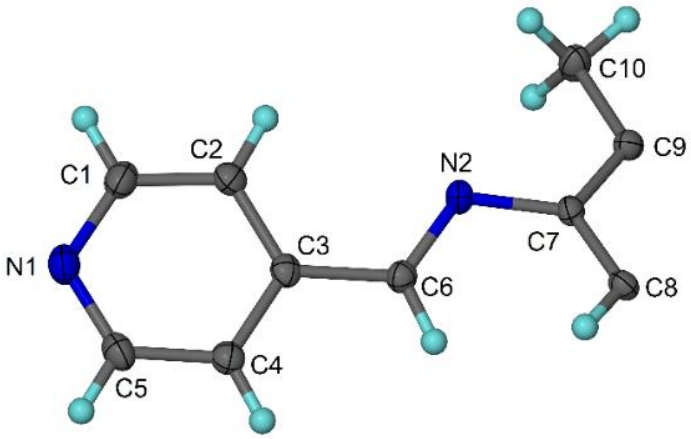

Figure 4.5: *N,N'*-Bis(4-pyridinylmethylene)-2,5-dimethylbenzene-1,4-diamine asymmetric unit of the crystal structure. Ellipsoids shown at 50 % probability levels.

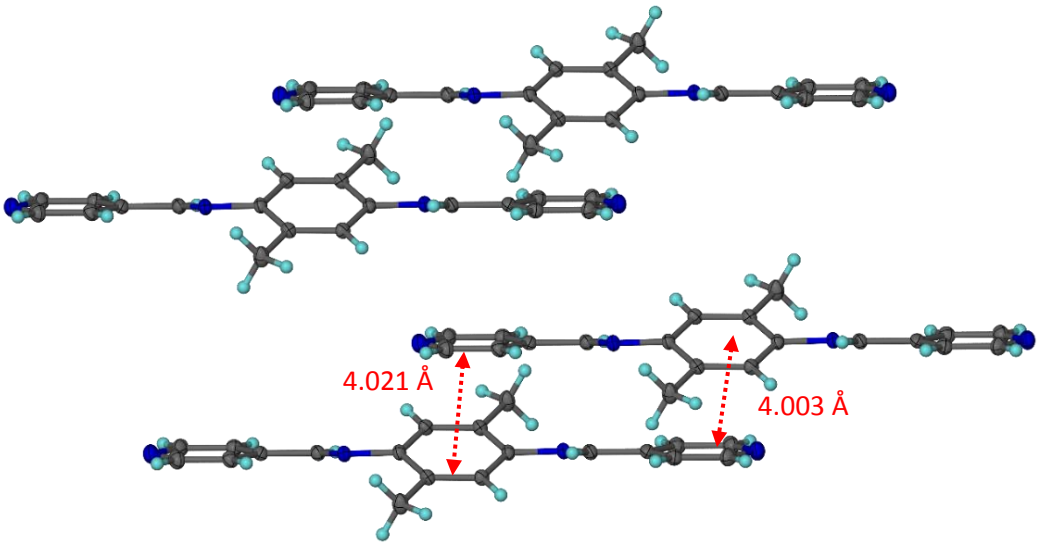

Figure 4.6: Crystal structure of ^{c}L ligand shows torsion angle of 178.78(11) ° between phenyl and 4-pyridyl rings, 4.003 or 4.021 Å distances between the aromatic rings.

Table 4.1: Selected bond lengths (Å) and angles (°) for ^{c}L ligand.

N1-C1	1.3491(19)	C8-C9^{1}	1.3900(18)	N1-C5-C4	123.35(13)
N1-C5	1.3367(19)	C9-C8^{1}	1.3899(18)	N2-C6-C3	122.74(12)
N2-C6	1.2758(17)	C9-C10	1.5020(18)	C8-C7-N2	123.12(12)
N2-C7	1.4199(16)	C5-N1-C1	116.52(12)	C8-C7-C9	119.59(12)
C1-C2	1.3813(19)	C6-N2-C7	118.51(11)	C9-C7-N2	117.29(11)
C2-C3	1.3958(19)	N1-C1-C2	124.09(13)	C9^{1}-C8-C7	122.05(12)
C3-C4	1.3877(18)	C1-C2-C3	118.85(13)	C7-C9-C10	121.17(12)
C3-C6	1.4713(17)	C2-C3-C6	122.70(12)	C8^{1}-C9-C7	118.32(12)
C4-C5	1.3895(19)	C4-C3-C2	117.50(12)	C8^{1}-C9-C10	120.49(12)
C7-C8	1.3959(18)	C4-C3-C6	119.80(12)		
C7-C9	1.4036(18)	C3-C4-C5	119.68(12)		

Table 4.2: Selected torsion angles (°) for ^{c}L ligand.

N1-C1-C2-C3	0.3(2)	C4-C3-C6-N2	-174.45(12)
N2-C7-C8-C9^{1}	178.18(11)	C5-N1-C1-C2	0.1(2)
N2-C7-C9-C8^{1}	-178.24(11)	C6-N2-C7-C8	-30.06(19)
N2-C7-C9-C10	0.53(18)	C6-N2-C7-C9	150.39(12)
C1-N1-C5-C4	-0.6(2)	C6-C3-C4-C5	179.82(12)
C1-C2-C3-C4	-0.17(19)	C7-N2-C6-C3	178.87(11)
C1-C2-C3-C6	179.71(12)	C8-C7-C9-C8^{1}	2.2(2)
C2-C3-C4-C5	-0.29(19)	C8-C7-C9-C10	-179.03(12)
C2-C3-C6-N2	5.7(2)	C9-C7-C8-C9^{1}	-2.3(2)
C3-C4-C5-N1	0.7(2)		

4.5.2 Crystal structure of the new ligand *N,N'*-bis(4-pyridinylmethyl)-2,5-dimethylbenzene-1,4-diamine (L3)

N,N'-Bis(4-pyridinylmethyl)-2,5-dimethylbenzene-1,4-diamine ligand was dissolved in dichloromethane and left to evaporate slowly to afford yellow single crystals after two days. A suitable crystal was selected for structure determination by X-ray diffraction. The structure was solved in the triclinic space group $P\bar{1}$ [30-34] and shows one L3 ligand molecule per asymmetric unit (figure 4.7). The crystal structure shows two torsion angles of 86.4(3) ° and -82.3(3) ° between the phenyl and 4-pyridyl rings. The crystal structure also shows 3.852 Å distance between 4-pyridyl rings from different L3 ligand molecules that is due to π-π interaction (figure 4.8). Selected bond lengths, angles and torsion angles of L3 ligand are listed in tables 4.3 and 4.4.

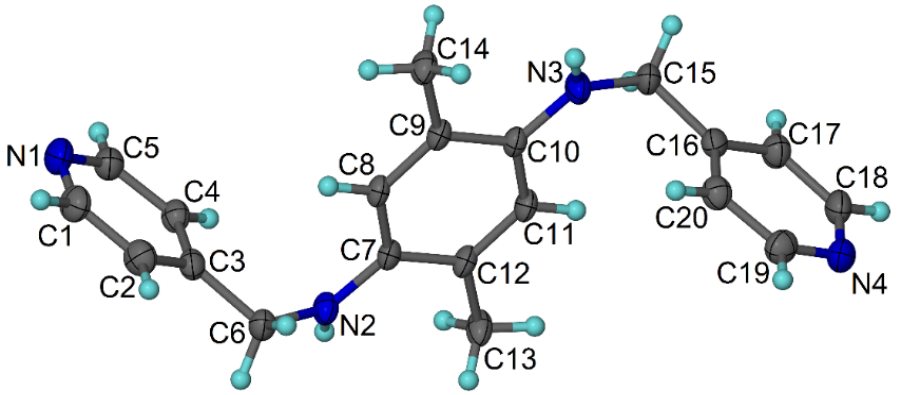

Figure 4.7: L3 asymmetric unit of the crystal structure. Torsion angles of 86.4 ° and -82.3° between the phenyl and 4-pyridyl rings. Ellipsoids shown at 50 % probability levels.

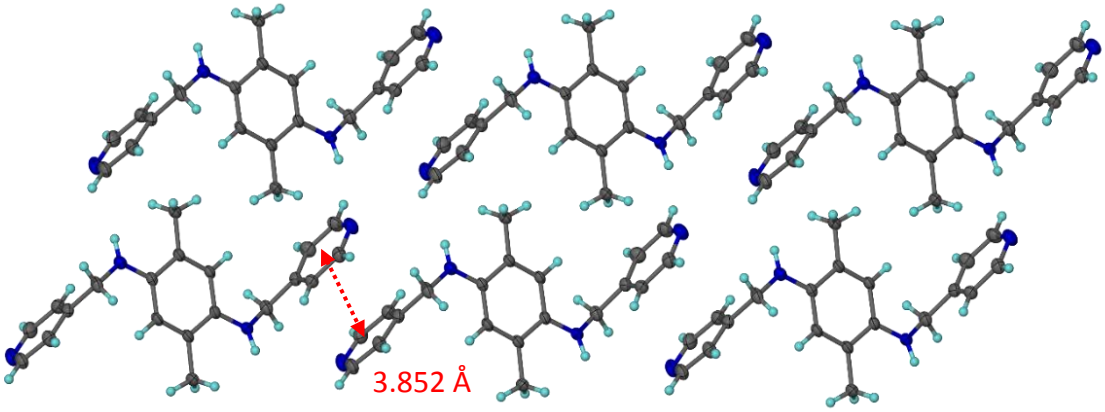

Figure 4.8: Packing diagram of L3 ligand molecules that shows 3.852 Å between 4-pyridyl rings from different L3 ligand molecules.

Table 4.3: Selected bond lengths (Å) and angles (°) for L3 ligand.

N1-C1	1.344(4)	C10-N3-C15	121.82(19)
N1-C5	1.337(3)	C19-N4-C18	116.6(2)
N2-C6	1.442(3)	N1-C1-C2	123.6(2)
N2-C7	1.400(3)	N1-C5-C4	123.8(2)
N3-C10	1.394(3)	N2-C6-C3	114.7(2)
N3-C15	1.439(3)	N2-C7-C8	121.46(19)
N4-C18	1.336(4)	N2-C7-C12	120.44(19)
N4-C19	1.328(4)	N3-C10-C9	120.2(2)
C3-C6	1.518(3)	N3-C10-C11	121.57(19)
C15-C16	1.521(3)	N3-C15-C16	115.1(2)
C5-N1-C1	116.5(2)	N4-C18-C17	123.4(2)
C7-N2-C6	119.94(18)	N4-C19-C20	124.5(2)

Table 4.4: Selected torsion angles (°) for L3 ligand.

N1-C1-C2-C3	-0.1(4)	C5-N1-C1-C2	0.5(4)
N2-C7-C8-C9	-177.2(2)	C6-N2-C7-C8	-27.9(3)
N2-C7-C12-C11	177.5(2)	C6-N2-C7-C12	155.0(2)
N2-C7-C12-C13	-2.4(3)	C7-N2-C6-C3	86.4(3)
N3-C10-C11-C12	178.6(2)	C8-C9-C10-N3	-178.3(2)
N3-C15-C16-C17	166.4(2)	C10-N3-C15-C16	-82.3(3)
N3-C15-C16-C20	-14.8(3)	C14-C9-C10-N3	1.4(3)
N4-C19-C20-C16	-1.4(4)	C15-N3-C10-C9	-164.1(2)
C1-N1-C5-C4	-0.8(4)	C15-N3-C10-C11	17.0(3)
C2-C3-C6-N2	-160.7(2)	C16-C17-C18-N4	1.3(4)
C3-C4-C5-N1	0.6(4)	C18-N4-C19-C20	0.9(4)
C4-C3-C6-N2	21.3(3)	C19-N4-C18-C17	-0.9(4)

4.5.3 Crystal structure of $([Fe_{0.5}(L3)Cl].MeOH)_n$ coordination polymer (14)

$([Fe_{0.5}(L3)Cl].MeOH)_n$ coordination polymer crystal structure was solved in monoclinic space group $P2_1/c$ [30-34] and shows half of Fe(II) ion on an inversion centre, two halves of L3 ligand molecules, one coordinated chloride anion and one methanol guest molecule per asymmetric unit (figure 4.9). Fe(II) ion is coordinated to four L3 ligand molecules by nitrogen atoms of 4-pyridyl rings and shows two Fe-N coordination distances of 2.198(2) and 2.358(2) Å for Fe-N1 and Fe-N3 respectively. Fe(II) ion is also coordinated to two chloride anions in a *trans* arrangement (Fe-Cl= 2.444(7) Å) to produce Fe(II) distortion octahedral coordination centres (figure 4.10).

Compound **14** was synthesised from Iron(III) but reduced to Fe(II) by methanol and water [54]. Compound **14** shows similar Fe-N and Fe-Cl coordination bond lengths in

comparison with Karsten reported crystal structure of *trans*-[$FeCl_2$(pyridine)$_4$].2[(HDBU)Cl] (HDBU= 1,8-diazabicyclo[5.4.0]undec-7-en-8-ium) that shows coordination distances of 2.279(3), 2.273(3) and 2.4067(8) Å for Fe-N or Fe-Cl [55]. Graziani reported [$FeCl_2$($tBuC_3H_3N_2$)$_4$] crystal structure that has Fe-N coordination bond lengths from 2.158(3) to 2.191(4) Å, and Fe-Cl coordination bonds of 2.533(12) or 2.565(12) Å [56]. Furthermore, ([$Fe_{0.5}$(L3)Cl].MeOH)$_n$ coordination polymer shows similar Fe-N and Fe-Cl coordination bond lengths in comparison with compound **11** coordination bond lengths.

L3 ligand behaves as a bi-dentate ligand to two Fe(II) coordination centres by nitrogen atoms of 4-pyridyl rings and shows two coordination distances of 2.198(2) and 2.358(2) Å for Fe-N1 and Fe-N3 respectively. The first coordinated L3 ligand molecule shows torsion angles of -86.515(3) ° between the phenyl and 4-pyridyl rings to produce L3 bent-S shape between Fe(II) coordination centres (Fe-L3-Fe= 16.951 Å) (figure 4.10). The second coordinated L3 ligand molecule is approximately linear and shows torsion angle of 175.1(2) ° between the phenyl and 4-pyridyl rings (Fe-L3-Fe= 20.478 Å) (figure 4.10). Four L3 ligand molecules are coordinated to four Fe(II) ions to produce M_4-$(L3)_4$ square cavity. The resulted structure is extending to form a two-dimensional network that has 4^4 topology and shows 16.951 × 20.478 Å sides, and 26.331 × 26.833 Å diagonals between Fe(II) coordination centres (figure 4.10). The resulted square units of four Fe(II) ions and four L3 ligand molecules are packing with two Fe(II) coordination centres from two different 2D networks in an inter-digitated fashion left no significant channels or voids in the lattice (figure 3.13). The resulted crystal structure shows hydrogen bond interaction between the coordinated chloride anion and methanol guest molecule (O⋯Cl= 3.141 Å). In addition to another hydrogen bond interaction between the secondary amines from different L3 ligand molecules (N1⋯N4= 3.091 Å) (figure 4.12). Powder X-ray analysis for compound **14** shows a good agreement with calculated XRD pattern which indicate phase purity and material stability (figure 4.13). Summary of bond lengths, angles and torsion angles of compound **14** are listed in tables 4.5 and 4.6.

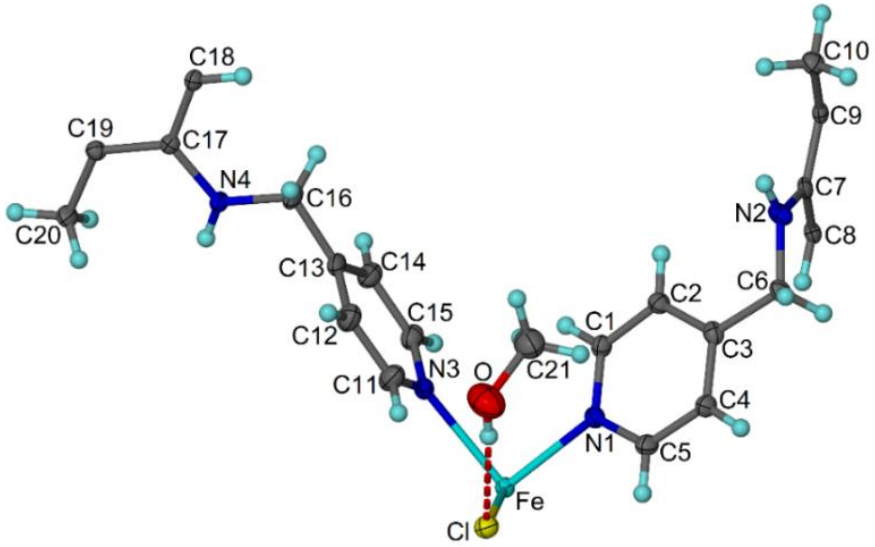

Figure 4.9: ([$Fe_{0.5}$(L3)Cl].MeOH)$_n$ CP asymmetric unit of the crystal structure. Ellipsoids shown at 50 % probability levels.

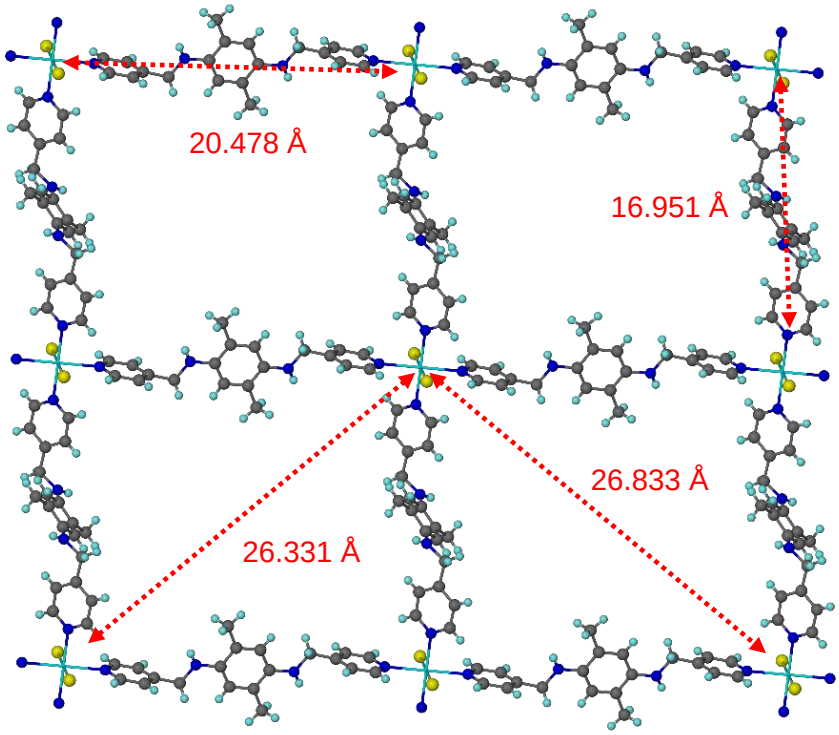

Figure 4.10: ([$Fe_{0.5}$(L3)Cl].MeOH)$_n$ CP network that has 20.478 × 16.951 Å sides and 26.331 × 26.833 Å diagonals between Fe(II) coordination centres.

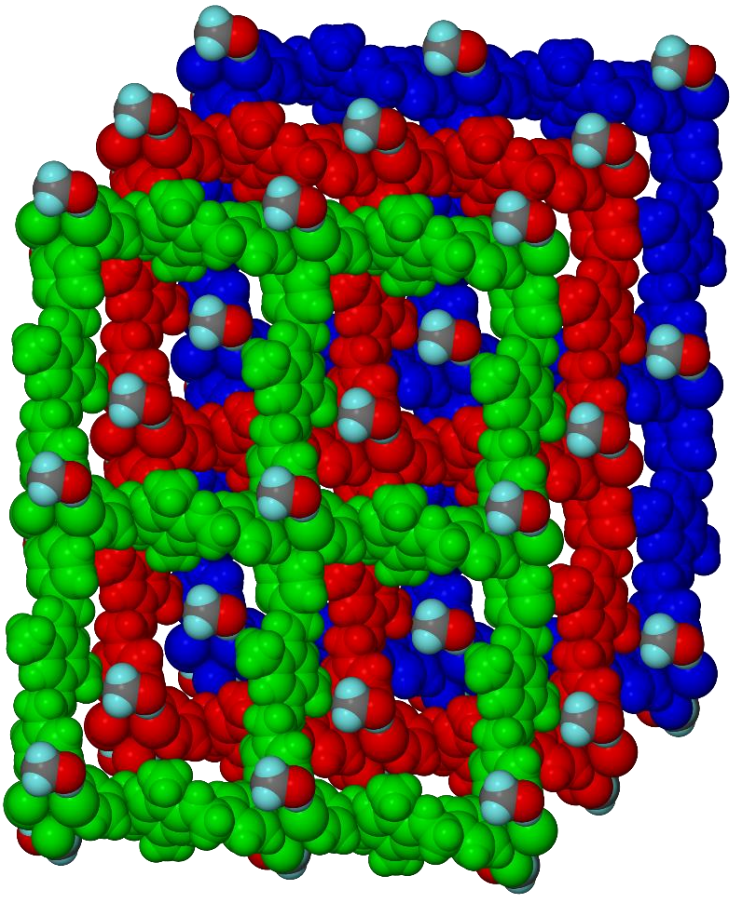

Figure 4.11: Packing diagram of $([Fe_{0.5}(L3)Cl].MeOH)_n$ CP. Square cavities are occupied by two Fe(II) coordination centres from two different networks and four MeOH solvent guest molecules.

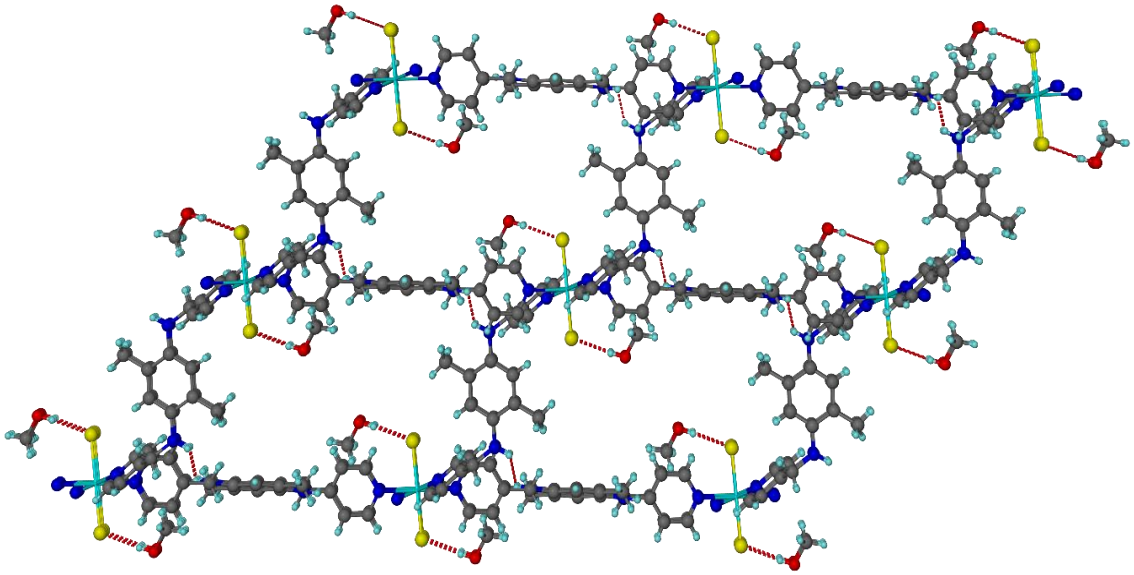

Figure 4.12: Hydrogen bond interactions between the coordinated chloride anions and methanol guest molecules (Cl⋯O= 3.141 Å). Hydrogen bond interaction between the secondary amines from different L3 ligand molecules (N1⋯N4= 3.091 Å).

Table 4.5: Selected bond lengths (Å) and angles (°) for $([Fe_{0.5}(L3)Cl].MeOH)_n$ CP.

Fe-Cl	2.4442(7)	$N1^1$-Fe-Cl	90.97(6)	N3-Fe-$N3^1$	180.0
Fe-N1	2.198(2)	N1-Fe-Cl^1	90.97(6)	C1-N1-Fe	123.66(19)
Fe-N3	2.358(2)	N1-Fe-Cl	89.03(6)	C5-N1-Fe	119.68(18)
N1-C1	1.350(3)	$N1^1$-Fe-Cl^1	89.03(6)	C7-N2-C6	122.1(2)
N1-C5	1.342(4)	N1-Fe-$N1^1$	180.0	C11-N3-Fe	119.68(19)
N2-C6	1.445(4)	$N1^1$-Fe-$N3^1$	89.15(8)	C15-N3-Fe	124.25(19)
N2-C7	1.393(4)	$N1^1$-Fe-N3	90.85(8)	C17-N4-C16	117.1(2)
N3-C11	1.336(4)	N1-Fe-$N3^1$	90.85(8)	N2-C6-C3	115.3(2)
N3-C15	1.339(4)	N1-Fe-N3	89.15(8)	N2-C7-C8	122.7(3)
N4-C16	1.452(4)	N3-Fe-Cl^1	88.46(6)	N2-C7-C9	119.0(2)
N4-C17	1.429(3)	N3-Fe-Cl	91.54(6)	N4-C16-C13	111.3(2)
O-C21	1.408(4)	$N3^1$-Fe-Cl^1	91.54(6)	C18-C17-N4	121.5(2)
Cl-Fe-Cl^1	180.0	$N3^1$-Fe-Cl	88.46(6)	C19-C17-N4	119.4(2)

Table 4.6: Selected torsion angles (°) for $([Fe_{0.5}(L3)Cl].MeOH)_n$ CP.

Fe-N1-C1-C2	-179.15(19)	C3-C4-C5-N1	0.3(4)
Fe-N1-C5-C4	178.5(2)	C4-C3-C6-N2	-174.0(2)
Fe-N3-C11-C12	173.7(3)	C5-N1-C1-C2	0.9(4)
Fe-N3-C15-C14	-173.8(2)	C6-N2-C7-C8	18.3(4)
N1-C1-C2-C3	0.9(4)	C6-N2-C7-C9	-164.6(2)
N2-C7-C8-$C9^1$	177.3(2)	C7-N2-C6-C3	-86.5(3)
N2-C7-C9-$C8^1$	-177.4(2)	C11-N3-C15-C14	0.3(4)
N2-C7-C9-C10	2.7(4)	C12-C13-C16-N4	-102.4(3)
N3-C11-C12-C13	0.6(5)	C13-C14-C15-N3	0.0(5)
N4-C17-C18-$C19^1$	178.6(2)	C14-C13-C16-N4	80.8(3)
N4-C17-C19-$C18^1$	-178.6(2)	C15-N3-C11-C12	-0.6(5)
N4-C17-C19-C20	-0.8(4)	C16-N4-C17-C18	9.0(4)
C1-N1-C5-C4	-1.6(4)	C16-N4-C17-C19	-172.3(2)
C2-C3-C6-N2	7.2(4)	C17-N4-C16-C13	175.1(2)

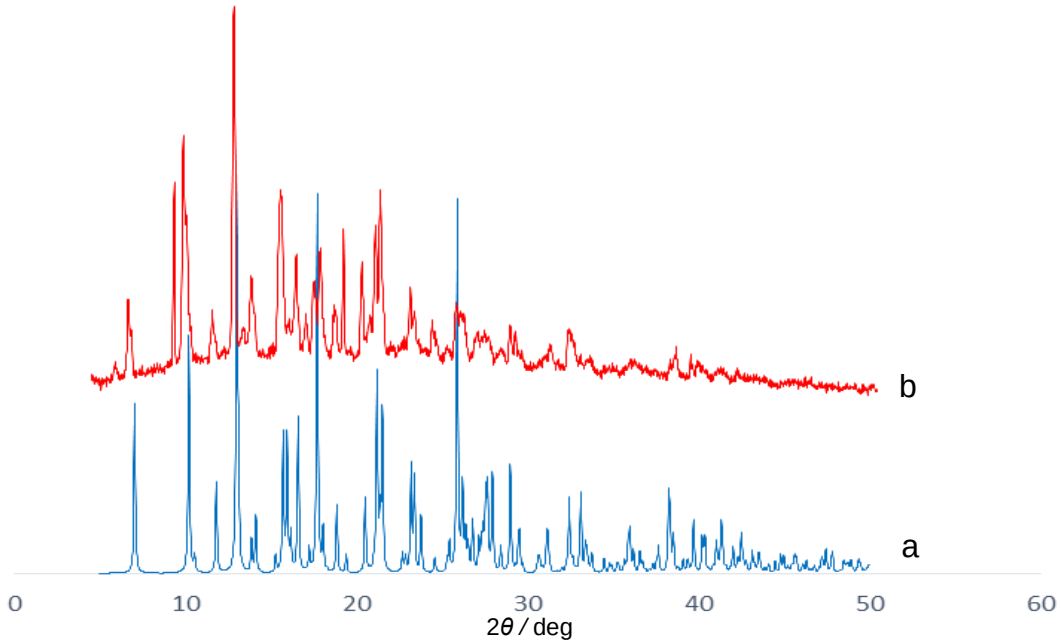

Figure 4.13: (a) Calculated powder XRD pattern of compound **14**. (b) Powder XRD pattern of compound **14**.

4.5.4 Crystal structure of $([Fe(L3)_{0.5}(SCN)])_n$ MOF (15)

$([Fe(L3)_{0.5}(SCN)])_n$ MOF crystal structure was solved in tetragonal space group $I4_1/a$ [30-34] and shows one iron(II) ion on four-fold inversion centre, one disordered thiocyanate anion and half of L3 ligand molecule per asymmetric unit (figure 4.14). Iron(II) ion is coordinated to four L3 ligand molecules along the equatorial axes (Fe-N1= 2.209(6) Å) and two thiocyanate anions on the axial axes (Fe-N3= 2.092(13) Å) to produce iron(II) distorted octahedral coordination centres (figure 4.15). $([Fe(L3)_{0.5}(SCN)])_n$ MOF shows similar coordination bond lengths in comparison with other reported Fe(II), SCN^- and 4-pyridyl coordination polymers [8, 25]. Halder reported $Fe_2(azpy)_4(NCS)_2$.(guest) MOF that has similar coordination bond lengths in comparison with compound **15** (Fe-(4-py)= 2.214(5)-2.221(5) Å) and (Fe-NCS= 2.080(5)-2.086(5) Å) [8]. $([Fe(L3)_{0.5}(SCN)])_n$ MOF also shows similar coordination bond lengths in comparison with Halder $Fe_2(azpy)_4(NCS)_2$.(azpy) reported MOF where (Fe-(azpy)= 2.204(7)-2.267(6) Å) and (Fe-(NCS)= 2.069(7)-2.081(8) Å) [25].

L3 ligand behaves as a bidentate ligand *via* nitrogen atoms of 4-pyridyl rings. The 4-pyridyl ring was refined as a disordered molecule across two sites each at 0.5 occupancy and shows rotation between the two planes approximately 55.69-58.51 ° (figure 4.14). The new ligand also shows torsion angle of -64.046 ° between the phenyl and 4-pyridyl rings to produce L3 bent S-shape between Fe(II) coordination centres (Fe-L3-Fe= 15.992 Å). After symmetry expansion the crystal structure shows 22 × 27 Å hexagonal channels consists of six L3 ligand molecules and six Fe(II) coordination centres along *a* and *c* axes (figure 4.16).

$([Fe(L3)_{0.5}(SCN)])_n$ crystal structure also shows 13 × 15 Å H-shape channels consists of four L3 ligand molecules and four Fe(II) ions along *c* and *b* axes (figure 4.17). Furthermore, the crystal structure shows 14 × 14 Å cross shape channels consists of four L3 ligand molecules and four Fe(II) ions along *a* and *b* axes (figure 4.17). However, each three-dimensional network is interpenetrating with four other three-dimensional networks with no significant space, hydrogen bond interactions or solvent guest molecules (figure 4.18). Powder XRD of the dried $([Fe(L3)_{0.5}(SCN)])_n$ MOF does not match the calculated pattern from the single crystal structures. The new phase is crystalline, but the structure could not be determined as the materials did not stay as a single crystal on drying out (figure 4.19). Selected bond lengths, angles and torsion angle for compound **15** are listed in tables 4.7 and 4.8.

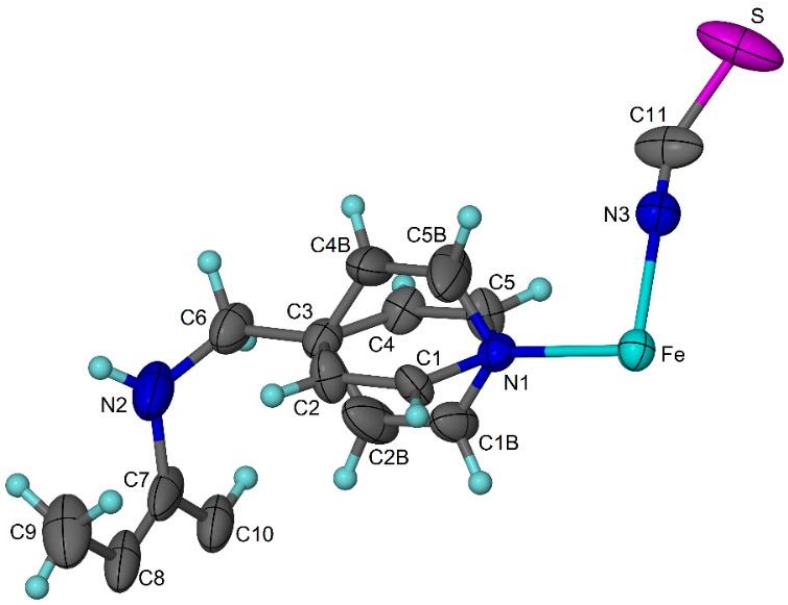

Figure 4.14: $([Fe(L3)_{0.5}(SCN)])_n$ MOF asymmetric unit of the crystal structure, torsion angle of -64.046 ° between C3-C6-N2-C7. Ellipsoids shown at 50 % probability levels.

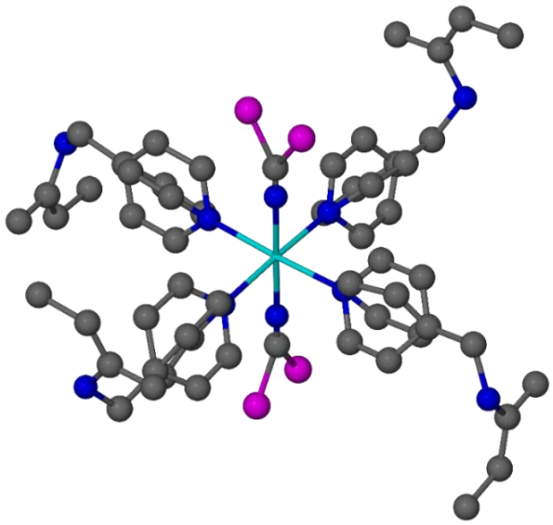

Figure 4.15: Compound **15** Fe(II) distorted octahedral coordination centre.

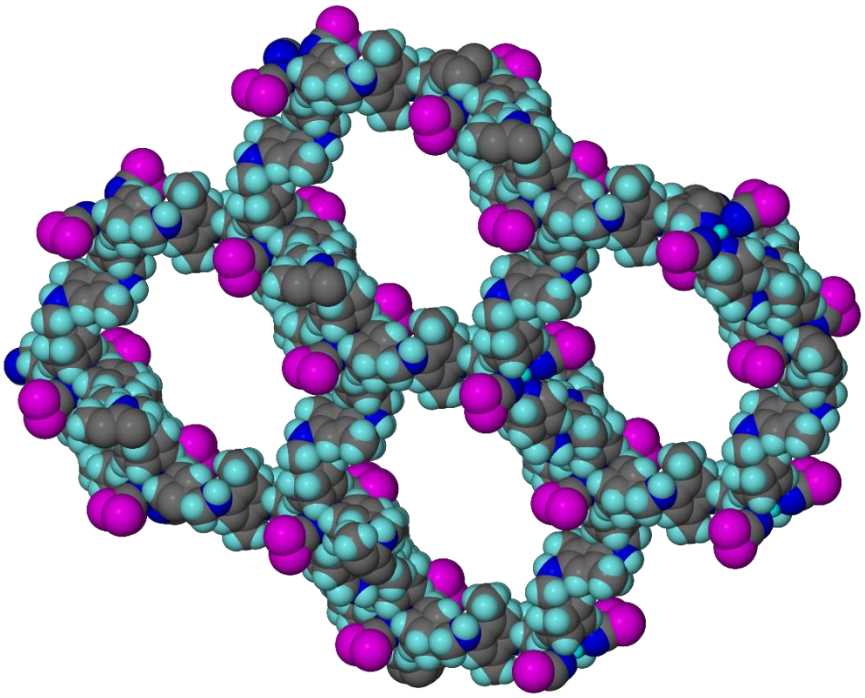

Figure 4.16: $([Fe(L3)_{0.5}(SCN)])_n$ MOF M_6-$(L3)_6$ hexagonal channels along *a* and *c* axes, Fe-L3-Fe= 15.992 Å.

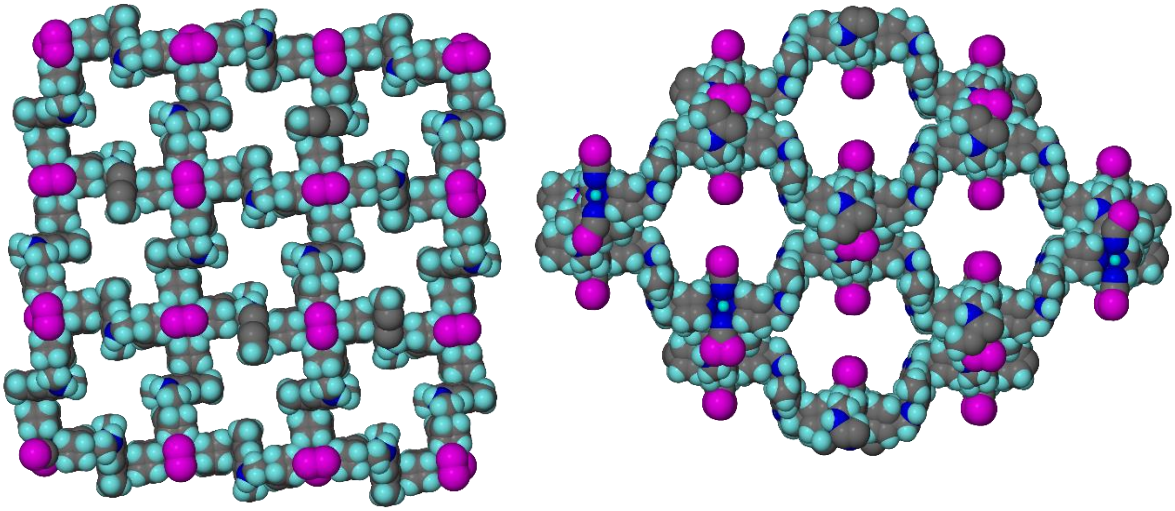

Figure 4.17: (left) 14 × 14 Å Cross shape channels consist of four L3 ligands and four Fe(II) ions *a* and *b* axes view. (right) 13 × 15 Å H-shape channels along *c* and *b* axes.

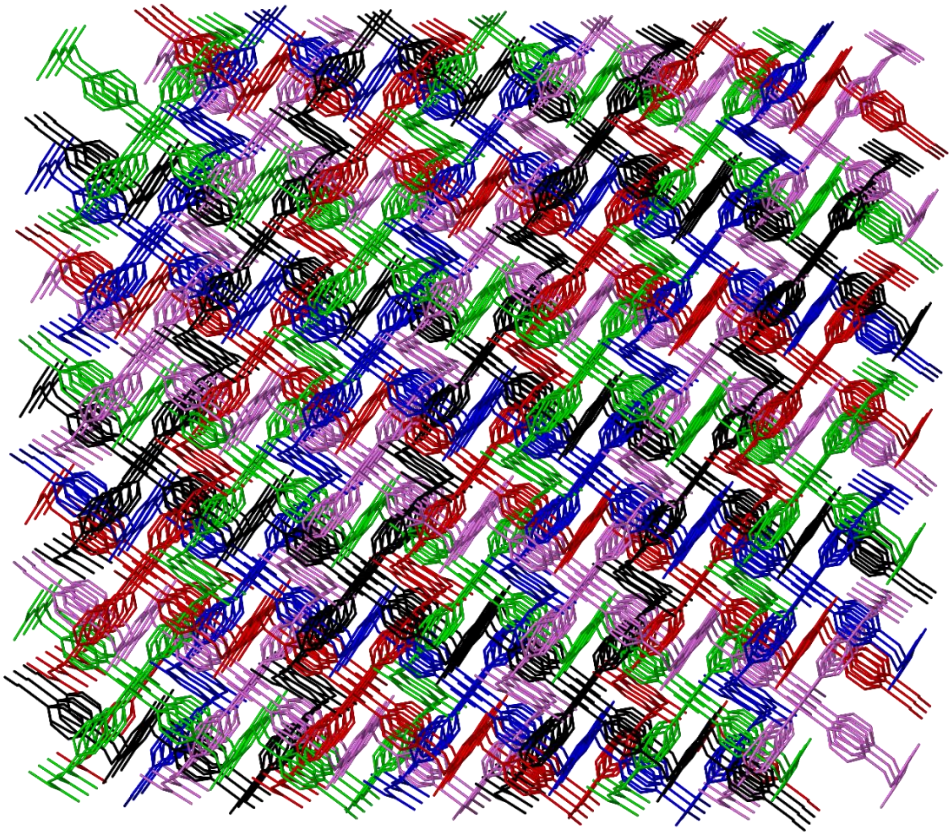

Figure 4.18: ([Fe(L3)$_{0.5}$(SCN)])$_n$ MOF crystal structure after symmetrical expanding where each three-dimensional network is interpenetrating with four networks and shows no significant spaces. Hydrogen atoms were removed for clarity.

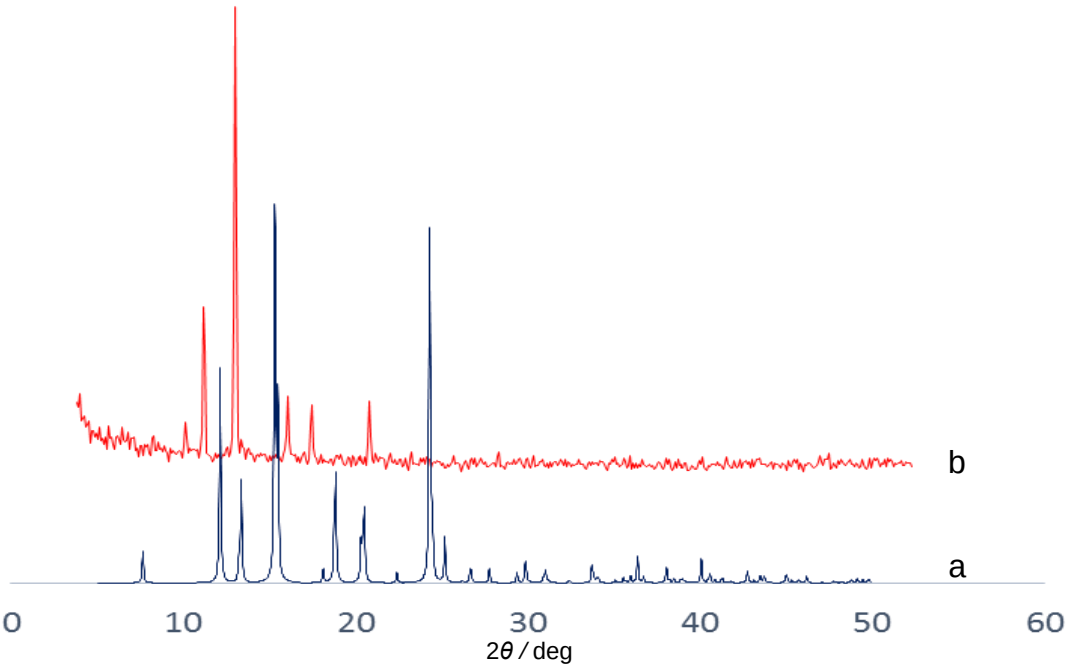

Figure 4.19: (a) Calculated powder XRD patterns of ([Fe(L3)$_{0.5}$(SCN)])$_n$ MOF. (b) Powder XRD pattern of compound **15**.

Table 4.7: Selected bond lengths (Å) and angles (°) for $([Fe(L3)_{0.5}(SCN)])_n$ MOF.

Fe-N1	2.209(6)	$N1^1$-Fe-$N1^3$	90.050(12)	C2B-C3-C6	127.4(12)
Fe-N3	2.092(13)	$N1^3$-Fe-N1	90.050(13)	C4B-C3-C6	119.1(14)
N1-C1	1.367(17)	$N1^2$-Fe-N1	90.049(12)	C4B-C3-C2B	112.7(17)
N1-C5	1.335(16)	$N1^2$-Fe-$N1^3$	176.6(4)	N2-C6-C3	116.5(11)
N1-C1B	1.21(2)	$N3^1$-Fe-$N1^1$	91.69(19)	C8-C7-N2	122.3(17)
N1-C5B	1.32(3)	N3-Fe-$N1^1$	88.31(19)	C10-C7-N2	118(2)
N2-C6	1.460(14)	N3-Fe-$N1^2$	91.69(19)	C10-C7-C8	119.2(13)
N2-C7	1.468(16)	$N3^1$-Fe-N1	91.69(19)	C7-C8-C9	121.4(17)
N3-C11	1.016(17)	N3-Fe-N1	88.31(19)	$C10^1$-C8-C7	117.6(13)
C3-C2	1.41(2)	$N3^1$-Fe-$N1^2$	88.31(19)	$C10^1$-C8-C9	121(2)
C3-C4	1.31(2)	N3-Fe-$N1^3$	91.69(19)	C7-C10-$C8^1$	123.2(14)
C3-C6	1.500(12)	$N3^1$-Fe-$N1^3$	88.31(19)	S-C11-S^1	59.8(10)
C3-C2B	1.34(3)	N3-Fe-$N3^1$	180.0	N3-C11-S	150.1(5)
C3-C4B	1.25(2)	C1-N1-Fe	124.2(8)	N3-C11-S^1	150.1(5)
C7-C8	1.41(2)	C5-N1-Fe	122.0(8)	C2-C1-N1	122.2(16)
C7-C10	1.338(18)	C5-N1-C1	113.7(11)	C1-C2-C3	120.7(16)
C8-C9	1.530(18)	C1B-N1-Fe	126.9(11)	C3-C4-C5	122.0(15)
$C8-C10^1$	1.372(18)	C1B-N1-C5B	112.1(15)	C4-C5-N1	125.7(16)
C1-C2	1.35(2)	C5B-N1-Fe	121.0(11)	N1-C1B-C2B	125(2)
C4-C5	1.33(2)	C6-N2-C7	118.1(11)	C3-C2B-C1B	123(2)
C1B-C2B	1.38(3)	C11-N3-Fe	180.0	C3-C4B-C5B	120(2)
C4B-C5B	1.41(4)	C2-C3-C6	123.9(11)	N1-C5B-C4B	124(2)
$N1^1$-Fe-$N1^2$	90.050(12)	C4-C3-C6	120.6(12)		
$N1^1$-Fe-N1	176.6(4)	C4-C3-C2	115.4(12)		

Table 4.8: Selected torsion angles (°) for $([Fe(L3)_{0.5}(SCN)])_n$ MOF.

Fe-N1-C1-C2	172.8(17)	C2-C3-C4-C5	-1(3)
Fe-N1-C5-C4	-177.4(18)	C2-C3-C2B-C1B	-69(3)
Fe-N1-C1B-C2B	-176(3)	C2-C3-C4B-C5B	39(3)
Fe-N1-C5B-C4B	167(3)	C4-C3-C6-N2	158.1(14)
N1-C1-C2-C3	5(4)	C4-C3-C2-C1	-3(3)
N1-C1B-C2B-C3	-6(6)	C4-C3-C2B-C1B	56(4)
N2-C7-C8-C9	-5.6(19)	C4-C3-C4B-C5B	-81(3)
N2-C7-C8-C10[1]	174.1(9)	C5-N1-C1-C2	-3(3)
N2-C7-C10-C8[1]	-174.1(9)	C5-N1-C1B-C2B	-46(3)
C3-C4-C5-N1	4(4)	C5-N1-C5B-C4B	57(3)
C3-C4B-C5B-N1	23(6)	C1B-N1-C1-C2	-73(2)
C6-N2-C7-C8	148.9(12)	C1B-N1-C5-C4	49(3)
C6-N2-C7-C10	-34.9(16)	C1B-N1-C5B-C4B	-15(5)
C6-C3-C2-C1	178.9(17)	C2B-C3-C6-N2	50(3)
C6-C3-C4-C5	176.9(17)	C2B-C3-C2-C1	62(2)
C6-C3-C2B-C1B	-179(2)	C2B-C3-C4-C5	-52(3)
C6-C3-C4B-C5B	171(3)	C2B-C3-C4B-C5B	-19(4)
C7-N2-C6-C3	-64.0(15)	C4B-C3-C6-N2	-142(2)
C8-C7-C10-C8[1]	2(2)	C4B-C3-C2-C1	-52(3)
C10-C7-C8-C9	178.2(10)	C4B-C3-C4-C5	72(2)
C10-C7-C8-C10[1]	-2.1(19)	C4B-C3-C2B-C1B	12(5)
C1-N1-C5-C4	-2(3)	C5B-N1-C1-C2	48(2)
C1-N1-C1B-C2B	75(3)	C5B-N1-C5-C4	-69(2)
C1-N1-C5B-C4B	-65(4)	C5B-N1-C1B-C2B	7(4)
C2-C3-C6-N2	-24.1(19)		

4.5.5 Crystal structures of $(Co(L3)(isoph)].DMF)_n$ (16) and $(Cd(L3)(isoph)].DMF.H_2O)_n$ (17) coordination polymers

$(Co(L3)(isoph)].DMF)_n$ and $(Cd(L3)(isoph)].DMF.H_2O)_n$ coordination polymers were synthesised by reaction of L3, isophthalic acid (H_2-isopoh), $Co(NO_3)_2.6H_2O$ or $Cd(NO_3)_2.4H_2O$ in DMF at 115 °C for 24 hours. Compounds **16** and **17** are isostructural CPs and their crystal structures were solved in the triclinic space group $P\bar{1}$ [30-34]. The resulted crystal structures show one M^{2+} ion on a general position, one L3 ligand molecule, one coordinated isophthalate anion and one DMF solvent molecule for compound **16** or one DMF and one water molecule for compound **17** per asymmetric unit (figure 4.20). Co(II) is coordinated to three carboxylate groups from three different isophthalate molecules along the equatorial axes and shows four coordination bond lengths of 2.054(3), 2.022(3), 2.193(3) and

2.159(3) Å for Co-O1, Co-O2, Co-O3 and Co-O4 (figure 4.21). The divalent metal is also coordinated to two L3 ligand molecules along the axial axes (Co-N1= 2.129(4) Å) and (Co-N4= 2.135(4) Å) to produce Co(II) distortion octahedral coordination centres. Cd(II) ion in compound **17** has similar coordination environment as Co(II) ion in compound **16** and shows coordination bond lengths of 2.331(2), 2.292(2), 2.393(2), 2.390(2), 2.304(3) and 2.286(3) Å for Cd-O1, Cd-O2, Cd-O3, Cd-O4, Cd-N1 and Cd-N4.

The isophthalate anion is fully deprotonated and behaves as a tetra-dentate ligand to three M^{2+} coordination centres. The first carboxylate group behaves as a bi-dentate ligand to two M^{2+} coordination centres and shows two coordination distances for M-O1 and M-O2. The second carboxylate group behaves as a chelate ligand to one M^{2+} coordination centre and shows two coordination distances for M-O3 and M-O4. A one-dimensional coordination polymer based on isophthalic acid, Co(II) and 2,6-bis((1H-1,2,4-triazol-1-yl)methyl)pyridine (Cbtp) was reported in 2010 Kim and co-workers [57]. Isophthalate molecules of Kim's reported structure show similar coordination style as compound **16** with Co-O coordination bond lengths from 2.008(2) to 2.169(17) Å. Another coordination polymer example based on isophthalate, dipyrido[3,2-*d*:2′,3′-*f*]quinoxaline and Cd(II) ion $[Cd_3(Dpq)_3(isoph)_3].4.5H_2O$ was reported in 2007 by Wang and co-workers. Wang's reported complex has similar Cd(II)-$isoph^{2-}$ coordination style in comparison with compound **17** and shows Cd-O coordination bond lengths from 2.293(2) to 2.393(2) Å [5].

L3 ligand behaves as a bi-dentate ligand *via* nitrogen atoms of 4-pyridyl rings to two different M^{2+} coordination centres from two different M(II)-$isoph^{2-}$ chains (Co-L3-Co^1= 19.873 Å) and (Cd-L3-Cd^1= 20.135 Å). L3 ligand molecule is approximately linear and shows torsion angles of 174.6(4) and -174.192(2) ° between the phenyl and 4-pyridyl rings in compound **16**, or 177.40(3) and -175.50(3) ° in compound **17**. Four L3 ligand molecules, four isophthalate molecules and eight divalent metals are coordinated to produce $(M^{2+})_8(L3)_4(isoph)_4$ tetragonal structure (figure 4.22). The resulted tetragonal structure shows 10.077 × 4.102 Å or 10.230 × 3.868 Å distances between M^{2+} ions and 3.818 or 3.872 Å as the closest distance between dimethylphenyl rings that due to π-π interactions (figure 4.22). The tetragonal structure shows another π-π interaction between 4-pyridyl rings (4-py to 4-py= 3.939 Å) and (4-py to 4-py= 3.746 Å or 3.738 Å).

After symmetrical expanding the resulted two-dimensional network shows 4^4 topology (figure-4.23), and one dimensional open channels that occupied by DMF solvent molecules for compound **16** or DMF and water guest molecules for compound **17**. Compound **17** also shows hydrogen bond interactions between water guest molecules and the deprotonated carboxylate

group (O4···O6= 2.837 Å) and (O4[1]···O6= 2.975 Å). Powder X-ray analysis for compounds **16** and **17** shows a good agreement between calculated and experimental patterns which indicate phase purity and materials stability after removing guest molecules figures 4.24 and 4.25. Summary of bond lengths, angles and torsion angles for compounds **16** and **17** are listed in tables 4.9 and 4.10.

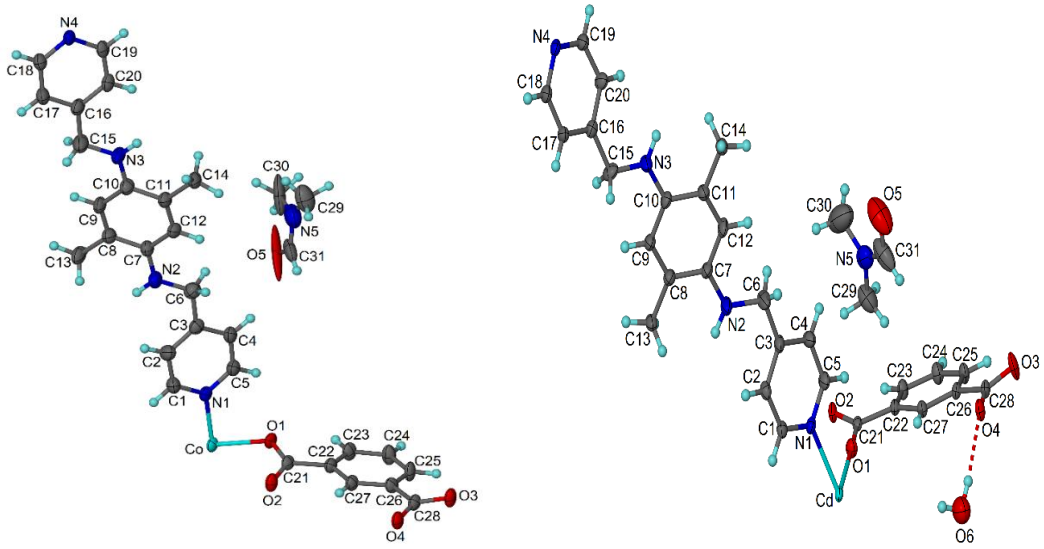

Figure 4.20: (left) Compound **16** asymmetric unit of the crystal structure. (right) Compound **17** asymmetric unit of the crystal structures, hydrogen bond interaction between O4···O6= 2.837 Å in compound **17**. Ellipsoids shown at 50 % probability levels.

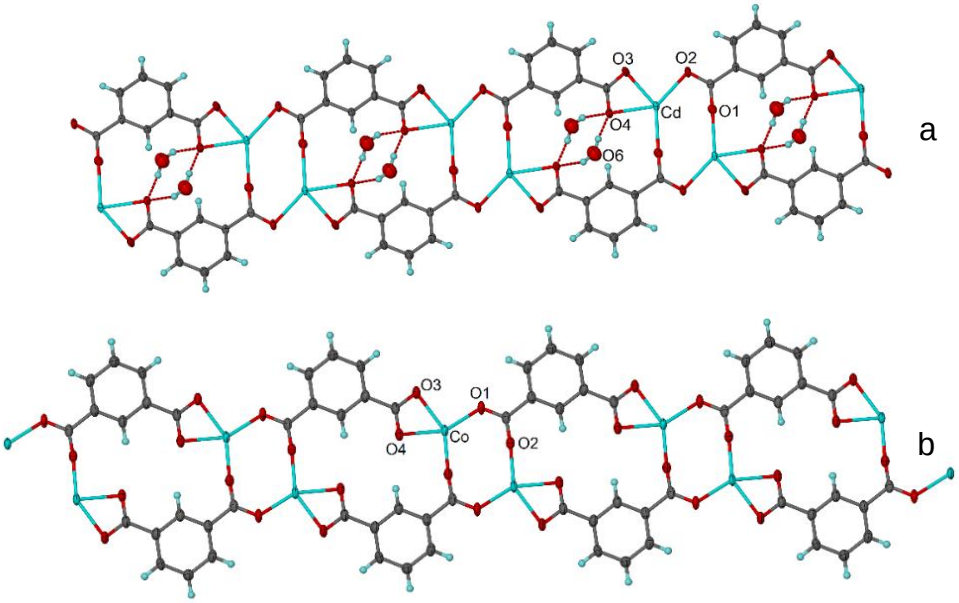

Figure 4.21: (a) Isophthalate and Co(II) coordination chains, (b) isophthalate and Cd(II) coordination chain. Each isophthalate behaves as a tetra-dentate ligand to three M^{2+} cations and shows four M-O coordination bond lengths. Hydrogen bond interaction between water guest molecules and carboxylate anions in compound **17**.

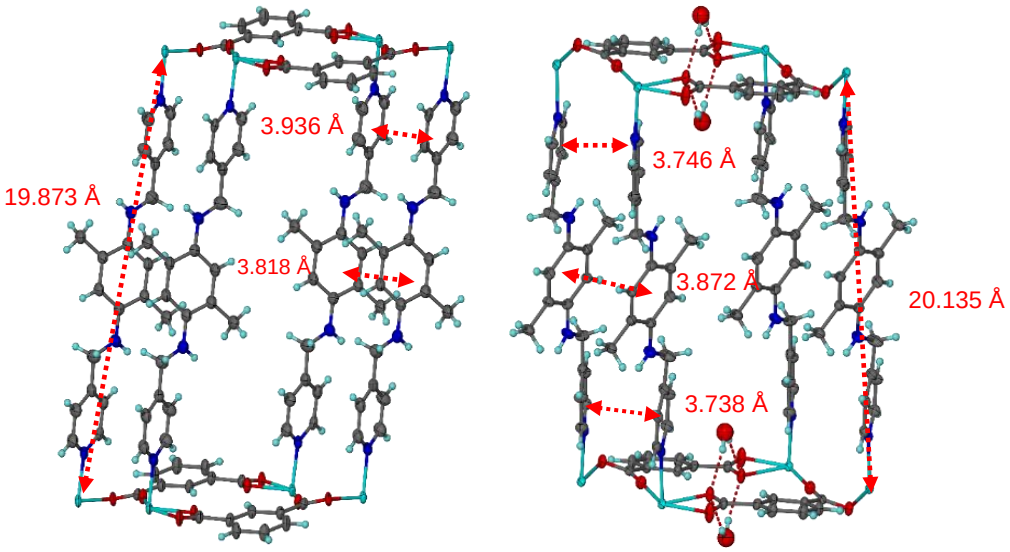

Figure 4.22: (left) $(Co)_8(L3)_4(isoph)_4$ tetragonal structure, (right) $(Cd)_8(L3)_4(isoph)_4$ tetragonal structure.

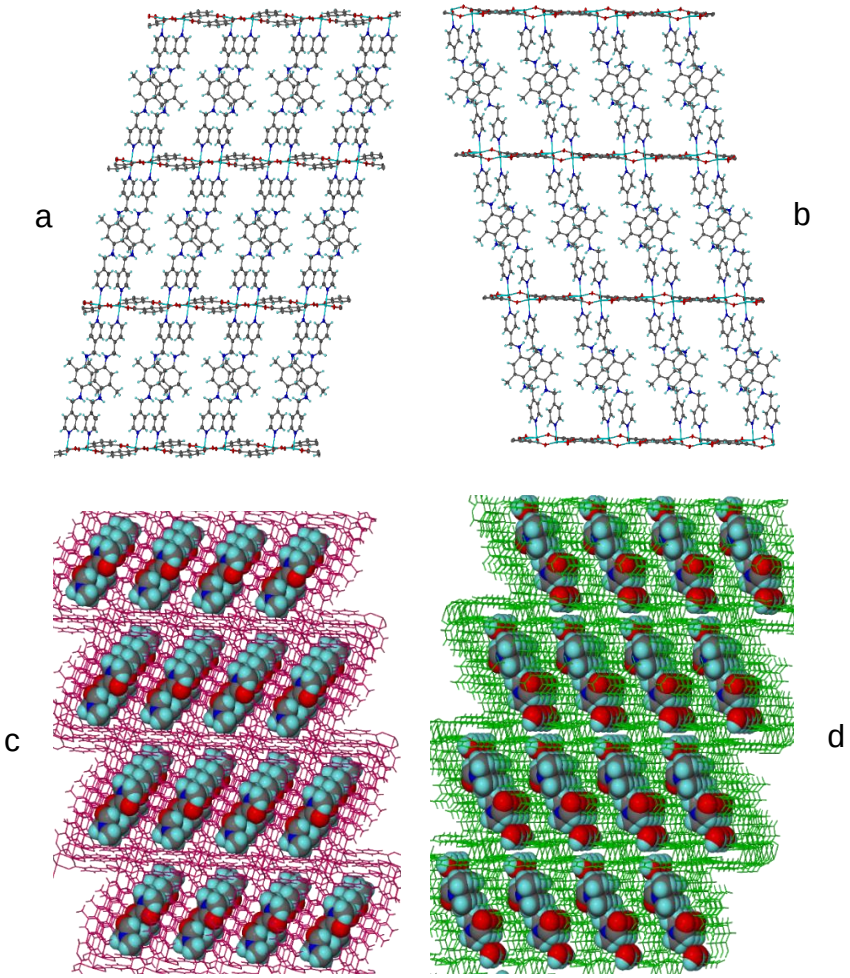

Figure 4.23: (a, b) Compounds **16** and **17** 2D networks. (c, d) Packing diagram of compounds **16** and **17** with guest molecules occupy the resulted one-dimensional channels.

Table 4.9: Selected bond lengths (Å) and angles (°) of $(Co(L3)(isoph)].DMF)_n$ and $(Cd(L3)(isoph)].DMF.H_2O)_n$ coordination polymers.

$(Co(L3)(isoph)].DMF)_n$				$(Cd(L3)(isoph)].DMF.H_2O)_n$			
Co-O1	2.054(3)	$O4^1$-Co-$O3^1$	60.35(11)	Cd-O1	2.331(2)	N1-Cd-$O4^1$	91.27(9)
Co-O2	2.022(3)	N1-Co-$O3^1$	89.12(13)	Cd-O2	2.292(2)	$N4^1$-Cd-O1	87.82(9)
Co-O3	2.193(3)	N1-Co-$O4^1$	92.07(13)	Cd-O3	2.393(2)	$N4^1$-Cd-$O2^2$	91.00(9)
Co-O4	2.159(3)	N1-Co-$N4^1$	177.57(13)	Cd-O4	2.390(2)	$N4^1$-Cd-$O3^1$	95.81(10)
Co-N1	2.129(4)	$N4^1$-Co-$O3^1$	93.27(13)	Cd-N1	2.304(3)	$N4^1$-Cd-$O4^1$	90.83(9)
Co-N4	2.135(4)	$N4^1$-Co-$O4^1$	89.52(12)	Cd-N4	2.286(3)	$N4^1$-Cd-N1	174.42(9)
N2-C6	1.370(6)	C21-O1-Co	119.5(3)	N2-C6	1.430(5)	$N4^1$-Cd-$C28^1$	93.74(10)
N2-C7	1.386(6)	C21-O2-Co^1	169.4(3)	N2-C7	1.395(5)	C21-O1-Cd	178.2(2)
N3-C10	1.391(6)	C28-O3-Co^1	88.4(3)	N3-C10	1.401(5)	C21-O2-Cd^1	104.93(19)
N3-C15	1.398(6)	C28-O4-Co^1	90.4(2)	N3-C15	1.389(5)	C28-O3-Cd^1	92.20(19)
O1-C21	1.263(5)	C1-N1-Co	122.1(3)	O1-C21	1.249(4)	C28-O4-Cd^1	91.73(18)
O2-C21	1.241(5)	C1-N1-C5	115.9(4)	O2-C21	1.256(4)	C1-N1-Cd	120.6(2)
O3-C28	1.266(5)	C5-N1-Co	122.1(3)	O3-C28	1.244(4)	C5-N1-Cd	121.7(2)
O4-C28	1.250(5)	C6-N2-C7	121.2(4)	O4-C28	1.267(4)	C7-N2-C6	121.5(3)
O1-Co-$O3^1$	93.30(11)	C10-N3-C15	122.3(4)	O1-Cd-$O3^1$	141.27(8)	C15-N3-C10	120.7(3)
O1-Co-$O4^1$	153.52(12)	C18-N4-Co^1	120.9(3)	O1-Cd-$O4^1$	86.93(8)	C18-N4-$Cd1^1$	120.6(2)
O1-Co-N1	89.91(12)	C19-N4-Co^1	123.4(3)	$O2^1$-Cd-O1	132.30(8)	C19-N4-$Cd1^1$	121.8(2)
O1-Co-$N4^1$	89.48(12)	N2-C6-C3	115.0(4)	$O2^1$-Cd-$O3^1$	86.29(8)	C19-N4-C18	117.3(3)
$O2^1$-Co-O1	118.71(12)	N2-C7-C8	117.9(4)	$O2^1$-Cd-$O4^1$	140.77(8)	N2-C6-C3	112.2(3)
$O2^1$-Co-$O3^1$	147.79(11)	N2-C7-C12	123.3(4)	$O2^1$-Cd-N1	90.64(9)	N2-C7-C8	118.1(3)
$O2^1$-Co-$O4^1$	87.76(11)	N3-C10-C9	122.5(4)	$O4^1$-Cd-$O3^1$	54.55(8)	N3-C10-C9	122.4(3)
$O2^1$-Co-N1	87.62(14)	N3-C10-C11	118.3(4)	N1-Cd-O1	87.13(9)	N3-C10-C11	118.6(3)
$O2^1$-Co-$N4^1$	90.60(13)	N3-C15-C16	113.8(4)	N1-Cd-$O3^1$	89.62(10)	N3-C15-C16	114.7(3)

Table 4.10: Selected torsion angles (°) for compounds **16** and **17**.

16		**17**	
Co-O1-C21-O2	-13.9(5)	Cd-O2-C21-O1	-12.6(4)
Co-O1-C21-C22	165.0(3)	Cd-O2-C21-C22	167.1(2)
Co-O2-C21-O1	-56.6(16)	Cd-O3-C28-O4	-0.1(4)
Co-O2-C21-C22	124.5(13)	Cd-O3-C28-C26	178.1(3)
Co-O3-C28-O4	-2.5(4)	Cd-O4-C28-O3	0.1(4)
Co-O3-C28-C26	175.7(4)	Cd-O4-C28-C26	-178.1(3)
Co-O4-C28-O3	2.5(4)	Cd-N1-C1-C2	175.1(2)
Co-O4-C28-C26	-175.6(4)	Cd-N1-C5-C4	-175.5(3)
Co-N1-C1-C2	179.9(4)	Cd-N4-C18-C17	-175.8(3)
Co-N1-C5-C4	-179.1(4)	Cd-N4-C19-C20	174.8(3)
Co-N4-C18-C17	-179.2(4)	N2-C7-C8-C9	179.6(3)
Co-N4-C19-C20	-179.9(3)	N2-C7-C8-C13	-0.5(5)
N2-C7-C8-C9	177.5(4)	N2-C7-C12-C11	-179.3(4)
N2-C7-C8-C13	-0.9(7)	N3-C10-C11-C12	-177.6(3)
N2-C7-C12-C11	-177.9(4)	N3-C10-C11-C14	1.1(5)
N3-C10-C11-C12	-178.4(4)	N3-C15-C16-C17	-153.5(3)
N3-C10-C11-C14	1.6(7)	N3-C15-C16-C20	28.0(5)
N3-C15-C16-C17	-163.9(5)	C6-N2-C7-C8	176.1(4)
N3-C15-C16-C20	19.9(8)	C6-N2-C7-C12	-3.8(6)
C6-N2-C7-C8	169.7(5)	C7-N2-C6-C3	177.7(3)
C6-N2-C7-C12	-13.5(7)	C8-C9-C10-N3	177.8(3)
C7-N2-C6-C3	174.6(4)	C10-N3-C15-C16	-175.5(3)
C8-C9-C10-N3	177.8(5)	C15-N3-C10-C9	12.4(5)
C10-N3-C15-C16	-174.2(5)	C15-N3-C10-C11	-170.9(3)
C15-N3-C10-C9	9.9(8)		
C15-N3-C10-C11	-171.0(5)		

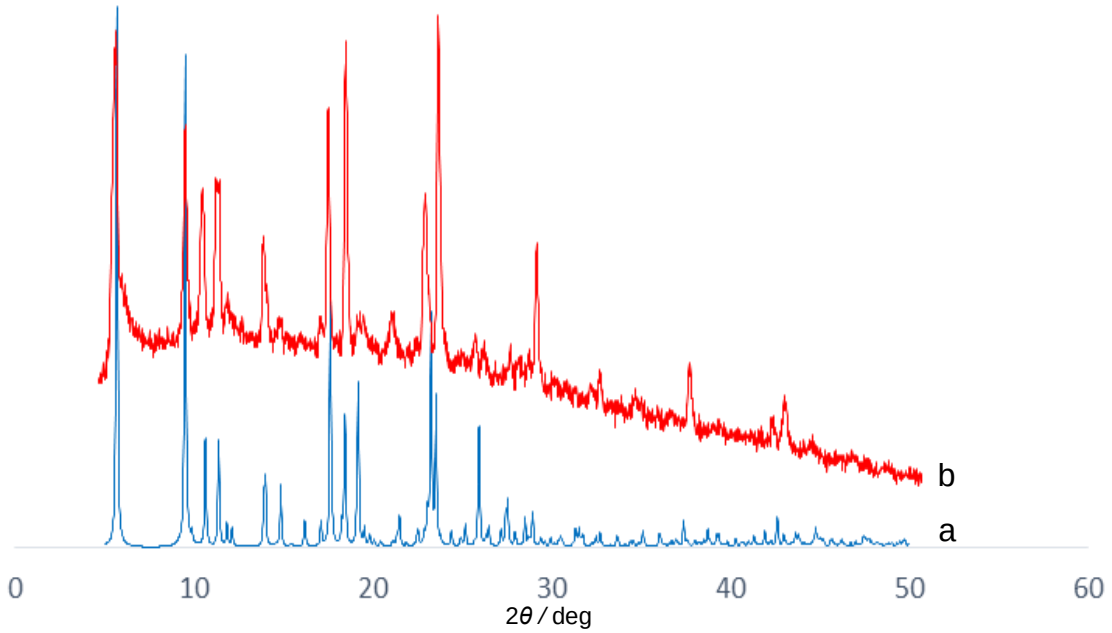

Figure 4.24: (a**)** Compound **16** calculated powder XRD pattern, (b) compound **16** powder XRD pattern.

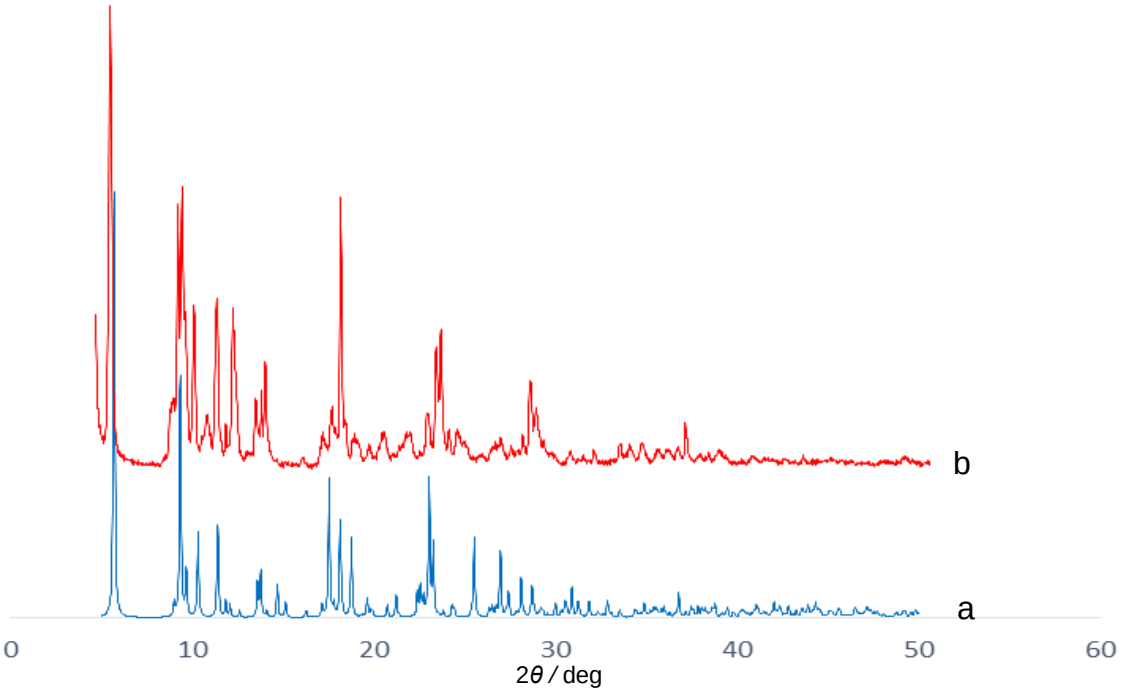

Figure 4.25: (a**)** Compound **17** calculated powder XRD pattern, (b) Compound **17** powder XRD pattern.

4.5.6 Crystal structures of $([Co(L3)(Meisoph)].DMF)_n$ (18) and $([Cd(L3)(Meisoph)].DMF)_n$ (19) coordination polymers

$([Co(L3)(Meisoph)].DMF)_n$ (**18**) and $([Cd(L3)(Meisoph)].DMF)_n$ (**19**) are isostructural coordination polymers, their crystal structures were solved in the triclinic space group $P\bar{1}$ [30-34] and show one Co(II) or Cd(II) ion on a general position, one L3 ligand molecule, one 5-methylisophthalate molecule and one DMF solvent molecule per asymmetric unit (figure 4.26). The divalent metal is coordinated to three 5-methylisophthalate molecules along the equatorial axes and shows four M-O bond lengths of 2.041(2), 2.044(2), 2.220(3) and 2.123(2) Å for Co-O1, Co-O2, Co-O3 and Co-O4, or 2.310(2), 2.317(2), 2.377(2) and 2.357(2) Å for Cd-O1, Cd-O2, Cd-O3 and Cd-O4. M^{2+} ion is also coordinated to two L3 ligand molecules along the axial axes Co-N1= 2.150(3) and Co-N4= 2.137(3) Å or Cd-N1= 2.293(3) and Cd-N4= 2.333(3) Å to produce the distortion octahedral coordination centre (Co-Co= 4.020 Å) and (Cd-Cd= 3.880 Å).

5-methylisophthalate molecules in compounds **18** and **19** are fully deprotonated and behave as tetra-dentate ligands to three M^{2+} coordination centres. The first carboxylate group behave as a bidentate ligand to two different coordination centres and shows two coordination distances between M-O1 and M-O2. The second carboxylate group behave as a bidentate ligand to one divalent coordination centre and shows two coordination distances between M-O3 and M-O4. 5-Methylisophthalate molecules in compounds **18** and **19** shows similar coordination style as isophthalate molecules in compounds **16** and **17**. To the best of our knowledge and according to CCDC the coordination style of 5-methylisophthalate in compounds **18** and **19** was not reported before.

L3 ligand behaves as a bidentate ligand by nitrogen atoms of 4-pyridyl rings to two M^{2+} coordination centres from two different M^{2+}-$Meisoph^{2-}$ chains (Co-L3-Co^1= 19.843 Å) and (Cd-L3-Cd^1= 20.227 Å). L3 ligand molecule in compound **18** and **19** is approximately linear and shows two torsion angles of -178.20(4) and -177.90(4) ° for compound **18** or 177.60(3) and 179.00(3) ° for compound **19** respectively. Four L3 ligand molecules, four 5-methylisophthalate molecules and eight M^{2+} cations are coordinated to produce $(M)_8(L3)_4(Meisoph)_4$ tetragonal structure that shows 4.020 × 10.028 or 3.880 × 10.189 Å distances between M^{2+} ions and 4.000 or 3.902 Å as the closest distance between dimethylphenyl rings that due to π-π stacking interaction (figure 4.28). The tetragonal structure shows another π-π stacking interaction between 4-pyridyl rings 4-py to 4-py= 3.854 and 3.852 Å for compound **18**, or 3.688 and 3.694 Å for compound **19** (figure 4.28). Bridging ligand

result in two-dimensional coordination polymers of 4^4 topology and one-dimensional open channels that occupied by solvent guest molecules (figure 4.29). Powder X-ray analysis for compounds **18** and **19** shows a good agreement between calculated and experimental patterns which indicate phase purity and materials stability after drying figures 4.30 and 4.31. Summary of bond lengths, angles and torsion angles for compounds **18** and **19** are listed in tables 4.11 and 4.12.

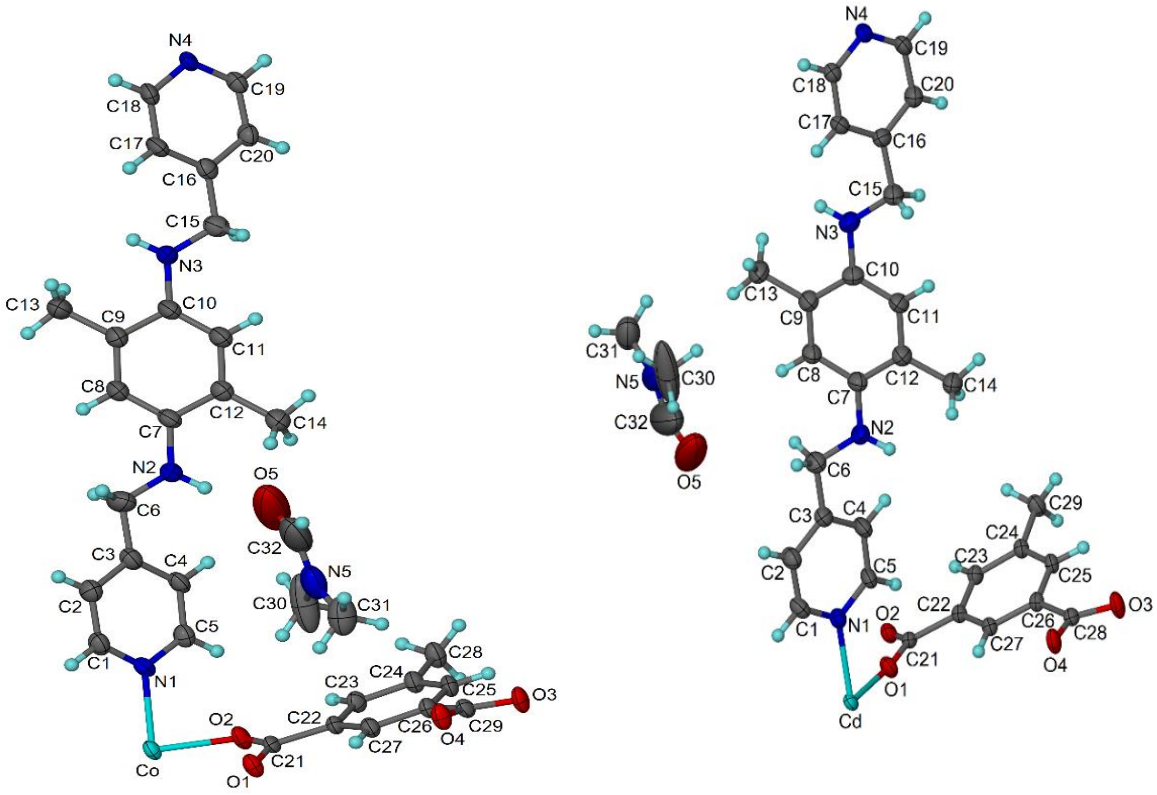

Figure 4.26: (left) ([Co(L3)(Meisoph)].DMF)$_n$ MOF asymmetric unit of the crystal structure, (right) ([Cd(L3)(Meisoph)].DMF)$_n$ MOF asymmetric unit of the crystal structure. Ellipsoids shown at 50 % probability levels.

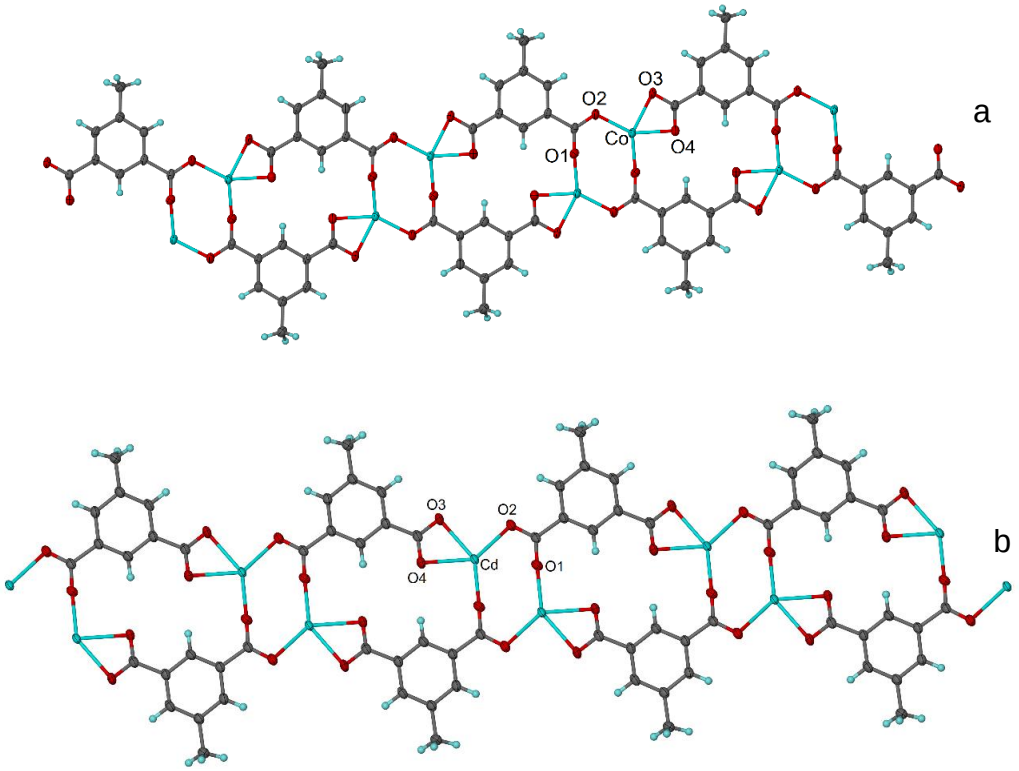

Figure 4.27: (a) Co(II) and 5-methylisophthalate one-dimensional coordination chain. (b) Cd(II) and 5-methylisophthalate coordination chain. Each 5-methylisophthalate is coordinated to three M^{2+} and shows four M-O coordination bond length.

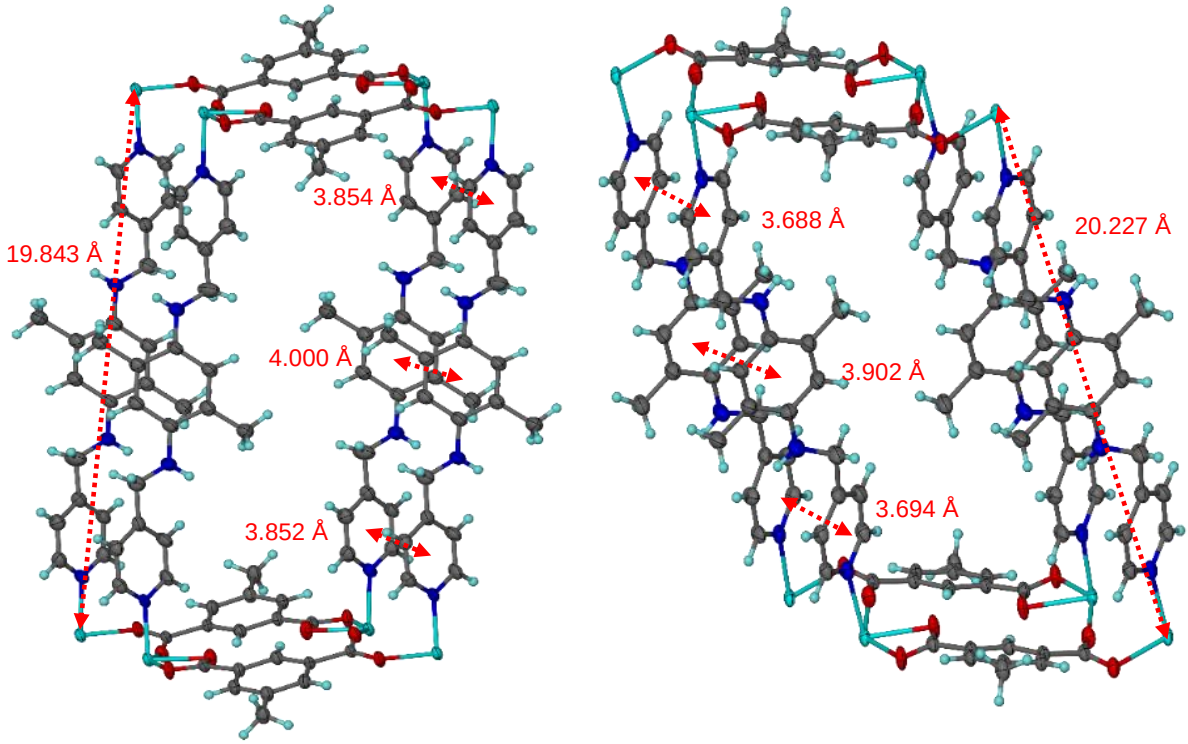

Figure 4.28: (left) $([Co(L3)(Meisoph)].DMF)_n$ tetragonal structure, (right) $([Cd(L3)(Meisoph)].DMF)_n$ tetragonal structure.

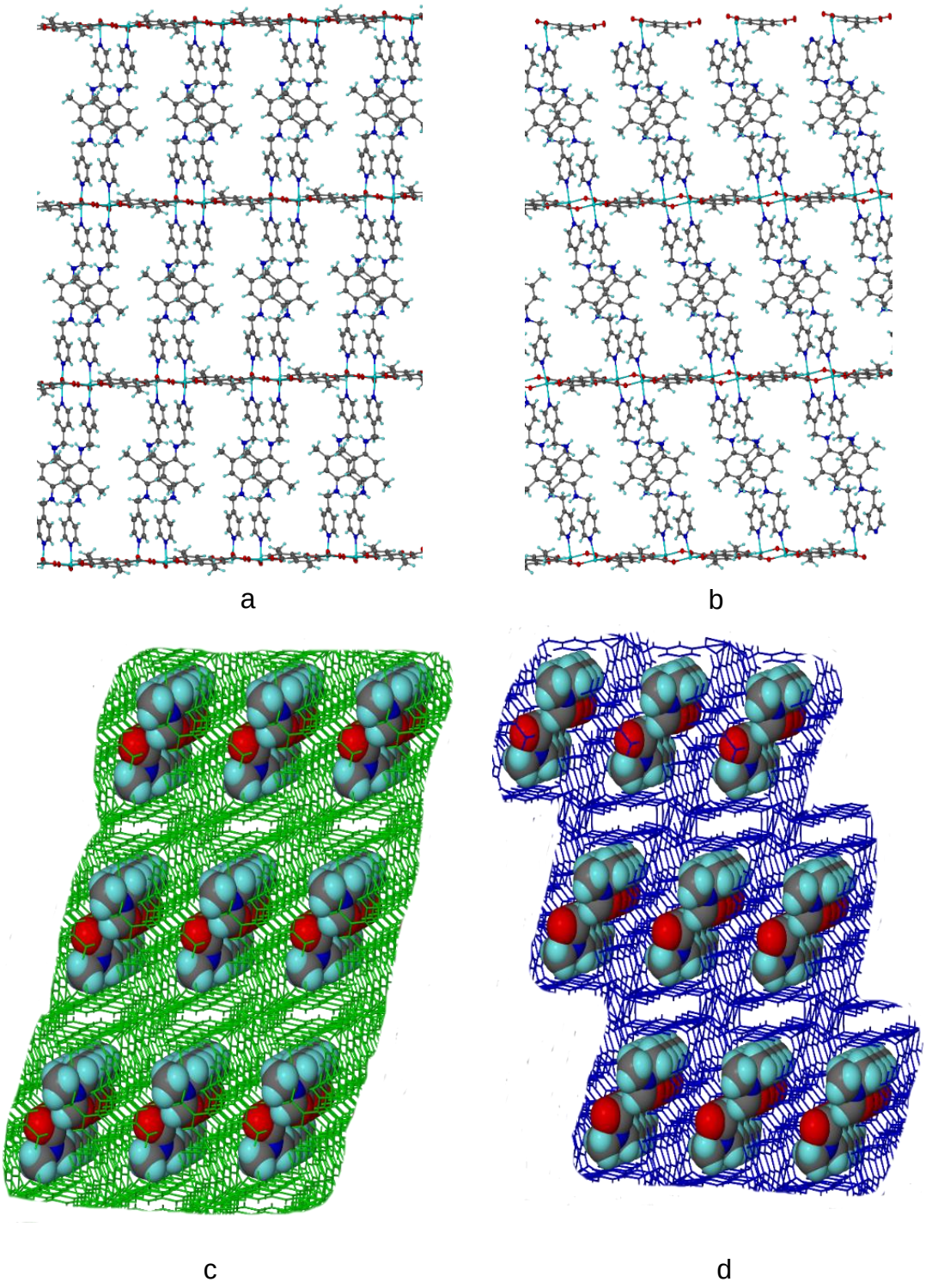

Figure 4.29: (a, b) Compounds **18** and **19** 2D networks. (c, d) Compounds **18** and **19** coordination polymers after symmetrical expanding, solvent guest molecules occupy the resulted one-dimensional channels.

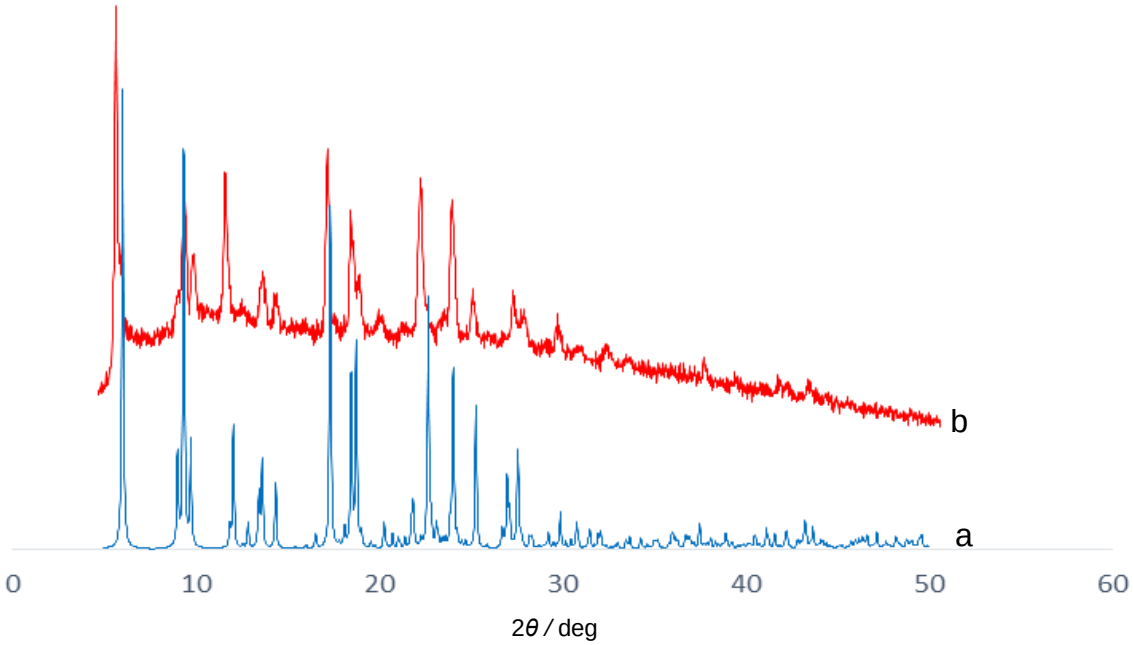

Figure 4.30: (a) Compound **18** calculated powder XRD pattern, (b) compound **18** powder XRD pattern.

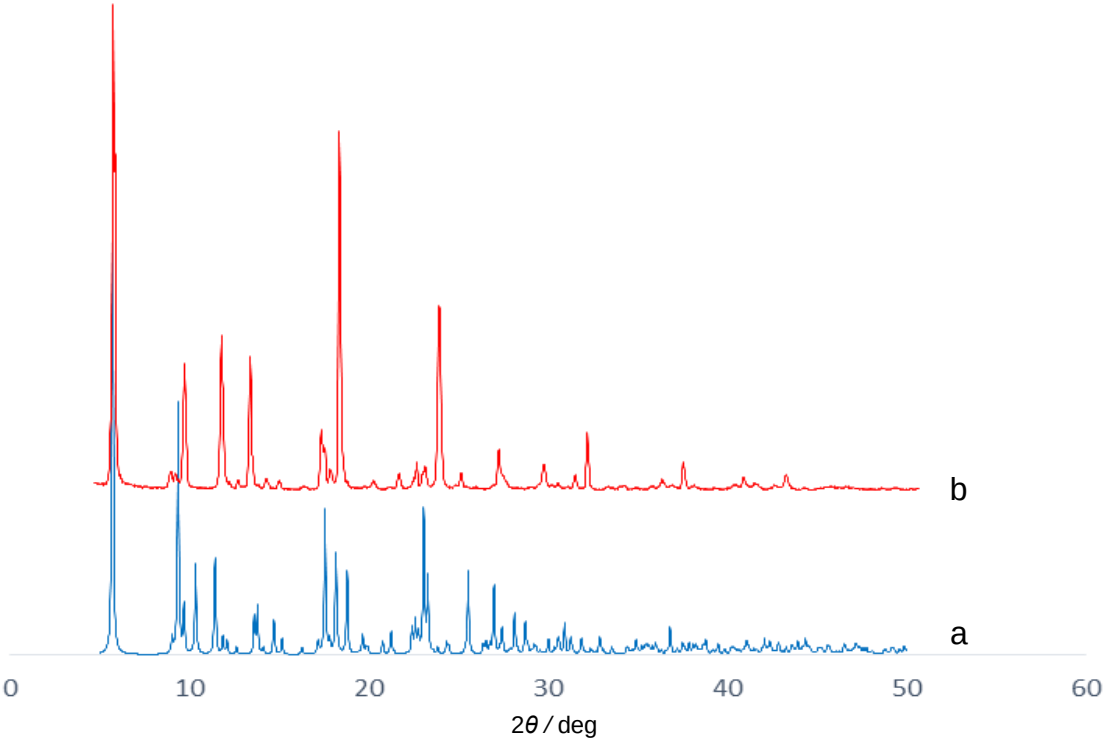

Figure 4.31: (a) Compound **19** calculated powder XRD pattern, (b) compound **19** powder XRD pattern.

Table 4.11: Selected bond lengths (Å) and torsion (°) angles of compounds **18** and **19**.

Compound **18**				Compound **19**			
Co-O1	2.041(2)	O2-Co-N4	90.32(10)	Cd-O1	2.310(2)	N1-Cd-O1	90.24(10)
Co-O2	2.044(2)	O4-Co-O3	60.41(9)	Cd-O2	2.317(2)	N1-Cd-O2	90.90(9)
Co-O3	2.220(3)	O4-Co-N1	94.34(11)	Cd-O3	2.377(2)	N1-Cd-O3	97.02(10)
Co-O4	2.123(2)	O4-Co-N4	90.23(11)	Cd-O4	2.357(2)	N1-Cd-O4	92.06(10)
Co-N1	2.150(3)	N1-Co-O3	89.31(11)	Cd-N1	2.293(3)	N1-Cd-N4	172.73(10)
Co-N4	2.137(3)	N4-Co-O3	93.35(11)	Cd-N4	2.333(3)	N4-Cd-O3	89.82(10)
O1-C21	1.251(4)	N4-Co-N1	175.41(11)	O1-C21	1.254(4)	N4-Cd-O4	93.87(10)
O2-C21	1.258(4)	C21-O1-Co	156.0(2)	O2-C21	1.266(4)	C21-O1-Cd	169.3(2)
O3-C29	1.264(4)	C21-O2-Co	119.8(2)	O3-C28	1.254(4)	C21-O2-Cd	101.96(19)
O4-C29	1.253(4)	C29-O3-Co	87.1(2)	O4-C28	1.247(4)	C28-O3-Cd	90.4(2)
N2-C6	1.364(5)	C29-O4-Co	91.8(2)	N2-C6	1.397(5)	C28-O4-Cd	91.53(19)
N2-C7	1.385(5)	C1-N1-Co	123.0(2)	N2-C7	1.410(5)	C1-N1-Cd	121.1(2)
N3-C10	1.407(5)	C6-N2-C7	122.3(3)	N3-C10	1.404(5)	C5-N1-Cd	121.5(2)
N3-C15	1.343(5)	C15-N3-C10	121.7(3)	N3-C15	1.424(5)	C6-N2-C7	119.1(3)
O1-Co-O2	121.99(10)	N2-C6-C3	115.6(4)	O1-Cd-O2	131.05(8)	C10-N3-C15	120.3(3)
O1-Co-O3	148.19(10)	N2-C7-C8	122.4(3)	O1-Cd-O3	143.35(8)	N2-C6-C3	114.1(3)
O1-Co-O4	88.42(10)	N2-C7-C12	118.6(3)	O1-Cd-O4	88.73(9)	C8-C7-N2	122.1(3)
O1-Co-N1	86.76(11)			O1-Cd-N4	85.70(9)	C12-C7-N2	119.3(3)
O1-Co-N4	92.91(11)			O2-Cd-O3	84.88(8)	C9-C10-N3	118.1(3)
O2-Co-O3	89.13(9)			O2-Cd-O4	140.10(8)	C11-C10-N3	122.7(3)
O2-Co-O4	149.51(10)			O2-Cd-N4	87.24(9)	N3-C15-C16	112.1(3)
O2-Co-N1	85.98(11)			O4-Cd-O3	55.27(8)		

Table 4.12: Selected torsion angles (°) for compounds **18** and **19**.

Compound **18**		Compound **19**	
Co-O1-C21-O2	-78.4(7)	Cd-O1-C21-O2	-115.7(11)
Co-O1-C21-C22	101.6(6)	Cd-O1-C21-C22	63.0(13)
Co-O2-C21-O1	11.4(5)	Cd-O2-C21-O1	17.9(3)
Co-O2-C21-C22	-168.6(2)	Cd-O2-C21-C22	-160.8(2)
Co-O3-C29-O4	-0.6(3)	Cd-O3-C28-O4	1.1(3)
Co-O3-C29-C26	178.6(3)	Cd-O3-C28-C26	-177.8(3)
Co-O4-C29-O3	0.6(4)	Cd-O4-C28-O3	-1.2(4)
Co-O4-C29-C26	-178.6(3)	Cd-O4-C28-C26	177.7(3)
Co-N1-C1-C2	-174.4(3)	Cd-N1-C1-C2	178.6(3)
Co-N1-C5-C4	174.2(3)	Cd-N1-C5-C4	-178.7(3)
Co-N4-C18-C17	-176.9(3)	Cd-N4-C18-C17	-167.6(3)
Co-N4-C19-C20	177.3(3)	Cd-N4-C19-C20	167.4(3)
N2-C7-C8-C9	-178.6(4)	N2-C7-C8-C9	-177.9(4)
N2-C7-C12-C11	178.5(4)	N2-C7-C12-C11	179.3(4)
N2-C7-C12-C14	-1.8(6)	N2-C7-C12-C14	-0.4(6)
N3-C10-C11-C12	177.8(4)	N3-C10-C11-C12	-177.8(4)
N3-C15-C16-C17	23.4(6)	N3-C15-C16-C17	45.9(5)
N3-C15-C16-C20	-155.5(4)	N3-C15-C16-C20	-136.1(4)
C2-C3-C6-N2	155.9(4)	C2-C3-C6-N2	146.2(4)
C4-C3-C6-N2	-26.6(7)	C4-C3-C6-N2	177.60(3)
C6-N2-C7-C8	-21.5(6)	C6-N2-C7-C8	-10.6(6)
C6-N2-C7-C12	160.4(4)	C6-N2-C7-C12	172.4(4)
C7-N2-C6-C3	-178.2(4)	C7-N2-C6-C3	177.6(3)
C8-C9-C10-N3	-178.1(4)	C8-C9-C10-N3	179.3(3)
C10-N3-C15-C16	-177.9(4)	C10-N3-C15-C16	179.0(3)
C13-C9-C10-N3	0.5(6)	C13-C9-C10-N3	-1.2(6)
C15-N3-C10-C9	-164.7(4)	C15-N3-C10-C9	179.7(4)
C15-N3-C10-C11	18.8(7)	C15-N3-C10-C11	-3.0(6)

Table 4.13: The crystallographic data of compounds ^{c}L, L3 and **14**.

Identification code	^{c}L	L3	**14**
Empirical Formula	$C_{20}H_{18}N_4$	$C_{20}H_{22}N_4$	$C_{21}H_{26}ClFe_{0.5}N_4O$
Formula weight	314.38	318.41	413.83
Temperature/K	120.00(10)	120.20(5)	120.00(10)
Crystal system	Monoclinic	Triclinic	Monoclinic
Space group	$P2_1/c$	$P\bar{1}$	$P2_1/c$
a/Å	7.4640(2)	7.3393(3)	12.6742(3)
b/Å	8.3794(2)	10.3396(4)	11.2556(4)
c/Å	12.6517(4)	12.2912(5)	13.6593(4)
α/°	90	96.336(4)	90
β/°	95.023(3)	106.392(4)	99.068(3)
γ/°	90	106.566(4)	90
Volume/Å^3	788.25(4)	839.00(7)	1924.24(9)
Z	2	2	4
ρ_{calc}g/cm^3	1.325	1.260	1.428
μ/mm^{-1}	0.635	0.597	4.810
F(000)	332.0	340.0	872.0
Crystal size/mm^3	0.216 × 0.180 × 0.149	0.164 × 0.093 × 0.059	0.208 × 0.143 × 0.099
Radiation	Cu$K\alpha$ (λ = 1.54184)	$CuK\alpha$ (λ = 1.54184)	$CuK\alpha$ (λ = 1.54184)
2Θ range for data collection/°	11.902 to 147.734	7.664 to 147.596	7.062 to 147.346
Index ranges	$-8 \le h \le 9$, $-10 \le k \le 7$, $-13 \le l \le 15$	$-7 \le h \le 9$, $-12 \le k \le 8$, $-14 \le l \le 15$	$-15 \le h \le 13$, $-11 \le k \le 13$, $-13 \le l \le 16$
Reflections collected	2895	5959	9062
Independent reflections	1534 [R_{int} = 0.0245, R_{sigma} = 0.0332]	3166 [R_{int} = 0.0365, R_{sigma} = 0.0430]	3652 [R_{int} = 0.0350, R_{sigma} = 0.0399]
Data/restraints/parameters	1534/0/110	3166/0/219	3652/0/254
Goodness-of-fit on F^2	1.026	1.048	1.023
Final R indexes [I>=2σ (I)]	R_1 = 0.0391, wR_2 = 0.1019	R_1 = 0.0748, wR_2 = 0.2028	R_1 = 0.0481, wR_2 = 0.1288
Final R indexes [all data]	R_1 = 0.0475, wR_2 = 0.1094	R_1 = 0.0891, wR_2 = 0.2212	R_1 = 0.0568, wR_2 = 0.1362
Largest diff. peak/hole / e Å^{-3}	0.22/-0.18	1.26/-0.47	0.63/-0.68

Table 4.14: The crystallographic data of compounds **15**, **16** and **17**.

Identification code	**15**	**16**	**17**
Empirical Formula	$C_{11}H_{11}FeN_3S$	$C_{31}H_{33}CoN_5O_5$	$C_{31}H_{35}CdN_5O_6$
Formula weight	356.8	614.57	686.06
Temperature/K	120.15	120.00(10)	120.00(13)
Crystal system	Tetragonal	Triclinic	Triclinic
Space group	$I4_1/a$	$P\bar{1}$	$P\bar{1}$
a/Å	13.3600(12)	9.1194(10)	9.3594(3)
b/Å	13.3600(12)	10.0774(9)	10.2299(3)
c/Å	22.845(4)	16.2617(16)	16.3773(5)
α/°	90	75.183(8)	73.946(3)
β/°	90	79.860(9)	78.064(2)
γ/°	90	82.924(8)	82.264(3)
Volume/Å^3	4077.6(11)	1417.4(2)	1469.33(8)
Z	4	3	3
ρ_{calc}g/cm^3	1.318	1.397	1.551
μ/mm^{-1}	4.265	5.132	6.397
F(000)	1696.0	622.0	704.0
Crystal size/mm^3	0.178 × 0.077 × 0.067	0.181 × 0.120 × 0.113	0.229 × 0.124 × 0.077
Radiation	*CuKα* (λ = 1.54184)	*CuKα* (λ = 1.54184)	*CuKα* (λ = 1.54184)
2*Θ* range for data collection/°	7.666 to 147.254	9.108 to 147.994	9.026 to 148.132
Index ranges	$-16 \le h \le 11$, $-15 \le k \le 16$, $-27 \le l \le 15$	$-8 \le h \le 11$, $-12 \le k \le 12$, $-20 \le l \le 19$	$-11 \le h \le 11$, $-12 \le k \le 12$, $-18 \le l \le 20$
Reflections collected	4018	11317	17364
Independent reflections	1993 [R_{int} = 0.0534, R_{sigma} = 0.0737]	5326 [R_{int} = 0.0478, R_{sigma} = 0.0566]	5676 [R_{int} = 0.0517, R_{sigma} = 0.0406]
Data/restraints/parameters	1993/0/167	5326/0/383	5676/0/395
Goodness-of-fit on F^2	1.011	1.052	0.984
Final *R* indexes [$I>=2\sigma(I)$]	R_1 = 0.0898, wR_2 = 0.2411	R_1 = 0.0755, wR_2 = 0.2093	R_1 = 0.0389, wR_2 = 0.1140
Final *R* indexes [all data]	R_1 = 0.1981, wR_2 = 0.3471	R_1 = 0.0869, wR_2 = 0.2219	R_1 = 0.0424, wR_2 = 0.1198
Largest diff. peak/hole / e Å^{-3}	0.47/-0.30	1.37/-0.85	1.27/-0.97

Table 4.15: The crystallographic data of compounds **18** and **19**.

Identification code	**18**	**19**
Empirical Formula	$C_{32}H_{35}CoN_5O_5$	$C_{32}H_{35}CdN_5O_5$
Formula weight	628.58	682.07
Temperature/K	120.00(10)	120.00(10)
Crystal system	Triclinic	Triclinic
Space group	$P\bar{1}$	$P\bar{1}$
a/Å	10.0276(6)	10.0304(4)
b/Å	10.1458(5)	10.1890(4)
c/Å	15.5412(7)	15.7214(7)
α/°	98.994(4)	73.025(4)
β/°	105.454(5)	75.635(4)
γ/°	99.562(4)	82.358(3)
Volume/Å^3	1468.94(13)	1485.49(11)
Z	2	3
ρ_{calc}g/cm^3	1.421	1.525
μ/mm^{-1}	4.995	6.299
F(000)	658.0	700.0
Crystal size/mm^3	0.180 × 0.112 × 0.076	0.700 × 0.184 × 0.165
Radiation	*CuKα* (λ = 1.54184)	*CuKα* (λ = 1.54184)
2*Θ* range for data collection/°	9.042 to 147.7	9.094 to 147.074
Index ranges	-12 ≤ *h* ≤ 10, -12 ≤ *k* ≤ 12, -14 ≤ *l* ≤ 18	-12 ≤ *h* ≤ 12, -9 ≤ *k* ≤ 11, -17 ≤ *l* ≤ 19
Reflections collected	11067	10645
Independent reflections	5522 [R_{int} = 0.0452, R_{sigma} = 0.0598]	5592 [R_{int} = 0.0393, R_{sigma} = 0.0393]
Data/restraints/parameters	5522/0/393	5592/0/393
Goodness-of-fit on F^2	1.028	1.046
Final *R* indexes [*I*>=2*σ*(*I*)]	R_1 = 0.0581, wR_2 = 0.1450	R_1 = 0.0388, wR_2 = 0.1026
Final *R* indexes [all data]	R_1 = 0.0785, wR_2 = 0.1590	R_1 = 0.0420, wR_2 = 0.1057
Largest diff. peak/hole / e Å^{-3}	1.16/-0.63	1.45/-1.24

4.6 Conclusion

Chapter four reports the synthesis and characterisation of the new ligand *N*,*N*′-bis(4-pyridinylmethyl)-2,5-dimethylbenzene-1,4-diamine (L3) and its self-assembly with Fe(III) chloride hydrate or Fe(II) thiocyanate in methanol at room temperature to produce $([Fe_{0.5}(L3)Cl].MeOH)_n$ (**14**) coordination polymer or $([Fe(L3)_{0.5}(SCN)])_n$ (**15**) MOF. The first L3 ligand molecule in compound **14** is approximately linear and coordinated to two iron(II) coordination centres by nitrogen atoms of 4-pyridyl rings. Whereas the second L3 ligand molecule shows bent S-shape between iron(II) coordination centres. Four L3 ligand molecules are coordinated to four Fe(II) ions to produce $(Fe)_4$-$(L3)_4$ square cavity that extending to form a two-dimensional network. The resulted two-dimensional network is packing with two networks in an inter-digitated fashion and shows no significant channels in the lattice. L3 ligand in compound **15** shows rotation of 4-pyridyl rings and torsion angle of -64.046 ° between the phenyl and 4-pyridyl rings to produce L3 bent S-shape between Fe(II) coordination centres. Compound **15** resulted structure is a three-dimensional open network and shows unusual channels shape along the three axes. Compound **15** shows hexagonal channels consist of $(Fe)_6$-$(L3)_6$ along *a* and *c* axes, cross shape channels along *a* and *b* axes and H-shape channels along *c* and *d* axes consisting of four L3 ligand molecules and four Fe(II) ions. The resulted network interpenetrating with other four networks leave no free space or significant voids along the three axes.

Solvothermal reaction of L3 ligand with isophthalic acid, 5-methylisophthalic acid, Co(II) nitrate or Cd(II) nitrate in DMF at 115 °C for 24 hours produced $(Co(L3)(isoph)].DMF)_n$ (**16**), $(Cd(L3)(isoph)].DMF.H_2O)_n$ (**17**), $([Co(L3)(Meisoph)].DMF)_n$ (**18**) or $([Cd(L3)(Meisoph)].DMF)_n$ (**19**) two-dimensional coordination polymers. Compounds **16** and **17** are isostructural two-dimensional coordination polymers as well as compounds **18** and **19**. L3 ligand in compounds **16-19** is approximately linear and behaves as a bidentate ligand to two M^{2+} coordination centres from two different chains. Four L3 ligand molecules, eight M^{2+} metal ions and four isophthalate or 5-methylisophthalate molecules are coordinated to produce $(M^{2+})_8(L3)_4(isoph)_4$ or $(M^{2+})_8(L3)_4(Meisoph)_4$ tetragonal structure that expands to produce a two-dimensional network structure. The resulted two-dimensional network shows 4^4 topology and packing with orther networks to produce one-dimensionl channels that ocuppied by DMF solvet guest molecules for componds **16**, **18** and **19** or DMF and water molecules for compound **17**. Powder XRD analysis for compounds **14** and **16-19** show a good agreement between calculated and experimental pattrens. On the other hand, compound **15** powder XRD pattern does not match

the calculated pattern. The new phase is crystalline, but the structure could not be determined as the materials did not stay as a single crystal on drying out.

4.7 References

1. N. R. Yousefnia, B. Shaabani, M. Kubicki, M. S. Zakerhamidi and A. M.Grzeskiewicz, 2D holodirected lead(II) halide coordination polymers based on rigid *N,N′*-bis(4-pyridylmethylidyne) phenylene-1,4-diamine ligand: Syntheses, crystal structures, NBO studies and luminescence properties. *Polyhedron*. 2017, **129**, 38-45.
2. F. Bigdeli, S. Abedi, H. H. Monfared and A. Morsali, An investigation of the catalytic activity in a series of isoreticular Zn(II)-based metal-organic frameworks. *Inorganic Chemistry Communications*. 2016, **72**, 122-127.
3. S. Abedi, A. A. Tehrani, H. Ghasempoura and A. Morsali, Interplay between hydrophobicity and basicity toward the catalytic activity of isoreticular MOF organocatalysts. *New Journal of Chemistry*. 2016, **40**(8), 6970-6976.
4. A. Ghorai, J. Mondal, R. Chandra and G. K. Patra, A reversible fluorescent-colorimetric imino-pyridyl bis-Schiff base sensor for expeditious detection of Al^{3+} and HSO_3^- in aqueous media. *Dalton Transactions*. 2015, **44**(29), 13261-13271.
5. X. L. Wang, Y. F. Bi, H. Y. Lin and G. C. Liu, Three Novel Cd(II) Metal-Organic Frameworks Constructed from Mixed Ligands of Dipyrido[3,2-d:*2′,3′-f*]quinoxaline and Benzene-dicarboxylate: From a 1-D Ribbon, 2-D Layered Network, to a 3-D Architecture. *Crystal Growth and Design*. 2007, **7**(6), 1086-1091.
6. M. C. Aragoni, M. Arca, N. R. Champness, A. V. Chernikov, F. A. Devillanova, F. Isaia, V. Lippolis, N. S. Oxtoby, G. V. Sergey, Z. Vatsadze and C. Wilson, Designed Assembly of Low-dimensional Molecular Units: Novel Neutral Coordination Polymers Based on (Phosphonodithioato)Ni^{II} Complexes. *European Journal of Inorganic Chemistry*. 2004, **2004**(10), 2008-2012.
7. S. Z. Vatsadze, V. N. Nuriev, A. V. Chernikov and N. V. Zyk, Synthesis of novel linear exo-bidentate bispyridine ligands and their complexes with silver(I) tetrafluoroborate. *Russian Chemical Bulletin*. 2002, **51**(10), 1957-1958.
8. G. J. Halder, C. J. Kepert, B. Moubaraki, K. S. Murray and J. D. Cashion, Guest-dependent spin crossover in a nanoporous molecular framework material. *Science*. 2002, **298**(5599), 1762-1765.
9. D. Sek, M. Siwy, K. Bijak, M. G. Zajac, G. Malecki, K. Smolarek, L. Bujak, S. Mackowski and E. S. Balcerzak, Comparative Studies of Structural, Thermal, Optical, and Electrochemical Properties of Azines with Different End Groups with Their Azomethine Analogues toward Application in (Opto)Electronics. *The Journal of Physical Chemistry A*. 2013, **117**(40), 10320-10332.
10. H. Zhou, C. X. Chua and Y. Z. Li, Poly[[aquatris(μ-benzene-1,4-dicarboxylato)tricobalt(II)] methanol monosolvate monohydrate]. *Acta Crystallographica Section E: Structure Reports Online*. 2011, **67**(7), m841-m842.
11. D. Grasso, G. Buemi, S. Fasone and C. Gandolfo, Electronic Spectra and Dipole Moments of *p*-Phenylendiamine-*N*-*N*′-dibenzylidene and Its Aza-derivatives. *Croatica Chemica Acta*. 1981, **45**(1), 85-90.
12. E. Tahmasebi, M. Y. Masoomi, Y. Yamini and A. Morsali, Application of Mechanosynthesized Azine-Decorated Zinc(II) Metal-Organic Frameworks for Highly Efficient Removal and Extraction of Some Heavy-Metal Ions from Aqueous Samples: A Comparative Study. *Inorganic Chemistry*. 2015, **54**(2), 425-433.

13. C. Janiak and J. K. Vieth, MOFs, MILs and more: concepts, properties and applications for porous coordination networks (PCNs). *New Journal of Chemistry*. 2010, **34**(11), 2366-2388.
14. L. F. Ma, L. Y. Wang, Y. Y. Wang, S. R. Batten and J. G. Wang, Self-Assembly of a Series of Cobalt(II) Coordination Polymers Constructed from H_2tbip and Dipyridyl-Based Ligands. *Inorganic Chemistry*. 2009, **48**(3), 915-924.
15. A. Rana, S. K. Jana, M. Bera, D. Hazari, D. S. Chowdhuri, E. Zangrando and S. Dalai, Two new metal-organic coordination polymers of lead with O-, N-donor ligands: Synthesis, characterization, luminescence and thermal behavior. *Journal of Solid State Chemistry*. 2013, **197**, 46-52.
16. A. Pichon, A. L. Garay and S. L. James, Solvent-free synthesis of a microporous metal-organic framework. *Crystal Engineering Communication*. 2006, **8**(3), 211-214.
17. S. L. James, Metal-organic frameworks. *Chemical Society Reviews*. 2003, **32**(5), 276-288.
18. Y. Tan, Z. Fu and J. Zhang, A layered amino-functionalized zinc-terephthalate metal organic framework: Structure, characterization and catalytic performance for Knoevenagel condensation. *Inorganic Chemistry Communications*. 2011, **14**(12), 1966-1970.
19. R. F. D. Luis, E. S. Larrea, J. Orive, A. F. Marijuan, L. Lezamaad and M. I. Arriortuaab, Open and closed forms of the interpenetrated $[Cu_2(Tae)(Bpa)_2](NO_3)_2{\cdot}nH_2O$: magnetic properties and high pressure CO_2/CH_4 gas sorption. *Dalton Transactions*. 2018, **47**(3), 958-970.
20. J. A. Gould, H. S. Athwal, A. J. Blake, W. Lewis, P. Hubberstey, N. R. Champness and M. Schröder, Gas adsorption and structural diversity in a family of Cu(II) pyridyl-isophthalate metal-organic framework materials. *Philosophical Transactions of the Royal Society A: Mathematical, Physical and Engineering Sciences*. 2017, **A 375**, (2084).
21. A. Husain, M. Ellwart, S. A. Bourne, L. Öhrstro and C. L. Oliver, Single-Crystal-to-Single-Crystal Transformation of a Novel 2-Fold Interpenetrated Cadmium-Organic Framework with Trimesate and 1,2-Bis(4-pyridyl)ethane into the Thermally Desolvated Form Which Exhibits Liquid and Gas Sorption Properties. *Crystal Growth and Design*. 2013, **13**(4), 1526-1534.
22. J. Y. Lee, J. Li and J. Jagiello, Gas sorption properties of microporous metal organic frameworks. *Journal of Solid State Chemistry*. 2005, **178**(8), 2527-2532.
23. Y. Lin, X. Zhang, W. Chen, W. Shi and P. Cheng, Three Cadmium Coordination Polymers with Carboxylate and Pyridine Mixed Ligands: Luminescent Sensors for Fe^{III} and Cr^{VI} Ions in an Aqueous Medium. *Inorganic Chemistry*. 2017, **56**(19), 11768-11778.
24. V. J. Catalano and A. O. Etogo, Luminescent coordination polymers with extended Au(I)–Ag(I) interactions supported by a pyridyl-substituted NHC ligand. *Journal of Organometallic Chemistry*. 2005, **690**(24), 6041-6050.
25. G. J. Halder and C. J. Kepert, Iron(II) Molecular Framework Materials with 4,4'-Azopyridine. *Australian Journal of Chemistry*. 2005, **58**(5), 311-314.
26. Z. X. Liu, Synthesis, Crystal Structure and Biological Activity of a Polymeric Silver(I) Complex Derived from Nicotinic Acid. *Synthesis and Reactivity in Inorganic, Metal-Organic, and Nano-Metal Chemistry*. 2016, **46**(6), 809-813.
27. L. Tabrizi, H. Chiniforoshan and P. M. Ardl, A novel one-dimensional manganese(II) coordination polymer containing both dicyanamide and pyrazinamide ligands: Synthesis, spectroscopic investigations, X-ray studies and evaluation of biological activities. *Spectrochimica Acta Part A: Molecular and Biomolecular Spectroscopy*. 2015, **139**, 307-312.

28. X. Han, C. An and Z. Zhang, Two novel Ag(I) coordination polymers with triazoles derivatives: synthesis, crystal structures and biological activity. *Applied Organometallic Chemistry*. 2008, **22**(10), 565-572.
29. H. Vardhan, A. Mehta, C. I. Ezugwu and F. Verpoort, Self-assembled arene ruthenium metalla-assemblies. *Polyhedron*. 2016, **112**, 104-108.
30. L. J. Bourhis, O. V. Dolomanov, R. J. Gildea, J. A. K. Howardd and H. Puschmannb, The anatomy of a comprehensive constrained, restrained refinement program for the modern computing environment-Olex2 dissected. *Acta Crystallographica Section A*. 2015, **71**(1), 59-75.
31. L. Palatinus, S. J. Prathapab and S. V. Smaalen, EDMA: a computer program for topological analysis of discrete electron densities. *Journal of Applied Crystallography*. 2012, **45**(3), 575-580.
32. O. V. Dolomanov, L. J. Bourhis, R. J. Gildea, J. A. K. Howarda and H. Puschmann, OLEX2: a complete structure solution, refinement and analysis program. *Journal of Applied Crystallography*. 2009, **42**(2), 339-341.
33. L. Palatinus and A. V. D. Lee, Symmetry determination following structure solution in *P*1. *Journal of Applied Crystallography*. 2008, **41**(6), 975-984.
34. L. Palatinus and G. Chapuis, SUPERFLIP-a computer program for the solution of crystal structures by charge flipping in arbitrary dimensions. *Journal of Applied Crystallography*. 2007, **40**(4), 786-790.
35. Robert M. Silverstein, Francis X. Webster and David J. Kiemle, Spectrometric identification of organic compounds. 7th Edition. 2005. John Wiley and Sons, Inc.
36. R. M. Issa, A. M. Khedr and H. F. Rizk, UV-vis, IR and ^{1}H NMR spectroscopic studies of some Schiff bases derivatives of 4-aminoantipyrine. *Spectrochemica Acta Part A-Molecular and Biomolecular Spectroscopy*. 2005, **62**(1-3), 621-629.
37. Donald L. Pavia, Gary M. Lampman and George S. Kriz, Introduction to spectroscopy: a guide for students of organic chemistry. 2nd Edition. 1996. Harcourt Brace College Publications.
38. Dudley Williams and Ian Fleming, Spectroscopic methods in organic chemistry. 6th Edition. 2008. McGraw-Hill Education.
39. Y. M. Issa, H. B. Hassib and H. E. Abdelaal, ^{1}H NMR, ^{13}C NMR and mass spectral studies of some Schiff bases derived from 3-amino-1,2,4-triazole. *Spectrochimica Acta Part A: Molecular and Biomolecular Spectroscopy*. 2009, **74**(4), 902-910.
40. R. J. Abraham, J. Fisher and P. Loftus, Introduction to NMR spectroscopy. 1988. John Wiley and Sons.
41. Y. Yang, S. Liu, J. Li, X. Tian, X. Zhen and J. Han, Convenient Method for Reduction of C-N Double Bonds in Oximes, Imines, and Hydrazones Using Sodium Borohydride-Raney Ni System. *Synthetic Communications*. 2012, **42**(17), 2540-2554.
42. G. W. Gribble, Sodium borohydride in carboxylic acid media: a phenomenal reduction system. *Chemical Society Reviews*. 1998, **27**(6), 395-404.
43. Alan K. Brisdon, Inorganic Spectroscopic Methods. 1998. Oxford University Press.
44. J. R. Ferraro, L. J. Basile and D. L. Kovacic, The Infrared Spectra of Rare Earth Metal Chloride Complexes of 2,2'-Bipyridyl and 1,10-Phenanthroline from 650 to 70 cm^{-1}. *Inorganic Chemistry*. 1966, **5**(3), 391-395.
45. L. H. Jones, Infrared Spectrum and Structure of the Thiocyanate Ion. *The Journal of Chemical Physics*. 1956, **25**(5), 1069-1072.

46. C. Baer and J. Pike, Infrared Spectroscopic Analysis of Linkage Isomerism in Metal-Thiocyanate Complexes. *Journal of Chemical Education*. 2010, **87**(7), 724-726.
47. X. L. Wang, B. Mu, H. Y. Lin and G. C. Liu, Three new two-dimensional metal-organic coordination polymers derived from bis(pyridinecarboxamide)-1,4-benzene ligands and 1,3-benzenedicarboxylate: Syntheses and electrochemical property. *Journal of Organometallic Chemistry*. 2011, **696**(11), 2313-2321.
48. X. Wang, H. Lin, B. Mu, A. Tian and G. Liu, Encapsulation of discrete $(H_2O)_{12}$ clusters in a 3D three-fold interpenetrating metal-organic framework host with (3,4)-connected topology. *Dalton Transactions*. 2010, **39**(27), 6187-6189.
49. F. Luo, Y. X. Che and J. M. Zheng, Layer-pillared metal-organic framework showing two-fold interpenetration and considerable solvent-accessible channels. *Microporous and Mesoporous Materials*. 2009, **117**(1), 486-489.
50. L. Zhang, L. Lin, D. Liu, Y. J. Lin, Z. H. Li and G. X. Jin, Stacking Interactions Induced Selective Conformation of Discrete Aromatic Arrays and Borromean Rings. *Journal of the American Chemical Society*. 2017, **139**(4), 1653-1660.
51. V. Safarifard, S. R. Hermida, V. Guillerm, I. Imaz, M. Bigdeli, A. A. Tehrani, J. Juanhuix, A. Morsali, M. E. Casco, J. S. Albero, E. V. R. Fernandez and D. Maspoch, Influence of the Amide Groups in the CO_2/N_2 Selectivity of a Series of Isoreticular, Interpenetrated Metal-Organic Frameworks. *Crystal Growth and Design*. 2016, **16**(10), 6016-6023.
52. X. L. Wang, X. T. Sha, G. C. Liu, N. L. Chen, C. H. Gong and Y. Qu, Assembly, Structures, and Properties of a Series of Metal-Organic Coordination Polymers Derived from a Semi-rigid Bis-pyridyl-bis-amide Ligand. *Journal of Inorganic and General Chemistry*. 2015, **641**(7), 1274-1281.
53. Y. Y. Niu, Y. L. Song, J. Wu, H. Hou, Y. Zhu and X. Wang, Nonlinear polymeric effect: synthesis, crystal structure and nonlinear optical properties of a new mercury iodide adduct polymer $[Hg(bpfb)I_2]_n \cdot 2DMF$ (bpfb=*N,N*′-bis(4-pyridyl formamide)-1,4-benzene). *Inorganic Chemistry Communications*. 2004, **7**(4), 471-474.
54. T. Iwasita, Electrocatalysis of methanol oxidation. *Electrochimica Acta*. 2002, **47**(22-23), 3663-3674.
55. P. Karsten and J. Strahle, Bis(1,8-diazabicyclo[5.4.0]undec-7-en-8-ium) *trans*-Dichlorotetra(pyridine-N)iron(II) Dichloride. *Acta Crystallographica Section C*. 1998, **54**(10), 1406-1408.
56. O. Graziani, L. Toupet, J. R. Hamon and M. Tilset, An unexpected deboronation of $[tBuB(3\text{-}tBuC_3H_2N_2)_3]-$ in a reaction with iron(II) chloride, and the X-ray crystal structure of *trans*-$FeCl_2(tBuC_3H_3N_2)_4$. *Inorganica Chimica Acta*. 2002, **341**, 127-131.
57. E. Y. Kim, Y. J. Song, H. G. Koo, J. H. Lee, H. M. Park, C. Kim, T. H. Kwon, S. Huh, S. J. Kim and Y. Kim, 1-D, 2-D and 3-D coordination polymers assembled from polynuclear Co^{II} units based on the isophthalate(-2) ligand. *Polyhedron.* 2010, **29**(18), 3335-3341.

N,N'-Bis(4-pyridinylmethyl)-2,5-dimethylbenzene-1,4-diamine metal-organic frameworks

5.1 Introduction

Metal-organic frameworks (MOFs) are two or three-dimensional coordination polymers constructed from metal ions or clusters and bridging organic linkers [1-11]. MOFs have repeated ordered coordination network structure, usually leading to produce open channels or voids where guest molecules can be bound [12-21]. Guest molecules binding ability leads to a range of possible applications for example, gas or liquid storage and separation [22-39], chemical catalysis [40-50] and drug delivery [51-57]. The behaviour of metal-organic frameworks or porous coordination polymers is different from other porous materials such as inorganic zeolites, as MOFs may be utilised in post-modification materials [58] or display structural dynamism [59-74] that normally associated with changes to guest inclusion. Guest molecules exchange leads to structural changes which is one of the first reported properties for metal-organic frameworks [74]. Structural behaviour changes of MOFs include changes in metal coordination style and rotations of ligands functional groups or rings. Some of the most common organic bridging ligands are aliphatic and aromatic dicarboxylates or bis-pyridyl. These materials can be combined to produce heteroleptic coordination polymers or MOFs [75-76]. A few examples based on carboxylate rigid linkers and bis-pyridyl ligands with diamine or azomethine were reported before [77-78] although other examples with diamides are more common [79-81].

This chapter reports four novel heteroleptic MOFs known as compounds **20**, **21**, **22** or **23** resulted from solvothermal reactions of Co(II) nitrate hydrate, L3 ligand and benzene-1,4-dicarboxylic acid, 4,4-biphenyldicarboxylic acid or naphthalene-2,6-dicarboxylic acid. Compound **20** shows complicated phase behaviour with two-fold interpenetrating 3D network structures. Compound **22** shows a new topologically-complex self-catenating structural type with one-dimensional open channels. Compound **23** shows three-fold interpenetrating network with no significant free spaces or channels for guest molecules. However, Compounds **20** and **22** showed good sorption properties for H_2 and EtOH. Moreover, compound **20** showed hysteretic EtOH adsorption that due to the complicated phase and structural transformation behaviour.

5.2 Experimental

5.2.1 Synthesis of ($[Co_2(L3)(bdc)_2].nDMF)_n$ (20) and ($[Co_2(L3)_2(bdc)_2].2H_2O)_n$ (21) MOFs

A solution of the ligand (L3) (31 mg, 0.1 mmol) and benzene-1,4-dicarboxylic acid (H_2-bdc) (17 mg, 0.1 mmol) in DMF (4 ml) was added dropwise to $Co(NO_3)_2.6H_2O$ (29 mg, 0.1 mmol) solution in DMF (2 ml). The reaction vial was sealed and placed in the thermal block and heated at 115 °C for 24 hours to result in $([Co_2(L3)(bdc)_2].nDMF)_n$ MOF (22 mg) as red block crystals and $([Co_2(L3)_2(bdc)_2].2H_2O)_n$ MOF (16.8 mg) as yellow-orange plates which were separated by hand prior to analysis and sorption measurements. IR (solid state) for compound **20**: $\bar{\nu}$ (cm^{-1}) 3431, 3028, 2928, 1671, 1605, 1522, 1384, 551 and 485. IR (solid state) for compound **21**: $\bar{\nu}$ (cm^{-1}) 3328, 3061, 2918, 1672, 1595, 1567, 1392, 517 and 432. Micro analysis found: C, 54.55; H, 4.82; N, 8.29 %, calculated for $([Co_2(L3)(bdc)_2]\cdot DMF\cdot H_2O)_n$: C, 54.75; H, 4.59; N, 8.19 %. Found: C, 57.72; H, 4.55; N, 11.42 %, calculated for $([Co_2(L3)_2(bdc)_2]\cdot 2(DMF)\cdot 3(H_2O))_n$: C, 58.03, H, 5.66, N 10.92.

5.2.2 Synthesis of $([Co_2(L3)(bpdc)_2])_n$ MOF (22)

A solution of the ligand (L3) (31 mg, 0.1 mmol) in DMF (2 ml) and 4,4′-biphenyldicarboxylic acid (H_2-bpdc) (24 mg, 0.1 mmol) in DMSO (2 ml) was added dropwise to a vial containing $Co(NO_3)_2.6H_2O$ (29 mg, 0.1 mmol) solution in DMF (2 ml). The reaction vial was sealed and placed in a thermal block and heated at 115 °C to give $([Co_2(L3)(bpdc)_2])_n$ MOF (32 mg) red crystals after two days. IR (solid state): $\bar{\nu}$ (cm^{-1}) 3025, 2925, 1608, 1523, 1391 and 466. Micro analysis found: C, 62.35; H, 4.34; N, 6.14 %, calculated for $([Co_2(L3)(bpdc)_2])_n$: C, 62.89; H, 4.18; N, 6.11 %.

5.2.3 Synthesis of $([Co(L3)_{0.5}(naph)].(H_2O).n(DMF))_n$ MOF (23)

A solution of the ligand (L3) (31 mg, 0.1 mmol) and naphthalene-2,6-dicarboxylic acid (H_2-naph) (21 mg, 0.1 mmol) in DMF (3.5 ml) was added dropwise to $Co(NO_3)_2.6H_2O$ (29 mg, 0.1 mmol) in DMF (3 ml). Then, the reaction vial was sealed and placed in the thermal block and left for solvothermal reaction at 115 °C to result in $([Co(L3)_{0.5}(naph)].(H_2O).n(DMF))_n$ MOF (48 mg) after 24 hours. IR (solid state): $\bar{\nu}$ (cm^{-1}) 3301, 3056, 2920, 1675, 1614, 1521, 1403, 1355, 582 and 487. Micro analysis found: C, 59.69; H, 5.41; N, 7.97 %, calculated for $([Co_2(L3)(naph)_2].2DMF)_n$: C, 59.41; H, 4.79; N, 8.31 %.

5.3 Crystallography experimental

Crystals were mounted under inert oil on a MiTeGen tip and flash frozen to 120(1) or 150 K using an OxfordCryosystems low temperature device. X-ray diffraction data were collected using Cu-*Kα* (λ= 1.54184 Å) or Mo-*Kα* (λ= 0.71073 Å) radiation using an Agilent Supernova dual-source diffractometer with Atlas S2 CCD detector and fine-focus sealed tube generator or using synchrotron radiation (λ= 0.6889 Å) with Pilatus detector at station I19 of Diamond Light Source, UK. Data were

corrected for Lorenztian and polarization effects, and absorption corrections were applied. The structures were solved by charge flipping methods using SUPERFLIP or by direct methods using SHELXS, and refined by Olex2.refine, ShelXL methods or by full-matrix least-squares on F^2 using SHELXL. All non-hydrogen atoms were refined as anisotropic, and hydrogen positions were included at geometrically estimated positions [82-86]. Experimental powder XRD patterns were measured on a Bruker Phaser D2 diffractometer using Cu-$K\alpha$ radiation or at SPring-8 BL02B2 Japan at room temperature, λ= 1.000414(2) Å. Calculated powder XRD patterns were obtained using Mercury. Summary of data collections and refinements are given in tables 5.32-5.37.

5.4 Results and discussions

A series of novel three-dimensional coordination polymers were synthesised from the reaction of L3 ligand, $Co(NO_3)_2.6H_2O$, benzene-1,4-dicarboxylic acid, 4,4-biphenyldicarboxylic acid or naphthalene-2,6-dicarboxylic acid to produce compounds **20-23**. IR spectra for complexes **20** and **21** show main peaks between 3431-3328, 3061-3028, 2928-2918, 1672-1671, 1605-1595, 1567-1522, 1392-1384, 551-517 and 485-432 cm^{-1} due to νN-H, $\nu C\text{-}H_{Ar,}$ $\nu C\text{-}H_{Al}$, νC=O, νC=C, νC-N, νCH_3, νM-N and νM-O functional groups and coordination bonds [87-90]. Compound **22** IR spectrum shows main bands at 3025, 2925, 1608, 1523 and 1391 cm^{-1} due to $\nu C\text{-}H_{Ar,}$ $\nu C\text{-}H_{Al}$, νC=C, νC-N and νCH_2. The spectrum also shows another band at 466 cm^{-1} due to νM-O coordination bond [91-95]. IR spectrum for compound **23** shows main bands at 3301, 3056, 2920, 1675, 1614, 1521, 1403 and 1355 cm^{-1} due to νN-H, $\nu C\text{-}H_{Ar,}$ $\nu C\text{-}H_{Al}$, νC=O, νC=C, νC-N, νCH_2 and νCH_3 functional groups [89-95]. The spectrum also shows two bands at 582 and 487 cm^{-1} due to νM-N and νM-O coordination bonds [96-99].

5.5. Crystal structures

5.5.1 Crystal structures of $([Co_2(L3)(bdc)_2].nDMF)_n$ (20) and $([Co_2(L3)_2(bdc)_2].2H_2O)_n$ (21) MOFs

Solvothermal reaction of L3 ligand, benzene-1,4-dicarboxylic acid (H_2-bdc) and cobalt(II) nitrate hexahydrate in DMF at 115 °C for 24 or 48 hours produced ($[Co_2(L3)(bdc)_2]\cdot nDMF$) (**20**) as block red crystals and a second product ($[Co_2(L3)_2(bdc)_2]\cdot 2H_2O$) (**21**) as yellow-orange microcrystals if L3 ligand sample is a few weeks old (figure 5.1). Crystals shape of the resulted compounds **20** and **21** are different and compound **21** orange crystals could be easily separated by hand from compound **20** large crystals (figure 5.1). Compound **20** shows complicated phase behaviour with two dominant phases, α-**20**(L) and β-**20**(S) where L is linear, and S is bent L3 ligand shape. Compound **20** also shows two minor amounts of closely related phases γ-**20**(L) and δ-**20**(L) (scheme 5.1). One hundred and seven crystals unit cell measurements on different vials of compound **20** indicated equal amounts of α-**20**(L) and β-**20**(S) being formed from the reaction of L3 ligand, benzene-1,4-dicarboxylic acid and $Co(NO_3)_2.6H_2O$ heated for 24

hours or a mixture of L3, $2H_2$-bdc and $2Co(NO_3)_2.6H_2O$ heated for 48 hours. On the other hand, the reaction of L3 ligand, $2H_2$-bdc and $2Co(NO_3)_2.6H_2O$ heated for 24 hours produced more of α-**20**(L), and the reaction of L3 ligand, H_2-bdc and $Co(NO_3)_2.6H_2O$ for 48 hours produced more of β-**20**(S).

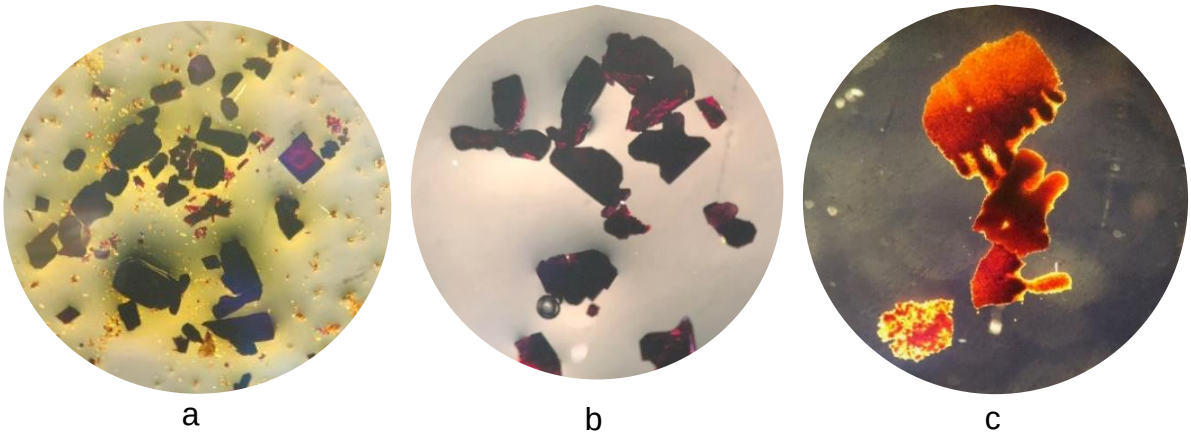

Figure 5.1: (a) Compounds **20** and **21** crystals as-synthesised in DMF, (b) compounds α-**20**(L), β-**20**(S), γ-**20**(L) and δ-**20**(L) crystals after separation, (c) compound **21** crystals after separation.

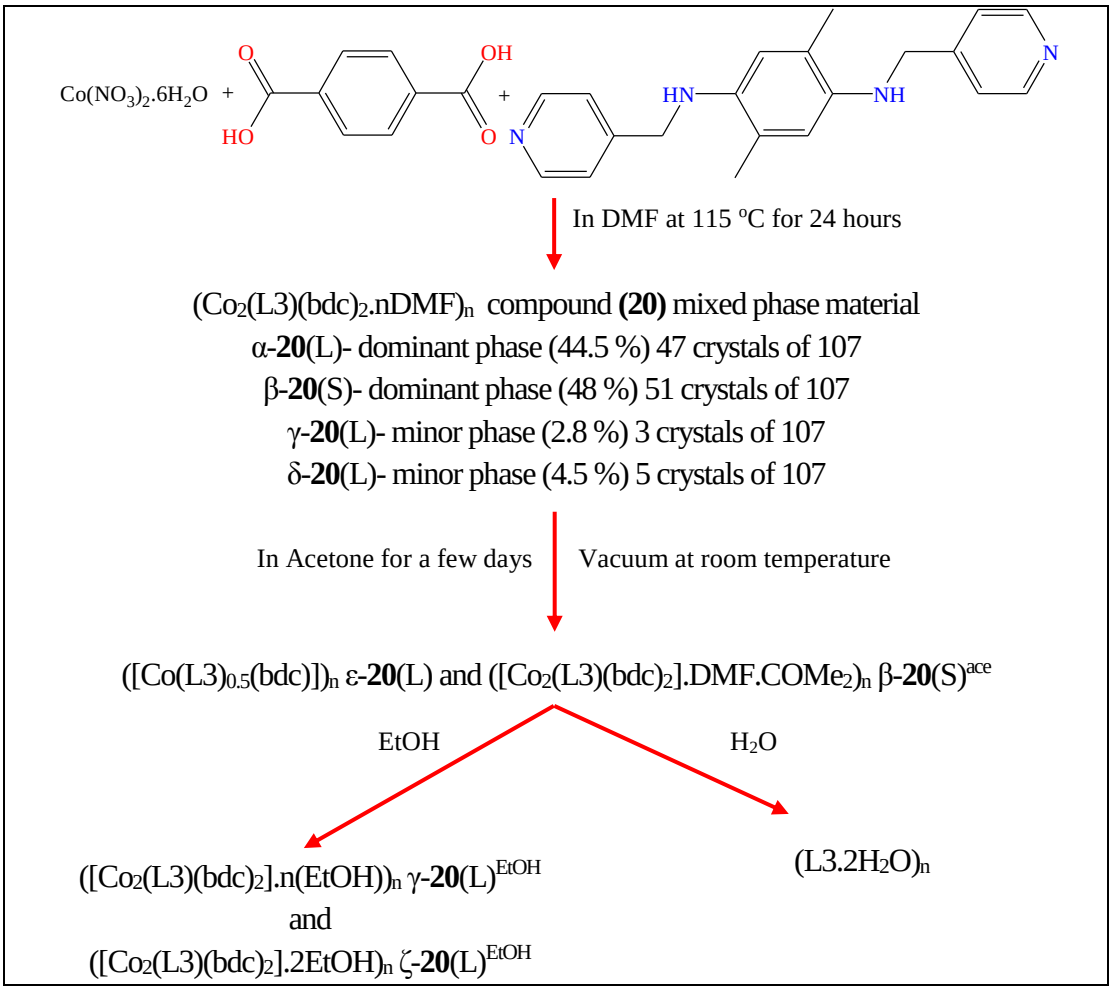

Scheme 5.1: Phase behaviour of compound **20** as-synthesised, dried and in EtOH or water.

5.5.1.1 Crystal structure of $(Co_2(L3)(bdc)_2.n(DMF))_n$ α-20(L) MOF

α-**20**(L) MOF crystal structure was solved in triclinic space group $P\bar{1}$ and shows two Co(II) ions on general positions, two bdc^{2-} ions and one L3 ligand molecule per asymmetric unit (figure 5.2). Each Co(II) ion is coordinated to four oxygen atoms from four different bdc^{2-} ions and shows four M-O coordination bond lengths of 2.014(5), 2.034(5), 2.012(5) and 2.085(5) Å for Co1-O1, Co1-O4, Co1-O6 and Co1-O7 or 2.020(5), 2.034(5), 2.071(5) and 2.013(5) Å for Co2-O2, Co2-O3, Co2-O5 and Co2-O8. Co(II) ion is also coordinated to one L3 ligand on the axial axis and shows coordination bond length of 2.060(6) Å for Co1-N4 or 2.050(6) Å for Co2-N1 to produce Co(II) square pyramidal structure. Benzene-1,4-dicarboxylate molecules behave as tetra-dentate ligands by the deprotonated carboxylate groups to four different Co(II) ions. Four bdc^{2-} ions are coordinated to one Co(II) dimer (Co1-Co2= 2.752(14) Å) to produce $Co_2(bdc)_4$ paddlewheel structure (figure 5.2). Moreover, four bdc^{2-} ions are coordinated to four different Co(II) dimers to produce $(Co_2)_4(bdc)_4$ square unit that shows 10.917 or 10.950 Å distances between bdc^{2-} ions and 15.902 × 15.010 Å diagonals between Co(II) dimers (figure 5.2). After symmetrical expansion the coordinated Co(II) dimers and bdc^{2-} ions produce a two-dimensional network structure that has 4^4 network topology (figure 5.2).

L3 ligand behaves as a bidentate ligand by nitrogen atoms of 4-pyridyl rings to two Co(II) coordination centres from two different 2D networks (Co1-L3-Co2= 19.636 Å) (figure 5.3). L3 ligand overall shape is approximately linear and shows torsion angles of 179.2 and 177.6 ° between the phenyl and 4-pyridyl rings. The 4-pyridyl ring is disordered and shows half occupancy for carbon atoms (figure 5.2). Four L3 ligand molecules, eight bdc^{2-} ions and eight Co(II) dimers are coordinated to produce $(Co_2)_8(L3)_4(bdc)_8$ tetragonal structure that shows 10.917 or 10.950 Å between L3 dimethylphenyl rings and expand to produce the 3D network structure (figure 5.3). The resulted 3D network is interpenetrating with another 3D network to produce a two-fold three-dimensional network MOF structure that shows two-dimensional open channels (figure 5.3). Selected bond lengths, angles and torsion angles for compound α-**20**(L) are listed in tables 5.1 and 5.2.

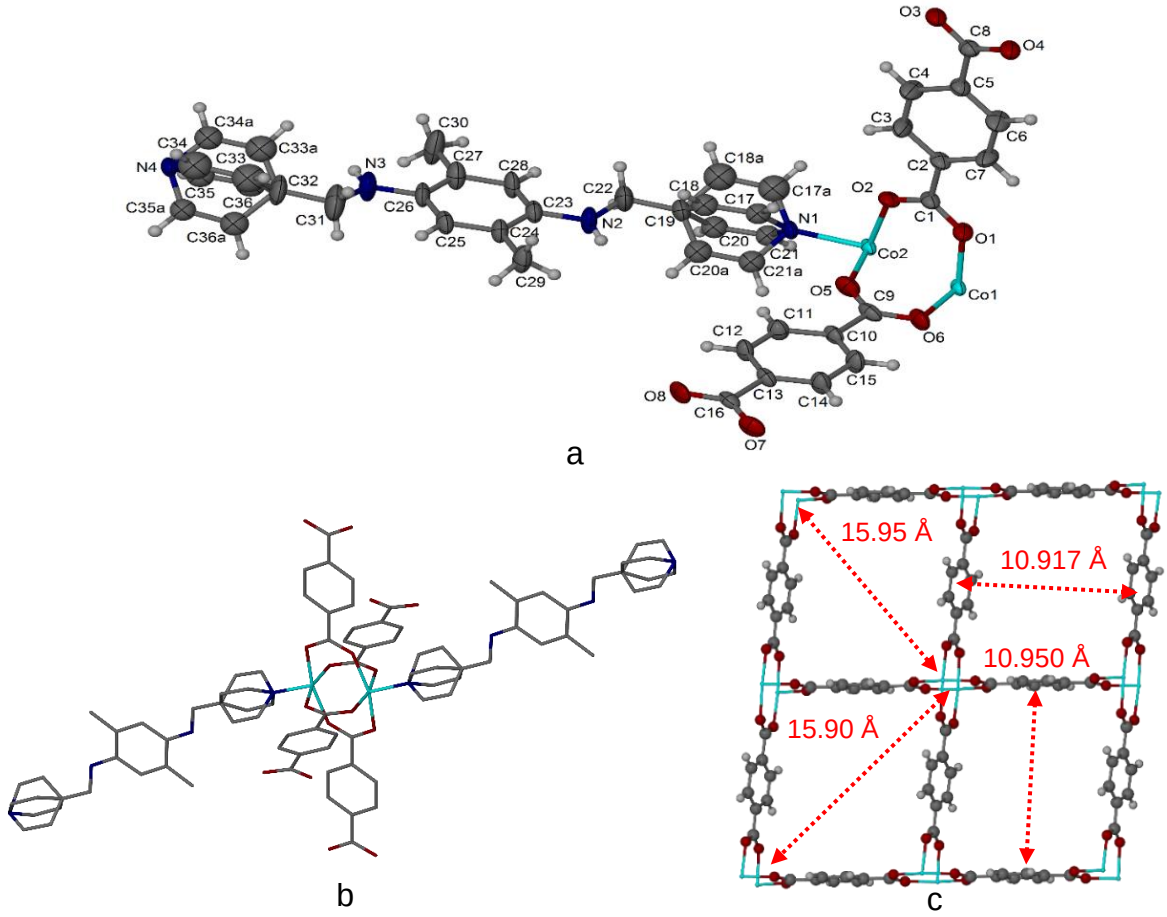

Figure 5.2: (a) α-**20**(L) Asymmetric unit of the crystal structure, ellipsoids shown at 50 % probability levels. (b) Coordination environment of α-**20**(L), (c) $(Co_2)_4(bdc)_4$ square units.

Table 5.1: Selected bond lengths (Å) and angles (°) for α-**20**(L) MOF.

Co1-Co2	2.752(14)	O6-Co1-Co2	95.82(16)	O5-Co2-O2	87.8(2)
Co1-O1	2.014(5)	O6-Co1-O1	91.4(2)	O5-Co2-O3	86.7(2)
Co1-O4	2.034(5)	O6-Co1-O4	91.0(2)	O8-Co2-Co1	96.31(16)
Co1-O6	2.012(5)	O7-Co1-Co2	69.19(17)	O8-Co2-O2	91.0(2)
Co1-O7	2.085(5)	O7-Co1-O1	87.2(2)	O8-Co2-O3	91.0(2)
Co1-N4	2.060(6)	O7-Co1-O4	87.1(2)	O8-Co2-O5	166.1(2)
Co2-O2	2.020(5)	O7-Co1-O6	165.0(2)	N1-Co2-Co1	160.82(17)
Co2-O3	2.034(5)	N4-Co1-Co2	160.36(18)	N1-Co2-O2	98.9(2)
Co2-O5	2.071(5)	N4-Co1-O1	96.8(2)	N1-Co2-O3	95.4(2)
Co2-O8	2.013(5)	N4-Co1-O4	95.4(2)	N1-Co2-O5	91.1(2)
Co2-N1	2.050(6)	N4-Co1-O6	103.8(2)	N1-Co2-O8	102.8(2)
N2-C23	1.384(12)	N4-Co1-O7	91.2(2)	C1-O1-Co1	124.2(4)
N3-C32	1.393(16)	O2-Co2-Co1	82.24(15)	C1-O2-Co2	125.5(4)
O1-Co1-Co2	83.34(15)	O3-Co2-Co1	82.55(15)	C8-O3-Co2	124.9(5)
O4-Co1-Co2	83.25(15)	O3-Co2-O2	164.8(2)	C8-O4-Co1	123.8(5)
O4-Co1-O1	166.5(2)	O5-Co2-Co1	69.79(16)		

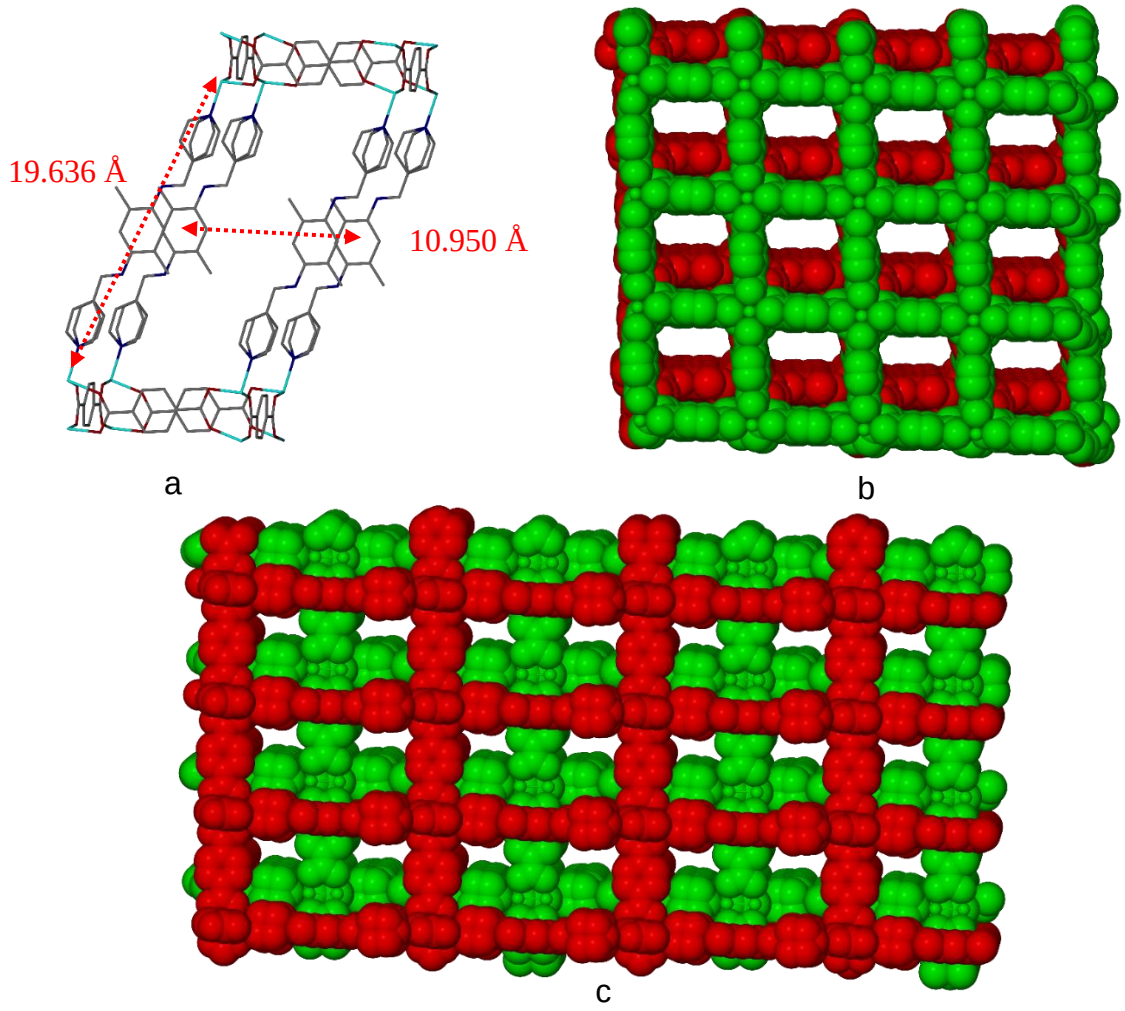

Figure 5.3: (a) α-**20**(L) $(Co_2)_8(L3)_4(bdc)_8$ Tetragonal structure Co1-L3-Co2= 19.63 Å, L3 to L3= 10.917 or 10.950 Å, (b) and (c) two-fold interpenetrating 3D networks.

Table 5.2: Selceted torsion angles (°) for compound α-**20**(L) MOF.

N1-Co2-O8-C16	179.9	C21a-N1-Co2-O5	47.6	C34-N4-Co1-O6	141.2
N1-Co2-O3-C8	-161.0	C21a-N1-Co2-O2	-45.3	C34a-N4-Co1-O4	132.6
N1-Co2-O5-C9	177.8	C17-N1-Co2-O3	46.9	C34a-N4-Co1-O7	45.5
N1-Co2-O2-C1	163.2	C17-N1-Co2-O8	139.1	C34a-N4-Co1-O1	-41.6
N4-Co1-Co2-N1	173.0	C17-N1-Co2-O5	-39.9	C34a-N4-Co1-O6	-134.8
N4-Co1-O7-C16	-178.0	C17-N1-Co2-O2	-128.0	C35-N4-Co1-O4	-144.1
N4-Co1-O1-C1	159.4	C17a-N1-Co2-O3	139.9	C35-N4-Co1-O7	128.8
N4-Co1-O4-C8	-161.5	C17a-N1-Co2-O5	52.6	C35-N4-Co1-O1	41.6
N4-Co1-C6-C9	-177.3	C17a-N1-Co2-O2	-35.6	C35-N4-Co1-O6	-51.6
C21-N1-Co2-O3	-39.7	C17a-N1-Co2-O8	-128.5	C35a-N4-Co1-O4	-144.1
C21-N1-Co2-O8	52.4	C32-C31-N3-C26	177.6	C35a-N4-Co1-O7	128.8
C21-N1-Co2-O5	-126.5	N23-N2-C22-C19	179.2	C35a-N4-Co1-O1	41.6
C21-N1-Co2-O2	145.4	C34-N4-Co1-O4	48.7	C35a-N4-Co1-O6	-51.6
C21a-N1-Co2-O3	-137.5	C34-N4-Co1-O7	-38.4		
C21a-N1-Co2-O8	135.8	C34-N4-Co1-O1	-125.6		

5.5.1.2 Crystal structure of $(Co_2(L3)(bdc)_2.2DMF)_n$ β-20(S) MOF

β-**20**(S) MOF crystal structure was solved in monoclinic space group $P2_1/c$ and shows two halves of L3 ligand molecules, two bdc^{2-} ions, two Co(II) ions on general positions and two DMF solvent molecules per asymmetric unit (figure 5.4). Co1 ion is coordinated to four oxygen atoms from four different bdc^{2-} ions and shows four different coordination bond lengths of 2.022(15), 2.029(15), 2.061(15) and 2.029(15) Å for Co1-O5, Co1-O6, Co1-O7 and Co1-O8. Co1 ion is also coordinated to one L3 ligand molecule by the nitrogen atom of 4-pyridyl ring (Co1-N3= 2.061(17) Å) to produce Co1 distortion square pyramid structure. Co2 ion shows similar coordination environment as Co1 with coordination bond lengths of 2.029(14), 2.032(14), 2.037(15), 2.216(15) and 2.058(18) Å for Co2-O1, Co2-O2, Co2-O3, Co2-O4 and Co2-N1. Compound β-**20**(S) shows two different paddlewheel structures resulted from four bdc^{2-} ions and a dimer of Co(II) ions (figure 5.5). Co2 resulted paddlewheel structure is more skewed in comparison with Co1 paddlewheel structure ($Co1\text{-}Co1^1$= 2.731(15) Å) and ($Co2\text{-}Co2^1$= 2.835(15) Å) (figure 5.5). Four bdc^{2-} ions are coordinated to four different Co1 dimers to produce $(Co_2)_4(bdc)_4$ square structure that shows 10.122 or 11.661 Å distances between bdc^{2-} ions, and 14.777 × 15.983 Å diagonals between Co(II) dimers. On the other hand, Co2 square structure shows 11.642 or 10.222 Å distances between bdc^{2-} ions, and 15.983 × 14.777 Å diagonals between Co(II) dimers (figure 5.5).

L3 ligand behaves as a bidentate ligand connecting between two different Co(II)-bdc^{2-} 2D networks (Co1-L3-Co1= 15.917 Å) and (Co2-L3-Co2= 15.907 Å) (figure 5.5). L3 ligand shows torsion angles of 68.56 or 77.30 ° between the phenyl and 4-pyridyl rings to produce L3 bent S-shape between Co(II) coordination centres. Four bdc^{2-} ions, eight Co(II) dimers and four L3 ligand molecules are coordinated to produce $(Co_2)_8(L3)_4(bdc)_8$ tetragonal structure that shows 10.887 × 10.897 Å or 10.893 × 10.874 Å between L3 ligand molecules and extending to produce a 3D open network structure (figure 5.6). The resulted 3D network is interpenetrating with another 3D network in two-fold fashion to produce a three-dimensional two-fold interpenetrating MOF structure (figure 5.6). The two networks have the same topology but are different structurally due to the conformation of the L3 ligand. The new MOF interpenetrating structure shows one-dimensional solvent accessible spaces at a total of 34 % of the unit cell filled by DMF solvent molecules (figure 5.7). Summary of bond lengths, angles and torsion angles for compound β-**20**(S) are listed in tables 5.3 and 5.4.

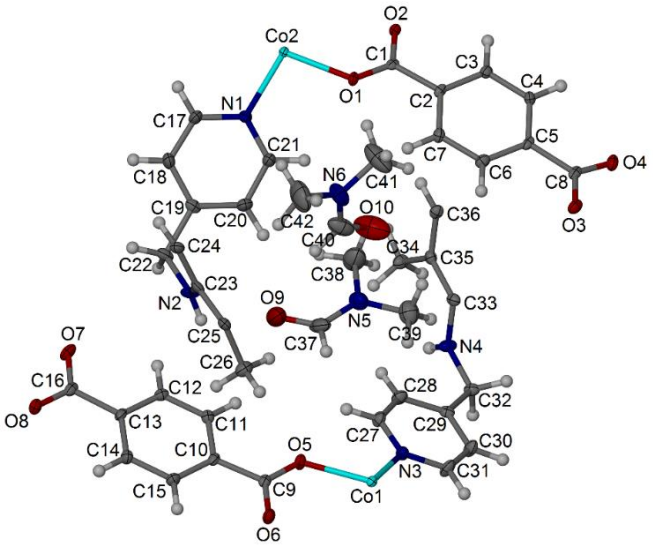

Figure 5.4: β-**20**(S) Asymmetric unit of the crystal structure, ellipsoids shown at 50 % probability levels

Table 5.3: Selected bond lengths (Å) and angles (°) for β-**20**(S) MOF.

Co1-Co1^1	2.7315(5)	O7-Co1-O5	89.59(6)	O3-Co2-O1	93.93(6)
Co1-O5	2.0226(15)	O7-Co1-O6	87.26(6)	O3-Co2-O2	93.58(6)
Co1-O6	2.0292(15)	O8-Co1-O5	89.61(6)	O4-Co2-O1	82.86(6)
Co1-O7	2.0617(16)	O8-Co1-O6	90.15(6)	O4-Co2-O2	85.63(6)
Co1-O8	2.0291(15)	O8-Co1-O7	165.87(6)	O4-Co2-O3	163.89(6)
Co1-N3	2.0613(17)	N3-Co1-O5	98.51(7)	N1-Co2-O1	97.48(7)
O5-C9	1.265(2)	N3-Co1-O6	95.14(7)	N1-Co2-O2	95.13(6)
O6-C9	1.261(3)	N3-Co1-O7	91.57(7)	N1-Co2-O3	107.08(7)
O7-C16	1.254(3)	N3-Co1-O8	102.50(7)	N1-Co2-O4	89.01(6)
O8-C16	1.268(3)	C9-O5-Co1	121.83(14)	C1-O1-Co2	125.28(13)
N3-C27	1.333(3)	C9-O6-Co1^1	126.23(14)	C1-O2-Co2^1	125.92(13)
N3-C31	1.348(3)	C16-O7-Co1^1	138.98(15)	C8-O3-Co2^1	100.97(13)
N4-C32	1.440(3)	C16-O8-Co1^1	110.40(14)	C8-O4-Co2^1	151.86(15)
N4-C33	1.397(3)	C27-N3-Co1	121.87(14)	C17-N1-Co2	121.91(16)
Co2-Co2^1	2.8359(5)	C31-N3-Co1	120.70(15)	C21-N1-Co2	120.76(15)
Co2-O1	2.0295(14)	C31-N3-C27	117.41(18)	C21-N1-C17	117.15(19)
Co2-O2	2.0322(14)	C33-N4-C32	121.25(18)	C23-N2-C22	121.3(2)
Co2-O3	2.0377(15)	C28-C27-N3	123.3(2)	C18-C17-N1	122.8(2)
Co2-O4	2.0216(15)	C30-C31-N3	122.7(2)	C20-C21-N1	123.0(2)
Co2-N1	2.058(18)	C29-C32-N4	114.36(18)	C19-C22-N2	115.42(18)
N2-C22	1.442(3)	C35-C33-N4	119.64(19)	C24-C23-N2	122.3(2)
N2-C23	1.402(3)	C36-C33-N4	122.0(2)	C25-C23-N2	119.2(2)
O6-Co1-O5	166.07(6)	O2-Co2-O1	162.74(6)		

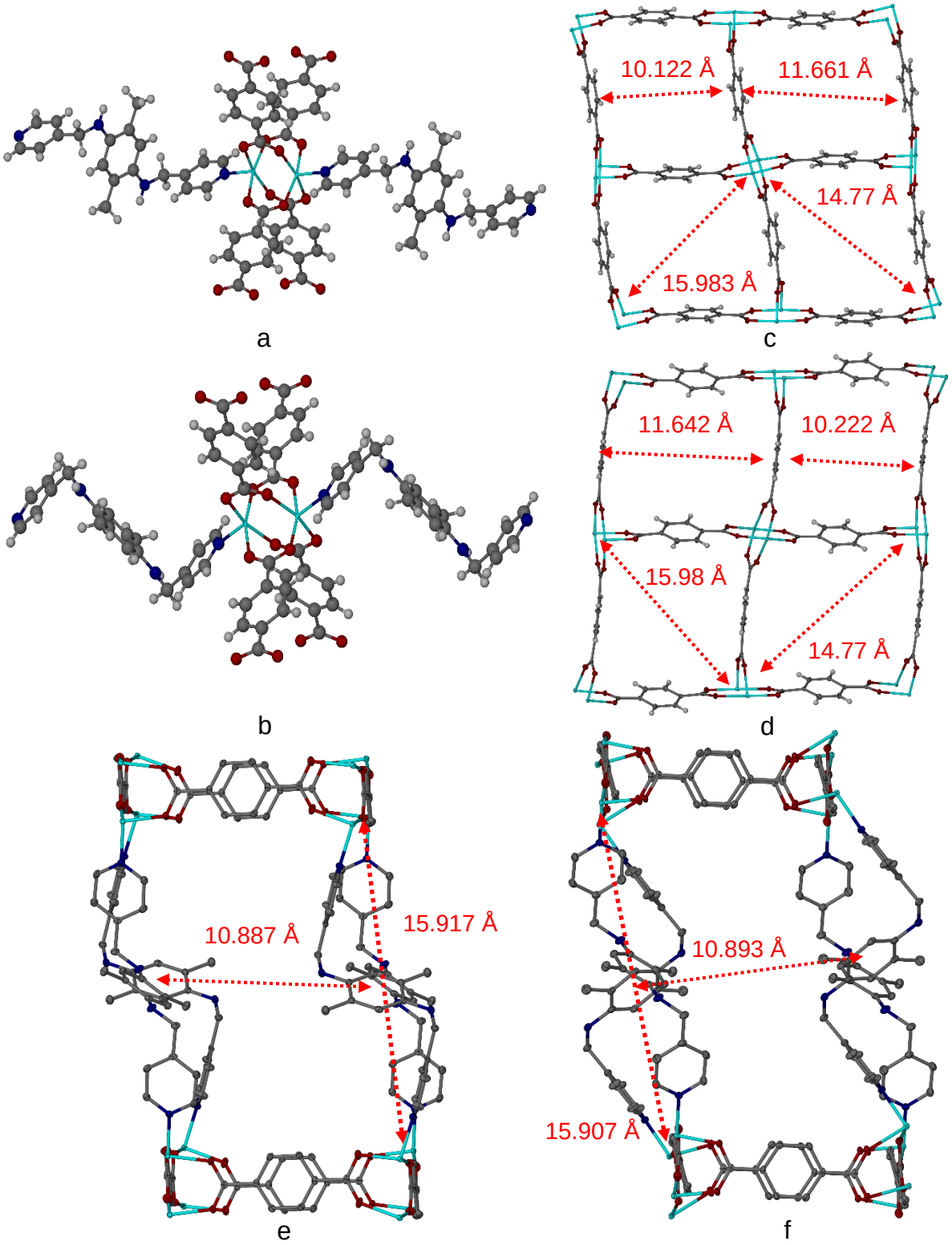

Figure 5.5: (a) Co1 paddlewheel structure, (b) Co2 paddlewheel structure of β-**20**(S) MOF, (c) and (d) $(Co_2)_4(bdc)_4$ square structures. (e) Co1 tetragonal structure, (f) Co2 tetragonal structures of $(Co_2)_8(L3)_4(bdc)_8$. DMF guest molecules and hydrogen atoms were removed for clarity.

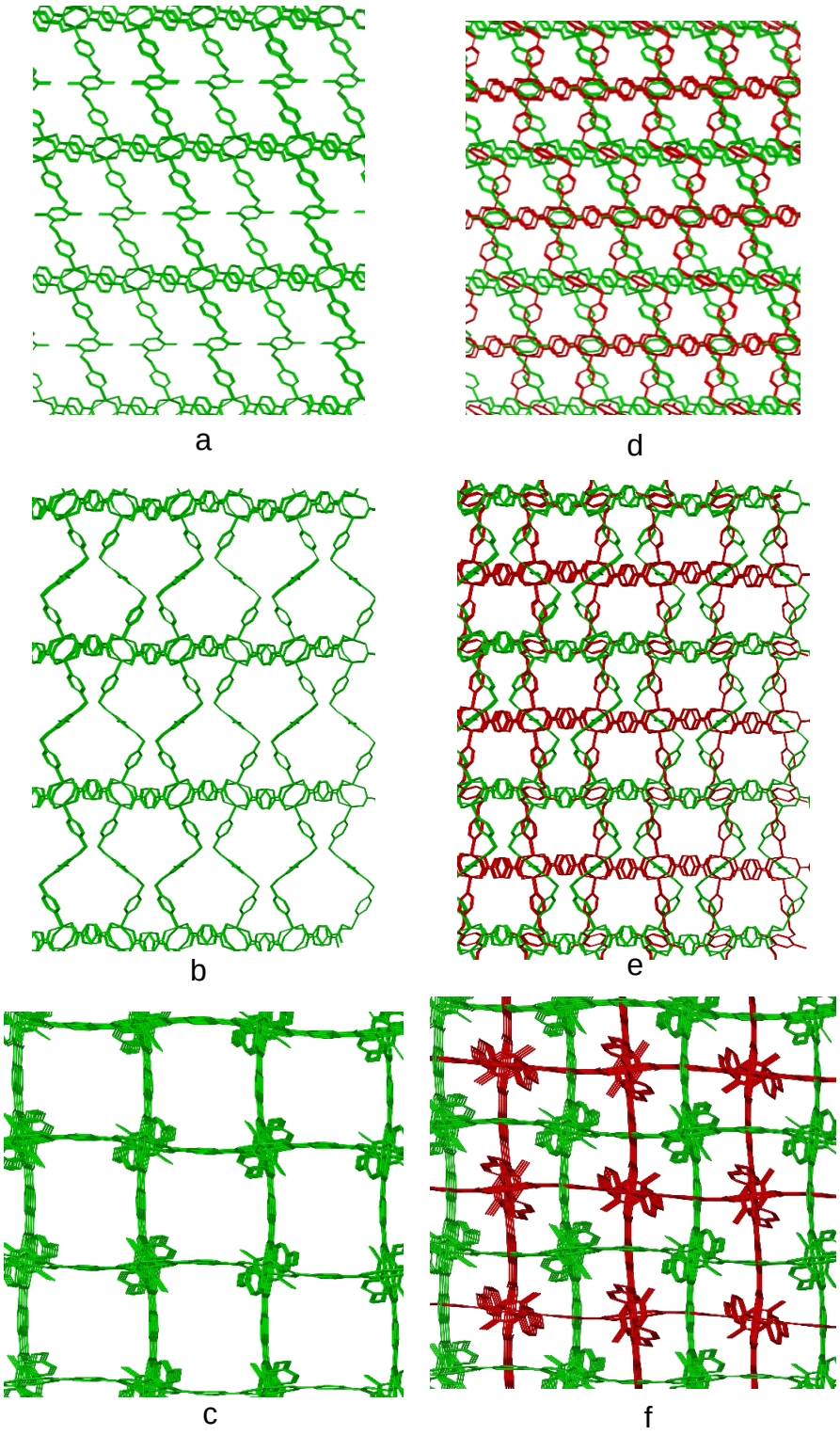

Figure 5.6: (a-c) β-**20**(S) MOF open network structure along the three axes, (d-f) two 3D interpenetrating networks. DMF molecules were removed for clarity.

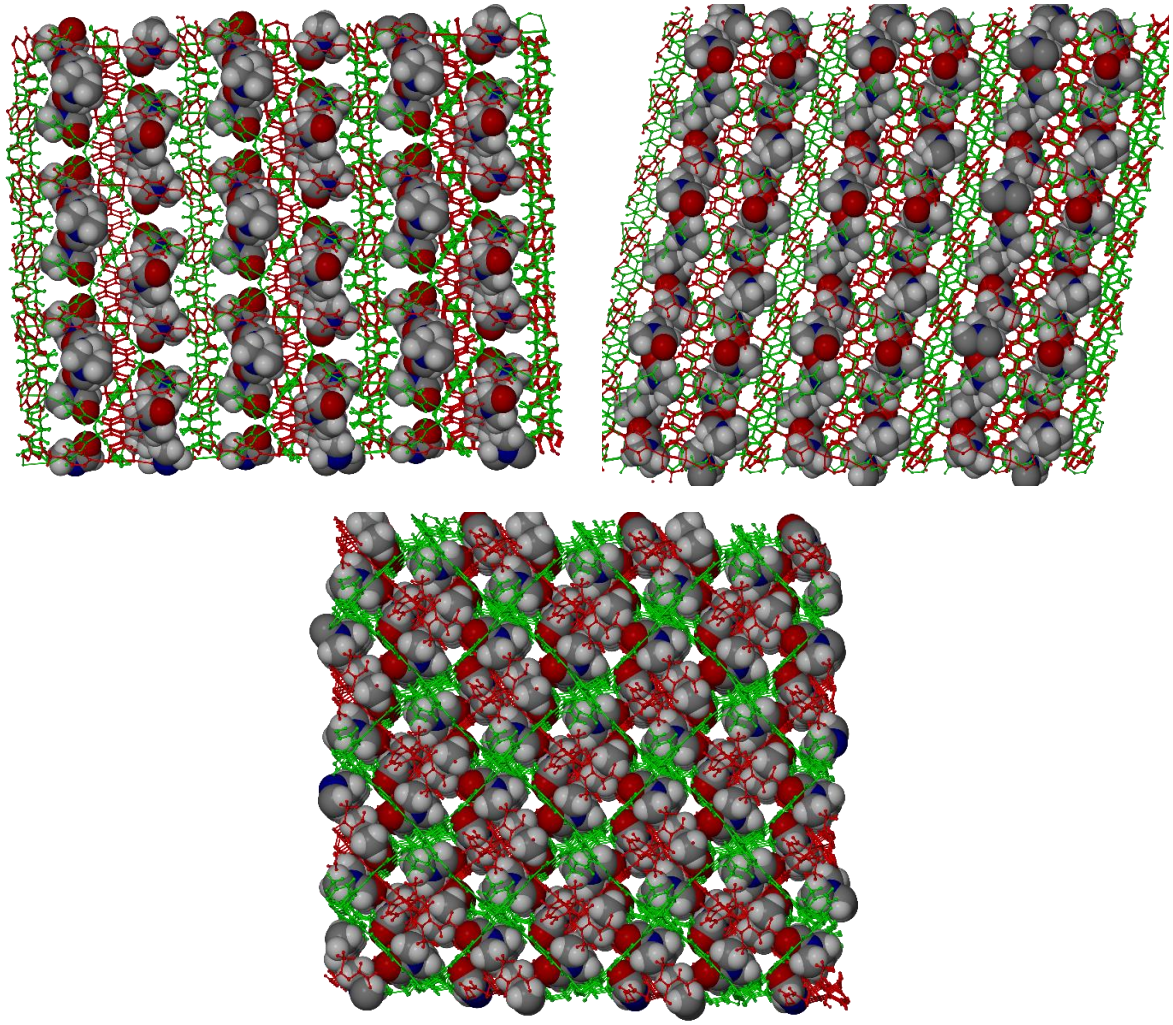

Figure 5.7: β-**20**(S) MOF crystal structure, DMF solvent molecules occupy the resulted channels.

Table 5.4: Selected torsion angles (°) for β-**20**(S) MOF.

N1-Co2-O1-C1	149.043	C27-N4-Co1-O7	108.8
N1-Co2-O4-C8	174.379	C27-N4-Co1-O6	-163.8
N1-Co2-O2-C1	-153.521	C31-N4-Co1-O8	106.1
N1-Co2-O3-C8	-176.644	C31-N4-Co1-O6	14.8
N3-Co1-O5-C9	164.020	C31-N4-Co1-O7	-72.6
N3-Co1-O7-C16	179.053	C31-N4-Co1-O5	-162.4
N3-Co1-O6-C9	-156.500	C21-N1-Co2-O1	-13.9
N3-Co1-O8-C16	-175.713	C21-N1-Co2-O3	-110.3
N1-Co2-$Co2^1$-$N1^1$	180	C21-N1-Co2-O2	145.3
N3-Co1-$Co1^1$-$N3^1$	-180.00	C21-N1-Co2-O4	68.8
C19-C22-N2-N23	68.563	C17-N1-Co2-O3	74.8
C29-C32-N4-C33	77.30	C17-N1-Co2-O2	-20.8
C27-N4-Co1-O8	-72.5	C17-N1-Co2-O4	-106.1
C27-N4-Co1-O5	19.0	C17-N1-Co2-O1	171.2

5.5.1.3 Crystal structure of $(Co_2(L3)(bdc)_2.(DMF).(H_2O))_n$ γ-20(L) MOF

γ-**20**(L) MOF crystal structure was solved in monoclinic space group *P*2/*n* and shows one L3 ligand molecule, two bdc^{2-} ions, two Co(II) ions on general positions, one water molecule and one DMF molecule per asymmetric unit (figure 5.8). Co1 is coordinated to five oxygen atoms from four different bdc^{2-} ions and shows five coordination bond lengths of 2.059(5), 2.196(6), 2.352(5), 2.021(4) and 2.038(5) Å for Co1-O1, Co1-O2, $Co1^{1}$-O2, Co1-O5 and Co1-O6. Co1 ion is also coordinated to one L3 ligand molecule through the nitrogen atom of 4-pyridyl ring (Co1-N1= 2.063(5) Å) to produce Co1 distortion octahedral coordination centre (figure 5.8). Co2 ion is coordinated to four oxygen atoms from four different bdc^{2-} ions along the equatorial axes and shows four coordination bond lengths of 2.163(4), 2.034(4), 2.026(4) and 2.012(4) for Co2-O3, Co2-O4, Co2-O7, Co2-O8. Co2 ion is also coordinated to one L3 ligand molecule (Co2-N4= 2.056(5) Å) to produce the distorted square pyramid coordination centre (figure 5.8).

Four bdc^{2-} ions are coordinated to a Co(II) dimer to produce a $Co_2(bdc)_4$ paddlewheel structure (figure 5.8). The Co1 paddlewheel structure has four coordinated carboxylate groups from four different bdc^{2-}. The first and the third coordinated carboxylate groups behave as tri-dentate ligands, whereas the second and the fourth coordinated carboxylate groups behave as bi-dentate ligands (figure 5.8). Co2 paddlewheel structure has four coordinated carboxylate groups from four different bdc^{2-} ions and all of the coordinated carboxylate groups behave as bidentate ligands (figure 5.8). In compound γ-**20**(L) the coordinated bdc^{2-} ions beave either as penta-dentate ligands to two Co(II) dimers or as tetra-dentate ligands to two Co(II) dimers (figure 5.8). Four bdc^{2-} ions are coordinated to four Co(II) dimers to produce $(Co_2)_4(bdc)_4$ square structure that has 10.935 or 10.770 Å distance between bdc^{2-} ions and 14.431 × 16.216 Å diagonals between Co(II) dimers (figure 5.9). Like compounds α-**20**(L) and β-**20**(S) $(Co_2)_4(bdc)_4$ square structure is extending to produce Co(II)-bdc^{2-} two-dimensional network structure that has 4^4 topology (figure 5.9).

L3 behaves as a bidentate ligand by nitrogen atoms of 4-pyridyl rings and connecting between two different Co(II)-bdc^{2-} two-dimensional networks (Co1-L3-Co2= 19.680 Å). L3 ligand overall shape is approximately linear and shows torsion angles of 178.8 and -177.7 ° between the phenyl and 4-pyridyl rings (figure 5.8). like compounds α-**20**(L) and β-**20**(S) four L3 molecules, eight bdc^{2-} ions and eight Co(II) dimers are coordinated to produce a $(Co_2)_8(L3)_4(bdc)_8$ tetragonal structure that shows 10.935 or 10.971 Å as the closest distance between L3 molecules (figure 5.9). Moreover, the resulted tetragonal structure is expanding to produce a three-dimensional open network that interpenetrating with another 3D network and shows 3.55 Å between bdc^{2-} ions and L3 phenyl rings that due to π-π stacking (figure 5.10). The resulted MOF channels are more diamond-shape than a rectangular-shape for compound α-**20**(L) (figure 5.10). Solvent accessible space is approximately 39.3 % of the crystal lattice volume with no strong

interaction with the new MOF network (figure 5.10). Selected bond lengths, angles and torsion angles for compound γ-**20**(L) are listed in tables 5.5 and 5.6.

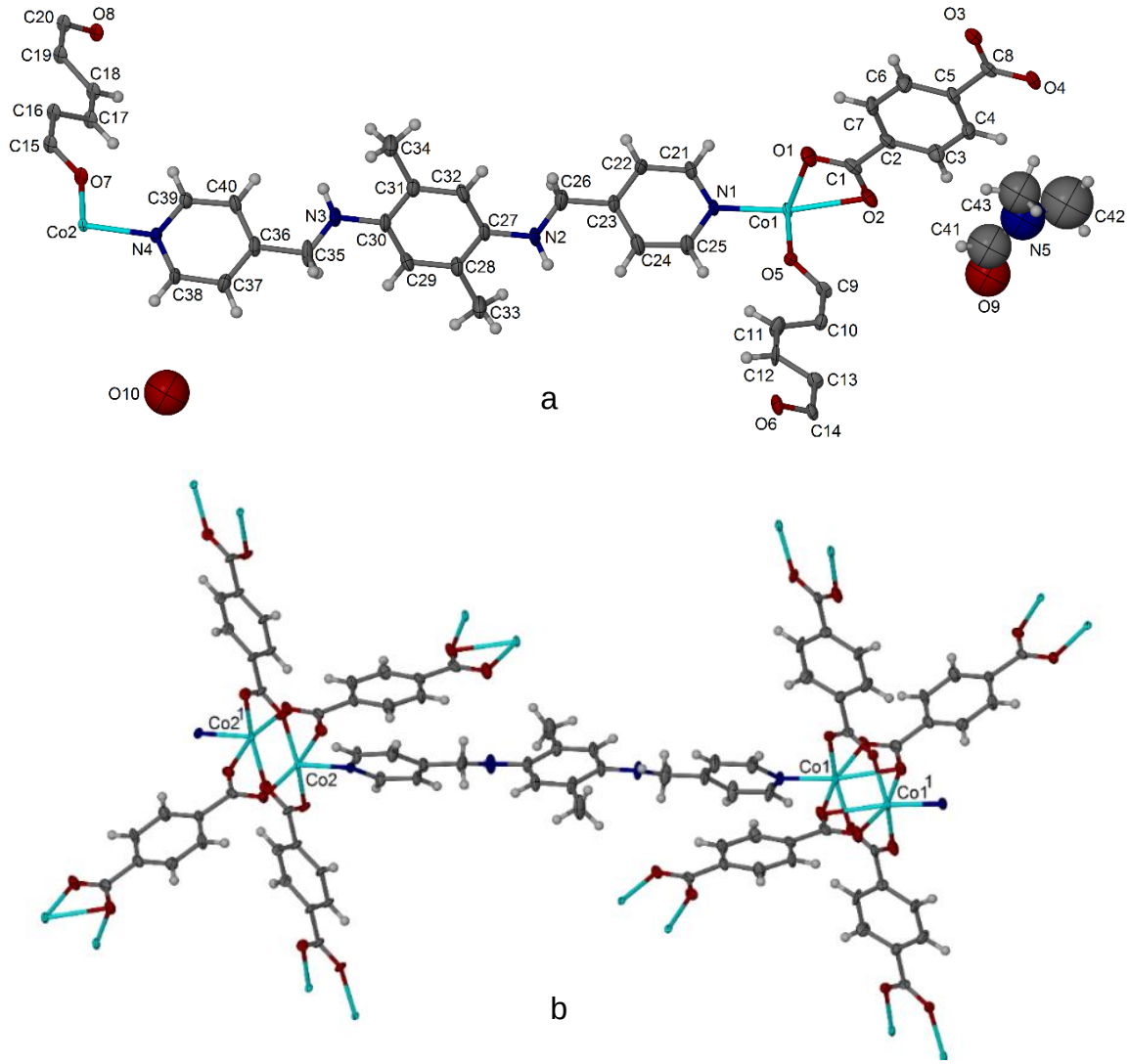

Figure 5.8: (a) γ-**20**(L) MOF asymmetric unit of the crystal structure, ellipsoids shown at 50 % probability levels. (b) Co1 octahedral and Co2 square pyramid coordination environments.

Table 5.5: Selected torsion angles (°) for compound γ-**20**(L).

N1-Co1-O2-C1	-161.1	C21-N1-Co1-O6	-35.1	C39-N4-Co2-O7	30.4
N1-Co1-O6-C14	-149.0	C21-N1-Co1-O2	-119.4	C39-N4-Co2-O3	-53.6
N1-Co1-O1-C1	176.2	C21-N1-Co1-O5	157.4	C39-N4-Co2-O8	-139.2
N1-Co1-O5-C9	149.9	C21-N1-Co1-O1	64.7	C39-N4-Co2-O4	123.4
N4-Co2-O7-C15	-151.8	C25-N1-Co1-O6	143.1	C38-N4-Co2-O7	-155.4
N4-Co2-O4^{1}-C8^{1}	-178.4	C25-N1-Co1-O2	58.9	C38-N4-Co2-O3	120.6
N4-Co2-O8-C20	149.5	C25-N1-Co1-O5	-24.4	C38-N4-Co2-O8	35.0
N4-Co2-O3^{1}-C8^{1}	170.5	C25-N1-Co1-O1	-117.1	C38-N4-Co2-O4	-62.4
C23-C26-N2-C27	178.8	C30-N3-C35-C36	-177.1		

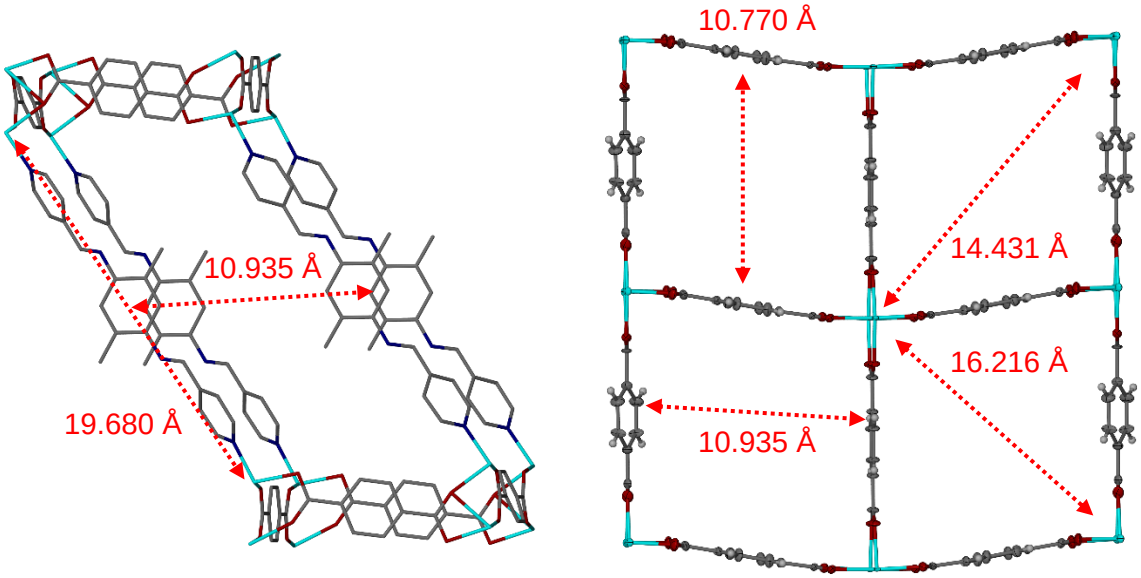

Figure 5.9: (left) γ-**20**(L) Tetragonal structure that shows 10.935 × 10.971 Å distanced between L3 ligand molecules and 19.680 Å between Co1-L3-Co2, (right) $(Co_2)_4(bdc)_4$ square structure.

Table 5.6: Selected bond lengths (Å) and angles (°) for γ-**20**(L) MOF.

Co1-Co1[1]	2.856(16)	O2-Co1-O1	161.45(19)	N4-Co2-O3	88.64(19)
Co1-O1	2.059(5)	O5-Co1-O1	91.16(19)	N4-Co2-O4	106.9(2)
Co1-O2	2.196(5)	O5-Co1-O2	83.08(18)	N4-Co2-O7	96.30(18)
Co1-O5	2.021(4)	O6-Co1-O1	97.3(2)	N4-Co2-O8	96.28(19)
Co1-O6	2.038(5)	O6-Co1-O2	84.10(19)	C1-O1-Co1	95.8(4)
Co1-N1	2.063(5)	O6-Co1-O5	162.54(18)	C1-O2-Co1	159.4(4)
Co2-Co2[1]	2.801(15)	N1-Co1-O1	106.2(2)	C8-O3-Co2	151.5(4)
Co2-O3	2.163(4)	N1-Co1-O2	91.9(2)	C8-O4-Co2	100.7(4)
Co2-O4	2.034(4)	N1-Co1-O5	95.14(19)	C9-O5-Co1	125.4(4)
Co2-O7	2.026(4)	N1-Co1-O6	97.1(2)	C14-O6-Co1	124.7(5)
Co2-O8	2.012(4)	O4-Co2-O3	164.16(18)	C15-O7-Co2	125.5(4)
Co2-N4	2.056(5)	O7-Co2-O3	84.19(17)	C20-O8-Co2	125.5(5)
N2-C26	1.262(10)	O7-Co2-O4	91.03(18)	C21-N1-Co1	121.8(4)
N2-C27	1.404(8)	O8-Co2-O3	85.77(18)	C25-N1-Co1	120.5(4)
N3-C30	1.409(8)	O8-Co2-O4	95.20(18)		
N3-C35	1.274(10)	O8-Co2-O7	163.68(18)		

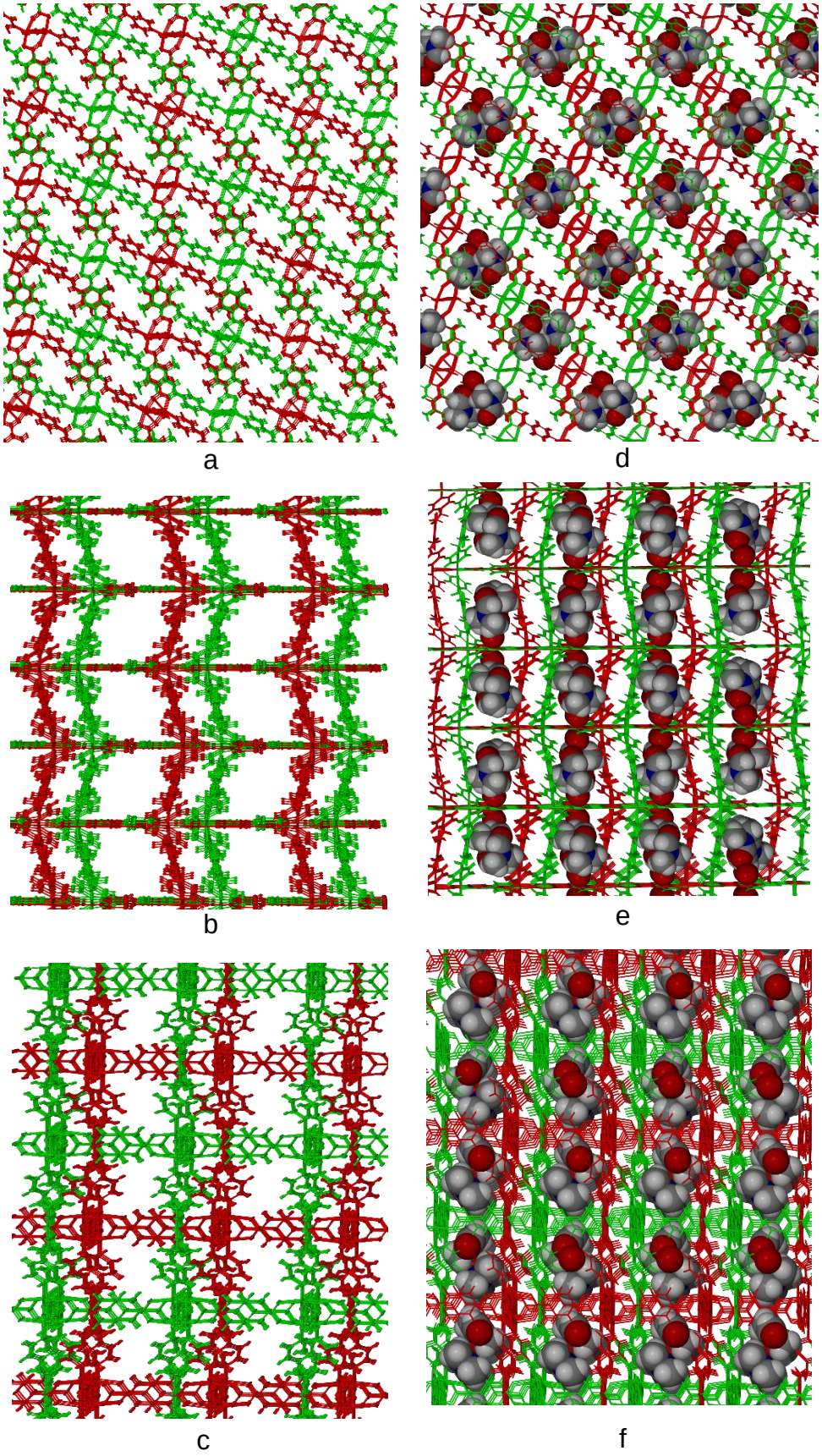

Figure 5.10: (a-c) γ-**20**(L) Interpenetrating three-dimensional networks without DMF and water molecules, (d-f) 3D networks with DMF and water molecules.

5.5.1.4 Crystal structure of δ-20(L) MOF

δ-**20**(L) MOF crystal structure was solved in tetragonal space group $P4_322$ and shows half of L3 ligand molecule, one Co(II) ion on a general position and two halves of bdc^{2-} ions per asymmetric unit (figure 5.11). Co(II) ion is coordinated to four oxygen atoms from four bdc^{2-} ions and shows four coordination distances of 2.031(3), 2.059(2), 2.001(2) and 2.028(3) Å for Co1-O1, Co1-O2, Co1-O3 and Co1-O4. Co(II) ion is also coordinated to one L3 molecule through the nitrogen atom of 4-pyridyl ring (Co-N1= 2.053(3)) to produce Co(II) distortion square pyramid structure (figure 5.12). Like compounds α-**20**(L) and β-**20**(S) the coordinated bdc^{2-} ions behave as tetra-dentate ligands to two different Co(II) dimers and show four M-O coordination bond lengths as discussed before. Four bdc^{2-} ions are coordinated to one Co(II) dimer to produce $Co_2(bdc)_4$ paddlewheel skewed structure (Co1-$Co1^1$= 2.702(8) Å) (figure 5.12). Four Co(II) dimers and four bdc^{2-} ions are coordinated to produce $(Co_2)_4(bdc)_4$ square unit that displays 10.983 Å distance between bdc^{2-} and 15.532 Å diagonal between Co(II) dimers (figure 5.12). Similar to compounds α-**20**(L), β-**20**(S) and γ-**20**(L) the resulted square unit is expanding to produce the two-dimensional network structure with 4^4 topology (figure 5.12).

L3 ligand behaves as a bi-dentate ligand *via* nitrogen atoms of 4-pyridyl rings and connecting between two different Co(II)-bdc^{2-} 2D networks (Co1-L3-$Co1^1$= 19.482 Å). The overall shape of L3 ligand is approximately linear and shows torsion angle of -176.3 ° between the phenyl and 4-pyridyl rings. Moreover, the 4-pyridyl ring is disordered as compound α-**20**(L) and shows half occupancy for carbon atoms figures 5.11 and 5.12. However, L3 ligands are axial to $Co_2(bdc)_4$ paddlewheel and show approximately a mirror plane symmetry (figure 5.12). δ-**20**(L) MOF $(Co_2)_8(L3)_4(bdc)_8$ tetragonal structure shows 10.983 Å between L3 ligand molecules and 19.482 Å between Co(II)-bdc^{2-} networks (figure 5.12). The tetragonal structure is expanding to produce a three-dimensional open network structure that interpenetrating with another 3D network (figure 5.13). There are π-π stacking interactions between bdc^{2-} ions of one network and dimethylphenyl group of an interpenetrating network with ring distances of 3.55 Å (figure 5.13). Selected bond lengths, angles and torsion angles for compound δ-**20**(L) are listed in tables 5.7 and 5.8. Powder XRD analysis of compound **20** as-synthesised in DMF has a good match with α-**20**(L), β-**20**(S), γ-**20**(L) and δ-**20**(L) compounds calculated patterns which indicate material stability and multiple phase existence (figure 5.14).

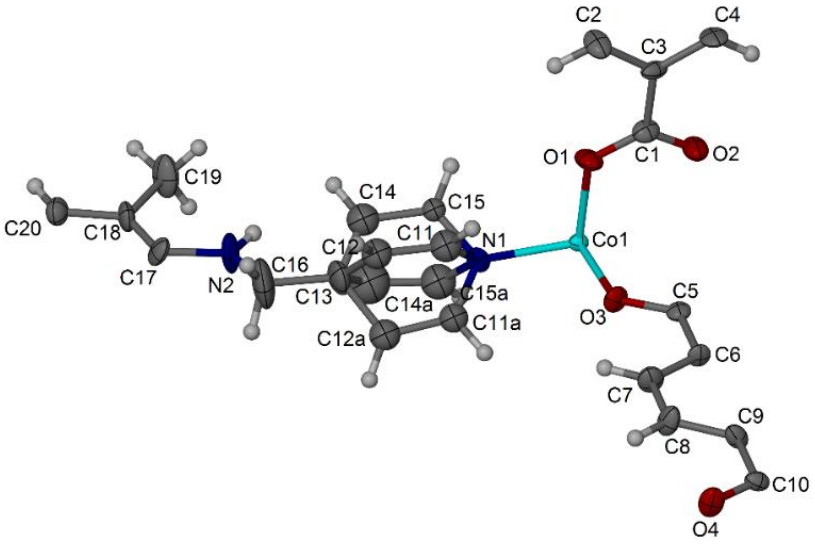

Figure 5.11: δ-**20**(L) MOF asymmetric unit of the crystal structure, ellipsoids shown at 50 % probability levels.

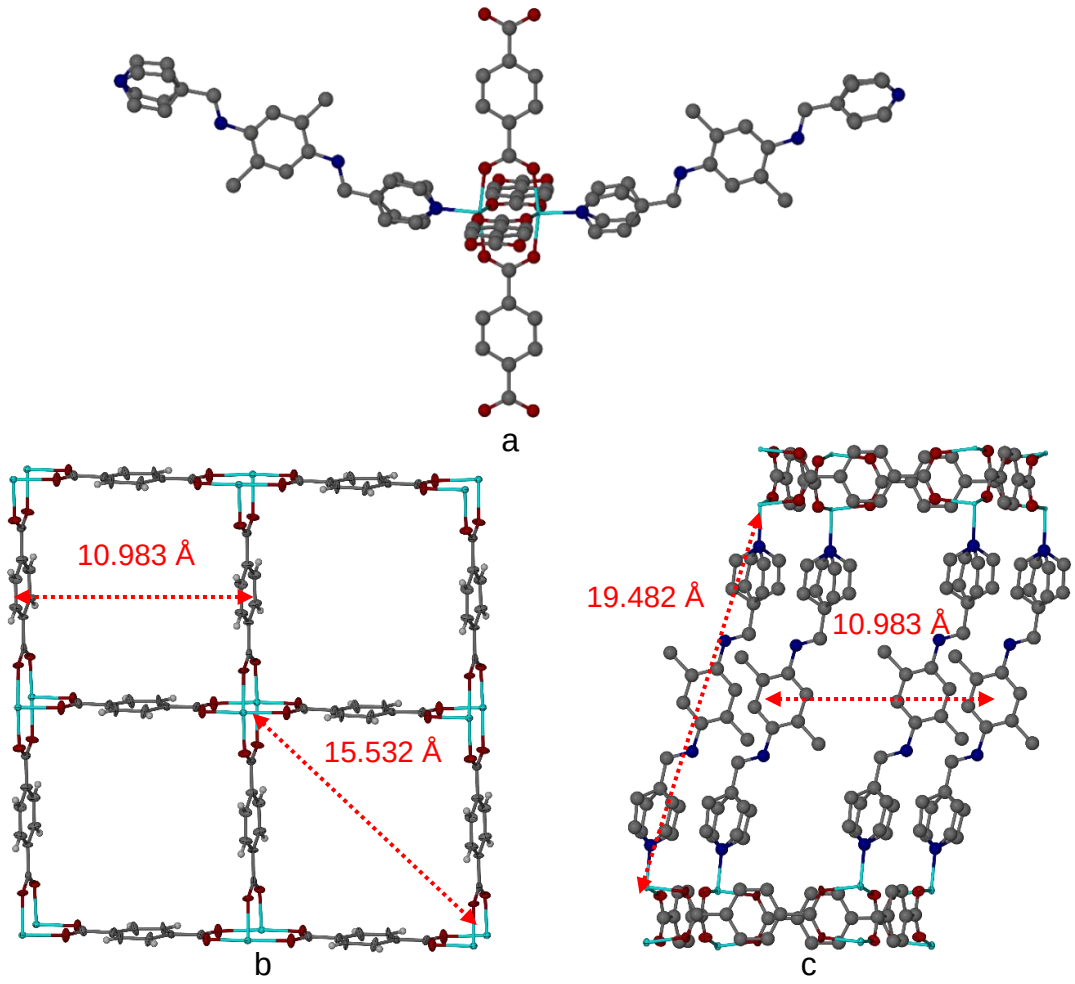

Figure 5.12: (a) δ-**20**(L) MOF coordination environment that shows a mirror plane for L3 ligand molecules. (b) $(Co_2)_4(bdc)_4$ Square structure. (c) $(Co_2)_8(bdc)_8(L3)_4$ Tetragonal structure that shows 10.983 Å between L3 ligand molecules and 19.482 between two different networks.

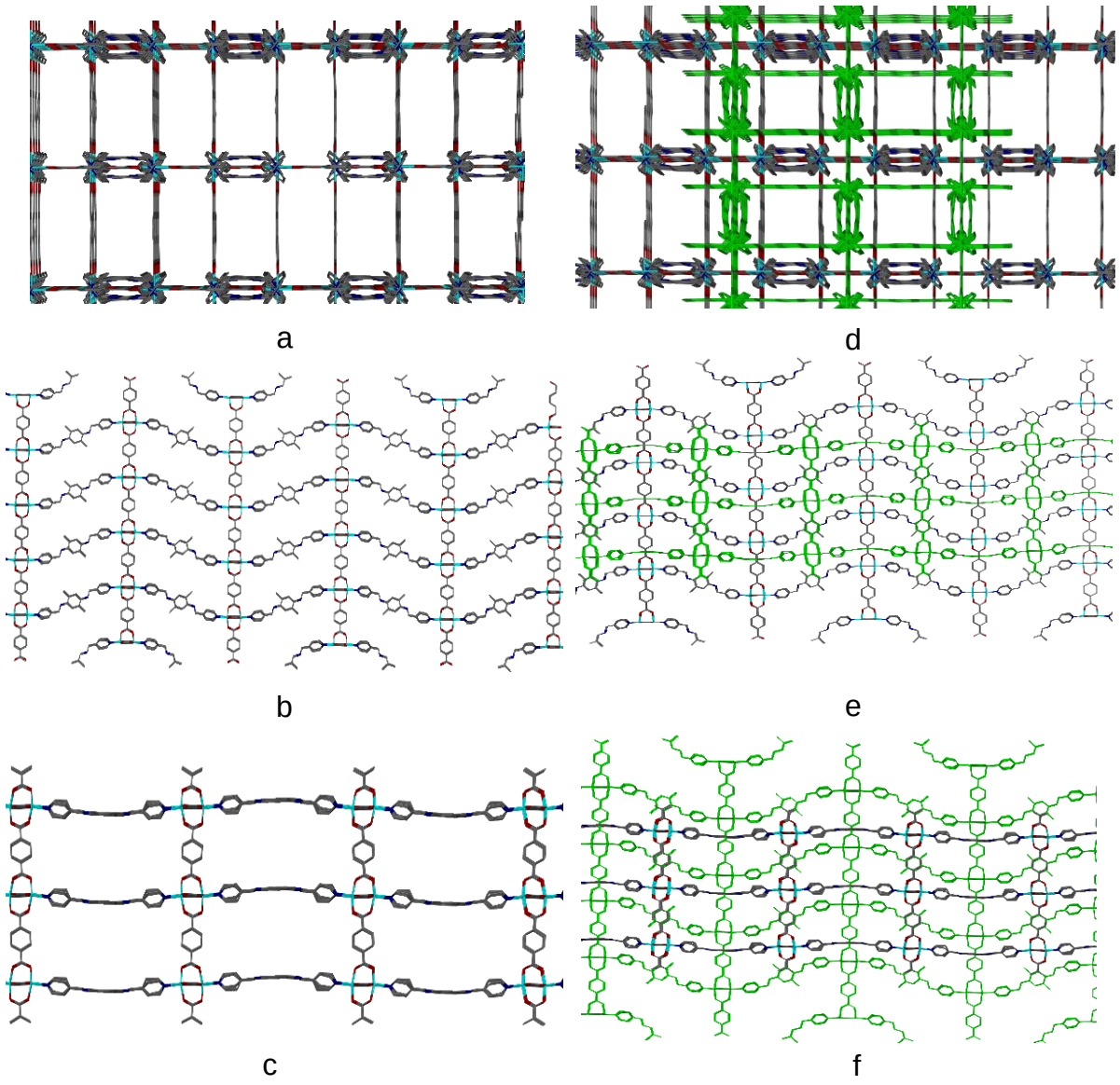

Figure 5.13: (a-c) δ-**20**(L) Three-dimensional open network, (d-f) interpenetrating of two three-dimensional networks.

Table 5.7: Selected bond lengths (Å) and angles (°) for compound δ-**20**(L).

Co1-Co1^1	2.7029(8)	O3-Co1-O1	90.03(11)	C1-O1-Co1	117.9(2)
Co1-O1	2.031(3)	O3-Co1-O2	89.68(11)	C1-O2-Co1	130.1(3)
Co1-O2	2.059(3)	O4-Co1-O1	88.55(11)	C5-O3-Co1	124.3(3)
Co1-O3	2.001(2)	O4-Co1-O2	88.70(12)	C10-O4-Co1	124.1(3)
Co1-O4	2.028(2)	O4-Co1-O3	167.06(10)	C13-C16-N2	115.2(5)
Co1-N1	2.052(3)	N1-Co1-O1	99.23(11)	C18-C17-N2	120.6(4)
N2-C16	1.319(6)	N1-Co1-O2	94.24(11)	C20-C17-N2	120.5(4)
N2-C17	1.433(5)	N1-Co1-O3	99.49(11)		
O2-Co1-O1	166.39(10)	N1-Co1-O4	93.43(11)		

Table 5.8: Selected torsion angles (°) for δ-**20**(L) MOF.

N1-Co1-O3-C5	172.3	C15a-N1-Co1-O1	141.8
N1-Co1-O1-C1	-176.0	C15a-N1-Co1-O4	52.8
N1-Co1-O4-C10	-169.6	C15a-N1-Co1-O2	-36.2
N1-Co1-O2-C1	178.3	C11a-N1-Co1-O1	-31.7
C13-C16-N2-C17	-176.3	C11a-N1-Co1-O3	59.9
C16-N2-C17-C18	175.8	C11a-N1-Co1-O4	-120.7
C11-N1-Co1-O3	-41.7	C11a-N1-Co1-O2	150.3
C11-N1-Co1-O2	48.7	C15-N1-Co1-O1	52.5
C11-N1-Co1-O4	137.6	C15-N1-Co1-O4	-36.6
C11-N1-Co1-O1	-133.3	C15-N1-Co1-O2	125.5
C15a-N1-Co1-O3	-126.6	C15-N1-Co1-O3	144.1

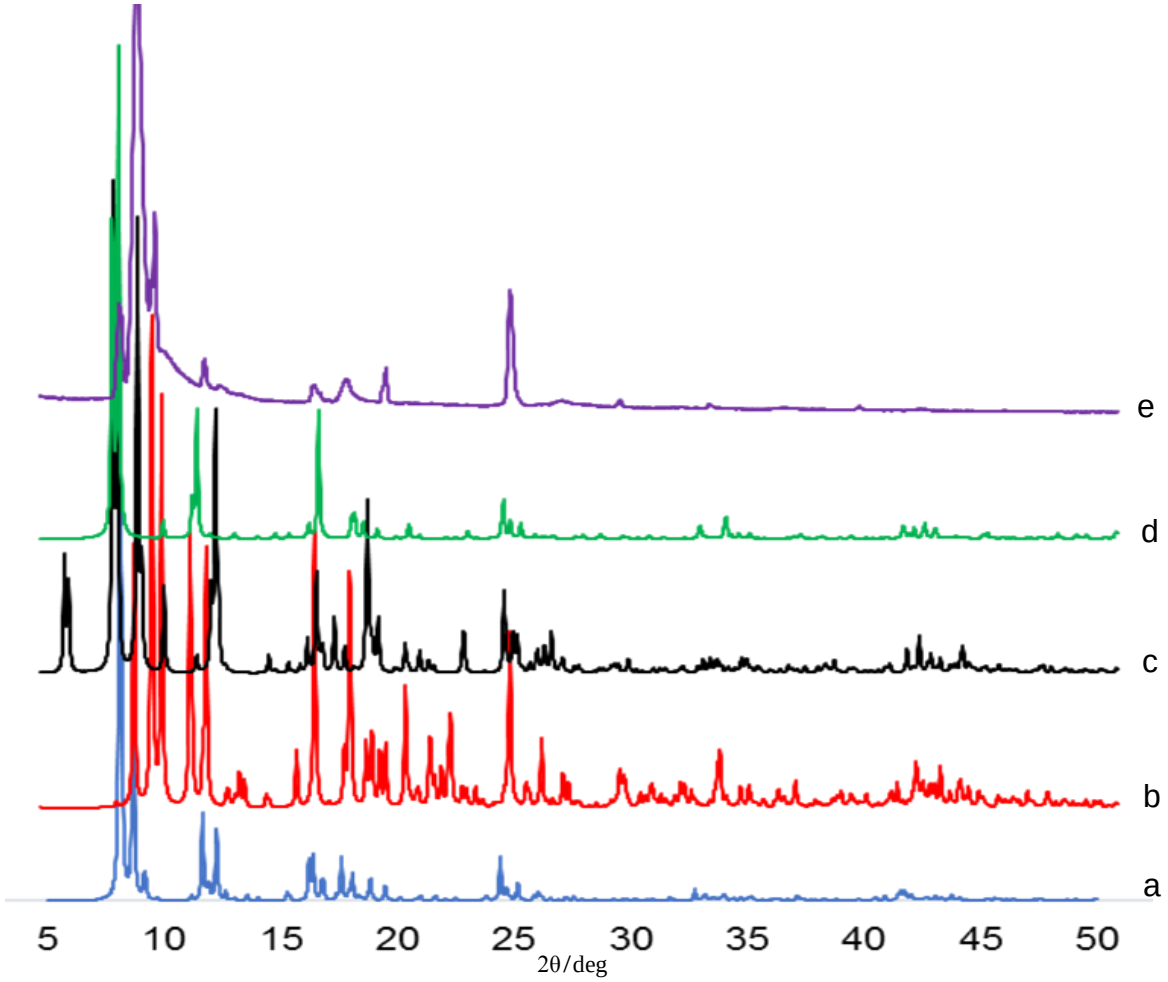

Figure 5.14: (a) Compound α-**20**(L) calculated powder XRD pattern, (b) compound β-**20**(S) calculated powder XRD pattern, (c) compound γ-**20**(L) calculated powder XRD pattern, (d) compound δ-**20**(L) calculated powder XRD pattern. (e) Compound **20** powder XRD pattern as-synthesised in DMF.

5.5.1.5 Crystal structure of ($[Co_2(L3)_2(bdc)_2].2H_2O)_n$ (21) MOF

Compound **21** crystal structure was solved in monoclinic space group *C*2/*c* and displays two L3 ligand molecules, two Co(II) ions on general positions, two bdc^{2-} ions and two water molecules per asymmetric unit (figure 5.15). Co1 ion is coordinated to four oxygen atoms from three different bdc^{2-} ions along the equatorial axes and shows four coordination bond lengths of 2.153(19), 2.195(17), 2.010(17) and 2.020(18) Å for Co1-O1, Co1-O2, Co1-O5 and Co1-O7. Co1 ion is also coordinated to two L3 ligand molecules along the axial axes (Co1-N1= 2.140(2) Å) and (Co1-N4= 2.165(2) Å) to produce Co1 distortion octahedral coordination centre. Co2 shows similar coordination environment as Co1 with coordination bond lengths of 2.191(19), 2.159(17), 2.010(19), 2.038(2), 2.162(2) and 2.161(2) Å for Co2-O3, Co2-O4, Co2-O6, Co2-O8, Co2-N5 and Co2-N8.

Coordinated bdc^{2-} ions show two different coordination styles to Co(II) ions. In the first coordination style the coordinated bdc^{2-} ions behave as tetra-dentate ligands to two Co(II) ions and show four different coordination distances (figure 5.16). In the second coordination style, bdc^{2-} ions behave as tetra-dentate ligands to four different Co(II) ions and show four coordination bond lengths (figure 5.16). To the best of our knowledge and according to CCDC the coordination style between bdc^{2-} and Co(II) ions in compound **21** was not reported before. Four Co(II) dimers and four bdc^{2-} ions are coordinated to produce $(Co_2)_4(bdc)_4$ rectangle structure that shows 14.919 × 10.045 Å sides and 16.084 × 19.704 Å diagonal between Co(II) coordination centres (figure 5.16). The resulted rectangle structure also shows 10.278 and 14.919 Å as the closest distance between bdc^{2-} ions (figure 5.16).

L3 ligand behaves as a bi-dentate ligand by nitrogen atoms of 4-pyridyl rings to two different Co(II)-bdc^{2-} 2D networks (Co1-L3-Co1= 19.915 Å) and (Co2-L3-Co2= 19.915 Å). L3 ligand shows five torsion angles of 178.3, 167.3, -177.7, -172.3 and 179.4 ° between dimethylphenyl rings and 4-pyridyl rings to produce L3 linear shape between Co(II)-bdc^{2-} networks. Unlike compounds α-**20**(L), β-**20**(S), γ-**20**(L) and δ-**20**(L) compound **21** shows disordered dimethylphenyl rings and ordered 4-pyridyl rings. Moreover, the asymmetric unit cell shows 3.898 Å distance between dimethylphenyl rings and 3.828 or 3.994 Å between 4-pyridyl rings that due to π-π interaction (figure 5.15). After symmetry expansion compound **21** shows three-dimensional open network that interpenetrating with another 3D network leaving no significant space for guest molecules (figure 5.17). Powder XRD analysis for compound **21** as-synthesised in DMF shows low agreement with calculated pattern. Moreover, the resulted pattern shows some amorphous material in present (figure 5.18). Selected bond lengths, angles and torsion angles for compound **21** are listed in tables 5.9 and 5.10.

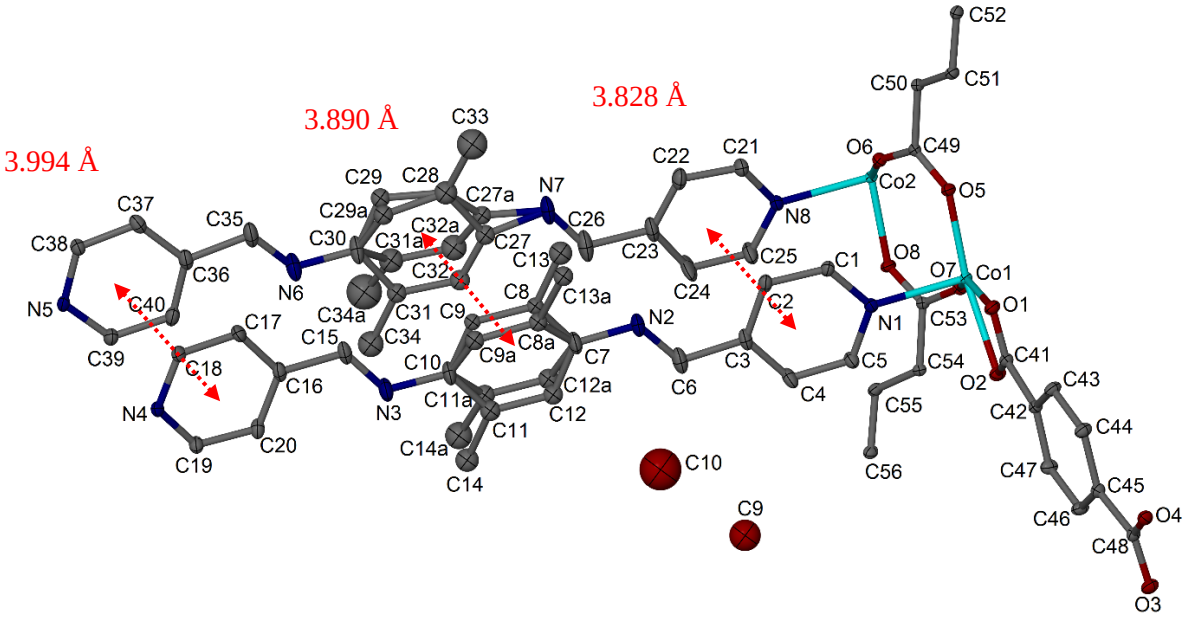

Figure 5.15: Compound **21** asymmetric unit of the crystal structure. Ellipsoids shown at 50 % probability levels. Hydrogen atoms were removed for clarity (4-py to 4-py= 3.828 or 3.994 Å) (dimethylphenyl-dimethylphenyl= 3.890 Å).

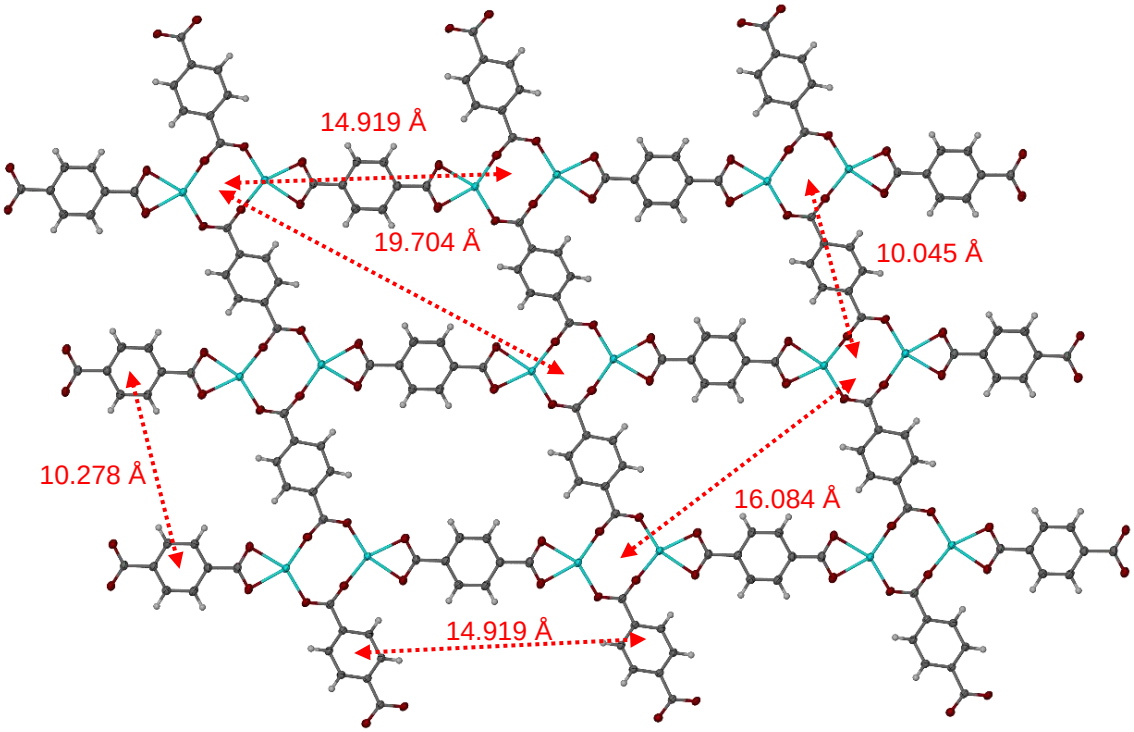

Figure 5.16: Co(II)-bdc^{2-} two-dimensional network. Each bdc^{2-} molecule behaves either as a tetra-dentate ligand to two Co(II) ions or as a tetra-dentate ligand to four Co(II) ions.

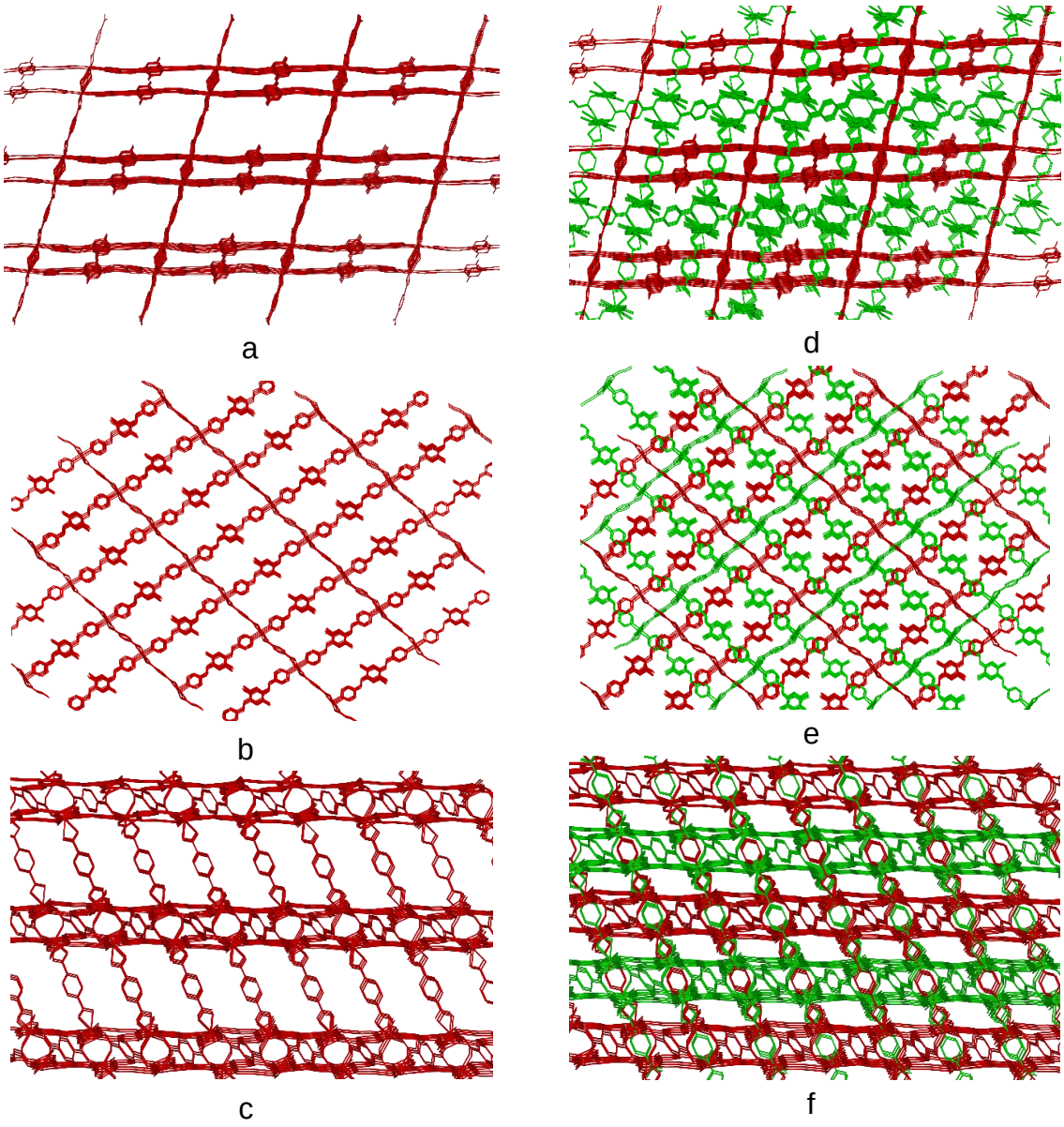

Figure 5.17: (a-c) Compound **21** three-dimensional open network, (d-f) two interpenetrating networks that shows π-π interaction between bdc^{2-} of one network and dimethylphenyl of another network.

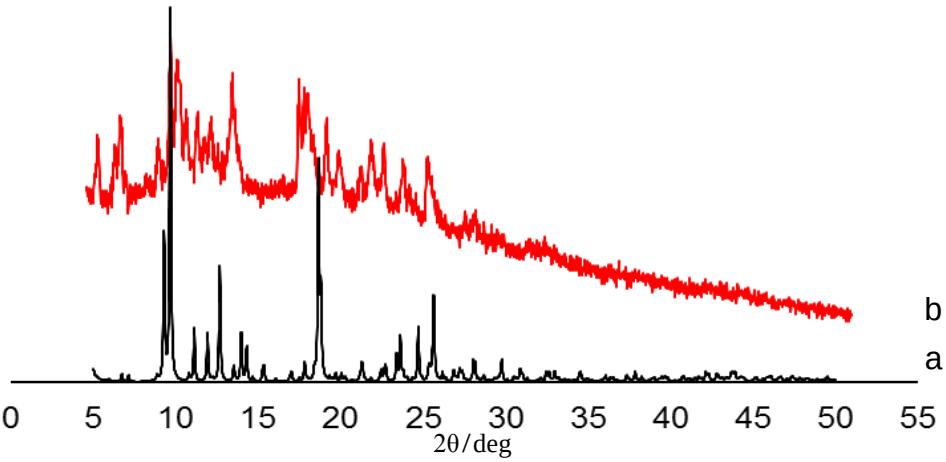

Figure 5.18: (a) Calculated powder XRD pattern of compound **21**, (b) powder XRD pattern of compound **21** as-synthesised in DMF.

Table 5.9: Selected bond lengths (Å) and angles (°) for compound **21**.

Co1-O1	2.153(19)	O5-Co1-O1	95.16(7)	O6-Co2-O8	115.29(7)
Co1-O2	2.195(17)	O5-Co1-O2	155.68(7)	O6-Co2-N5	88.47(8)
Co1-O5	2.010(17)	O5-Co1-O7	110.28(7)	O6-Co2-N8	85.85(8)
Co1-O7	2.020(18)	O5-Co1-N1	92.97(8)	O6-Co2-C48	122.79(8)
Co1-N1	2.140(2)	O5-Co1-N4	87.26(8)	O8-Co2-O3	90.72(7)
Co1-N4	2.165(2)	O5-Co1-C41	125.27(8)	O8-Co2-O4	151.23(7)
Co2-O3	2.191(19)	O7-Co1-O1	153.73(7)	O8-Co2-N5	96.04(8)
Co2-O4	2.159(17)	O7-Co1-O2	93.51(7)	O8-Co2-N8	89.01(8)
Co2-O6	2.010(19)	O7-Co1-N1	91.72(8)	O8-Co2-C48	120.92(8)
Co2-O8	2.037(17)	O7-Co1-N4	84.73(8)	N5-Co2-O3	95.53(8)
Co2-N5	2.162(2)	O7-Co1-C41	123.71(8)	N5-Co2-C48	95.38(8)
Co2-N8	2.161(2)	N1-Co1-O1	93.47(8)	N8-Co2-O3	88.28(8)
N2-C6	1.317(5)	N1-Co1-O2	91.25(7)	N8-Co2-N5	173.62(9)
N2-C7	1.409(4)	N1-Co1-N4	176.29(9)	N8-Co2-C48	85.30(8)
N3-C10	1.410(4)	N1-Co1-C41	93.72(8)	C41-O1-Co1	90.10(15)
N3-C15	1.263(4)	N4-Co1-O2	90.05(8)	C41-O2-Co1	87.96(14)
N6-C30	1.414(4)	N4-Co1-C41	89.17(8)	C48-O3-Co2	87.48(16)
N6-C35	1.307(5)	O3-Co2-C48	30.48(8)	C48-O4-Co2	89.10(15)
N7-C26	1.242(6)	O4-Co2-O3	60.73(7)	C49-O5-Co1	129.77(16)
N7-C27a	1.422(8)	O4-Co2-N5	90.59(7)	C49-O6-Co2	147.59(17)
O1-Co1-O2	60.66(7)	O4-Co2-N8	86.80(8)	C53-O7-Co1	141.98(17)
O1-Co1-N4	90.20(8)	O4-Co2-C48	30.35(8)	C53-O8-Co2	124.87(16)
O1-Co1-C41	30.23(7)	O6-Co2-O3	153.18(7)	C1-N1-Co1	123.44(17)
O2-Co1-C41	30.46(7)	O6-Co2-O4	92.79(7)		

Table 5.10: Selected torsion angles (°) for compound **21**.

N1-Co1-O1-C41	91.4	N8-Co2-O6-C49	165.3
N1-Co1-O2-C41	-95.2	N5-Co2-O3-C48	-91.2
N1-Co1-O5-C49	-63.9	N5-Co2-O4-C48	99.7
N1-Co1-O7-C53	-0.5	N5-Co2-O6-C49	-17.6
N4-Co1-O2-C41	88.3	N5-Co2-O8-C53	64.8
N4-Co1-O1-C41	-88.0	C23-C26-N7-C27	178.3
N4-Co1-O5-C49	112.4	C23-C26-N7-C27a	167.3
N4-Co1-O7-C53	-179.4	C36-C35-N6-C30	-177.7
N8-Co2-O3-C48	83.7	C16-C15-N3-C10	-172.3
N8-Co2-O4-C48	-86.2	C7-N2-C6-C3	179.4
N8-Co2-O8-C53	-111.3		

5.5.1.6 Crystal structure of ($[Co_2(L3)(bdc)_2].DMF.COMe_2)_n$ β-20(S)^{ace} MOF

Compound **20** resultant crystals were immersed in acetone for a few days and dried under vacuum to remove DMF solvent molecules. Two new materials ($[Co_2(L3)(bdc)_2].DMF.COMe_2)_n$ β-**20**(S)^{ace} and $([Co(L3)_{0.5}(bdc)])_n$ ε-**20**(L) were successfully characterised by single X-ray analysis. β-**20**(S)^{ace} crystal structure was solved in monoclinic space group $P2_1/c$ and shows two Co(II) ions on general positions, two halves of L3 ligand molecules, two bdc^{2-} ions, one DMF molecule and one acetone molecule per asymmetric unit (figure 5.19). β-**20**(S)^{ace} shows similar unit cell and Co(II) coordination environment in comparison with compound β-**20**(S) but differs in guest molecules positions and L3 ligand molecules torsion angles (figure 5.19). Co1 is coordinated to four oxygen atoms from four different bdc^{2-} ions along the equatorial axes and shows four coordination bond lengths of 2.022(2), 2.028(2), 2.015(2) and 2.045(3) Å for Co1-O1, Co1-O2, Co1-O3 and Co1-O4. Co1 is also coordinated to one L3 ligand molecule along the axial axis (Co1-N1= 2.053(3) Å) to produce the distortion square pyramid structure. Co2 shows similar coordination environment as Co1 and shows coordination bond lengths of 2.215(2), 2.044(2), 2.030(2), 2.035(2) and 2.061(3) Å for Co2-O5, Co2-O6, Co2-O7, Co2-O8 and Co2-N3 (figure 5.19).

The coordinated bdc^{2-} ions behave as tetra-dentate ligands to four Co(II) ions and shows four different coordination bond lengths as discussed previously. Compound β-**20**(S)^{ace} shows skewed paddlewheel structures resulted from a Co(II) dimer and four bdc^{2-} ions (Co1-$Co1^1$= 2.740(9) Å) and (Co2-$Co2^1$= 2.839(9) Å) (figure 5.20). Four bdc^{2-} and four Co(II) dimers are coordinated to produce $(Co_2)_4(bdc)_4$ square structure that shows 10.080 or 11.683 Å distance between bdc^{2-} ions and 14.704 × 16.037 Å diagonal between Co1 dimers. On the other hand, Co2 square structure shows 10.174 or 11.680 Å between bdc^{2-} and 14.705 × 16.037 Å diagonals between Co2 dimers (figure 5.20). Moreover, $(Co_2)_4(bdc)_4$ square structure is extending to produce a two-dimensional network that shows 4^4 network topology (figure 5.20).

L3 ligand behaves as a bi-dentate ligand *via* nitrogen atoms of 4-pyridyl rings and connecting between two different Co(II)-bdc^{2-} 2D networks. The ligand shows torsion angles of -69.6 or -71.6° between the phenyl and 4-pyridyl rings to produce L3 bent S-shape between Co(II) dimers Co1-L3-Co1= 15.781 Å and Co2-L3-Co2= 15.770 Å (figure 5.20). Eight bdc^{2-}, eight Co(II) dimers and four L3 ligand molecules are coordinated to produce $(Co_2)_8(L3)_4(bdc)_8$ tetragonal structure that extending to produce a three-dimensional network open structure (figure 5.21). The resulted network is interpenetrating with another 3D network to produce a two-fold interpenetrating 3D networks (figure 5.21). Moreover, the two-fold interpenetrating network shows one-dimensional channels occupied by DMF and acetone guest molecules (figure 5.22). Selected bond lengths, angles and torsion angles for compound β-**20**(S)^{ace} are listed in tables 5.11 and 5.12.

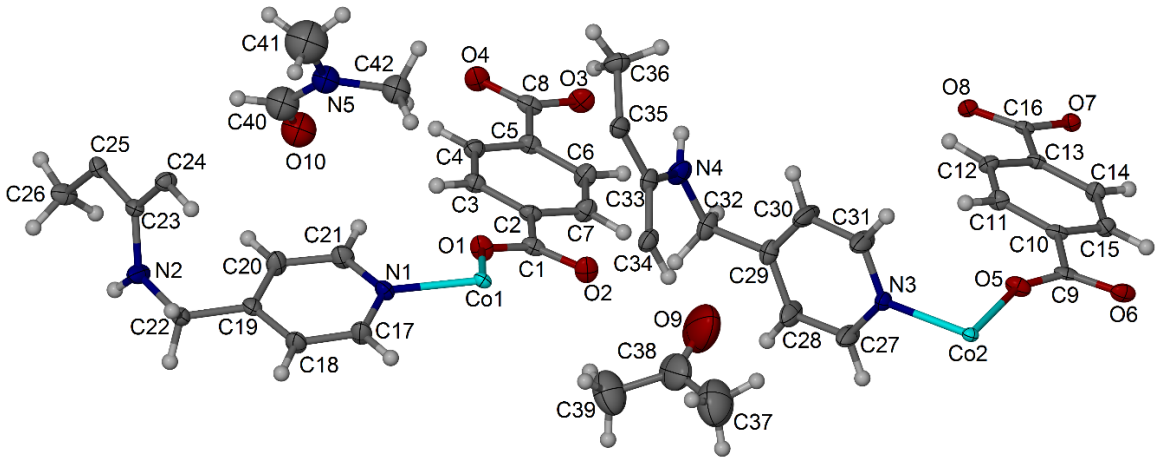

Figure 5.19: Compound β-**20**(S)^{ace} asymmetric unit of the crystal structure, ellipsoids shown at 50 % probability levels.

Table 5.11: Selected bond lengths (Å) and angles (°) for β-**20**(S)^{ace} MOF.

Co1-Co1^{1}	2.730(9)	O7-Co2-O5	83.25(9)	O3-Co1-N1	103.75(12)
Co1-O1	2.022(2)	O7-Co2-O6	93.53(9)	O4-Co1-Co1^{1}	73.91(8)
Co1-O2	2.028(2)	O7-Co2-O8	162.76(10)	O4-Co1-N1	90.35(12)
Co1-O3	2.015(2)	O7-Co2-N3	97.00(10)	N1-Co1-Co1^{1}	163.71(9)
Co1-O4	2.045(3)	O8-Co2-Co2^{1}	80.85(7)	O5-Co2-Co2^{1}	58.21(7)
Co1-N1	2.053(3)	O8-Co2-O5	85.49(9)	O6-Co2-Co2^{1}	105.45(8)
Co2-Co2^{1}	2.839(9)	O8-Co2-O6	93.60(10)	O6-Co2-O5	163.60(10)
Co2-O5	2.215(2)	O8-Co2-N3	95.62(10)	O6-Co2-N3	108.26(11)
Co2-O6	2.044(2)	N3-Co2-Co2^{1}	146.26(8)	O7-Co2-Co2^{1}	82.13(7)
Co2-O7	2.030(2)	O1-Co1-O4	89.53(11)	N3-Co2-O5	88.11(11)
Co2-O8	2.035(2)	O1-Co1-N1	98.41(11)	C1-O1-Co1	120.3(2)
Co2-N3	2.061(3)	O2-Co1-Co1^{1}	79.97(8)	C1-O2-Co1	127.3(2)
N2- C22	1.445(5)	O2-Co1-O4	87.64(11)	C8-O3-Co1	114.1(2)
N2- C23	1.400(4)	O2-Co1-N1	95.53(11)	C8-O4-Co1	134.8(2)
N4- C32	1.438(5)	O3-Co1-Co1^{1}	91.97(8)	C9-O5-Co2	152.6(2)
N4- C33	1.410(5)	O3-Co1-O1	89.25(11)	C9-O6-Co2	100.4(2)
O1-Co1-Co1^{1}	85.87(8)	O3-Co1-O2	90.11(11)	C16-O7-Co2	125.1(2)
O1-Co1-O2	165.79(11)	O3-Co1-O4	165.87(11)	C16-O8-Co2	126.4(2)

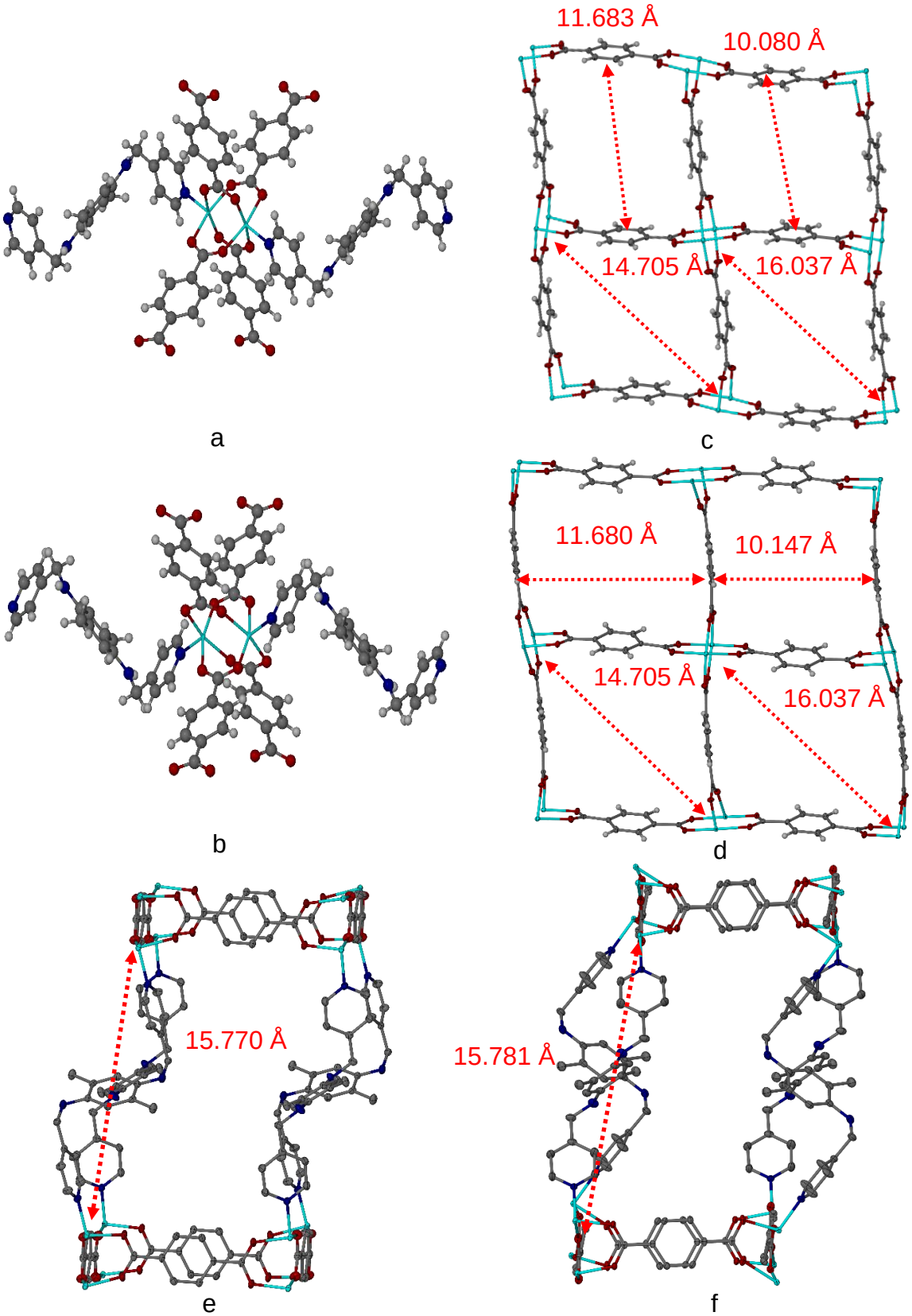

Figure 5.20: (a-b) Co1 and Co2 paddlewheel structures, (c-d) Co1 and Co2 $(Co_2)_4(bdc)_4$ square structures. (e-f) Co1 and Co2 $(Co_2)_8(L3)_4(bdc)_8$ tetragonal structures.

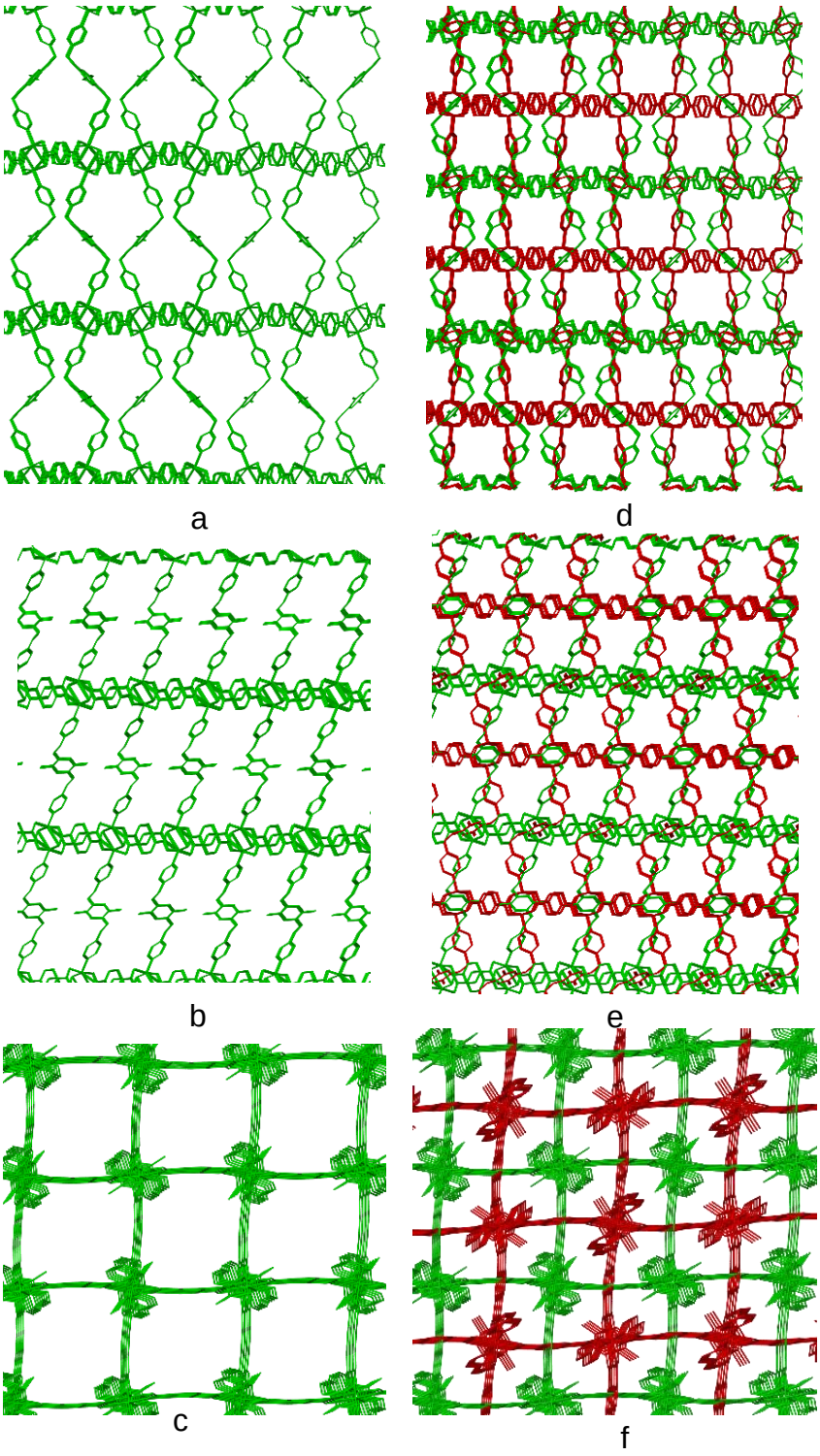

Figure 5.21: (a-c) β-**20**(S)^{ace} MOF three-dimensional open network, (d-f) β-**20**(S)^{ace} two-fold interpenetrating networks. Guest molecules were removed for clarity.

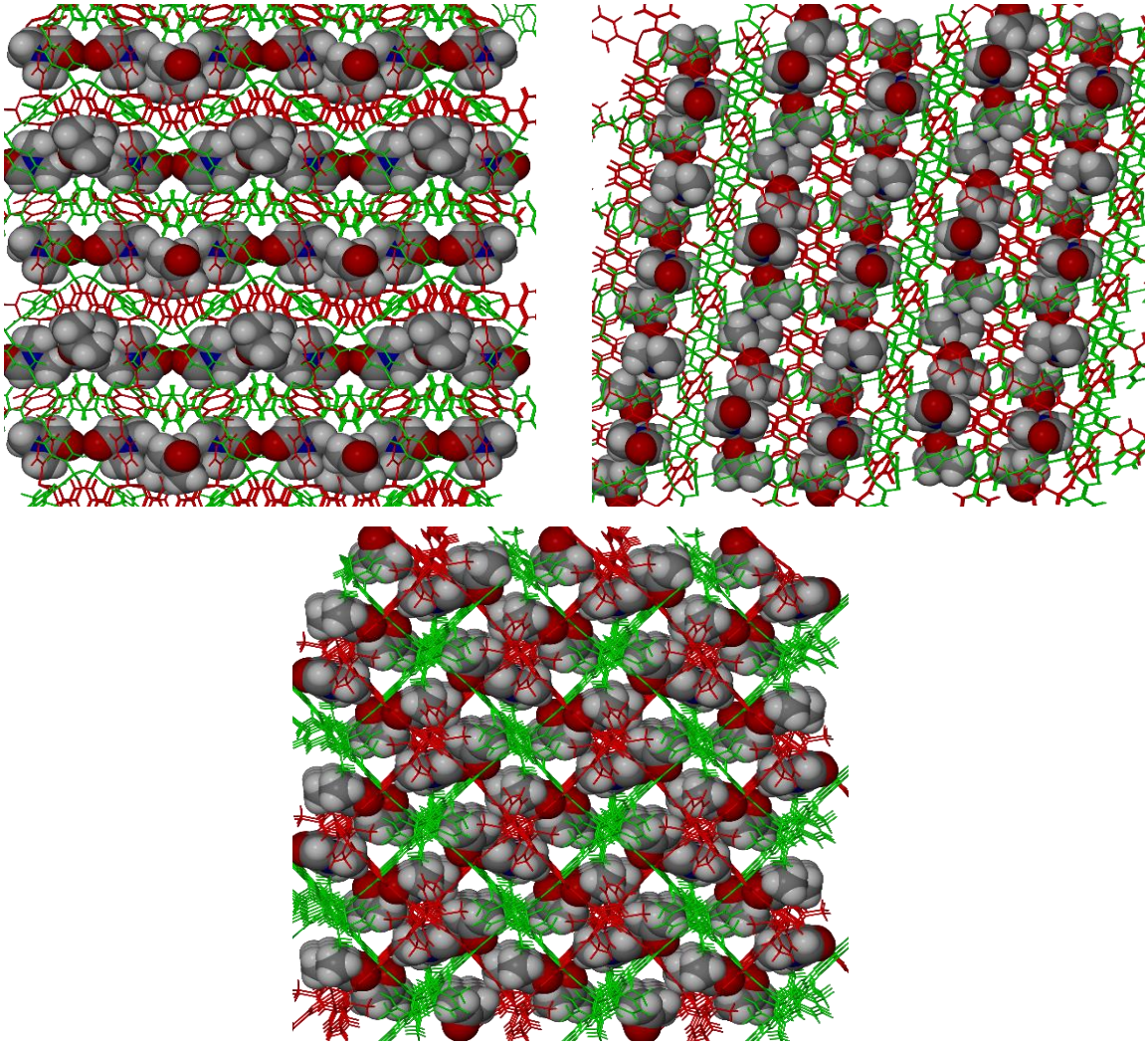

Figure 5.22: β-**20**(S)^{ace} MOF two-fold interpenetrating networks with guest molecules occupy the resulted channels.

Table 5.12: Selected torsion angles (°) for β-**20**(S)^{ace} MOF.

N1-Co1-O2-C1	158.4	C21-N1-Co1-O2	158.7
N1-Co1-O4-C8	-176.3	C21-N1-Co1-O3	67.2
N1-Co1-O1-C1	-166.8	C17-N1-Co1-O4	64.0
N1-Co1-O3-C8	174.8	C17-N1-Co1-O4	-23.7
N3-Co2-O5-C9	-174.8	C17-N1-Co1-O4	-115.1
N3-Co2-O8-C16	151.8	C17-N1-Co1-O4	153.6
N3-Co2-O6-C9	176.9	C27-N3-Co2-O8	5.3
N3-Co2-O7-C16	-147.3	C27-N3-Co2-O6	-90.3
C23-N2-C22-C19	-69.6	C27-N3-Co2-O7	173.6
C33-N4-C32-C29	-71.6	C27-N3-Co2-O5	90.6
N1-Co1-Co1^{1}-N1^{1}	180.00	C31-N3-Co2-O8	-17.01
N3-Co2-Co2^{1}-N1^{1}	180.00	C31-N3-Co2-O6	94.3
C21-N1-Co1-O1	-24.1	C31-N3-Co2-O7	-1.8
C21-N1-Co1-O4	-113.6	C31-N3-Co2-O5	-84.8

5.5.1.7 Crystal structure of ([Co(L3)$_{0.5}$(bdc)])$_n$ ε-20(L) MOF

The de-solvated ε-**20**(L) MOF crystal structure was solved in triclinic space group $P\bar{1}$ and shows one Co(II) ion on a general position, half of L3 ligand molecule and two halves of bdc^{2-} ions per asymmetric unit (figure 5.23). Co(II) ion is coordinated to five oxygen atoms from four different bdc^{2-} ions and shows five coordination bond lengths of 2.125(2), 2.231(2), 2.201(17), 2.004(14) and 2.030(17) Å for Co1-O1, Co1-O2, Co1-O2^1, Co1-O3 and Co1-O4. Co1 ion is also coordinated to one L3 ligand molecule by the nitrogen atom of 4-pyridyl ring (Co1-N1= 2.107(17) Å) to produce Co1 distortion octahedral coordination centre (figure 5.24). Coordinated bdc^{2-} ions show two different coordination styles toward Co(II) coordination centres (figure 5.24). In the first coordination style bdc^{2-} ions behave as hexa-dentate ligands to four different Co(II) ions and show three different coordination distances for Co-O1, Co-O2^1 and Co-O2. Whereas in the second coordination style bdc^{2-} ions behave as tetra-dentate ligands to four Co(II) ions and show two coordination distances for Co-O3 and Co-O4. Four bdc^{2-} ions are coordinated to one Co(II) dimer to produce a very skewed $Co_2(bdc)_4$ paddlewheel structure (figure 5.24). A square unit of Co(II)-bdc^{2-} is resulted from four bdc^{2-} ions and four Co(II) dimers that shows 10.822 or 10.958 Å between bdc^{2-} ions and 15.064 × 15.710 Å diagonal between Co(II) dimers (figure 5.24). Furthermore, $(Co_2)_4(bdc)_4$ square unit is extending to produce a two-dimensional network structure that shows 4^4 topology (figure 5.24).

L3 ligand behaves as a bi-dentate ligand by nitrogen atoms of 4-pyridyl ring and coordinated to two different Co(II) dimers from two different 2D networks (Co1-L3-Co1^1= 19.639 Å). L3 ligand is approximately linear and shows torsion angle of -172.8 ° between dimethylphenyl and 4-pyridyl rings. Four L3 ligands ions, eight bdc^{2-} ions and eight Co(II) dimers are coordinated to produce $(Co_2)_8(L3)_4(bdc)_8$ tetragonal structure that shows 10.943 or 8.616 Å between L3 ligands molecules (figure 5.24). The resulted tetragonal structure expands to produce a three-dimensional open network that is interpenetrating with another network to produce a two-fold interpenetrating structure (figure 5.25). Powder XRD analysis pattern of compound **20** dried sample has a good match with compounds β-**20**(S)^{ace} and ε-**20**(L) calculated patterns which indicates materials stability (figure 5.26). Selected bond lengths, angles and torsion angles for compound ε-**20**(L) are listed in tables 5.13 and 5.14.

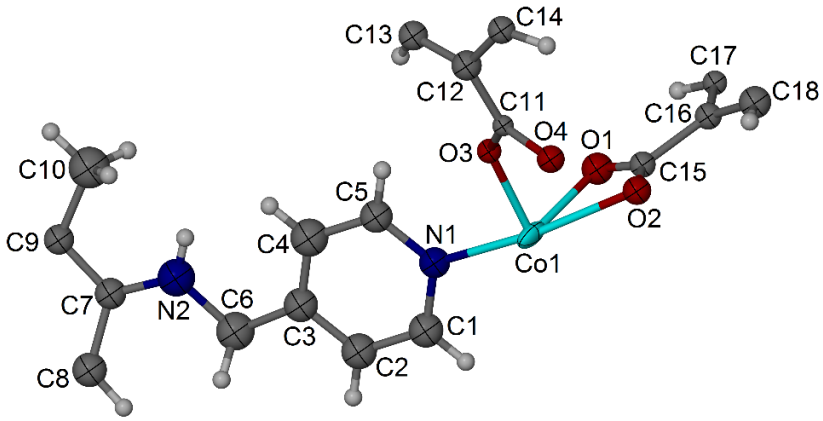

Figure 5.23: ε-**20**(L) MOF asymmetric unit of the crystal structure, ellipsoids shown probability at 50 % levels.

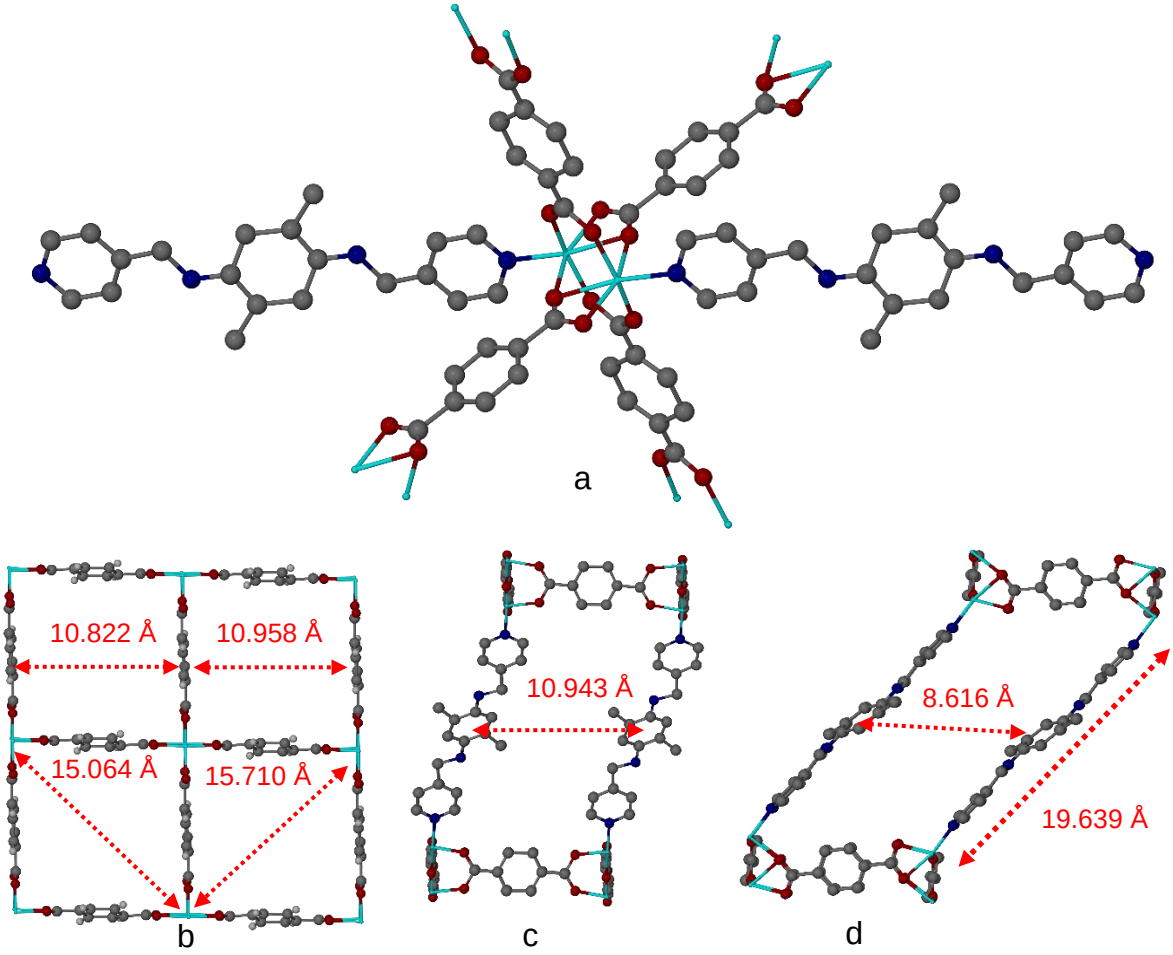

Figure 5.24: (a) ε-**20**(L) MOF skewed paddlewheel structure, each bdc^{2-} molecule behaves either as a hexa-dentate or as a tetra-dentate ligand to four Co(II) ions. (b) $(Co_2)_4(bdc)_4$ Square unit, (c-d) $(Co_2)_8(L3)_4(bdc)_8$ tetragonal structure.

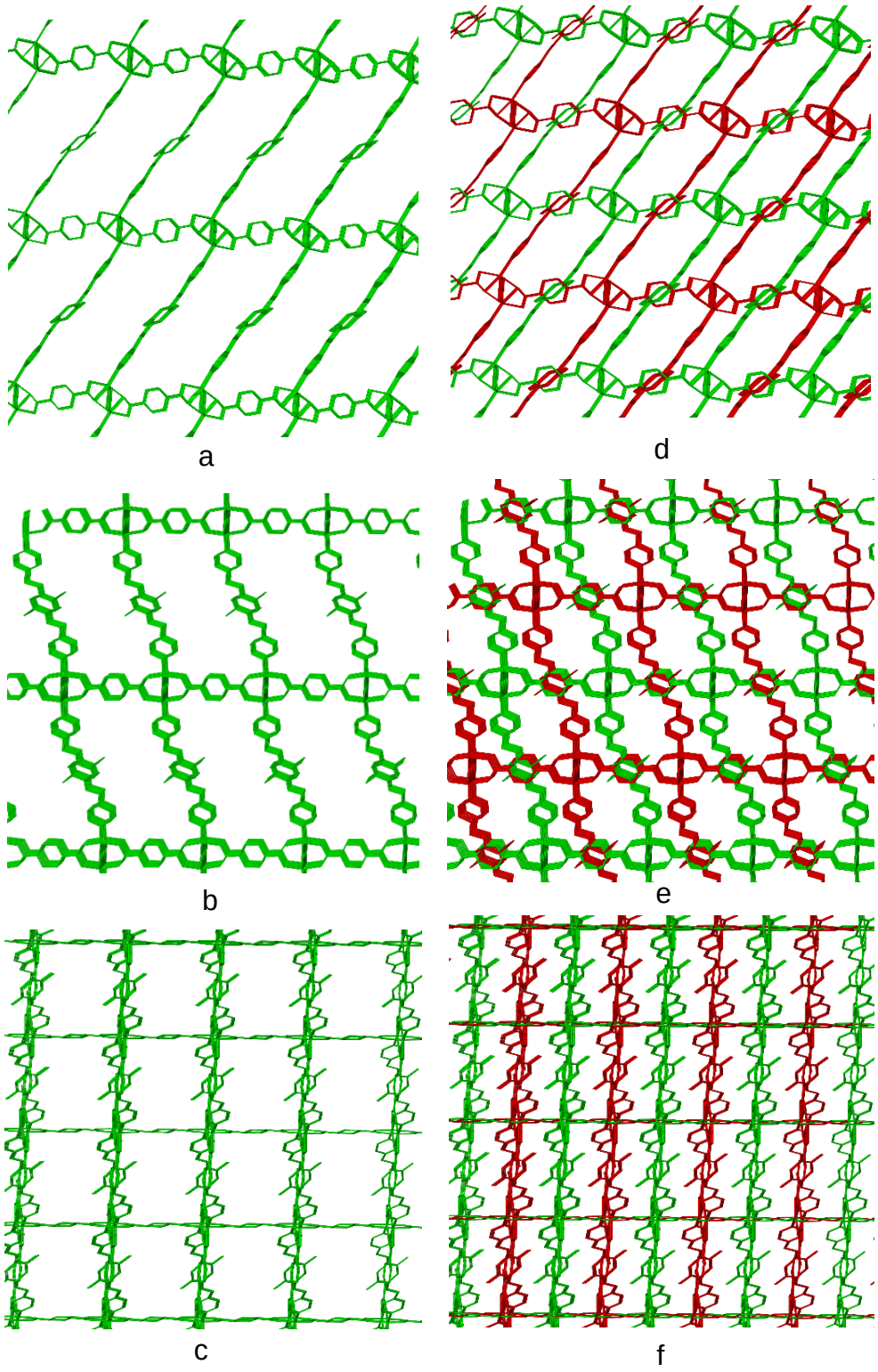

Figure 5.25: (a-c) ε-**20**(L) MOF three-dimensional open network, (d-f) two-fold interpenetrating networks.

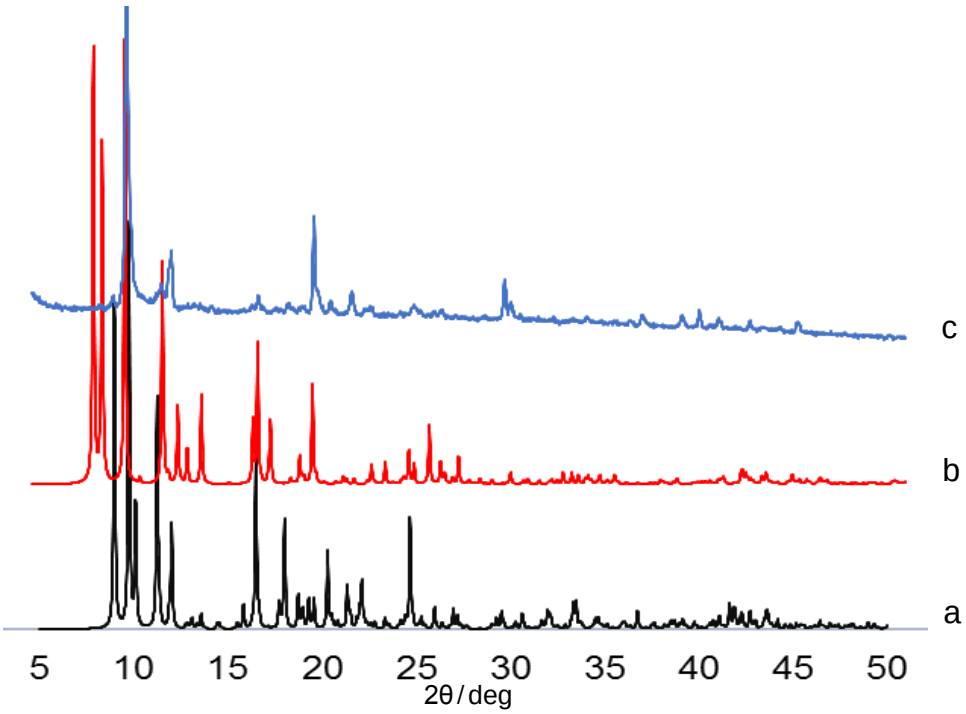

Figure 5.26: (a) Compound β-**20**(S)^{ace} calculated powder XRD pattern, (b) compound ε-**20**(L) calculated powder XRD pattern, (c) compound **20** powder XRD pattern after washing with acetone for a few days and drying under vacuum for 48 hours.

Table 5.13: Selected bond lengths (Å) and angles (°) for ε-**20**(L) MOF.

Co1-Co1^{1}	2.843(8)	O4-C11	1.35(3)	C7-N2-C6	117(3)
Co1-O1	2.125(2)	N2-C6	1.52(4)	C8-C7-N2	120(3)
Co1-O2^{1}	2.201(17)	N2-C7	1.34(5)	C9-C7-N2	117(3)
Co1-O2	2.231(2)	O2-Co1-O1	56.1(7)	O4-Co1-O2^{1}	84.8(6)
Co1-O3	2.004(14)	O2^{1}-Co1-O1	156.3(9)	O4-Co1-O3	163.6(7)
Co1-O4	2.030(17)	O3-Co1-O1	93.2(7)	C15-O1-Co1	94.1(16)
Co1-N1	2.107(17)	O3-Co1-O2	84.9(7)	C15-O2-Co1	87.8(16)
O1-C15	1.15(3)	O3-Co1-O2^{1}	83.3(6)	C15-O2-Co1^{1}	167.4(18)
O2-C15	1.19(3)	O4-Co1-O1	93.3(7)	C11-O3-Co1	130.9(13)
O3-C11	1.28(2)	O4-Co1-O2	86.3(7)	C11-O4-Co1^{1}	125.0(15)

Table 5.14: Selcted torsion angles (°) for ε-**20**(L) MOF.

N1-Co1-O4-C11	-143.6	C1-N1-Co1-O3	-162.6
N1-Co1-O1-C15	-179.7	C5-N1-Co1-O1	-86.8
N1-Co1-O2-C15	-170.6	C5-N1-Co1-O4	176.9
N1-Co1-O3-C11	146.0	C5-N1-Co1-O3	8.7
C1-N1-Co1-O4	5.7	C5-N1-Co1-O2	92.0
C1-N1-Co1-O1	102.0	C7-N2-C6-C3	-172.8
C1-N1-Co1-O2	-79.2		

5.5.1.8 Crystal structure of ($[Co_2(L3)(bdc)_2].n(EtOH))_n$ γ-20(L)^{EtOH} MOF

γ-**20**(L)^{EtOH} MOF crystals are poor-quality that required synchrotron radiation. The crystal structure was solved in monoclinic space group *P*2/*n* and shows one L3 ligand molecule, two Co(II) ions on general positions and two bdc^{2-} ions per asymmetric unit (figure 5.27). Co1 is coordinated to five oxygen atoms from four different bdc^{2-} ions and shows five different coordination bond lengths of 2.069(8), 2.190(9), 2.402(8), 2.051(9) and 1.985(8) Å for Co1-O1, Co1-O2, Co1-$O2^1$, Co1-O5 and Co1-O6. Co1 is also coordinated to one L3 ligand molecule (Co1-N1= 2.062(10) Å) to produce Co1 distortion octahedral geometry. Co2 shows similar coordination environment in comparison with Co1 and displays coordination bond lengths of 2.044(10), 2.069(8), 2.190(9), 2.367(8), 2.003(7) and 2.104(9) Å for Co2-N4, Co2-O3, Co2-O4, Co2-$O4^1$, Co2-O7 and Co2-O8.

Coordinated bdc^{2-} ions behave either as hexa-dentate ligands to four Co(II) ions and shows six coordination bond lengths or as tetra-dentate ligands to four Co(II) ions and shows four different coordination bond lengths. Four bdc^{2-} ions are coordinated to two Co(II) ions in a dimer style to produce $Co_2(bdc)_4$ skewed paddlewheel structure that has 2.826(3) Å distance between Co1-$Co1^1$ ions or 2.841(3) Å distance between Co2-$Co2^1$ ions (figure 5.28). $(Co_2)_4(bdc)_4$ square structure shows 10.924 or 10.769 Å distances between bdc^{2-} ions and 16.006 × 14.640 Å diagonals between Co(II) dimers (figure 5.28). Furthermore, Co(II) dimers and bdc^{2-} ions square structure is expanding to produce a two-dimensional network that has 4^4 topology (figure 5.28).

L3 ligand behaves as a bi-dentate ligand and coordinated to two different networks (Co1-L3-Co2= 19.690 Å). L3 ligand shape is approximately linear and shows torsion angles of 177.37(15) and -173.55(14) ° between the phenyl and 4-pyridyl rings (figure 5.27). Four L3 ligand molecules, eight bdc^{2-} ions and eight Co(II) dimers are coordinated to produce a tetragonal structure that shows 10.585 or 10.924 Å distances between L3 ligand molecules (figure 5.28). Moreover, the tetragonal structure is expanding to produce a 3D open network that interpenetrating with another 3D network and shows face-to-face π-π stacking interaction between dimethylphenyl and bdc^{2-} ions from two different network (ring centroid separation= 3.68 Å) (figure 5.29). Selected bond lengths, angles and torsion angles for γ-**20**(L)^{EtOH} MOF are listed in tables 5.15 and 5.16.

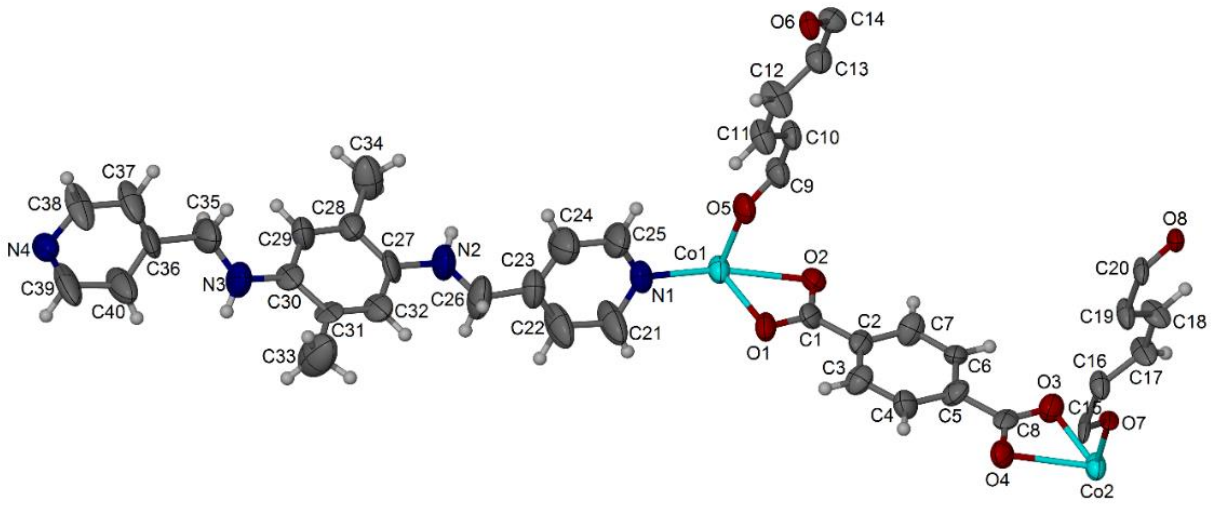

Figure 5.27: γ-**20**(L)^{EtOH} MOF asymmetric unit of the crystal structure, ellipsoids shown at 50 % probability levels.

Table 5.15: Selected bond lengths (Å) and angles (°) for γ-**20**(L)^{EtOH} MOF.

Co1-Co1^1	2.826(3)	O5-Co1-O2	84.8(3)	O7-Co2-N4	96.3(4)
Co1-O1	2.069(8)	O5-Co1-N1	97.4(4)	O8^1-Co2-Co2^1	81.9(2)
Co1-O2^1	2.402(8)	O6^1-Co1-Co1^1	81.9(2)	O8^1-Co2-O4	86.3(3)
Co1-O2	2.190(9)	O6^1-Co1-O1	94.7(3)	O8^1-Co2-O4^1	83.5(3)
Co1-O5	2.051(9)	O6^1-Co1-O2^1	85.0(3)	N4^1-Co2-Co2^1	143.9(3)
Co1-O6	1.985(8)	O6^1-Co1-O2	85.7(3)	N4^1-Co2-O3	107.6(4)
Co1-N1	2.062(10)	O6^1-Co1-O5	162.8(4)	N4^1-Co2-O4^1	89.7(4)
Co2-Co2^1	2.841(3)	O6^1-Co1 N1	95.4(4)	N4^1-Co2-O4	167.4(4)
Co2-O3	2.069(8)	N1-Co1-Co1^1	145.8(3)	N4^1-Co2-O8	94.6(4)
Co2-O4	2.190(9)	N1-Co1-O1	106.7(4)	C1-O1-Co1	97.9(8)
Co2-O4^1	2.367(8)	N1-Co1-O2^1	90.4(4)	Co1^1-O2-Co1	75.8(3)
Co2-O7	2.003(7)	N1-Co1-O2	165.4(4)	C1-O2-Co1	82.6(7)
Co2-O8	2.104(9)	O3-Co2-Co2^1	108.5(3)	C1-O2-Co1^1	158.2(8)
Co2-N4	2.044(10)	O3-Co2-O4^1	162.7(3)	C8-O3-Co2	95.4(7)
N2-C26	1.234(17)	O3-Co2-O4	59.8(3)	Co2^1-O4-Co2	77.0(3)
N2-C27	1.410(17)	O3-Co2-O8	93.1(3)	C8-O4-Co2	82.5(7)
N3-C30	1.368(17)	O4^1-Co2-Co2^1	54.3(2)	C8-O4-Co2^1	159.1(8)
N3-C35	1.341(18)	O4-Co2-Co2^1	48.7(2)	C9-O5-Co1	126.3(10)
O2-Co1-Co1^1	48.7(2)	O4^1-Co2-O4	103.0(3)	C14-O6-Co1^1	126.4(8)
O2^1-Co1-Co1^1	55.5(2)	O7-Co2-Co2^1	82.1(2)	C15-O7-Co2	122.4(8)
O2^1-Co1-O2	104.2(3)	O7-Co2-O3	95.1(3)	C20-O8-Co2^1	118.2(9)
O5-Co1-Co1^1	81.1(2)	O7-Co2-O4^1	84.4(3)	O7-Co2-O8	163.7(4)
O5-Co1-O1	92.5(3)	O7-Co2-O4	85.7(3)	O5-Co1-O2^1	83.5(3)

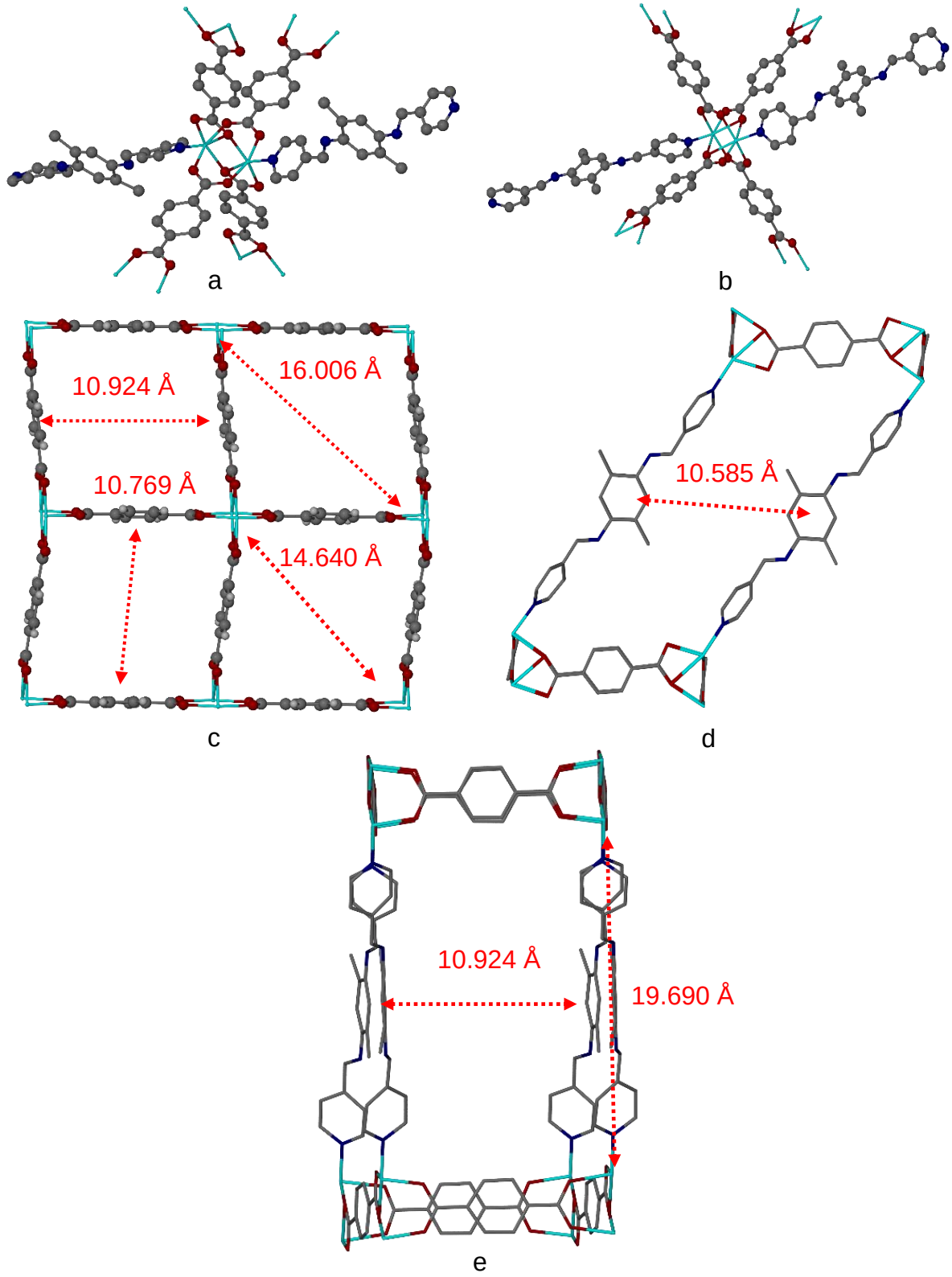

Figure 28: (a) Co1 paddlewheel structure, (b) Co2 paddlewheel structure. (c) Co(II)-bdc^{2-} two-dimensional network structure, (d) and (f) $(Co_2)_8(L3)_4(bdc)_8$ tetragonal structures.

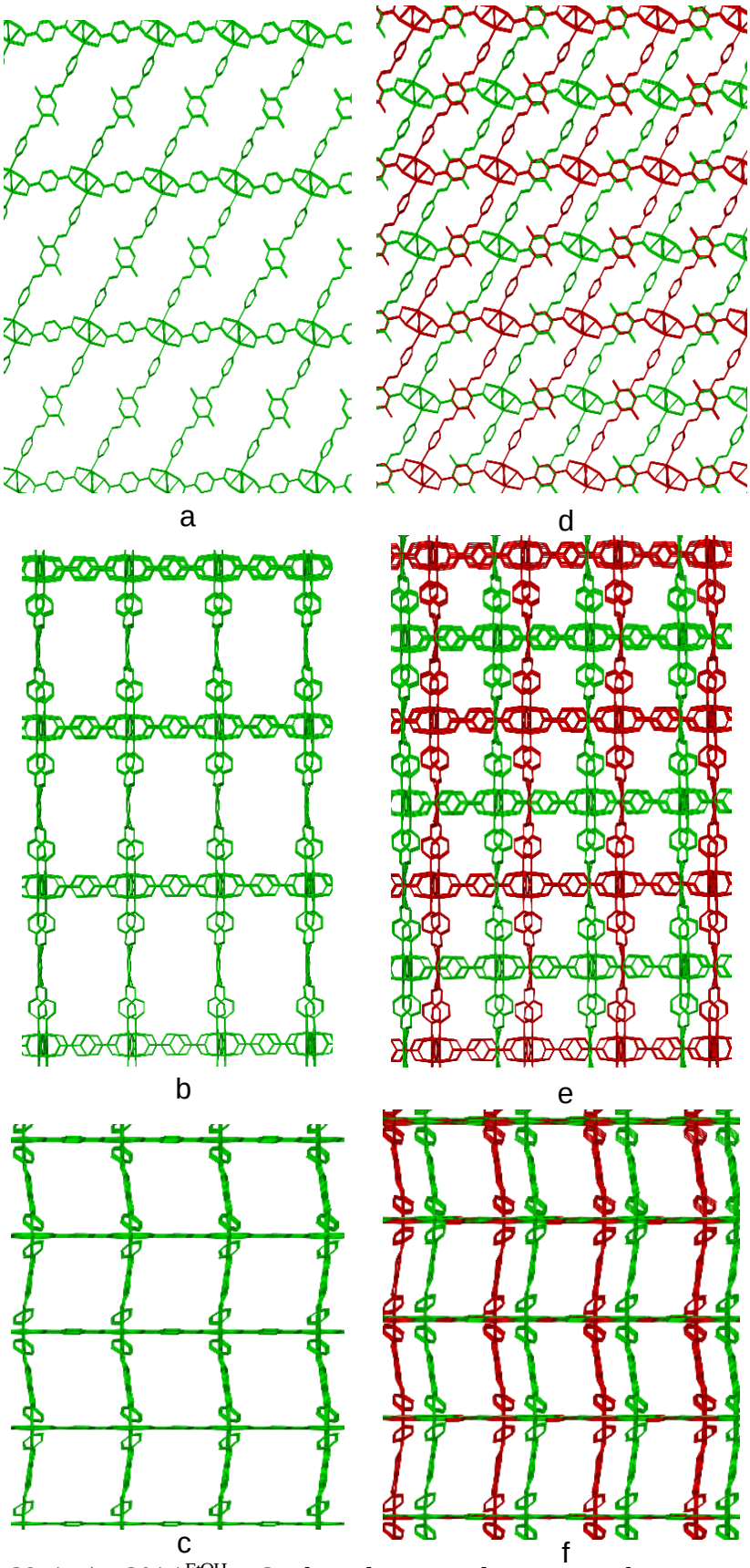

Figure 5.29: (a-c) γ-**20**(L)^{EtOH} MOF three-dimensional open network structure, (d-f) two interpenetrating networks (π-π interactions= 3.68 Å).

Table 5.16: Selected torsion angles (°) for γ-**20**(L)^{EtOH} MOF.

Co1-O1-C1-O2	-3.4(12)	Co2-O3-C8-O4	5.1(11)
Co1-O1-C1-C2	174.3(9)	Co2-O3-C8-C5	-172.8(8)
Co1-O2-C1-O1	2.9(10)	Co2-O4-C8-O3	-4.5(10)
Co1^{1}-O2-C1-O1	11(3)	Co2^{1}-O4-C8-O3	-17(3)
Co1^{1}-O2-C1-C2	-167.2(14)	Co2-O4-C8-C5	173.4(9)
Co1-O2-C1-C2	-174.8(10)	Co2^{1}-O4-C8-C5	160.9(15)
Co1-O5-C9-O5^{1}	2.1(4)	Co2-O7-C15-O7^{1}	1.7(3)
Co1-O5-C9-C10	-177.9(4)	Co2-O7-C15-C16	-178.3(3)
Co1^{1}-O6-C14-O6^{1}	-1.5(3)	Co2^{1}-O8-C20-O8^{1}	-3.1(3)
Co1^{1}-O6-C14-C13	178.5(3)	Co2^{1}-O8-C20-C19	176.9(3)
Co1-N1-C21-C22	-179.6(13)	Co2^{1}-N4-C38-C37	-177.2(14)
Co1-N1-C25-C24	175.8(14)	Co2^{1}-N4-C39-C40	-177.6(17)
C30-N3-C35-C36	177.372(15)	C23-C26-N2-C27	173.55(14)

5.5.1.9 Crystal structure of ([Co_2(L3)(bdc)$_2$].2EtOH)$_n$ ζ-20(S)^{EtOH} MOF

ζ-**20**(S)^{EtOH} MOF shows some structural similarities with β-**20**(S) but it is a distinct phase. The new MOF crystal structure shows one Co(II) ion on a general position, one bdc^{2-} ion, half of L3 ligand molecule and two ethanol molecules one of them is disordered (figure 5.30). Co(II) ion is coordinated to four oxygen atoms from four different bdc^{2-} ions and shows four different coordination bond lengths of 2.030(19), 2.043(19), 2.035(18) and 2.037(18) Å for Co1-O1, Co1-O2, Co1-O3 and Co1-O4. Moreover, Co(II) is coordinated to one L3 ligand molecule along the axial axis (Co1-N1= 2.065(3) Å) to produce Co(II) distortion square pyramid coordination centre (figure 5.31). The coordinated bdc^{2-} ions behave as tetra-dentate ligands to four different Co(II) ions and show four different M-O bond lengths. Four bdc^{2-} ligands are coordinated to two Co(II) ions in a dimer style to produce $Co_2(bdc)_4$ paddlewheel ordered structure (Co1-Co1^{1}= 2.708(8) Å) (figure 5.31). Four Co(II) dimers and four bdc^{2-} ions are coordinated to produce $(Co_2)_4(bdc)_4$ square unit that shows 11.678 and 10.268 Å distances between bdc^{2-} ions and 15.255 × 15.771 Å diagonals between Co(II) dimers, and expands to produce Co(II)-bdc^{2-} two-dimensional network (figure 5.31).

The ligand L3 is connecting between two different Co(II)-bdc^{2-} 2D networks (Co1-L3-Co1^{1}= 16.562 Å) and shows torsion angle of 75.8 ° between the dimethylphenyl and 4-pyridyl ligands to produce L3 bent S-shape between Co(II) coordination centres. ζ-**20**(S)^{EtOH} MOF also has $(Co_2)_8(L3)_4(bdc)_8$ tetragonal structure that shows 10.959 or 10.973 Å between L3 ligand molecules and extending to produce a three-dimensional network structure (figure 5.31). The resulted three-dimensional open network structure is interpenetrating with another three-dimensional network to produce a two-fold interpenetrated MOF structure (figure 5.32). Ethanol guest molecules could be located inside the new

MOF channels and form hydrogen bond interactions with each other (O5-O6= 2.992 Å) (figure 5.33). Selected bond lengths, angles and torsion angles for ζ-**20**(S)^{EtOH} MOF are listed in tables 5.17 and 5.18. Calculated powder XRD patterns for compounds ζ-**20**(L)^{EtOH} and γ-**20**(L)^{EtOH} show a low agreement with compound **20** as-synthesised in DMF or dried powder XRD patterns, that could due to the structural changes after removing DMF solvent molecules and replacing them with ethanol guest molecules (figure 4.34).

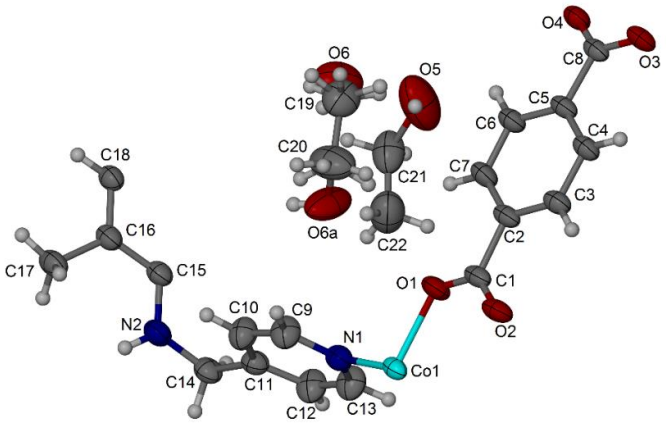

Figure 5.30: ζ-**20**(S)^{EtOH} MOF asymmetric unit of crystal structure, ellipsoids shown at 50 % probability levels.

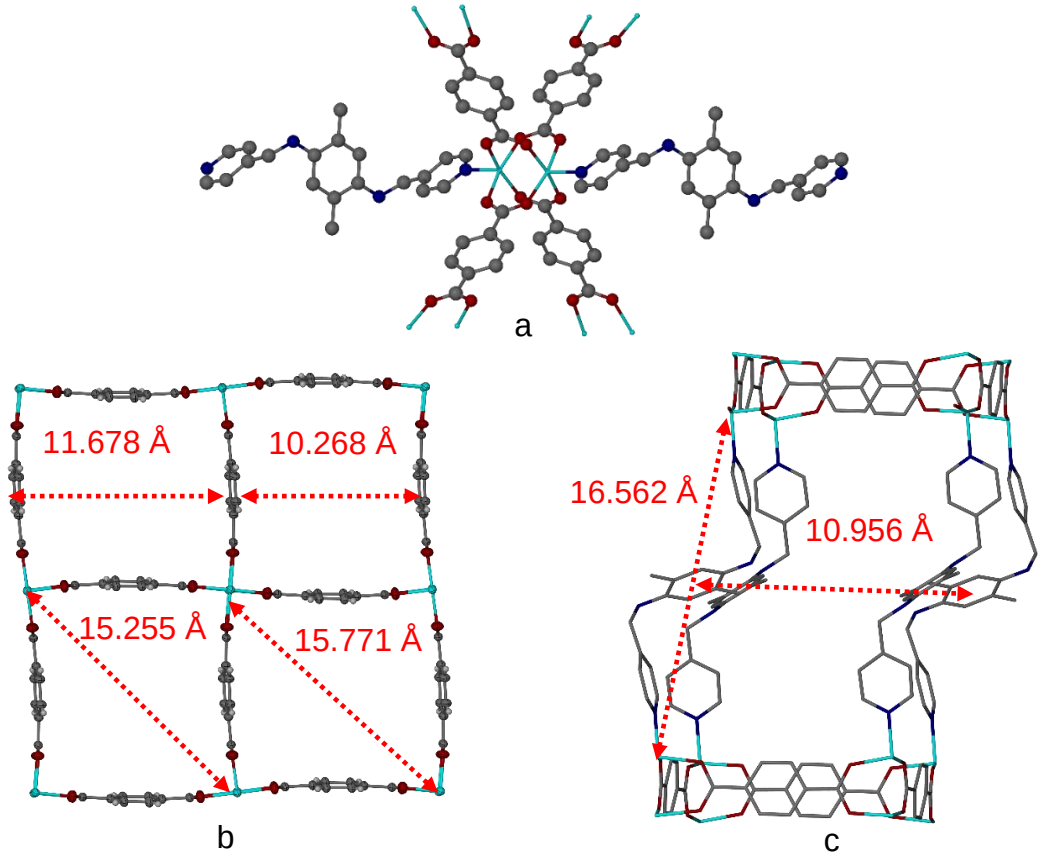

Figure 5.31: (a): ζ-**20**(S)^{EtOH} MOF paddlewheel structure (Co1-Co1^{1}= 2.708(8) Å). (b) Co(II)-bdc^{2-} two-dimensional network, (c) ζ-**20**(S)^{EtOH} MOF $(Co_2)_8(L3)_4(bdc)_8$ tetragonal structure.

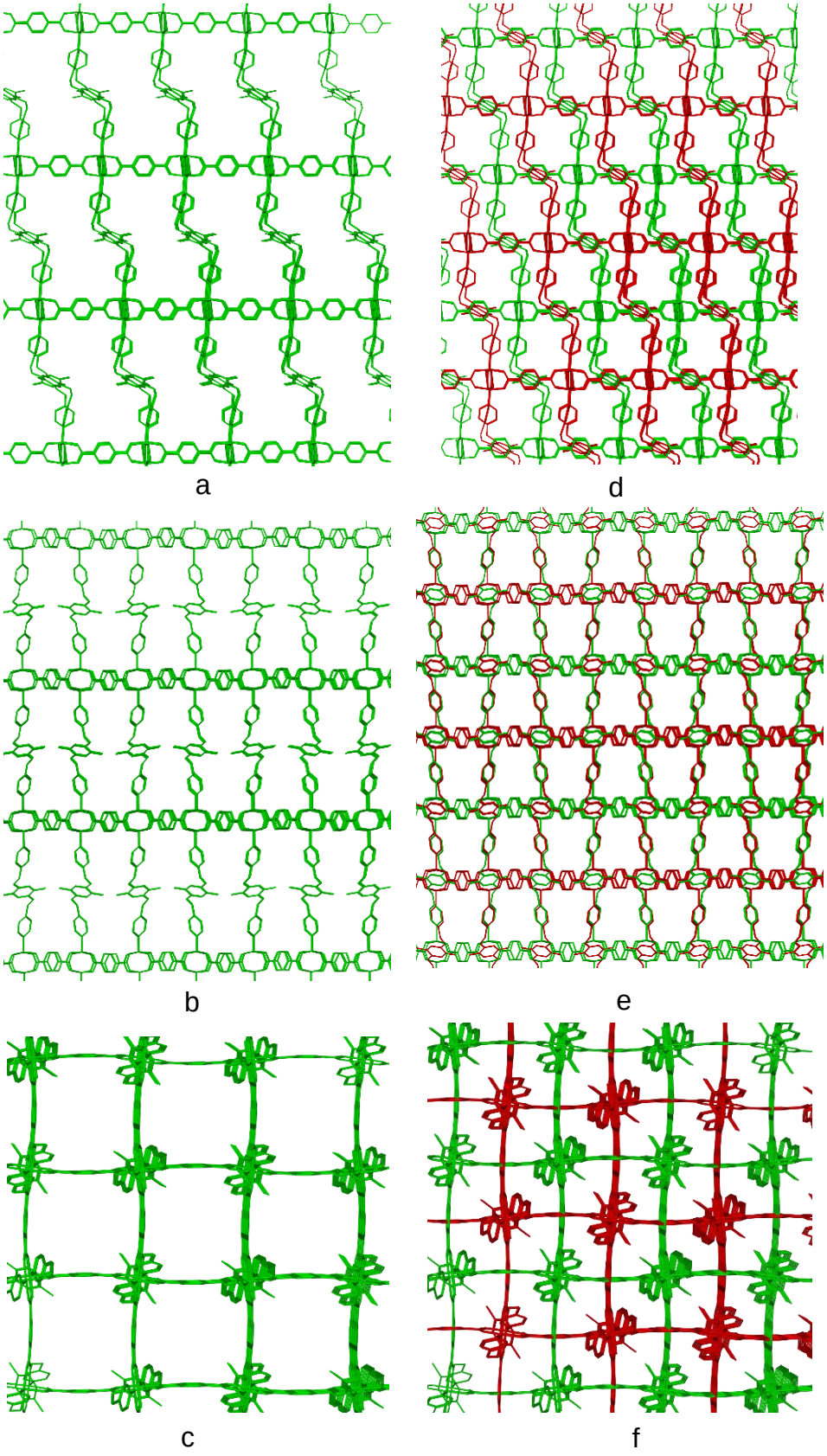

Figure 5.32: (a-c) ζ-**20**(S)^{EtOH} MOF three-dimensional open network, (d-f) two-fold interpenetrating three-dimensional networks.

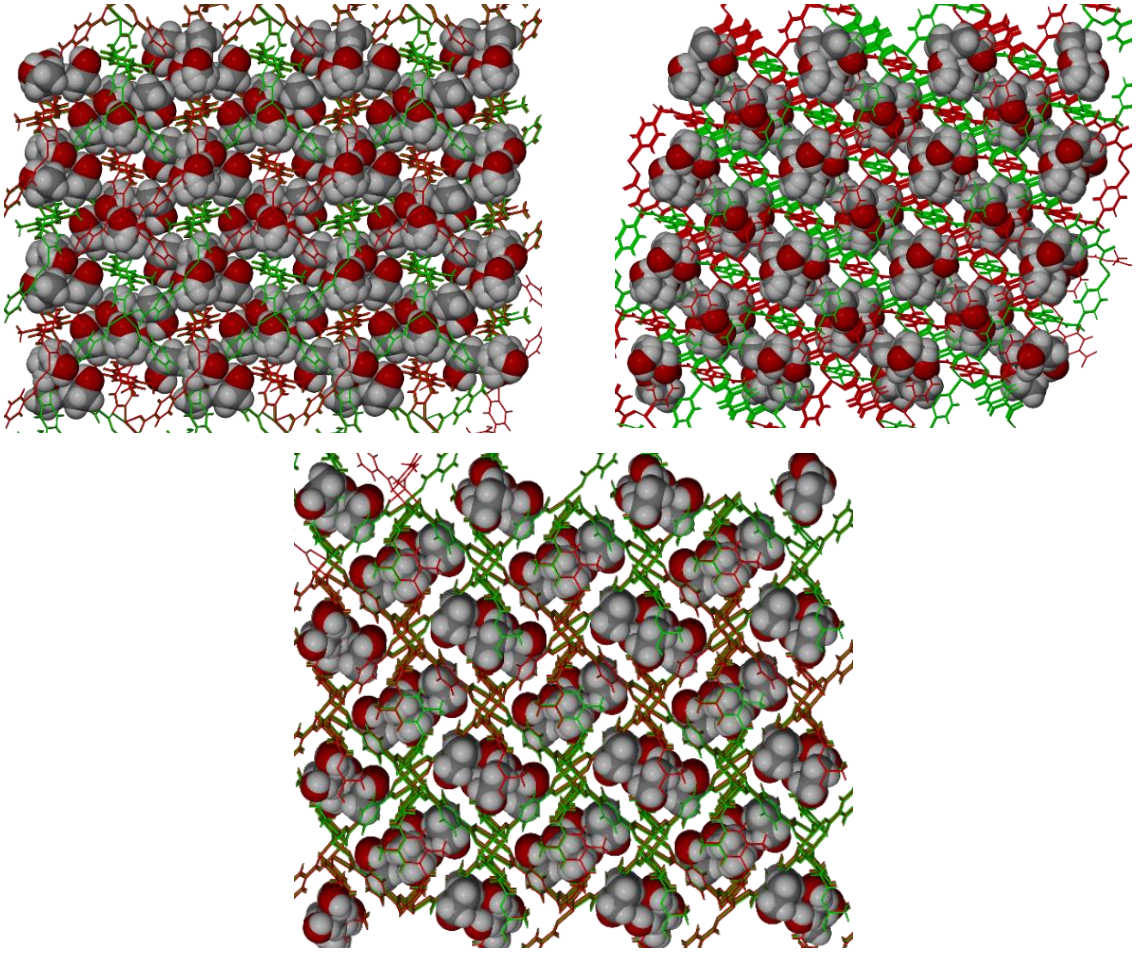

Figure 5.33: Ethanol molecules located in ζ-**20**(S)^{EtOH} MOF channels.

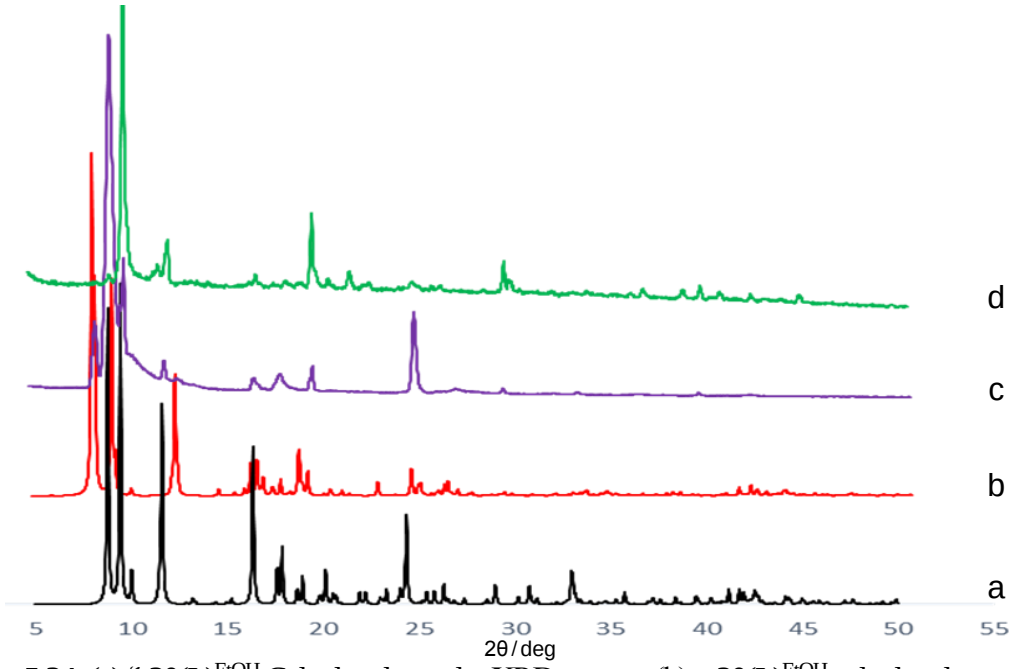

Figure 5.34: (a) ζ-**20**(L)^{EtOH} Calculated powder XRD pattern, (b) γ-**20**(L)^{EtOH} calculated powder XRD pattern, (c) compound **20** powder XRD pattern as-synthesised in DMF, (d) powder XRD pattern of compound **20** dried sample.

Table 5.17: Selected bond lenghts (Å) and angles (°) for ζ-**20**(S)^{EtOH} MOF.

Co1-Co1^{1}	2.708(8)	O2^{1}-Co1-N1	92.48(10)
Co1-O1	2.030(19)	O3^{1}-Co1-Co1^{1}	86.05(6)
Co1-O2	2.043(19)	O3^{1}-Co1-O2^{1}	89.60(9)
Co1-O3	2.034(18)	O3^{1}-Co1-O4^{1}	166.63(9)
Co1-O4	2.037(18)	O3^{1}-Co1-N1	96.80(9)
Co1-N1	2.065(3)	O4^{1}-Co1-Co1^{1}	80.58(6)
O1-C1	1.262(3)	O4^{1}-Co1-O2^{1}	88.58(8)
O2-C1	1.257(4)	O4^{1}-Co1-N1	96.51(9)
N2-C14	1.428(4)	N1-Co1-Co1^{1}	173.73(8)
N2-C15	1.386(3)	C1-O1-Co1	122.12(18)
O1-Co1-Co1^{1}	84.93(7)	C1-O2-Co1^{1}	125.25(18)
O1-Co1-O2^{1}	166.83(10)	C8-O3-Co1^{1}	120.70(17)
O1-Co1-O3^{1}	88.68(9)	C8-O4-Co1^{1}	127.34(17)
O1-Co1-O4^{1}	90.08(8)	C9-N1-Co1	121.3(2)
O1-Co1-N1	100.69(10)	C13-N1-Co1	121.4(2)
O2^{1}-Co1-Co1^{1}	81.92(7)	C13-N1-C9	116.8(3)

Table 5.18: Selected torsion angle (°) for ζ-**20**(S)^{EtOH} MOF.

N1-Co1-O1-C1	-175.1	C9-N1-Co1-O4	-176.4
N1-Co1-O3-C8	175.9	C9-N1-Co1-O2	94.7
N1-Co1-O2-C1	177.2	C13-N1-Co1-O3	-166.3
N1-Co1-O4-C8	-172.6	C13-N1-Co1-O1	103.8
C11-C14-N2-C15	75.8	C13-N1-Co1-O4	12.5
C9-N1-Co1-O3	4.9	C13-N1-Co1-O2	-76.4
C9-N1-Co1-O1	-85.1		

5.5.1.10 Crystal structure of compound 20 in water

Compound **20** de-solvated crystals are not stable in water after a few days and decomposed to produce $(L3.2H_2O)_n$ material. $(L3.2H_2O)_n$ crystal structure was solved in monoclinic space groups $P2_1/c$ and shows half of L3 ligand molecule and a water molecule per asymmetric unit (figure 5.35). $(L3.2H_2O)_n$ crystal structure shows torsion angle of 86.9 ° between the dimethylphenyl and 4-pyridyl rings to produce L3 bent S-shape (figure 5.35). $(L3.2H_2O)_n$ Crystal structure shows hydrogen bond interaction between L3 and water molecules (N1-O1= 3.832 Å). The crystal structure shows another hydrogen bond interaction between water molecules (O1-O1^{1}= 2.744 Å) (figure 5.35). Selected bond lengths, angles and torsion angles for compound $(L3.3H_2O)_n$ are listed in table 5.19.

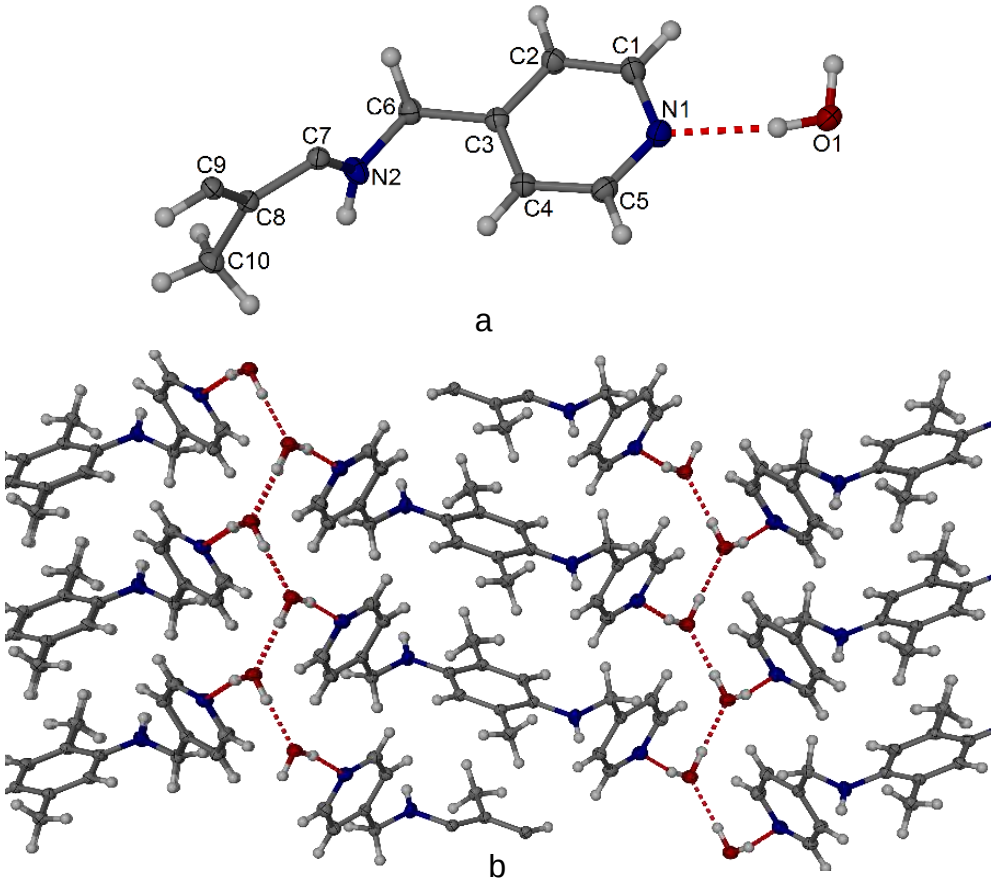

Figure 5.35: (a) $(L3.2H_2O)_n$ Asymmetric unit of the crystal structure, ellipsoids shown at 50 % probability levels. (b) Packing diagram of $(L3.2H_2O)_n$ material.

Table 5.19: Selected bond lengths (Å), angles and torsion angles (°) for compound $(L3.2H_2O)_n$.

N1-C1	1.346(10)	C7-C8	1.406(9)
N1-C5	1.338(11)	C7-C9	1.402(9)
N2-C6	1.447(9)	C8-C9	1.396(10)
N2-C7	1.401(9)	C8-C10	1.506(9)
C1-C2	1.387(11)	C7-N2-C6	120.92(6)
C2-C3	1.398(10)	C3-C6-N2	114.65(6)
C3-C4	1.390(10)	C8-C7-N2	120.44(6)
C3-C6	1.516(10)	C9-C7-N2	121.00(6)
C4-C5	1.394(11)	C3-C6-N2-C7	86.9

5.5.2 Crystal structure of $([Co_2(L3)(bpdc)_2])_n$ MOF (22)

Solvothermal reaction of L3 ligand, 4,4-biphenyldicarboxylic acid and $Co(NO_3)_2.6H_2O$ in a mixture of 2DMF and DMSO at 115 °C for 48 hours produced $([Co_2(L3)(bpdc)_2])_n$ MOF (**22**). Immersion of compound **22** resultant crystals in acetone for a few days and drying under vacuum for two days gave the de-solvated $([Co_2(L3)(bpdc)_2])_n$ MOF (**22**)^a. Then, immersion of compound **22**^{a} in ethanol or water produced $([Co_2(L3)(bpdc)_2].n(EtOH))_n$ (**22**)^{EtOH} or $([Co_2(L3)(bpdc)_2].(H_2\text{-}bpdc).n(H_2O))_n$ (**22**)^{H_2O} MOFs (scheme 5.2). Moreover, as-synthesised, dried, in ethanol or water MOFs are isostructural and their crystal structures were solved in orthorhombic space group *Ccce*.

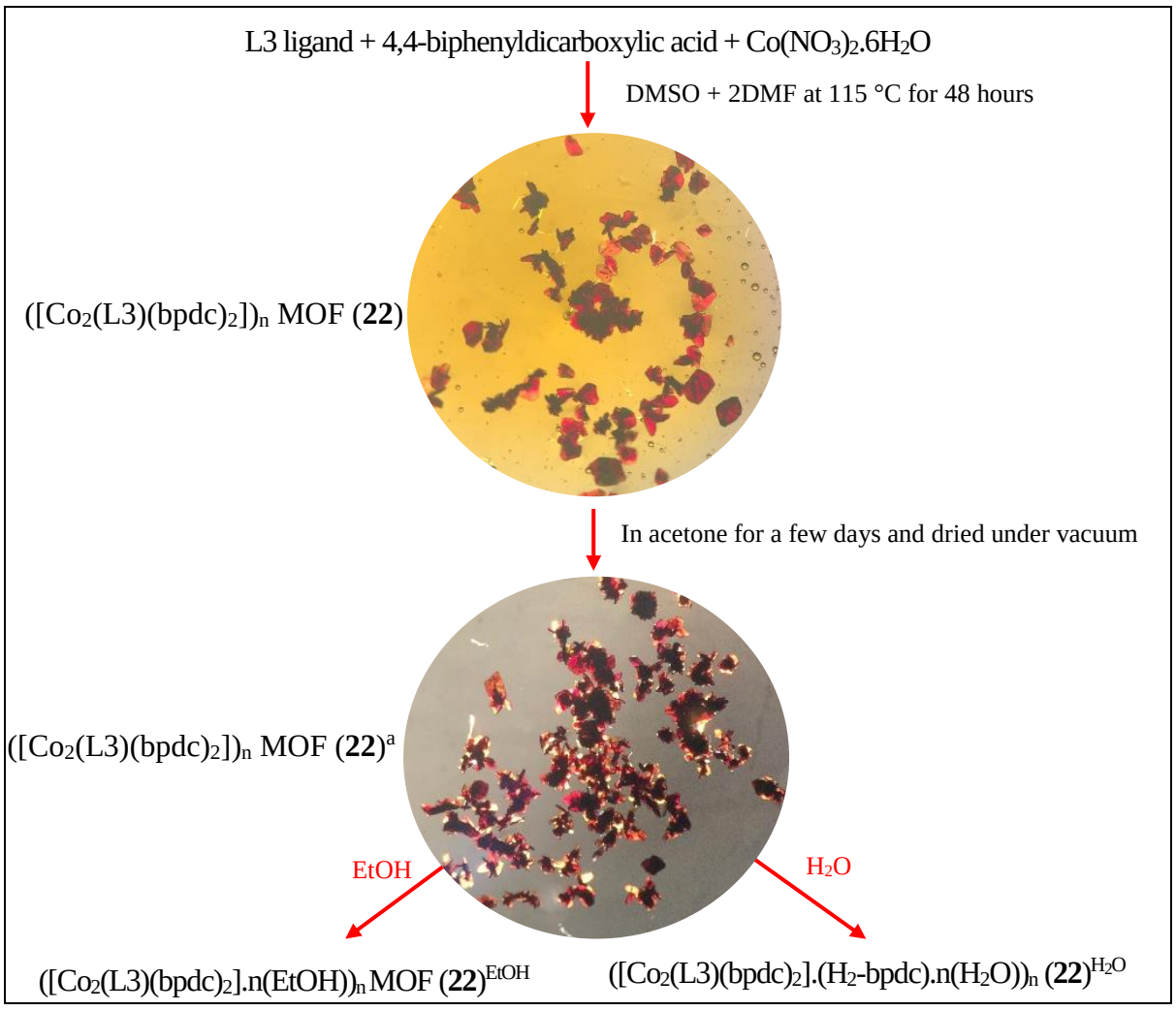

Scheme 5.2: Compound **22** as-synthesised, dried, in ethanol or water.

5.5.2.1 Crystal structure of $([Co_2(L3)(bpdc)_2])_n$ MOF (22)

Compound **22** crystal structure was solved in orthorhombic space group *Ccce* and shows one Co(II) ion on a general position, half of L3 ligand molecule and two halves of $bpdc^{2-}$ ligand molecules, one of them has disordered phenyl groups (figure 5.36). Co(II) ion is coordinated to four oxygen atoms from four different $bpdc^{2-}$ molecules and shows four different coordination bond lengths of 2.027(3), 2.020(3), 2.026(3) and 2.033(3) Å for Co1-O1, Co1-O2, Co1-O3 and Co1-O4. Co(II) ion is also coordinated to one L3 ligand molecule by nitrogen atom of 4-pyridyl ring to produce Co(II) distortion square pyramidal structure (figure 5.37).

Four $bpdc^{2-}$ molecules are coordinated to one Co(II) dimer (Co1-$Co1^1$= 2.696(12) Å) to produce $Co_2(bpdc)_4$ paddlewheel structure that shows torsion angles of 136.8, -161.6 and -148.8 ° between $bpdc^{2-}$ phenyl rings (figure 5.37). Torsion angles between $bpdc^{2-}$ phenyl rings have a great effect on the network expanding and produce Co(II)-$bpdc^{2-}$ three-dimensional open network structure (figure 5.38). Coordinated $bpdc^{2-}$ molecules behave as tetra-dentate ligands to four different Co(II) ions and show four M-O coordination bond lengths. Six Co(II) dimers and six $bpdc^{2-}$ molecules are coordinated to produce $(Co_2)_6(bpdc)_6$ rectangle structure that has 30.487 × 15.196 Å sides and 34.064 Å diagonal between Co(II) dimers (figure 5.38). The resulted $(Co_2)_6(bpdc)_6$ rectangle structure expands to produce a two-dimensional network structure that has 4^4 topology (figure 5.38). Two Co(II) dimers from the $(Co_2)_6(bpdc)_6$ rectangle structure are coordinated to two different two-dimensional networks by four $bpdc^{2-}$ molecules (Co_2-bpdc-Co_2= 15.196 Å) to produce Co(II)-$bpdc^{2-}$ three-dimensional open network structure (figure 5.38). The resulted 3D network shows $(Co_2)_4(bpdc)_4$ rhombic channels along *a* and *b* axes (figure 5.39). $(Co_2)_4(bpdc)_4$ square channels along *b* and *c* axes and $(Co_2)_6(bpdc)_6$ rectangle channels along *a* and *c* axes (figure 5.39). There are two Co(II)-$bpdc^{2-}$ three-dimensional networks in the overall lattice and L3 molecules are connecting between them to form a single 3D network (figure 5.39).

L3 ligand behaves as a bidentate ligand *via* nitrogen atoms of 4-pyridyl rings to two different Co(II)-$bpdc^{2-}$ three-dimensional networks and shows torsion angle of -93.1 ° between dimethylphenyl and pyridyl rings to produce L3 bent S-shape between Co(II) centres (Co1-L3-$Co1^1$= 17.383 Å). The resulted network is topologically complex and self-catenates. To the best of our knowledge this 6-connected self-catenating network has not been reported, although other types of self-catenating MOFS with mixed carboxylate and N-donor ligands are known [100-105]. Solvent accessible void space comprises approximately 34 % of the cell overall volume but could not be resolved within the crystal structure. Selected bond lengths, angles and torsion angles for compound **22** are listed in tables 5.20 and 5.21.

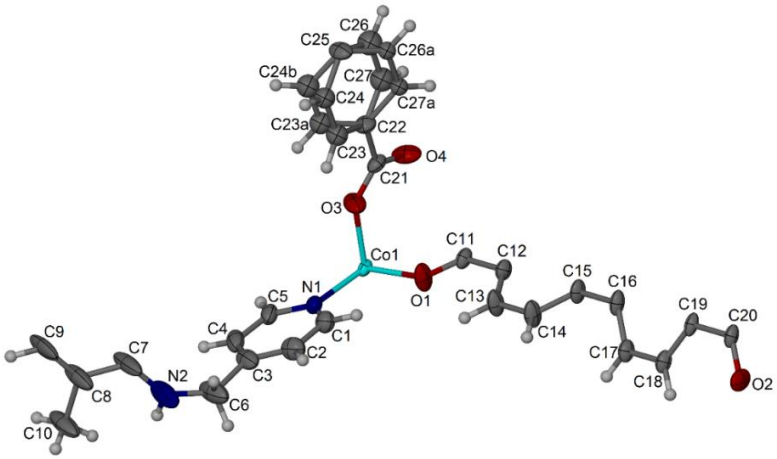

Figure 5.36: Compound **22** asymmetric unit of the crystal structure. Ellipsoids shown at 50 % probability levels.

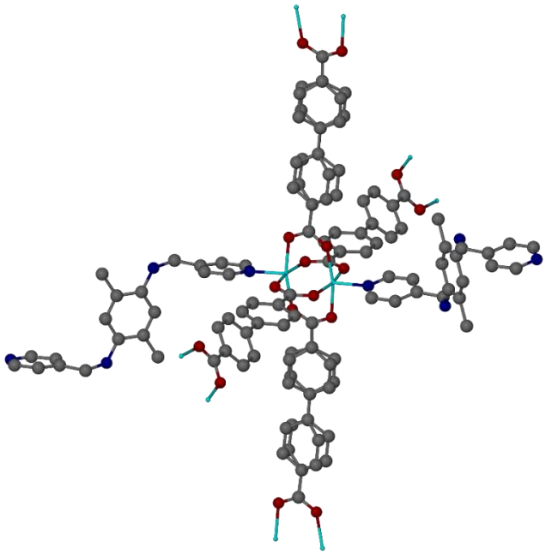

Figure 5.37: Compound **22** paddlewheel structure that has torsion angles of 136.8 or -148.8 ° between $bpdc^{2-}$ rings. Torsion angle of -93.1 ° between dimethylphenyl and 4-pyridyl rings to produce L3 bent S-shape.

Table 5.20: Selected bond lengths (Å) and angles (°) for compound **22**.

$Co1-Co1^{1}$	2.696(12)	O2-Co1-O1	166.37(16)	$N1-Co1-Co1^{1}$	172.65(10)
Co1-O1	2.027(3)	O2-Co1-O3	90.10(14)	C11-O1-Co1	124.4(3)
Co1-O2	2.020(3)	O2-Co1-O4	91.87(14)	$C20-O2-Co1^{1}$	124.1(3)
Co1-O3	2.026(3)	O2-Co1-N1	94.94(12)	C21-O3-Co1	130.4(3)
Co1-O4	2.033(3)	$O3-Co1-Co1^{1}$	77.68(11)	$C21-O4-Co1^{1}$	117.5(3)
Co1-N1	2.062(4)	O3-Co1-O1	87.10(15)	C1-N1-Co1	120.8(3)
$O1-Co1-Co1^{1}$	83.15(10)	O3-Co1-O4	165.73(15)	C1-N1-C5	117.5(4)
O1-Co1-O4	87.67(14)	O3-Co1-N1	95.23(14)	C5-N1-Co1	121.6(3)
O1-Co1-N1	98.60(12)	$O4-Co1-Co1^{1}$	88.52(11)		
$O2-Co1-Co1^{1}$	83.22(10)	O4-Co1-N1	98.68(15)		

Table 5.21: Selected torsion angles (°) for compound **22**.

C3-C6-N2-C7	-93.1	C5-N1-Co1-O4	-82.3
C14-C15-C16-C17	136.8	C5-N1-Co1-O1	-171.3
C24-C25-C25[1]-C24b	-148.8	C5-N1-Co1-O3	100.9
N1-Co1-O2-C20	170.6	C1-N1-Co1-O2	-172.6
N1-Co1-O3-C21	175.3	C1-N1-Co1-O4	94.9
N1-Co1-O1-C11	-174.8	C1-N1-Co1-O1	5.9
N1-Co1-O4-C21	178.9	C1-N1-Co1-O3	-81.9
C5-N1-Co1-O2	10.3	C26a-C25-C25[1]-C26	-161.6

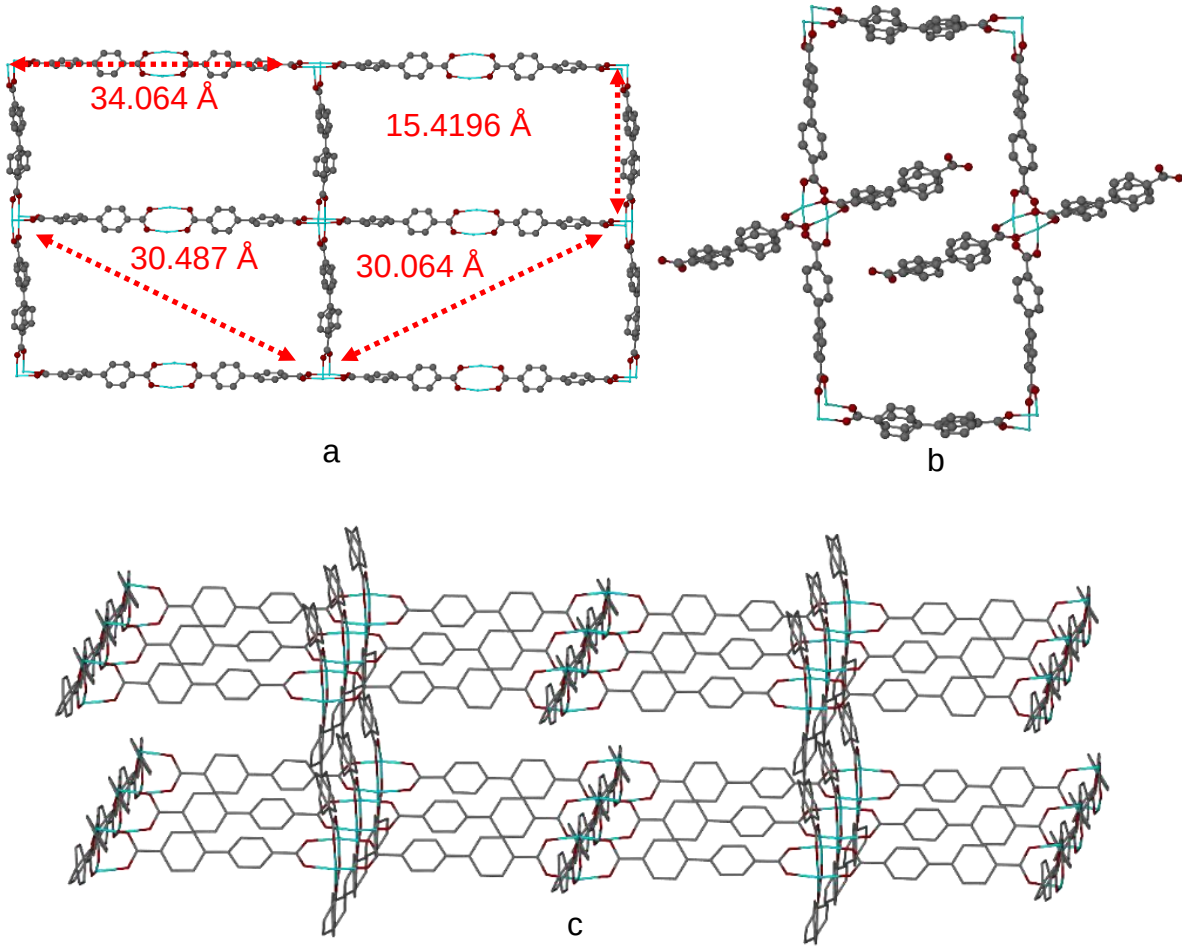

Figure 5.38: (a) $(Co_2)_6(bpdc)_6$ rectangle structure that expand to produce a 2D network. (b) Two Co(II) dimers from the rectangle structure are connecting between two different 2D networks by four $bpdc^{2-}$ molecules. (c) Co(II)-$bpdc^{2-}$ three-dimensional open network.

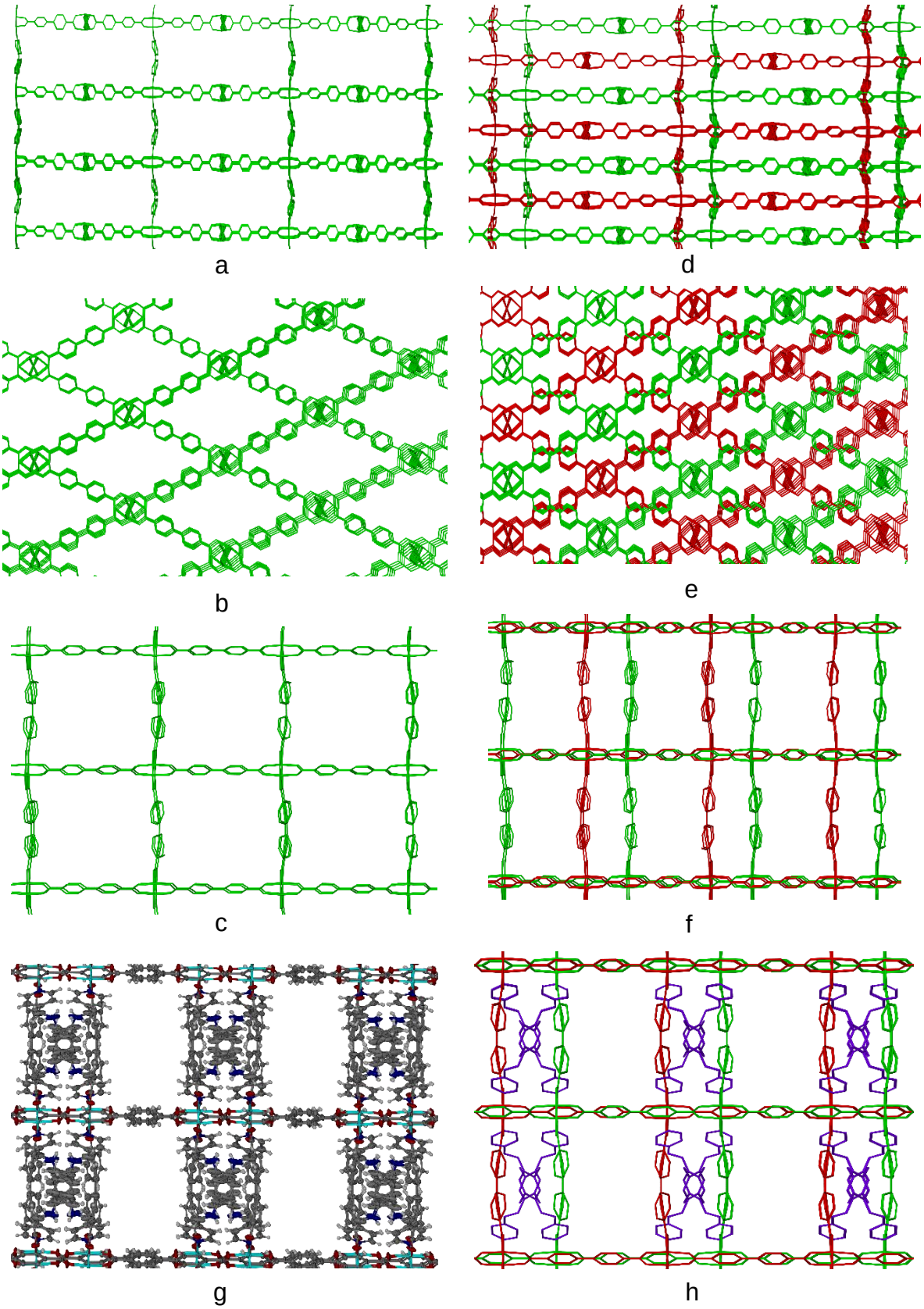

Figure 5.39: (a-c) Rectangle, rhombic and square shape channels for Co(II)-bpdc^{2-} 3D network. (d-f) Two interpenetrating Co(II)-bpdc^{2-} 3D networks. (g) Compound **22** single 3D network. (h) L3 ligand molecules (blue colour) connecting between two different Co(II)-bpdc^{2-} 3D networks to produce a single 3D network.

5.5.2.2 Crystal structure of $([Co_2(L3)(bpdc)_2])_n$ MOF (22)[a]

Compound **22** resultant crystals were washed with acetone to remove DMSO and DMF solvent guest molecules. Then, dried under vacuum for two days and exposed to the atmosphere to give the de-solvated material **22**[a]. Compound **22**[a] crystal structure was solved in orthorhombic space group *Ccce* and shows one Co(II) ion on a general position, half of L3 ligand molecule and two halves of $bpdc^{2-}$ molecules per asymmetric unit (figure 5.40). Co(II) ion in compound **22**[a] has similar coordination environment like compound **22** and shows coordination bond lengths of 2.031(3), 2.032(3), 2.028(3), 2.029(3) and 2.055(4) Å for Co1-O1, Co1-O2, Co1-O3, Co1-O4 and Co1-N1 to produce Co(II) square pyramid coordination centre (figure 5.41).

Coordinated $bpdc^{2-}$ molecules behave as tetra-dentate ligands to four different Co(II) ions and show four M-O coordination bond lengths (figure 5.41). $Co_2(bpdc)_4$ paddlewheel structure shows 2.664(12) Å distance between Co(II) ions and torsion angles of 142.8, -165.8 and 179.4 ° between $bpdc^{2-}$ phenyl rings (figure 5.41). Compound **22**[a] also forms $(Co_2)_6(bpdc)_6$ rectangle structure that shows 30.578 × 15.259 Å sides and 34.174 Å diagonal between Co(II) ions (figure 5.42). The resulted rectangle structure is expanding to produce Co(II)-$bpdc^{2-}$ two-dimensional network with 4^4 network topology (figure 5.42). Two Co(II) dimers from the rectangle structure are coordinated to two different 2D networks by four $bpdc^{2-}$ molecules and show 15.259 Å distance between Co(II) centres (figure 5.42). Co(II)-$bpdc^{2-}$ resulted three-dimensional network shows $(Co_2)_4(bpdc)_4$ square channels along *b* and *c* axes. $(Co_2)_4(bpdc)_4$ rhombic channels along *a* and *b* axes and $(Co_2)_6(bpdc)_6$ rectangle channels along *c* axis and between *a* and *b* axes (figure 5.43). Like compound **22** there are two Co(II)-$bpdc^{2-}$ 3D networks in the lattice and L3 ligand molecules are linking between them to produce a single 3D network (figure 5.43).

L3 ligand behaves as a bi-dentate ligand by nitrogen atoms of 4-pyridyl rings to two different Co(II) ions from two different Co(II)-$bpdc^{2-}$ 3D networks (Co1-L3-$Co1^1$= 17.494 Å) and shows torsion angle of -96.1 ° between dimethylphenyl and 4-pyridyl rings to produce L3 bent S-shape (figure 5.41). The resulted network is topologically identical to compound **22** and solvent accessible void space comprises approximately 34 % of the cell overall volume. Selected bond lengths, angles and torsion angles for compound **22**[a] are listed in tables 5.22 and 5.23.

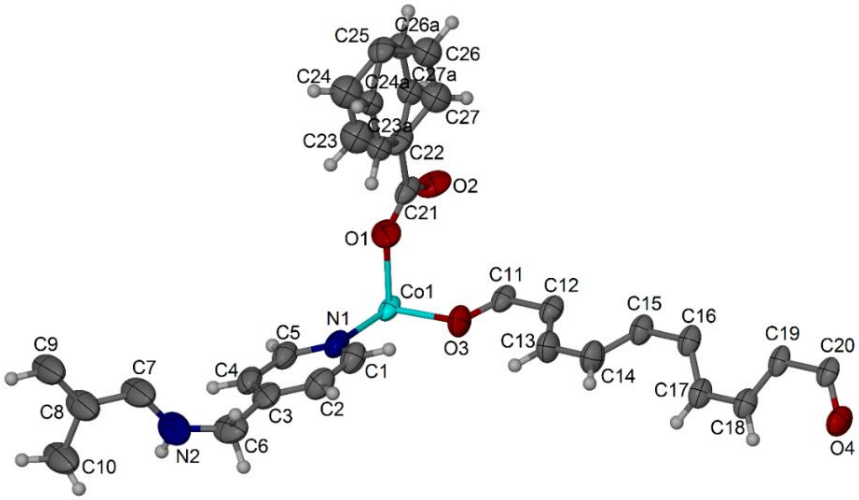

Figure 5.40: Compound **22**[a] asymmetric unit of the crystal structure. Ellipsoids shows at 50 % probability levels.

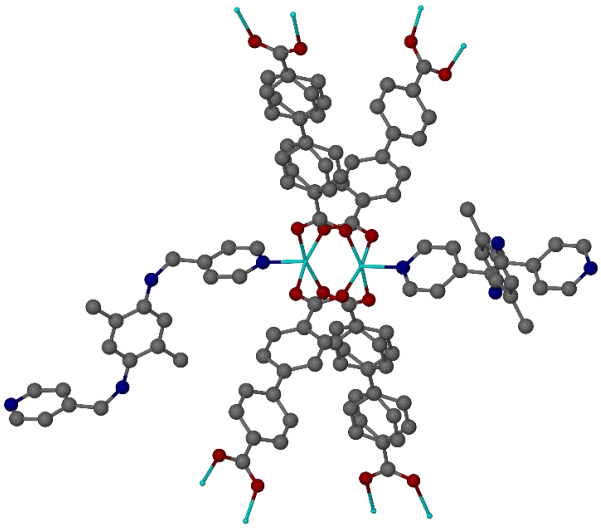

Figure 5.41: $Co_2(bpdc)_4(L3)_2$ structure that shows 2.664(12) Å distance between Co(II) ions. Torsion angles of 142.8, -165.8 and 179.4 ° between $bpdc^{2-}$ molecules. Torsion angle of -96.1 ° between dimethylphenyl and 4-pyridyl rings.

Table 5.22: Selected torsion angles (°) for compound **22**[a].

NI-Co1-O2-C21	-173.8	C5-N1-Co1-O2	-77.7
N1-Co1-O3-C11	-168.0	C5-N1-Co1-O3	-167.2
N1-Co1-O1-C21	-175.2	C18-C19-C20-O4	-8.1
N1-Co1-O4-C20	178.6	O2-C21-C22-C27a	-24.4
C1-N1-Co1-O1	-76.5	O2-C21-C22-C27	13.5
C1-N1-Co1-O4	-167.3	C24-C25-C25[1]-C24a	-165.8
C1-N1-Co1-O2	101.5	C26-C25-C25[1]-C26a	179.4
C1-N1-Co1-O3	11.9	C3-C6-N2-C7	-96.1
C5-N1-Co1-O1	104.3	C17-C16-C15-C14	142.8
C5-N1-Co1-O4	13.5	C13-C12-C11-O3	-5.5

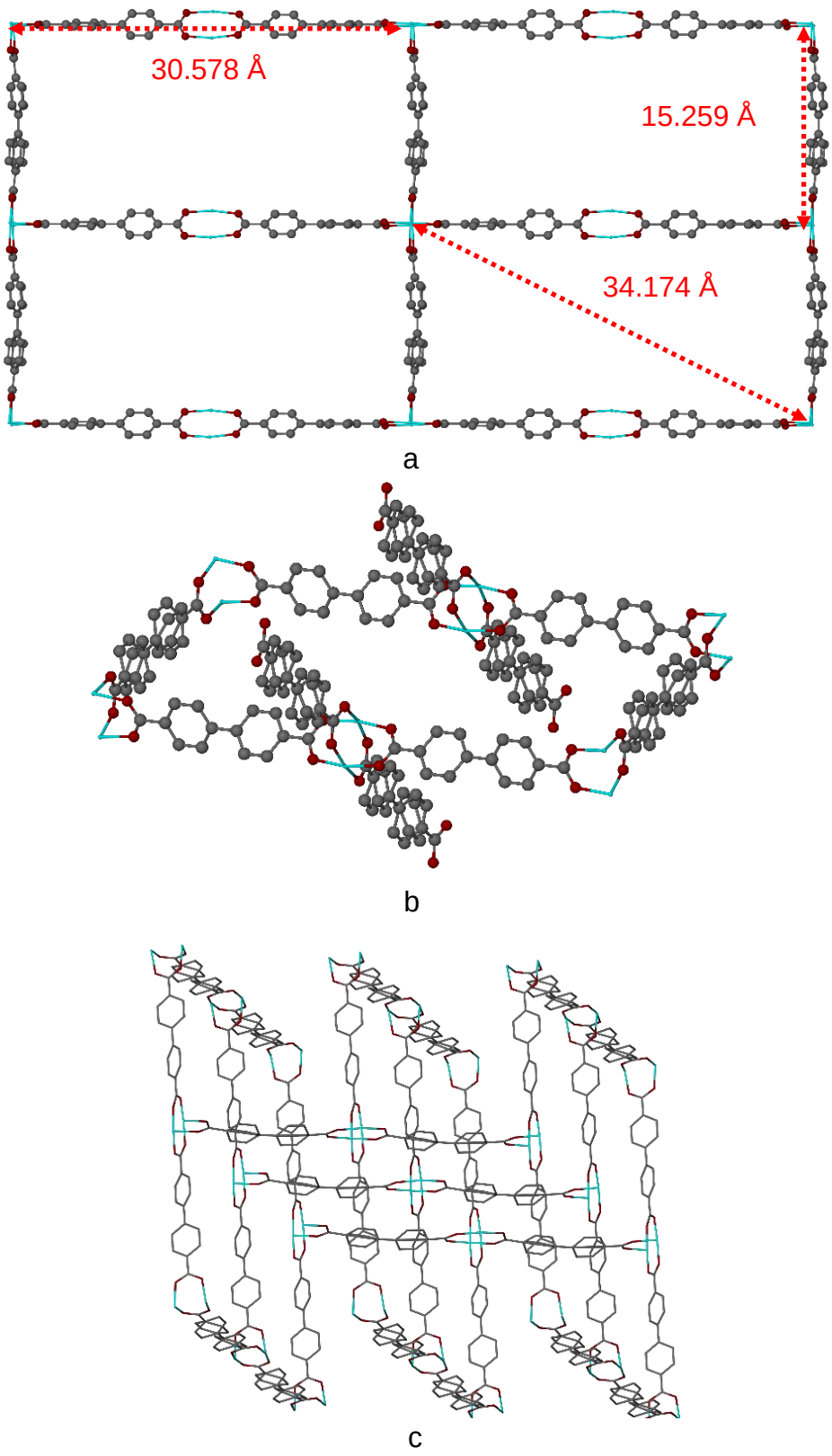

Figure 5.42: (a) $(Co_2)_6(bpdc)_6$ rectangle structure that shows 30.578 × 15.259 Å sides and 34.174 Å diagonal between Co(II) dimers and expands to produce a 2D network. (b) Two Co(II) dimers from $(Co_2)_6(bpdc)_6$ rectangle structure are coordinated to two different two-dimensional networks by four $bpdc^{2-}$ molecules. (c) Co(II)-$bpdc^{2-}$ three-dimensional open network.

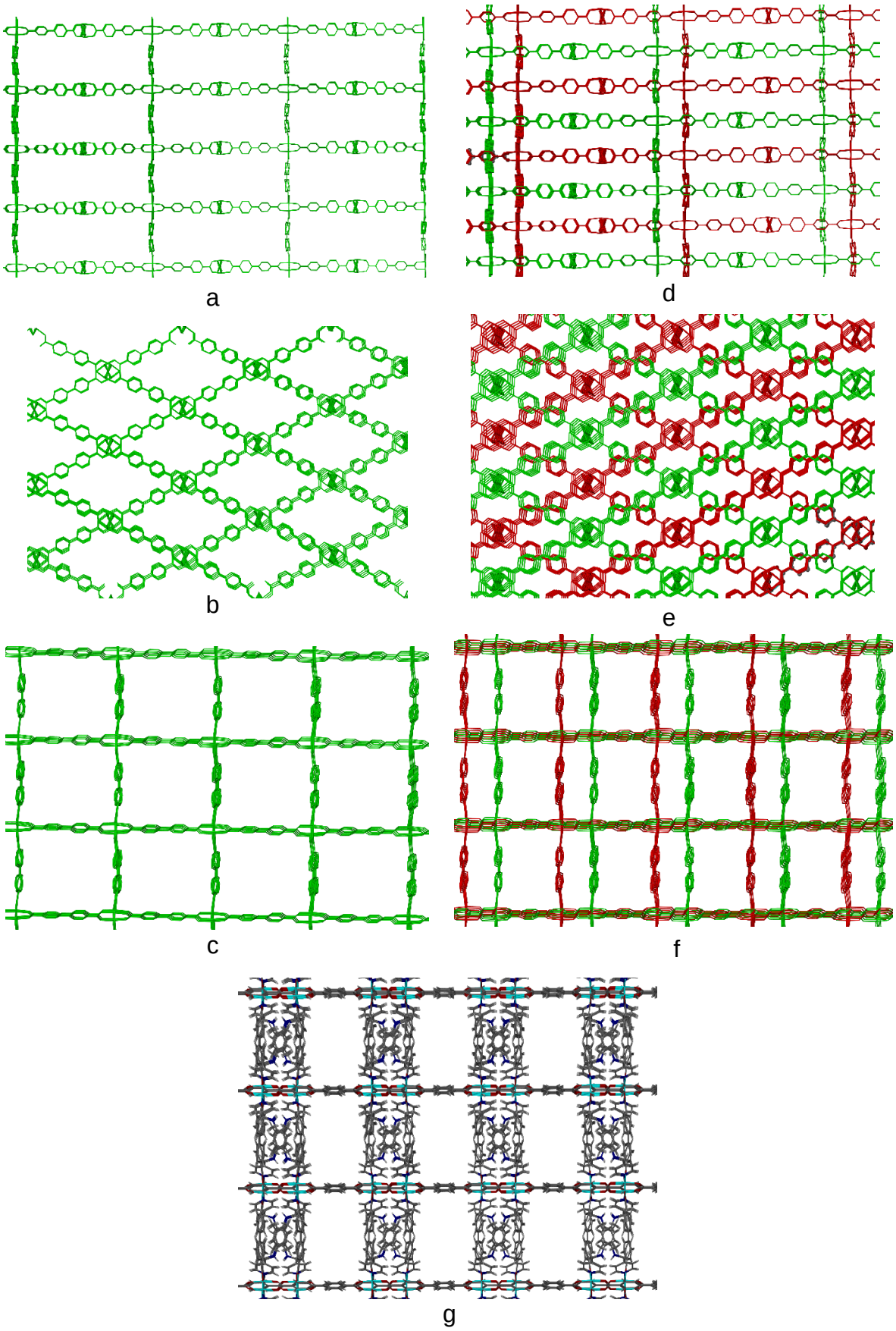

Figure 5.43: (a-c) Co(II)-bpdc^{2-} 3D open network rectangle, square and rhombic channels. (d-f) Two Co(II)-bpdc^{2-} interpenetrating 3D networks. (g) Compound **22**^{a} single 3D network.

Table 5.23: Selected bond lengths (Å) and angles (°) for compound **22**[a].

Co1-Co1[1]	2.664(12)	O4-Co1-O2	90.71(13)
Co1-O1	2.031(3)	O4-Co1-O3	167.78(14)
Co1-O2	2.032(3)	N1-Co1-O1	95.02(14)
Co1-O3	2.028(3)	N1-Co1-O2	97.82(14)
Co1-O4	2.029(3)	N1-Co1-O3	98.64(13)
Co1-N1	2.055(4)	N1-Co1-O4	93.56(13)
N2-C6	1.422(3)	C21-O1-Co1	128.7(3)
N2-C7	1.410(3)	C21-O2-Co1	117.2(3)
O2-Co1-O1	167.01(15)	C11-O3-Co1	123.0(3)
O3-Co1-O1	87.72(13)	C20-O4-Co1	123.2(3)
O3-Co1-O2	88.37(13)	C1-N1-Co1	121.0(3)
O4-Co1-O1	90.49(13)	C5-N1-Co1	122.1(3)

5.5.2.3 Crystal structure of ($[Co_2(L3)(bpdc)_2].n(EtOH))_n$ MOF (22)^{EtOH}

Compound **22**^{EtOH} crystal structure was solved in orthorhombic space group *Ccce* and shows one Co(II) ion on a general position, half of L3 ligand molecule, two halves of $bpdc^{2-}$ molecules and one and a half of ethanol molecule per asymmetric unit (figure 5.44). L3 ligand molecule shows ordered 4-pyridyl ring and disordered dimethylphenyl ring that refined at half occupancy. Like compounds **22** and **22**[a] one of the coordinated $bpdc^{2-}$ molecules is disordered and carbon atoms of phenyl rings were refined at half occupancy. Moreover, both ethanol molecules are refined at half occupancy. One also showed symmetry-related disorder and one position was refined with mixed C:O character, hydrogen atoms were not included for this ethanol molecule (figure 5.44). Co(II) ion has similar coordination environment in comparison with compounds **22** and **22**[a] and shows coordination bond lengths of 2.015(17), 2.023(18), 2.026(19), 2.028(19) and 2.062(2) Å for Co1-O1, Co1-O2, Co1-O3, Co1-O4 and Co1-N1 to form Co(II) square pyramid coordination centre (figure 5.45).

Coordinated $bpdc^{2-}$ molecules behave as tetra-dentated ligands by the deprotonated carboxylate groups to four different Co(II) ions and shows torsion angles of 142.1, 168.1 or 153.0 ° between phenyl rings (figure 5.45). Four $bpdc^{2-}$ molecules are coordinated to one Co(II) dimer to produce $Co_2(bpdc)_4$ paddlewheel structure Co1-Co1[1]= 2.677(6) Å (figure 5.45). Compound **22**^{EtOH} also forms $(Co_2)_6(bpdc)_6$ rectangle structure that has 30.510 × 15.246 Å sides and 34.107 Å diagonal between Co(II) dimers. Two Co(II) dimers from the rectangle structure are connecting between three Co(II)-$bpdc^{2-}$ 2D networks to produce Co(II)-$bpdc^{2-}$ three-dimensional network.

L3 ligand behaves as a bidentate ligand by nitrogen atoms of 4-pyridyl rings and shows torsion angles of 93.5 or 95.5 ° between the disordered dimethylphenyl ring and 4-pyridyl rings to produce L3 ligand bent S-shape. There are two Co(II)-$bpdc^{2-}$ three-dimensional network in the overall crystal lattice

and L3 ligand molecules are connecting between them to produce a single three-dimensional network (figure 5.46). Ethanol guest molecules occupy the resulted one-dimensional channels and show hydrogen bond interaction between them (EtOH-EtOH= 2.635 Å). Selected bond lengths, angles and torsion angles for compound **22**^{EtOH} are listed in tables 5.24 and 5.25.

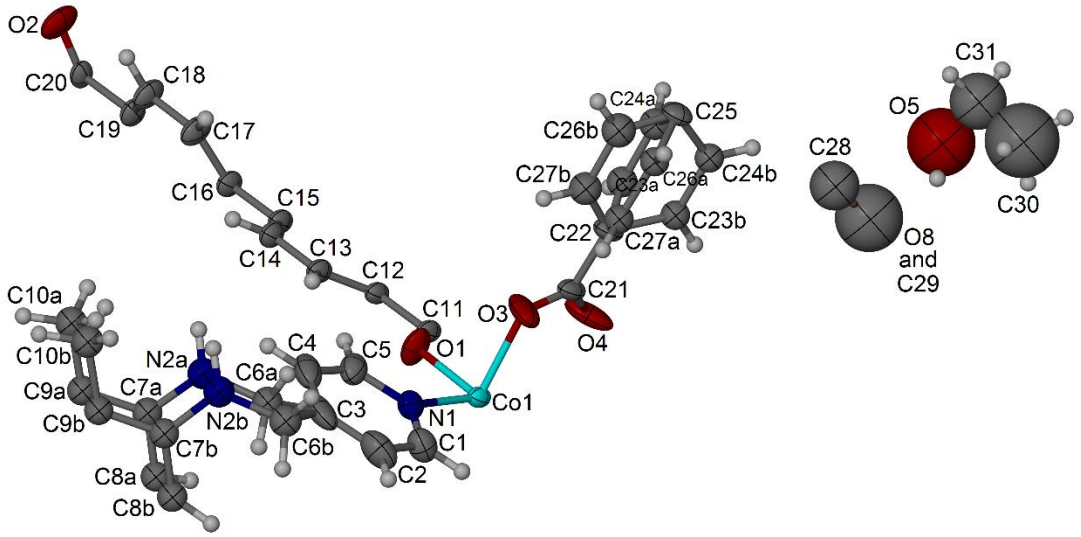

Figure 5.44: Compound **22**^{EtOH} asymmetric unit of the crystal structure, ellipsoids shows at 50 % probability levels.

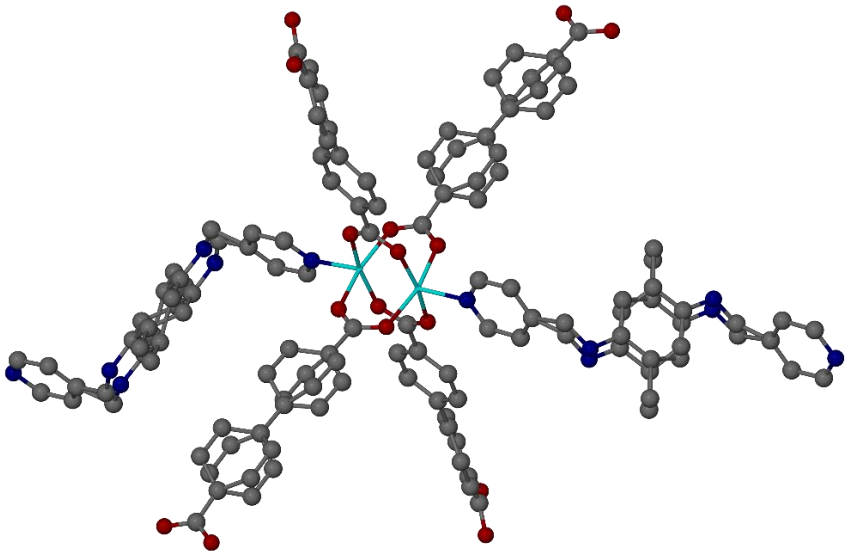

Figure 5.45: $Co_2(L3)_2(bpdc)_4$ structure that shows torsion angles of 142, 168.1 or 153 ° between $bpdc^{2-}$ phenyl rings, and 93.5 or 95.5 ° between dimethylphenyl and 4-pyridyl rings.

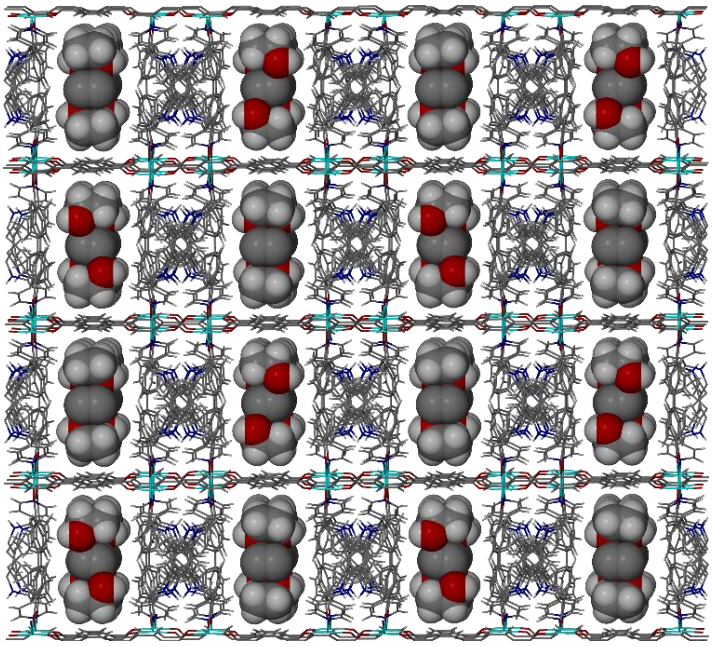

Figure 5.46: Compound **22**^{EtOH} 3D network that has one-dimensional open channels occupied by ethanol guest molecules.

Table 5.24: Selected bond lengths (Å) and angles (°) for compound **22**^{EtOH}.

Co1-Co1^{1}	2.677(6)	O4-Co1-O1	90.20(10)
Co1-O1	2.015(17)	O4-Co1-O2	87.59(10)
Co1-O2	2.023(18)	O4-Co1-O3	166.10(10)
Co1-O3	2.026(19)	N1-Co1-O1	93.71(8)
Co1-O4	2.028(19)	N1-Co1-O2	99.05(8)
Co1-N1	2.062(2)	N1-Co1-O3	99.01(10)
C7a-N2a	1.402(7)	N1-Co1-O4	94.70(9)
C6a-N2a	1.430(7)	C11-O1-Co1	123.84(16)
N2b-C6b	1.448(7)	C20-O2-Co1^{1}	123.66(17)
N2b-C7b	1.412(7)	C21-O3-Co1	118.37(18)
O2-Co1-O1	167.19(10)	C21-O4-Co1^{1}	130.58(19)
O3-Co1-O1	91.19(10)	C1-N1-Co1	120.97(17)
O3-Co1-O2	88.00(10)	C5-N1-Co1	121.80(19)

Table 5.25: Selected torsion angles (°) for compound **22**^{EtOH}.

N1-Co1-O1-C11	-174.5	C5-N1-Co1-O3	79.2
N1-Co1-O2-C20	170.2	C5-N1-Co1-O2	168.6
N1-Co1-O3-C21	178.2	C5-N1-Co1-O1	-12.6
N1-Co1-O4-C21	178.4	C5-N1-Co1-O4	-103.1
C1-N1-Co1-O2	-94	C14-C6a-N2a-C7a	93.5
C1-N1-Co1-O3	-98.8	C3-C6b-N2b-C7b	95.5
C1-N1-Co1-O1	169.4	C26a-C25-C25^{1}-C26b	168.1
C1-N1-Co1-O4	78.9	C24a-C25-C25^{1}-C24b	153.0
C14-C15-C16-C17	142.1		

5.5.2.4 Crystal structure of ($[Co_2(L3)(bpdc)_2].(H_2\text{-}bpdc).n(H_2O))_n$ MOF (22)^{H_2O}

Immersion of compound **22**^{a} crystals in water for one week produced compound **22**^{H_2O}. The resulted compound is isostructural with compounds **22**, **22**^{a} and **22**^{EtOH} materials with small differences in L3 ligand and $bpdc^{2-}$ torsion angles. Compound **22**^{H_2O} crystal structure was solved in orthorhombic space groups *Ccce* and shows one Co(II) ion on a general position, half of L3 ligand molecule, two coordinated $bpdc^{2-}$ half molecules and half H_2-bpdc guest molecule per asymmetric unit (figure 5.47). Co(II) ion has similar coordination environment like compound **22** with coordination bond lengths of 2.056(4), 2.020(3), 2.035(3), 2.043(3) and 2.033(3) Å for Co1-N1, Co1-O1, Co1-O2, Co1-O3 and Co1-O4 to produce Co(II) square pyramid coordination centre (figure 5.48).

Coordinated $bpdc^{2-}$ molecules behave as tetradentate ligands to four different Co(II) ions and shows torsion angles of -146.360, -179.495 and -175.261 ° between phenyl rings (figure 5.48). Four $bpdc^{2-}$ molecules are coordinated to one Co(II) dimer (Co1-Co1^{1}= 2.675(10) Å) to produce $Co_2(bpdc)_4$ paddlewheel structure (figure 5.48). Six Co(II) dimers and six $bpdc^{2-}$ molecules are coordinated to produce $(Co_2)_6(bpdc)_6$ rectangle structure that has 30.565 × 15.268 Å sides and 34.166 Å diagonal between Co(II) dimers (figure 5.48). The rectangle structure expands to produce Co(II)-$bpdc^{2-}$ two-dimensional network (figure 5.48). Moreover, two Co(II) dimers from the $(Co_2)_6(bpdc)_6$ rectangle structure are coordinated to two different Co(II)-$bpdc^{2-}$ 2D networks by four $bpdc^{2-}$ ligands to produce a single Co(II)-$bpdc^{2-}$ three-dimensional open network (figure 5.48). The resulted Co(II)-$bpdc^{2-}$ three-dimensional network shows $(Co_2)_4(bpdc)_4$ square channels along *b* and *c* axes. $(Co_2)_4(bpdc)_4$ rhombic channels along *a* and *b* axes and $(Co_2)_6(bpdc)_6$ rectangle channels along *c* and between *a* and *b* axes. There are two Co(II)-$bpdc^{2-}$ 3D networks in the overall crystal lattice and L3 ligand molecules are connecting between them.

L3 ligand behaves as a bi-dentate ligand to two different Co(II) ions from two different Co(II)-$bpdc^{2-}$ 3D networks (Co1-L3-Co1^{1}= 17.560 Å) and shows torsion angles of 98.201 ° between dimethylphenyl and 4-pyridyl rings to produce L3 bent S-shape and a single three-dimensional network. **22**^{H_2O} MOF crystal structure shows one dimensional open network channels occupied by H_2-bpdc molecules resulted from the MOF decomposition in water (figure 5.49). H_2-bpdc molecules were refined at half occupancy and show π-π stacking interaction with the ordered $bpdc^{2-}$ coordinated molecules (ring centroid separation= 3.61 Å). Selected bond lengths, angles and torsion angles for compound **22**^{H_2O} are listed in tables 5.26 and 5.27. Calculated powder XRD patterns for compounds **22**, **22**^{a}, **22**^{EtOH} and **22**^{H_2O} are consistent with each other and show a good match with compound **22** dried powder XRD pattern (figure 5.50).

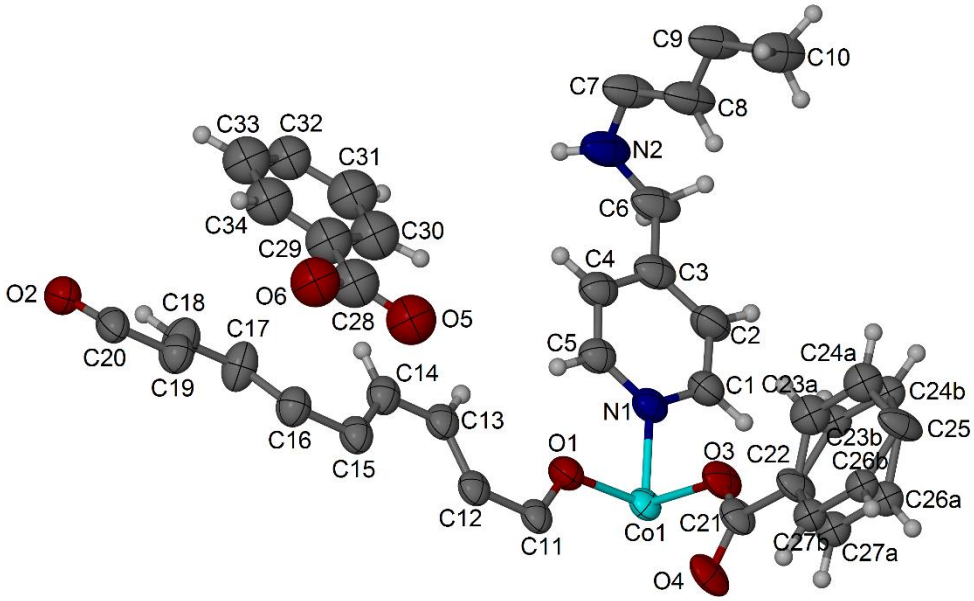

Figure 5.47: Compound **22**^{H_2O} asymmetric unit of the crystal structure, ellipsoids shown at 50 % probability levels.

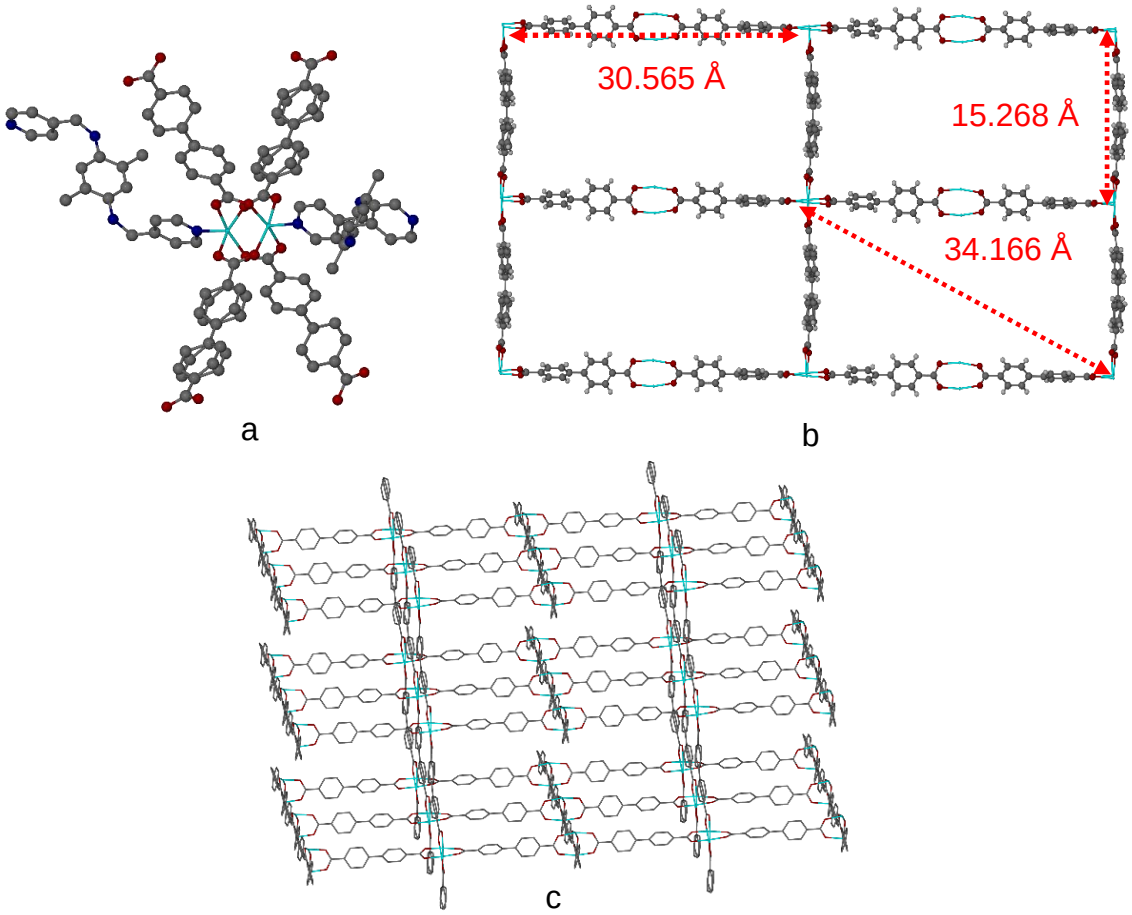

Figure 5.48: (a) $Co_2(bpdc)_4(L3)_2$ structure that shows torsion angles of -146.360, -179.495 or -175.261 ° for $bpdc^{2-}$ molecules and 98.201 ° for L3 ligand molecules. (b) Co(II)-$bpdc^{2-}$ 2D network that shows 30.565 × 15.265 Å sides and 34.166 Å diagonal between Co(II) dimers. (c) Co(II)-$bpdc^{2-}$ 3D network.

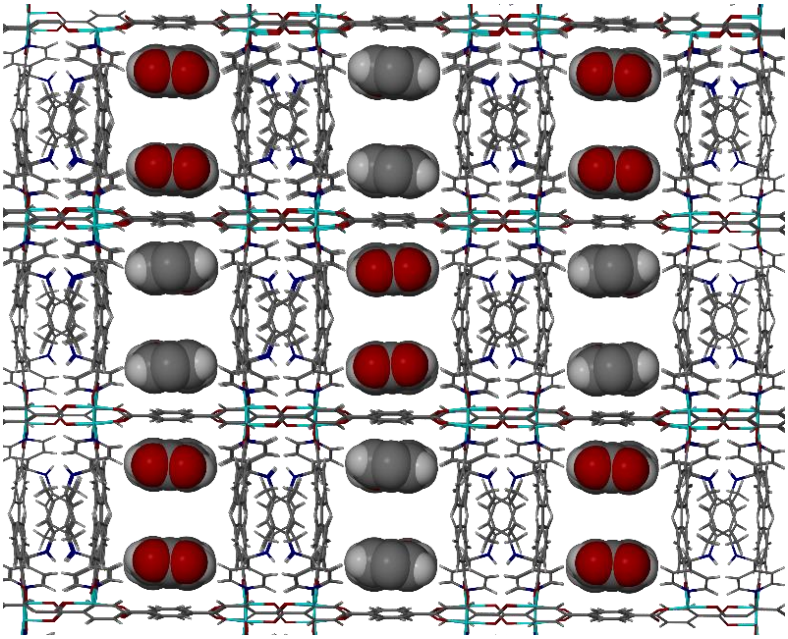

Figure 5.49: Compound **22**^{H_2O} one-dimensional open network that occupied by H_2-bpdc molecules (π-π interactions= 3.61 Å).

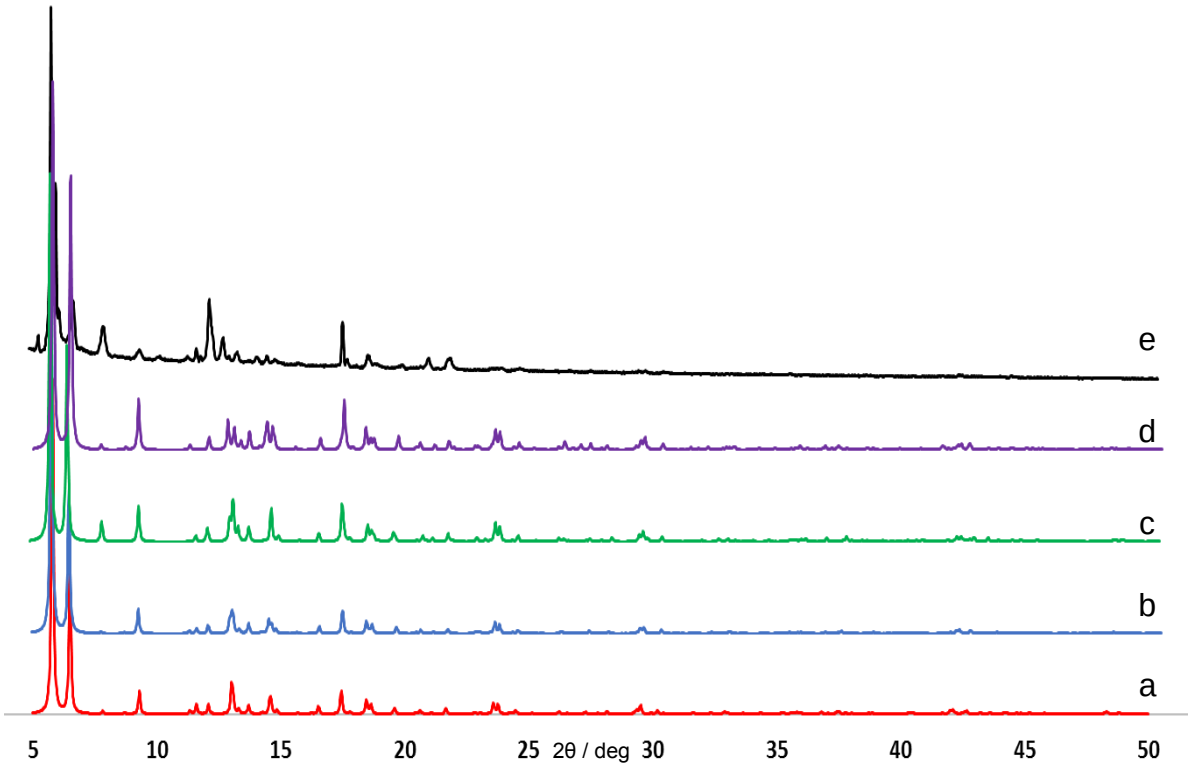

Figure 5.50: (a) Calculated powder XRD pattern for compound **22**. (b) Calculated powder XRD pattern for compound **22**^{a}. (c) Calculated powder XRD pattern for compound **22**^{EtOH}. (d) Calculated powder XRD pattern for compound **22**^{H_2O}. (e) Powder XRD pattern for compound **22**^{a}.

Table 5.26: Selected bond lengths (Å) and angles (°) for compound **22**^{H_2O}.

Co1-Co1^{1}	2.6754(10)	O3-Co1-O1	90.55(12)
Co1-O1	2.020(3)	O3-Co1-O2	87.64(13)
Co1-O2	2.035(3)	O4-Co1-O1	91.05(12)
Co1-O3	2.043(3)	O4-Co1-O2	87.87(12)
Co1-O4	2.033(3)	O4-Co1-O3	166.69(14)
Co1-N1	2.056(4)	N1-Co1-O1	93.68(12)
O1-C11	1.268(4)	N1-Co1-O2	99.16(12)
O2-C20	1.248(4)	N1-Co1-O3	94.91(13)
O3-C21	1.257(5)	N1-Co1-O4	98.17(14)
O4-C21	1.251(5)	C11-O1-Co1	123.0(3)
N1-C1	1.346(5)	C20-O2-Co1^{1}	122.3(3)
N1-C5	1.346(5)	C21-O3-Co1	127.1(3)
N2-C6	1.448(6)	C21-O4-Co1^{1}	118.2(3)
N2-C7	1.405(5)	C1-N1-Co1	120.4(3)
O2-Co1-O1	167.13(14)	C5-N1-Co1	121.5(3)

Table 5.27: Selected torsion angles (°) for compound **22**^{H_2O}.

C7-N2-C6-N3	98.201	N1-Co1-O1-C11	175.657
C1-N1-Co1-O2	-13.973	N1-Co1-O4-C12	170.252
C1-N1-Co1-O4	-103.117	N1-Co1-O2-C20	163.379
C1-N1-Co1-O1	165.294	C14-C15-C16-C17	-146.360
C1-N1-Co1-O3	74.425	C24b-C25-C25^{1}-C24a	-179.495
N1-Co1-O3-C21	168.992	C26a-C25-C25^{1}-C26b	-175.261

5.5.3 Thermogravimetric Analysis

5.5.3.1 Thermogravimetric analysis of compound 20

Thermal gravimetric analysis (TAG) trace for compound **20** as-synthesised in DMF at a fixed average of heating 5 °C per minute showed three weight losses. The first weight loss was equal to 33 % of the sample weight and occurred between 0-70 °C due to release of water guest molecules. The second weight loss was equal to 15 % of the sample weight and occurred from 71 to 202 °C due to release of DMF solvent molecules. Then, compound **20** was thermally stable from 203 to 380 °C. The third weight loss was equal to 21 % of the sample weight and happened between 385-465 °C due to decomposition of compound **20** (figure 5. 51). However, compound **20** resultant crystals as-synthesised in DMF showed a high uptake of water and DMF guest molecules up to 48 % of the sample weight. Compound **20** dried crystals TGA trace showed two weight losses, the first weight loss was equal to 13 % of the sample weight and occurred between 75-140 °C due to release of water and DMF guest molecules. Then, the activated

MOF was thermally stable from 145 to 372 °C. The second weight loss was equal to 40 % weight of the sample and occurred between 385-469 °C due to decomposition of activated MOFs (figure 5.51).

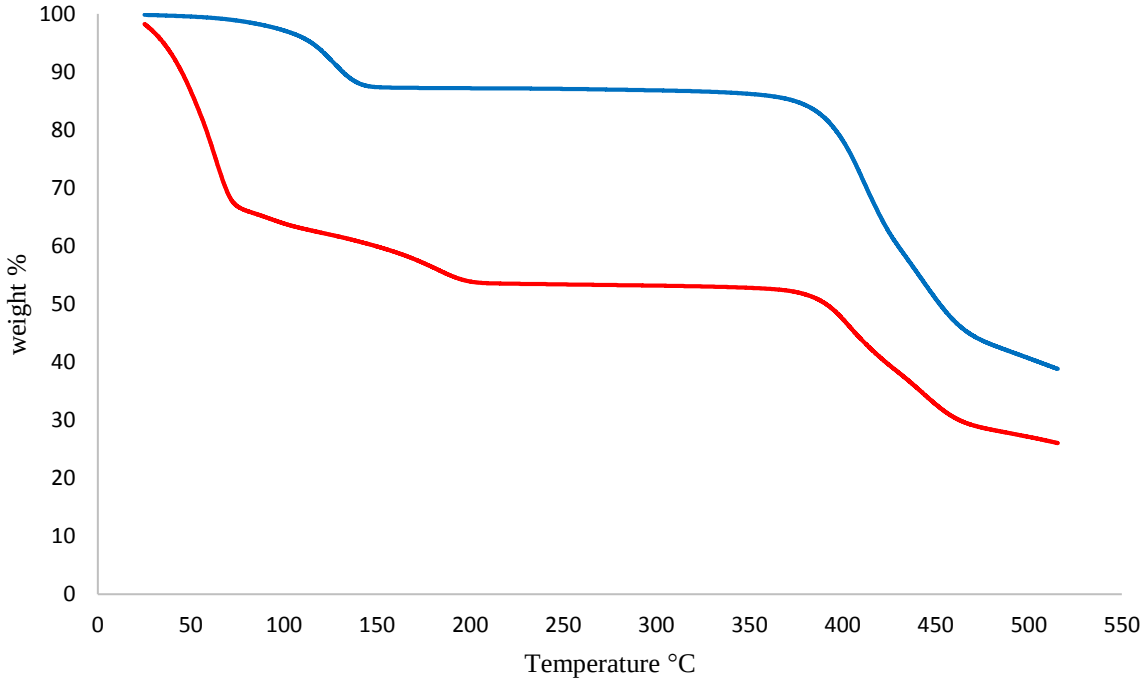

Figure 5.51: (red) TGA trace of compound **20** as-synthesised in DMF. (blue) TGA trace of activated compound **20**.

5.5.3.2 Thermogravimetric analysis of compound 22

Thermal gravimetric analysis trace for compound **22** as-synthesised in a mixture of DMSO and DMF at a fixed average of heating 5 °C per minute showed four weight losses. The first weight loss was equal to 42 % of the sample weight and occurred between 0-87 °C due to release of water guest molecules. The second weight loss was equal to 11 % of the sample weight and occurred between 88-218 °C due to release of DMF and DMSO solvent molecules. Then, compound **22** was thermally stable from 226 to 357 °C. The third weight loss was equal to 13 % of the sample weight and occurred between 358-401 °C due to L3 ligand molecules decomposition. The final weight loss was equal to 17 % of the sample weight and happened from 405 to 497 °C due to Co(II)-bpdc^{2-} 3D network decomposition (figure 5.52). Compound **22** TGA trace in a mixture of DMSO and DMF shows high solvents uptake up to 53 % of the sample weight that may due to L3 ligand amines hydrogen bond interaction with guest molecules and the significant open one-dimensional channels. Compound **22**^{a} was thermally stable from 0 to 347 °C and showed only 6 % weight loss of the sample weight. Then compound **22**^{a} showed two weight losses. The first weight loss was equal to 23 % of the sample weight and occurred between 358-394 °C due to L3 ligand molecules decomposition. The second weight loss was equal to 38 % weight of the sample and happened between 396-494 °C due to Co(II)-bpdc^{2-} 3D network decomposition (figure 5. 52).

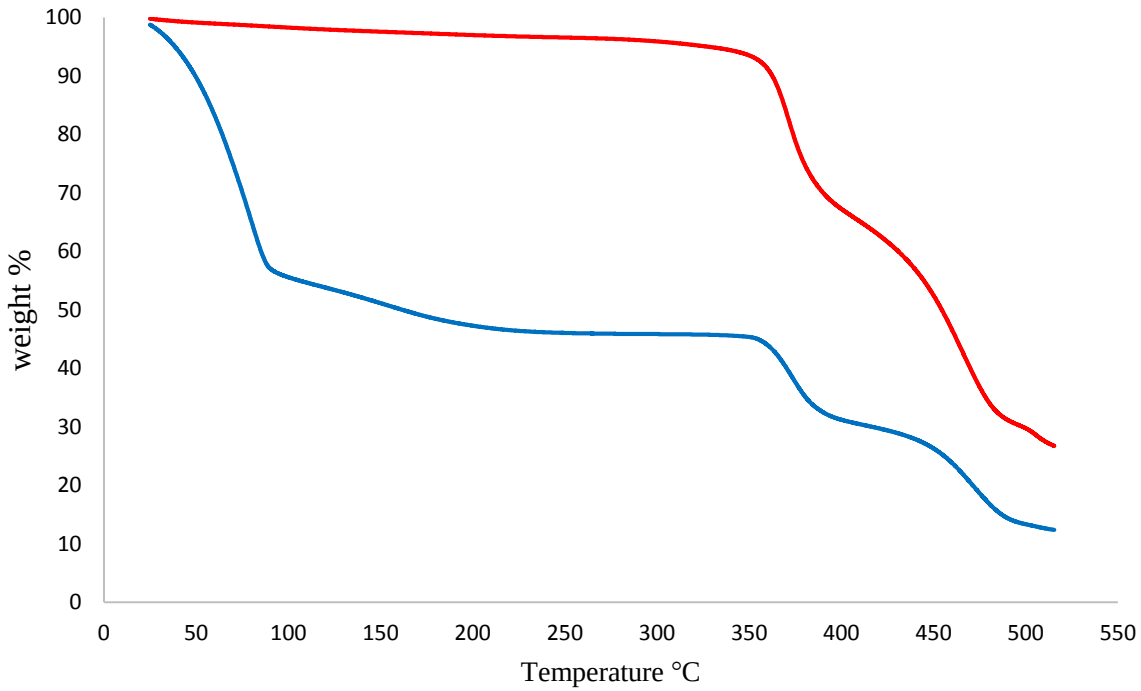

Figure 5.52: (blue) Thermal gravimetric analysis trace of compound **22** as-synthesised. (red) TGA trace of compound **22**[a] .

5.5.4 Gas sorption studies

Compounds **20** and **22** resultant crystals were washed with acetone for a few days and dried under vacuum for two days to produce compounds **20** and **22** activated crystals. The activated crystals were heated at 100 °C for 900 minutes to remove any possible guest molecules and evacuated for 180 minutes on the sample port prior to the gas measurement starting. Compounds **20** and **22** are porous with Brunauer–Emmett–Teller (BET) and Langmuir surface areas equal to 378.093 and 428.776 m^2/g for compound **20** or 502.300 and 569.198 m^2/g for compound **22** through N_2 sorption. Compound **20** showed gas uptake equal to 4.778, 4.061, 1.391 or 0.297 mmol /g for N_2, H_2, CO_2 or CH_4 at 77 or 298 K (figure 5.53). On the other hand, compound **22** showed gas uptake equal to 6.255, 5.227, 1.002 or 0.203 mmol/g for N_2, H_2, CO_2 or CH_4 at 77 or 298 K (figure 5.54). However, hydrogen uptake for compounds **20** and **22** are equal to 20.30 or 26.1 % of H_2 uptake for NU-100 MOF which is one of the leading MOF H_2 absorbers [20].

Compounds **20** and **22** have pendant amine groups capable of forming hydrogen bond interactions. Both materials showed ethanol uptake equal to 97.16 or 91.36 cm^3/g with relative pressure equal to 0.9 at 289 K (figure 5.55). These are relatively high uptakes of ethanol for a metal-organic framework or a coordination polymer [106-109]. Moreover, compound **22** shows a simple isotherm but the sorption profile for compound **20** shows a stepped hysteresis that due to structural changes during the

guest uptake as we investigated this behaviour by single crystal determination before in sections 5.5.1.8, 5.5.1.9 and 5.5.2.3.

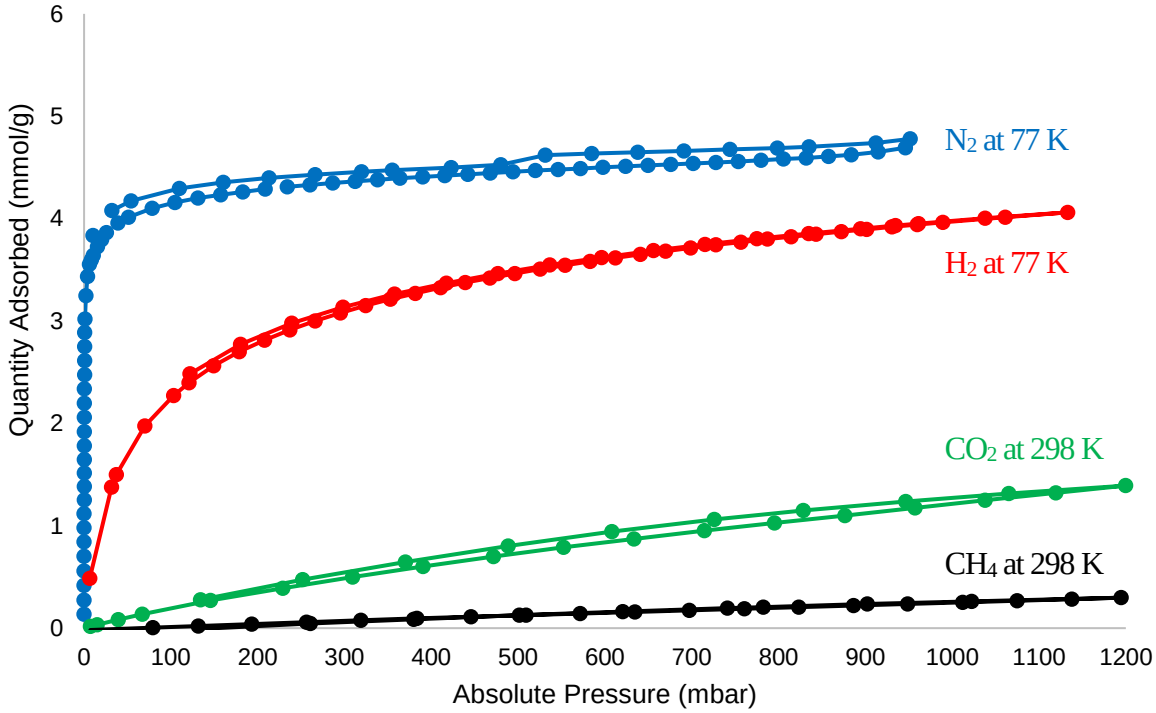

Figure 5.53: Gas sorption properties of activated compound **20**.

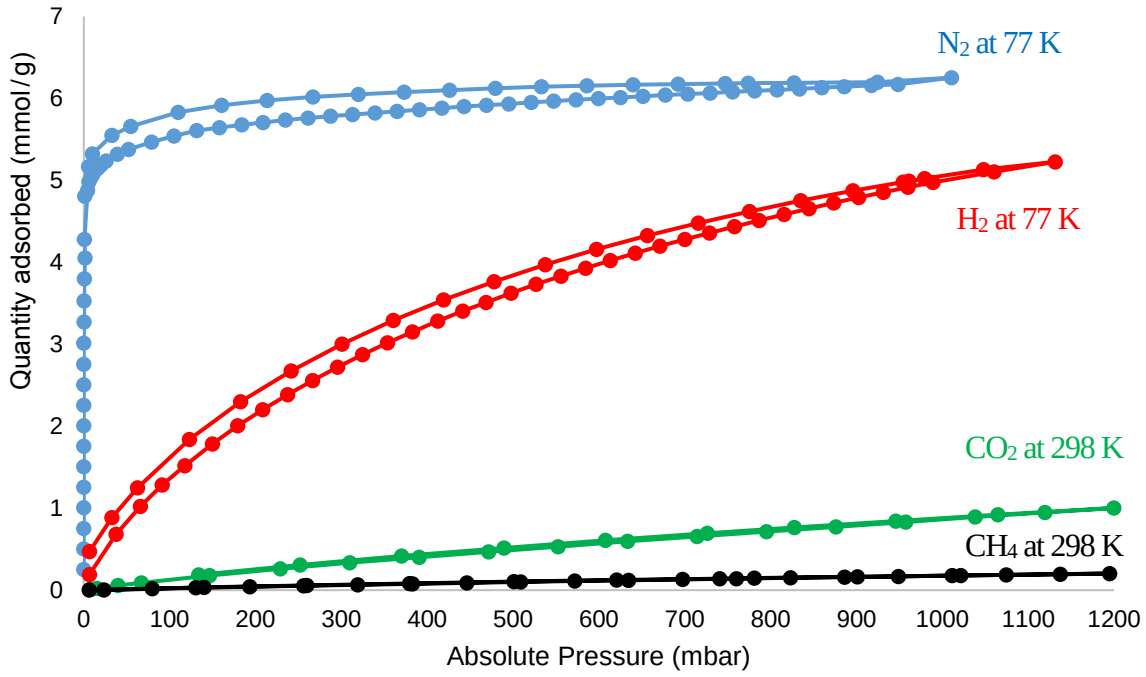

Figure 5.54: Gas sorption properties of activated compound **22**.

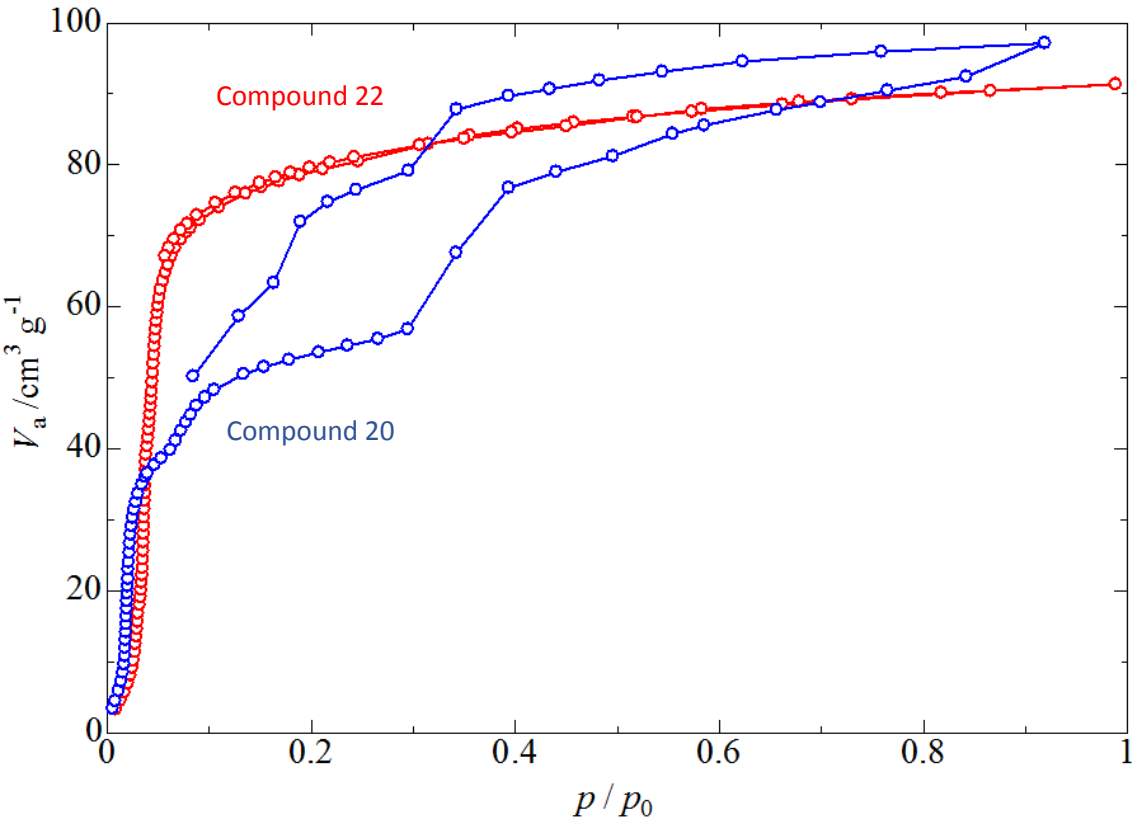

Figure 5.55: Ethanol isotherms of Compounds **20** and **22** at 298 K.

5.5.5 Crystal structure of $([Co(L3)_{0.5}(naph)])_n$ MOF

Solvothermal reaction of L3 ligand, naphthalene-2,6-dicarboxylic acid (H_2-naph) and $Co(NO_3)_2.6H_2O$ in DMF at 115 °C for 24 hours produced $([Co(L3)_{0.5}(naph)](H_2O).n(DMF))_n$ MOF (**23**). Compound **23** resultant crystals were washed by acetone for one week and dried under vacuum for two days to produce $([Co_2(L3)(naph)_2].H_2O)_n$ MOF $(\mathbf{23})^{H_2O}$. Immersion of compound $(\mathbf{23})^{H_2O}$ activated crystals in ethanol or water for one week produced a very poor diffracting crystals or an amorphous material unsuitable for single X-ray or powder XRD analysis. Powder XRD analysis for activated compound $\mathbf{23}^{H_2O}$ shows a good match with compound **23** and $\mathbf{23}^{H_2O}$ calculated powder XRD patterns. Moreover, activated compound $\mathbf{23}^{H_2O}$ shows low nitrogen and hydrogen gases uptake of 0.692 or 0.538 mmol/g and BET surface area equal to 12.261 m^2/g.

5.5.5.1 Crystal structure of $([Co(L3)_{0.5}(naph)].(H_2O).n(DMF))_n$ MOF (23)

Compound **23** crystal structure was solved in triclinic space group $P\bar{1}$ and shows one Co(II) ion on a general position, half of L3 ligand molecule, two halves of naphthalene-2,6-dicarboxylate molecules and one disordered water molecule per asymmetric unit (figure 5.56). Co(II) ion is coordinated to four oxygen atoms from four different $naph^{2-}$ molecules along the equatorial axes and shows four coordination bond lengths of 2.109(4), 2.021(4), 2.024(4) and 2.033(4) Å for Co1-O1, Co1-O2, Co1-O3 and Co1-O4. Co(II) ion is also coordinated to one L3 ligand molecule along the axial axis (Co1-N1= 2.057(4) Å) to

produce Co(II) distorted square pyramid coordination centre (figure 5.57). Coordinated $naph^{2-}$ molecules behave as tetradentate ligands to four different Co(II) ions and shows four different M-O bond lengths. Four $naph^{2-}$ molecules are coordinated to one Co(II) dimer ($Co1\text{-}Co1^{1}$= 2.7522(14) Å) to produce $Co_2(naph)_4$ paddlewheel structure (figure 5.57). Four Co(II) dimers and four $naph^{2-}$ molecules are coordinated to produce $(Co_2)_4(naph)_4$ square unit that shows 12.929 × 13.099 Å between $naph^{2-}$ molecules and 19.840 × 16.848 Å diagonals between Co(II) dimers (figure 5.57). $(Co_2)_4(naph)_4$ square unit is expanding to produce Co(II)-$naph^{2-}$ two-dimensional network that has 4^4 network topology (figure 4.57).

L3 ligand behaves as a bidentate ligand by nitrogen atoms of 4-pyridyl rings to two different Co(II) ions from two different Co(II)-$naph^{2-}$ 2D networks ($Co1\text{-}L3\text{-}Co1^{1}$= 19.717 Å) and shows torsion angle of -178.961 Å between dimethylphenyl and 4-pyridyl rings. Eight Co(II) dimers, eight $naph^{2-}$ molecules and four L3 ligand molecules are coordinated to produce $(Co_2)_8(L3)_4(naph)_8$ tetragonal structure that shows 12.929 and 13.099 Å between L3 ligand molecules (figure 5.57). The resultant tetragonal structure is expanding to form a three-dimensional open network that shows $(Co_2)_4(L3)_2(naph)_2$ rectangle channels along *a* and *b* axes, $(Co_2)_4(L3)_2(naph)_2$ rectangle channels along *c* axis and between *a*-*b* axes, $(Co_2)_4(naph)_4$ square channels along *b* and *c* axes. The resulted 3D open network is interpenetrating with two 3D networks to produce the three-fold interpenetrating MOF structure (figure 5.58). Moreover, the resulted 3D MOF shows one-dimensional open channels occupied by water guest molecules (figure 5.58). Selected bond lengths angles and torsion angles for compound **23** are listed in tables 5.28 and 5.29.

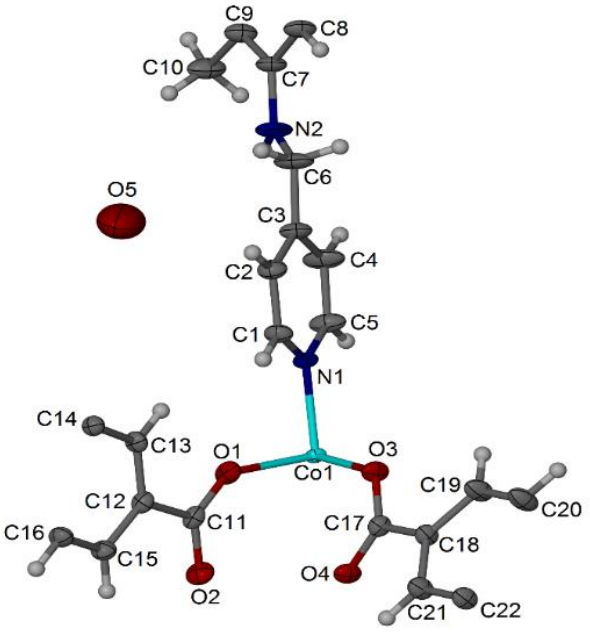

Figure 5.56: Compound **23** asymmetric unit of the crystal structure, ellipsoids shown at 50 % probability levels.

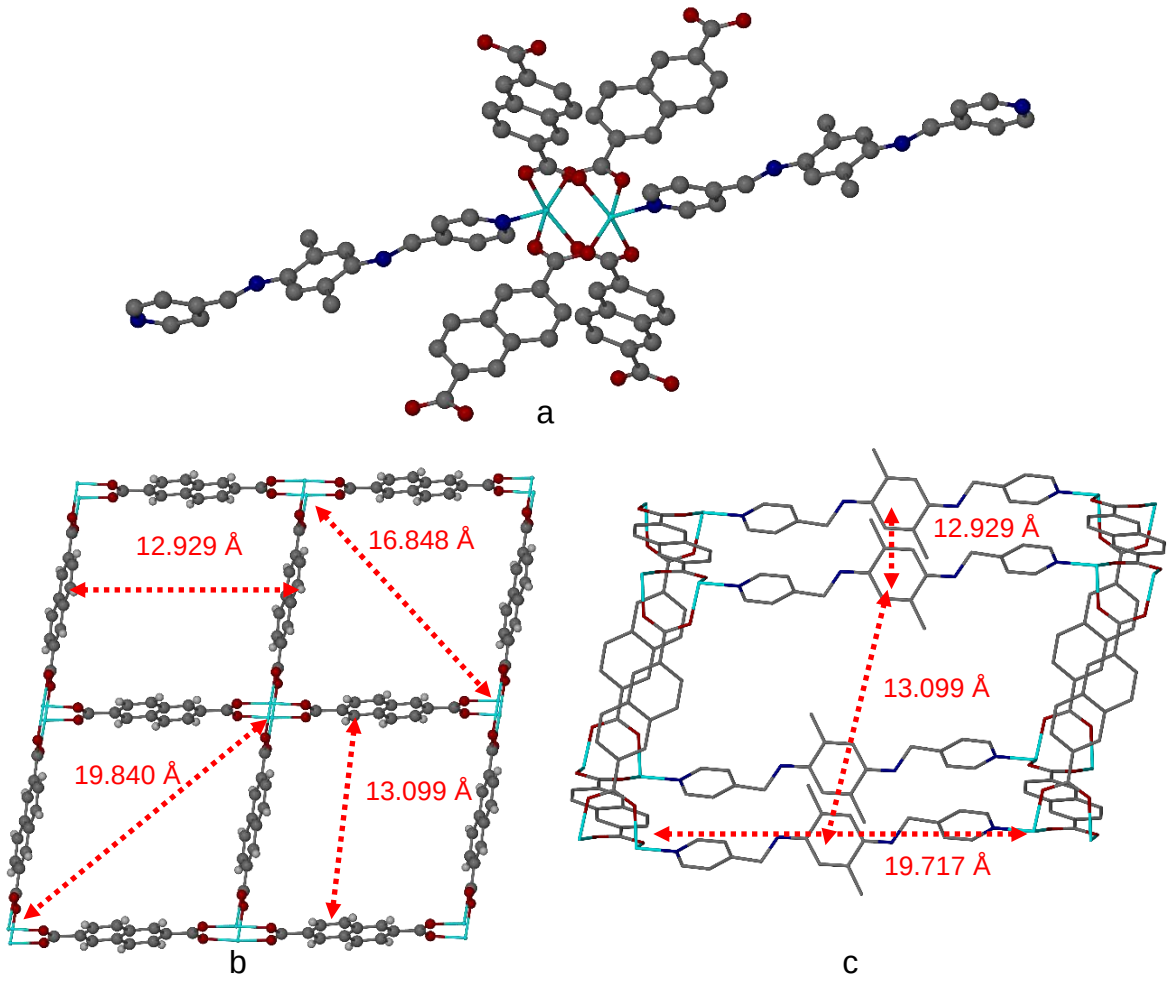

Figure 5.57: (a) Compound **23** paddlewheel structure that shows torsion angle of -178.961 ° for L3 ligand molecules and 2.7522(14) Å distance between Co1 and Co1[1]. (b) Co(II)-naph^{2-} 2D network that shows 12.929 × 13.099 Å between naph^{2-} molecules and 19.840 × 16.848 Å diagonals between Co(II) dimers. (c) $(Co_2)_8(L3)_4(naph)_8$ Tetragonal structure that shows 12.929 or 13.099 Å between L3 ligand molecules and 19.717 Å between Co(II) dimers.

Table 5.28: Selected bond lengths (Å) and angles angles (°) for compound **23**.

Co1-Co1[1]	2.752(14)	N1-C1	1.332(7)	N1-Co1-O1	92.99(17)
Co1-O1	2.109(4)	N1-C5	1.340(7)	N1-Co1-O2	101.30(18)
Co1-O2	2.021(4)	N2-C6	1.416(8)	N1-Co1-O3	98.94(16)
Co1-O3	2.024(4)	N2-C7	1.407(7)	N1-Co1-O4	94.52(16)
Co1-O4	2.033(4)	O2-Co1-O1	165.45(17)	C11-O1-Co1	140.6(4)
Co1-N1	2.057(4)	O3-Co1-O1	86.98(16)	C11-O2-Co1[1]	108.4(4)
O1-C11	1.256(7)	O3-Co1-O2	93.44(17)	C17-O3-Co1	120.2(3)
O2-C11	1.256(7)	O4-Co1-O1	87.18(16)	C17-O4-Co1[1]	128.5(3)
O3-C17	1.260(7)	O4-Co1-O2	88.94(17)	C1-N1-Co1	121.9(4)
O4-C17	1.262(7)	O4-Co1-O3	165.59(16)	C5-N1-Co1	120.2(4)

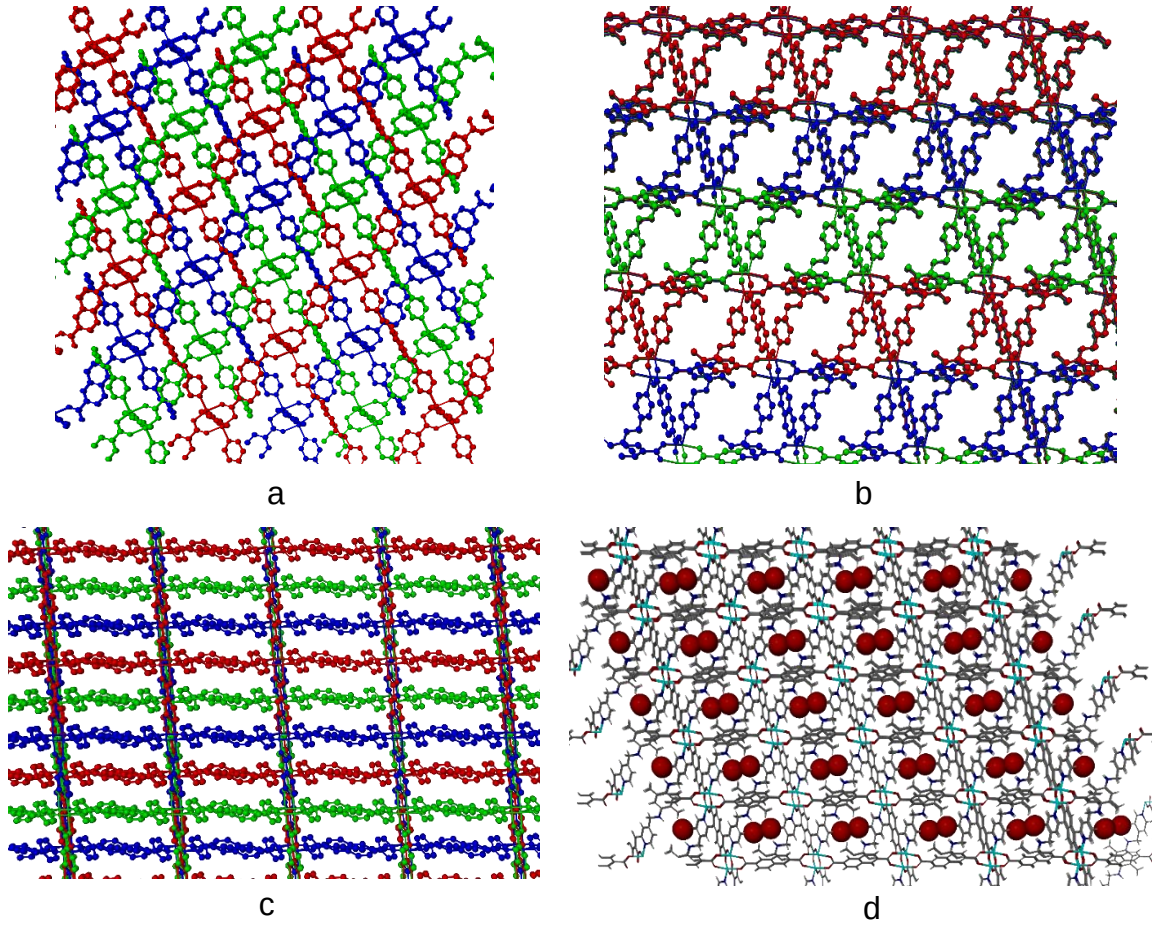

Figure 5.58: (a-c) Compound **23** three-fold interpenetrating network, water and hydrogen atoms were removed for clarity. (d) Water molecules occupy the resulted one-dimensional channels.

Table 5.29: Selected torsion angles (°) for compound **23**.

N1-Co1-O3-C17	162.051
N1-Co1-O1-C11	-178.588
N1-Co1-O4-C17	-160.090
N1-Co1-O2-C11	-170.877
C1-N1-Co1-O1	29.846
C1-N1-Co1-O3	-57.562
C1-N1-Co1-O4	117.253
C1-N1-Co1-O2	-152.923
C5-N1-Co1-O1	-151.365
C5-N1-Co1-O3	121.227
C5-N1-Co1-O4	25.866
C5-N1-Co1-O2	-63.958
C7-N2-C6-C3	-178.961

5.5.5.2 Crystal structure of $([Co(L3)_{0.5}(naph)].H_2O)_n$ MOF 23^{H_2O}

Compound **23** as-synthesised crystals were immersion in acetone for one week and dried under vacuum for two days to produce compound $\mathbf{23}^{H_2O}$. Compound $\mathbf{23}^{H_2O}$ crystal structure is isostructural with compound **23** and shows one Co(II) ion on general position, half of L3 ligand molecule, two halves of $naph^{2-}$ molecules and one disordered water molecule per asymmetric unit (figure 5.59). Co(II) ion has similar coordination environment in comparison with compound **23** and shows coordination bond lengths of 2.020(6), 2.111(6), 2.016(5), 2.035(5) and 2.059(6) Å for Co1-O1, Co1-O2, Co1-O3, Co1-O4 and Co1-N1. Four $naph^{2-}$ molecules are coordinated to Co(II) dimer ($Co1\text{-}Co1^1$= 2.752 Å) to produce $Co_2(naph)_4$ paddlewheel structure. Like compound **23**, compound $\mathbf{23}^{H_2O}$ forms $(Co_2)_4(naph)_4$ square unit that has 12.940 × 13.093 Å sides and 16.819 × 19.870 Å diagonal between Co(II) dimers and expanding to produce Co(II)-$naph^{2-}$ 2D network. L3 ligand behaves as a bidentate ligand and connecting between two Co(II)-$naph^{2-}$ 2D networks (Co1-L3-Co2= 19.714 Å) to produce a three-dimensional open network. The resulted 3D network is interpenetrating with two other 3D networks to produce a three-fold interpenetrating MOF structure with water molecules occupied the resulted one-dimensional channels (figure 5.59). Selected bond lengths, angles and torsion angles for compound $\mathbf{23}^{H_2O}$ are listed in tables 5.30 and 5.31.

Powder XRD analysis for compound $\mathbf{23}^{H_2O}$ shows a good match with compounds **23** and $\mathbf{23}^{H_2O}$ calculated powder XRD patterns which indicates phase purity and materials stability (figure 5.60). Thermal gravimetric analysis (TGA) for compound **23** at a fixed average of heating 5 °C per minute showed three weight losses. The first weight loss was equal to 48 % of the sample weight and occurred between 0-100 °C due to release of water guest molecules. The second weight loss was equal to 7 % of the sample weight and happened from 100 to 225 °C due to release of DMF solvent molecules. Then, the new MOF was thermally stable from 200 to 425 °C. The third weight loss was equal to 25 % of the sample weight and occurred between 410-475 °C due to decomposition of compound **23** (figure 5.61). Compound $\mathbf{23}^{H_2O}$ TGA trace showed two weight losses, the first weight loss was equal to 15 % of the sample weight and occurred between 150-211 °C due to guest molecules release. Then, the new MOF was thermally stable from 200 to 410 °C. The second weight loss was equal to 50 % weight of the sample and occurred from 410 to 465 °C due to the MOF decomposition (figure 5.61).

Compound $\mathbf{23}^{H_2O}$ resultant crystals were heated at 100 °C and held to 900 minutes to remove any possible guest molecules. Then, evacuated for 180 minutes on the sample port prior to the gas measurement starting. Compound **23** dried crystals showed low nitrogen (0.692 mmol/g) and hydrogen (0.538 mmol/ g) gases uptake at 77 K. Moreover, according to nitrogen gas sorption experiment compound **23** dried sample shows Brunauer–Emmett–Teller surface area equal to 12.2611 m^2/ g (figure 5.62).

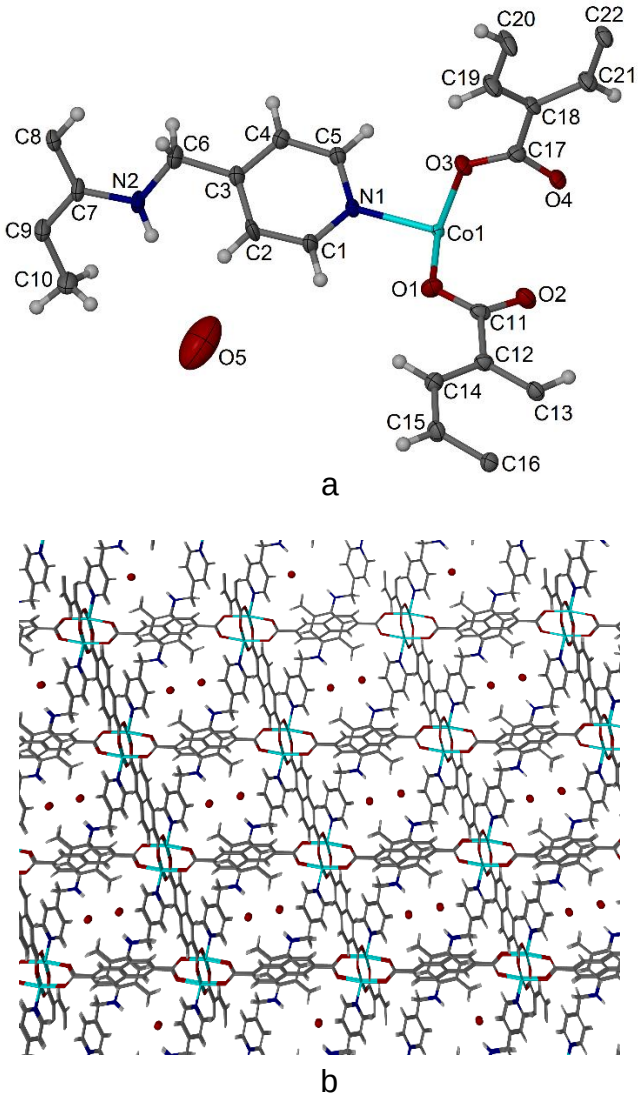

Figure 5.59: (a) Compound **23**^{H_2O} asymmetric unit of the crystal structure, ellipsoids shown at 50 % probability levels. (b) Three-fold MOF structure with water molecules occupy the one-dimensional channels.

Table 5.30: Selected torsion angles (°) for compound **23**^{H_2O}.

N1-Co1-O1-C11	170.8	C1-N1-Co1-O4	63.9
N1-Co1-O2-C11	179.0	C5-N1-Co1-O1	153.0
N1-Co1-O3-C17	-162.5	C5-N1-Co1-O2	-29.8
N1-Co1-O4-C17	160.2	C5-N1-Co1-O3	57.6
C1-N1-Co1-O1	-25.8	C5-N1-Co1-O4	-117.3
C1-N1-Co1-O2	151.3	C3-C6-N2-C7	178.9
C1-N1-Co1-O3	57.6		

Table 5.31: Selected bond lengths (Å) and angles (°) for compound **23**^{H_2O}.

Co1-O1	2.020(6)	O4-Co1-O3	165.5(2)
Co1-O2	2.111(6)	N1-Co1-O1	101.1(2)
Co1-O3	2.016(5)	N1-Co1-O2	93.0(2)
Co1-O4	2.034(5)	N1-Co1-O3	99.1(2)
Co1-N1	2.059(6)	N1-Co1-O4	94.4(2)
O1-C11	1.260(9)	C11-O1-Co1	108.7(5)
O2-C11	1.258(10)	C11-O2-Co1	140.3(5)
O3-C17	1.268(9)	C17-O3-Co1	120.8(5)
O4-C17	1.263(10)	C17-O4-Co1	128.9(5)
N1-C1	1.330(10)	C1-N1-Co1	120.7(5)
N1-C5	1.342(10)	C5-N1-Co1	121.6(5)
N2-C6	1.415(11)	C5-N1-C1	117.7(6)
N2-C7	1.418(10)	C7-N2-C6	118.4(7)
O2-Co1-O1	165.6(2)	C2-C1-N1	123.2(7)
O3-Co1-O1	93.5(2)	C4-C5-N1	123.3(7)
O3-Co1-O2	87.0(2)	C3-C6-N2	112.6(7)
O4-Co1-O1	88.9(2)	C8-C7-N2	121.8(7)
O4-Co1-O2	87.2(2)	C9-C7-N2	118.6(7)

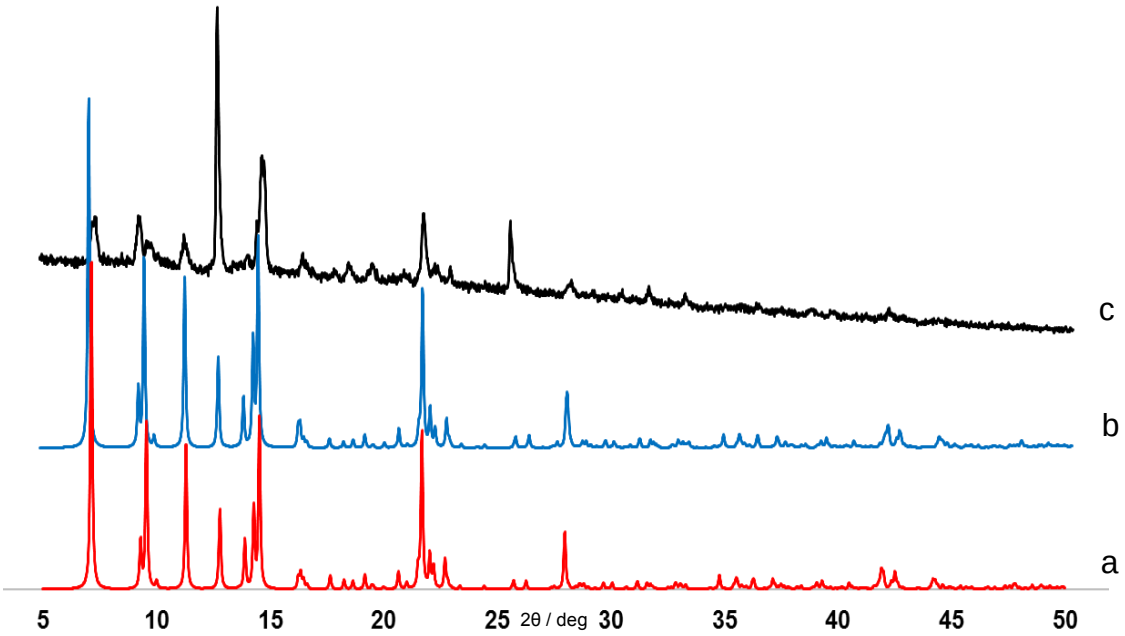

Figure 5.60: (a) Calculated powder XRD pattern for compound **23** as-synthesised in DMF. (b) Calculated powder XRD pattern for compound **23**^{H_2O}, (c) Powder XRD pattern for compound **23**^{H_2O}.

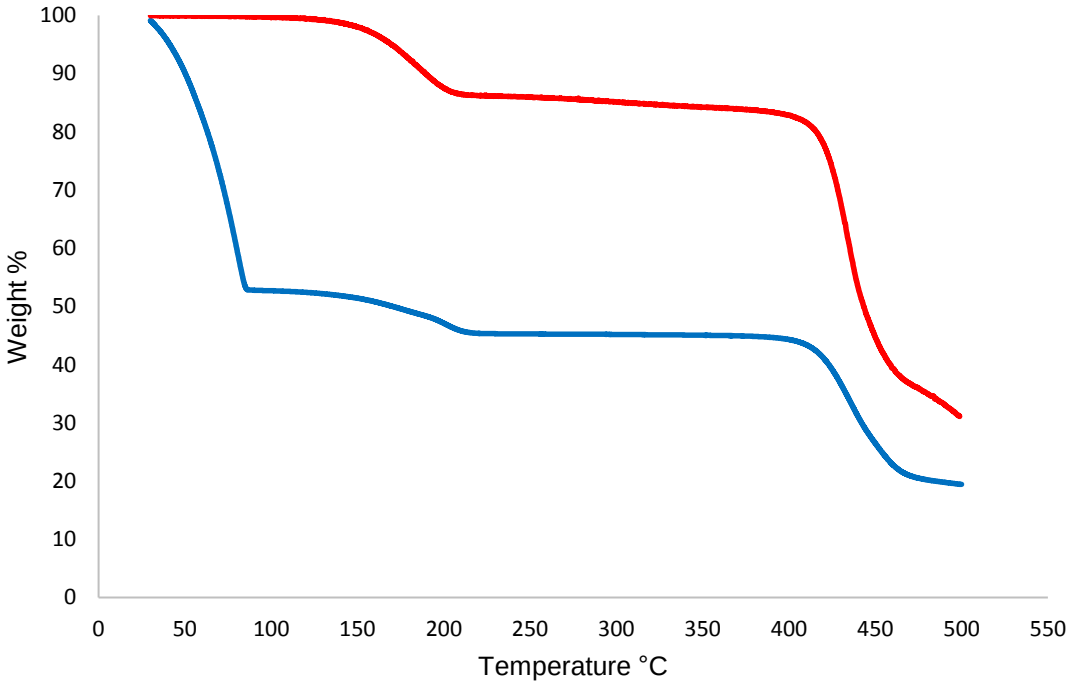

Figure 5.61: (blue) Thermal gravimetric analysis trace of compound **23** as-synthesised in DMF. (red) Thermal gravimetric analysis trace of compound **23**^{H_2O} dried sample.

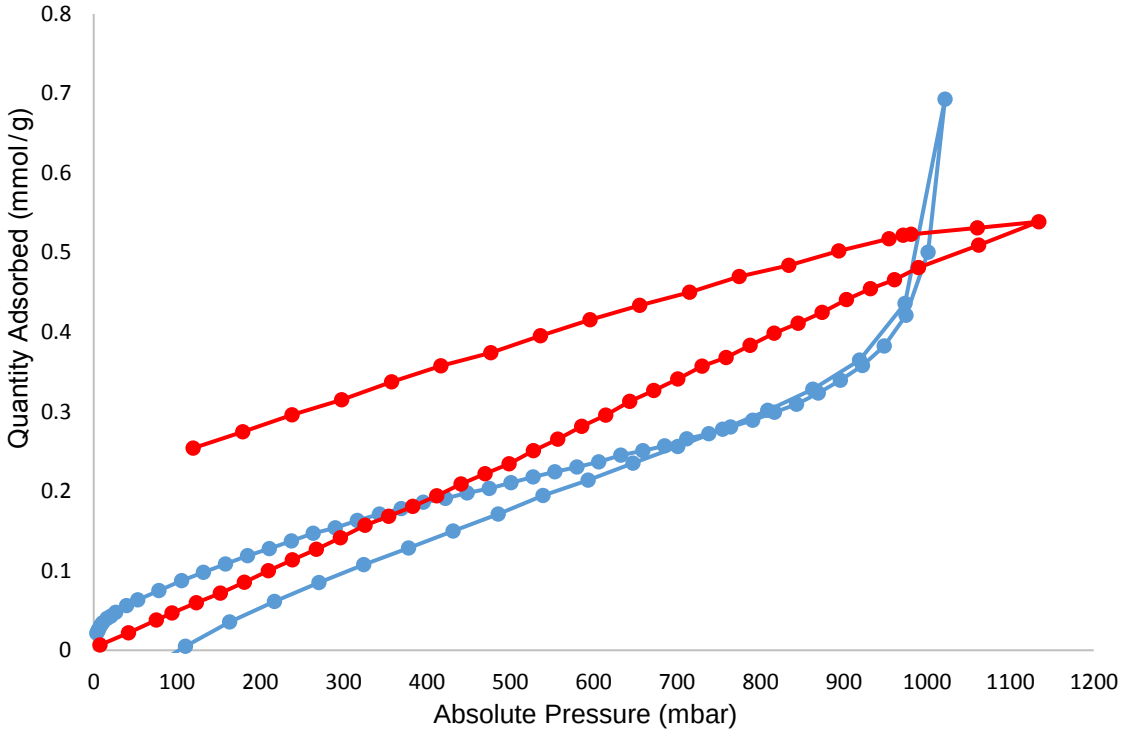

Figure 5.62: Nitrogen (blue) and hydrogen (red) gases isotherms sorption properties at 77 K for activated compound **23**.

Table 5.32: Crystallographic data of compounds α-**20**(L), β-**20**(S) and γ-**20**(L).

Identification code	α-**20**(L)	β-**20**(S)	γ-**20**(L)
Empirical Formula	$C_{36}H_{30}Co_2N_4O_8$	$C_{42}H_{44}Co_2N_6O_{10}$	$C_{39}H_{39}Co_2N_5O_{10}$
Formula weight	764.50	910.69	857.61
Temperature/*K*	120.0(2)	120.00(10)	150.00(10)
Crystal system	Triclinic	Monoclinic	Monoclinic
Space group	$P\bar{1}$	$P2_1/c$	$P2/n$
a/Å	10.9168(4)	18.6020(6)	19.4426(7)
b/Å	10.9505(4)	14.7768(4)	10.9351(4)
c/Å	20.5461(9)	15.9831(5)	21.3976(7)
α/°	90.147(3)	90	90
β/°	96.942(3)	101.524(3)	91.615(3)
γ/°	93.306(3)	90	90
Volume/Å^3	2433.99(17)	4304.8(2)	4547.5(3)
Z	2	4	4
ρ_{calc}g/cm^3	1.043	1.405	1.250
μ/mm^{-1}	5.684	0.834	0.784
F(000)	784.0	1888.0	1768.0
Crystal size/mm^3	0.25 × 0.12 × 0.09	0.53 × 0.32 × 0.26	0.38 × 0.25 × 0.137
Radiation	Cu *Kα* (λ = 1.54184)	Mo *Kα* (λ = 0.71073)	Mo *Kα* (λ = 0.71073)
2*Θ* range for data collection/°	8.088 to 148.034	6.658 to 59.292	6.52 to 49.998
Index ranges	-13 ≤ h ≤ 13, -11 ≤ k ≤ 13, -25 ≤ l ≤ 24	-25 ≤ h ≤ 24, -20 ≤ k ≤ 18, -16 ≤ l ≤ 21	-23 ≤ h ≤ 19, -13 ≤ k ≤ 12, -25 ≤ l ≤ 25
Reflections collected	18373	28170	25113
Independent reflections	9177 [R_{int} = 0.0408, R_{sigma} = 0.0559]	10480 [R_{int} = 0.0351, R_{sigma} = 0.0515]	7990 [R_{int} = 0.0363, R_{sigma} = 0.0425]
Data/restraints/parameters	9177/3/445	10480/0/547	7990/0/443
Goodness-of-fit on F^2	1.444	1.028	1.106
Final *R* indexes [*I*>=2*σ*(*I*)]	R_1 = 0.1203, wR_2 = 0.3526	R_1 = 0.0446, wR_2 = 0.0895	R_1 = 0.0942, wR_2 = 0.2660
Final *R* indexes [all data]	R_1 = 0.1438, wR_2 = 0.3722	R_1 = 0.0646, wR_2 = 0.0984	R_1 = 0.1074, wR_2 = 0.2756
Largest diff. peak/hole / e Å^{-3}	1.64/-0.78	1.08/-0.50	1.61/-0.70

Table 5.33: Crystallographic data of compounds δ-**20**(L), **21** and β-**20**(S)[ace].

Identification code	δ-**20**(L)	**21**	β-**20**(S)[ace]
Empirical Formula	$C_{36}H_{30}Co_2N_4O_8$	$C_{56}H_{53}Co_2N_8O_9$	$C_{40.5}H_{39.5}Co_2N_{4.5}O_{9.5}$
Formula weight	764.53	1099.92	859.12
Temperature/*K*	150.00(10)	100.15	173.15
Crystal system	Tetragonal	Monoclinic	Monoclinic
Space group	$P4_322$	$C2/c$	$P2_1/c$
a/Å	10.9831(3)	26.6119(4)	18.4764(5)
b/Å	10.9831(3)	29.6356(4)	14.7048(3)
c/Å	42.6078(16)	14.9189(2)	16.0370(4)
α/°	90	90	90
β/°	90	111.5000(10)	101.241(3)
γ/°	90	90	90
Volume/Å^3	5139.7(3)	10947.2(3)	4273.53(19)
Z	4	8	4
ρ_{calc}g/cm^3	0.9879	1.335	1.335
μ/mm^{-1}	0.684	0.618	0.834
F(000)	1571.5	4568.0	1776.0
Crystal size/mm^3	0.41 × 0.25 × 0.26	0.09 × 0.01 × 0.005	0.7 × 0.24 × 0.21
Radiation	Mo *Kα* (λ = 0.71073)	synchrotron (λ = 0.6889)	Mo *Kα* (λ = 0.71073)
2*Θ* range for data collection/°	6.5 to 59.3	3.188 to 72.002	6.69 to 59.416
Index ranges	-14 ≤ h ≤ 12, -15 ≤ k ≤ 10, -59 ≤ l ≤ 37	-44 ≤ h ≤ 43, -48 ≤ k ≤ 48, -24 ≤ l ≤ 24	-17 ≤ h ≤ 25, -17 ≤ k ≤ 20, -20 ≤ l ≤ 22
Reflections collected	15901	118396	29162
Independent reflections	6108 [R_{int} = 0.0594, R_{sigma} = 0.0860]	26414 [R_{int} = 0.0852, R_{sigma} = 0.1001]	10401 [R_{int} = 0.0342, R_{sigma} = 0.0498]
Data/restraints/parameters	6108/27/225	26414/4/661	10401/0/514
Goodness-of-fit on F^2	0.979	1.025	1.053
Final *R* indexes [$I>=2\sigma(I)$]	R_1 = 0.0571, wR_2 = 0.1470	R_1 = 0.0711, wR_2 = 0.2108	R_1 = 0.0630, wR_2 = 0.1640
Final *R* indexes [all data]	R_1 = 0.0762, wR_2 = 0.1573	R_1 = 0.1423, wR_2 = 0.2399	R_1 = 0.0881, wR_2 = 0.1784
Largest diff. peak/hole / e Å^{-3}	0.47/-0.55	1.54/-0.96	1.92/-0.47

Table 5.34: Crystallographic data of compounds ε-**20**(L), γ-**20**(L)^{EtOH} and ζ-**20**(S)^{EtOH}.

Identification code	ε-**20**(L)	γ-**20**(L)^{EtOH}	ζ-**20**(S)^{EtOH}
Empirical Formula	$C_{18}H_{15}CoN_2O_4$	$C_{36}H_{30}Co_2N_4O_8$	$C_{21}H_{24}CoN_2O_{5.5}$
Formula weight	382.26	764.50	451.35
Temperature/*K*	119.98(14)	100.15	100(1)
Crystal system	Triclinic	Monoclinic	Monoclinic
Space group	$P\bar{1}$	$P2/n$	$P2_1/n$
a/Å	9.634(5)	19.4488(4)	11.0172(5)
b/Å	10.822(5)	10.9238(9)	15.2551(5)
c/Å	10.943(4)	21.4481(9)	13.6887(8)
α/°	87.59(3)	90	90
β/°	69.58(4)	91.636(3)	101.478(4)
γ/°	87.10(4)	90	90
Volume/Å^3	1067.5(9)	4554.9(4)	2254.63(19)
Z	2	4	4
ρ_{calc}g/cm^3	1.1892	1.115	1.330
μ/mm^{-1}	6.481	0.714	0.790
F(000)	388.4	1568.0	940.0
Crystal size/mm^3	0.25 × 0.22 × 0.15	0.03 × 0.015 × 0.005	0.13 × 0.11 × 0.06
Radiation	Cu *Kα* (λ = 1.54184)	synchrotron (λ = 0.6889)	synchrotron (λ = 0.6889)
2*Θ* range for data collection/°	9.8 to 100	3.614 to 40.438	3.918 to 72.018
Index ranges	-10 ≤ h ≤ 11, -13 ≤ k ≤ 7, -12 ≤ l ≤ 13	-19 ≤ h ≤ 19, -10 ≤ k ≤ 10, -21 ≤ l ≤ 21	-18 ≤ h ≤ 18, -25 ≤ k ≤ 25, -22 ≤ l ≤ 23
Reflections collected	3770	33621	46540
Independent reflections	1641 [R_{int} = 0.0863, R_{sigma} = 0.0832]	4794 [R_{int} = 0.1741, R_{sigma} = 0.0774]	10868 [R_{int} = 0.1094, R_{sigma} = 0.0771]
Data/restraints/parameters	1641/3/94	4794/448/456	10868/0/294
Goodness-of-fit on F^2	2.266	1.806	1.106
Final *R* indexes [*I*>=2*σ*(*I*)]	R_1 = 0.2188, wR_2 = 0.5333	R_1 = 0.1776, wR_2 = 0.4472	R_1 = 0.0977, wR_2 = 0.2949
Final *R* indexes [all data]	R_1 = 0.2506, wR_2 = 0.5574	R_1 = 0.1865, wR_2 = 0.4569	R_1 = 0.1288, wR_2 = 0.3244
Largest diff. peak/hole / e Å^{-3}	2.30/-1.09	3.18/-1.01	3.82/-0.48

Table 5.35: Crystallographic data of compounds L3.2H_2O, **22** and **22**[a].

Identification code	L3.2H_2O	**22**	**22**[a]
Empirical Formula	$C_{20}H_{26}N_4O_2$	$C_{48}H_{38}Co_2N_4O_8$	$C_{48}H_{38}Co_2N_4O_8$
Formula weight	354.46	916.68	916.68
Temperature/*K*	100.15	120.0(2)	100.15(1)
Crystal system	Monoclinic	Orthorhombic	Orthorhombic
Space group	$P2_1/c$	*Ccce*	*Ccce*
a/Å	7.00330(10)	13.5858(2)	13.7228(3)
b/Å	27.2227(3)	27.1868(3)	27.2586(2)
c/Å	4.90870(10)	30.4870(4)	30.5782(3)
α/°	90	90	90
β/°	102.5150(10)	90	90
γ/°	90	90	90
Volume/Å^3	913.60(3)	11260.5(3)	11438.2(3)
Z	2	8	8
ρ_{calc}g/cm^3	1.2884	1.081	1.065
μ/mm^{-1}	0.080	4.992	0.621
F(000)	380.1	3776.0	3776.0
Crystal size/mm^3	0.08 × 0.04 × 0.023	0.24 × 0.12 × 0.09	0.175 × 0.065 × 0.03
Radiation	synchrotron (λ = 0.6889)	Cu *Kα* (λ = 1.54184)	synchrotron (λ = 0.6889)
2*Θ* range for data collection/°	2.9 to 71.72	7.832 to 147.52	2.582 to 49.998
Index ranges	-11 ≤ h ≤ 11, -45 ≤ k ≤ 44, -7 ≤ l ≤ 8	-16 ≤ h ≤ 16, -33 ≤ k ≤ 22, -37 ≤ l ≤ 36	-16 ≤ h ≤ 16, -33 ≤ k ≤ 33, -37 ≤ l ≤ 37
Reflections collected	19323	13937	68928
Independent reflections	4415 [R_{int} = 0.0517, R_{sigma} = 0.0380]	5553 [R_{int} = 0.0254, R_{sigma} = 0.0262]	5546 [R_{int} = 0.2081, R_{sigma} = 0.0765]
Data/restraints/parameters	4415/0/127	5553/0/280	5546/0/280
Goodness-of-fit on F^2	1.037	1.365	1.092
Final *R* indexes [I>=2σ (I)]	R_1 = 0.0426, wR_2 = 0.1285	R_1 = 0.0858, wR_2 = 0.2967	R_1 = 0.0909, wR_2 = 0.2465
Final *R* indexes [all data]	R_1 = 0.0516, wR_2 = 0.1341	R_1 = 0.0925, wR_2 = 0.3095	R_1 = 0.0981, wR_2 = 0.2538
Largest diff. peak/hole / e Å^{-3}	0.59/-0.63	1.46/-0.53	1.77/-0.65

Table 5.36: Crystallographic data of compounds **22**^{EtOH} and **22**^{H_2O}.

Identification code	**22**^{EtOH}	**22**^{H2O}
Empirical Formula	$C_{51}H_{45.5}Co_2N_4O_{9.5}$	$C_{55}H_{43}Co_2N_4O_{10}$
Formula weight	984.81	1036.83
Temperature/*K*	100(1)	100.15
Crystal system	Orthorhombic	Orthorhombic
Space group	*Ccce*	*Ccce*
a/Å	13.5202(2)	13.8627(2)
b/Å	27.3301(3)	27.2087(3)
c/Å	30.5099(3)	30.5649(5)
α/°	90	90
β/°	90	90
γ/°	90	90
Volume/Å^3	11273.7(2)	11528.7(3)
Z	8	8
ρ_{calc}g/cm^3	1.1580	1.1946
μ/mm^{-1}	0.592	0.583
F(000)	4065.6	4273.7
Crystal size/mm^3	0.2 × 0.15 × 0.06	0.23 × 0.08 × 0.04
Radiation	synchrotron (λ = 0.6889)	synchrotron (λ = 0.6889)
2Θ range for data collection/°	2.88 to 71.8	2.58 to 71.8
Index ranges	-22 ≤ h ≤ 21, -45 ≤ k ≤ 44, -50 ≤ l ≤ 51	-23 ≤ h ≤ 23, -46 ≤ k ≤ 46, -51 ≤ l ≤ 49
Reflections collected	114536	117849
Independent reflections	14032 [R_{int} = 0.0864, R_{sigma} = 0.0468]	14241 [R_{int} = 0.0746, R_{sigma} = 0.0475]
Data/restraints/parameters	14032/0/294	14241/0/316
Goodness-of-fit on F^2	1.080	1.720
Final *R* indexes [I>=2σ (I)]	R_1 = 0.0849, wR_2 = 0.2812	R_1 = 0.1575, wR_2 = 0.4557
Final *R* indexes [all data]	R_1 = 0.1065, wR_2 = 0.2988	R_1 = 0.1935, wR_2 = 0.4752
Largest diff. peak/hole / e Å^{-3}	1.30/-0.88	6.25/-1.28

Table 5.37: Crystallographic data of compounds **23** and **23**^{H_2O}.

Identification code	**23**	**23**^{H2O}
Empirical Formula	$C_{22}H_{19}CoN_2O_5$	$C_{22}H_{19}CoN_2O_5$
Formula weight	450	450
Temperature/*K*	150.01(10)	150.01(10)
Crystal system	Triclinic	Triclinic
Space group	$P\bar{1}$	$P\bar{1}$
a/Å	9.5946(4)	9.5882(5)
b/Å	9.7889(4)	9.7942(5)
c/Å	13.0988(5)	13.0926(6)
α/°	71.500(3)	71.441(4)
β/°	83.948(3)	84.137(4)
γ/°	83.667(3)	83.758(4)
Volume/Å^3	1156.31(8)	1155.68(10)
Z	2	2
ρ_{calc}g/cm^3	1.2875	1.2882
μ/mm^{-1}	6.098	6.102
F(000)	456.7	456.7
Crystal size/mm^3	0.177 × 0.257 × 0.313	0.134 × 0.185 × 0.388
Radiation	Cu *Kα* (λ = 1.54184)	Cu *Kα* (λ = 1.54184)
2*Θ* range for data collection/°	9.56 to 148.08	9.3 to 147.82
Index ranges	-11 ≤ h ≤ 10, -12 ≤ k ≤ 12, -16 ≤ l ≤ 15	-10 ≤ h ≤ 11, -12 ≤ k ≤ 12, -16 ≤ l ≤ 16
Reflections collected	12715	12746
Independent reflections	4442 [R_{int} = 0.0418, R_{sigma} = 0.0335]	4437 [R_{int} = 0.0517, R_{sigma} = 0.0465]
Data/restraints/parameters	4442/0/272	4437/0/272
Goodness-of-fit on F^2	0.985	1.032
Final *R* indexes [I>=2σ (I)]	R_1 = 0.0849, wR_2 = 0.2648	R_1 = 0.1053, wR_2 = 0.3247
Final *R* indexes [all data]	R_1 = 0.0871, wR_2 = 0.2674	R_1 = 0.1109, wR_2 = 0.3301
Largest diff. peak/hole / e Å^{-3}	3.26/-0.55	2.94/-0.75

5.6 Conclusion

In conclusion, simple ligands were utilised to produce novel MOF materials known as compounds **20**, **21**, **22** and **23**. Compounds **20**, **22** and **23** showed common structural transformations after desolvation or solvation for example, rings rotation, changes in torsion angles, changes in coordination bond lengths and angles. The conformational flexibility of L3 ligand in compound **20** produced four different phases consisting of two-fold interpenetrating 3D networks with one-dimensional or two-dimensional open network channels. All phases of compound **20** showed significant accessible void spaces between 34-39 % of the unit cell overall volume. Dimethylphenyl and 4-pyridyl rings rotation and torsion angles lead to more accessibility of L3 ligand secondary amines with potential for hydrogen bonding interactions. This, in addition to conformational flipping of L3 ligand in S-shape phases may account for complex isotherm ethanol sorption. Compound **21** shows two-fold interpenetrating 3D network MOF structure with no significant void spaces or open network channels suitable for guest molecules exchange. Compound **22** has a single MOF network that is self-catenating consisting of two Co(II)-bpdc^{2-} interpenetrating 3D networks and L3 ligand molecules connecting between them to produce a single three-dimensional MOF structure that has one-dimensional open channels. Compound **22** shows no significant changes after desolvation or solvation with ethanol. This due to the additional rigidity of the single 3D network structure in comparison with compound **20** two-fold interpenetrating networks. Moreover, compound **22** showed partial decomposition in water after one week where digested H_2-bpdc molecules could be located in the MOF channels. Compound **23** has a three-fold interpenetrating network structure with one-dimensional open channels occupied by guest molecules. However, compound **23** is not stable after solvation with water or ethanol and showed low uptake of H_2 and N_2 gases.

5.7 References

1. O. M. Yaghi, G. Li and H. Li, Selective binding and removal of guests in a microporous metal-organic framework. *Nature*. 1995, **378**, 703-706.
2. A. Schneemann, V. Bon, I. Schwedler, I. Senkovska, S. Kaskel and R. A. Fischer, Flexible metal-organic frameworks. *Chemical Society Reviews*. 2014, **43**(16), 6062-6096.
3. J. Gascon, A. Corma, F. Kapteijn and F. X. L. Xamena, Metal Organic Framework Catalysis: Quo vadis ?. *Journal of the American Chemical Society Catalysis*. 2014, **4**(2), 361-378.
4. T. Yamada, K. Otsubo, R. Makiurac and H. Kitagawa, Designer coordination polymers: dimensional crossover architectures and proton conduction. *Chemical Society Reviews*. 2013, **42**(16), 6655-6669.
5. J. R. Li, J. Sculley and H. C. Zhou, Metal-Organic Frameworks for Separations. *Chemical Reviews*. 2012, **112**(2), 869-932.
6. L. E. Kreno, K. Leong, O. K. Farha, M. Allendorf, R. P. Van Duyne and J. T. Hupp, Metal-Organic Framework Materials as Chemical Sensors. *Chemical Reviews*. 2012, **112**(2), 1105-1125.
7. D. J. Tranchemontagne, J. L. Mendoza-Cortés, M. O'Keeffea and O. M. Yaghi, Secondary building units, nets and bonding in the chemistry of metal-organic frameworks. *Chemical Society Reviews*. 2009, **38**(5), 1257-1283.
8. J. J. Perry IV, J. A. Perman and M. J. Zaworotko, Design and synthesis of metal-organic frameworks using metal-organic polyhedra as supermolecular building blocks. *Chemical Society Reviews*. 2009, **38**(5), 1400-1417.
9. S. Kitagawa, R. Kitaura and S. I . Noro, Functional Porous Coordination Polymers. *Angewandte Chemie International Edition*. 2004, **43**(18), 2334-2375.
10. S. L. James, Metal-organic frameworks. *Chemical Society Reviews*. 2003, **32**(5), 276-288.
11. R. Robson, A net-based approach to coordination polymers. *Dalton Transactions*. 2000, **21**, 3735-3744.
12. H. D. J. Arkawazi, R. Clowes, A. I. Cooper, T. Konno, N. Kuwamura, C. M. Pask and M. J. Hardie, Complex Phase Behaviour and Structural Transformations of Metal-Organic Frameworks with Mixed Rigid and Flexible Bridging Ligands. *Chemistry A European Journal*. 2019, **25**(5), 1353-1362.
13. R. F. d. Luis, E. S. Larrea, J. Orive, A. F. Marijuan, L. Lezamaad and M. I. Arriortuaab, Open and closed forms of the interpenetrated $[Cu_2(Tae)(Bpa)_2](NO_3)_2{\cdot}nH_2O$: magnetic properties and high pressure CO_2/CH_4 gas sorption. *Dalton Transactions*. 2018, **47**(3), 958-970.
14. Q. Qiu, L. Gu, H. Ma, L. Yan, M. Liuc and H. Li, Double layer zinc-UDP coordination polymers: structure and properties. *Dalton Transactions*. 2018, **47**(40), 14174-14178.
15. D. Geng, M. Zhang, X. Hang, W. Xie, Y. Qin, Q. Li, Y. Bi and Z. Zhengab, A 2D metal-thiacalix[4]arene porous coordination polymer with 1D channels: gas absorption/separation and frequency response. *Dalton Transactions*. 2018, **47**(27), 9008-9013.
16. S. Q. Bai, I. H. K. Wong, N. Zhang, K. L. Ke, M. Lin, D. J. Young and T. S. A. Hor, A new 3-D coordination polymer as a precursor for CuI-based thermoelectric composites. *Dalton Transactions*. 2018, **47**(45), 16292-16298.
17. Y. Lin, X. Zhang, W. Chen, W. Shi and P. Cheng, Three Cadmium Coordination Polymers with Carboxylate and Pyridine Mixed Ligands: Luminescent Sensors for Fe^{III} and Cr^{VI} Ions in an Aqueous Medium. *Inorganic Chemistry*. 2017, **56**(19), 11768-11778.

18. L. Wang, D. C. Tranca, J. Zhang, Y. Qi, S. Sfaelou, T. Zhang, R. Dong, X. Zhuang, Z. Zheng and G. Seifert, Toward Activity Origin of Electrocatalytic Hydrogen Evolution Reaction on Carbon-Rich Crystalline Coordination Polymers. *Small Communication*. 2017, **13**(37), 1700783.
19. K. Vellingiri, L. Philip and K. H. Kim, Metal-organic frameworks as media for the catalytic degradation of chemical warfare agents. *Coordination Chemistry Reviews*. 2017, **353**, 159-179.
20. O. K. Farha, A. Ö. Yazaydın, I. Eryazici, C. D. Malliakas, B. G. Hauser, M. G. Kanatzidis, S. B. T. Nguyen, R. Q. Snurr and J. T. Hupp, De novo synthesis of a metal-organic framework material featuring ultrahigh surface area and gas storage capacities. *Nature Chemistry*. 2010, **2**, 944-948.
21. G. Férey and C. Serre, Large breathing effects in three-dimensional porous hybrid matter: facts, analyses, rules and consequences. *Chemical Society Reviews*. 2009, **38**(5), 1380-1399.
22. H. Li, K. Wang, Y. Sun, C. T. Lollar, J. Li and H. C. Zhou, Recent advances in gas storage and separation using metal-organic frameworks. *Materials Today*, 2018, **21**(2), 108-121.
23. K. Chen, L. Zhang and W. Zhang, Preparation and evaluation of open-tubular capillary column combining a metal-organic framework and a brush-shaped polymer for liquid chromatography. *Journal of Separation Science*. 2018, **41**(11), 2347-2353.
24. X. Yang and Q. Xu, Bimetallic Metal-Organic Frameworks for Gas Storage and Separation. *Crystal Growth and Design*. 2017, **17**(4), 1450-1455.
25. M. P. Singh, N. R. Dhumal, H. J. Kim, J. Kiefer and J. A. Anderson, Removal of Confined Ionic Liquid from a Metal Organic Framework by Extraction with Molecular Solvents. *The Journal of Physical Chemistry* C. 2017, **121**(19), 10577-10586.
26. A. Singh, R. Vedarajan and N. Matsumi, Modified Metal Organic Frameworks (MOFs)/Ionic Liquid Matrices for Efficient Charge Storage. *Journal of The Electrochemical Society*. 2017, **164**(8), H5169-H5174.
27. M. S. Shah, M. Tsapatsis and J. I. Siepmann, Hydrogen Sulfide Capture: From Absorption in Polar Liquids to Oxide, Zeolite, and Metal-Organic Framework Adsorbents and Membranes. *Chemical Reviews*. 2017, **117**(14), 9755-9803.
28. J. Cho and Y. Ishida, Macroscopically Oriented Porous Materials with Periodic Ordered Structures: From Zeolites and Metal-Organic Frameworks to Liquid-Crystal-Templated Mesoporous Materials. *Advanced Materials*. 2017, **29**(25), 1605974.
29. M. I. Nandasiri, S. R. Jambovanea, B. P. M. Grailb, H. T. Schaefc and S. K. Nune, Adsorption, separation, and catalytic properties of densified metal-organic frameworks. *Coordination Chemistry Reviews*. 2016, **311**, 38-52.
30. D. De, T. K. Pal, S. Neogi, S. Senthilkumar, D. Das, S. S. Gupta and P. K. Bharadwaj, A Versatile Cu^{II} Metal-Organic Framework Exhibiting High Gas Storage Capacity with Selectivity for CO_2: Conversion of CO_2 to Cyclic Carbonate and Other Catalytic Abilities. *Chemistry A European Journal*. 2016, **22**(10), 3387-3396.
31. S. Kayal, B. Sun and A. Chakraborty, Study of metal-organic framework MIL-101(Cr) for natural gas (methane) storage and compare with other MOFs (metal-organic frameworks). *Energy*. 2015, **91**, 772-781.
32. J. A. Mason, M. Veenstra and J. R. Long, Evaluating metal-organic frameworks for natural gas storage. *Chemical Science*. 2014, **5**(1), 32-51.
33. L. Li, S. Tang, C. Wang, X. Lv, M. Jiang, H. Wua and X. Zhao, High gas storage capacities and stepwise adsorption in a UiO type metal-organic framework incorporating Lewis basic bipyridyl sites. *Chemical Communications*. 2014, **50**(18), 2304-2307.

34. B. Li, H. M. Wen, W. Zhou and B. Chen, Porous Metal-Organic Frameworks for Gas Storage and Separation: What, How, and Why?. *The Journal of Physical Chemistry Letters*. 2014, **5**(20), 3468-3479.
35. M. Yadav and Q. Xu, Liquid-phase chemical hydrogen storage materials. *Energy and Environmental Science*. 2012, **5**(12), 9698-9725.
36. C. Tan, S. Yang, N. R. Champness, X. Lin, A. J. Blake, W. Lewisa and M. Schröder, High capacity gas storage by a 4,8-connected metal-organic polyhedral framework. *Chemical Communications*. 2011, **47**(15), 4487-4489.
37. D. Frahm, M. Fischer, F. Hoffmann and M. Fröba, An interpenetrated metal-organic framework and its gas storage behavior: simulation and experiment. *Inorganic Chemistry*. 2011, **50**(21), 11055-11063.
38. S. Ma and H. C. Zhou, Gas storage in porous metal-organic frameworks for clean energy applications. *Chemical Communications*. 2010, **46**(1), 44-53.
39. Y. Li and R. T. Yang, Gas adsorption and storage in metal-organic framework MOF-177. *Langmuir*. 2007, **23**(26), 12937-12944.
40. L. Zhu, X. Q. Liu, H. L. Jiang and L. B. Sun, Metal-Organic Frameworks for Heterogeneous Basic Catalysis. *Chemical Reviews*. 2017, **117**(12), 8129-8176.
41. Q. Yang, Q. Xu and H. L. Jiang, Metal-organic frameworks meet metal nanoparticles: synergistic effect for enhanced catalysis. *Chemical Society Reviews*. 2017, **46**(15), 4774-4808.
42. Y. B. Huang, J. Liang, X. S. Wanga and Rong Cao, Multifunctional metal-organic framework catalysts: synergistic catalysis and tandem reactions. *Chemical Society Reviews*. 2017, **46**(1), 126-157.
43. X. Chen, Y. Peng, X. Han, Y. Liu, X. Lin and Y. Cui, Sixteen isostructural phosphonate metal-organic frameworks with controlled Lewis acidity and chemical stability for asymmetric catalysis. *Nature Communications*. 2017, **8**(1), 1-9.
44. S. Wang, J. Lin and X. Wang, Semiconductor-redox catalysis promoted by metal-organic frameworks for CO_2 reduction. *Physical Chemistry Chemical Physics*. 2014, **16**(28), 14656-14660.
45. A. Dhakshinamoorthy and H. Garcia, Catalysis by metal nanoparticles embedded on metal-organic frameworks. *Chemical Society Reviews*. 2012, **41**(15), 5262-5284.
46. F. Song, C. Wang and W. Lin, A chiral metal-organic framework for sequential asymmetric catalysis. *Chemical Communications*. 2011, **47**(29), 8256-8258.
47. M. Ranocchiari and J. A. V. Bokhoven, Catalysis by metal-organic frameworks: fundamentals and opportunities. *Physical Chemistry Chemical Physics*. 2011, **13**(14), 6388-6396.
48. X. Gu, Z. H. Lu, H. L. Jiang, T. Akita and Q. Xu, Synergistic catalysis of metal-organic framework-immobilized Au-Pd nanoparticles in dehydrogenation of formic acid for chemical hydrogen storage. *Journal of the American Chemical Society*. 2011, **133**(31), 11822-11825.
49. D. Dang, P. Wu, C. He, Z. Xie and C. Duan, Homochiral metal-organic frameworks for heterogeneous asymmetric catalysis. *Journal of the American Chemical Society*. 2010, **132**(41), 14321-14323.
50. L. Ma, C. Abney and W. Lin, Enantioselective catalysis with homochiral metal-organic frameworks. *Chemical Society Reviews*. 2009, **38**(5), 1248-1256.
51. I. A. Lázaro and R. S. Forgan, Application of zirconium MOFs in drug delivery and biomedicine. *Coordination Chemistry Reviews*. 2019, **380**, 230-259.

52. K. R. Stefaniak, C. C. Epley, J. J. Novak, M. L. McAndrew, H. D. Cornell, J. Zhu, D. K. McDaniel, J. L. Davis, I. C. Allen, A. J. Morris and T. Z. Grove, Photo-triggered release of 5-fluorouracil from a MOF drug delivery vehicle. *Chemical Communications*. 2018, **54**(55), 7617-7620.
53. M. Pander, A. Żelichowska and W. Bury, Probing mesoporous Zr-MOF as drug delivery system for carboxylate functionalized molecules. *Polyhedron*. 2018, **156**, 131-137.
54. Z. Nadizadeh, M. R. Naimi-Jamal and L. Panahi, Mechanochemical solvent-free in situ synthesis of drug-loaded $\{Cu_2(1,4\text{-bdc})_2(dabco)\}_n$ MOFs for controlled drug delivery. *Journal of Solid State Chemistry*. 2018, **259**, 35-42.
55. M. X. Wu and Y. W. Yang, Metal-Organic Framework (MOF)-Based Drug/Cargo Delivery and Cancer Therapy. *Advanced Materials*. 2017, **29**(23), 1606134.
56. J. D. Rocca, D. Liu and W. Lin, Nanoscale Metal-Organic Frameworks for Biomedical Imaging and Drug Delivery. *Accounts of Chemical Research*. 2011, **44**(10), 957-968.
57. A. C. McKinlay, R. E. Morris, P. Horcajada, G. Férey, R. Gref, P. Couvreur and C. Serre, BioMOFs: Metal-Organic Frameworks for Biological and Medical Applications. *Angewandte Chemie International Edition.* 2010, **49**(36), 6260-6266.
58. S. M. Cohen, Postsynthetic Methods for the Functionalization of Metal-Organic Frameworks. *Chemical Reviews*. 2012, **112**(2), 970-1000.
59. Q. Y. Yang, P. Lama, S. Sen, M. Lusi, K. J. Chen, W. Y. Gao, M. Shivanna, T. Pham, N. Hosono, S. Kusaka, J. J. Perry IV, S. Ma, B. Space, L. J. Barbour, S. Kitagawa and M. J. Zaworotko, Reversible Switching between Highly Porous and Nonporous Phases of an Interpenetrated Diamondoid Coordination Network That Exhibits Gate-Opening at Methane Storage Pressures. *Angewandte Chemie International Edition.* 2018, **57**(20), 5684-5689.
60. H. Y. Yang, Y. Z. Li, C. Y. Jiang, H. H. Wang, L. Hou, Y. Y. Wang and Z. Zhu, An Interpenetrated Pillar-Layered Metal-Organic Framework with Novel Clusters: Reversible Structural Transformation and Selective Gate-Opening Adsorption. *Crystal Growth and Design*. 2018, **18**(5), 3044-3050.
61. M. Shivanna, Q. Y. Yang, A. Bajpai, E. P. Kazmierczak and M. J. Zaworotko, A dynamic and multi-responsive porous flexible metal-organic material. *Nature Communications*. 2018, **9**(1), 3080.
62. A. Halder and D. Ghoshal, Structure and properties of dynamic metal-organic frameworks: a brief accounts of crystalline-to-crystalline and crystalline-to-amorphous transformations. *Crystal Engineering Communications*. 2018, **2**(1), 1322-1345.
63. X. Sun, S. Yao, G. Li, L. Zhang, Q. Huo and Y. Liu, A Flexible Doubly Interpenetrated Metal-Organic Framework with Breathing Behavior and Tunable Gate Opening Effect by Introducing Co^{2+} into Zn_4O Clusters. *Inorganic Chemistry*. 2017, **56**(11), 6645-6651.
64. R. E. Morris and L. Brammer, Coordination change, lability and hemilability in metal-organic frameworks. *Chemical Society Reviews*. 2017, **46**(17), 5444-5462.
65. J. P. Zhang, P. Q. Liao, H. L. Zhou, R. B. Lina and X. M. Chen, Single-crystal X-ray diffraction studies on structural transformations of porous coordination polymers. *Chemical Society Reviews*. 2014, **43**(16), 5789-5814.
66. A. Schneemann, V. Bon, I. Schwedler, I. Senkovska, S. Kaskel and R. A. Fischer, Flexible metal-organic frameworks. *Chemical Society Reviews*. 2014, **43**(16), 6062-6096.
67. C. R. Murdock, B. C. Hughes, Z. Lu and D. M. Jenkins, Approaches for synthesizing breathing MOFs by exploiting dimensional rigidity. *Coordination Chemistry Reviews*. 2014, **258**-**259**, 119-136.

68. G. K. Kole and J. J. Vittal, Solid-state reactivity and structural transformations involving coordination polymers. *Chemical Society Reviews*. 2013, **42**(4), 1755-1775.
69. J. S. Grosch and F. Paesani, Molecular-Level Characterization of the Breathing Behavior of the Jungle-Gym-type DMOF-1 Metal-Organic Framework. *Journal of the American Chemical Society*. 2012, **134**(9), 4207-4215.
70. S. Kitagawa and R. Matsuda, Chemistry of coordination space of porous coordination polymers. *Coordination Chemistry Reviews*. 2007, **251**(21), 2490-2509.
71. G. J. Halder and C. J. Kepert, Single Crystal to Single Crystal Structural Transformations in Molecular Framework Materials. *Australian Journal of Chemistry*. 2006, **59**(9), 597-604.
72. A. J. Fletcher, K. M. Thomas and M. J. Rosseinsky, Flexibility in metal-organic framework materials: Impact on sorption properties. *Journal of Solid State Chemistry*. 2005, **178**(8), 2491-2510.
73. D. N. Dybtsev, H. Chun and K. Kim, Rigid and flexible: a highly porous metal-organic framework with unusual guest-dependent dynamic behavior. *Angewandte Chemie International Edition*. 2004, **43**(38), 5033-5036.
74. B. F. Abrahams, M. J. Hardie, B. F. Hoskins, R. Robson and G. A. Williams, Topological rearrangement within a single crystal from a honeycomb cadmium cyanide $[Cd(CN)_2]_n$ 3D net to a diamond net. *Journal of the American Chemical Society*. 1992, **114**(26), 10641-10643.
75. Z. Yin, Y. L. Zhou, M. H. Zeng and M. Kurmooc, The concept of mixed organic ligands in metal-organic frameworks: design, tuning and functions. *Dalton Transactions*. 2015, **44**(12), 5258-5275.
76. H. Y. Lin, J. Luan, X. L. Wang, J. W. Zhang, G. C. Liua and A. X. Tiana, Construction and properties of cobalt(II)/copper(II) coordination polymers based on N-donor ligands and polycarboxylates mixed ligands. *Royal Society of Chemistry Advances*. 2014, **4**(107), 62430-62445.
77. S. Abedi, A. A. Tehrani, H. Ghasempoura and A. Morsali, Interplay between hydrophobicity and basicity toward the catalytic activity of isoreticular MOF organocatalysts. *New Journal of Chemistry*. 2016, **40**(8), 6970-6976.
78. M. Y. Masoomi, S. Beheshti and A. Morsali, Mechanosynthesis of new azine-functionalized Zn(II) metal-organic frameworks for improved catalytic performance. *Journal of Materials Chemistry A*. 2014, **2**(40), 16863-16866.
79. R. G. Lin, G. J. Cao, J. D. Lina and Y. L. Wanga, A novel 3-fold interpenetration metal-organic framework with tunable luminescence and selective adsorption of CO_2 properties. *New Journal of Chemistry*. 2015, **39**(12), 9075-9078.
80. P. J. Kitson, R. J. Marshall, D. Long, R. S. Forgan and L. Cronin, 3D Printed High-Throughput Hydrothermal Reactionware for Discovery, Optimization, and Scale-Up. *Angewandte Chemie International Edition*. 2014, **126**(47), 12937-12942.
81. Y. Gong, J. Li, J. B. Qin, T. Wu, R. Cao and J. H. Li, Metal(II) Coordination Polymers Derived from Bis-pyridyl-bis-amide Ligands and Carboxylates: Syntheses, Topological Structures, and Photoluminescence Properties. *Crystal Growth and Design*. 2011, **11**(5), 1662-1674.
82. L. J. Bourhis, O. V. Dolomanov, R. J. Gildea, J. A. K. Howardd and H. Puschmannb, The anatomy of a comprehensive constrained, restrained refinement program for the modern computing environment-Olex2 dissected. *Acta Crystallographica Section A*. 2015, **71**(1), 59-75.
83. L. Palatinus, S. J. Prathapab and S. V. Smaalen, EDMA: a computer program for topological analysis of discrete electron densities. *Journal of Applied Crystallography*. 2012, **45**(3), 575-580.

84. O. V. Dolomanov, L. J. Bourhis, R. J. Gildea, J. A. K. Howarda and H. Puschmann, OLEX2: a complete structure solution, refinement and analysis program. *Journal of Applied Crystallography*. 2009, **42**(2), 339-341.
85. L. Palatinus and A. V. D. Lee, Symmetry determination following structure solution in P1. *Journal of Applied Crystallography*. 2008, **41**(6), 975-984.
86. L. Palatinus and G. Chapuis, SUPERFLIP-a computer program for the solution of crystal structures by charge flipping in arbitrary dimensions. *Journal of Applied Crystallography*. 2007, **40**(4), 786-790.
87. S. L. Huang, Y. J. Lin, Z. H. Li and G. X. Jin, Self-Assembly of Molecular Borromean Rings from Bimetallic Coordination Rectangles. *Angewandte Chemie International Edition*. 2014, **53**(42), 11218-11222.
88. A. Hu, X. Chen, H. Zhou, Y. Y. Chen and A. Yuan, Syntheses, structures, and host-guest interactions of 2-D grid-type cyanide-bridged compounds $[Zn(L)(H_2O)_2][M(CN)_4]\cdot 3H_2O$ (L= *N,N*'-bis(4-pyridylformamide)-1,4-benzene; M = Ni, Pd or Pt). *Journal of Coordination Chemistry*. 2013, **66**(18), 3241-3248.
89. Robert M. Silverstein, Francis X. Webster and David J. Kiemle, Spectrometric identification of organic compounds. 7th Edition. 2005. John Wiley and Sons, Inc.
90. Donald L. Pavia, Gary M. Lampman and George S. Kriz, Introduction to spectroscopy: a guide for students of organic chemistry. 2nd Edition. 1996. Harcourt Brace College Publishers.
91. Y. Lu, Y. Lin, Z. Li and G. Jin, Highly Stable Molecular Borromean Rings. *Chinese Journal of Chemistry*. 2018, **36**(2), 106-111.
92. H. Y. Lin, P. Liu, X. L. Wang, B. Mu, F. F. Sui and G. C. Liu, Two New 3-D Supramolecular Complexes Based on Tetradentate Carboxylate Linker and Bis-pyridyl-bis-amide Ligand: Syntheses, Structures and Electrochemical Properties. *Journal of Chemical Crystallography*. 2013, **43**(1), 44-50.
93. X. Wang, H. Lin, B. Mu, A. Tiana and G. Liua, Encapsulation of discrete $(H_2O)_{12}$ clusters in a 3D three-fold interpenetrating metal-organic framework host with (3,4)-connected topology. *Dalton Transactions*. 2010, **39**(27), 6187-6189.
94. Alan K. Brisdon, Inorganic Spectroscopic Methods. 1998. Oxford University Press.
95. Dudley Williams and Ian Fleming, Spectroscopic methods in organic chemistry. 6th Edition. 1995. McGraw-Hill Education.
96. G. Xu, M. Xie, X. Li, W. Shi, H. Yu, Y. Hu, X. Xuna and Y. Xie, Four binuclear coordination polymers with a 6^3 net and self-assembly of 2D 6^3 topology into different supramolecular networks using unit-unit H-bonds. *Crystal Engineering Communications*. 2015, **17**(19), 3677-3686.
97. L. P. Hsu, J. Y. Wu and K. L. Lu, Self-Recognition of 3D Porous Frameworks: Fourfold Diamondoid or Threefold Cuboidal Interpenetrating Nets Formed by Varying Pillar Motifs. *Journal of Inorganic and Organometallic Polymers and Materials*. 2007, **17**(1), 259-265.
98. E. Y. Choi, K. Park, C. M. Yang, H. Kim, J. H. Son, S. W. Lee, Y. H. Lee, D. Min and Y. U. Kwon, Benzene-Templated Hydrothermal Synthesis of Metal-Organic Frameworks with Selective Sorption Properties. *Chemistry A European Journal*. 2004, **10**(21), 5535-5540.
99. S. W. Lee, H. J. Kim, Y. K. Lee, K. Park. J. H. Son and Y. U. Kwon, Triply interpenetrating coordination polymers based on paddle-wheel type secondary-building units of $M_2(CO_2R)_4$: $[Ni_3(2,6\text{-NDC})_3(bipy)_{1.5}]$, $[Co_3(2,6\text{-NDC})_3(bipy)_{1.5}]$, and [Co(1,3-BDC)(bipyen)] (2,6-NDC=2,6-

naphthalenedicarboxylate; 1,3-BDC=1,3-benzenedicarboxylate; bipy=4,4'-bipyridine; bipyen=trans-1,2-bis(4-pyridyl)ethylene). *Inorganica Chimica Acta*. 2003, **353**, 151-158.

100. X. D. Zhu, Y. Li, W. X. Zhou, R. M. Liu, Y. J. Ding, J. Lü and D. M. Proserpiocd, Metal-organic frameworks assembled from flexible alicyclic carboxylate and bipyridyl ligands for sensing of nitroaromatic explosives. *Crystal Engineering Communication*. 2016, **18**(24), 4530-4537.
101. J. M. Hu, V. A. Blatov, B. Yu, K. Van Heckec and G. H. Cui, An unprecedented "strongly" self-catenated MOF containing inclined catenated honeycomb-like units. *Dalton Transactions*. 2016, **45**(6), 2426-2429.
102. T. Jacobs, R. Clowes, A. I. Cooper and M. J. Hardie, A Chiral, Self-Catenating and Porous Metal-Organic Framework and its Post-Synthetic Metal Uptake. *Angewandte Chemie International Edition.* 2012, **51**(21), 5192-5195.
103. Y. Gong, Y. C. Zhou, T. F. Liu, J. Lü, D. M. Proserpioc and R. Cao, Interpenetrated metal-organic frameworks of self-catenated four-connected mok nets. *Chemical Communications*. 2011, **47**(21), 5982-5984.
104. L. F. Ma, Q. L. Meng, C. P. Li, B. Li, L. Y. Wang, M. Du and F. P. Liang, Delicate Substituent Effect of Benzene-1,2,3-Tricarboxyl Tectons on Structural Assembly of Unusual Self-Penetrating Coordination Frameworks. *Crystal Growth and Design*. 2010, **10**(7), 3036-3043.
105. D. S. Li, L. Tang, F. Fu, M. Du, J. Zhao, N. Wang and P. Zhang, Coordination assemblies of $Cd^{II}/Zn^{II}/Co^{II}$ with the 3-(pyridin-4-yl) benzoate tecton: Structural diversity and properties. *Inorganic Chemistry Communications*. 2010, **13**(10), 1126-1130.
106. Q. Q. Zhang, X. D. Yang, L. Sun, R. Y. Guo, M. Chen and J. Zhang, Structural adjustment of bipyridinium-bearing Cu(II) coordination polymers and the adsorption properties toward methanol, water and ethanol vapors. *Inorganic Chemistry Communications*. 2018, **87**, 27-29.
107. Y. Xiong, Y. Z. Fan, D. D. Borges, C. X. Chen, Z. W. Wei, H. P. Wang, M. Pan, J. J. Jiang, G. Maurin and C. Y. Su, Ligand and Metal Effects on the Stability and Adsorption Properties of an Isoreticular Series of MOFs Based on T-Shaped Ligands and Paddle-Wheel Secondary Building Units. *Chemistry A European Journal*. 2016, **22**(45), 16147-16156.
108. T. R. C. Van Assche, T. Duerinck, J. J. G. Sevillano, S. Calero, G. V. Baron and J. F. M. Denayer, High Adsorption Capacities and Two-Step Adsorption of Polar Adsorbates on Copper–Benzene-1,3,5-tricarboxylate Metal-Organic Framework. *The Journal of Physical Chemistry* C. 2013, **117**(35), 18100-18111.
109. M. P. Suh, Y. E. Cheon and E. Y. Lee, Reversible Transformation of Zn^{II} Coordination Geometry in a Single Crystal of Porous Metal-Organic Framework $[Zn_3(ntb)_2(EtOH)_2]\cdot 4\,EtOH$. *Chemistry A European Journal*. 2007, **13**(15), 4208-4215.